



**HAL**  
open science

# Analysis of the Protein Arginine Methyltransferases 1 (PRMT1) and 4 (PRMT4) in Triple-Negative Breast Cancer

Samyuktha Suresh

► **To cite this version:**

Samyuktha Suresh. Analysis of the Protein Arginine Methyltransferases 1 (PRMT1) and 4 (PRMT4) in Triple-Negative Breast Cancer. Cancer. Université Paris-Saclay, 2021. English. NNT : 2021UP-ASL060 . tel-03917555

**HAL Id: tel-03917555**

**<https://theses.hal.science/tel-03917555>**

Submitted on 2 Jan 2023

**HAL** is a multi-disciplinary open access archive for the deposit and dissemination of scientific research documents, whether they are published or not. The documents may come from teaching and research institutions in France or abroad, or from public or private research centers.

L'archive ouverte pluridisciplinaire **HAL**, est destinée au dépôt et à la diffusion de documents scientifiques de niveau recherche, publiés ou non, émanant des établissements d'enseignement et de recherche français ou étrangers, des laboratoires publics ou privés.

Analysis of the protein arginine  
methyltransferases 1 (PRMT1) and 4  
(PRMT4) in triple-negative breast cancer

*Analyse des protéines arginine  
méthyltransférases 1 (PRMT1) et 4 (PRMT4) dans  
les cancers du sein triple-négatifs*

**Thèse de doctorat de l'université Paris-Saclay  
Préparée à l'Institut Curie – Centre de Recherche**

École doctorale n°582  
Cancérologie : biologie - médecine - santé (CBMS)  
Spécialité de doctorat: recherche clinique, innovation technologique, santé  
publique  
Unité de recherche: Institut Curie - PSL Research University, Translational Research  
Department, Breast Cancer Biology Group, 75005 Paris, France.  
Réfèrent : Faculté de médecine

**Thèse présentée et soutenue à Paris-Saclay,  
le 20/09/2021, par**

**Samyuktha SURESH**

**Composition du Jury**

<b>Emmanuelle CHARAFE-JAUFFRET</b> Professeure, Institut Paoli-calmettes	Présidente
<b>Jocelyn CÔTÉ</b> Professeur, Ottawa University	Rapporteur & Examineur
<b>Julie PANNEQUIN</b> Directrice de recherche, Université de Montpellier	Rapporteur & Examinatrice
<b>Céline VALLOT</b> Chargée de recherche, Institut Curie	Examinatrice
<b>Renaud LEGOUIS</b> Directeur de recherche, I2BC, Paris- Saclay	Examineur

**Direction de la thèse**

<b>Thierry DUBOIS</b> Responsable d'équipe, Institut Curie	Directeur de thèse
---	--------------------



*Dedicated to*

*my beloved mom and dad  
and the loving memory of my maternal grandparents*

*என் அன்பான அம்மா மற்றும் அப்பாவிற்஑ு  
என் தாய்வழி தாத்தா மற்றும் பாட்டியின் நினைவாக*



# ACKNOWLEDGEMENTS

*First, I would like to thank Dr. Thierry Dubois, my thesis director, first for selecting me as a PhD candidate for the IC3i PhD program and for giving me the opportunity to work at the Breast Cancer Biology Group. Thierry, you have been an incredibly supportive supervisor and mentor during these last four years. I have learnt a lot from you, both scientifically and personally. Thank you for your guidance, support, and motivation without which this journey would not have been possible.*

*I would like to thank my two rapporteurs, Prof. Jocelyn Côté and Dr. Julie Pannequin for agreeing to read and comment on my thesis manuscript. I would also like to thank the other members of the jury, Prof. Emmanuelle Charafe-Jauffret, Dr. Celine Vallot, and Dr. Renaud Legouis, for accepting to be a part of my thesis jury.*

*I would also like to thank the members of my thesis monitoring committee, Dr. Muriel Le Romancer, Dr. Claire Hivroz, Dr. Francisco Cruzalegui, Dr. Nicolas Reynoird, Prof. Christian Auclair, and Dr. Sergio Roman-Roman for their expertise, guidance, and valuable feedback during these four years and for advising me on which direction to follow during each committee meeting. Claire, thank you for being a kind mentor. Muriel, thank you for the insightful interactions and discussions during the visits to Lyon. Francisco, apart from being on my thesis committee, you were also a part of my selection committee for the IC3i PhD program. Thank you for asking me challenging questions that really stimulated my critical thinking on the spot.*

*I would like to thank the collaborators and my lab mates whose expertise and advice have been helpful for the completion of my thesis. For the PRMT1 project, Dr. Coralie Poulard and Dr. Muriel Le Romancer (for the ChIP of PRMT1 though I would have liked to learn this technique from you at Lyon); Dr. Fariba Némati (for all the in vivo work, and replying to my late-night emails!); Solène Huard (for doing the drug combination experiments); the Pathology department; Mengliang Ye, and the previous members of the BCBG lab who started this work (Amelie Brisson, Dr. David Silvestre, Dr. Faisal Mahmood, Bérengère-Marty prouvost). For the CARM1 project, Dr. Damarys Loew, Vanessa Masson and Florent Dingli at the Mass spectrometry Platform (for all your help with the different kinds of analysis we wanted to do); Dr. Arnaud Echard, Dr. Tamara Advedissian, Dr. Adrien Presle, Dr. Cyril Addi for all their help with cytokinesis related experiments; Laetitia Lesage, Dr. Andre Nicolas, Dr. Didier Meseure, Dr. Anne Vincent-Salomon and Laetitia Fuhrmann at the Pathology department and platform; Sophie Vacher and Dr. Ivan Bièche at the Genetic Department; Dr. Ahmed El Marjou at the Recombinant platform (and Solène Huard for purifying CARM1); Dr. Greg Towers (for his help and discussion on the HIV experiments); Dr. Clotilde Thèry (for help and discussion on the exosomes experiments) and Mathilde Mathieu (for showing me how to purify exosomes); Dr. Amulya Priya and Nguyen Huyen Nhung.*

*A big thanks to my lab mates; Virginie Maire, Amelie Brisson, Clarisse Monchecourt, Olivier Zajac, Dr. Ramón García Areas, Dr. Mathilde Vinet, Benjamin Marande, Solène Huard, and Rayan Dakroub. Virginie, thanks for being a great teacher and for a lively atmosphere in the office and for helping me improve my French skills because of your "Vitesse de parole". Amelie, Clarisse, Olivier, and Mathilde, for a friendly and welcoming experience at the BCBG lab, it was a pleasure to work by your sides. Ramón, for being a great companion, and late-night lab buddy during your time here in the lab. Ben, it was a lot of fun to work with you. Solène, a big thanks for your help experimentally, and I hope you find interesting results with ALIX (and maybe CARM1 at the midbody?). Solène and Rayan, I have truly enjoyed working and discussing with you both and Goodluck with your PhDs.*

*Un grand merci à Dominique Gallier. Dominique, merci de m'avoir appris le français et d'être un professeur formidable, que je peux le parler "couramment" et évidemment de l'écrire !*

*Thank you, Rania El Botty, Malcy Tarin, Adeline Durand, and all the members of the Translational department for your inputs and help.*

*I would like to thank the Cofund – IC3i international PhD program for giving me this fantastic opportunity to pursue my PhD at Institut Curie. To the European Union's Horizon 2020 research and innovation programme (Marie Skłodowska-Curie grant no: 666003) for financial support during the last four years.*

*Melanie Herrbach and Anemone Trysavath for accommodating us during the IC3i interviews and also all the help during the settling down period in Paris, and of course for introducing the IC3i family!*

*My IC3i friends, Raquel, Sandra, Darine, Silvia, Anne-Céline and Özge for being my family away from home and the extraordinary support from each of them during the last four years. Raquel, my constant companion in the lab, even though we were not in the same office/team, I am grateful for your incredible support through all the highs and lows, gràcies, amic meu. Sandra, my first friend in Paris, and for being a forever friend. Cheers to the intense thesis writing and all our memorable trips. Darine, thanks for always feeding me, our movie/dinner nights, and the amazing couple trip of 2020. Silvia and Annie for all the beautiful memories we have made. Tommaso, Deep and Danny, for being good friends and for your support.*

*Tushar, for all your support, motivation, and for being there.*

*Mom and Dad, for your tremendous support, love, and encouragement since 1994, even from thousands of kilometers away, without which I would not be where I am. A big Thank you!*

*Thank you to everyone who has been a part of this amazing journey, for your help and support however small or big.*

*Thank you, Merci, நன்றி.*

*Samyuktha*

# RESUMÉ

Le cancer du sein triple-négatifs (TNBC) est le cancer du sein le plus agressif avec un taux élevé de rechute dans les cinq années suivant la chimiothérapie. L'identification de nouvelles pistes thérapeutiques pour éviter les rechutes est une priorité en oncologie. Les protéines arginine méthyltransférases (PRMTs) constituent une nouvelle famille de neuf enzymes qui catalysent l'ajout de groupements méthyle sur les arginines de leurs substrats (histones et non-histones). Cette modification post-traductionnelle régule ainsi de nombreux processus cellulaires fondamentaux tels que la transcription (activation et/ou répression), le métabolisme de l'ARN, la réparation de l'ADN et la transduction du signal. Certaines PRMTs sont surexprimées dans divers cancers, dont le cancer du sein, et ont été proposées comme des cibles thérapeutiques intéressantes. En analysant des biopsies de tumeurs de sein, nous avons observé que PRMT1 et PRMT4 sont plus exprimées, au niveau ARN, dans les tumeurs TNBC par rapport aux tissus « normaux » de sein. Par conséquent, l'objectif principal de ma thèse a été de caractériser les fonctions de PRMT1 et PRMT4 dans des lignées cellulaires TNBC.

Nous avons montré, par immunohistochimie (IHC), que la protéine PRMT1 est exprimée à des niveaux plus élevés dans les tumeurs du sein par rapport aux tissus normaux. Nous n'avons pas observé de variation d'expression entre les différents sous-types de cancer du sein. Nous avons ensuite démontré qu'une diminution de l'expression de PRMT1 par des ARN interférents ralentit la prolifération cellulaire et la formation de colonies et induit l'apoptose dans plusieurs lignées cellulaires de cancer du sein. Nous avons également montré que l'inhibition de PRMT1 (à l'aide d'inhibiteurs des PRMTs de type I, dont PRMT1 est l'enzyme principale) diminue *in vitro* la prolifération cellulaire et la formation de colonies. L'inhibiteur des PRMTs de type I, GSK3368715, est actuellement évalué dans un essai clinique de phase I. Nous avons traité des souris avec cet inhibiteur et avons observé un ralentissement de la croissance tumorale dans un modèle murin de cancer TNBC. Nos travaux suggèrent donc que PRMT1 pourrait être une cible thérapeutique pour le traitement des cancers du sein. Pour déterminer son rôle fonctionnel, nous avons comparé le transcriptome de cellules TNBC MDA-MB-468 transfectées avec des ARN interférents contrôle ou ciblant PRMT1. Cette étude a révélé que PRMT1 régule les voies de signalisation de l'EGFR et de Wnt. Nous avons constaté que la déplétion de PRMT1 diminue l'expression de l'ARNm de l'EGFR et de deux composants de la voie Wnt, LRP5 et Porcupine. De plus, nous avons



démontré que PRMT1 est directement recrutée sur les promoteurs de ces trois gènes pour activer leur transcription. Porcupine est une enzyme qui modifie de manière post-traductionnelle les ligands Wnt permettant ainsi leur sécrétion dans le milieu extracellulaire ; ces ligands vont ensuite interagir avec les récepteurs transmembranaires de la voie Wnt, dont LRP5, pour activer cette voie de signalisation. Nous avons ensuite montré que la diminution de l'expression de PRMT1 ou son inhibition, réduisait l'activité de la voie Wnt. Nos résultats suggèrent donc que PRMT1 active la voie de signalisation Wnt, en contrôlant l'expression de LRP5 et Porcupine. La voie Wnt étant souvent associée à la chimiorésistance, nous avons émis l'hypothèse que cibler PRMT1 pourrait éventuellement éradiquer les cellules chimiorésistantes. Nous avons réalisé des combinaisons de médicaments entre les inhibiteurs des PRMTs de type I (MS023 et GSK3368715) et les chimiothérapies utilisées en clinique pour traiter les patientes présentant un cancer TNBC. Nous avons observé une synergie avec le cisplatine, le cyclophosphamide et la camptothécine, mais pas avec le docétaxel ou le paclitaxel. Nous avons aussi rapporté qu'il existe une synergie entre les inhibiteurs de PRMT1 et de l'EGFR. Ainsi, nous proposons qu'inhiber PRMT1, en combinaison avec des chimiothérapies, pourrait représenter une nouvelle stratégie de traitement pour les patientes atteintes d'un cancer TNBC.

Nous avons aussi constaté, par IHC, que l'expression protéique de PRMT4 est plus élevée dans les tumeurs de sein que dans les tissus normaux. Nous avons montré qu'une diminution de l'expression de PRMT4 par des ARN interférents compromet la prolifération cellulaire et la formation de colonies, et entraîne des cassures de l'ADN et de l'apoptose. En revanche, l'inhibition de son activité avec des inhibiteurs spécifiques récemment décrits (TP064, EZM2302) n'a pas ou peu d'effet sur la viabilité cellulaire. Ces observations suggèrent que PRMT4 pourrait contrôler la viabilité indépendamment de son activité enzymatique, à travers des interactions avec ses partenaires. Ainsi, afin de mieux comprendre les fonctions de PRMT4, nous avons recherché ses partenaires protéiques par spectrométrie de masse et avons identifié la protéine ALIX comme partenaire principal de PRMT4. ALIX est une protéine interagissant avec les protéines de transport ESCRT, et est impliquée dans le trafic cellulaire et la cytokinèse. Nous avons montré que PRMT4 interagit avec le domaine C-terminal d'ALIX et le méthyle au niveau de deux arginines. Comme ce domaine d'ALIX sert de point d'ancrage à de nombreuses protéines, sa méthylation par PRMT4 pourrait ainsi réguler certaines fonctions d'ALIX. Nous avons observé qu'une diminution de l'expression de PRMT4 entraîne des défauts de cytokinèse, altérant la localisation de la protéine ESCRT, CHMP4B, au site d'abscission, et conduisant à la

formation de cellules binucléées. Cependant, le rôle exact de PRMT4 dans la cytokinèse et la pertinence fonctionnelle de la méthylation d'ALIX médiée par PRMT4, restent à démontrer.

Nos travaux ont permis de mieux caractériser les fonctions cellulaires de PRMT1 et PRMT4, et de proposer d'inhiber PRMT1, en combinaison avec certaines chimiothérapies, pour le traitement des cancers TNBC.

# Table of Contents

<b>ACKNOWLEDGEMENTS .....</b>	<b>1</b>
<b>RESUMÉ.....</b>	<b>3</b>
<b>LIST OF FIGURES.....</b>	<b>12</b>
<b>LIST OF TABLES .....</b>	<b>16</b>
<b>LIST OF ABBREVIATIONS .....</b>	<b>17</b>
<b>CHAPTER 1: INTRODUCTION .....</b>	<b>24</b>
<b>I. GENERALITIES OF BREAST CANCER .....</b>	<b>25</b>
1.1 BREAST CANCER INCIDENCE AND MORTALITY RATE .....	25
1.2 RISK FACTORS .....	25
1.3 DIAGNOSIS AND SCREENING.....	26
1.4 ANATOMY OF BREAST.....	27
1.5 BREAST CANCER DEVELOPMENT AND TERMINOLOGIES.....	27
1.6 MOLECULAR SUBTYPES OF BREAST CANCER.....	29
1.6.1 Luminal A (ER+/PR+/Her2-).....	30
1.6.2 Luminal B (ER+/PR+ and Her2+ or Her2-) .....	30
1.6.3 Non-luminal Her2+ (ER-/PR- and Her2+) .....	31
1.6.4 Basal-like (ER-/PR-/Her2-).....	31
1.6.5 Normal-like (ER+/PR+/Her2-).....	31
1.7 BREAST CANCER TREATMENT .....	31
1.7.1 Surgery.....	32
1.7.2 Radiation therapy.....	34
1.7.3 Chemotherapies.....	34
1.7.4 Hormone therapies .....	35
1.7.5 Immunotherapy .....	36
1.7.6 Targeted therapy .....	37
<b>II. TRIPLE-NEGATIVE BREAST CANCER .....</b>	<b>40</b>
1.8 CLINICAL FEATURES, RISK FACTORS, PROGNOSIS .....	40
1.9 GENERAL MOLECULAR FEATURES .....	40
1.10 MOLECULAR SUBTYPES OF TNBC (LEHMANN CLASSIFICATION) .....	41
1.10.1 Basal-like 1 and 2 (BL1, BL2) .....	43
1.10.2 Mesenchymal (M) and Mesenchymal stem-like (MSL) .....	43
1.10.3 Immunomodulatory (IM).....	43
1.10.4 Luminal-androgen receptor (LAR).....	43

1.11	APPROVED THERAPY FOR TNBC .....	44
1.12	CHEMORESISTANCE, TNBC STEM CELLS AND THEIR UNDERLYING MECHANISMS.....	45
1.12.1	<i>ATP-binding cassette (ABC) transporters</i> .....	45
1.12.2	<i>Breast cancer stem cells and contributing signaling pathways</i> .....	45
1.13	CONCLUDING REMARKS .....	50
<b>III. PROTEIN-ARGININE METHYLTRANSFERASES (PRMTs) .....</b>		<b>52</b>
1.14	STRUCTURE OF THE PRMTs .....	54
1.15	GENERALITIES OF PRMTs .....	56
1.16	SUBSTRATE MOTIFS .....	56
1.17	CROSSTALK AMONG PRMTs AND SUBSTRATE SCAVENGING .....	57
1.18	CELLULAR FUNCTIONS AND ROLE IN DISEASES .....	57
1.18.1	<i>The many cellular functions of PRMTs</i> .....	57
1.18.2	<i>Pathological conditions associated with PRMTs</i> .....	61
1.19	PRMT INHIBITORS.....	70
<b>IV. PROTEIN-ARGININE METHYLTRANSFERASE 1 (PRMT1) .....</b>		<b>72</b>
1.20	CRYSTAL STRUCTURE .....	72
1.21	SEVEN SPLICED VARIANTS OF PRMT1.....	73
1.22	PHOSPHORYLATION AND UBIQUITINATION OF PRMT1.....	75
1.23	SUBSTRATES OF PRMT1.....	76
1.24	REGULATION OF SIGNAL TRANSDUCTION BY PRMT1 .....	77
1.24.1	<i>Wnt signaling pathway</i> .....	77
1.25	ROLE IN CANCER .....	79
1.25.1	<i>Breast cancer</i> .....	79
1.25.2	<i>Other solid cancer types</i> .....	81
1.25.3	<i>Hematological cancer</i> .....	82
<b>V. COACTIVATOR-ASSOCIATED ARGININE METHYLTRANSFERASE 1 (CARM1) .....</b>		<b>84</b>
1.26	CRYSTAL STRUCTURE OF CARM1 .....	84
1.26.1	<i>Generalities of the structure</i> .....	84
1.26.2	<i>Domain-specific features</i> .....	85
1.26.3	<i>Catalytic-dead mutants</i> .....	86
1.26.4	<i>Insights into ternary structures</i> .....	86
1.26.5	<i>CARM1 complexed with small-molecule inhibitors</i> .....	87
1.26.6	<i>Limitations of existing structures</i> .....	87
1.27	ALTERNATIVELY SPLICED ISOFORMS OF CARM1 .....	87
1.28	REGULATION OF CARM1.....	89
1.28.1	<i>Post-translational modifications</i> .....	89

1.28.2	<i>CARM1 regulation by nucleic acids</i> .....	90
1.29	THE KNOWN METHYLOME OF CARM1 .....	91
1.30	MAJOR CELLULAR FUNCTIONS .....	92
1.30.1	<i>Transcriptional regulation</i> .....	92
1.30.2	<i>RNA metabolism</i> .....	94
1.30.3	<i>Autophagy</i> .....	96
1.30.4	<i>Metabolism</i> .....	98
1.30.5	<i>Early-embryo development and cellular differentiation</i> .....	100
1.31	ROLE IN CANCER .....	102
1.31.1	<i>Breast Cancer</i> .....	103
1.31.2	<i>Ovarian cancer</i> .....	105
1.31.3	<i>Other solid cancer</i> .....	106
1.31.4	<i>Hematopoietic cancer</i> .....	106
1.31.5	<i>Liver and pancreatic cancer</i> .....	107
1.32	CONCLUDING REMARKS .....	107
<b>VI. ALIX: A MULTIFUNCTIONAL ADAPTOR PROTEIN .....</b>		<b>108</b>
1.33	STRUCTURE, DOMAINS AND THE INTERACTOME OF ALIX .....	109
1.33.1	<i>Bro1 domain of ALIX</i> .....	110
1.33.2	<i>V domain</i> .....	111
1.33.3	<i>Proline-rich domain</i> .....	112
1.33.4	<i>Consequences of protein-protein interactions at the PRD</i> .....	113
1.34	POST-TRANSLATIONAL MODIFICATIONS AND THEIR REPERCUSSIONS .....	114
1.34.1	<i>Phosphorylation</i> .....	116
1.34.2	<i>Ubiquitination</i> .....	116
1.34.3	<i>Palmitoylation</i> .....	117
1.34.4	<i>Methylation</i> .....	117
1.35	CELLULAR FUNCTIONS.....	118
1.35.1	<i>Budding of viruses</i> .....	120
1.35.2	<i>Intracellular membrane vesicle trafficking</i> .....	122
1.35.3	<i>Cytokinesis</i> .....	123
1.36	CONCLUDING REMARKS .....	127
<b>CHAPTER 2: RESULTS AND DISCUSSION .....</b>		<b>129</b>
<b>CHAPTER 2: PART I.....</b>		<b>130</b>
<b>PRMT1 REGULATES THE EGFR AND WNT SIGNALING PATHWAYS .....</b>		<b>131</b>
<b>ABSTRACT .....</b>		<b>132</b>
INTRODUCTION.....		133

RESULTS.....	134
<i>PRMT1 is overexpressed in breast tumors</i> .....	134
<i>RNAi-mediated depletion of PRMT1 decreases BC cell viability, clonogenicity and induces apoptosis</i> ....	138
<i>Type I PRMT inhibitors decrease cell viability, colony formation and show anti-tumor effects</i> .....	142
<i>EGFR and Wnt pathway identified in the transcriptome of PRMT1-depleted cells</i> .....	147
<i>PRMT1 activates the canonical Wnt signaling pathway</i> .....	151
<i>Synergistic interaction between Type I PRMT inhibitors and Erlotinib/standard of care chemotherapy</i> ..	155
DISCUSSION .....	160
CONCLUSION AND FUTURE PERSPECTIVES.....	164
(i) <i>Is PRMT1 inhibition effective as a monotherapy for all breast cancer patients?</i> .....	165
(ii) <i>Can anti-EGFR/anti-PRMT1 combination be used as a treatment for breast cancer patients?</i> .....	165
(iii) <i>Can PRMT1 inhibition be combined with chemotherapy in vivo?</i> .....	165
(iv) <i>Does PRMT1 regulate the secretion of Wnt ligands?</i> .....	165
(v) <i>Is the regulation of Wnt signaling by PRMT1 specific to MDA-MB-468? What is Wnt activity status in our BC cohort?</i> .....	165
(vi) <i>Does PRMT1 regulate the Wnt signaling pathway in colorectal cancer or hepatocellular carcinomas? Can Type I PRMT inhibitors be beneficial in these cancer types?</i> .....	166
<b>CHAPTER 2: PART II.....</b>	<b>167</b>
<b>THE ESCRT-BINDING PROTEIN ALIX IS A NOVEL CARM1 SUBSTRATE .....</b>	<b>168</b>
<b>ABSTRACT .....</b>	<b>169</b>
INTRODUCTION.....	170
RESULTS.....	170
<i>CARM1 mRNA is overexpressed breast tumors</i> .....	170
<i>Higher CARM1 expression correlates with worse prognosis in Her2+ and LA BC subtypes</i> .....	171
<i>CARM1 depletion decreases cell proliferation, colony formation and induces apoptosis</i> .....	175
<i>CARM1 inhibition does not impact cell viability of two TNBC cell lines</i> .....	177
<i>ALIX was identified as the principal protein partner of CARM1</i> .....	178
<i>CARM1 interacts with the proline-rich domain of ALIX</i> .....	184
<i>Enzymatic activity of CARM1 is required for interaction with ALIX</i> .....	186
<i>ALIX is monomethylated in cells and the methylation is dependent on CARM1</i> .....	187
<i>Endogenous ALIX is mono- and di-methylated on Arg745 and Arg757</i> .....	188
<i>CARM1 mono- and di-methylates ALIX on Arg745 and Arg757, in vitro</i> .....	190
<i>CARM1 regulates cytokinetic abscission in HeLa cells</i> .....	192
DISCUSSION .....	195
<i>CARM1 as a potential therapeutic target for TNBC</i> .....	195
<i>The CARM1-interactome reveals a novel partner and new function for CARM1</i> .....	198
CONCLUSION AND FUTURE PERSPECTIVES.....	202

(i) Is CARM1 important for the cell survival of all breast cancer cells? .....	203
(ii) What are the cell types in the stroma that express CARM1? Does CARM1 in the stroma influence tumor progression? .....	203
(iii) Are there underlying mechanisms contributing to CARM1 inhibition resistance in BC cells? .....	204
(iv) Can CARM1 inhibition potentiate cell death when combined with other inhibitors/chemotherapies (used in the clinic)?.....	204
(v) Does ALIX influence the methyltransferase activity of CARM1? .....	204
(vi) What are the other cellular functions of the CARM1/ALIX complex besides cytokinesis? .....	204
(vii) What is the role of CARM1 in cytokinesis?.....	204
(viii) Does ALIX methylation impact its partner interactions? Does the methylation impact the conformation of ALIX?.....	205
(ix) Can ALIX methylation be compensated for by other PRMTs (in CARM1 KO condition)?.....	205
(x) What is the role of ALIX in BC? Does ALIX methylation correlate with BC progression? .....	205
<b>CHAPTER 3: ADDITIONAL RESULTS AND DISCUSSIONS .....</b>	<b>207</b>
<b>THE FUNCTION OF CARM1 ISOFORMS IN BREAST CANCER .....</b>	<b>208</b>
ARE BOTH CARM1 ISOFORMS EXPRESSED IN BC? .....	208
<b>IS CARM1 INVOLVED IN OTHER FUNCTIONS REGULATED BY ALIX, APART FROM CYTOKINESIS?.....</b>	<b>212</b>
DOES CARM1 PLAY A ROLE IN THE BIOGENESIS OF EXOSOMES? .....	212
IS CARM1 NECESSARY FOR THE BUDDING OF HIV FROM THE CELLS? .....	215
<b>CHAPTER 4: MATERIALS AND METHODS .....</b>	<b>219</b>
CELL LINES AND CELL CULTURE .....	219
HUMAN SAMPLES AND IMMUNOHISTOCHEMISTRY .....	219
PLASMID CONSTRUCTS .....	220
SMALL-INTERFERING RNA (SIRNA) TRANSFECTION .....	220
PLASMID TRANSFECTION.....	220
WNT3A CONDITIONED MEDIUM PREPARATION .....	221
WNT TARGET GENE EXPRESSION ASSAY.....	221
REAL-TIME – QUANTITATIVE PCR ASSAY (RT-QPCR).....	221
B-CATENIN-ACTIVATED LUCIFERASE (BAR) ASSAY .....	221
IMMUNOPRECIPITATION .....	222
WESTERN BLOTTING .....	222
PROXIMITY LIGATION ASSAY (PLA).....	223
IMMUNOFLUORESCENCE .....	223
RECOMBINANT PROTEIN PRODUCTION .....	224
IMMUNOPRECIPITATION FOLLOWED BY MASS SPECTROMETRY ANALYSIS.....	224
IN VITRO METHYLATION ASSAY (FOR MASS SPECTROMETRY ANALYSIS).....	224

LC-MS/MS ANALYSIS .....	225
DATA PROCESSING OF LC-MS/MS .....	225
CELLTITERGLO CELL VIABILITY ASSAY – FOR siRNA TREATMENTS .....	226
CELLTITERGLO CELL VIABILITY ASSAY – FOR DRUG/INHIBITOR TREATMENTS.....	226
2D COLONY FORMATION ASSAY – FOR siRNA TREATMENTS .....	227
2D COLONY FORMATION ASSAY – FOR DRUG/INHIBITORS TREATMENTS .....	227
DRUG COMBINATIONS .....	228
CHROMATIN IMMUNOPRECIPITATION (CHIP) .....	228
MICE, TREATMENT AND TUMOR GROWTH MEASUREMENTS.....	229
GENERATION OF METHYLATED ALIX ANTIBODIES.....	229
<b>SUPPLEMENTARY MATERIALS AND METHODS .....</b>	<b>245</b>
CARM1 ISOFORM ANALYSIS IN BC CELL LINES AND HUMAN BC TUMORS.....	245
EXTRACELLULAR VESICLES AND EXOSOME ISOLATION .....	245
HIV VIRAL-LIKE PARTICLE PRODUCTION.....	247
<b>BIBLIOGRAPHY.....</b>	<b>253</b>
<b>ANNEXE I: CARM1/PRMT4: MAKING ITS MARK BEYOND ITS FUNCTION AS A TRANSCRIPTIONAL COACTIVATOR .....</b>	<b>298</b>
<b>ANNEXE II: KNOWN CARM1 SUBSTRATES .....</b>	<b>300</b>
<b>ANNEXE III: PROTEIN ARGININE METHYLTRANSFERASE 5: A NOVEL THERAPEUTIC TARGET FOR TRIPLE- NEGATIVE BREAST CANCER.....</b>	<b>302</b>



# LIST OF FIGURES

FIGURE 1: INCIDENCE AND MORTALITY OF THE CANCER OCCURRING IN FEMALES. ....	25
FIGURE 2: ANATOMY OF THE HUMAN FEMALE BREAST. ....	27
FIGURE 3: TYPE OF CELLS FOUND IN NON-INVASIVE AND INVASIVE BREAST CANCER. ....	28
FIGURE 4: SUMMARY OF BREAST CANCER CLASSIFICATION BY DIFFERENT TEAMS UNTIL DATE. ....	30
FIGURE 5: SCHEME OF THE DIFFERENT KINDS OF SURGICAL PROCEDURES AVAILABLE TO TREAT BREAST CANCER. ....	33
FIGURE 6: USE OF PARP INHIBITORS IN BREAST CANCER. ....	39
FIGURE 7: LEHMAN CLASSIFICATION OF TNBC CELL LINE MODELS. ....	41
FIGURE 8: TNBC SUBTYPE CLUSTERING BY LEHMANN ET AL. ....	42
FIGURE 9: SCHEMATIC REPRESENTATION OF TGF-B PATHWAY. ....	46
FIGURE 10: SUMMARY OF THE NOTCH SIGNALING PATHWAY. ....	47
FIGURE 11: HEDGEHOG SIGNALING PATHWAY IN ITS “ON” AND “OFF” STATE. ....	48
FIGURE 12: SCHEMATIC OVERVIEW OF THE WNT/B-CATENIN PATHWAY IN ITS “OFF” AND “ON” STATE. ....	49
FIGURE 13: CURRENT AND UPCOMING TREATMENT STRATEGIES FOR TNBC.]. ....	51
FIGURE 14: OVERVIEW OF PROTEIN METHYLATION ON LYSINE AND ARGININE RESIDUES. ....	53
FIGURE 15: METABOLIC CYCLE GENERATING THE METABOLITE, SAM. ....	54
FIGURE 16: FAMILY OF NINE MAMMALIAN PRMTS. ....	55
FIGURE 17: FUNCTION OF PRMTS IN PRE-MRNA SPLICING. ....	58
FIGURE 18: REGULATION OF THE DNA DAMAGE RESPONSE PATHWAY BY THE PRMTS. ....	59
FIGURE 19: SIGNAL TRANSDUCTION PATHWAYS MODULATED BY PRMTS. ....	60
FIGURE 20: PRMT2, CARM1, AND PRMT5 ACTIVATE THE WNT PATHWAY. ....	61
FIGURE 21: CARDIOVASCULAR DISEASE CONDITIONS UPON PRMT DYSREGULATION. ....	62
FIGURE 22: PRMTS METHYLATE VIRAL PROTEINS. ....	63
FIGURE 23: ROLE IN NEURODEGENERATIVE DISEASES. ....	65
FIGURE 24: EXPRESSION AND ACTIVITY OF PRMTS IN METABOLIC DISEASES. ....	66
FIGURE 25: PRMT5 DEPENDENCY OF CANCER CELLS DELETED FOR MTAP. ....	69
FIGURE 26: TIMELINE OF PRMT INHIBITOR DEVELOPMENT. ....	70
FIGURE 27: SPLICED ISOFORMS OF PRMT1 (V1-V7). ....	74
FIGURE 28: MODIFICATIONS OCCURRING ON PRMT1. ....	75
FIGURE 29: PRMT1 ACTIVATES OR INHIBITS THE WNT PATHWAY. ....	79
FIGURE 30: PRMT1 CONTRIBUTES TO DRUG RESISTANCE, EMT AND METASTATIC PHENOTYPES. ....	81
FIGURE 31: PRMT1 CONTROLS ONCOGENESIS IN HEMATOPOIETIC CANCER. ....	83
FIGURE 32: STRUCTURE AND DOMAINS OF CARM1. ....	85
FIGURE 33: ALTERNATIVELY SPLICED ISOFORMS OF CARM1. ....	88
FIGURE 34: VARIOUS MODIFICATIONS REGULATING CARM1 ACTIVITY. ....	89

FIGURE 35: REGULATION OF CARM1 BY LNCRNAS AND MIRNAS. ....	91
FIGURE 36: REGULATION OF TRANSCRIPTION BY CARM1.....	92
FIGURE 37: CO-ACTIVATOR FUNCTION BY CARM1 ON NUCLEAR RECEPTORS. ....	93
FIGURE 38: CARM1 REGULATES SPLICING BY METHYLATING FACTORS. ....	95
FIGURE 39: MRNA METABOLISM IN PARASPECKLES MEDIATED BY CARM1. ....	96
FIGURE 40: CARM1 REGULATES AUTOPHAGY THROUGH TWO DIFFERENT MECHANISMS. ....	97
FIGURE 41: CARM1 MODULATES METABOLIC PATHWAYS IN CANCER.....	99
FIGURE 42: CARM1 REGULATES EARLY EMBRYO DEVELOPMENT.....	100
FIGURE 43: CELLULAR DIFFERENTIATION CONTROLLED BY CARM1.....	102
FIGURE 44: CARM1 ACTIVATES LUMINAL BREAST CANCER PROGRESSION.....	103
FIGURE 45: CARM1 IS A BIOMARKER OF RESPONSE TO EZH2 INHIBITION IN OVARIAN CANCER.....	105
FIGURE 46: ALIX-RELATED PROTEINS IN HUMANS. ....	108
FIGURE 47: DOMAINS AND STRUCTURE OF ALIX.....	110
FIGURE 48: STRUCTURAL ARCHITECTURE OF ALIX BRO1 DOMAIN. ....	111
FIGURE 49: OPEN AND CLOSED CONFORMATIONS OF ALIX V DOMAIN.....	112
FIGURE 50: PROTEINS INTERACTING WITH THE PROLINE-RICH DOMAIN OF ALIX. ....	113
FIGURE 51: POST-TRANSLATIONAL MODIFICATIONS AND CONFORMATIONS OF ALIX. ....	115
FIGURE 52: THE MAJOR FUNCTIONS OF ESCRT PROTEINS WHERE ALIX IS ALSO INVOLVED.....	118
FIGURE 53: SCHEMATIC OF EGFR RECYCLING MEDIATED BY ALIX AND ITS PARTNERS. ....	120
FIGURE 54: VIRAL BUDDING PROCESS USING ESCRTS AND ALIX. ....	121
FIGURE 55: BIOGENESIS OF VESICLES (MVBS, EXOSOMES). ....	122
FIGURE 56: GRAPHICAL ABSTRACT SUMMARIZING THE KEY FINDINGS OF MONNYPENNY ET AL. ....	123
FIGURE 57: OVERVIEW OF CYTOKINESIS. ....	124
FIGURE 58: DETAILS OF BRIDGE MATURATION AND ABSCISSION. ....	125
FIGURE 59: SCHEMATIC OF THE CYTOKINETIC ABSCISSION CHECKPOINT SIGNALING.....	126
FIGURE 60: PRMT1 IS MORE HIGHLY EXPRESSED IN BC SAMPLES THAN NORMAL BREAST TISSUE. ....	136
FIGURE 61: CORRELATION, SURVIVAL ANALYSIS AND VALIDATION OF PRMT1 ANTIBODY FOR IHC. ....	138
FIGURE 62: PRMT1 DEPLETION USING SIRNA INDUCES APOPTOSIS AND DECREASES THE VIABILITY AND CLONOGENICITY OF MDA-MB-468 CELLS. ....	140
FIGURE 63: PRMT1 DEPLETION IN A LARGE PANEL OF BREAST CANCER CELL LINES DECREASES THEIR VIABILITY, COLONY FORMATION AND INDUCES APOPTOSIS. ....	142
FIGURE 64: PRMT1 INHIBITION DECREASES THE BC CELL PROLIFERATION IN MDA-MB-468 CELLS. ....	145
FIGURE 65: GSK3368715 INHIBITS PRMT1 ACTIVITY, SHOWS NO TOXICITY TO MICE AND IMPAIRS TUMOR GROWTH.....	146
FIGURE 66: PRMT1 REGULATES THE TRANSCRIPTION OF EGFR AND WNT COMPONENTS (LRP5, PORCN)....	149
FIGURE 67: PRMT1 REGULATES EGFR TRANSCRIPTION BY BINDING TO ITS PROMOTER. ....	149
FIGURE 68: WNT PATHWAY GENES DEREGULATED BY PRMT1 DEPLETION.....	150
FIGURE 69: PRMT1 POSITIVELY REGULATES THE WNT SIGNALING PATHWAY.....	153

FIGURE 70: PRMT1 DEPLETION DECREASES LRP5 AND PORCN EXPRESSION. ....	154
FIGURE 71: SYNERGISTIC INTERACTION BETWEEN TYPE I PRMT INHIBITORS AND CHEMOTHERAPIES OR ERLOTINIB. ....	158
FIGURE 72: NEUTRAL EFFECT BETWEEN TYPE I PRMT INHIBITORS AND CERTAIN CHEMOTHERAPIES (DOCETAXEL, PACLITAXEL, DOXORUBICIN). ....	160
FIGURE 73: SCHEME OF THE METHIONINE AND FOLATE CYCLES. ....	164
FIGURE 74: CARM1 MRNA IS MORE EXPRESSED IN BC THAN NORMAL BREAST TISSUE.. ....	171
FIGURE 75: DISTANT METASTASIS-FREE (DMFS) SURVIVAL OUTCOMES IN CARM1 HIGH AND LOW BC PATIENTS.. ....	172
FIGURE 76: CARM1 PROTEIN IS OVEREXPRESSED IN ALL BREAST TUMORS THAN NORMAL BREAST TISSUE BY IMMUNOHISTOCHEMICAL STAINING.. ....	174
FIGURE 77: CARM1 DEPLETION IMPAIRS CELL VIABILITY, COLONY FORMATION AND INDUCES APOPTOSIS.. .....	176
FIGURE 78: VALIDATION OF CARM1 SIRNA AND CARM1 DEPLETION DECREASES THE VIABILITY OF VARIOUS BREAST CELL LINES. ....	177
FIGURE 79: CARM1 INHIBITION DOES NOT IMPAIR TNBC CELL VIABILITY. ....	178
FIGURE 80: CARM1 INTERACTOME REVEALS ALIX AS ITS MAIN PARTNER. ....	181
FIGURE 81: ALIX INTERACTS WITH CARM1 IN THE BT-549 TNBC CELL LINE. ....	183
FIGURE 82: ALIX INTERACTS WITH CARM1 THROUGH ITS PROLINE-RICH DOMAIN. ....	185
FIGURE 83: ALIX DOES NOT INTERACT WITH CATALYTICALLY INACTIVE CARM1 MUTANTS. ....	186
FIGURE 84: ALIX METHYLATION IN CELLS IS CARM1-MEDIATED. ....	187
FIGURE 85: FRAGMENTATION MS/MS SPECTRA OF IMMUNOPRECIPITATED ALIX DIGESTED BY LYSARGINASE .....	189
FIGURE 86: CARM1 METHYLATES <i>IN VITRO</i> ALIX ON ARG745 AND ARG757.. ....	191
FIGURE 87: ENDOGENOUS STAINING OF CARM1 AND ALIX IN DIVIDING HELA CELLS.. ....	193
FIGURE 88: CARM1 IS INVOLVED IN CYTOKINESIS.. ....	195
FIGURE 89: MAJOR CARM1 ISOFORMS IN HUMAN CELL LINES AND BINDING SITE OF CARM1 ANTIBODY USED IN OUR IHC ANALYSIS. ....	197
FIGURE 90: PROTEIN-PROTEIN INTERACTIONS OCCURRING THROUGH THE PRD OF ALIX. ....	200
FIGURE 91: SUMMARY OF CYTOKINETIC DEFECTS CAUSED BY CARM1 DEPLETION. ....	202
FIGURE 92: SCHEMATIC HYPOTHESIS OF THE EFFECT OF CYTOKINETIC DEFECTS ON TUMOR CELL DEATH. ..	203
FIGURE 93: CARM1 TOTAL AND ISOFORM MRNA EXPRESSION IN NON-TUMORIGENIC AND BREAST CANCER LINES. ....	209
FIGURE 94: COMPARISON OF CARM1 ISOFORM EXPRESSION IN BREAST TUMORS VS NORMAL BREAST TISSUES. ....	210
FIGURE 95: COMPARISON OF CARM1 ISOFORM EXPRESSION IN THE DIFFERENT BC SUBTYPES.. ....	210
FIGURE 96: EXOSOME/EXTRACELLULAR VESICLES (EVS) ISOLATION.. ....	214
FIGURE 97: ANALYSIS OF VIRAL-LIKE PARTICLE RELEASE IN HEK293T CELLS.. ....	216

<b>FIGURE 98: SCHEME OF A 96-WELL CELL CULTURE PLATE FOR IC50 CALCULATIONS. ....</b>	<b>227</b>
<b>FIGURE 99: SCHEME OF A 96-WELL CELL CULTURE PLATE FOR DRUG COMBINATION ANALYSIS. ....</b>	<b>228</b>
<b>FIGURE 100: SCHEMATIC PROCESS OF IMAGE ANALYSIS FOR 2D COLONY FORMATION ASSAY USING IMAGEJ SOFTWARE. ....</b>	<b>244</b>
<b>FIGURE 101: SCHEMA OF EXTRACELLULAR VESICLE ISOLATION PROTOCOL. ....</b>	<b>246</b>

# LIST OF TABLES

TABLE 1: SUMMARY OF ARGININE METHYLATION SITES IDENTIFIED ON ALIX .....	117
TABLE 2: CORRELATION BETWEEN PRMT1 <sup>1</sup> MRNA AND KI67 <sup>2</sup> MRNA FROM KM-PLOTTER DATABASE .....	134
TABLE 3: IC <sub>50</sub> VALUES OF DRUGS USED IN THE COMBINATION ANALYSIS. ....	155
TABLE 4: CELL CULTURE CONDITIONS USED .....	230
TABLE 5: LIST OF ANTIBODIES USED .....	232
TABLE 6: LIST OF PRIMERS USED .....	235
TABLE 7: LIST OF SIRNA USED .....	238
TABLE 8: LIST OF DRUGS AND INHIBITORS USED .....	239
TABLE 9: LIST OF SYNTHETIC PEPTIDES USED (FROM COVALAB) .....	240
TABLE 10: 1X LAEMMLI SAMPLE BUFFER COMPOSITION .....	241
TABLE 11: 1X IMMUNOPRECIPITATION LYSIS BUFFER COMPOSITION .....	242
TABLE 12: ACQUISITION LIST FROM THE ALIX SYNTHETIC PEPTIDES GENERATED IN THE PARALLEL REACTION MONITORING MODE DURING LC-MS/MS ANALYSIS. ....	243
TABLE 13: SUPPLEMENTARY LIST OF ANTIBODIES .....	248
TABLE 14: SUPPLEMENTARY LIST OF PRIMERS .....	249
TABLE 15: SUPPLEMENTARY LIST OF SIRNA .....	250

# LIST OF ABBREVIATIONS

<b>ABC</b>	ATP-binding Cassette Transporters
<b>ADMA</b>	Asymmetric Dimethylarginine
<b>AI</b>	Aromatase Inhibitors
<b>AJCC</b>	American Joint Committee on Cancer
<b>ALDH</b>	Aldehyde dehydrogenase
<b>ALIX</b>	ALG-2 Interacting Protein X
<b>ALL</b>	Acute Lymphoblastic Leukaemia
<b>ALS</b>	Amyotrophic Lateral Sclerosis
<b>AML</b>	Acute myeloid leukaemia
<b>AMPK</b>	AMP-activated protein kinase
<b>APC</b>	Adenomatous Polyposis Coli
<b>AR</b>	Androgen Receptor
<b>ASK</b>	Apoptosis Signal-regulating Kinase
<b>ATCC</b>	American Type Culture Collection
<b>ATF4</b>	Activating Transcription Factor 4
<b>ATP</b>	Adenosine triphosphate
<b>AURKA</b>	Aurora kinase A
<b>AURKB</b>	Aurora kinase B
<b>BAR</b>	$\beta$ -catenin-activated luciferase reporter
<b>BCA</b>	Bicinchoninic Acid assay
<b>BL</b>	Basal Like
<b>BMP</b>	Bone Morphogenetic Protein
<b>BRAF</b>	v-raf murine sarcoma viral oncogene homolog B
<b>BRCA</b>	BReast CAncer gene.
<b>BSA</b>	Bovine Serum Albumin
<b>BTG1</b>	B-cell translocation gene 1
<b>cAMP</b>	cyclic Adenosine MonoPhosphate
<b>CARM 1</b>	Coactivator Associated Arginine Methyltransferase 1
<b>CBP</b>	C-AMP Response Element-binding protein (CREB) Binding Protein
<b>CDK</b>	Cyclin-Dependent Kinases
<b>CHTOP</b>	Chromatin Target of PRMT1
<b>CMF</b>	Cyclophosphamide
<b>CML</b>	Chronic myeloid leukemia
<b>CRC</b>	Colorectal Cancer Cells
<b>CSC</b>	Cancer Stem Cells

<b>DCIS</b>	Ductal Carcinoma In Situ
<b>DMEM</b>	Dulbecco's modified version Minimal Essential Medium
<b>DMSO</b>	Dimethylsulfoxide
<b>DNA</b>	Deoxyribonucleic acid
<b>Dvl</b>	Dishevelled
<b>DZIP</b>	DAZ-interacting protein
<b>EBRT</b>	External-Beam Radiation Therapy
<b>EBV</b>	Epstein-Barr Virus
<b>EGF</b>	Epidermal Growth Factor
<b>EGFR</b>	Epidermal Growth Factor Receptor
<b>EMT</b>	Epithelial-to-Mesenchymal Transition
<b>ER</b>	Estrogen
<b>ERD</b>	Estrogen Receptor Downregulator
<b>ERK</b>	Extracellular signal-regulated kinase
<b>ERV</b>	Endogenous retrovirus
<b>ESC</b>	Embryonic Stem Cell
<b>ESCRT</b>	Endosomal Sorting Complexes Required for Transport
<b>EZH</b>	Enhancer of Zeste Homologue
<b>FBS</b>	Fetal Bovine Serum
<b>FDA</b>	Food and Drug Administration
<b>FEN</b>	Flap endonuclease
<b>FLT3</b>	Fms Related Receptor Tyrosine Kinase 3
<b>FOXM1</b>	Forkhead transcription factor M1
<b>FOXO</b>	Forkhead box transcription factors
<b>FTD</b>	Frontotemporal Dementia
<b>FTLD</b>	Frontotemporal Lobar Degeneration
<b>FUS</b>	Fused in Sarcoma
<b>FZD</b>	Frizzleds
<b>GAR</b>	Glycine Arginine Rich
<b>GBM</b>	Glioblastoma
<b>GFP</b>	Green Fluorescent Protein
<b>GLI</b>	Glioma-associated oncogene
<b>GOF</b>	Gain-Of-Function
<b>GRIP1</b>	Glutamate receptor-interacting protein 1
<b>GSK</b>	Glycogen Synthase Kinase
<b>GST</b>	Glutathione S-transferases
<b>HCC</b>	Hepatocellular carcinoma
<b>HDAC</b>	Histone deacetylases
<b>Her2</b>	Human Epidermal growth factor 2

<b>HIV</b>	Human Immunodeficiency Virus
<b>hnRNP</b>	Heterogenous Ribonucleoproteins
<b>HR</b>	Hormone Receptor
<b>HSPC</b>	Hematopoietic Stem and Progenitor Cells
<b>HSV</b>	Herpes Simplex Virus
<b>Htt</b>	Huntingtin
<b>ICB</b>	Intercellular bridge
<b>ICM</b>	Inner Cell Mass
<b>IGF</b>	Insulin-like growth factor
<b>IHC</b>	Immunohistochemistry
<b>IM</b>	Immunomodulatory
<b>INM</b>	Inner Nuclear Membrane
<b>IRAlus</b>	Inverted Repeated Alu elements
<b>KO</b>	Knockout
<b>LAR</b>	Luminal-Androgen Receptor
<b>LCIS</b>	Lobular Carcinoma In Situ
<b>LEF</b>	Lymphoid enhancer-binding factor
<b>LHRH</b>	Luteinizing Hormone-Releasing Hormone
<b>LINAC</b>	Linear Accelerator
<b>LOF</b>	Loss-Of-Function
<b>LPS</b>	LipoPolySaccharide
<b>LRP</b>	Low- Density Lipoproteins
<b>LSD</b>	Lysine-Specific Histone Demethylase
<b>LTED</b>	Long Term Estrogen Deprivation
<b>LTR</b>	Long Terminal Repeat
<b>M</b>	Mesenchymal
<b>mAb</b>	Monoclonal Antibody
<b>MAPK</b>	Mitogen-Activated Protein Kinase
<b>MBC</b>	Medullary Breast Cancer
<b>MBR</b>	Mid Body Remnant
<b>MDH</b>	Malate Dehydrogenase
<b>MDR</b>	Multi-Drug Resistance
<b>MED12</b>	Mediator Complex Subunit 12
<b>MEF</b>	Mouse Embryonic Fibroblast
<b>MLL</b>	Mixed Lineage Leukemia
<b>MMA</b>	MonomethylArginine
<b>MPTAC</b>	Molybdopterin Synthase Associating Complex
<b>MRE</b>	Magnetic resonance elastography
<b>MRI</b>	Magnetic Resonance Imaging



<b>mRNA</b>	Messenger ribonucleic acid
<b>MSL</b>	Mesenchymal Stem-Like
<b>MTA</b>	Methylthioadenosine
<b>MTAP</b>	5-Methylthioadenosine phosphorylase
<b>mTOR</b>	Mammalian Target Of Rapamycin
<b>NEC</b>	Nuclear Egress Complex
<b>NHEJ</b>	Non- Homologous End-Joining
<b>NICD</b>	NOTCH intracellular domain
<b>NMD</b>	Nonsense-Mediated Decay
<b>NMR</b>	Nuclear Magnetic Resonance
<b>NO</b>	Nitric Oxide
<b>NOS</b>	Nitric Oxide Synthase
<b>NSCLC</b>	Non-Small Cell Lung Carcinoma
<b>OC</b>	Ovarian Cancer
<b>OGT</b>	O-GlcNAc-Transferase
<b>PABP</b>	poly(A)-binding protein
<b>PAK</b>	p21-activated kinase
<b>PARP</b>	Poly (ADP-ribose) Polymerase
<b>PCR</b>	Pathological complete response
<b>PD-L</b>	Programmed Cell Death Ligand 1
<b>PDAC</b>	Pancreatic ductal adenocarcinoma
<b>PDCD</b>	Programmed Cell Death
<b>PDGFR</b>	platelet-derived growth factor receptor
<b>PELP</b>	Proline-, glutamic acid- and leucine-rich protein
<b>PET</b>	Positron Emission Tomography
<b>PFA</b>	Paraformaldehyde
<b>PGM</b>	Proline Glycine Motif
<b>PH</b>	Plekstrin Homology
<b>PHP</b>	PseudoHypoParathyroidism
<b>PKM2</b>	Pyruvate kinase M2
<b>PLA</b>	Proximity Ligation Assay
<b>PLK1</b>	Polo-like kinase 1
<b>PR</b>	Progesterone
<b>PRC1</b>	Protein Regulator of Cytokinesis 1
<b>PRD</b>	Proline-Rich Domain
<b>PRMT</b>	Protein Arginine MethylTransferases
<b>PSPC1</b>	Para Speckles Protein 1
<b>PTEN</b>	Phosphatase and tensin homolog
<b>PTM</b>	Post-Translational Modifications

<b>PTP</b>	Protein Tyrosine Phosphatase
<b>PXR</b>	Pregane- x Receptor
<b>RB</b>	Retinoblastoma
<b>RBP</b>	RNA-Binding Proteins
<b>RGG</b>	Arginine Glycine Glycine motif
<b>ROS</b>	Reactive oxygen species
<b>RPM</b>	Revolutions per minute
<b>RT-qPCR</b>	Real-time – quantitative polymerase chain reaction
<b>RTV</b>	Relative Tumor Volume
<b>RUNX1</b>	Runt-related transcription factor 1
<b>SAH</b>	S-Adenosylhomocysteine
<b>SAM</b>	S-Adenosyl-L- Methionine
<b>SAP49</b>	Spliceosome associated protein 49
<b>SCF</b>	SKP1-cullin1-F-box protein
<b>SDMA</b>	Symmetric Dimethylarginine
<b>SDS-PAGE</b>	Sodium dodecyl sulphate–polyacrylamide gel electrophoresis
<b>SERM</b>	Selective Estrogen Receptor Modulators
<b>SF</b>	Splicing Factor
<b>siRNA</b>	Small interfering RNA
<b>SKP2</b>	S phase kinase-associated protein 2
<b>SMA</b>	Spinal Muscular Atrophy
<b>SMAD</b>	small Mothers Against Decapentaplegic
<b>SMARCA4</b>	SWI/SNF Related, Matrix Associated, Actin Dependent Regulator of Chromatin, Subfamily A, Member 4
<b>SMN</b>	Survival Motor Neuron
<b>snRNP</b>	small nuclear Ribonucleoprotein
<b>SRSF</b>	Serine/arginine-rich splicing factors
<b>TAM</b>	Tumor-Associated Macrophages
<b>TBST</b>	Tris-Buffered Saline with Tween
<b>TCA</b>	Trichloroacetic acid
<b>TCF</b>	T-cell factor
<b>TCGA</b>	The Cancer Genome Atlas
<b>TDBP</b>	Tudor domain-binding proteins
<b>TF</b>	Transcription Factors
<b>TFEB</b>	Transcription factor EB
<b>TGF</b>	Transforming Growth factor
<b>THW</b>	Threonine Histidine Tryptophan
<b>TIC</b>	Tumor Initiating Cells

<b>TMA</b>	Tissue Microarrays
<b>TNBC</b>	Triple negative breast Cancer
<b>TNM</b>	Tumor Node Metastasis
<b>TSG</b>	Tumor suppressor genes
<b>TTK</b>	Threonine Tyrosine Kinase
<b>TWIST1</b>	Twist Family BHLH Transcription Factor 1
<b>VEGF</b>	Vascular Endothelial Growth Factor
<b>VEGFR</b>	Vascular Endothelial Growth Factor Receptor
<b>Wnt</b>	Wingless/Integrated
<b>ZEB</b>	Zinc finger E-Box binding Homeobox

# **CHAPTER 1**

# CHAPTER 1: INTRODUCTION

In the introductory chapter for this thesis, I will give an overview of three main topics important to follow the results obtained during the course of my PhD. The first part will describe breast cancer and its subtypes, with emphasis on triple-negative breast cancer. In the second part, I will give a comprehensive summary of the family of enzymes called protein arginine methyltransferases (PRMTs) with a detailed description of the structure and function of PRMT1 and PRMT4, two members of this family that were the subject of my thesis. In the last part of the introduction, I will discuss the protein, ALIX, as we identified it as a protein partner of PRMT4 in my thesis.

# I. Generalities of breast cancer

## 1.1 Breast cancer incidence and mortality rate

Breast cancer is the most commonly diagnosed disease in women worldwide and remains the leading cause of death in more than one hundred countries [1]. Breast cancer accounts for 24.5% of cancer incidence and 15.5% mortality in females (**Figure 1**) [1]. In France, more than 58,000 new cases were recorded in 2020 [1]. Worldwide, breast cancer is ranked number one in female cancer incidence and cancer-related mortality [1]. Although rare, breast cancer also affects men and it is estimated that the lifetime risk of getting breast cancer is 1 in 883 [2] as opposed to 1 in 8 for women [3] in the United States. Therefore, understanding the biology of breast cancer is warranted from the perspectives of the general public, oncologists and researchers.

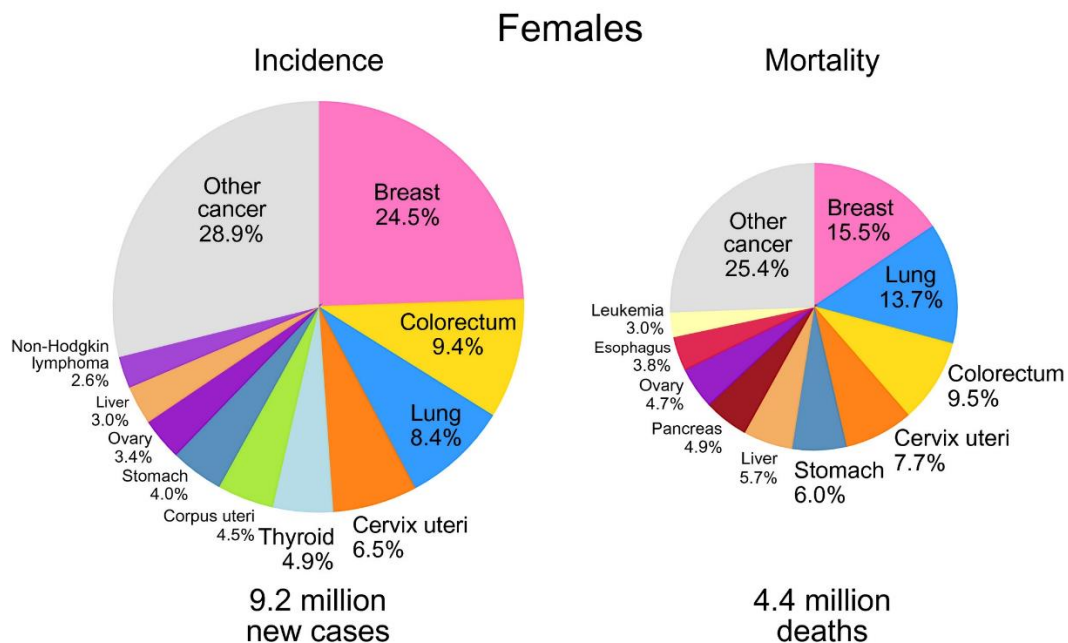


**Figure 1: Incidence and mortality of the cancer occurring in females.** Modified and adapted from [1].

## 1.2 Risk factors

Several risk factors have been identified as causal reasons to develop breast cancer. These can be intrinsic or extrinsic factors. The intrinsic factors sometimes also referred to as established risk factors are:

- i. Sex – the disease is most prevalent in women and therefore belonging to the female gender already increases the risk of developing this disease [4].

- ii. Age – Older women (usually those around menopausal age or greater than 45 years) have a higher risk of developing breast cancer than younger women [4].
- iii. Family history – women with first-degree female relatives (such as sister, mother, daughter) who have been diagnosed with the disease have a higher risk of developing it [4].
- iv. Genetics - mutations in certain germline genes can predispose women to breast cancer. The most common gene mutation associated with a high risk of breast cancer is *BRCA1* or *BRCA2* [5].
- v. Race/ethnicity – White Caucasian women develop breast cancer more frequently as compared to the African-American or the Hispanic population. However, African-American and Hispanic women are usually diagnosed with a more aggressive subtype of breast cancer and usually at a younger age [6].
- vi. Pregnancy, breastfeeding and menstrual history – having the first child after the age of 30, a shorter period of breastfeeding, and starting menstruation younger than the age of 12 are all associated with a higher risk of breast cancer [4].

Extrinsic factors such as, (i) being overweight, (ii) having dense breasts, (iii) lack of exercise, (iv) smoking, and (v) drinking alcohol are linked to a higher risk of developing the disease [4].

Other factors such as high endogenous estrogen hormone levels or using hormone replacement therapy for long periods (>10 years) are associated with a higher risk of developing breast cancer [4, 7].

Despite having several high-risk factors, the key to better treatment is early detection and diagnosis. In the next section, I will discuss the various diagnostic methods used for detecting breast cancer.

### **1.3 Diagnosis and screening**

Mammography, typically performed during routine health checks, is the preferred method to screen for breast cancer. A mammogram, the output of a mammography test, can detect different kinds of lesions and is essentially an X-ray of the breast. Ultrasonography is a complementary test to a mammogram and helps to identify the type of abnormality (solid lumps or fluid-filled lumps) but cannot determine if the abnormality is cancerous. Other imaging techniques, such as magnetic resonance imaging (MRI) or positron emission tomography (PET) scan can be used as adjunct screening methods in addition to mammography [8]. In certain cases, a Lymphoscintigraphy can be performed to track the spread of breast cancer into the nearby lymph nodes [8].

The sure way of diagnosing if a woman has developed breast cancer, once a lesion is identified by any of the above-mentioned methods, is by performing a biopsy. A biopsy

is an interventional procedure by which a small piece of breast tissue from the suspected area is extracted and analyzed by a pathologist. Once cancerous growth is confirmed, several molecular tests (like MammaPrint – 70 gene signature analysis or Oncotype DX – 21 gene expression array) can be performed to accurately diagnose breast cancer [9, 10].

## 1.4 Anatomy of breast

In order to understand the development of this disease, we must first understand the anatomy of the breast. The female breast is composed of adipose, glandular, and connective tissue. The glandular tissue is responsible for producing milk and is organized into 15 to 20 sections, called lobes. Each lobe contains smaller structures called lobules and at the end of the lobules are dozens of bulbs where the milk is produced. The network of tubes that connects all these structures are called ducts (**Figure 2**). The breast also contains blood and lymph vessels along with lymph nodes.

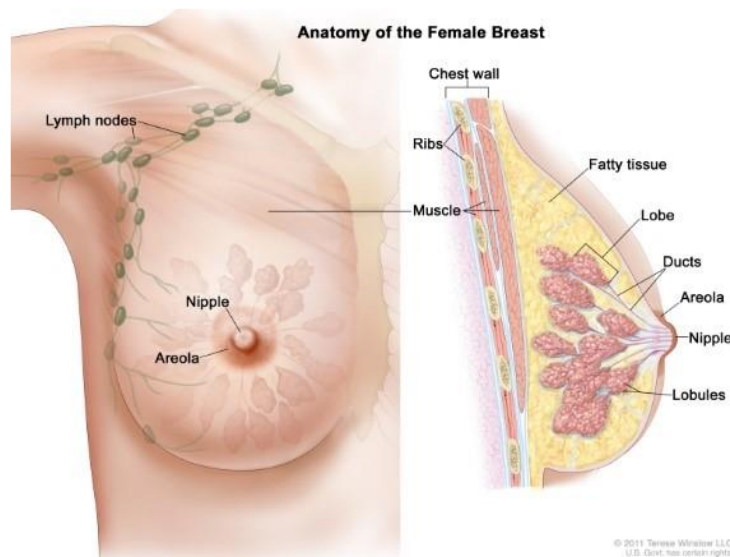


**Figure 2: Anatomy of the human female breast.** (©Terese Winslow).

## 1.5 Breast cancer development and terminologies

Breast cancer can develop in any part of the breast, but not all conditions have the same outcome. The term 'breast cancer' is usually used to describe malignant cells, that abnormally divide in the breast and eventually metastasize to the rest of the body (most frequently to the bone, lung, brain, and liver). Cancerous cell growth that does not spread to the rest of the body but arises in the duct cells is referred to as Ductal carcinoma in situ (DCIS) while those that occur in the lobular cells is called Lobular carcinoma in situ (LCIS). The problem is deepened when these *in situ* growths start invading the rest of the breast, with the potential of spreading to the rest of the body (**Figure 3**). Invasive ductal carcinoma, as the name suggests originates in the duct cells and represents the most common type



of invasive breast cancer. However, invasive lobular carcinoma, originating in the lobular cells, is less common.

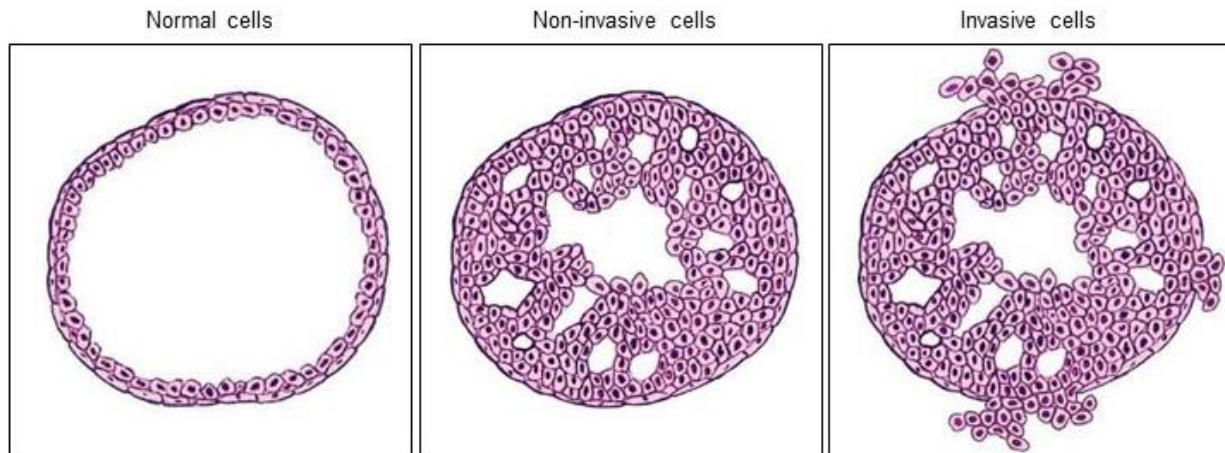


**Figure 3: Type of cells found in non-invasive and invasive breast cancer.** Adapted from [4].

Historically, breast cancer stage was categorized using the **Tumor Node Metastasis** (TNM) system, where the size of the tumor (**T**), if it had spread to the lymph nodes (**N**) and whether the tumor metastasized (**M**) were assessed [nomenclature by American Joint Committee on Cancer (AJCC)]. The different stages of breast cancer are clinically described as follows:

**Stage 0:** Mostly non-invasive breast cancer such as DCIS with a 5-year survival rate of 100% [8].

**Stage I-III:** describes invasive breast cancer based on the tumor size and the extent to which the tumor has spread to the nearby lymph nodes.

**Stage IV:** describes advanced invasive breast cancer that has metastasized beyond the breast to other body parts, such as the lung, distant lymph node, skin, bone, liver, or brain and has a 5-year survival rate of around 22% [8].

In 2018, the American Joint Committee on Cancer updated this classical TNM system to include more details such as the **tumor grade** and **biomarkers** (hormone receptor or Human epidermal growth factor 2, Her2 status) [11]. Although including these details make it more complicated to diagnose the different types of breast cancer patients, it is more accurate aiding the oncologists to provide the best suitable therapy for the patient.

Tumor grade is used to describe the abnormality of the cells and tissues when compared to their healthy counterparts while tumor stage explains the size of the tumor and how far the cancer has spread in the patient.

**Grade 1** or low grade (sometimes also called well-differentiated): When the cancer cells differ slightly from normal cells and are not dividing at high rates.

**Grade 2** or intermediate/moderate grade (moderately differentiated): When the cancer cells differ from normal cells and are actively dividing and growing.

**Grade 3** or high grade (poorly differentiated): The cells look very different from normal cells and are rapidly dividing to produce new cancer cells in a highly disorganized manner.

## 1.6 Molecular subtypes of breast cancer

As previously mentioned, using biomarker status in classifying breast cancer stages aids to differentiate between the different types of breast cancer. The subtypes of breast cancer are broadly categorized based on their hormone receptor (estrogen: ER and progesterone: PR) status and Her2 status when analyzed by immunohistochemistry (IHC). Tumors expressing hormone receptors are called "**Luminal**" breast cancer (ER+/PR+). The tumors that overexpress the Her2 gene (either ER+/PR+/Her2+ or ER-/PR-/Her2+) are termed "**Her2+**" breast cancer. Lastly, there exists a subgroup that does not express the hormone receptors nor has an overexpression of Her2 (i.e., ER-/PR-/Her2-), called "**Triple-negative**". These broad subgroups have been further classified based on intrinsic gene expression as (i) Luminal A, (ii) Luminal B, (iii) Non-luminal Her2+, (iv) Basal-like, and (v) Normal-like [12]. Recently, Mathews et al., have summarized the way breast cancer subtypes have been classified, and also proposed a new method of classification (**Figure 4**) [13]. Here, I will discuss five subgroups described by Sorlie et al.

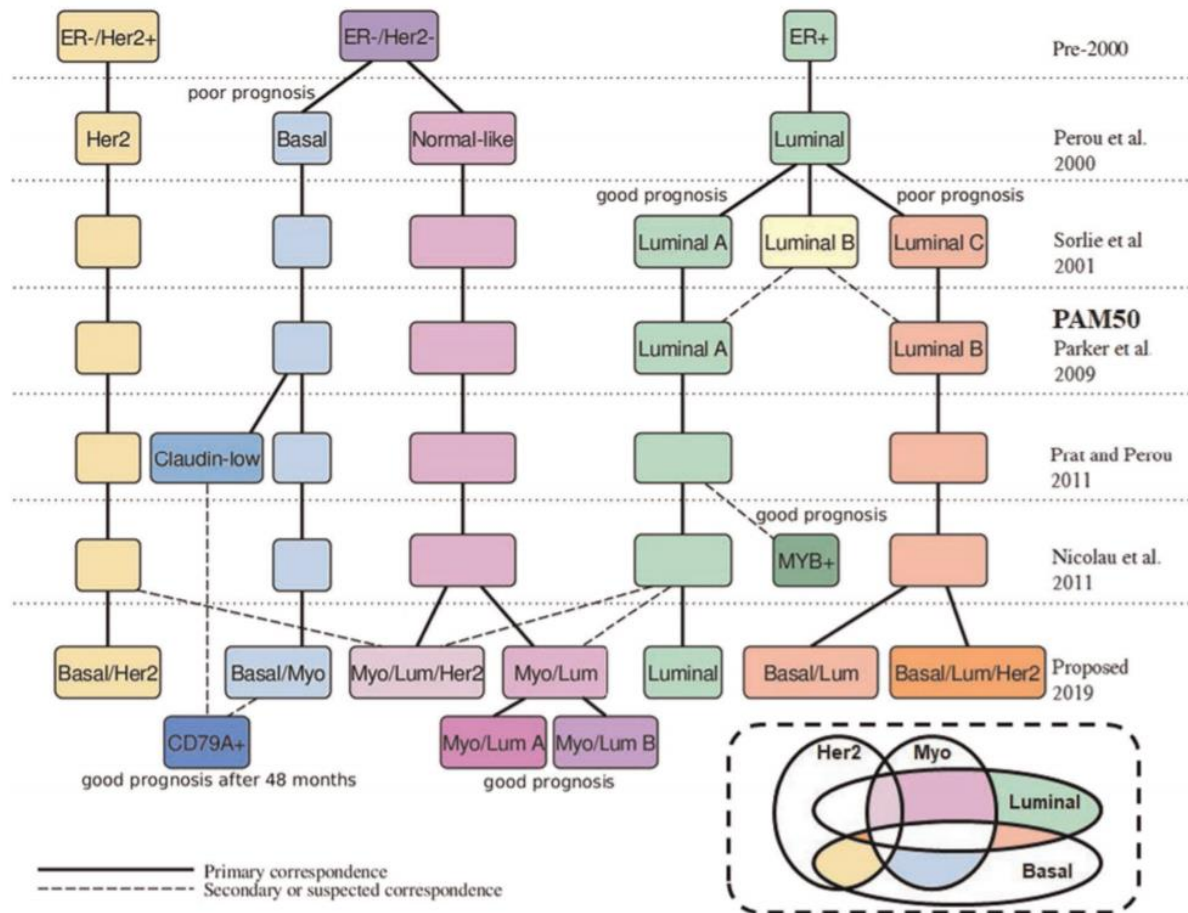


**Figure 4: Summary of breast cancer classification by different teams until date.** Adapted from [13].

### 1.6.1 Luminal A (ER+/PR+/Her2-)

Accounting for ~50% of invasive breast cancer, the luminal A subtype displays high ER signaling and expresses low levels of the protein Ki-67 (a proliferative marker), making this cancer grow more slowly than the other subtypes. At the DNA level, they show a lower number of mutations and copy-number changes [14] but around 45% of the tumors are mutated for *PIK3CA* [15]. Moreover, they are often of low tumor grade and patients diagnosed with luminal A have the best prognosis.

### 1.6.2 Luminal B (ER+/PR+ and Her2+ or Her2-)

These tumors are ER+/PR+ but can be either Her2+ or Her2- and account for 20 – 30% of breast cancer. Unlike luminal A, luminal B have higher levels of Ki-67 and other cell-cycle markers [14], thereby more proliferative and have a worse prognosis than luminal A. They also have a higher number of mutations and copy-number changes than luminal A [14]. A key distinguishing marker for luminal B tumors is higher DNA methylation frequency than any other subtype [16].

### 1.6.3 Non-luminal Her2+ (ER-/PR- and Her2+)

These tumors represent around 20% of all breast cancer and are characterized by an overexpression/amplification of Her2 (also known as *ERBB2*) and other proliferation-related genes. Her2-enriched tumors have the highest genome instability, with mutations in the known oncogenes *TP53* and *PIK3CA* [14]. They are of high grade, highly proliferative and have an unfavorable prognosis [17].

### 1.6.4 Basal-like (ER-/PR-/Her2-)

The basal-like subtype (based on gene expression, around 15% of breast cancer) is the most distinct among all breast cancer and are often referred to as triple-negative breast cancer (based on Immunohistochemical staining) as they are negative for ER, PR and lack overexpression of Her2. However, only around 75% of TNBCs are basal-like while the remaining 25% show markers of the other subtypes [18]. The basal-like tumors have high expression of basal<sup>1</sup> epithelial genes and basal cytokeratins (e.g., cytokeratins 5/6 and cytokeratin 14), high proliferation, *TP53* mutation, and a subset have *BRCA1* dysfunction [15, 17]. They are also high-grade tumors and have the worst prognosis among all the subtypes of breast cancer. They are also characterized by having the least DNA methylation frequency among all the subtypes [16]. I will discuss TNBC in detail in Chapter 1, part II.

### 1.6.5 Normal-like (ER+/PR+/Her2-)

The fifth subtype according to Sorlie et al., called the normal-like breast cancer are hormone receptor-positive (ER+/PR+) and Her2- like the luminal A subtype and have low Ki-67 levels and low rates of proliferation [12]. They usually have a good prognosis but are slightly worse than luminal A.

Therefore, knowing the existence of these different subtypes, it becomes evident that breast cancer is highly heterogeneous, and each subtype must be treated differently. The next section will discuss the available types of treatment for breast cancer in general and the existing targeted treatments for the different subtypes.

## 1.7 Breast cancer treatment

Treating breast cancer usually involves more than one type of therapy, such as primary therapy (often surgery or radiation therapy) along with adjuvant and/or neoadjuvant therapy. Neoadjuvant treatment is typically chemotherapy or hormone therapy while adjuvant therapies include chemotherapy, hormone therapy, immunotherapy, or targeted therapy.

---

<sup>1</sup> Basal epithelium: cells located on the lower surface of the epithelium, closer to the basement membrane.

Neoadjuvant therapy is the first treatment given to the patients, to reduce the tumor size or to destroy the metastatic cancer cells before radical treatment interventions. On the other hand, adjuvant therapy is given after the primary treatment to eradicate the remaining cancer cells.

The choice of treatment depends on many factors, including the stage and grade of breast cancer, the subtype and if the patient is willing to undergo surgery. Chemotherapy given as a neoadjuvant was hypothesized to be more advantageous rather than when given in the adjuvant setting, particularly in patients who wished for breast-conserving therapy [19]. However, a study analyzing ten randomized trials found no significant difference between neoadjuvant or adjuvant chemotherapy in the risk of distant recurrence or mortality [20].

### **1.7.1 Surgery**

Most breast cancer patients might have to undergo surgery to eliminate the cancer. Depending on the stage and tumor grade, the patient could undergo any of the following procedures (**Figure 5**).

#### *1.7.1.1 Mastectomy*

It is the surgical procedure in which the entire breast is removed and is sometimes referred to as total or simple mastectomy [4, 8]. Before or after this surgery, some lymph nodes under the arm may be removed to check for the presence of cancer cells (**Figure 5A**).

Modified radical mastectomy is the most common type of mastectomy performed, where the entire affected breast, surrounding lymph nodes and the underlying chest muscles are surgically removed [4, 8] (**Figure 5B**).

#### *1.7.1.2 Breast-conserving surgery*

Breast-conserving surgery is the procedure where the cancer and some normal tissues surrounding it will be removed while preserving the breast itself. If the cancer is found close to the underlying chest lining, that may also be removed. This type of surgery has also been referred to as lumpectomy, partial mastectomy, segmental mastectomy, quadrantectomy, or breast-sparing surgery [4]. This surgery is recommended only for patients still in the early stages of breast cancer (stage I or II) and the cancer is benign [8] (**Figure 5C**).

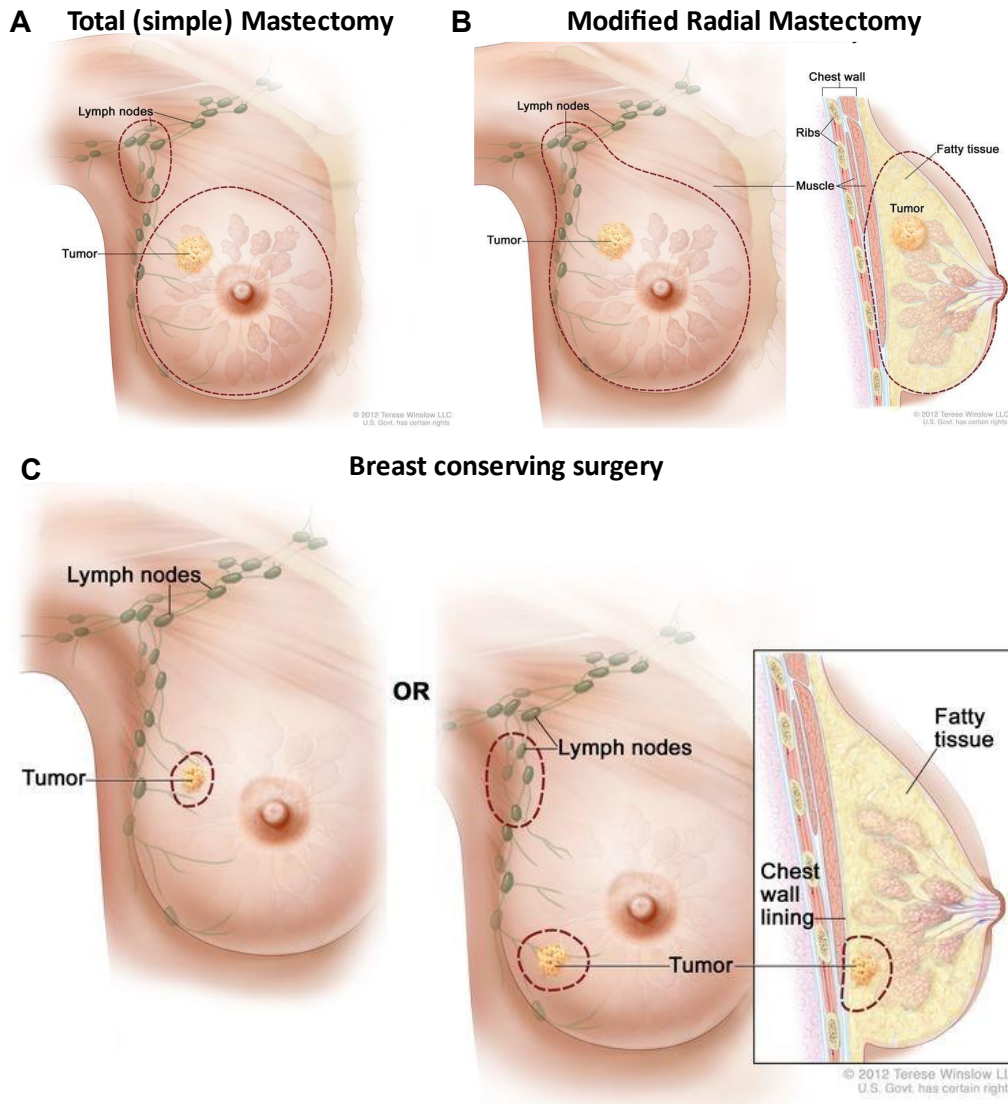


**Figure 5: Scheme of the different kinds of surgical procedures available to treat breast cancer.** (A) Simple mastectomy where the entire breast is removed. (B) Radial mastectomy is when the entire breast along with its neighboring lymph nodes is removed. (C) In order to conserve the breast, only the tumor and/or the nearby lymph nodes infected will be removed. (© Therese Winslow).

### 1.7.1.3 Lymph node biopsy

A lymph node biopsy (also called axillary lymph node dissection) is when some or all the lymph nodes surrounding the breast are surgically removed to test for the presence of cancer cells. This procedure is typically performed after a mastectomy/breast-conserving surgery. However, the lymph node biopsy has been deemed unnecessary and a sentinel lymph node biopsy is recommended by researchers [8]. Sentinel lymph node biopsy is the removal of the first lymph node to which the cancer is likely to have spread from the primary tumor and it is a minimally invasive procedure as compared to the lymph node biopsy [4, 8].

## 1.7.2 Radiation therapy

The accidental discovery of X-rays by Prof. Wilhelm Roentgen in 1895 proved to be useful particularly in cancer treatment. High-energy radiation is used to kill the cancer cells or to limit their growth while not affecting the remaining areas of the body. The use of a linear accelerator (LINAC) became the backbone of radiation therapy delivery since the 1950s [21]. This type of therapy is given either as primary therapy or as an adjuvant (with surgery and/or chemotherapy). Two types of radiation therapy are given:

### 1.7.2.1 External radiation therapy

External-beam radiation therapy (EBRT) is usually given once a day for 6 to 7 weeks and is delivered using a LINAC, to specifically target the affected region. Radiation is thought to kill cancer cells by inducing DNA damage. Beam-shaping blocks and multileaf collimators are used to protect the normal cells from receiving the radiation [8].

### 1.7.2.2 Internal radiation therapy

In this type of therapy, the radiation source is delivered internally and is given for 3 to 5 days, unlike EBRT [8]. A radioactive substance is rendered directly to the affected site using needles, wires and/or catheters [4]. Sometimes, the radionuclide strontium-89 is given to breast cancer patients where the cancer has metastasized to the bones to relieve bone pain [4].

## 1.7.3 Chemotherapies

Another commonly used breast cancer treatment is chemotherapy. It is the use of drugs to kill cancer cells or arrest their growth. Chemotherapy can be given as an adjuvant to surgery and/or radiation therapy or as a neoadjuvant. Chemotherapy is quite often given as a combination of different drugs. These drugs can be broadly categorized as alkylating agents, DNA intercalants, anti-metabolites, and microtubule-targeting agents.

### 1.7.3.1 Alkylating agents

Alkylating agents directly target the DNA of proliferative cells causing cross-linking of DNA strands, abnormal base pairing, or DNA strand breaks, thus preventing the cancer cells from dividing. They work on all cell cycle phases and usually work better on slow-growing cancer. Examples of common alkylating agents are **cyclophosphamide** and Thiothepa. Platinum-based drugs such as **cisplatin** and carboplatin function similarly to classical alkylating agents and are used to treat metastatic breast cancer [22].

### 1.7.3.2 DNA intercalants

As the name suggests, these agents intercalate with the DNA of proliferative cells and inhibit the cells from dividing. They particularly inhibit the enzyme, topoisomerase II, thereby leading to DNA cleavage which is a critical event responsible for killing the cancer cells [23]. Anthracyclines such as **doxorubicin** (also called adriamycin) and epirubicin are the most used DNA intercalants for breast cancer.

### 1.7.3.3 *Anti-metabolites*

They function during the S-phase of the cell cycle, acting as purine/pyrimidine antagonists or interfering with the enzymes required for metabolism and protein synthesis. The standard antimetabolites that have been used to treat breast cancer for decades are 5-fluorouracil (5-FU) – a nucleoside analogue – and **methotrexate**, an inhibitor of the enzyme dihydrofolate reductase [24]. Gemcitabine, a pyridine antimetabolite, was identified later and is used to treat metastatic breast cancer both as a single agent or in combination therapy [25].

### 1.7.3.4 *Mitotic inhibitors (or microtubule-targeting agents)*

These classes of drugs affect proliferative cells by targeting microtubule formation (either by stabilizing or destabilizing its polymerization dynamics) and chromosome segregation, thereby inducing mitotic arrest [26]. Taxanes, which include **paclitaxel** and **docetaxel**, fall under the standard regimen of treatment for breast cancer patients, either as monotherapy or in combination with anthracyclines [27].

### 1.7.3.5 *Standard drug combination therapies*

The general clinical practice for treating breast cancer patients is to give multiple chemotherapeutic agents belonging to different categories. Since each drug targets and kills the cancer cells in different ways, a complete anti-tumor response can be expected, preventing a relapse. The most traditional combination included an alkylating agent (cyclophosphamide) along with anti-metabolites (methotrexate and 5-FU), commonly referred to as the CMF regimen [28]. Other drug combinations approved by the Food and Drug Administration (FDA) for treating breast cancer include AC (doxorubicin, cyclophosphamide), AC-T (doxorubicin, cyclophosphamide, followed by paclitaxel), CAF (cyclophosphamide, doxorubicin, 5-FU), FEC (5-FU, epirubicin, cyclophosphamide), and TAC (docetaxel, doxorubicin, cyclophosphamide) [3].

## 1.7.4 **Hormone therapies**

It is typically used to treat breast cancer expressing hormone receptors (i.e., the luminal subtypes). It can either be given as an adjuvant or neoadjuvant to surgery [2].

### 1.7.4.1 *Selective estrogen receptor modulators (SERMs)*

The earliest use of hormone therapy can be traced back to the 1970s, where the drug Tamoxifen was given to patients with ER+ breast cancer [29]. It acts as an anti-estrogen drug, preventing estrogen from binding to its receptor thereby cutting off ER supply to the growing cancer cells. Raloxifene, similar in activity to Tamoxifen has been in clinical use since 2007 since it shows lesser side effects as compared to Tamoxifen [8]. However, these drugs must be used with caution as the drug acts on the entire body (including normal cells) and may cause an increased risk of developing endometrial cancer [4].



#### *1.7.4.2 Estrogen receptor down regulator (ERDs)*

Fulvestrant is the commonly used ERD and is recommended to treat ER+ metastatic breast cancer in postmenopausal women [2]. It functions by competitively binding to the ER and downregulates cellular levels of ER [30].

#### *1.7.4.3 Aromatase inhibitors (AIs)*

These are another class of drugs that inhibit an enzyme called aromatase, involved in the estrogen synthesis pathway [31]. Examples of aromatase inhibitors are anastrozole, exemestane, and letrozole [2]. Aromatase inhibitors are typically given either as an initial adjuvant therapy, sequentially adjuvant i.e., 2-3 years after tamoxifen treatment or after 5 years of tamoxifen and all three have shown better efficacy over tamoxifen alone [31].

#### *1.7.4.4 Ovarian suppression*

The different hormone therapies, particularly ERDs and AIs, discussed until now are mostly recommended for postmenopausal women. However, in pre-menopausal women, the main source of estrogen production is the ovary. Hence, the main type of treatment offered to pre-menopausal women is to suppress the ovaries thereby making them postmenopausal and susceptible to treatment by the above-mentioned methods [2]. One method is surgery to permanently remove the ovaries (called Oophorectomy or ovarian ablation). A less invasive and more common procedure is to give drugs, called Luteinizing hormone-releasing hormone (LHRH) analogs such as goserelin and leuprolide, that temporarily shut down the function of the ovaries [2].

### **1.7.5 Immunotherapy**

The use of the body's immune system to target and kill cancer cells has been an intriguing concept for more than one hundred years, particularly in the mind of the pioneer surgeon William B. Coley [32]. But practical use of this type of therapy has been fairly recent. In general, immunotherapy is divided into two main groups:

#### *1.7.5.1 Passive immunotherapies*

The traditional use of immunotherapies against breast cancer has been to provide the body with immune system components that will fight the cancer rather than actively stimulating the immune system. The commonly used passive immunotherapy is immune checkpoint inhibitors. Pembrolizumab and atezolizumab which target the PD-1/PD-L1 immune checkpoint pathway have been FDA approved for treating metastatic TNBC (will be addressed in Chapter 1, part II).

#### *1.7.5.2 Active immunotherapies*

Here, the immune system is actively stimulated using specific antigens found on the tumor cell surface. Breast cancer vaccines [33] and adoptive cell therapy [34] are common examples, although they are all still under different phases of clinical trials and none has yet been approved for clinical use.

The use of immunotherapy to treat breast cancer is an attractive option and has gained popularity in recent years, leading to several clinical trials, especially for the Her2+ and TNBC subtypes [35].

### **1.7.6 Targeted therapy**

As we understand the molecular subtleties of breast cancer, we are able to develop specific therapies that target the cancer cells and cause less harm to the surrounding normal cells. Several such targeted therapies have been identified to treat the different subtypes of breast cancer.

#### *1.7.6.1 Anti-Her2 therapy*

A crucial step in targeted therapy was the development of trastuzumab, a monoclonal antibody (mAb) against Her2 in 1998, that targeted the extracellular domain of Her2, preventing further downstream signaling [36]. Trastuzumab (commonly referred to as Herceptin), has been found effective in Her2 overexpressing breast tumors either as a single agent or as an adjuvant with taxane-based or anthracycline-based chemotherapies [36]. Another example of anti-Her2 therapy is Pertuzumab, a mAb that prevents the dimerization of the Her receptors [37]. Other anti-Her2 mediated targeted therapies include Trastuzumab-DM1 (trastuzumab is conjugated with a fungal toxin DM1) and Ertumaxomab (targeting Her2 on the tumor cells and CD3 on the T-cells) [38]. A major drawback with trastuzumab treatment has been the development of resistance in patients and the inability of this drug to cross the blood-brain barrier, resulting in brain metastasis post-trastuzumab treatment [36].

This led to the development of dual inhibitors that targeted the tyrosine kinase epidermal growth factor receptor (EGFR) along with Her2. Lapatinib is one such dual inhibitor of EGFR and Her2, targeting their intracellular domains and blocking the downstream signaling cascade [36, 38]. Lapatinib could potentially be used to treat Her2-breast cancer that express one or more of the Her family receptors [36].

#### *1.7.6.2 Vascular endothelial growth factor (VEGF) inhibitors*

This class of inhibitors block angiogenic pathways, which is a common hallmark of breast cancer [39]. Two major ways to inhibit angiogenesis in breast cancer is (i) using an agent that blocks the ligand (VEGF-A) from binding to the VEGF receptor (e.g., bevacizumab) or (ii) multi-tyrosine kinase inhibitors that are involved in the VEGF pathway such as, sorafenib, sunitinib [36, 38]. The FDA approved VEGF inhibitors (bevacizumab) in 2008 for treating breast cancer patients but withdrew this approval in 2011 [4], which may be due to adverse side-effects. However, the national comprehensive cancer network guidelines still recommend the use of bevacizumab with paclitaxel [40].

#### 1.7.6.3 *PI3K/Akt/mTOR pathway inhibitors*

Downstream signaling of growth factor receptors (EGFR, Her2) is mediated by phosphatidylinositol-3 kinase (PI3K), protein kinase B (Akt) and mammalian target of rapamycin (mTOR) [38]. Aberrant activation of these kinases is frequently observed in breast cancer, particularly through mutations in *PI3K* [41] or *PTEN* (mutation and deletion) [42]. Hence, targeting this pathway using small-molecular inhibitors has been one method to treat breast cancer. All the different inhibitors that exist targeting this pathway are in various phases of clinical trials; however, Everolimus, an mTOR inhibitor, and Alpelisib, a PI3K inhibitor are the only two drugs targeting this pathway, that are currently approved for treating luminal breast cancer (HR+/Her2-) [2, 43].

#### 1.7.6.4 *Cell cycle inhibitors*

Typically, cyclin-dependent kinases (CDKs) are misregulated in the different phases of the cell cycle, leading to uncontrolled proliferative signals in breast cancer cells [44]. Drugs such as palbociclib, ribociclib, and abemaciclib that target certain CDKs, namely CDK4 and 6, were FDA approved recently to treat advanced or metastatic luminal breast cancer [45]. Notably, a subgroup called the luminal androgen receptor (LAR) that belongs to the TNBC subtype is also sensitive to CDK inhibition due to the association of the androgen receptor with the tumor suppressor retinoblastoma (Rb1) [15, 46].

#### 1.7.6.5 *PARP inhibitors for BRCA 1/2 mutants*

A characteristic of breast cancer is that it can be heritable if a woman possesses mutations in the *BRCA1/2* genes. *BRCA1/BRCA2* germline mutations, accounting for around 5% of all breast cancer are key genes involved in the homologous recombination DNA repair pathway [47]. Patients with *BRCA1* mutation tend to develop TNBC phenotype while *BRCA2* mutation leads to ER+/PR+ breast tumors [48]. Poly (ADP-ribose) polymerases (PARPs) are another family of enzymes that repair DNA damage through alternative mechanisms (e.g., Base-excision repair or non-homologous end joining). In breast cancer mutated for *BRCA*, the cells rely on PARP-mediated DNA repair and hence, introducing PARP inhibitors in this setting will introduce a “synthetic lethality” causing cell death and controlling tumor progression (**Figure 6**). Olaparib and talazoparib, two PARP inhibitors, have been approved for Her2- breast cancer since 2019 that exhibit *BRCA1/2* mutations. [2, 4].

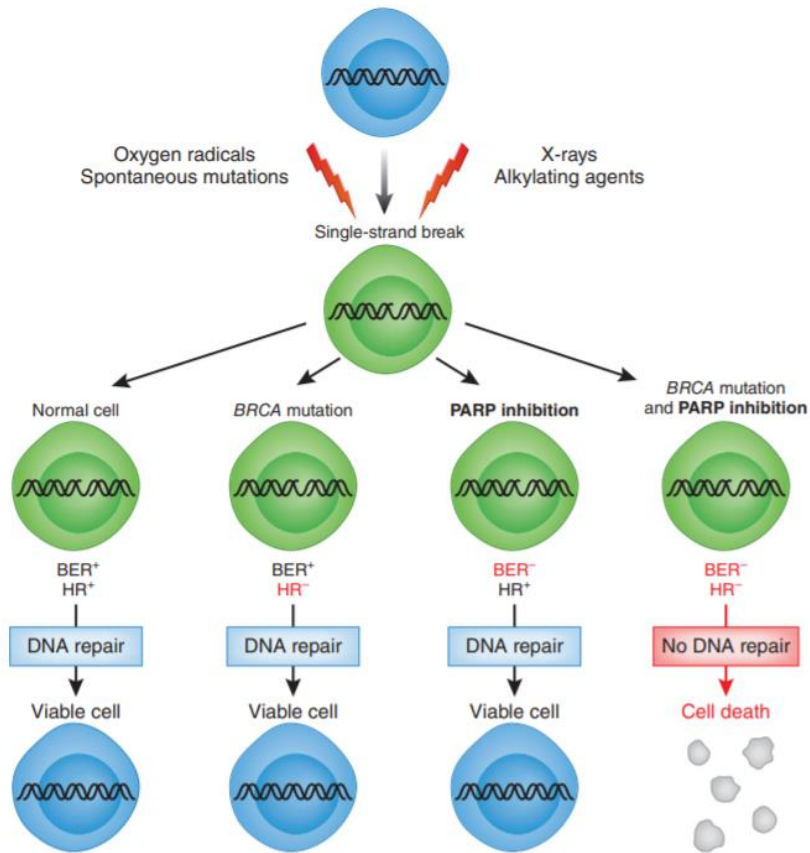


**Figure 6: Use of PARP inhibitors in breast cancer.** DNA damage can be repaired by base-excision repair (BER) which depends on PARP or homologous recombination which requires BRCA1/2. BRCA mutated cells rely on BER for DNA repair so introducing PARP inhibitors in these cells introduces synthetic lethality causing cell death. Adapted from [49].

#### 1.7.6.6 Other pathways under clinical trials

Several other molecular targets or pathways, such as histone deacetylase, insulin-like growth factor, HSP90, src-family tyrosine kinases, matrix metalloproteinases and the RAS/MEK/ERK pathway can also be inhibited using small molecules. These inhibitors are currently in different phases of clinical trials for breast cancer treatment [36, 38].

## II. Triple-negative breast cancer

The breast cancer subtype that belongs to the basal-like is the study model in this thesis and the subject matter for this chapter. The term TNBC was coined almost 15 years ago and represents around 15% of all breast cancer [50]. These tumors are generally more aggressive and highly proliferative. Although most basal-like are also triple-negative and vice-versa, they are not synonymous. The term triple-negative was assigned based on the absence of the hormone receptors (ER and PR) and lacking an overexpression of Her2 while basal-like is an intrinsic molecular subtype defined by specific gene expression profiling [51]. TNBC also encompass another subtype, called the claudin-low group, identified by Hershkowitz and colleagues as a separate cluster by microarray analysis [52]. A characteristic of this subtype is the low expression level of critical cell-cell adhesion molecules, like claudins (3, 4, and 7), occludin, and E-cadherin and is related to mesenchymal TNBC [53].

### 1.8 Clinical features, risk factors, prognosis

Some common clinical features of TNBC include high tumor grade, larger tumor size and are found associated with age (diagnosed more in younger women  $\leq 45$  years) and race (African-American and Hispanic women more susceptible) [50, 51]. TNBC tumors are more likely to metastasize to either the lungs or the brain, and less likely to the bones, unlike other subtypes [54]. TNBC is usually associated with a poor prognosis within 5-years after diagnosis although they are sensitive to primary chemotherapy. The main reason is a higher relapse among those with a residual disease [51].

Interestingly, germline mutations in *BRCA1* are associated with the TNBC subtype, making *BRCA1* a potential specific risk factor for TNBC over other breast subtypes [55]. Other risk factors for TNBC include higher parity and lack of breastfeeding, young age at first full-term pregnancy, and higher body weight [56-58].

### 1.9 General molecular features

TNBCs are also highly heterogeneous (like the whole breast cancer population) warranting a need to subclassify them, further. The first classification of TNBC was by Lehmann and colleagues in 2011 and I will discuss this in the next section. First, I will describe certain general molecular features that have been identified in the TNBC cluster compared to non-TNBC. The Cancer Genome Atlas (TCGA) analysis did not distinguish between TNBC and basal-like in their clustering and found around 80% of the tumors were mutated for *TP53*, and there were losses in other tumor suppressor genes such as retinoblastoma 1 (*RBT*) or the previously mentioned *BRCA1*. Another striking observation

was the increased activity of the PI3K/Akt pathway, either through mutations/amplifications in *PI3CKA* or loss of *PTEN* [42] and *INPP4B* [15]. The oncogenes (30% *KRAS*) and proto-oncogenes (30% *BRAF*, 23% *EGFR*) were found amplified in the basal-like subgroup. The last key feature was the hyperactivation of transcriptional factors FOXM1 and cMyc, which appeared to contribute to the highly proliferative nature of basal-like breast cancer [15].

### 1.10 Molecular subtypes of TNBC (Lehmann classification)

Perhaps the most extensively used system of TNBC classification is the one proposed by Lehmann and colleagues where they identified six subgroups of TNBC by analyzing gene expression profiles [59]. Such a classification highlighted not only the intrinsic heterogeneity characteristic of TNBC but also emphasized the need to identify targeted therapy by understanding the underlying biology of TNBC tumors. The six subgroups were (i) basal-like 1, (ii) basal-like 2, (iii) mesenchymal, (iv) mesenchymal stem-like, (v) immunomodulatory, and (vi) luminal-androgen receptor (**Figure 8**). Note, they also clustered several TNBC cell lines into similar groups, which has helped the entire TNBC research community while working with these models to understand their clinical relevance (**Figure 7**). Notably, several others have proposed different models of TNBC classifications [60-63] but I will focus on the subgroups identified by Lehmann and colleagues.

Cell line	TNBC subtype
HCC1395	UNS
BT20	
HCC1599	BL1
HCC1937	
HCC1143	
<b>MDA-MB-468</b>	
HCC38	
SUM149PT	BL2
<b>HCC70</b>	IM
<b>HCC1187</b>	M
<b>BT-549</b>	
CAL-51	
<b>Hs578T</b>	MSL
MDA-MB-157	
SUM159PT	
MDA-MB-436	
<b>MDA-MB-231</b>	
<b>MDA-MB-453</b>	LAR

**Figure 7: Lehman classification of TNBC cell line models [59].** The cell lines listed here are those routinely used in our lab and the ones highlighted in bold are those used in this thesis. UNS: unstable, BL1: basal-like 1, BL2: basal-like 2, IM: immunomodulatory, M: mesenchymal, MSL: mesenchymal stem-like, LAR: luminal androgen receptor.

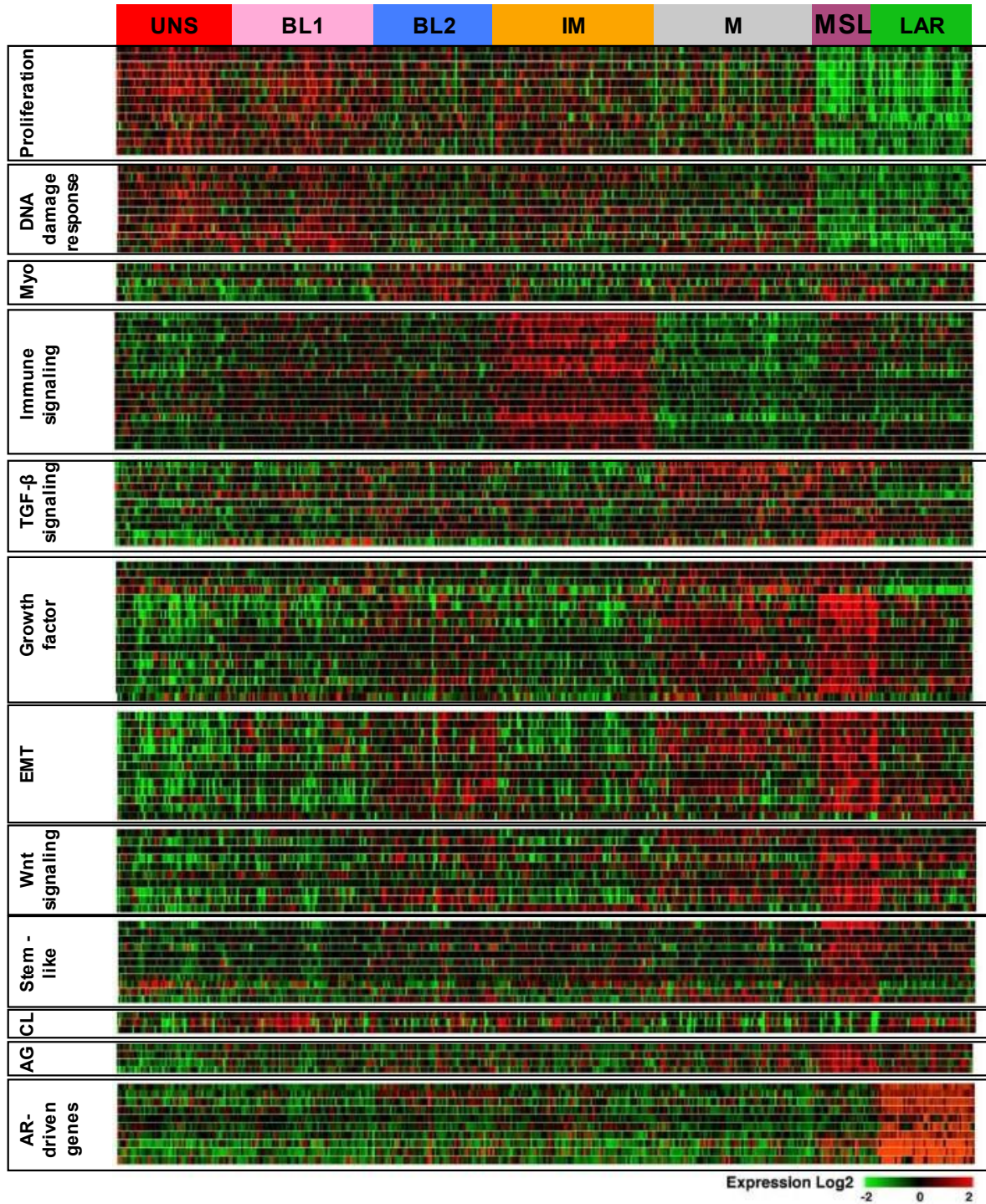


**Figure 8: TNBC subtype clustering by Lehmann et al.** This gene expression profiling highlights the enriched pathways unique to each TNBC subtype. UNS: unstable, BL1: basal-like 1, BL2: basal-like 2, IM: immunomodulatory, M: mesenchymal, MSL: mesenchymal stem-like, LAR: luminal androgen receptor, Myo: myoepithelial, CL: claudin, AG: angiogenesis. Modified and adapted from [59].

### **1.10.1 Basal-like 1 and 2 (BL1, BL2)**

The key pathways up regulated in the BL1 subtype were cell cycle and cell division pathways associated with proliferation genes like *PLK1*, *TTK*, *PRC1*, *AURKA*, *AURKB*, etc along with increased DNA damage response pathways. They also displayed high Ki67 expression, suggesting that these subtypes would respond better to a taxane treatment regime (as taxanes target highly proliferative cells).

BL2 subtype differs from BL1 as it is enriched in growth factor signaling pathways like EGF, IGF, Wnt/ $\beta$ -catenin and is accompanied by increases in the receptors of these pathways like EGFR. They were also uniquely enriched in metabolic pathways like glycolysis and gluconeogenesis.

### **1.10.2 Mesenchymal (M) and Mesenchymal stem-like (MSL)**

The M and MSL subgroups displayed mesenchymal features and majorly differed from the BL group as they were enriched in cell motility (Rho pathway), cell differentiation, and growth factor pathways (ALK, TGF- $\beta$ , and Wnt/ $\beta$ -catenin signaling). They were also enriched in genes responsible for the epithelial-to-mesenchymal transition (EMT) like *TWIST1*, and *ZEB1*.

The MSL subgroup differed from the mesenchymal subgroup as it was uniquely enriched in growth factor pathways (EGFR, G-protein coupled receptor, inositol phosphate metabolism, etc.) and angiogenetic genes (*VEGFR2*). They expressed low levels of proliferation genes but showed enrichment in stem-cell markers, HOX genes and mesenchymal stem-cell markers. The MSL subgroup also displayed low claudin expression, correlating with the other breast cancer subgroup "claudin-low" mentioned before.

### **1.10.3 Immunomodulatory (IM)**

The IM subgroup was highly enriched in classical immune signaling pathways like NF $\kappa$ B, TNF, JAK/STAT and immune cell response pathways like NK cell and B-cell receptor pathways. The gene signatures identified by Lehmann et al. for the IM subgroup overlapped with those found by Bertucci et al. in a very rare subtype of breast cancer known as the medullary breast cancer (MBC) [64]. MBC is a very rare form of breast cancer accounting for <2% of all breast cancer and falls under the intrinsic subtype of basal-like breast cancer (ER-/PR-/Her2-), but surprisingly has a favorable prognosis [64-66]

### **1.10.4 Luminal-androgen receptor (LAR)**

This last subgroup differed the most from the others especially since the gene ontologies were enriched in hormone-regulated pathways (steroid synthesis, androgen, and estrogen metabolism), though they did not express ER. They showed high expression of the androgen receptor (AR) mRNA and were enriched in downstream targets of AR. LAR group also showed luminal gene enrichment patterns, hence the name.



Lehmann and colleagues refined their stratification of TNBC subtypes in 2016, to have only 4 subtypes – BL1, BL2, M, and LAR since the high immune signature in the IM subtype and the mesenchymal signature in the MSL subtype were contributed from the lymphocyte infiltrates and stromal cells, respectively, rather than the tumor cells themselves [67].

## 1.11 Approved therapy for TNBC

As previously discussed, due to the lack of hormone receptors or overexpression of Her2 receptors on TNBC cell surface they cannot be treated with existing targeted therapies such as a hormone or anti-Her2 treatment. Typically, for early-stage TNBC, surgery or radiation is recommended depending on the tumor size. The most standard systemic treatment available for TNBC is chemotherapy, such as anthracyclines, taxanes, and capecitabine [2]. These conventional neoadjuvant treatments (composed of adriamycin, cyclophosphamide, and paclitaxel) result in a pathological complete response rate of 35-45% [68].

Recently, two targeted therapies have been approved by the FDA for TNBC patient treatment: **PARP inhibitors** and **anti-programmed cell death ligand 1 (PD-L1) therapy**.

PARP inhibitors (like Olaparib and talazoparib) have been approved only for TNBC patients having a *BRCA1/2* mutation (see **PARP inhibitors** for ). The platinum-based drugs – cisplatin and carboplatin are also used for *BRCA* mutated TNBC treatment [2, 4] or in the neoadjuvant or metastatic setting [69].

TNBC patients express high levels of PD-L1 and the tumor-infiltrating immune cells in these patients expressed programmed cell death 1 (PD-1) [70]. Therefore, targeting PD-1/PD-L1 was thought to be beneficial and the FDA approved anti-PD-L1 therapy (e.g., pembrolizumab) for the subset of metastatic TNBC patients who expressed PD-L1 [4]. Notably, anti-PD-L1 therapy was found more efficient in patients who had already received first-line chemotherapy, especially since this treatment increased PD-L1 expression on the surface of these tumors [71].

In 2020, a new antibody-drug conjugate **sacituzumab-govitecan** was approved by the FDA for the treatment of metastatic TNBC patients, who have already received at least two prior treatments [72]. This therapy contains two components: Sacituzumab, which is a monoclonal antibody that targets the trophoblast cell-surface antigen (Trop-2) while the drug conjugate govitecan is a camptothecin-derivative (called as SN-38), a chemotherapeutic drug that inhibits topoisomerase-I activity [4]. This antibody-drug conjugate was developed to specifically direct this drug to the cancer cells rather than targeting all proliferative cells (which is the case with conventional chemotherapy). Trop-

2 is overexpressed in many solid cancer types, including TNBC, and is an important biomarker for the EMT phenotype in breast cancer, possibly explaining the success of this drug-conjugate. However, it must be noted that the efficacy of this antibody-drug conjugate was studied in heavily pretreated metastatic TNBC patients and not as a single-agent treatment.

## **1.12 Chemoresistance, TNBC stem cells and their underlying mechanisms**

Despite the new therapies recently approved for TNBC patients, the prevailing systemic treatment strategy remains chemotherapy. The main limitation is that patients often develop resistance to chemotherapy. Several underlying mechanisms, often a dysregulation in developmental pathways, have been identified to contribute to chemoresistance.

### **1.12.1 ATP-binding cassette (ABC) transporters**

These transporters use ATP to efflux the drugs across the cell membrane and are implicated in chemoresistance [73]. Some ABC transporters are found more expressed in TNBC such as ABCC1, ABCG2, and ABCC11 and confer resistance to anthracyclines, taxanes, methotrexate, 5-FU, and doxorubicin [74]. Hence, targeting these transporters could help in overcoming chemoresistance in TNBC and pre-clinical evidences support this hypothesis [74].

### **1.12.2 Breast cancer stem cells and contributing signaling pathways**

Another major contributor to chemoresistance is a subset of tumor cells with self-renewing ability regardless of their nomenclature (cancer stem cells, CSCs; tumor initiating cells, TICs; or as a subpopulation of cells resistant to treatment) [75, 76]. They often increase in residual breast tumors following chemotherapy, implying that these cells are resistant [77]. These cells can be identified by probing for certain distinct molecular markers such as CD44<sup>+</sup>/CD24<sup>-/low</sup> [78, 79] or aldehyde dehydrogenase 1 positive (ALDH1<sup>+</sup>) [80] though each marker represents different populations of CSCs. The CD44<sup>+</sup>/CD24<sup>-/low</sup> population of cells show mesenchymal and quiescent phenotypes (meaning they had undergone EMT) while the ALDH1<sup>+</sup> cells display more epithelial, proliferative phenotypes (i.e., having undergone mesenchymal-to-epithelial transition) as analyzed by gene expression profiling [81, 82].

Several signaling pathways, particularly those involved in developmental processes like the TGF- $\beta$ , Notch, Hedgehog, BMP and Wnt/ $\beta$ -catenin, are known to fuel the self-renewing ability of these CSCs.

### 1.12.2.1 Transforming growth factor-beta (TGF- $\beta$ )/Smad pathway

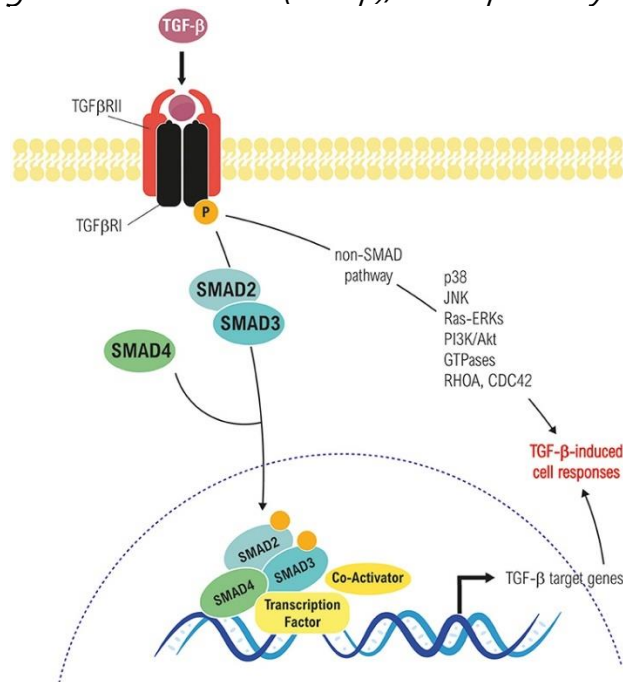


**Figure 9: Schematic representation of TGF- $\beta$  pathway.** TGF- $\beta$  binds to the transmembrane receptor TGF- $\beta$ RII which leads to the phosphorylation of TGF- $\beta$ RI. This causes the phosphorylation of the different SMAD proteins, leading to their translocation to the nucleus, activating TGF- $\beta$  induced target gene expression. Adapted from [83].

TGF- $\beta$  is part of the cytokine family and binds to the type II TGF- $\beta$  receptor (TGF- $\beta$ R). This ligand-receptor interaction recruits and phosphorylates another receptor counterpart, type I TGF- $\beta$  receptor (TGF- $\beta$ R), activating the signaling pathway. The effectors of this pathway are the Smad family proteins, which are phosphorylated by the receptor complex and translocate to the nucleus to activate the transcription of the target genes (**Figure 9**) [84]. TGF- $\beta$  signaling is implicated in many cancer hallmarks such as EMT, proliferation, angiogenesis, metastasis [85], but mainly in CSC renewal in breast cancer [86]. In TNBC, this pathway is known to play a vital role in conferring resistance and increasing stemness/tumor-initiating properties, responsible for the relapse of the disease. For example, it was found that treatment with chemotherapy increased TGF- $\beta$  signaling and inhibiting this pathway, prevented the re-establishment of tumors in a xenograft model [87]. Targeting the main receptor of this pathway, TGF- $\beta$ R, is in the early stages of clinical investigation, but still needs to be refined before being used as a TNBC therapy regimen.

### 1.12.2.2 Notch pathway

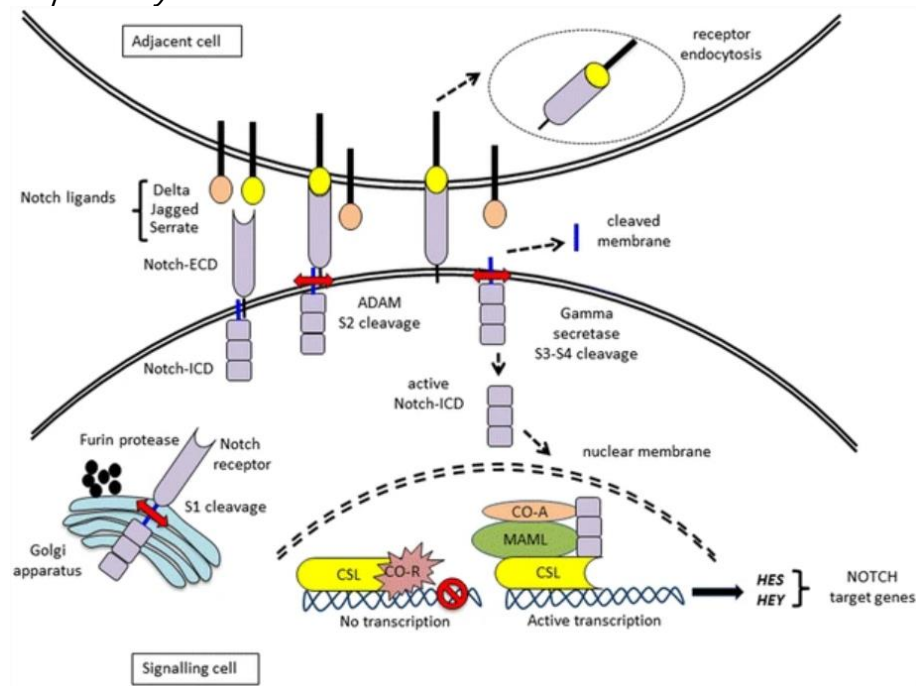


**Figure 10: Summary of the Notch signaling pathway.** This pathway uses a paracrine mode of activation where the ligands (Delta, Jagged, Serrate) bind to the receptors of the adjacent cell to activate the cleavage of the intracellular receptor domain. This domain translocates to the nucleus to activate the transcription of NOTCH target genes. Adapted from [88].

This pathway requires cell-to-cell contact to be activated. NOTCH family of receptors are activated when ligands (DELTA or JAGGED) from adjacent cells bind to these receptors. This interaction initiates sequential cleavages by proteases and secretases of the intracellular domain of the NOTCH receptor (NICD), which translocates to the nucleus to activate target gene transcription [89] (**Figure 10**).

Similar to TGF- $\beta$  signaling, the Notch pathway is also implicated in several hallmarks of cancer, particularly in immune system invasion, EMT, and proliferative signaling. In TNBC, the NOTCH receptors (1/3/4) are either overexpressed or amplified and associated with the above-mentioned cancer hallmarks [90]. Some inhibitors of the NOTCH pathway, particularly those that target the  $\gamma$ -secretase are in Phase-I clinical trials for advanced TNBC in combination with docetaxel [91, 92]. Apart from these two inhibitors, there are no other available inhibitors of the NOTCH pathway that show clinical benefit for TNBC patients, but it remains a valuable pathway to be targeted.

### 1.12.2.3 Hedgehog pathway

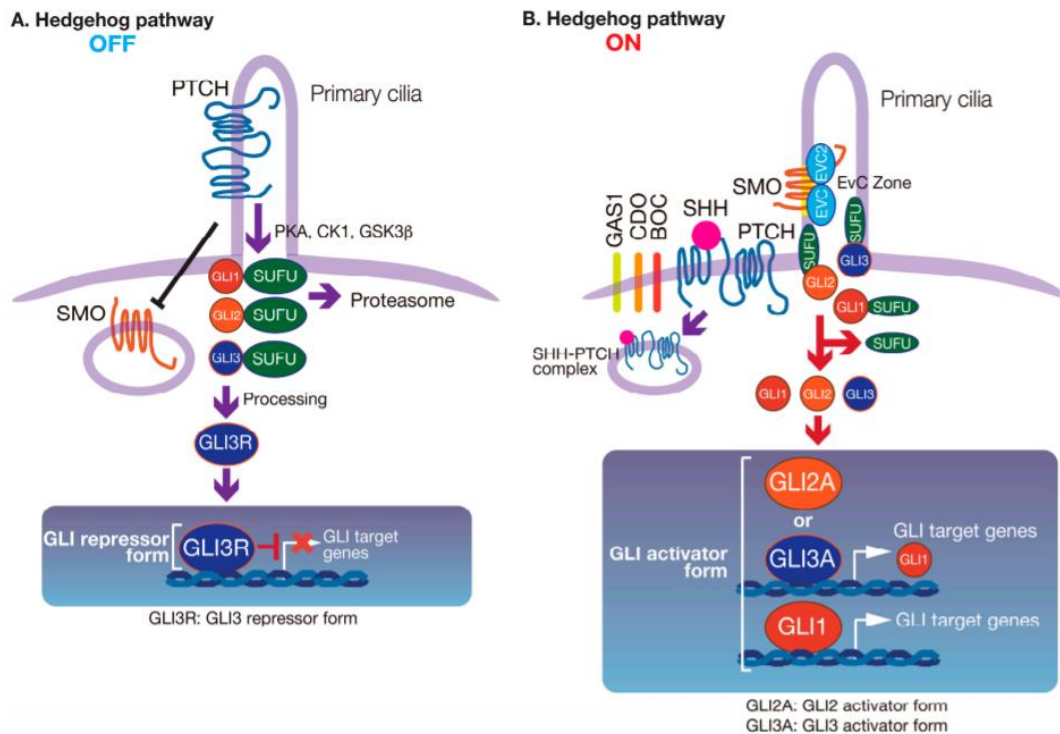


**Figure 11: Hedgehog signaling pathway in its “on” and “off” state.** (A) In the absence of Hedgehog (HH) ligand, Patched (PTCH) prevents the localization of Smoothed (SMO) to the cilia, and the GLI repressor form – GLI3R, represses the target genes. (B) The pathway is activated when HH binds to PTCH, aiding in the ciliary localization of SMO. This activates the GLI family of transcription factors to translocate to the nucleus and activate target gene expression. Adapted from [93].

This is one of the crucial pathways in embryonic development and has been linked to carcinogenesis. The main ligand is Sonic HedgeHog that binds to the transmembrane receptors Patched and Smoothened. The downstream signaling activates the transcription factors GLI1-3 to regulate the expression of target genes, which include ABCG2 and VEGF (**Figure 11**). The most druggable target of this pathway is Smoothened, but none of them have shown clinical efficacy for breast cancer in general or TNBC in particular [74].

### 1.12.2.4 Wnt/ $\beta$ -catenin pathway

The last major pathway involved in TNBC chemoresistance [94, 95] and maintenance of CSC [96, 97] is the Wnt/ $\beta$ -catenin pathway (is a subject of my thesis). As with all signal transduction mechanisms, the major receptors of this pathway are the Frizzleds (FZDs) and low-density lipoproteins LRP5/6. In the absence of Wnt ligands, there is a destruction complex in the cytosol composed of casein kinase 1 (CK1), glycogen synthase kinase 3 (GSK3), Dishevelled (Dvl), Axin, and adenomatous polyposis coli (APC), that sequesters  $\beta$ -catenin (main effector). Both GSK3 and CK1 phosphorylate  $\beta$ -catenin and prime it for ubiquitin-mediated proteasomal destruction, and the repressor factor

Groucho is bound to the TCF/LEF1 transcription factor preventing the activation of Wnt target genes. On the other hand, the signaling is initiated when the Wnt ligands bind to the Frizzleds and LRP5/6, recruiting Dvl and phosphorylating LRP5/6, which interact with Axin. This destabilizes the destruction complex, freeing  $\beta$ -catenin and leading to its accumulation in the cytosol. Increased cytosolic  $\beta$ -catenin level leads to its nuclear translocation where it displaces Groucho and binds to the transcription factors TCF/LEF1, thereby activating Wnt target genes (*Axin2*, *NKD1*, *APCDD1*). A crucial step to initiate the signaling cascade is the palmitoylation of the Wnt ligands catalyzed by the enzyme Porcupine (PORCN) in the endoplasmic reticulum. This modification aids in the extracellular secretion of these ligands, to then bind to the transmembrane receptors [98] (Figure 12).

Nonetheless, this is the simplest model of the canonical Wnt signaling and there exist other mechanisms often called non-canonical which include the planar cell polarity pathway or the Wnt/Calcium pathway [94].

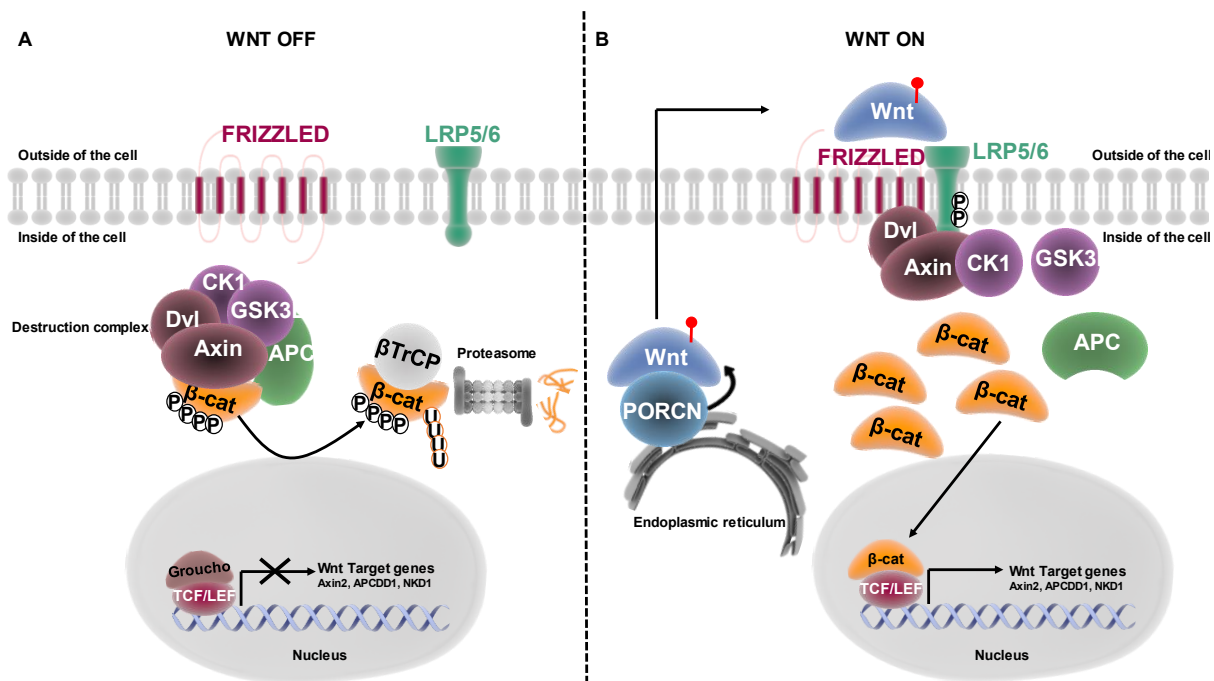


**Figure 12: Schematic overview of the Wnt/ $\beta$ -catenin pathway in its "OFF" and "ON" state.** (A) In its "OFF" state, the cytosolic destruction complex sequesters  $\beta$ -catenin ( $\beta$ -cat) and phosphorylates it. Phosphorylated  $\beta$ -cat is bound to the E3 ubiquitin ligase  $\beta$ -TrCP which poly-ubiquitinates  $\beta$ -cat and targets it to proteasomal degradation. (B) The pathway is activated when the Wnt ligands are palmitoylated by the enzyme porcupine (PORCN) in the endoplasmic reticulum and secreted out of the cell, binding to the transmembrane receptors Frizzled and LRP5/6. This dissociates the destruction complex causing  $\beta$ -cat to translocate to the nucleus, where it interacts with TCF/LEF to activate Wnt target gene expression.

As with the other key developmental pathways, Wnt/ $\beta$ -catenin dysregulation is implicated in TNBC tumorigenesis, metastasis and is responsible for stem cell-like features

and chemoresistance in TNBC [95]. A key feature of aberrant Wnt signaling in TNBC is that it is not driven by mutations in the  $\beta$ -catenin (*CTNBB1*) gene [99]. Rather, the transmembrane receptors, FZDs and LRPs are overexpressed. For example, *FZD6* is amplified while *FZD7* is overexpressed in TNBC, and reducing their expression decreased tumorigenic features like proliferation, invasion, and others [100, 101]. *FZD8* is upregulated in TNBC residual cells treated with cisplatin, suggesting that the Wnt pathway was involved in chemoresistance via *FZD8* [102]. The co-receptors LRP5 and LRP6 are both overexpressed in TNBC and like FZDs, they can be potential therapeutic targets for TNBC [103-106]. LRP8, sharing conserved domains with LRP5/6, was later found to positively regulate the Wnt pathway, particularly to induce osteoblast differentiation [107]. Recently, LRP8 was also found overexpressed in TNBC (and Her2+) and shown to be a potential therapeutic target [108].

Therefore, targeting the Wnt/ $\beta$ -catenin pathway could prove beneficial to TNBC patients. However, among all the existing inhibitors targeting this pathway such as  $\beta$ -catenin inhibitors, TCF/LEF inhibitors, and others, only the porcupine inhibitor **LGK-974** is in Phase I clinical trial for Wnt ligand-dependent tumors, including TNBC (NCT01351103).

Crosstalk among the above pathways is one major challenge in developing inhibitors for clinical use due to potential off-target effects. Identifying regulatory mechanisms, such as epigenetic/post-translational modifications on the components of these pathways might prove useful to design better inhibitors.

### 1.13 Concluding remarks

Treatments targeting other pathways dysregulated and/or implicated in the tumorigenesis of TNBC are being investigated either in pre-clinical or clinical models (**Figure 13**). Several of these studies are performed using these targeted therapies in combination with chemotherapies. Some of the examples for targeted therapies include inhibitors against (i) angiogenetic receptors, (ii) Src, (iii) mTOR, (iv) PI3K, (v) AKT, (vi) Histone deacetylase (HDAC), (vii) androgen receptor, (viii) Hsp90 [109].

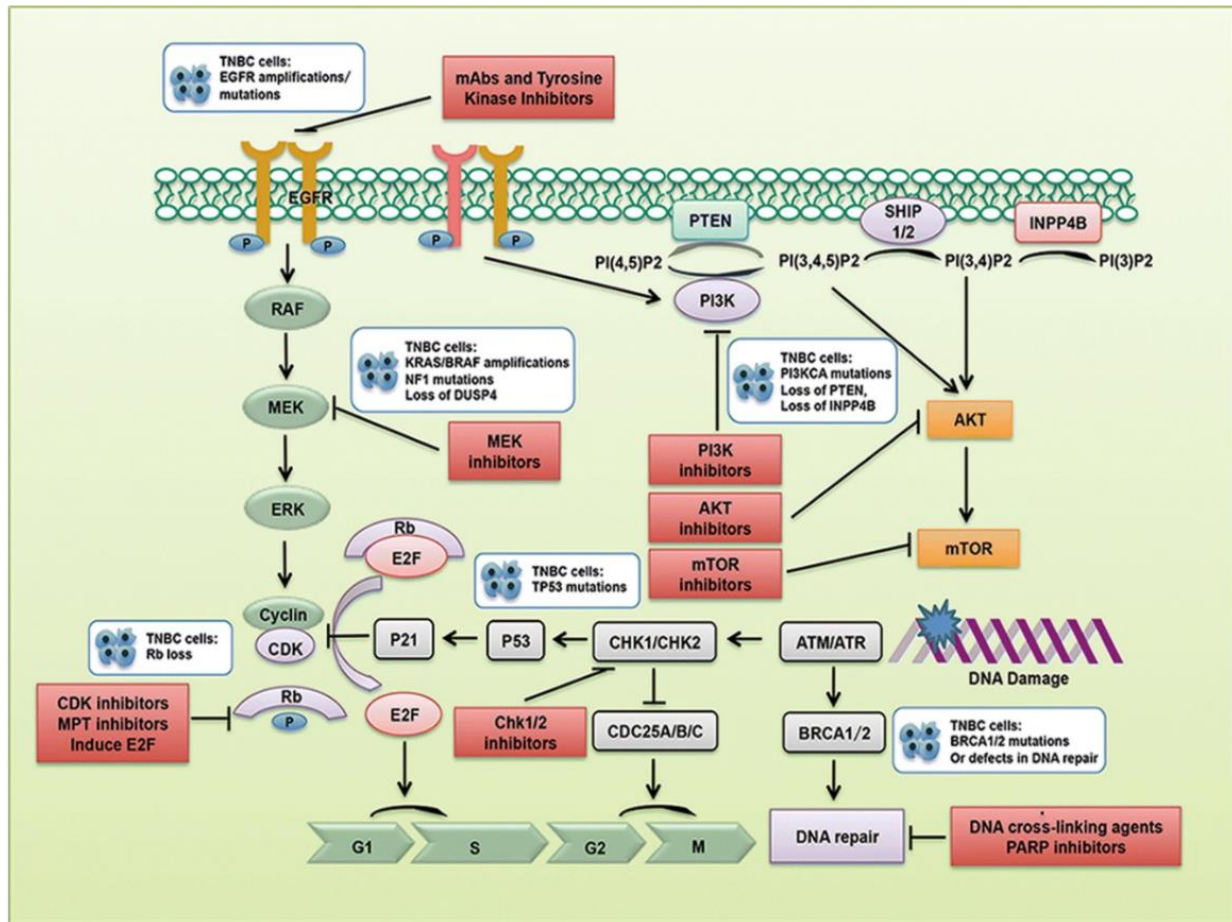


**Figure 13: Current and upcoming treatment strategies for TNBC.** The genetic alterations are indicated in white boxes while the upcoming therapies are mentioned in the red boxes. Adapted from [110].

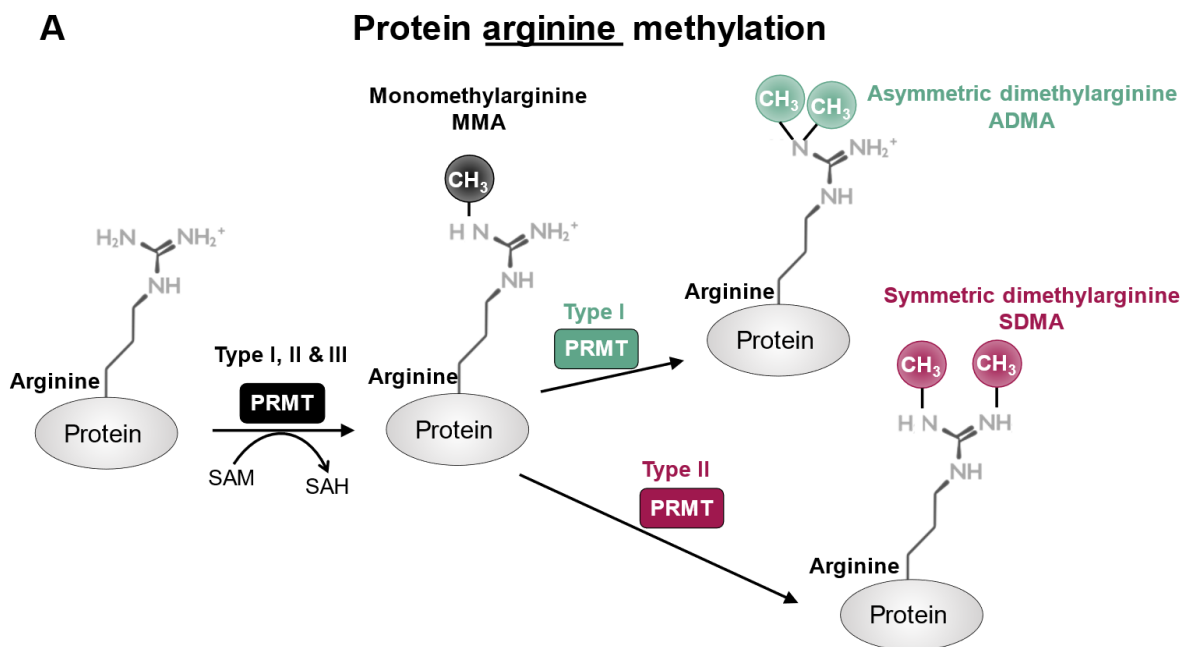
One of the most disappointing trials in the clinic for TNBC has been the EGFR inhibitors. Given that more than 80% of TNBC tumors overexpress EGFR, it appeared to be a very promising target, leading to the development of inhibitors - erlotinib and lapatinib or mAbs – cetuximab and panitumumab. Erlotinib, for example, showed a very poor response in a phase II trial of advanced/metastatic BC as a monotherapy [111]. However, a combination of anti-EGFR with other agents such as chemotherapy, PARP inhibitors or potentially several of the above-mentioned inhibitors seem promising and remain to be fully evaluated [109]

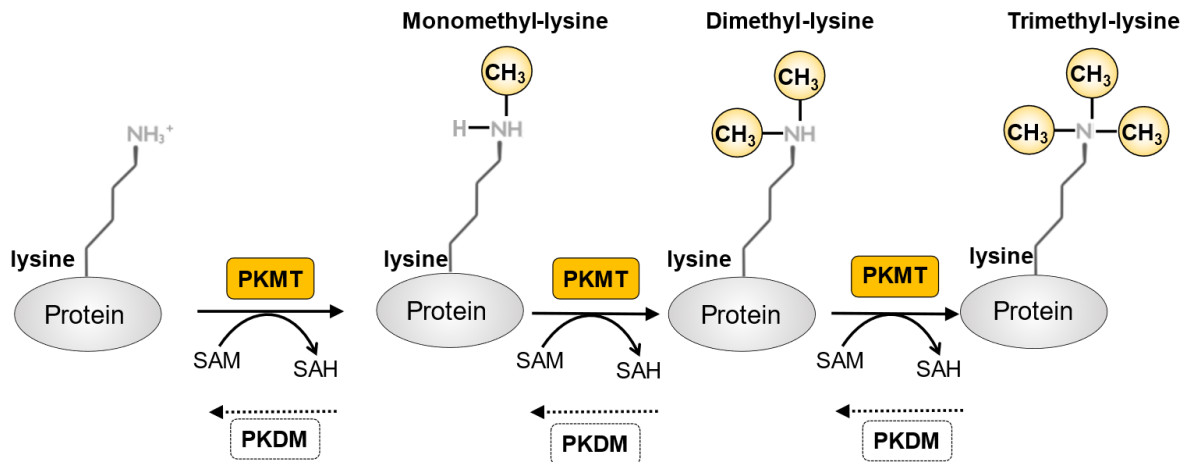
In conclusion, there is an urgent clinical need to identify specific therapeutic targets for treating TNBC patients. An in-depth understanding of the underlying biology of TNBC would surely prove resourceful in achieving the above goal.



### III. Protein-arginine methyltransferases (PRMTs)

The occurrence of protein-methylation on the two basic amino acids, lysine or arginine has been known since the 1960s [112] and the first PRMT (called protein-methylase I at the time) was isolated from calf-thymus in 1968 [113]. Protein-methylation has a high energy cost associated with it (net usage of 12 ATP molecules) unlike the more commonly known PTM of phosphorylation (1 ATP molecule). Hence, one would imagine that this costly process would be rare. However, we now know that protein-methylation is as ubiquitous as phosphorylation [114]. Most importantly, this process has been evolutionarily conserved in all eukaryotes [115]. Protein methylation on arginines is catalyzed by protein arginine methyltransferases (**PRMTs**) (**Figure 14A**) while methylation on lysine residues is carried out by lysine methyltransferases (**PKMTs**) (**Figure 14B**). Only the PRMTs will be described in detail in the upcoming sections as the focus of this thesis is on PRMTs.



**B****Protein lysine methylation**

**Figure 14: Overview of protein methylation on lysine and arginine residues.** (A) PRMTs methylate their substrate proteins on the arginine residue and generate monomethylated (all PRMTs) or dimethylated arginines (Type I – asymmetric, Type II – symmetric). (B) The lysine residues on proteins can be methylated by protein lysine methyltransferases (PKMT) generating mono-, di-, and tri-methylated lysines. These modifications are reversible by lysine demethylases (PKDM). SAM: S-Adenosyl-L-methionine; SAH: S-Adenosylhomocysteine.

Within a span of five years (1998-2005), almost nine enzymes were identified from the human genome to belong to the PRMT family by various groups and were termed as PRMT1-9 (in their order of discovery) [116]. It must be noted here that PRMT4 is also called CARM1 and for the sake of consistency, I will refer to this protein as CARM1 in the rest of my thesis. All nine enzymes share a common central methyltransferase domain and unique N- and C-terminal domains attributing different cellular functions to the PRMTs. The first step in the enzymatic reaction for all nine PRMTs is the addition of one methyl group from S-Adenosyl-L- methionine (SAM) to the guanidino nitrogen of the arginine residue. SAM is the universal methyl donor in the cell and is generated through the metabolism of the essential amino acid methionine (**Figure 15**).

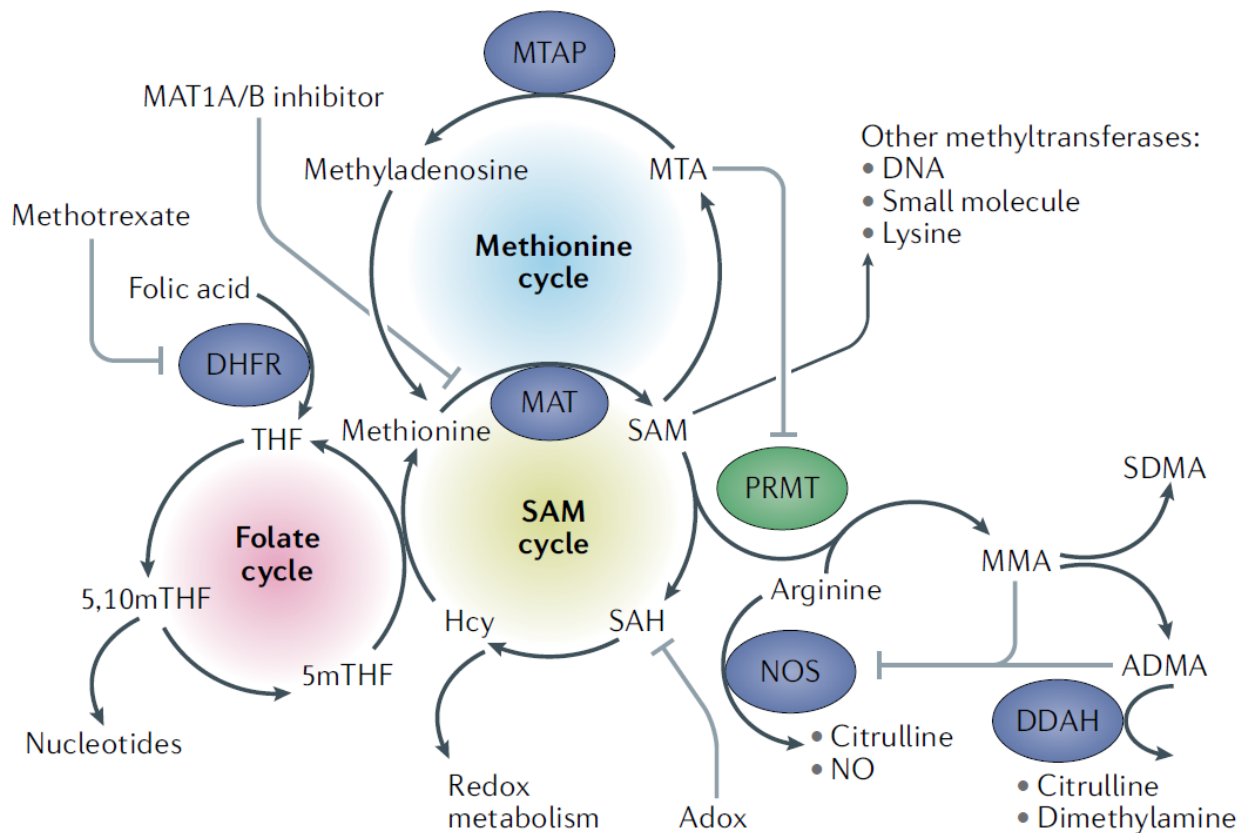


**Figure 15: Metabolic cycle generating the metabolite, SAM.** SAM is generated through the methionine metabolic cycle which is the methyl donor for all the methylation reactions in the cell, such as DNA, lysine, and arginine methylation. The by-product of methylation reaction using SAM generated SAH. Methionine is regenerated from SAH either through the folate cycle or through the methionine cycle. Modified and adapted from [117].

The first step of the methylation reaction generates a “methyl mark” called monomethyl arginine (MMA). For PRMT7, a type III PRMT, this is the only mark it can generate. Type I PRMTs (PRMT1-3, CARM1, PRMT6, and PRMT8), catalyze another methylation step, adding a second methyl group to the same terminal nitrogen group, generating an asymmetric dimethylarginine mark (ADMA). Type II PRMTs (PRMT5 and PRMT9) catalyze the addition of a second methyl group like type I PRMTs, but add it on the other terminal nitrogen, producing the symmetric dimethylarginine (SDMA) mark. PRMT1 is responsible for the bulk-arginine methylation in cells and is the major type I PRMT, while PRMT5 is the major type II PRMT. ADMA mark is the most prevalent, followed by the MMA (50% of ADMA) and SDMA (20% of ADMA) [116].

### 1.14 Structure of the PRMTs

All nine PRMTs have a central catalytic methyltransferase domain composed of conserved signature motifs (Figure 16). These are **motif I (VLD/VGxGxG)**, **post-motif I (V/I-X-G/A-X-D/E)**, **motif II (E/K/VDII)**, **double-E loop (SExMGxxLxxExM)**, **motif III**

(LK/xxGxxxP), and the **THW loop** [118]. Structurally, the core methyltransferase domain is composed of an N-terminal Rossmann-fold (common to the super-family of protein methyltransferases) and a C-terminal  $\beta$ -barrel, unique to the subfamily of PRMTs [119]. The Rossmann fold is associated with binding to the cofactor (and methyl donor), SAM. The double E and THW loops are crucial for binding to the substrate arginine, where the two highly conserved glutamic acid residues (highlighted in red earlier) orient the substrate arginine and this interaction is stabilized by a hydrogen bond with a histidine residue located in the THW loop. A common feature of all PRMTs is their ability to dimerize through a dimerization arm located in the N-terminal of the  $\beta$ -barrel region, and this dimerization is necessary for their enzymatic activity [118]. Higher-order oligomerization has also been shown for certain PRMTs, such as PRMT5 [120] and PRMT8 [121]. Type I PRMTs have an additional motif (YFxxY) upstream of motif I that forms an  $\alpha$ -helical structure [122]. The uniqueness of each PRMT arises from their respective N- and C-terminal regions (**Figure 16**). For example, CARM1 has a PH-like fold in its N-terminal that is important for substrate/long-non coding RNA recognition and binding [123].

The full-length crystal structure of all PRMTs is fully solved [119-121, 124-127], except for CARM1 [123] but none of them has been crystallized with a protein partner except PRMT5 with its partner MEP50 [120]. The structure of PRMT9 is yet to be solved.

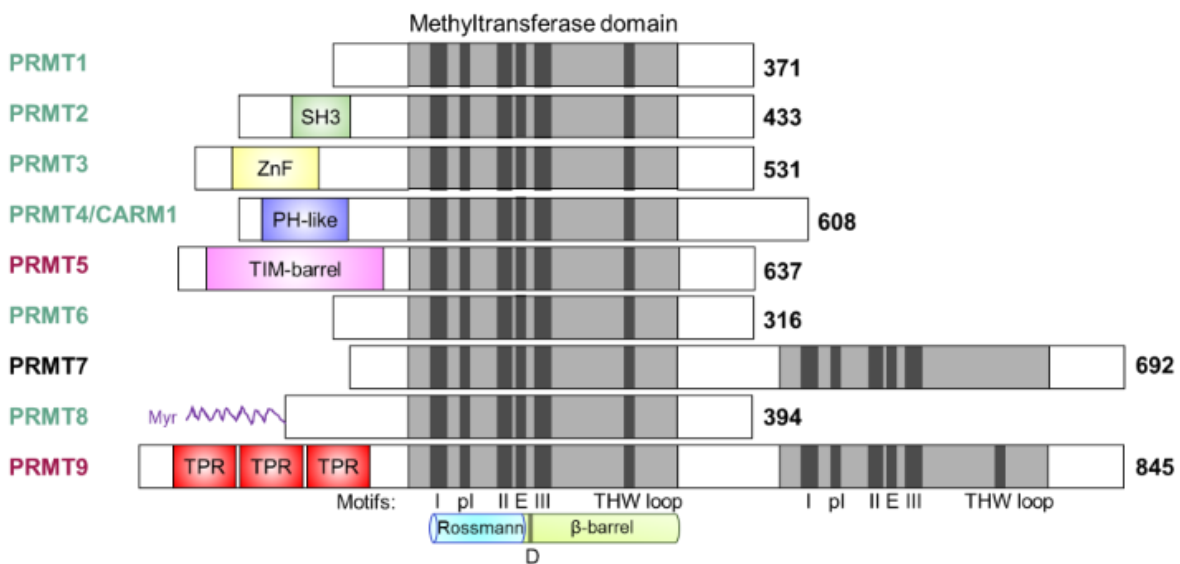


**Figure 16: Family of nine mammalian PRMTs.** All the PRMTs share structural homology in their central catalytic domain with certain conserved residues and motifs. The signature PRMT motifs (marked in black lines) are labeled motif I, post I (pI), II, E (double E loop), III and the THW loop. The dimerization arm common to all PRMTs is labeled as D. Some of the PRMTs have unique motifs at the N-terminus (shown in different colors). Type I PRMTs are labeled in green, Type II PRMTs in red and Type III in black. SH3: SRC Homology 3 Domain; ZnF: Zinc-finger; PH: Pleckstrin homology; TIM: triose phosphate isomerase; Myr: Myristoylation; TPR: Tetratricopeptide repeat.

## 1.15 Generalities of PRMTs

The distinctive roles of the PRMTs are achieved by various means: unique N and C-terminus regions, different subcellular localization, alternative splicing, and post-translational modifications (PTMs). PRMT1, PRMT2, CARM1, PRMT5, and PRMT7 are both nuclear and cytoplasmic [128]. PRMT3 [129] and PRMT9 [130] are exclusively cytoplasmic while PRMT6 [131] is only nuclear. PRMT8 is the only one localized to the plasma membrane owing to myristoylation at its N-terminus [132]. In addition, PRMT8 is the only known PRMT to display tissue-specific expression, exclusively in the brain [132]. Several PTMs for each PRMT are also known that regulate their activity such as phosphorylation, glycosylation, ubiquitination, and methylation.

Further, alternatively spliced isoforms have been identified for certain PRMTs, like PRMT1 [133], CARM1 [134], and PRMT7 [135]. These isoforms would no doubt enhance the individual function of each PRMT since these enzymes do not appear to be redundant. Further, the essential functions of PRMTs have been highlighted when full-body knockout (KO) mice were generated for PRMT1-6, with each displaying unique phenotypes. PRMT1 and PRMT5 mice KO are embryonically lethal [136, 137], while PRMT2 [138], PRMT3 [139], and PRMT6 [140] KO mice are viable. CARM1 KO mice die shortly after birth [141].

## 1.16 Substrate motifs

Historically, the substrate motif preferred by the PRMTs has been defined as glycine arginine-rich (GAR) [142], as some of the first identified substrates, mainly RNA-binding proteins, such as the heterogeneous ribonucleoproteins (hnRNPs), often harbored a GAR motif. This motif is also frequently referred to as the RGG/RG motif [143]. Two members of the PRMT differ greatly in this aspect. PRMT7, the only type III PRMT specifically targets an RXR motif [144]. The other unique PRMT is CARM1. It was first shown that CARM1 preferred a proline glycine motif (PGM) [145]. This preference of CARM1 towards proline-rich motifs has been recently reinforced by a few high-throughput mass spectrometry studies [146-148]. Moreover, using an oriented peptide library, PRMT9 was also found to methylate arginines within a proline-rich motif [149], however, the only PRMT9-specific substrate (SAP145) does not harbor this motif [150]. Some viral proteins, like Tat, shown to be methylated by PRMT6, harbor yet another sequence motif i.e., lysine residues in the vicinity of the substrate arginine (RKKRR) [151]. The specific motif requirements by CARM1, PRMT6, PRMT7 and PRMT9 point towards a “division of labor” hypothesis suggesting that each PRMT has its subset of protein interactors (and therefore function) further highlighting the non-redundancy of the different mammalian PRMTs.

## 1.17 Crosstalk among PRMTs and substrate scavenging

The idea that the PRMTs compensate for each other's activities exists in the field. This was brought to light by an elegant study from the labs of Richard, Clarke and Bedford [152]. They demonstrated that when PRMT1 was knocked out (KO), the cellular levels of MMA were significantly upregulated, and similar dramatic changes were not observed when other type I PRMTs (PRMT3, CARM1, PRMT6) or PRMT5 levels were perturbed. They also showed that after a few days of PRMT1 KO, MMA and SDMA levels increased, and surprisingly, ADMA levels as well (after an initial decrease), suggesting that the other type I PRMTs were probably compensating for the loss of PRMT1. Recent large-scale mass spectrometry analyses in search of PRMT substrates have shown that they share many substrates and methylate the same arginine residue within the protein [146, 148, 153].

Apart from sharing substrates, some PRMTs even methylate each other or regulate their activity. For example, CARM1 methylates PRMT5 regulating its dimerization ability and catalytic activity [154]. PRMT2 interacts with PRMT1 via its SH3 domain to increase PRMT1 enzymatic activity and this interaction was lost if global methylation was inhibited using Adox [155]. Together, this shows that there is definitive crosstalk among the PRMTs in cells, and an in-depth understanding of the physiological conditions that permit substrate scavenging could shed light on novel PRMT functions.

## 1.18 Cellular functions and role in diseases

The principal function of PRMTs has been linked to transcription – either as transcriptional activators or repressors. All the PRMTs methylate histones, each having their specific histone mark, but in certain cases also methylating the same histone residues. For example, both PRMT1 [156, 157] and PRMT5 [158] methylate histone H4 on Arg3, generating H4R3me2a or H4R3me2s marks, respectively. CARM1 methylates histone H3 on Arg 17 and 26 [159], and PRMT5 symmetrically dimethylates H3 on Arg 8 [160].

### 1.18.1 The many cellular functions of PRMTs

Inside the nucleus, apart from transcriptional regulation, the PRMTs are mainly involved in pre-mRNA splicing, DNA damage response, cell cycle, embryonic development, signaling, and RNA stability [116, 161-165]. Cytoplasmic functions of PRMTs include immune surveillance, and signal transduction [116, 161-164].

#### 1.18.1.1 *Pre-mRNA splicing*

PRMT5 has a key role in the maturation of snRNPs by methylating several of the Sm proteins which directly bind to snRNPs [166, 167]. Methylated Sm proteins are recognized by the Tudor domain of SMN to aid in the maturation of snRNPs [166, 167] (**Figure 17a**). Similarly, PRMT9 methylates the splicing factor SF3B2 (or SAP145) and

methylated SF3B2 is also recognized by the Tudor domain of SMN, and this interaction is important for the maturation of the snRNP, U2 [130, 150] (**Figure 17a**). CARM1 also regulates splicing by methylating splicing factors like SAP49, CA150 and others [145] (**Figure 17b**, see **Pre-mRNA splicing** for details). PRMT1 regulates alternative splicing by methylating and reducing the protein concentration of the RBP, RBM15 in leukemia cell lines [168]. RBM15 recruits the splicing factor, SF3B1, to the intronic gene regions that it binds [168].

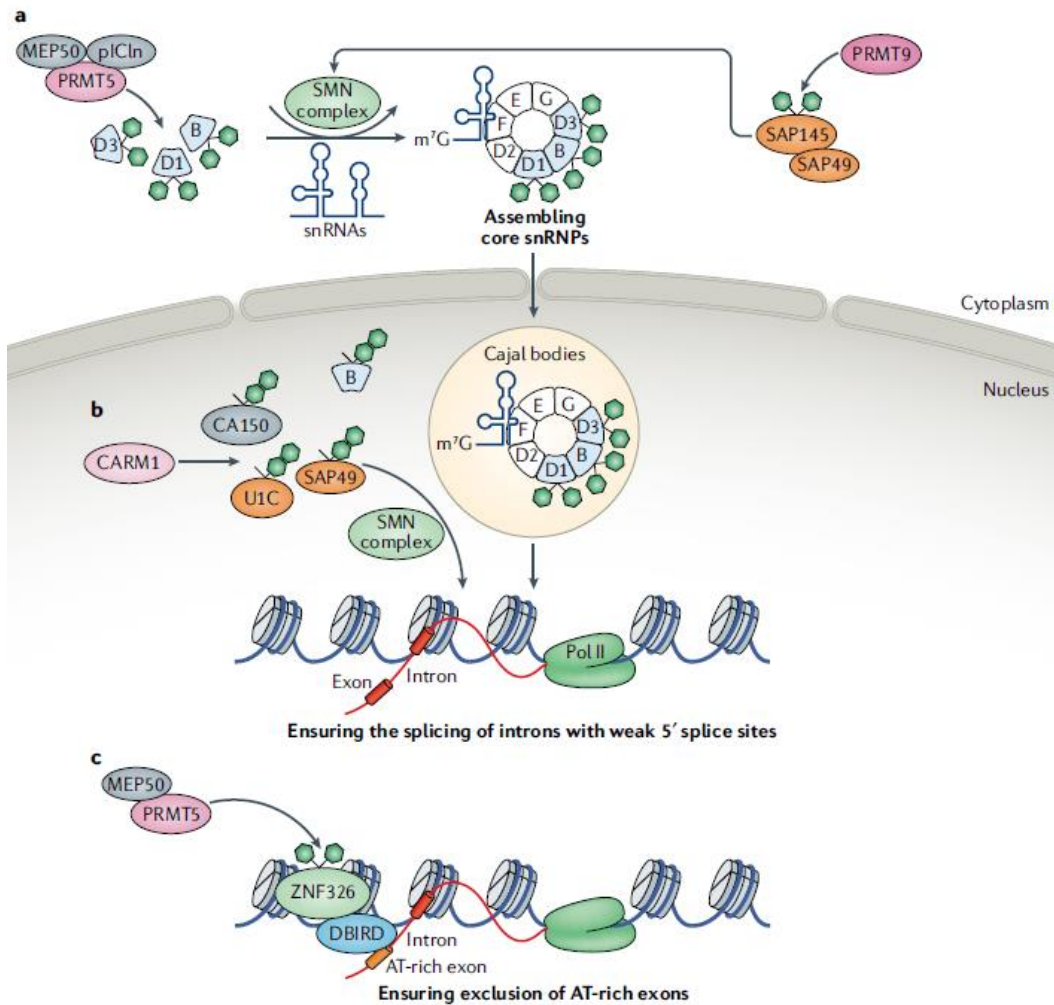


**Figure 17: Function of PRMTs in pre-mRNA splicing.** (a) PRMT5 methylates core members of the splicing complex while PRMT9 methylates the splicing factor SAP145, to promote the maturation of the snRNPs. (b, c) Inside the nucleus, CARM1 (labeled as CARM1 in the scheme) and PRMT5 methylate different splicing factors or Zinc-finger containing proteins to regulate pre-mRNA splicing. Adapted from [163].

#### 1.18.1.2 Cell cycle regulation and DNA damage response

PRMT1 and PRMT5 are mainly involved in the DNA damage response pathway [165]. PRMT1 methylates two proteins MRE11 and 53BP1 (p53 binding protein 1) which are key proteins in the DNA damage repair pathways [169-171] (**Figure 18a**). PRMT5 has

been identified as an important protein in homologous recombination-mediated DNA repair [172, 173]. Therefore, a loss of PRMT5 causes DNA damage in cells [172-174] (**Figure 18b**). Interestingly, PRMT5 regulates the DNA repair pathway particularly by affecting the alternative splicing of genes involved in this pathway (e.g., TIP60/KAT5, RUVBL1) [172-174]. PRMT6 methylates DNA polymerase beta enhancing its activity in the DNA base excision repair mechanism [175].

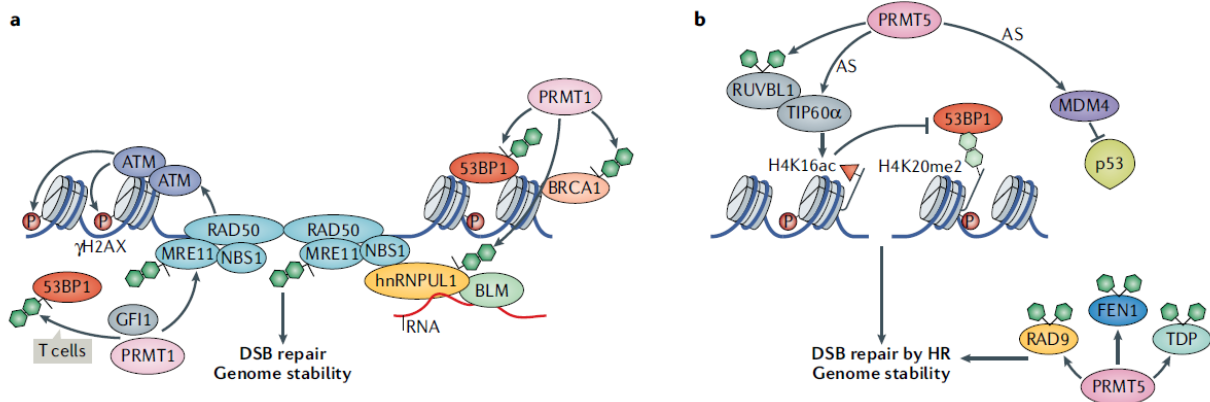


**Figure 18: Regulation of the DNA damage response pathway by the PRMTs.** (a) PRMT1 methylates 53BP1, BRCA1, and MRE11 to promote their function in double-strand break repair. (b) PRMT5 similarly methylates proteins involved in the DNA damage response pathway to promote DNA double-strand repair by homologous recombination. Modified and adapted from [163].

PRMTs (PRMT1, PRMT2, CARM1, PRMT5, and PRMT6) also control cell cycle, by methylating cell-cycle dependent kinases (CDKs) (PRMT1 and PRMT5 methylate CDK4) [176, 177], or proteins involved in the progression of cell cycle (like p16, p21, p27, p53, pRb) [138, 178-186].

### 1.18.1.3 Signal transduction

PRMTs participate in signal transduction, i.e., in relaying the “message” from the plasma membrane to the nucleus to activate the appropriate gene expression program. Some of these signaling include TGF-β/Smad, NF-κB, BMP, EGFR and Wnt pathways.



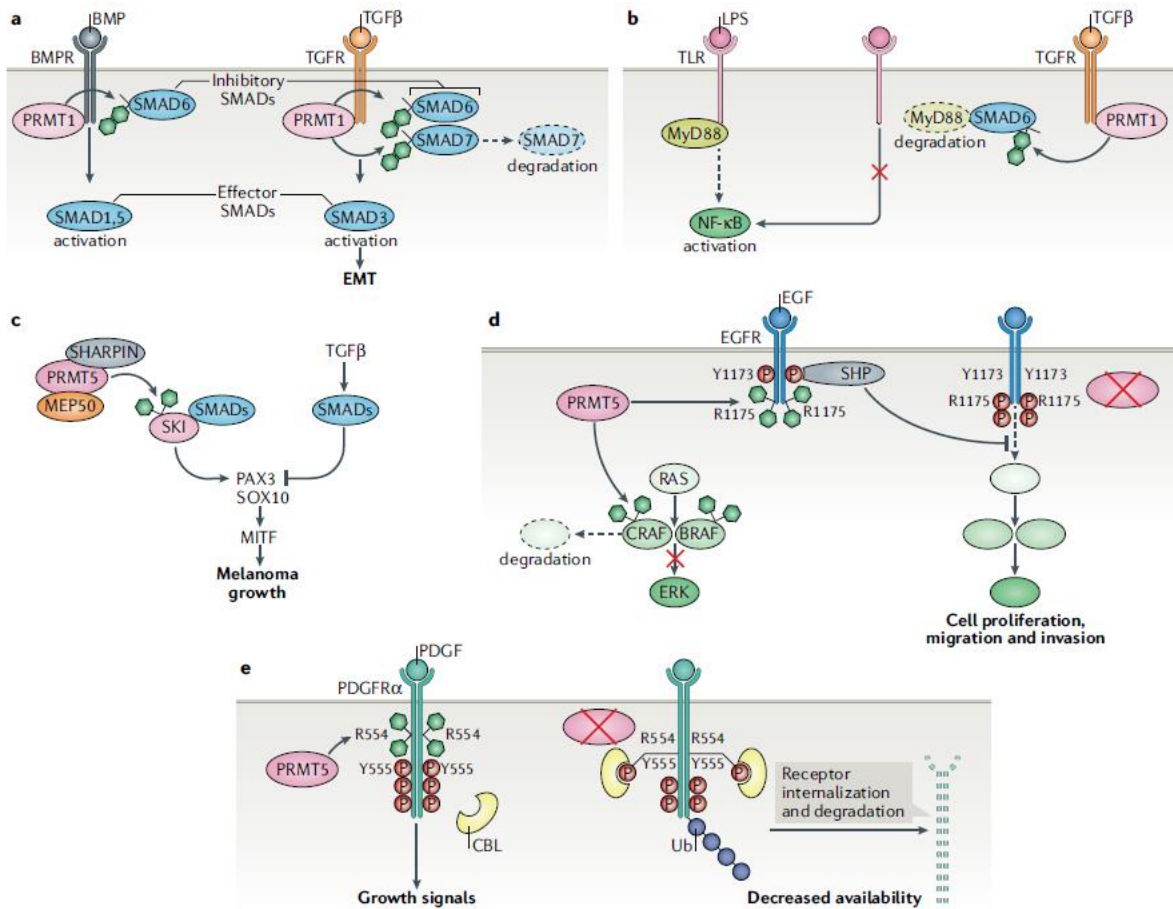


**Figure 19: Signal transduction pathways modulated by PRMTs.** (a) PRMT1 methylates SMAD6 and SMAD7 (inhibitory SMADs) to activate BMP and TGF- $\beta$  signaling pathways leading to EMT. (b) TGF- $\beta$  inhibits TLR signaling by PRMT1-mediated methylation of SMAD6, which causes MyD88 degradation. (c) PRMT5/MEP50 methylate the repressor SKI, activating PAX3/SOX10 expression causing MITF expression and thereby melanoma growth. (d) PRMT5 methylates the intracellular domain (ICD) of EGFR or CRAF to inhibit EGFR and ERK signaling, respectively. (e) PRMT5 methylates ICD of PDGFR $\alpha$  to growth factor signaling. Adapted from [163].

PRMT5 methylates NF- $\kappa$ B subunits to enhance their binding to the chromatin and activate transcription [187]. PRMT1 and CARM1 function as coactivators for NF- $\kappa$ B-mediated signaling [188, 189]. PRMT1 and PRMT5 have opposing roles on the BMP signaling pathway. For example, deleting PRMT1 leads to defective SMAD activation and inhibits the BMP pathway (**Figure 19a**) [190] while deleting PRMT5 can activate the BMP-SMAD pathway [191]. Alternatively, PRMT5 inhibits the TGF- $\beta$ /SMAD pathway by methylating a transcription factor of this pathway, Ski [192, 193] (**Figure 19c**). PRMT1 and PRMT5 also regulate the growth-factor signaling pathways such as EGFR or PDGFR $\alpha$  (**Figure 19d, e**). Remarkably, both PRMT1 and PRMT5 methylate EGFR at its extracellular and intracellular domains, respectively [194, 195] and are recruited to methylate the histones on its promoter region [196]. However, only PRMT5 is involved in PDGFR $\alpha$

signaling and it methylates the intracellular region of PDGFR to promote its phosphorylation and activates downstream signaling (**Figure 19e**) [197].

Certain PRMTs regulate the Wnt/ $\beta$ -catenin pathway (**Figure 20**), but there are some conflicting reports regarding their function in the pathway, especially for PRMT1 (**see Wnt signaling pathway**). PRMT2 is recruited by  $\beta$ -catenin to methylate H3 at Arg8 (H3R8me2a) to upregulate its target genes, and this plays a critical role in the dorsal development of *Xenopus* [198]. The Tudor domain in Spindlin-1 recognizes the H3R8me2a mark of PRMT2 to activate the Wnt signaling pathway [199]. On the other hand, CARM1 indirectly regulates the Wnt pathway by acting as a co-activator for  $\beta$ -catenin [200-203].

PRMT5 activates the Wnt/ $\beta$ -catenin pathway in various cancer types like hematopoietic, liver, laryngeal, and breast [204-208]. PRMT5 tends to activate the Wnt pathway by silencing the different antagonists such as Disheveled3 [204], *Axin2* and *WIF1* [205], DKK1 and DKK3 [208]. PRMT5 and  $\beta$ -catenin are recruited to the promoter of *Dkk-1*, a Wnt target gene, by *Copr5* to regulate early adipogenesis [209].

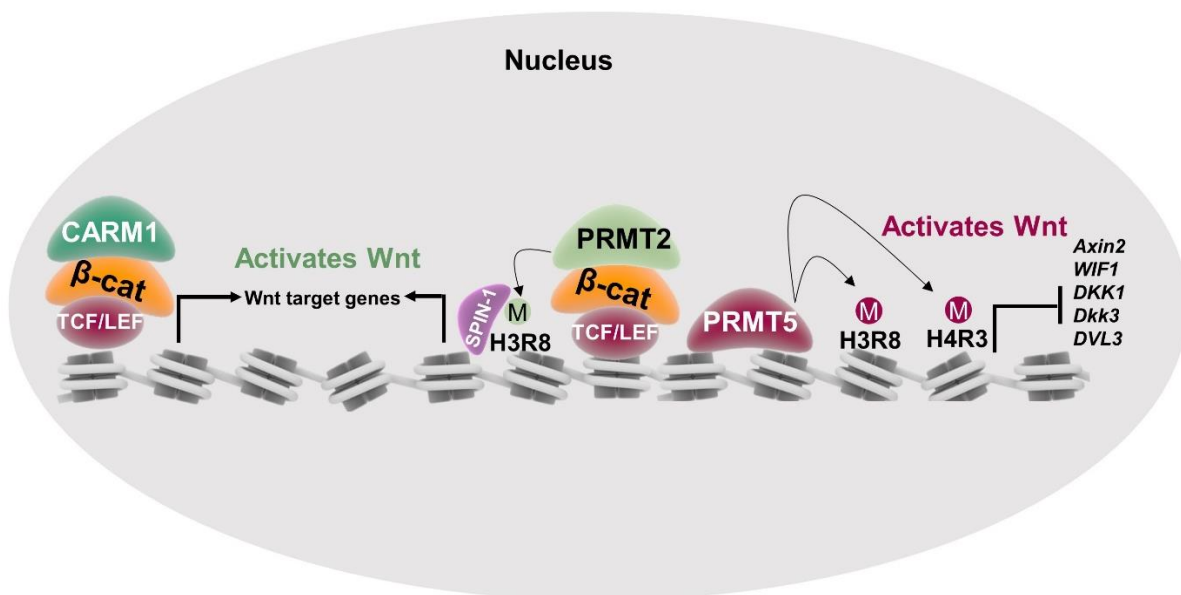


**Figure 20: PRMT2, CARM1, and PRMT5 activate the Wnt pathway.** CARM1 and PRMT2 are recruited by  $\beta$ -catenin to activate Wnt target genes. Methylation of H3R8 (me2a) by PRMT2 is a docking site for spindlin-1 (SPIN-1). PRMT5 activates the Wnt pathway by epigenetically silencing (H3R8me2s, H4R3me2s) the antagonists, *Axin2*, *WIF1*, *DKK1*, *DKK3*, and *DVL3*.

### 1.18.2 Pathological conditions associated with PRMTs

The importance of the cellular functions of PRMTs is reflected by their deregulation in pathological conditions. They are mainly implicated in cancer but also other conditions such as cardiovascular diseases, viral pathogenesis, neurodegenerative diseases, and metabolic diseases [116, 161].

### 1.18.2.1 Cardiovascular diseases

The first evidence that PRMTs could be involved in cardiovascular diseases came from a study in 2001 that showed an inhibitory role of MMA and ADMA on nitric oxide synthase (NOS) [210]. The product synthesized by NOS, nitric oxide (NO), plays multiple crucial roles in the cardiovascular system [211]. Apart from the interplay between ADMA and NO levels, some of the PRMTs are emerging to be directly involved in the pathogenesis of the cardiovascular system (**Figure 21**).

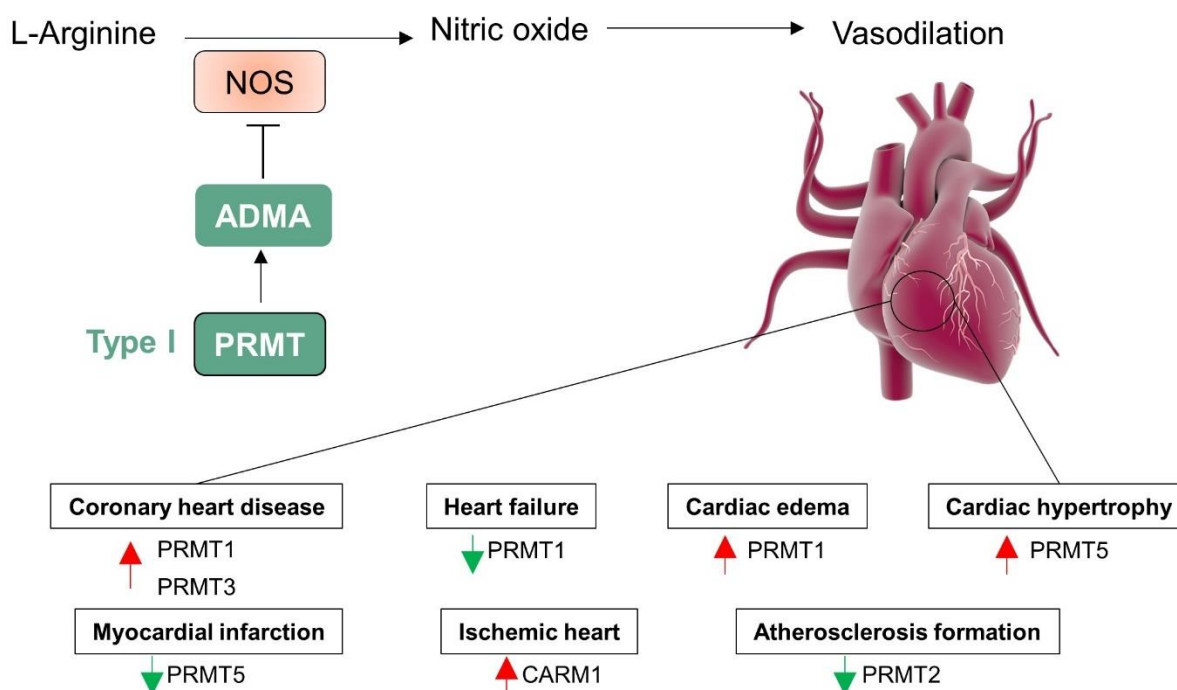


**Figure 21: Cardiovascular disease conditions upon PRMT dysregulation.** Asymmetric dimethylated arginines (ADMA) inhibits the enzyme nitric oxide synthase (NOS), thereby inhibiting the formation of nitric oxide (NO). Cellular NO usually acts as a vasodilator. Differential PRMT levels are associated with varying cardiac failures where the red arrow indicates an increased level while a green arrow indicates a decreased level of the PRMT shown.

This has been very recently reviewed [212]. For example, mice null of cardiac PRMT1 result in cardiomyocyte hypertrophy and fibrosis, leading to heart failure [213]. Overexpression of CARM1 [214] leads to the apoptosis of cardiomyocytes [214]. Further, overexpression of either PRMT3 or PRMT5 increased the expression of the sodium channel in cardiac muscles, and abnormal PRMT3 expression could lead to cardiac dysfunction [215]. Indeed, PRMT3 is overexpressed in patients with coronary heart disease [216]. Nevertheless, the role of PRMTs is still emerging in cardiovascular diseases.

### 1.18.2.2 Viral pathogenesis

The role of PRMTs in viral pathogenesis is limited apart from some viral proteins being discovered as PRMT substrates or PRMTs acting as coactivators for transcribing the

viral genes (**Figure 22**). For instance, the transcription elongation factor SPT5 is methylated by both PRMT1 and PRMT5, reducing its interaction to RNA polymerase II thereby decreasing the translation of the human immunodeficiency virus (HIV-1) Tat protein [217]. CARM1-mediated histone H3 methylation increases Tax transactivation of the HTLV-1 long terminal repeat (LTR) (methylation of R2, R17, R26 on Histone H3) [218] and represses the transcription of HIV-1 LTR (methylation of R26 on histone H3) [219]. On the contrary, a more recent study has shown that PRMT5 and PRMT7 could promote HIV-1 replication by stabilizing its Vpr protein [220]. PRMT6 is shown to be involved in multiple steps of the HIV-1 replicative cycle. For example, the Tat protein of HIV-1 is methylated by PRMT6, inhibiting Tat transactivation [221]. Moreover, PRMT6 increases the Tat half-life [222] and prevents its retention in the nucleolus [151]. Further studies have confirmed that PRMT6 acts as a restriction factor for HIV-1 infection, by many mechanisms including methylating other HIV-1 proteins (Rev, nucleocapsid protein p7) [223–227] (**Figure 22A**).

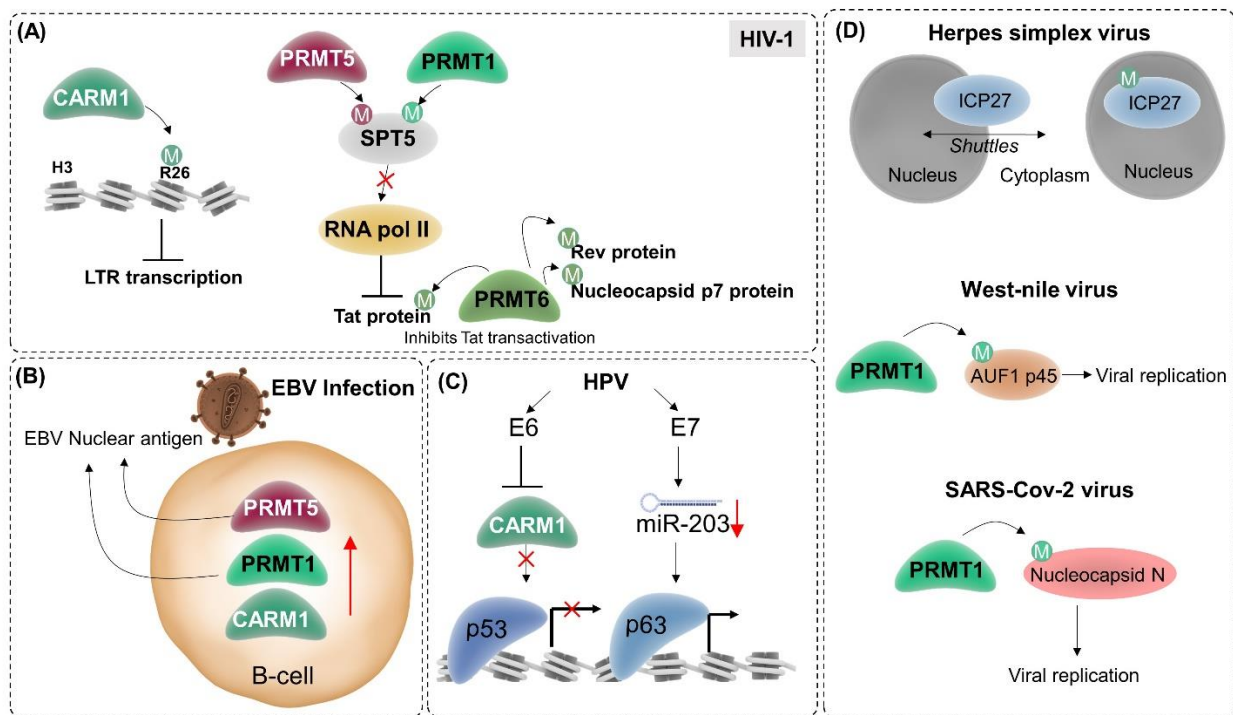


**Figure 22: PRMTs methylate viral proteins.** (A) CARM1 inhibits HIV-LTR transcription by methylating histone H3 (H3R26me2a). PRMT1, PRMT5 and PRMT6 inhibit HIV-1 Tat protein directly (PRMT6 methylation) or indirectly (inhibiting RNA pol II). (B) Epstein-Barr virus (EBV) infection increases PRMT1, CARM1, and PRMT5 levels in B-cells and both PRMT1 and PRMT5 control EBV nuclear antigens. (C) CARM1 levels are regulated in the human papillomavirus (HPV) by two mechanisms. HPV-E6 protein inhibits CARM1, preventing its role in activating p53-mediated transcription or HPV-E7 protein decreases miRNA203, which promotes the expression of all p63-mediated transcription, including CARM1. (D) PRMT1 methylates viral proteins (AUF1 p45 in the West Nile virus or N protein in SARS-Cov-2) to promote their replication. Arginine methylation of ICP27 prevents its shuttling from the nucleus to the cytosol in herpes simplex virus-1.

Epstein-Barr virus (EBV) is regulated by PRMT1 and PRMT5 [228-231] while EBV infection upregulates PRMT expression (PRMT1, CARM1, PRMT5) [232] (**Figure 22B**). Besides, PRMT-mediated arginine methylation has been linked to promoting viral replication in other viruses like the human papillomavirus [233, 234] (**Figure 22C**), herpes simplex virus 1 [235], West Nile virus [236], and the infamous SARS-COV-2 virus [237] (**Figure 22D**).

#### 1.18.2.3 *Neurodegenerative diseases*

The link between arginine methylation and neurodegenerative diseases is fairly recent and was uncovered through the finding that PRMT1 methylated the RNA-binding protein FUS [238] (**Figure 23A**). Accumulation of FUS has been linked to two conditions, amyotrophic lateral sclerosis (ALS) and frontotemporal lobar degeneration (FTLD) [239]. Knocking down PRMT1 or inhibiting the activity of both PRMT1 and PRMT8 prevented FUS accumulation [238, 240]. In contrast, Jun and colleagues show that loss of PRMT1 increases ALS-linked FUS accumulation enhancing degeneration of neurites [241] (**Figure 23A**). Interestingly, MMA FUS is found only in the FTLD pathology and not in ALS [242].

Genetic changes (both loss and gain of function) in C9orf72 can also lead to ALS and Frontotemporal Dementia (FTD) [243] (**Figure 23A**). C9orf72 is responsible for targeting CARM1 towards lysosomal-mediated degradation [244] (**see Autophagy**). Unsurprisingly, in ALS/FTD patients with C9orf72 deficiency, there is an abnormal accumulation of CARM1, leading to aberrant autophagy and lipid metabolism [244].

PRMT5 plays a protective role in Alzheimer's disease [245, 246] (**Figure 23B**).  $\beta$ -amyloid proteins decrease PRMT5 levels via the transcription factor E2F1, and this causes apoptosis of the neurons by several downstream signaling pathways (NF- $\kappa$ B, and GSK-3 $\beta$ ) [246]. In contrast, the association of the Molybdopterin Synthase Associating Complex (MPTAC) with PRMT5 and snRNPs prevents the accumulation of the  $\beta$ -amyloid proteins [245]. PRMT5 and PRMT6 are both involved in Huntington's disease [247, 248]. PRMT5 co-localizes with mutant huntingtin (Htt) protein and this interaction could impair the transcriptional and splicing function of PRMT5 [247] (**Figure 23C**). PRMT6 directly methylates Htt in vesicles and without this methylation event, Htt no longer associates with vesicles, leading to neuronal death [248] (**Figure 23C**). PRMT6 is also indirectly implicated in polyglutamine diseases (such as Huntington's) since PRMT6 binds to polyglutamine extended androgen receptor mutant leading to spinobulbar muscular atrophy [249]. Furthermore, PRMT1, CARM1 and PRMT5 are critical to Duchenne muscular dystrophy [250] and spinal muscular atrophy (SMA) [145, 251-255]. PRMT1 and CARM1 levels are higher in dystrophic as compared to normal muscle [250]. SMA is caused when there is a defect of the survival motor neuron 1 (SMN1) gene, decreasing SMN protein levels [256]. CARM1 and PRMT5 regulate SMA by methylating proteins that bind to the Tudor domain of SMN, affecting SMN function in mRNA splicing and transport [145, 251-

255] (Figure 23D). Further, CARM1-mediated methylation of a transcription factor involved in muscle-atrophy related gene expression, FoxO3, contributes to muscle wasting (atrophy) [257] (Figure 23D).

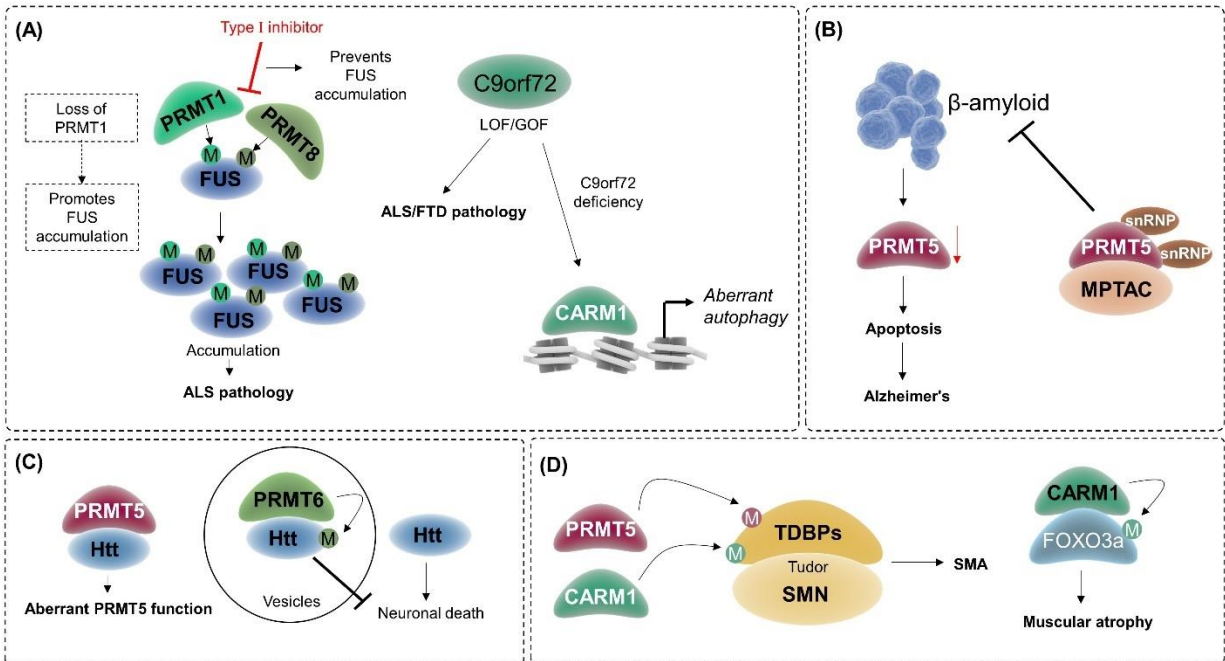


**Figure 23: Role in neurodegenerative diseases.** (A) PRMT1 or PRMT8 methylates FUS, causing its accumulation and/or C9orf72 mutations to cause the ALS phenotype. (B)  $\beta$ -amyloid protein accumulation decreases PRMT5 level leading to apoptosis of neurons in Alzheimer's patients. Conversely, the PRMT5/MPTAC/snRNP complex inhibits  $\beta$ -amyloid accumulation. (C) PRMT5 binding to Htt causes it to function abnormally while PRMT6 methylates Htt inside vesicles inhibiting neuronal death. (D) Both PRMT5 and CARM1 methylates Tudor domain-binding proteins (TDBPs) which bind to the Tudor domain of SMN to cause spinal muscular atrophy (SMA) or CARM1-mediated methylation of FOXO3a causes muscular atrophy. LOF: loss-of-function, GOF: gain-of-function.

#### 1.18.2.4 Metabolic diseases

Some of the PRMTs are also involved in metabolic diseases and the frequently studied metabolic condition in the context of PRMTs is in diabetes and obesity (Figure 24).

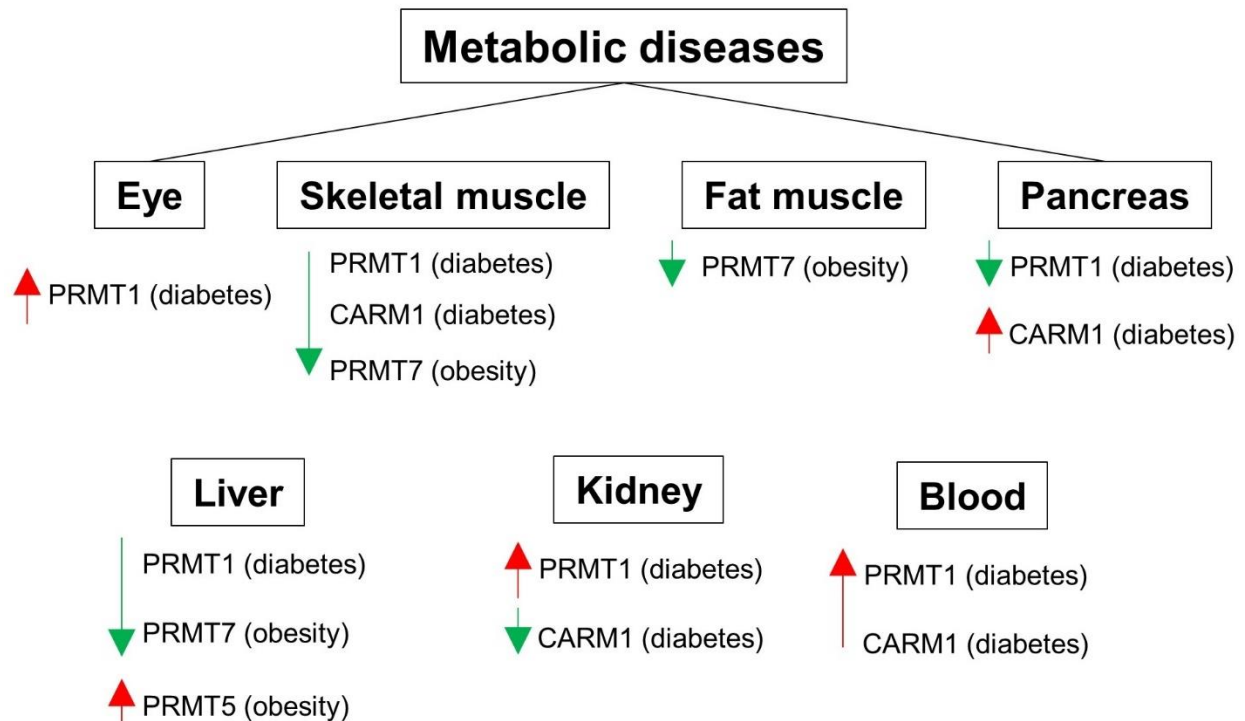


**Figure 24: Expression and activity of PRMTs in metabolic diseases.** The red arrow indicates upregulation, and the green arrow shows downregulation.

PRMT1 was shown to activate the glucose uptake pathway in skeletal muscle cells [258]. In support of this, lower PRMT1 activity was identified in the liver and pancreas of diabetic Goto-Kakizaki rats [259]. On the contrary, PRMT1 is also shown to contribute to the type II diabetic phenotype. For example, decreasing PRMT1 levels could lead to hyperglycemia [260] while overexpressing PRMT1 led to diabetic complications like retinopathy or nephropathy [261, 262]. CARM1 regulates some metabolic pathways in the context of cancer (see **Metabolism under CARM1**). In addition, CARM1 impacts both obesity and type II diabetes [263-265]. PRMT5-mediated histone methylation controls glucose production in the liver [266] and a high-fat diet increases PRMT5 expression in the liver [267]. This suggests that inhibiting PRMT5 could be beneficial to diabetic patients or patients suffering from a fatty liver. PRMT7 is the only member to have a genetic implication in patients suffering from a metabolic disease. *PRMT7* was found mutated in patients with features of pseudohypoparathyroidism (PHP) [268]. Moreover, loss of PRMT7 or a deficiency of PRMT7 causes syndromic intellectual disability and age-related obesity, respectively [269-271].

#### 1.18.2.5 Cancer

Thus far, the role of PRMTs in diseases has been extensively studied in cancer mainly since many PRMTs are overexpressed in several cancer types. The function of

PRMT1 and CARM1 in each cancer type will be discussed in detail in later sections. Here, I will describe the known roles of the other PRMTs in different cancer types.

#### *1.18.2.5.1 Breast cancer*

Almost all the PRMTs are directly or indirectly implicated in breast cancer [272]. However, their role has mainly been studied in luminal breast cancer compared to the other subtypes, since several of these PRMTs interact with  $E\alpha$  [273-277]. For example, PRMT3 has so far only been indirectly implicated in breast cancer as the tumor suppressor DAL1/4.1B interacts with and inhibits PRMT3 activity in MCF7 cells [278]. Further, by inhibiting global methylation using Adox, DAL1/4.1B-mediated apoptosis was upregulated in MCF7 cells via caspase 8 [279].

PRMT2 mRNA and protein expression is increased in ER+ breast tumors and cell lines as compared to ER- tumors [280]. PRMT2 also undergoes splicing to produce five isoforms, and the mRNA and protein expression of each isoform is increased in a panel of ER+ breast cancer cell lines and tumors (mRNA only) [280, 281]. In contrast, Oh and colleagues found lesser PRMT2 mRNA expression in breast cancer vs normal tissue [181]. They further showed that PRMT2 expression was inversely correlated with retinoid-related orphan receptor- $\gamma$  (ROR $\gamma$ ) in ER+ breast cancer [181]. Less PRMT2 in the nucleus was correlated with high tumor grade [282] while the overexpression of a splice variant, PRMT2 $\beta$ , suppressed cell proliferation in MCF7 cells, inducing apoptosis by regulating cyclin D1 expression [283]. Recently, PRMT2 was also shown to regulate ER- $\alpha$ 36 and inhibit its downstream activity on the PI3K/Akt or MAPK/ERK signaling pathways [284]. PRMT2-mediated inhibition of ER- $\alpha$ 36 was shown to sensitize the TNBC cell line MDA-MB-231 to tamoxifen [284]. Notably, ER- $\alpha$ 36 is a new variant of  $E\alpha$  that has been found to be expressed in both ER+ and ER-negative breast cancer [285].

Similarly, PRMT6 co-activates and methylates  $E\alpha$  and is required for estrogen-mediated cell proliferation in MCF7 cells [277, 286]. Low PRMT6-dependent gene expression was also found to correlate with worse relapse-free and distant metastasis-free survival in ER+ breast cancer [287]. Further, PRMT6 has both oncogenic and tumor suppressive functions. For example, PRMT6-mediated interaction with PELP1 or p21 promotes breast cancer cell growth [288, 289]. On the other hand, overexpressing PRMT6 suppresses migration and invasion by MCF7 breast cancer cells by upregulating thrombospondin-1 [290]. Only one study has explored the oncogenic potential of PRMT6 in Her2+ breast tumors [291]. They showed that PRMT6 accelerated Her2 oncogene-induced mammary tumors and promotes the activity of the PI3K/Akt pathway [291].

PRMT7 was first identified through meta-analysis as a gene to be involved in breast cancer metastasis [292] and later functionally shown to promote invasion, EMT and metastasis in breast cancer [293-297].



PRMT5 is one of the most studied PRMTs in the context of breast cancer as it is overexpressed [148, 208, 298-300]. High PRMT5 has been linked to poor prognosis in TNBC [301, 302] or all BC patients [298]. In contrast, high PRMT5 has also been associated with a good prognosis [303] in BC patients. Circulating-PRMT5 RNA has also been shown to be upregulated in breast cancer and associated with a poor prognosis [304]. PRMT5 maintains stemness in breast cancer [301] by several mechanisms: (i) methylating Kruppel-like factor 5 [305], (ii) methylating histone H3 (H3R2me2s) [306], or (iii) regulating the function of stem cell factors like Oct4, KLF4, C-MYC [307]. PRMT5 also methylates KLF4, and this methylation plays a role in breast tumor initiation and progression [308]. Therefore, inhibiting this complex induces cell death [309]. PRMT5 was also shown to play an important role in resistance to doxorubicin [307]. Further, PRMT5 is essential to promote invasion, metastasis and EMT markers [310]. The sub-cellular localization of PRMT5 can be a prognostic factor. For example, high nuclear PRMT5 was found in ER+ breast tumors and correlated with better overall survival [301, 311]. Similarly, a high nuclear expression was found in Her2+ tumors [299]. By either methylating histones or other proteins, PRMT5 can control tumor progression. For instance, the PHD finger protein 1 (PHF1) was found to be a novel reader protein of the H4R3me2s mark by PRMT5 and this coordination was implicated in tumor progression [312]. In addition, PRMT5 alters the function of the tumor suppressor programmed cell death 4 (PDCD4), possibly by methylating it, to accelerate tumor growth [313].

Therefore, PRMT5 has emerged as a valuable therapeutic target for breast cancer and inhibiting its activity induces cell death [208, 298, 301]. Moreover, a natural compound (curcumin) was shown to have an inhibitory effect on PRMT5/MEP50 in MCF7 cells at micromolar concentrations (2 or 20 $\mu$ M) [314].

The role of PRMT8 in cancer is just being explored and high PRMT8 expression was found to correlate with increased patient survival in breast cancer [315]. So far, the function of PRMT9 has not been explored in cancer.

#### *1.18.2.5.2 Hematopoietic cancer*

PRMT1, CARM1 and PRMT5 are the major PRMTs studied in the context of various hematopoietic cancer. Interestingly, PRMT5 was first discovered as a binding partner of JAK2 [316] and a decade later, it was found that constitutively active JAK2 could phosphorylate PRMT5, inhibiting its methyltransferase activity, and promoting myeloproliferation [317]. PRMT5 is overexpressed in lymphomas [205, 318-320] and high PRMT5 is associated with decreased progression-free and overall survival [321]. An important finding in the field was cancer deleted for the gene *MTAP*, involved in the methionine cycle (**Figure 15**), which made them more dependent on PRMT5 (**Figure 25**) [322-324].

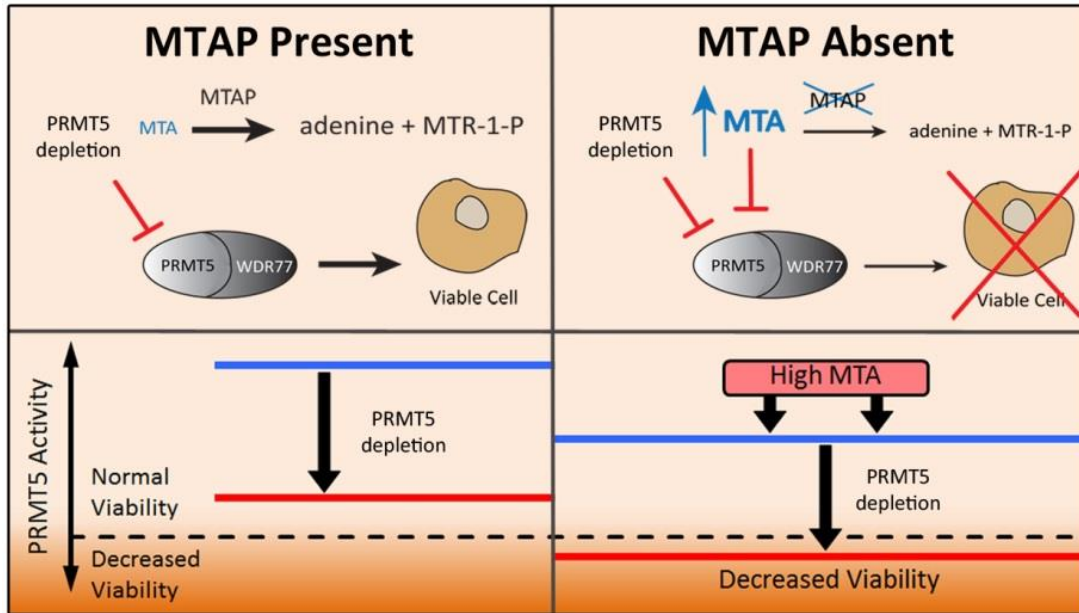


**Figure 25: PRMT5 dependency of cancer cells deleted for MTAP.** In the presence of MTAP, MTA is converted to adenine and PRMT5 depletion only shows a modest effect on cell viability. When MTAP is lost, there is an accumulation of intracellular MTA level, which inhibits PRMT5 activity as MTA is a SAM analog (thus binds to the SAM pocket within PRMT) and depleting PRMT5 in this setting severely decreases cancer cell viability. Adapted from [324].

This dependency was thought to make these *MTAP*-deleted cancer cells vulnerable to PRMT5 inhibition and the proof-of-concept was demonstrated *in vitro* in malignant mesothelioma [325]. Further, this concept of “synthetic lethality” was taken advantage of in acute myeloid leukemia (AML) cells. In *MTAP*-deleted cells, PRMT5 activity was inhibited (see Figure 25 for mechanism) and this further sensitized these cells to the type I PRMT inhibitor, GSK3368715 [326]. Moreover, in a recent review exploring synthetic lethality associated with PRMT inhibitors in cancer cells, Guccione and colleagues proposed a threshold model for PRMT5 inhibition, where normal cells require certain levels of PRMT5 activity while cancer cells are accustomed to high PRMT5 activity, providing a small therapeutic window to target PRMT5 [327]. Given the clinical importance of PRMT5 in hematological cancer, it is of no surprise that PRMT5 inhibitors are in two different phase I clinical trials for B cell non-Hodgkin lymphoma (NCT03573310; NCT02783300).

#### 1.18.2.5.3 Brain cancer

Unlike the above-mentioned cancer types, not all PRMTs have been studied in the development of brain cancer. PRMT1 and PRMT5 contribute to the oncogenesis of glioblastoma. PRMT8, the only PRMT with a tissue-specific localization to the brain, is necessary for neuronal cell differentiation [328] and proper neurological functions [329]. However, the role of PRMT8 in brain cancer is limited apart from one study showing that PRMT8 is absent in glioblastoma tissues and depleting PRMT8 alters gliomagenesis

markers [330]. PRMT5 on the other hand is involved in glioma [331, 332], glioblastoma [333-337], and medulloblastoma [338] development. In gliomas, PRMT5 is required to activate HOXC10-mediated VEGFA upregulation, important for the proliferation and migration of glioma cells [331]. PRMT5 is particularly implicated in glioblastoma because an increase in PRMT5 expression has been associated with a worse prognosis [336, 337] and tumor grade [336]. In addition, PRMT5 regulates stem-cell-like features in GBM cells by upregulating oncogenic pathways such as the PTEN/Akt [334], *MYC* [335], or the ERK pathways [334]. These studies indicated the oncogenic potential of PRMT5 in glioblastomas and its inhibition is shown to impair the stemness of GBM and decreases tumor growth [339]. Moreover, a combination of PRMT5 inhibition with mTOR inhibition shows a synergistic anti-tumor effect against GBMs [333].

The entire family of PRMTs are dysregulated in one or the other type of cancer and have emerged as attractive therapeutic targets in various disease pathologies including cancer. This has greatly encouraged the development of small-molecular inhibitors targeting these enzymes for clinical use and these inhibitors will be discussed in the next section.

### 1.19 PRMT inhibitors

It is quite remarkable that there are already specific small-molecule inhibitors targeting a family of enzymes discovered only twenty years ago. The first pan-type I inhibitor (AMI-1) was developed as early as 2004 [340] and the first PRMT5 specific inhibitor (EPZ015666) was developed in 2015 [341] (**Figure 26**). The chemical biology community has now developed PRMT-specific inhibitors against PRMT3 [342], CARM1 [343, 344], PRMT5 [341, 345-348], PRMT6 [349], and PRMT7 (Unpublished, SGC). Two pan-type I inhibitors, MS023 [350] and GSK5568715 [326] have also been developed.

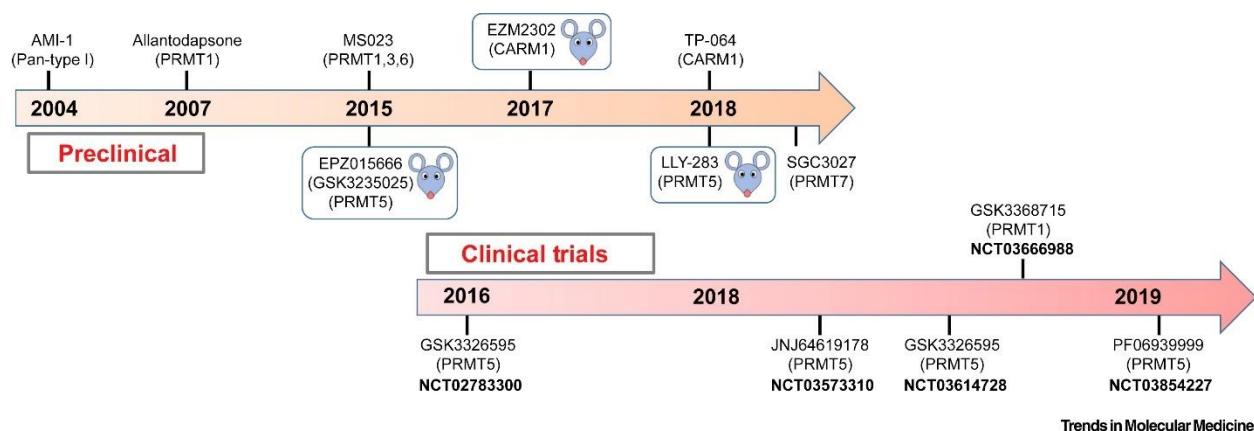


**Figure 26: Timeline of PRMT inhibitor development.** Adapted from [162].

The development of specific inhibitors against PRMT5 has been the most successful because (i) it is the major type II PRMT (PRMT9 is still being characterized), so fewer

chances of targeting other PRMTs and (ii) it varies from the type I PRMTs structurally. This success has led to several clinical trials for different cancer types such as advanced solid tumors and hematological malignancies (NCT03573310, NCT03854227, NCT03614728, NCT02783300, NCT04676516, NCT03886831). Specific inhibitors against PRMT1 are yet to be developed, and the major challenge is the similarity in the substrate pocket among all type I PRMTs. Notably, the recent type I PRMT inhibitor, GSK3368715, “specific to PRMT1 at low concentrations”, is also in phase I clinical trial for solid tumors and diffuse large B cell lymphomas (NCT03666988).

## IV. Protein-arginine methyltransferase 1 (PRMT1)

PRMT1 is the first member of the PRMT family to be mapped on the human genome [351] in 1997 and was identified as the predominant type I PRMT, proposed to contribute to around 85% of the cellular asymmetric dimethylation [352].

### 1.20 Crystal structure

The full-length structure of rat PRMT1 (rPRMT1) was solved in 2003 [125]. rPRMT1 contains 353 amino acids and the first 40 residues (in the N-terminal region) were not observed in the crystal structure, possibly because it is disordered [125]. The structure of PRMT1 is fairly “simple” when compared to the other members, containing predominantly the central catalytic domain and no characteristic N- and C-terminal regions. However, the core PRMT characteristics were conserved in PRMT1, such as the Rossman fold,  $\beta$ -barrel region, dimerization arm and the different signature motifs previously described [125]. PRMT1 forms a dimer or an extended polymer through di-sulfide bonds made by Cys254 [125]. While rPRMT1 exists as an oligomer, yeast PRMT1 (known as HMT1) exists as a dimer in solution [353]. However, this Cys254 residue is not conserved between PRMT1 sequences of different species, hence, the physiological relevance of this di-sulfide bond is unknown. The double E-loop (Glu144 and Glu153 in rPRMT1) forms hydrogen bonds with the target arginine as with all PRMTs, however, the side chain of Glu153 points away from the active site [125], unlike CARM1 [123].

#### 1.20.1.1 Catalytic-dead mutants

Mutating both the Glu residues, Glu144 and Glu153 to Gln, completely abolished catalytic activity [125] highlighting their importance in substrate arginine recognition and providing residues to mutate for developing catalytically dead mutants for PRMT1. Surprisingly, a double mutant of Glu144 and Glu153 to Ala retains considerable catalytic activity unlike the single mutants [354]. The authors of this study suggest that maybe the change in hydrophobicity upon mutating both Glu residues is compensated by nearby hydrophilic residues (like Tyr39, Arg54 or His293); however, no other group has tested these double mutants for *in vitro* or *in vivo* experiments.

#### 1.20.1.2 Unique features of PRMT1

One key difference between PRMT1 and PRMT3 is in the length of the  $\beta$ -barrel region, where PRMT1 has a deletion in the  $\beta$ 10 and  $\beta$ 11 strands and an insertion of 8 residues between  $\beta$ 14 and  $\beta$ 15 strands [125]. Another feature highlighted particularly for PRMT1 is the involvement of two Met residues in the active site, Met66 (Met48 in rPRMT1) and Met173 (Met155 in rPRMT1) [355]. Both Met residues are shown to be important for PRMT1 catalytic activity and also substrate binding [355]. Interestingly, mutating either

Met residue, generated a PRMT1 mutant capable of auto-methylation, wherein the authors have speculated that substrate recognition was modified upon mutation, and PRMT1 recognized itself as a substrate, resulting in auto-methylation [355]. Notably, Frankel and colleagues have shown that a histidine-tagged human PRMT1 can auto-methylate [356]. Though Met155 is strictly conserved among all type I PRMTs, its importance in catalytic activity or substrate recognition has not been explored for the other members so far.

#### *1.20.1.3 PRMT1 complexed with an inhibitor*

The only structure of PRMT1 complexed with an inhibitor (the type I inhibitor GSK3368715) was recently solved showing that this inhibitor is bound to PRMT1 in a substrate-competitive manner [326]. The inhibitor made hydrogen bond interactions with the double-E loop and the His residue of the THW loop, like the substrate arginine would make [326].

## **1.21 Seven spliced variants of PRMT1**

Three splice variants of PRMT1, differing in their N-terminal regions were first identified from the human *PRMT1* gene (with a total of 12 exons) [357, 358]. These variants termed v1, v2, and v3 generate proteins containing 343 (v1), 361 (v2) or 347 (v3) amino acids, respectively [358]. Subsequently, Goulet and colleagues identified that the 5' region of the *PRMT1* gene gave rise to seven alternatively spliced isoforms, v1-v7 which differed in exons (1-5) [133] (**Figure 27**). PRMT1-v2 is the full-length protein with a predicted molecular weight of 42.5kDa while PRMT1-v7 is the shortest isoform with 36.7kDa [133]. All seven splice variants display varying tissue-specificity.

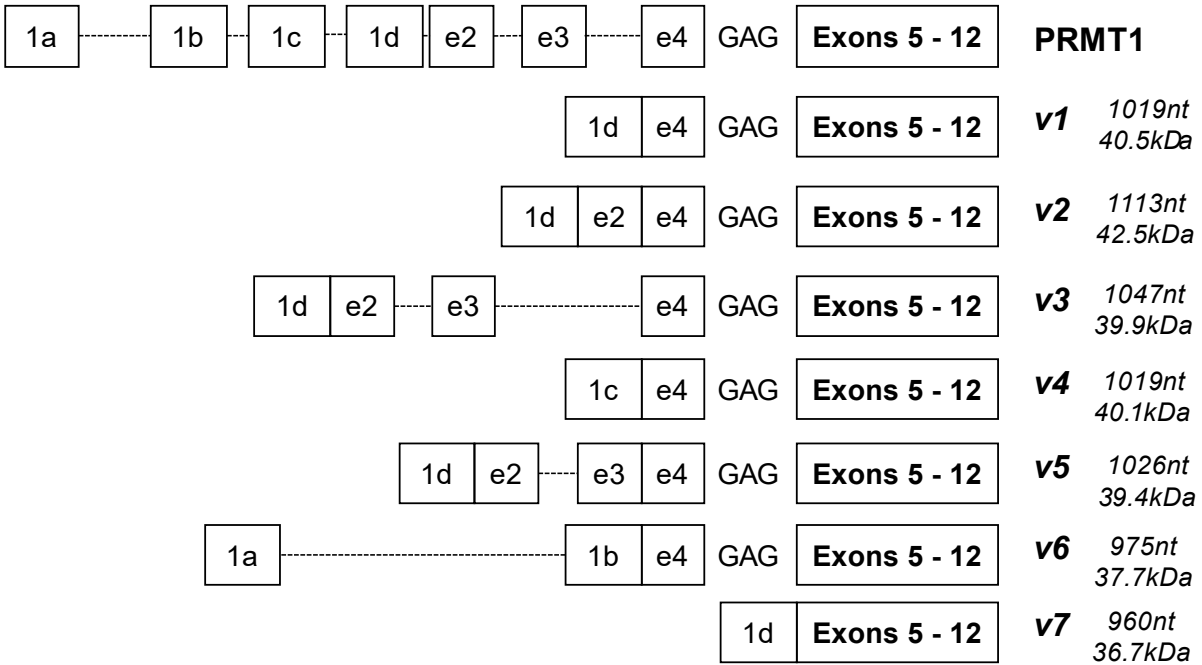


**Figure 27: Spliced isoforms of PRMT1 (v1-v7).** The nomenclature of the PRMT1 isoforms follows what has been described by Goulet and colleagues [133]. The alternative splicing occurs at the N-terminus of PRMT1 represented by the different exons (in boxes). The intronic sequences incorporated into the transcripts are shown in dotted lines between the exons. Exons 5-12 are conserved between all seven isoforms. GAG: Conserved nucleotide residues, guanine, and adenine.

For example, PRMT1-v1 and PRMT1-v2 are expressed in the kidney and liver, while v1 was also found in the lung, skeletal muscle, and spleen [133]. In contrast, PRMT1-v3 was expressed in all tissues at lower levels [133]. PRMT1-v4 is detectable only in the heart [133]. PRMT1-v2 and PRMT1-v5 are found in the pancreas [133]. PRMT1-v7 is also expressed in the heart and skeletal muscle [133]. However, PRMT1-v6 could not be detected in their study. [133] Notably, using GFP-fused proteins, they showed that PRMT1-v2 was uniquely localized to the cytoplasm (containing a nuclear export signal NES in exon 2), while PRMT1-v1 and PRMT1-v7 were predominantly nuclear, and the other variants were both nuclear and cytoplasmic [133]. However, their sub-cellular localization can vary depending on the cell type studied [128, 359]. Furthermore, all variants were catalytically active except PRMT1-v7 and the variants displayed substrate specificity, such as PRMT1-v1 preferring SmB, while PRMT-v6 prefers MRE11, *in vitro* [133]. Furthermore, another study from the group of Fackelmayer identified a PRMT1 variant lacking the dimerization arm (PRMT1 $\Delta$ arm) which was catalytically dead but still interacted with endogenous PRMT1 substrates. This variant localized to the nucleoli when the proteasomal machinery was inhibited [360]. The same group has recently identified numerous putative PRMT1 spliced variants by employing next-generation sequencing,

even identifying a novel exon between exons 11 and 12, but the relative abundance in the cell and their functionality are yet to be validated [361]. Multiple variants of PRMT1 could explain how this PRMT is responsible for more than 85% of cellular methylation. Nevertheless, these isoforms are implicated in disease conditions such as breast cancer and will be discussed in a later section.

## 1.22 Phosphorylation and ubiquitination of PRMT1

Reported PTMs on PRMT1 are limited, identified only since the last six-seven years. Only two types of modifications have been found so far: phosphorylation and ubiquitination (Figure 28).

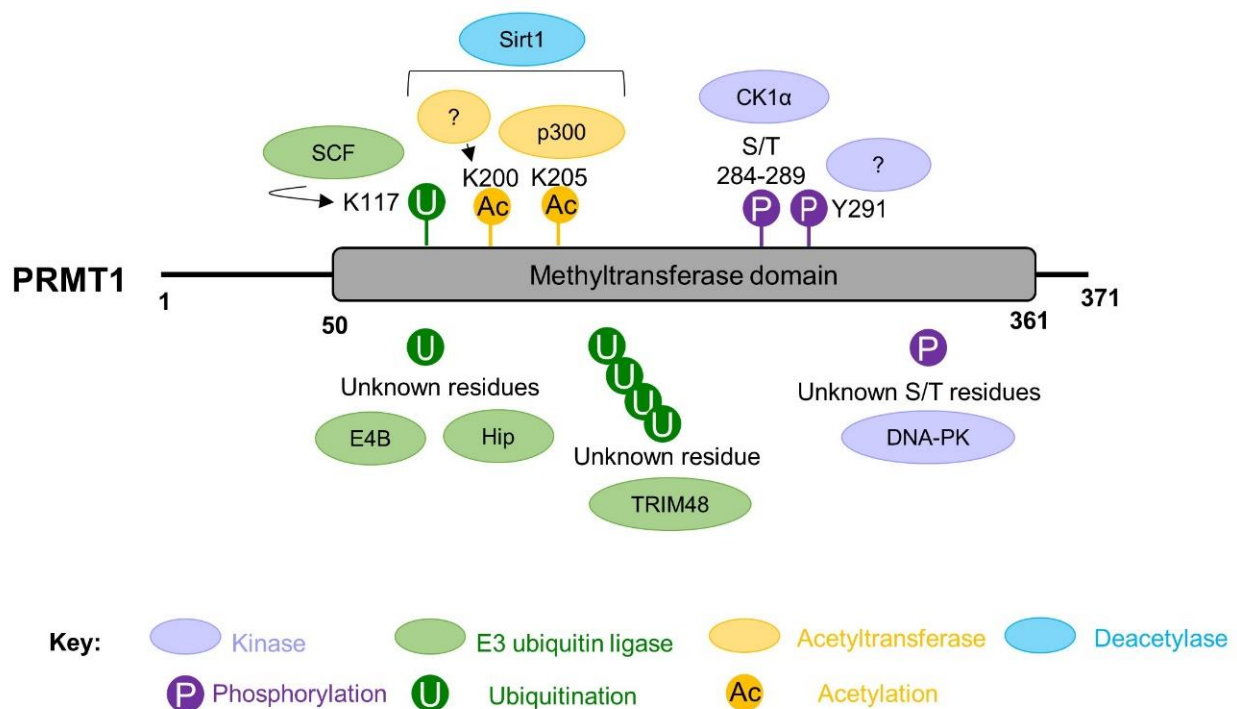


**Figure 28: Modifications occurring on PRMT1.** Most of the known modifications occur within its methyltransferase domain and question marks represent modifications on unknown residues.

Casein kinase 1 alpha 1 (CK1α) interacts with and phosphorylates PRMT1 on many Ser/Thr residues (particularly between 284-289) [362]. This phosphorylation event is required for PRMT1 to suppress a differentiation gene marker *GRHL3*, while promoting proliferative gene expression, to maintain epidermal cells in a progenitor state [362]. Mass spectrometry analysis identified Tyr291 of PRMT1 to be phosphorylated by an as yet unknown kinase [363]. Tyr291 is close to the THW loop of PRMT1, and the phosphorylation alters protein-protein interaction and substrate recognition [363]. For example, mutating Tyr291 to an unnatural amino acid p-carboxymethyl-L-phenylalanine results in a loss of interaction between PRMT1 and its substrate hnRNPA1 [363]. More



recently, the DNA-dependent protein kinase (DNA-PK) was shown to recruit and phosphorylate PRMT1 (at unidentified Ser/Thr sites) to increase its association to the chromatin [364]. This was mainly observed upon cisplatin treatment, as PRMT1 was required for maintaining the transcription of SASP genes, possibly contributing to chemoresistance [364].

Further, a few independent studies show that PRMT1 is ubiquitinated and targeted for degradation, having varied downstream consequences [365-367]. PRMT1 was identified as a substrate of the E3 ubiquitin ligases E4B and carboxyl terminus of Hsc70-interacting protein, however, the residues and their functional relevance have not been studied [366]. Another study found tripartite motif 48 (TRIM48) to polyubiquitinate PRMT1, preventing arginine methylation on Apoptosis signal-regulating kinase 1 (ASK1), thereby inducing cell death and suppressing cancer development [365]. PRMT1 was also found to be ubiquitinated on Lys117 by the SCF-E3 ligase complex Fbxl17 [367]. This ubiquitination event depended on the acetylation status of PRMT1 on the lysine residues K200 and K205 [367]. PRMT1 is acetylated on K205 by p300 while the acetylase responsible for K200 is unknown [367]. However, both K200 and K205 are deacetylated by Sirt1 [367]. This elegant study demonstrates a highly coordinated reaction of acetylation, deacetylation, and ubiquitination to regulate PRMT1 activity. PRMT1 is accumulated upon lipopolysaccharide (LPS) treatment (from gram-negative bacteria) since both Sirt1 and p300 are downregulated by LPS [367]. Lastly, a large-scale mass spectrometry screen identified several putative ubiquitination sites for PRMT1 [368], but none have been functionally validated, highlighting the importance of research required in understanding the PTMs that PRMT1 undergoes.

### **1.23 Substrates of PRMT1**

PRMT1 methylates histones, specifically histone H4 at Arg 3 (H4R3me2a) [156, 157]. Depending on the context, PRMT1-mediated H4 methylation can lead to transcriptional activation [369] or repression [370]. PRMT1 also methylates numerous non-histone proteins reflecting its diverse cellular roles. These include transcription factors such as STAT1 [371], SMAD6 [372] and SMAD7 [373],  $E\alpha$  [273]; transcription elongation factors [217] and methyl-DNA binding proteins [374] and others to regulate transcription and downstream signal transduction mechanisms. PRMT1 also methylates DNA damage response proteins such as MRE11 [170, 171, 375] and 53BP1 [169]. PRMT1 methylates a host of RNA-binding proteins (RBPs) like hnRNP K [376], Sam68 [377], and many others. The above-mentioned substrates are just a small subset of the PRMT1 methylome and there are definitely more known substrates [378], with plenty more still being discovered. Some PRMT1 substrates (related to my thesis) have been pointed out in later sections.

## 1.24 Regulation of signal transduction by PRMT1

Indeed, PRMT1-mediated arginine methylation is responsible for a host of signaling pathways, such as TGF- $\beta$ , BMP, EGFR, PI3K/Akt, and Wnt/ $\beta$ -catenin (**Figure 19**). PRMT1 activates both BMP and TGF- $\beta$  signaling by methylating the antagonists SMAD6 and SMAD7 [373, 379]. PRMT1-mediated SMAD6 methylation also inhibits toll-like receptor signaling since methylated SMAD6 interacts with MyD88 and targets it for degradation [380]. PRMT1 is crucial in the EGFR signaling pathway since it directly methylates EGFR extracellular domain promoting dimerization [194] and also its transcription by methylating the histones on the promoter [196]. Activation of EGFR signaling has been implicated in cancer progressions like TNBC and colorectal [381-383]. For instance, PRMT1-mediated H4R3me2a recruits the SWI/SNF subunit SMARCA4 to activate EGFR signaling in colorectal cancer [381]. Furthermore, PRMT1 methylates the transcription factor FOXO1 at residues within its Akt phosphorylation site to activate the PI3K/Akt pathway [384]. PRMT1 was also shown to regulate the Hedgehog pathway by methylating the transcription factor, Gli1, in pancreatic cancer [385].

### 1.24.1 Wnt signaling pathway

Thus far, there are contradictory reports concerning the role of PRMT1 in the Wnt signaling pathway (**Figure 29**). A few studies have shown that PRMT1 inhibits the Wnt pathway by different mechanisms (**Figure 29A**). PRMT1 interacts with and methylates the scaffolding protein Axin [386]. Methylation of Axin stabilizes the protein and therefore the destruction complex, causing  $\beta$ -catenin to be degraded [386]. Similarly, PRMT1 also methylates Dishevelled, another key component of the Wnt pathway [387]. Normally, when the Wnt pathway is activated by the Wnt ligands, Dishevelled is recruited to the plasma membrane to prevent the destruction complex from degrading  $\beta$ -catenin; however, methylated Dishevelled can no longer go to the plasma membrane and thus  $\beta$ -catenin is degraded and the Wnt pathway is inhibited [387]. On the contrary, the same group showed that PRMT1 activates the Wnt pathway by methylating two Dishevelled associated proteins G3BP1 and G3BP2 [388, 389] (**Figure 29B**). Overexpressed PRMT1 in esophageal squamous cell carcinoma was also shown to activate the Wnt pathway [390]. Activation of the Wnt pathway by Wnt3a promotes the methylation of both G3BP1 and G3BP2, and this methylation event is required for activating downstream signaling of Wnt through  $\beta$ -catenin by two different mechanisms [388, 389]. Methylated-G3BP1 aids in the dissociation of  $\beta$ -catenin mRNA from the disheveled super complex, thus promoting its translation and accumulation in the cytosol [388]. Methylated G3BP2 is required for GSK3 $\beta$ -mediated phosphorylation of LRP6 [389]. Interestingly, they also showed that inhibiting global cellular methylation (using MTA or Adox) blocked LRP6 phosphorylation [389], implying that arginine methylation on LRP6 might be required for it to be phosphorylated (**Figure 29C**). Although there has been no direct evidence for this, there

are a few studies from two labs that support this idea. First, LRP6 was identified as a partner of PRMT1 by MS analysis in vascular smooth muscles [391] (**Figure 29C**). Second, Albrecht and colleagues showed that 33% of cellular proteins containing putative phosphorylation sites for GSK3 $\beta$  were also methylated on adjacent arginine residues and this methylation event was required for GSK3 $\beta$ -mediated phosphorylation [392] (**Figure 29C**). They validated this using Smad4 (a known substrate of GSK3 $\beta$ ) as an example [392]. In addition, the same group showed for the first time that the process of endocytosis was involved in Wnt signaling [392-394]. Mechanistically, PRMT1 and GSK3 $\beta$  co-localize into the same subset of vesicles upon Wnt3a stimulation and the methyl donor SAM was crucial for GSK3 $\beta$  to be sequestered into these vesicles (**Figure 29C**) [392, 394]. Interestingly, they showed that the chemotherapeutic agent, methotrexate, functioned as a Wnt pathway inhibitor in this context [394]. Moreover, Wnt3a-induced sequestration of PRMT1 and GSK3 $\beta$  in vesicles was proposed as a novel mechanism for Wnt-driven cancer cells to acquire nutrients from the extracellular matrix by macropinocytosis since these vesicles fuse with lysosomes [393].

Other recent evidences suggest that PRMT1 is regulated by TCF7/L2 or MYC since the enhancer region upstream of PRMT1 was identified to be binding sites for both these transcription factors in chronic myeloid leukemia cells [395] (**Figure 29C**). Furthermore, a novel compound being developed as a PRMT1 inhibitor, compound9a, was found to downregulate the Wnt signaling pathway [396].

Therefore, PRMT1 is involved at multiple steps in regulating the Wnt signaling pathway, and this may be context dependent.

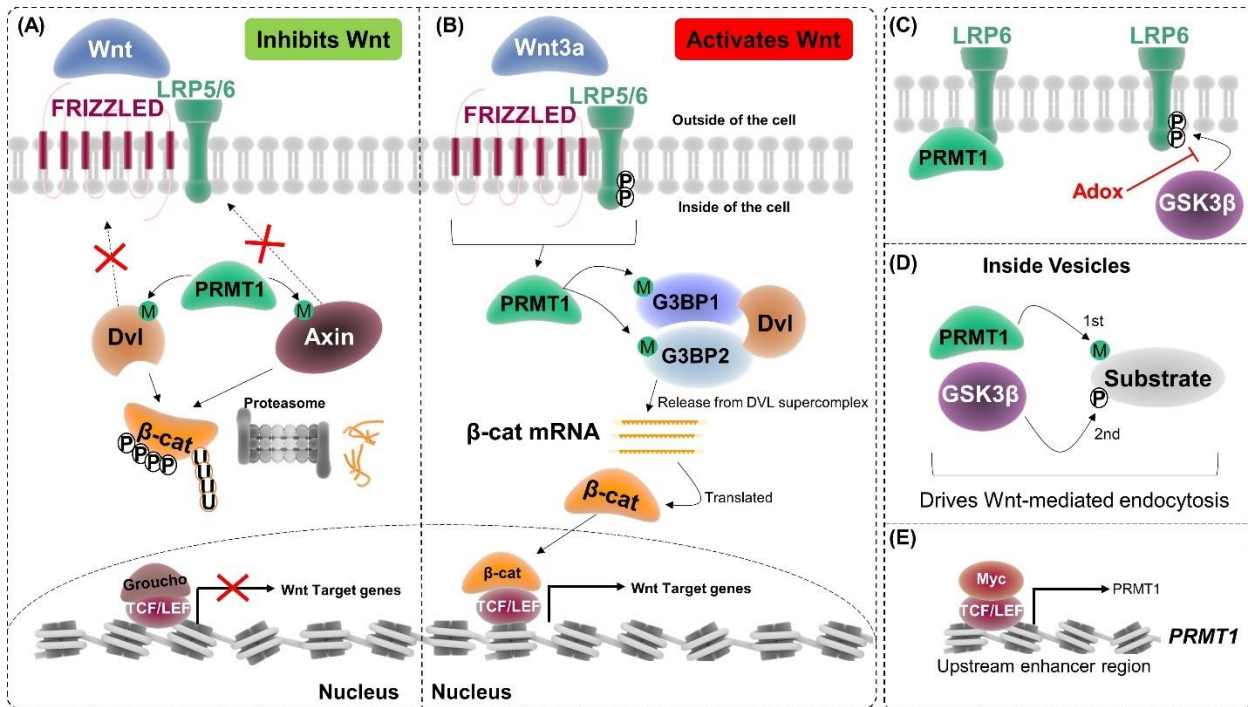


**Figure 29: PRMT1 activates or inhibits the Wnt pathway.** (A) PRMT1 inhibits the Wnt pathway by methylating Disheveled (Dvl) or Axin preventing their recruitment to the transmembrane receptors Frizzleds and LRP5/6. (B) PRMT1 activates the Wnt pathway by methylating proteins in DVL super complex (G3BP1, G3BP2) aiding in the release of  $\beta$ -catenin ( $\beta$ -cat) mRNA which is then translated and activates Wnt target genes. (C) PRMT1 binds to LRP6 and global methylation inhibition using Adox prevents GSK3 $\beta$ -mediated phosphorylation of LRP6. (D) In vesicles, PRMT1-mediated methylation primes a substrate for phosphorylation by GSK3 $\beta$  driving endocytosis. (E) Myc and TCF/LEF bind to the promoter of PRMT1 and aid in its transcription.

## 1.25 Role in cancer

PRMT1 is overexpressed and/or aberrantly spliced in several cancer types such as **breast** [133, 397-399], **prostate** [400], **lung** and **bladder** [401], **colon** [402, 403] cancer, and **leukemia** [404-406]. A study this year identified *PRMT1* as one of the cancer driver genes for metastatic breast cancer using a machine-learning algorithm [407].

### 1.25.1 Breast cancer

As mentioned above, PRMT1 is overexpressed in breast cancer and has been more studied in ER+ positive than ER- breast cancer. Only one study has explored the role of PRMT1 in Her2+ tumors, where PRMT1 was found to drive tumorigenesis in a Her2+ mouse model by activating the PI3K/Akt pathway [291]. In TNBC cell line models, depleting PRMT1 decreased tumor growth [399] and using the pan-methylation inhibitor AMI-1 sensitized TNBC cells to an EGFR inhibitor, cetuximab [383]. PRMT1 further aids in breast cancer progression by methylating and inhibiting the tumor suppressive function of C/EBP $\alpha$  [399].

Thus far, only one study reports that PRMT1 could play a protective role in breast cancer. Upon irradiation, PRMT1 methylates BRCA1 and aids in DNA double-strand break repair [408].

#### *1.25.1.1 ER+ breast cancer*

PRMT1 contributes to the tumorigenesis of ER+ breast cancer by several mechanisms. For example, PRMT1 methylates progesterone receptor and increases its turnover, activating downstream target genes involved in breast cancer cell proliferation and migration [409]. Alternatively, inhibiting PRMT1 decreased ER $\alpha$  methylation and IGF-1 signaling in ER $\alpha$ + breast cancer [410]. PRMT1-mediated hypermethylation of EGFR methylation causes activation of the non-genomic ER $\alpha$  pathway, leading to hyperactivation of signaling pathways like Akt in ER $\alpha$ + positive breast cancer cells [273, 411]. PRMT1 cooperates with its chromatin target CHTOP to induce ER $\alpha$ -related gene expression [196, 412]. Further, in ER $\alpha$ + breast cancer, tamoxifen or Adox treatment induces cell cycle arrest by reducing PRMT1 mRNA and ADMA levels and combination treatment was found synergistic [413].

#### *1.25.1.2 Role of PRMT1 isoforms in breast cancer*

PRMT1 isoforms expression could differ between breast cancer cells and normal mammary gland cells [358]. PRMT1v2 was identified as an oncogenic isoform and that it was responsible for the invasive phenotype of breast cancer cells [414, 415]. The abundance of this isoform was regulated positively and negatively by two RBPs, RALY and SNW1, respectively and in breast cancer patients with poor survival, RALY was upregulated, causing an increase in PRMT1v2 [416].

#### *1.25.1.3 EMT, metastasis and drug resistance*

Many reports suggest that PRMT1 drives the metastatic phenotype of breast cancer and that it could contribute to drug resistance (**Figure 30A**). By interacting with pregnane x-receptor (PXR), PRMT1 upregulates the expression of multidrug resistance 1 (MDR1) in MCF7 cells resistant to doxorubicin [417]. On the contrary, depleting PRMT1 aids in enhancing the apoptosis induced by the chemotherapeutic drug, paclitaxel, as PRMT1 methylates the Apoptosis signal-regulating kinase 1 (ASK1) which is typically upregulated during paclitaxel-induced cell death [418].

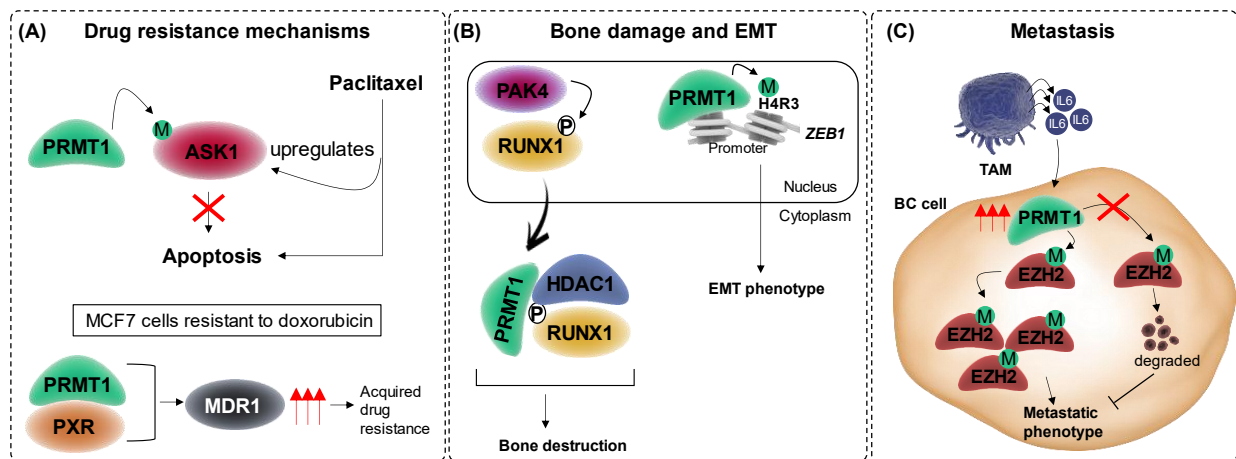


**Figure 30: PRMT1 contributes to drug resistance, EMT and metastatic phenotypes.** (A) Paclitaxel treatment induces cell death by increasing ASK1 levels but PRMT1 methylates ASK1 preventing apoptosis. PRMT1 causes an accumulation of multidrug resistance 1 (MDR1) by binding to pregnane-x receptor (PXR). (B) PAK4 phosphorylates RUNX1 in the nucleus and aids in its translocation to the cytoplasm. In the cytoplasm, phosphorylated RUNX1 binds to PRMT1 and HDAC1 leading to bone destruction. PRMT1 methylates the promoter of ZEB1 (H4R3me2a), activating it and leading to an EMT phenotype. (C) Tumor-associated macrophages (TAM) secrete IL-6 which stimulates PRMT1 expression in the nearby breast cancer (BC) cell, leading to methylation and stabilization of EZH2 causing a metastatic phenotype.

An induced effect of breast cancer is bone damage. Tang and colleagues demonstrated that the downstream target genes of phosphorylated RUNX1 were responsible for bone destruction [419] (**Figure 30B**). PAK4 phosphorylates RUNX1, promoting its translocation to the cytoplasm; here phosphorylated RUNX1 interacts with both HDAC1 and PRMT1 [419]. Besides, inhibiting methyltransferase activity using a non-hydrolysable SAM mimic, Sinefungin, decreased myofibroblast activity and breast cancer-mediated metastasis to the lung in mice [420]. Additionally, PRMT1 participates in the EMT of breast cancer cells by depositing the H4R3me2a mark on the promoter of ZEB1, a key gene involved in invasion, metastasis and EMT [421] (**Figure 30B**). Further, tumor-associated macrophages in breast cancer secrete the cytokine IL-6 to stimulate PRMT1 expression, thereby driving it to methylate EZH2 and stabilizing it, leading to a metastatic phenotype [422] (**Figure 30C**). Without this methylation, EZH2 would be ubiquitinated and degraded in the cell [422, 423].

### 1.25.2 Other solid cancer types

Apart from breast cancer, PRMT1 also regulates other solid cancer types, like lung, colorectal, and brain cancer. Notably, we can observe many similarities in the molecular mechanisms by which PRMT1 drives all these cancer types. Similar to breast cancer, PRMT1 co-operates with CHTOP to induce gene expression of EGFR, AKT3, BRAF, and other genes involved in the tumorigenesis of glioblastomas [196]. PRMT1 (like PRMT5) regulates *Myc* stability in glioblastoma stem cells [424]. PRMT1 also methylates EGFR in

colorectal (CRC) like in breast cancer, and methylated-EGFR is responsible for resistance to cetuximab in CRC and expressing a methylation-defective EGFR decreases CRC tumor growth in mice [194]. PRMT1 contributes to the EMT phenotype of lung cancer by methylating TWIST-1 (in BC, ZEB1 is methylated for the same phenotype) [425] or by controlling genes downstream of Src phosphorylation involved in EMT or migration [426]. PRMT1-mediated methylation of hnRNP A2 sequesters it in the nucleus [427]. The overexpression of cytosolic hnRNP A2 is a biomarker for lung cancer and is also observed in brain cancer [427]. Therefore, we can speculate that PRMT1 is playing a protective role in these cancer by methylating hnRNP A2 (causing its nuclear retention). High PRMT1 mRNA in lung cancer patients was found to correlate with poor prognosis [428]. Interestingly, in lung and pancreatic cancer cell models, the loss of PRMT1 sensitized these cells to PRMT5 inhibition [429], supporting the idea of crosstalk among PRMTs (see **Crosstalk among PRMTs and substrate scavenging**). More evidence points towards PRMT1 functioning in DNA repair mechanisms in lung cancer. Such as, PRMT1 could help overcome resistance to radiotherapy by methylating plakophilin 2, to activate genes required for the NHEJ pathway [430]. Otherwise, PRMT1 methylates FEN1, a protein critical in the BER pathway and contributes to drug resistance against chemotherapies like cisplatin [431]. Indeed, this suggests that combining chemotherapeutic agents with PRMT1 inhibitors could prove beneficial to lung cancer patients.

### 1.25.3 Hematological cancer

Since PRMT1 is required for normal hematopoiesis and is needed for the self-renewal capacity of the hematopoietic stem cell compartment [432], it was speculated to be involved in hematological cancer as well. PRMT1 expression is elevated in AML [433], MLL [434], and Hodgkin's lymphoma [232]. PRMT1 directly controls the oncogenesis of leukemia by methylating the tyrosine kinase FLT3 or its internal tandem duplicate (FLT3-ITD) counterpart to maintain AML progression [433, 434]. Both FLT3 and FLT3-ITD are genetic alterations frequently found in AML [433, 434]. Consequently, inhibiting PRMT1 alone decreased AML cell proliferation and this effect was enhanced when PRMT1 was inhibited in combination with FLT3 inhibitor [433, 434] (**Figure 31A**). Additionally, there is also some indirect evidence to implicate PRMT1 in the oncogenesis of leukemia (**Figure 31B**). For example, the tumor suppressor gene BTG1, which is often lost in leukemia, recruits PRMT1 to ATF4 to methylate it [435]. This methylation aids ATF4 to upregulate pro-apoptotic signals, but in the absence of BTG1, ATF4 activates pro-survival genes [435], and perhaps, this is what is happening in the leukemia cells deleted for BTG1. Otherwise, co-operativity between two transcription factors, TCF7L2 and Myc, on the PRMT1 genomic region during a blast crisis in CML could lead to tumor progression [395] (**Figure 31C**). Another vital factor in hematological cancer (also solid cancer) is the frequency of splicing factor (SF) mutations. Besides, a correlation between PRMT1 expression and that of the SF, SRSF1, was found in acute lymphoblastic leukemia (ALL) patients and SRSF1 was

responsible for anti-apoptotic signals [404]. Cancer mutated for SF were envisioned to be more vulnerable to certain drug treatments by exploiting the concept of “synthetic lethality”. An impressive recent study identified that indeed, leukemias mutated for splicing factors were more sensitive to combinatorial inhibition of PRMT5 and type I PRMTs than their wild-type counterparts [436] (**Figure 31D**).

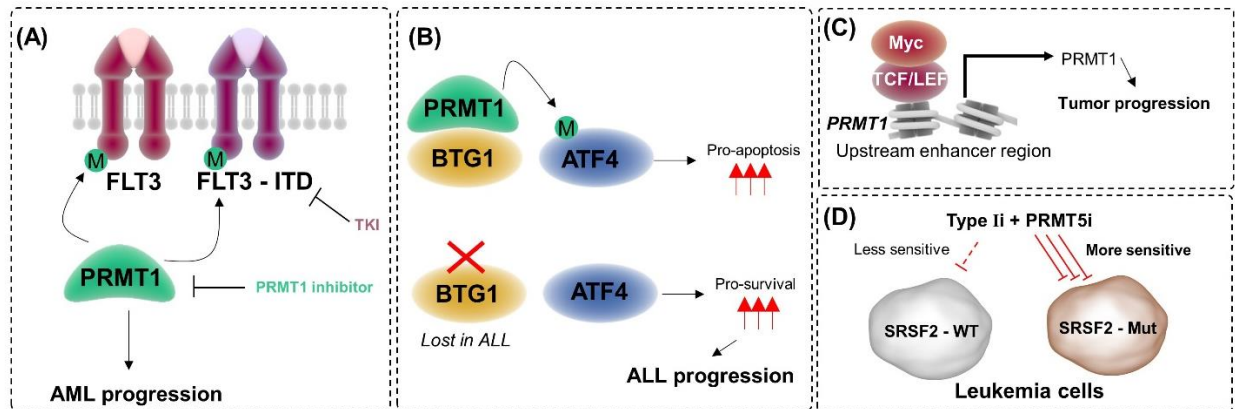


**Figure 31: PRMT1 controls oncogenesis in hematopoietic cancer.** (A) PRMT1 methylates transmembrane receptors FLT3 or the mutated form, FLT3 internal tandem repeat (ITD) leading to AML progression. (B) BTG1 protects against ALL progression by recruiting PRMT1 to methylate ATF4 upregulating pro-apoptotic signals. (C) Myc and TCF/LEF transcription factors bind and activate the PRMT1 promoter leading to tumor progression. (D) Leukemia cells mutated for the SRSF2 splicing factor are more sensitive to the combined inhibition of PRMT5 and type I PRMTs.



## V. Coactivator-assoaciated arginine methyltransferase 1 (CARM1)

We published a review article this year that focused on CARM1 in *Trends in Cell Biology* [437] (see **ANNEXE I: CARM1/PRMT4: Making Its Mark beyond Its Function as a Transcriptional Coactivator**) and the following section is a more detailed version of this review article.

CARM1 was discovered in 1999 as the first PRMT linked to transcriptional co-activation and hence its name [438]. Due to its sequence homology with the PRMTs family, it was renamed as PRMT4, but both names are used interchangeably in the literature.

### 1.26 Crystal structure of CARM1

#### 1.26.1 Generalities of the structure

CARM1 contains 608 amino acids and is the only PRMT harboring a C-terminal domain [439]. The N- and C-terminal domains of CARM1 are not necessary for its methyltransferase activity but essential for its co-activator function [439]. The N-terminal domain may be important for the methylation of Arg2 and Arg26 on Histone H3 [440].

The first crystallographic structures of mouse CARM1 (mCARM1) were published in 2007 by two different teams [123, 440]. The structure of the catalytic domain of CARM1, residues 140-480<sup>2</sup> or 147-478, was solved on its own (apo form) and with the cofactor SAH [123, 440]. These structures confirmed that CARM1 exists as a dimer [123, 440] and that dimerization is necessary for its methyltransferase activity [441].

---

<sup>2</sup> All residue numbering described in the crystal structure section are with respect to mouse CARM1 amino acid sequence.

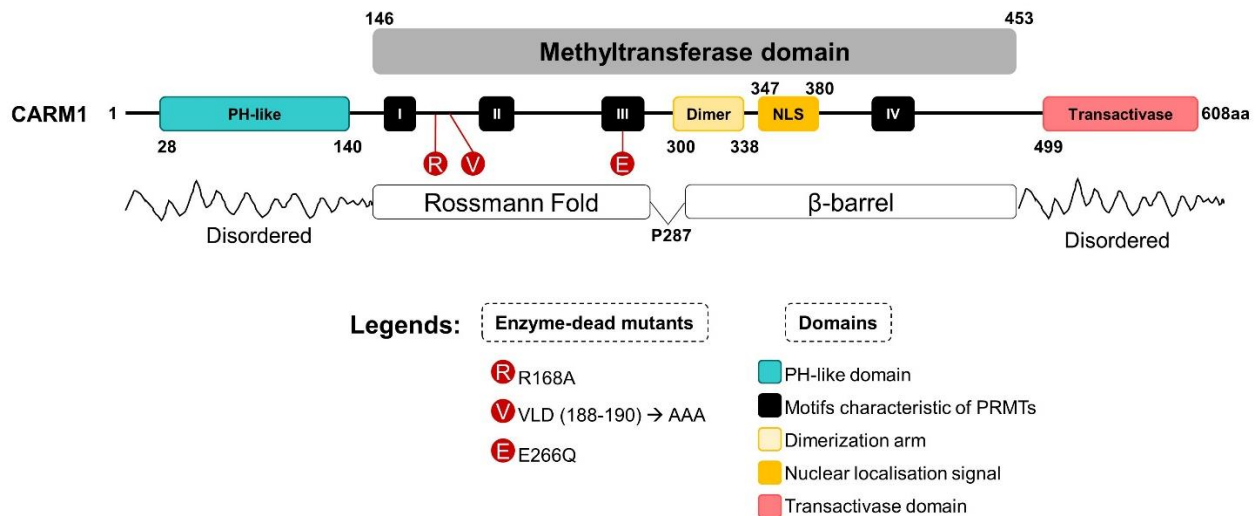


**Figure 32: Structure and domains of CARM1.** The N-terminal PH-like and C-terminal transactivase domains are disordered while the central methyltransferase domain has a Rossmann fold connected to a  $\beta$ -barrel region by a proline residue. The catalytic domain has the PRMT motif signatures (I, II, III, and IV), dimerization arm and the nuclear localization signal. Amino acid numbering is according to human CARM1.

## 1.26.2 Domain-specific features

### 1.26.2.1 N-terminal PH-like fold

The structure of the N-terminal domain (residues 28-140) reveals the presence of a Pleckstrin Homology (PH)-like domain [123], which is involved in protein-protein or protein-RNA interactions (**Figure 32**). However, this PH-like domain diverges from those already known, suggesting that it may interact with specific CARM1 partners which need to be identified. The N-terminal domain on its own behaves as a dimer [123].

### 1.26.2.2 Central catalytic domain with conserved features from PRMTs

The structure of the catalytic domain (residues 140-480) indicates the presence of two sub-domains connected by a proline residue (Pro-287) (**Figure 32**). The first sub-domain contains two  $\alpha$  helices ( $\alpha$ X (residues 144–154) and  $\alpha$ Y (residues 157–164)) followed by the typical Rossmann fold (residues 166–287) common to all PRMTs. This entire sub-domain comprises two of the four PRMT motif signatures (I and II) and the additional motif common to all type I PRMTs (**YFxxY**). The second sub-domain contains a  $\beta$ -barrel (residues 290–299 and 378–478), the dimerization arm (residues 300–338) and the THW loop (residues 413–417). The dimerization arm of CARM1 contains a unique insertion of 9/10 residues modifying the orientation of the two monomers in the final dimer structure. Further, these extra residues contain 5 acidic residues as compared to 20 acidic residues in the PRMT1 dimer [440]. Therefore, the central cavity of CARM1 is larger and less negatively charged than PRMT1, perhaps explaining why CARM1 has less affinity for basic Arg-rich motifs [123, 440].

The cofactor and methyl donor for PRMTs, SAM, is converted to S-Adenosylhomocysteine (SAH) upon hydrolysis, i.e., when SAM is demethylated. This SAH molecule is buried in a deep pocket of the CARM1 catalytic domain and is surrounded by all PRMT motif signatures. The adenine ring, ribose moiety and homocysteine carboxylate of SAH are recognized in the cofactor pocket through hydrogen bonds to Glu244, Glu215 and Arg169, respectively, all of which are strictly conserved within the PRMT family. Few changes are observed between the apo and the SAH-complexed CARM1 structures of the catalytic domain of CARM1 [123, 440]. For example, residues 144-154 which are disordered in the apo structure transform into a helix ( $\alpha$ X) in the presence of SAH.

### 1.26.3 Catalytic-dead mutants

Mutating key residues in the catalytic domain could disrupt the methyltransferase activity of CARM1 (**Figure 32**). For example, mutating Val189, Leu190, and Asp191 to Ala shows complete loss of activity since these residues are important for SAM binding [438]. The more commonly used mutations to inhibit its enzymatic activity reported in the literature is changing Glu267 to Gln267 [188, 442, 443] or Arg169 to Ala169 [444-446].

### 1.26.4 Insights into ternary structures

The attempts to obtain a ternary complex comprising CARM1 and SAH with a substrate have been unsuccessful so far [440, 447]. The first ternary complex composed of the catalytic domain of CARM1 with a peptide substrate has been obtained in 2016 using a non-hydrolysable SAM mimic (sinefungin) [447]. They used proline-rich peptide sequences from known CARM1 substrates such as histone H3 (Arg17), PABP1(Arg455), and PABP1(Arg460) [447]. The arginine residue bound in the substrate pocket makes several hydrogen bond interactions with the double E loop (Glu257, Glu266) and the THW loop (His414) [447]. These interactions allow for the presence of flanking proline residues, conformationally constrained compared to other amino acids, around the substrate arginine [447]. This may explain why, unlike most other type I PRMTs, CARM1 substrates tend to have proline residues flanking the substrate arginine. PABP1(Arg455) peptide was found in the CARM1 binding site when Arg455 was unmethylated and monomethylated [447]. When the Arg455 was dimethylated, only the monomethylated Arg460 bound in the CARM1 substrate site [447]. This agrees with the fact that CARM1 has less affinity to dimethylated compared to monomethylated products [447, 448].

An alternative approach using peptide-based transition state mimics has been employed to obtain the structure of CARM1 with a peptide substrate [449]. Here, they covalently linked two PABP1 peptide sequences – PABP1(Arg455) and PABP1(Arg460) - to an adenosine moiety (as in SAM) to mimic the transition state of the first methylation reaction catalyzed by CARM1 [449]. The molecules form stable complexes with CARM1 and inhibit its methyltransferase activity [449]. The conformations observed for the peptide components of the CARM1-bound transition state mimics are identical to those

observed with unmodified PABP1 fragments bound to CARM1 since they do not induce perturbations to the SAM binding site (Boriak-Sjodin, 2016), unlike sinefungin [449].

### **1.26.5 CARM1 complexed with small-molecule inhibitors**

The structure of CARM1 inhibitors complexed with the catalytic domain of CARM1 has been solved [124, 343, 344, 450, 451]. These inhibitors bind to the substrate-binding site interacting with the same residues as the substrate arginine, i.e., Glu257, Glu266 of the double-E loop and His414 of the THW loop.

### **1.26.6 Limitations of existing structures**

So far, it has been almost impossible to obtain the full-length crystallographic structure of CARM1. In reality, it appears that constructs containing the C-terminal domain of CARM1 are prone to proteolysis possibly due to its unfolded characteristic [123, 440, 449]. The longest CARM1 structures that have been reported are those for CARM1 (28-507) [123] and CARM1 (147-585) [440]. However, there was no electron density for the N- (residues 28-146) and the C- (residues 479-507) terminal domains [123], suggesting that both regions were disordered. Interestingly, the PH-like fold was observed only when the N-terminal domain (28-140) was crystallized on its own and not when the N-terminal domain was combined with the catalytic domain of CARM1 (28-507) suggesting that the PH-like fold may not be present in the full-length structure [123]. Nevertheless, obtaining the full-length structure would be valuable to the CARM1 community as we might be missing key interactions involving the N- and C-terminal domains which could play an important role in substrate recognition.

## **1.27 Alternatively spliced isoforms of CARM1**

Several spliced forms of CARM1 have been reported, and this may explain some apparent discrepancies in the literature regarding CARM1 function and its involvement in cancer (**Figure 33**).

Five rat CARM1 isoforms (v1 to v5) have been isolated [134, 452]: CARM1-v1 is the full-length version of CARM1 (referred to later as CARM1-FL), containing all 16 exons, whereas CARM1-v2 is generated by the retention of intron 15, CARM1-v3 by the retention of introns 14 and 15, CARM1-v4 by exon 15 skipping (referred to later as CARM1- $\Delta$ E15), and CARM1-v5, which includes a part of intron 15. In *Xenopus*, CARM1a (exon 14 skipping) and CARM1b (equivalent to CARM1-FL) have been reported, and only CARM1a activates the transcription of liganded thyroid hormone receptor [453].

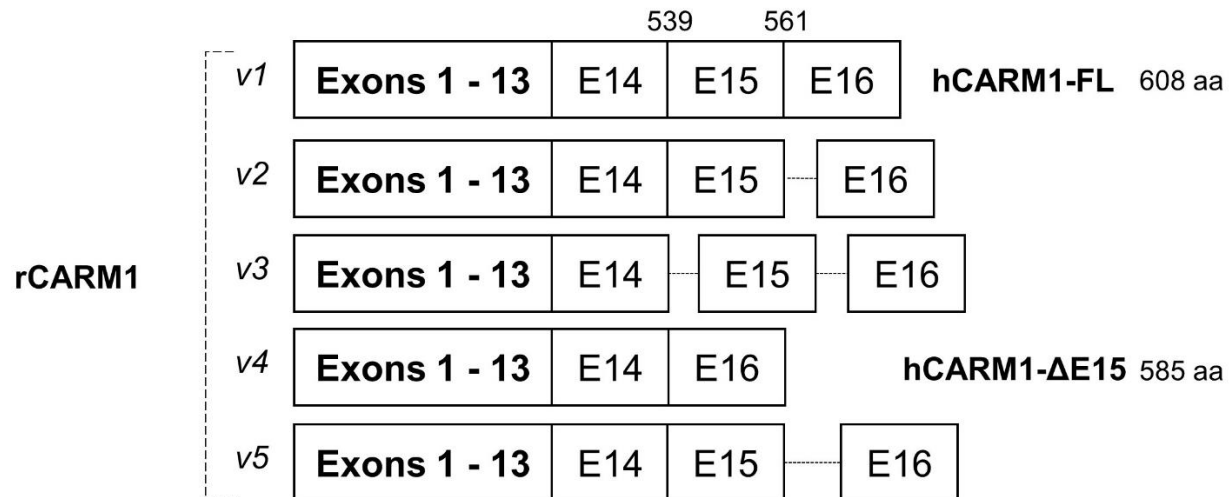


**Figure 33: Alternatively spliced isoforms of CARM1.** Rat CARM1 (rCARM1) has five isoforms that differ in the C-terminal region. rCARM1 v1 and rCARM1 v4 are the full-length (hCARM1-FL) and ΔE15 (hCARM1-ΔE15) isoform in humans, respectively. The amino acid residue number of exon 15 (539-561) is according to hCARM1.

In contrast, only two variants, CARM1-FL and CARM1-ΔE15 (**Figure 33**), are well expressed in breast [454] and hematopoietic [455] cell lines and are capable of forming homo- and heterodimers [454]. CARM1-FL is the most highly expressed form of CARM1 in a healthy brain, heart, skeletal muscle, and testis [134, 454], whereas CARM1-ΔE15 is predominant in a panel of breast cancer cell lines and breast tumors [454, 456]. Interestingly, the auto-methylation site (R550) of CARM1 occurs only in the CARM1-FL isoform, crucial to transduce ERα transcriptional activation [457]. Moreover, differential subcellular localization has been proposed for these two variants: nuclear for CARM1-FL, and potentially mainly cytosolic for CARM1-ΔE15 [456]. However, such localization may vary depending on the cell type and/or tissue studied. Both variants show similar *in vitro* methyltransferase activity towards histone H3 [134, 452, 454, 458], TP2 [452], and PABP1 [454]. Pax7 is preferentially methylated by CARM1-ΔE15 [458], possibly due to constrained accessibility to CARM1-FL.

So far very few studies have considered the presence of these two major CARM1 isoforms, although their apparent differential subcellular localization suggests compartment-specific functions. We still have a lot to learn about their common and specific roles and the physiological/pathological relevance of their existence.

## 1.28 Regulation of CARM1

### 1.28.1 Post-translational modifications

CARM1 catalyzes the methylation of proteins but is itself subjected to various PTMs, such as phosphorylation, O-GlcNAcylation, ubiquitination, and methylation (**Figure 34**).

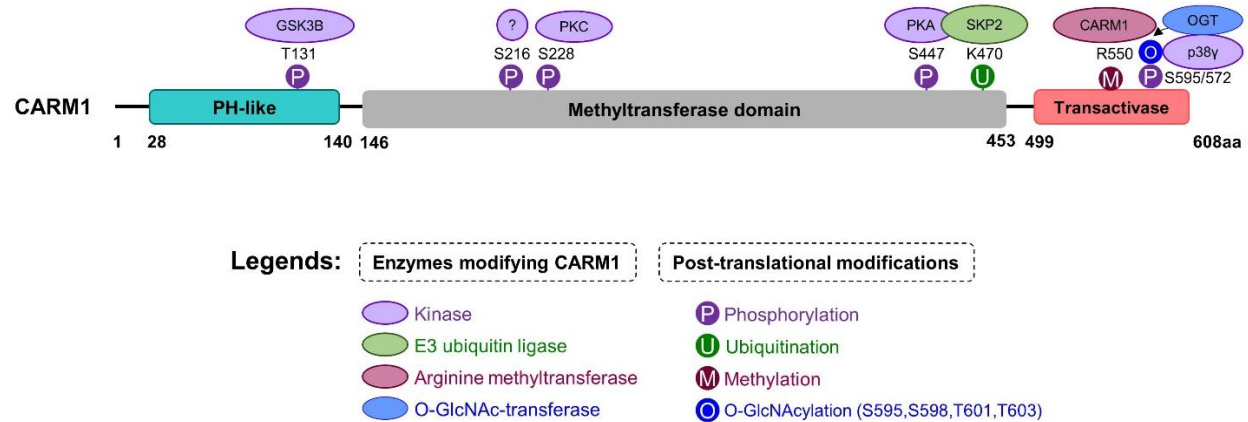


**Figure 34: Various modifications regulating CARM1 activity.** Known modifications, residues on which these modifications occur, and the regulation enzyme are indicated. The unknown kinase phosphorylating S216 is indicated with a question mark. Amino acid numbering is according to human CARM1.

#### 1.28.1.1 Phosphorylation

CARM1 is phosphorylated on several residues, T131 [459], S216 [460], S228 [441, 461], S447 [462], and S595/S572 [458]. Glycogen synthase kinase 3 beta (GSK3 $\beta$ ) phosphorylates CARM1 on T131, within the PH-like domain, to protect it from ubiquitin-mediated proteasomal degradation [459]. S216 [460] and S228 [441, 461] are located within the catalytic domain and are phosphorylated by an unknown kinase and protein kinase C (PKC) [461], respectively. Mutants mimicking their phosphorylated state (S216E and S228E) impair CARM1 methyltransferase activity by interfering with SAM binding, as well as transactivation of ER-dependent transcription [441, 460, 461]. Although S228E affects CARM1 dimerization [441, 460], S216E neither affects CARM1 dimerization nor its interaction with co-activators such as p300 [460]. Both S216 and S228 are phosphorylated during mitosis [441, 460], suggesting CARM1 is involved in cell-cycle progression. The phosphorylation of S447 by protein kinase A (PKA) promotes the interaction of CARM1 with the hormone-binding domain of unliganded ER $\alpha$ , leading to its cAMP (cyclic Adenosine Monophosphate)-dependent transcriptional activity [462], which is further enhanced by PKA-mediated phosphorylation of LSD1 (Lysine-Specific histone Demethylase 1) [463]. p38y MAPK (Mitogen-Activated Protein Kinase) phosphorylates S572 of CARM1- $\Delta$ E15 (and S595 of CARM1-FL) within its C-terminal domain without affecting its methyltransferase activity [458]. Phosphorylation of S216 [460] and S572

(CARM1- $\Delta$ E15) [458] has been shown to prevent nuclear localization of CARM1, leading to its accumulation in the cytosol. Furthermore, the authors of a study in *Saccharomyces cerevisiae* hypothesized that T413 (within motif IV) of human CARM1 could be phosphorylated, but this remains to be demonstrated [464].

#### 1.28.1.2 *O*-GlcNAcylation

Another PTM of S/T residues is *O*-GlcNAcylation, catalyzed by *O*-GlcNAc-transferase (OGT), which is also a CARM1 protein partner [465]. CARM1 is highly *O*-GlcNAcyated at four residues: S595 (corresponding to S572 of CARM1- $\Delta$ E15, also phosphorylated by p38y MAPK), S598, T601, and T603 [466]. *O*-GlcNAcylation of CARM1 does not alter its stability, nuclear-cytoplasmic distribution, dimerization capacity, or co-activator activity but may affect substrate specificity [466]. The overexpression of OGT prevents CARM1 phosphorylation (possibly on S216 and S228) and affects its localization (possibly on S572/S595 of CARM1- $\Delta$ E15/CARM1-FL) during mitosis [458, 466, 467]. Such crosstalk between phosphorylation and *O*-GlcNAcylation regulates the ability of CARM1 to methylate histone H3 at Arg17 [467].

#### 1.28.1.3 Ubiquitination

CARM1 is also ubiquitinated [264, 468, 469], particularly on K470, by the SKP2-containing SCF (SKP1-cullin1-F-box protein) E3 ligase complex [468, 469].

#### 1.28.1.4 Methylation

Finally, nearly 100% of CARM1-FL is auto-methylated on R550 (absent in CARM1- $\Delta$ E15) [454, 470]. This modification does not affect methyltransferase activity [454, 470] but is required for ER $\alpha$ -mediated transcription and pre-mRNA splicing [454, 470].

### 1.28.2 CARM1 regulation by nucleic acids

It was previously thought that CARM1 could only interact with proteins and not RNA, but recent studies indicate it associates with several lncRNAs (**Figure 35A**). Indeed, the lncRNA termed suppressor of tumorigenicity 7 antisense RNA 1 (ST7-AS1) interacts to the N-terminal of CARM1 and protects it from ubiquitin-dependent degradation [471]. ST7-AS1 further promotes CARM1-induced Sox-2 methylation/self-association, thereby acting as an oncogenic factor in laryngeal squamous cell carcinoma [471]. CARM1 co-expresses and binds to lncRNA PVT1 in non-small-cell lung carcinoma (NSCLC) and is associated with radiosensitivity [472]. LincGET (endogenous retrovirus ERV-associated lncRNA) induces the nuclear localization of CARM1 which turns on inner cell mass (ICM)-specific genes to bias embryo development [473]. Finally, the lncRNA NEAT1 recruits CARM1 to the paraspeckles and is itself negatively regulated transcriptionally by CARM1 [474, 475].

In addition, at the mRNA level, CARM1 is regulated by another subset of RNAs - the microRNAs (miRNA/miR) (**Figure 35B**). CARM1 has been shown to be targeted by miR-

195 and miR-195-5p in colorectal cancer cells [476, 477], by miR-424-5p in NSCLC [472] and by miR-223 in HSPCs [478]. In HSPCs, as part of a feedback loop, CARM1 also represses miR-223 expression by methylating RUNX1 [478]. The overexpression of miR-195, miR-195-5p, and miR-424-5p impairs cell proliferation [472, 476, 477]. It would be exciting to explore if there are more lncRNAs or other subsets of RNAs that interact with CARM1.

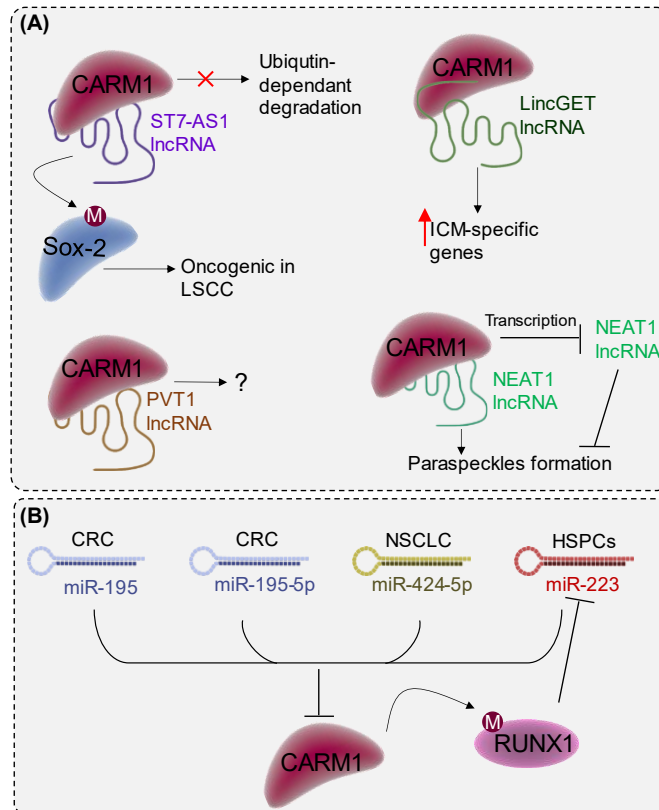


**Figure 35: Regulation of CARM1 by lncRNAs and miRNAs.** (A) Long-noncoding RNAs bind to CARM1 and regulate its function. (B) micro-RNAs (miR) degrade CARM1 in colorectal cancer cells (CRC), non-small cell lung carcinoma (NSCLC) or hematopoietic stem and progenitor cells (HSPCs).

## 1.29 The known methylome of CARM1

As previously discussed, CARM1 is unique among the PRMTs to preferentially methylate substrate arginines within a proline-rich [146] or a proline-glycine motif (PGM) [145] rather than a glycine-rich motif [143]. Here, I list all the known substrates of CARM1, which shed light on the diverse functions that CARM1 is involved in (see ANNEXE II: ).



## 1.30 Major cellular functions

### 1.30.1 Transcriptional regulation

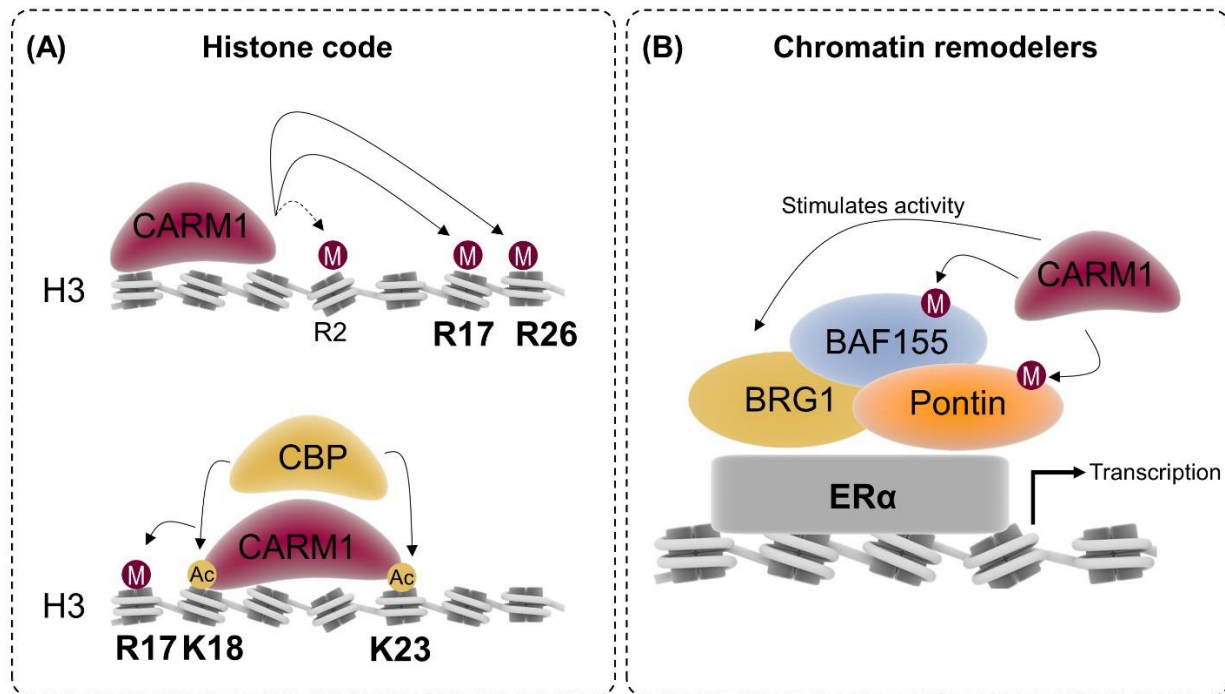


**Figure 36: Regulation of transcription by CARM1.** (A) CARM1 methylates histone H3 on Arg 17 and 26 and weakly on Arg 2. Acetylation on Lys 18 and 23 on histone H3 aids CARM1 binding and methylating Arg 17. (B) CARM1 methylates (BAF155, Pontin) or stimulates (BRG1, also called SMARCA4) chromatin remodeling complex subunits to activate ER $\alpha$  mediated transcription.

#### 1.30.1.1 Part of the "histone code"

Like the members of the PRMT family, CARM1 also methylates histones on several arginine residues. The two major histone sites methylated by CARM1 are on histone H3 at Arg17 and Arg26 [159] (**Figure 36A**). Arg2 was also identified to be weakly methylated *in vitro* by CARM1 [159], but there have been no cellular implications or *in vivo* evidence associated with the H3R2me2a mark (**Figure 36A**). Bauer and colleagues were the first to show that the H3R17me2a mark was linked to gene activation [479]. Subsequently, almost all studies showing transcriptional activation by CARM1 via histone methylation has been through H3R17me2a (examples: [480, 481]). Methylation on Arg26 is also responsible for transcriptional activation [481-483], but also to transcriptional repression in one study [219]. Interestingly, a recent study showed that CARM1 prefers to methylate H3R17 over H3R26 [448], although the physiological relevance is still unknown. Since these histone marks were fundamental in defining CARM1 activity, they have often been used as a read-out in CARM1 inhibition studies. However, it was always surprising that CARM1 inhibition never reduced the H3R17me2a mark [343, 344]. This discrepancy was solved by the group of Bedford last year, when they showed that Arg17 was methylated both by CARM1 and

PRMT6, as a possible compensatory mechanism [484]. Only a complete inhibition or knock-out of both CARM1 and PRMT6 could decrease the H3R17 methylation mark [484]. Substrate scavenging and compensation by other PRMTs is not new and has been known for other histone and non-histone substrates [152].

These arginine methylation marks often crosstalk with other histone modifications such as acetylation, lysine methylation and or ubiquitination to tightly regulate gene expression [482, 485, 486], and therefore CARM1 is considered an epigenetic “writer” part of the “histone code”. For example, lysine acetylation on histone H3 at K18 and K23 by CREB-binding protein (CBP) allows binding of CARM1 to histone H3 and methylating R17 [486] (**Figure 36A**).

### 1.30.1.2 Chromatin remodelers and CARM1

CARM1 also regulates transcription by interacting with and methylating some components of the chromatin remodeling complex (**Figure 36B**). Chromatin remodelers are large, multiprotein complexes that hydrolyze ATP to restructure nucleosomes, thus allowing better access to the DNA, to enable transcription. CARM1 stimulates the ATPase activity of BRG1, a core component of the SWI/SNF chromatin remodeling complex, and this interaction activates ER-dependent transcription [487]. Further evidence has shown that CARM1 interacts with and methylates two other components of the chromatin remodeling complex, BAF155 [488] and Pontin [446], to activate transcription. These methylation events have downstream implications in the oncology of breast [488] and ovarian [489] cancer and autophagy [446]. Both these topics will be discussed in detail in later sections.

### 1.30.1.3 Co-activator function

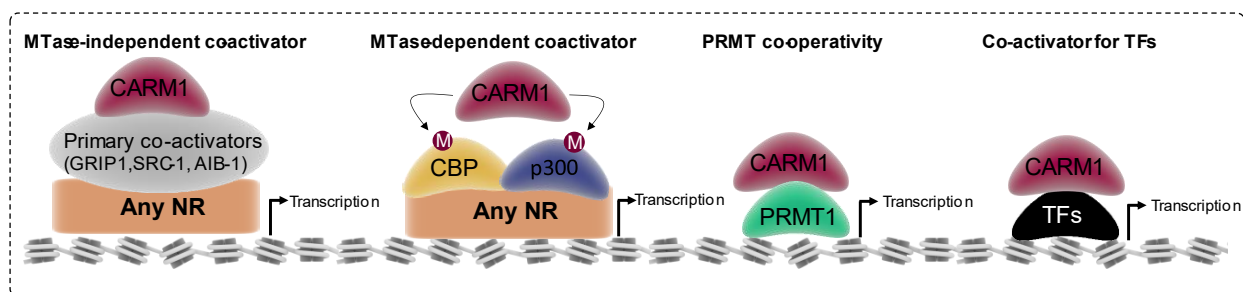


**Figure 37: Co-activator function by CARM1 on nuclear receptors.** CARM1 can bind to any primary co-activator on nuclear receptors to enhance transcription. CARM1 methylates co-activators CBP/p300 to enhance NR-mediated transcription. CARM1 can co-operate with PRMT1 or transcription factors (TFs) to mediate transcription.

The well-known and fully characterized function of CARM1 is its role in transcriptional co-activation (**Figure 37**). This was how it was first discovered in 1999, as a

co-factor bound to the c-terminal region of the nuclear hormone receptor GRIP1 and other members of the p160 family of co-activators [438].

Typically, CARM1 functions as a secondary co-activator with the p160 family, such as GRIP1, SRC-1, and AIB-1 proteins, to enhance their co-activator function on the nuclear receptors [275, 438, 490] (**Figure 37**). In other instances, CARM1 interacts with the histone acetyltransferases p300 and CBP, to synergistically enhance nuclear receptor (NR) function [442, 491] (**Figure 37**). Several of these co-activators were later identified as substrates of CARM1, such as p300 [485, 492-494], CBP [485, 495, 496], AIB-1 [497], to name a few (**see ANNEXE II:** ).

CARM1 in complex with these co-activators binds and regulates the promoters of estrogen receptor (ER) [498, 499], matrix metalloproteinase 9 (MMP-9) [500], cyclin E1 [482], and others. Further, CARM1 can bind to transcription factors such as p53 [501], myocyte enhancer factor 2C [502],  $\beta$ -catenin and TCF4/LEF1 [491], nuclear factor  $\kappa$  of B-cells (NF- $\kappa$ B) [188, 189, 503], and NF-E2-related factor 2 (Nrf2) [504] to activate transcription of their target genes (**Figure 37**). Though in most cases CARM1's methyltransferase activity is indispensable for its co-activator function, some evidence suggests the opposite. For example, NF- $\kappa$ B-mediated gene transcription required the presence of CARM1 in the complex for protein stabilization, independent of its methyltransferase activity [503], suggesting that CARM1 might also have scaffolding functions (**Figure 37**).

Apart from interacting with primary co-activators and transcription factors, as described above, CARM1 can also cooperate with PRMT1 to activate gene transcription [370, 490, 491] (**Figure 37**).

### **1.30.2 RNA metabolism**

In addition to its function as a transcriptional co-activator, nuclear CARM1 regulates mRNA stability by promoting mRNA degradation of a subset of transcripts via the nonsense-mediated decay (NMD) pathway [253], pre-mRNA splicing (**Figure 38**) [114, 134, 145, 253, 277, 326, 436, 470, 505], and mRNA export through paraspeckles (**Figure 39**) [474].

#### *1.30.2.1 Pre-mRNA splicing*

The first study implying a role for CARM1 in splicing showed that amongst the five rat isoforms, only the minor isoform CARM1-v3 regulates splicing by promoting the use of a 5' distal splice site, independent of its methyltransferase activity [134]. In contrast, Chen et al. showed that CARM1-FL regulates splicing, possibly due to different experimental conditions, and depends on its methyltransferase activity [145]. CARM1-FL methylates several splicing factors (SmB, SF3B4, U1C, and CA150) and promotes exon skipping through the methylation of CA150 [145] (**Figure 38**). More recently, additional

studies have highlighted the involvement of CARM1 in splicing: methylation of the splicing factor SRSF2 [114], exon skipping of VEGF [277], a requirement of auto-methylation of CARM1-FL for its splicing activity [470] (**Figure 38**), and involvement in other splicing events, such as intron retention in *Arabidopsis thaliana* [505]. Moreover, two major studies have shown that type I PRMT inhibitors and PRMT5 inhibitors alter splicing events and act synergistically when targeting cancer cells mutated for splicing factors [326, 436]. However, the importance of specifically inhibiting CARM1 (a Type I PRMT) in this context is yet to be determined.

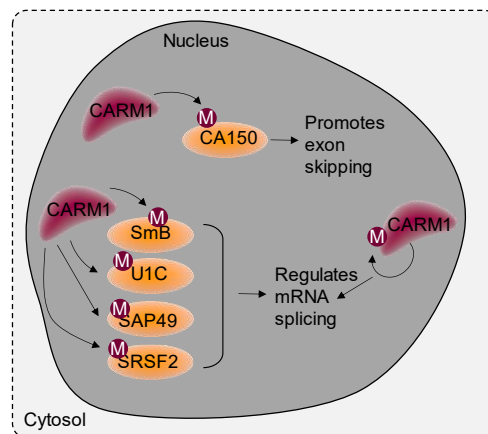


**Figure 38: CARM1 regulates splicing by methylating factors.** CARM1-mediated methylation of CA150 promotes exon skipping. CARM1 methylates splicing factors (SmB, U1C, SAP49, SRSF2) or automethylates itself to regulate mRNA splicing.

### 1.30.2.2 mRNA export through paraspeckles

Paraspeckles are a new class of membrane-less structures located in the interchromatin space inside the nucleus organized around the lncRNA NEAT1. It recruits several RNA binding proteins such as paraspeckles protein 1 (PSPC1), p54nrb (also known as NonO), and Splicing Factor Pro/Glu-rich (SFPQ) [506]. More recently, it was shown that CARM1 is also recruited to this protein-RNA complex [474, 475] (**Figure 39**). Paraspeckles are rich hubs of RNA-protein interactions involved in the regulation of gene expression. These structures regulate gene expression by sequestering specific mRNA molecules, such as those containing inverted repeated Alu elements (IRAlus) in their 3'UTR, through their binding to p54nrb [474].

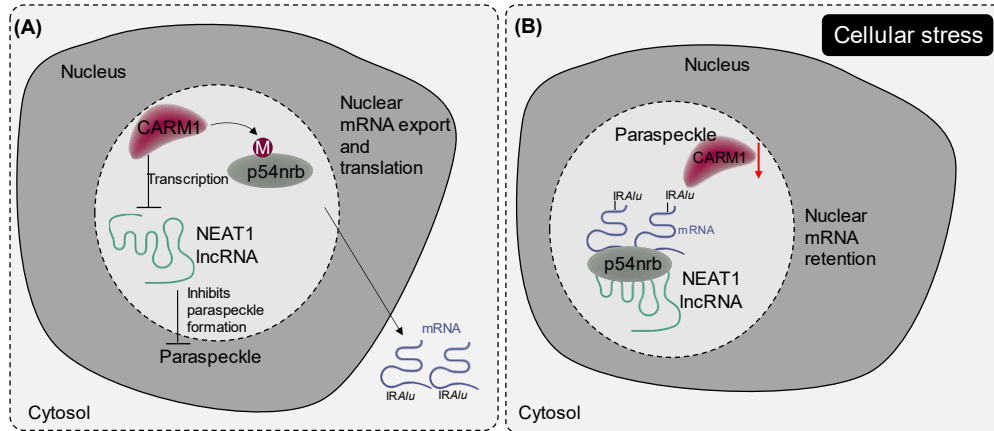


**Figure 39: mRNA metabolism in paraspeckles mediated by CARM1.** (A) Under normal conditions, CARM1 methylates p54nrb and inhibits the transcription of NEAT1 lncRNA, inhibiting paraspeckle formation. This aids in the cytosolic transport of mRNAs contains IRAlu elements. (B) When cellular stress is induced, the CARM1 level inside the paraspeckle is decreased, and the mRNAs containing IRAlus are sequestered by p54nrb.

CARM1 regulates paraspeckle formation and function. On the one hand, CARM1 represses the transcription of NEAT1 by binding to its promoter, thus impairing paraspeckle formation [474, 475] (**Figure 39A**). On the other hand, CARM1 methylates p54nrb, decreasing its binding affinity to IRAlus-containing mRNAs [474] (**Figure 39A**). This activity allows the export of these mRNAs from the nucleus to the cytosol, leading to their translation, and represents an additional molecular mechanism for CARM1 to regulate gene expression [474]. Inducing stress by treatment with polyinosine-polycytidylic acid (poly (I:C)) reduces CARM1 levels in paraspeckles, leading to the nuclear retention of IRAlus containing mRNAs [474] (**Figure 39B**). In addition, CARM1 appears to regulate paraspeckle localization of the splicing factor SRSF2, a potential CARM1 substrate [114], and p54nrb [475].

### 1.30.3 Autophagy

Autophagy is a lysosome-mediated cellular self-digestion process, which guarantees the quality of proteins and organelles by eliminating those that are damaged and allows cell survival during starvation and stress [507, 508].

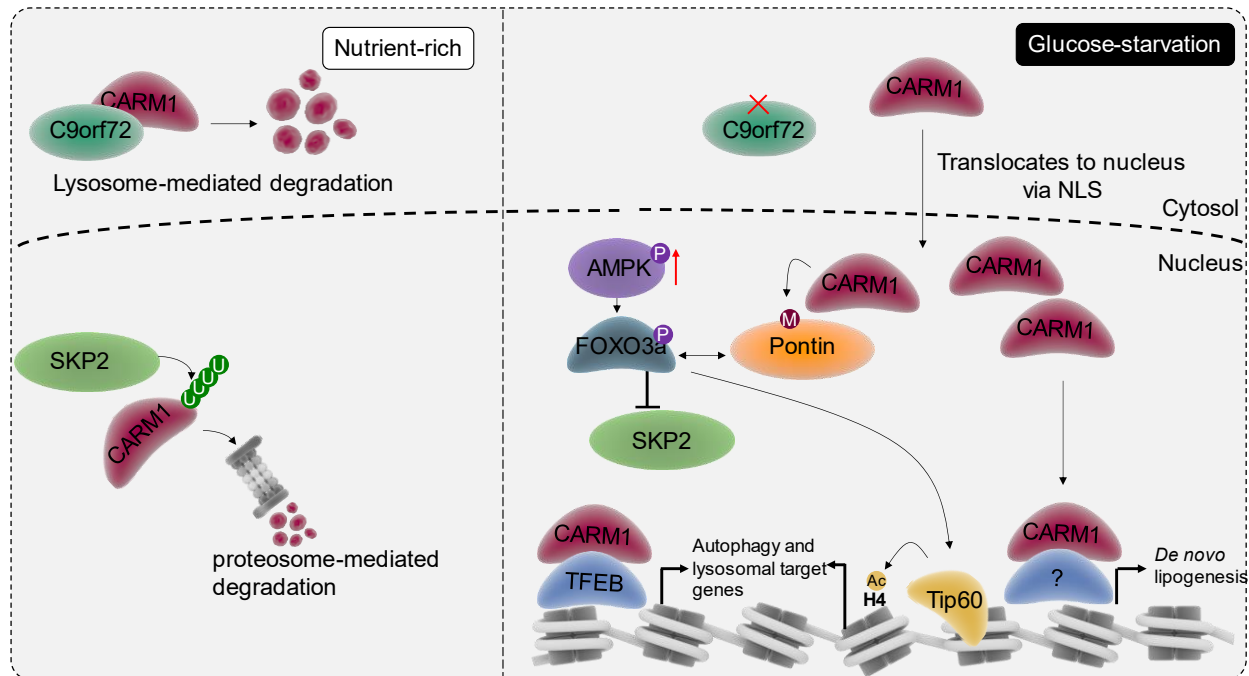


**Figure 40: CARM1 regulates autophagy through two different mechanisms.** CARM1 is degraded by C9orf72 or SKP2 in nutrient-rich conditions. Under glucose starvation, CARM1 translocates to the nucleus to directly or indirectly activate autophagy and lysosomal target genes and de novo lipogenesis. The double-headed arrow indicates direct binding between pontin and phosphorylated FOXO3a.

The role of CARM1 in autophagy is relatively new, first identified in a landmark paper by Shin and colleagues in 2016 [468]. Since then, many groups have identified certain nuances in the signaling axis, but the overall mechanism involving cytosolic and nuclear CARM1 has been highlighted in two studies [468, 509].

Under normal/nutrient-rich conditions, CARM1 is degraded via two different mechanisms: nuclear CARM1 through SKP2-mediated ubiquitination (K470) and subsequent proteasomal degradation [468, 469] and cytosolic CARM1 through C9orf72-dependent lysosomal proteolysis [509]. By contrast, CARM1 accumulates in the nucleus under glucose-starved conditions [468, 509] (**Figure 40**).

Upon glucose starvation, AMPK level increases in the nucleus and it phosphorylates FOXO3a, which is then recruited to the promoter of SKP2, leading to its repression; nuclear CARM1 is no longer degraded and interacts with TFEB, inducing the expression of various autophagy and lysosomal target genes by methylating histone H3 (H3R17me2a) [468]. Alternatively, increased nuclear CARM1 methylates the chromatin remodeler, Pontin, and methylated-pontin binds to FOXO3a [446]. This interaction recruits the histone acetylase Tip60, increasing H4 acetylation, activating autophagy genes [446]. These studies suggest that nuclear CARM1 can directly (via TFEB) [468] or indirectly (via Pontin) [446] activate

autophagy gene transcription. This pathway has since been reported as the AMPK-SKP2-CARM1 signaling pathway [468, 469, 510] (**Figure 40**).

C9orf72, which interacts with the PH-like domain of CARM1, regulates lipid metabolism [509] upon glucose starvation. The loss of C9orf72 prevents lysosomal-mediated degradation of CARM1, leading to its accumulation in the cytoplasm and nucleus (Figure 1b) [509]. The nuclear localization signal identified within CARM1 is responsible for its translocation to the nucleus to induce the de novo biogenesis of lipids as a stress response [509] (**Figure 40**).

#### **1.30.4 Metabolism**

Normal cells metabolize glucose to carbon dioxide and water in the presence of oxygen but convert glucose to lactic acid in the absence of oxygen. A hallmark of cancer cells is that they have altered metabolism, whereby they metabolize glucose to lactate even in the presence of oxygen and this has been called the Warburg effect after Otto Warburg [39]. CARM1 regulates some of these metabolic pathways (oxidative phosphorylation, glycolysis, and glutamine metabolism) in different cancer (**Figure 41**). In breast cancer, CARM1-dependent methylation of PKM2 decreases the expression of inositol-1,4,5-trisphosphate receptors (InsP3Rs), therefore switching the metabolism from oxidative phosphorylation to aerobic glycolysis [511] (**Figure 41A**). Blocking PKM2 methylation increases the calcium flux from the endoplasmic reticulum to mitochondria leading to oxidative phosphorylation [511].

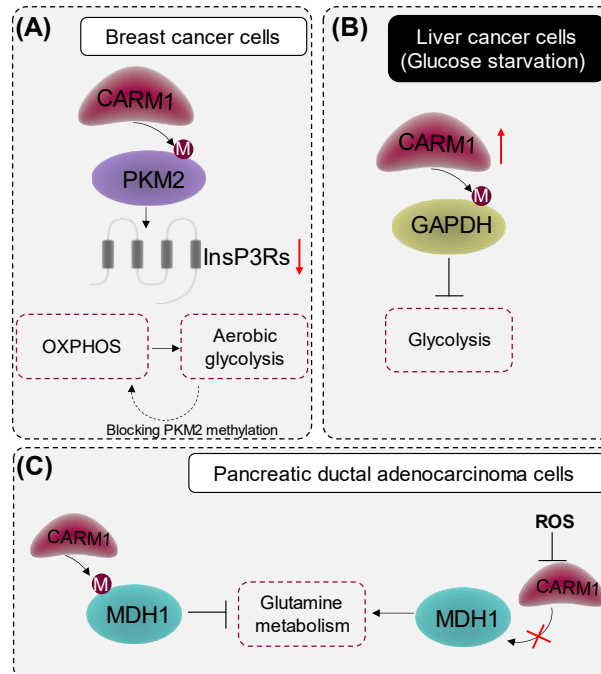


**Figure 41: CARM1 modulates metabolic pathways in cancer.** (A) CARM1 methylates PKM2 which decreases the inositol-1,4,5-trisphosphate receptors (InsP3Rs), changing the metabolism from oxidative phosphorylation (OXPHOS) to aerobic glycolysis. (B) Glucose starvation increases the CARM1 level and leads to methylation of GAPDH, inhibiting glycolysis. (C) CARM1 methylates MDH1 to inhibit glutamine metabolism. Reactive oxygen species (ROS) inhibits CARM1, activating glutamine metabolism.

Upon glucose starvation in liver cancer cells, CARM1 is upregulated in an AMPK-dependent manner and inhibits glycolysis through the methylation of glyceraldehyde-3-phosphate dehydrogenase (GAPDH) [512] (**Figure 41B**).

In normal conditions, CARM1-mediated methylation of malate dehydrogenase 1 (MDH1) inhibits its activity and therefore glutamine metabolism [513]. Conversely, under stress conditions, the inhibition of CARM1 activity by reactive oxygen species (ROS), activates glutamine metabolism in pancreatic ductal adenocarcinoma [513] (**Figure 41C**).



### 1.30.5 Early-embryo development and cellular differentiation

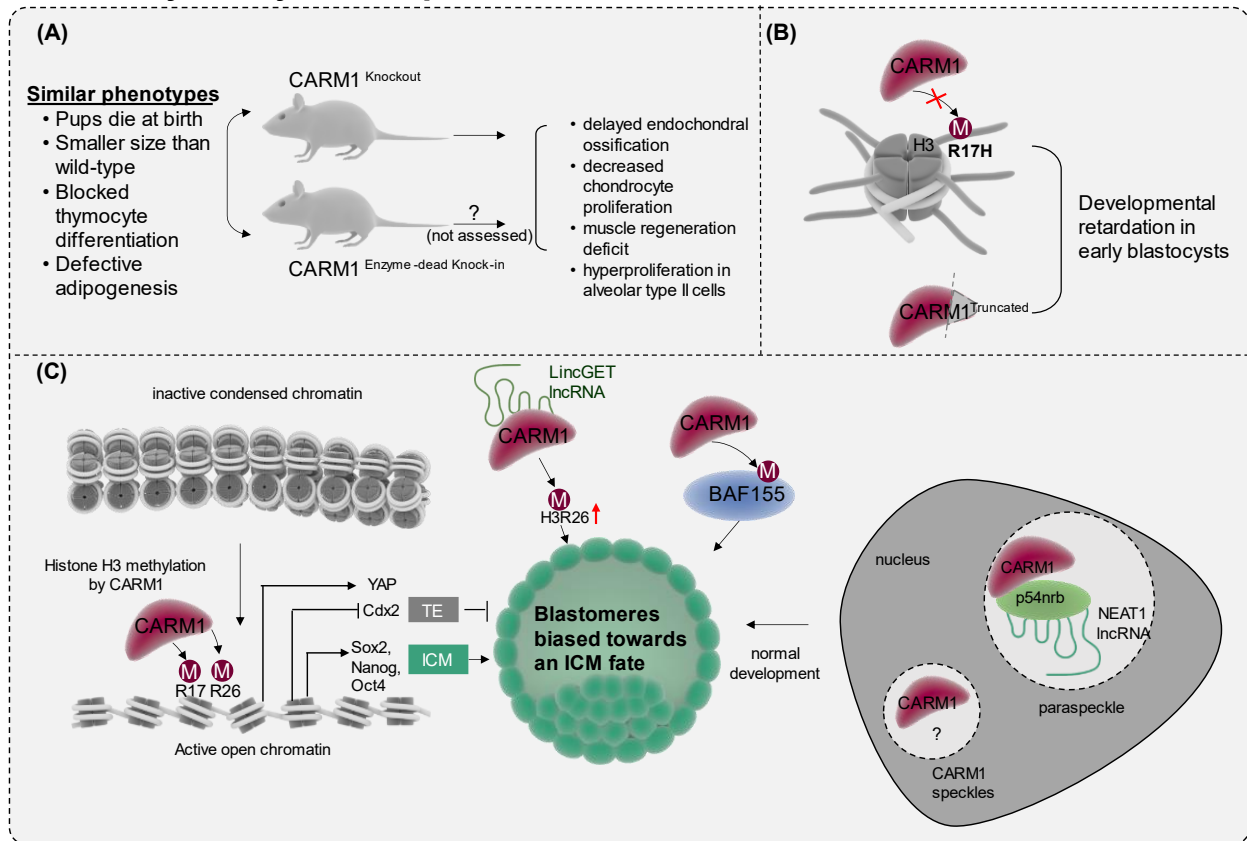


**Figure 42: CARM1 regulates early embryo development.** (A) Phenotypes of CARM1 knockout and enzyme-dead knock-in mice. (B) Substituting arginine 17 of histone H3 or truncating CARM1 at its C terminus causes developmental retardation. (C) CARM1-mediated methylation of histone H3 and/or BAF155 induces the expression of ICM-specific factors and blocks TE differentiation. Paraspeckles are necessary for normal development dependent on H3R26 methylation by CARM1.

#### 1.30.5.1 CARM1 activity is essential for embryonic development

CARM1 regulates early mouse development and plays a role in the determination of cell fate. In contrast to PRMT1 and PRMT5 (the major Type I and Type II PRMTs), whose knock-out (KO) cause embryonic lethality [136, 137], CARM1 KO mice display recessive neonatal lethality, with pups dying at birth due to breath failure [141, 444] (**Figure 42A**). Furthermore, CARM1 KO mice are smaller than their wild-type (WT) littermates [141], show delayed endochondral ossification and decreased chondrocyte proliferation [514], reduced thymopoiesis, resulting from a defect in the fetal hematopoietic compartment [515, 516], impaired adipocyte differentiation [517], muscle regeneration deficit [518], and hyperproliferation of alveolar type II cells [519] (**Figure 42A**). Interestingly, a CARM1 enzyme-dead knock-in mutant mouse phenocopies CARM1 KO mice [444], showing blocked thymocyte differentiation [444, 515, 516] and defective adipogenesis [444, 517], indicating CARM1 activity is essential for development (**Figure 42A**). In parallel, substituting R17 on histone H3 with histidine causes developmental retardation at embryo day E4.5

[480]. A similar phenotype was observed with a C-terminal truncated CARM1 mutant [480], suggesting that certain CARM1 partners may also be involved in early embryogenesis (**Figure 42B**).

#### *1.30.5.2 CARM1 biases cells towards an inner cell mass fate in early embryos*

The function of CARM1 at earlier stages of mammalian development was unknown until an elegant study by Torres-Padilla et al. showed that CARM1 can contribute to cell fate decisions in the mouse four-cell-stage embryo [481]. CARM1 levels, along with its specific histone marks (H3R17me2a and H3R26me2a), varied between the four-cell blastomeres and higher levels of H3R26me2a were associated with a global increase in transcription [481]. During mammalian embryo development, the blastomeres have two lineages or fates, either to become part of the ICM or trophectoderm (TE), contributing to embryonic and extra-embryonic cells, respectively. CARM1 activity and expression biases the blastomeres towards an ICM fate by inducing the expression of *Nanog*, *Sox2*, *Sox21*, and *Oct4* [481, 483], while repressing the expression of *Cdx2*, a transcription factor for TE differentiation [483, 520] (**Figure 42C**). Additionally, CARM1-mediated methylation of BAF155 influences the cell fate towards ICM [521]. Unmethylated BAF155 induces the expression of TE differentiation markers, whereas methylated BAF155 switches on the expression of pluripotent markers, such as *Nanog* [521] (**Figure 42C**). The heterogeneous distribution of CARM1 in the four-cell stage embryo is also regulated by the microRNA miR-181a [522]. Interestingly, it is a balance in CARM1 levels that determines the resulting fate of the blastomeres [481, 483, 520, 523].

Recent evidence suggests that CARM1 is involved in cell fate determination at earlier stages of the mouse embryo (two to four cells) by interacting with LincGET, an endogenous retroviral long-non coding RNA (lncRNA) [473] and localizing to the membrane-free nuclear body – paraspeckles [475] (**Figure 42C**). LincGET induces nuclear localization of CARM1 by interacting with its transactivation domain, resulting in high H3R26me2a levels and ICM-specific gene expression [473]. Moreover, the presence of CARM1 in paraspeckles is required for the methylation of histone H3 at R26 and to ensure proper lineage allocation to facilitate normal embryo development [475]. CARM1 is also present in other nuclear bodies called 'CARM1 speckles' [475], but its function in such structures is yet to be elucidated.

#### *1.30.5.3 CARM1 maintains the pluripotency of ESCs*

Mirroring its function in embryonic cell fate determination, CARM1 induces the expression of pluripotency genes (*Oct4*, *Sox2*) through the methylation of histone H3, impairing embryonic stem cell (ESC) differentiation [524-526]. Further, CARM1 is essential for retinoic-acid induced differentiation of mouse ESC [527]. Conversely, the miR-181 family promotes ESC differentiation by targeting CARM1 for degradation [524] (**Figure 43A**).

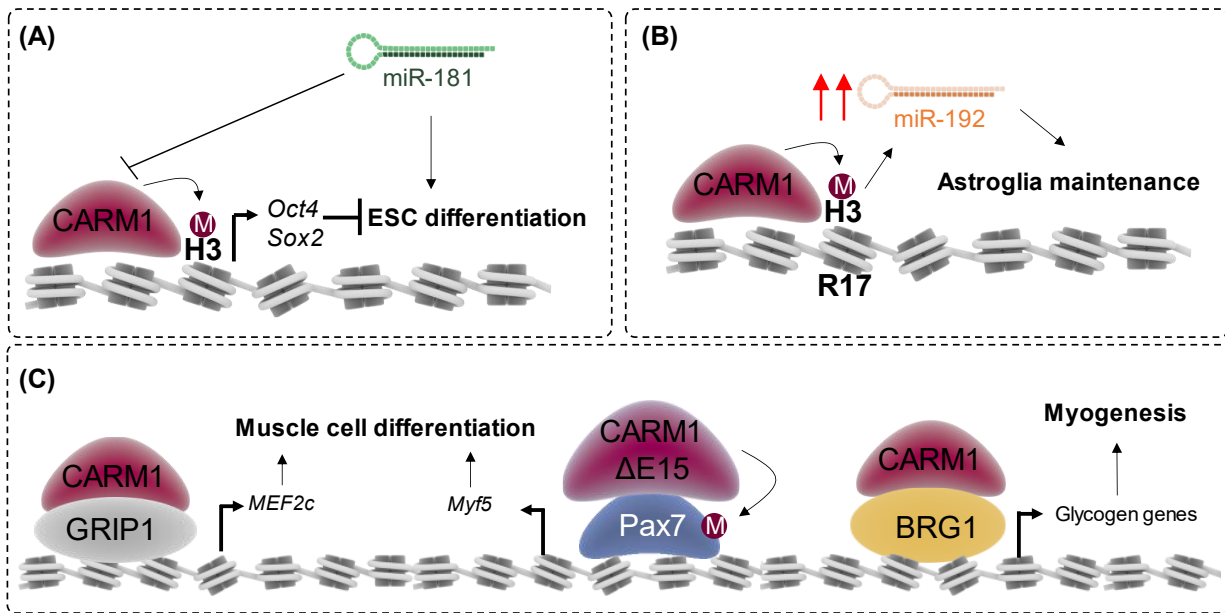


**Figure 43: Cellular differentiation controlled by CARM1.** (A) CARM1-mediated methylation of histone H3 inhibits embryonic stem cell (ESC) differentiation. microRNA (miR)-181 promotes ESC differentiation directly or by inhibiting CARM1. (B) CARM1 methylates histone H3 on arginine 17 to increase the miR-192 level for astroglial maintenance. (C) CARM1 (with GRIP1) activates MEF2c transcription or CARM1- $\Delta$ E15-mediated Pax7 methylation activates Myf5 transcription, leading to muscle cell differentiation. CARM1 with BRG1 activates glycogen genes to activate myogenesis.

#### 1.30.5.4 CARM1 controls neuronal and skeletal muscle differentiation

CARM1 is involved in both neuronal (**Figure 43B**) and skeletal muscle differentiation (**Figure 43C**). However, CARM1's role in neuronal differentiation is limited unlike in skeletal muscle. For example, CARM1-mediated methylation of histone H3 (H3R17me2a) enhances miR-92 expression, which is essential for the maintenance of the astroglial lineage [528]. On the other hand, CARM1 regulates myogenesis by several mechanisms. CARM1 enhances *MEF2c* transcription [502] and CARM1-dependent methylation of Pax7 activates *Myf5* expression [518], both leading to the differentiation of muscle cells. Moreover, CARM1 is needed for late-stage myogenesis by interacting with BRG1 [529, 530] and inducing the glycogen gene expression program [265].

### 1.31 Role in cancer

CARM1 is overexpressed in several cancer types, such as **breast** [147, 531-533], **ovarian** [489, 534], **colorectal** [476, 535], **prostate** [536], **bone** [537], **hematopoietic** [232, 478], **oral** [538], **non-small cell lung** [539] and **melanoma** [540]. CARM1 is required for the survival of many of these cancer types as its depletion impairs cell proliferation [476, 489, 536, 537, 539]. Moreover, in an attempt to identify cancer-driving genes, Buljan and colleagues recently identified a hotspot mutation at A202V of *CARM1*, which is

located in its methyltransferase domain [541]. Hence, CARM1 is emerging as an attractive therapeutic target for cancer and has gained interest to characterize its tumorigenic potential.

### 1.31.1 Breast Cancer

CARM1 is more expressed in breast tumors compared to normal breast tissues or tissues adjacent to the tumor [147, 531-533]. High levels of CARM1 correlate with young age, high grade, ER and PR negative status, increased p53 expression, and high proliferative index that are all hallmarks of TNBC and with high Her2 expression [531, 532]. CARM1 is expressed both in the nucleus and in the cytoplasm of breast cancer cells [531-533]. Higher cytoplasmic CARM1 levels are associated with ER-negative status whereas higher nuclear CARM1 levels are associated with Her2 receptor status [533]. Both the CARM1 isoforms (FL and  $\Delta E15$ ) are more expressed in breast tumors compared to normal breast samples at the RNA level and are not correlated with breast cancer subtypes [456]. However, their protein expression levels are still unknown. Furthermore, CARM1 regulates breast cancer cell migration and metastasis to the lung via the methylation of the SWI/SNF core subunit BAF155 [488].

#### 1.31.1.1 Luminal breast cancer

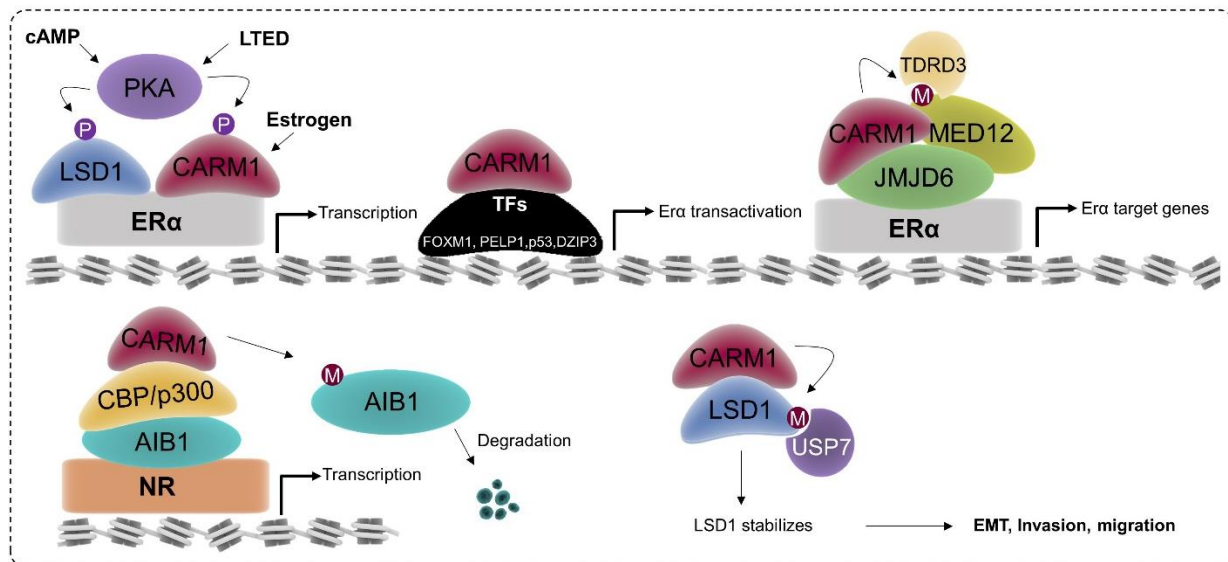


**Figure 44: CARM1 activates luminal breast cancer progression.** cAMP or LTED promotes PKA-mediated phosphorylation of LSD1 and CARM1 to activate ER $\alpha$ -mediated transcription. CARM1 binds to transcription factors (TFs) or methylates MED12 to activate ER $\alpha$  target genes. CARM1 can enhance nuclear receptor-mediated transcription or methylate AIB1 targeting it for degradation. CARM1-mediated LSD1 stabilizes it leading to EMT phenotype. cAMP: cyclic AMP, LTED: long-term estrogen deprivation.

Among the different subtypes of breast cancer, CARM1 has been mostly studied in luminal breast cancer which express ER (Figure 44). ER $\alpha$  is a transcription factor that can be activated with ligands (i.e., estrogens) or in a ligand-independent manner (unliganded

pathway). cAMP leads to activation of the unliganded ER $\alpha$  through the phosphorylation of CARM1 and LSD1 (histone lysine demethylase 1) by PKA [462]. Phosphorylated CARM1 binds to and activates ER $\alpha$  [462, 463]. CARM1 dimethylates LSD1, allowing the binding of the deubiquitinase USP7, resulting in LSD1 stabilization [542]. LSD1 stabilization leads to an epithelial-to-mesenchymal transition which regulates invasion and metastasis [542]. The levels of methylated LSD1 correlate with tumor grade in human breast tumors [542]. *PTGER4* is required for the proliferation of the luminal MCF7 breast cancer cells subjected to long-term estrogen deprivation (LTED), through PKA-mediated activation of CARM1, which binds to ER $\alpha$  and promotes ligand-independent activation of ER response genes [543]. CARM1 has been more extensively studied in estrogen-stimulated luminal cells, where it has been shown to bind to liganded ER $\alpha$  and to activate ER $\alpha$ -dependent gene transcription. Several proteins have been reported to associate with CARM1 to enhance ER $\alpha$  transactivation such as PELP1 [544], FOXM1 [545], p53 [546], DZIP3 [499], and others. AIB1 binds liganded nuclear hormone receptors and facilitates transcription by the histone acetyltransferases CBP/p300 and CARM1 [497]. AIB1 is methylated *in vitro* by CARM1 in a glutamine-rich region which is conserved among all steroid receptor coactivator proteins, and *in vivo* in MCF7 cells [497]. The methylation of AIB1 leads to its degradation and impairs its association to CBP [497]. Upon estrogen stimulation and depending on the presence of AIB1, CARM1 dimethylates histone H3 (H3R17me2a) at the *E2F1* promoter [547]. By analyzing MCF7 cells treated or not with estrogen, a recent comprehensive study confirms that CARM1 binds to ER $\alpha$ -bound active enhancers upon estrogen treatment leading to transcriptional activation [147]. Further, the authors identified 780 potential CARM1 partners/substrates involved in the regulation of intracellular estrogen receptor-mediated signaling, chromatin organization and chromatin remodeling [147]. JMJD6 allows the binding of CARM1 to MED12 [548], and the CARM1-mediated methylation of MED12 allows the recruitment of the tudor-domain-containing protein 3 (TDRD3), to CARM1-bound active enhancers to activate estrogen/ER $\alpha$ -target genes [147]. CARM1 is essential for estrogen-induced cell cycle progression in the MCF7 breast cancer cell line [547]. The depletion of CARM1 in MCF7 cells impairs proliferation, induces a G1 arrest, and delays tumor growth [147].

#### 1.31.1.2 *Her2+ breast cancer*

The oncogenic potential of some type I PRMTs (PRMT1, CARM1, PRMT6) has been evaluated in a Her2-driven mammary gland tumorigenesis model (NIC mice). Compared to NIC mice alone, PRMT1 and PRMT6 accelerated tumorigenesis and increased tumor growth [291]. However, CARM1 delayed tumor initiation but the tumors grew more quickly once the tumor was established suggesting that CARM1 might play a dual role in tumorigenesis, i.e., there might be a certain threshold level of CARM1 (or other proteins) which when exceeded causes rapid tumor growth [291]. The PRMT1- and PRMT6-dependent tumorigenesis involved the PI3K/Akt pathway and the regulation of cell-cycle,

but this was not the case for CARM1-dependent tumorigenesis [291]. CARM1 overexpression alone was sufficient to promote tumorigenesis, albeit with a long latency (>20months) period [291]. This elegant study demonstrates that CARM1 is involved in the tumorigenesis of Her2-driven breast tumors.

### 1.31.1.3 TNBC

Very few studies have been performed in TNBC cells although higher expression of CARM1 mRNA has been associated with TNBC and Her2-positive breast tumors [531, 533]. Nevertheless, CARM1 has been reported to be required for the migration of the TNBC cell line, MDA-MB-231 [147].

### 1.31.2 Ovarian cancer

An elegant study comparing CARM1-expressing OC cells to their counterpart CARM1 knockout cells revealed that two EZH2 inhibitors impaired cell viability and tumor growth specifically towards CARM1-expressing cells/tumors [489]. Importantly, the ectopic expression of CARM1 in OC cells expressing low levels of endogenous CARM1 sensitizes the cells to EZH2 inhibitors [489]. These results indicate that CARM1 expression could represent a biomarker of response to EZH2 inhibitors [489]. Further, *CARM1* amplification appears to be mutually exclusive to *BRCA1/2* mutation in these OC samples [489, 549].

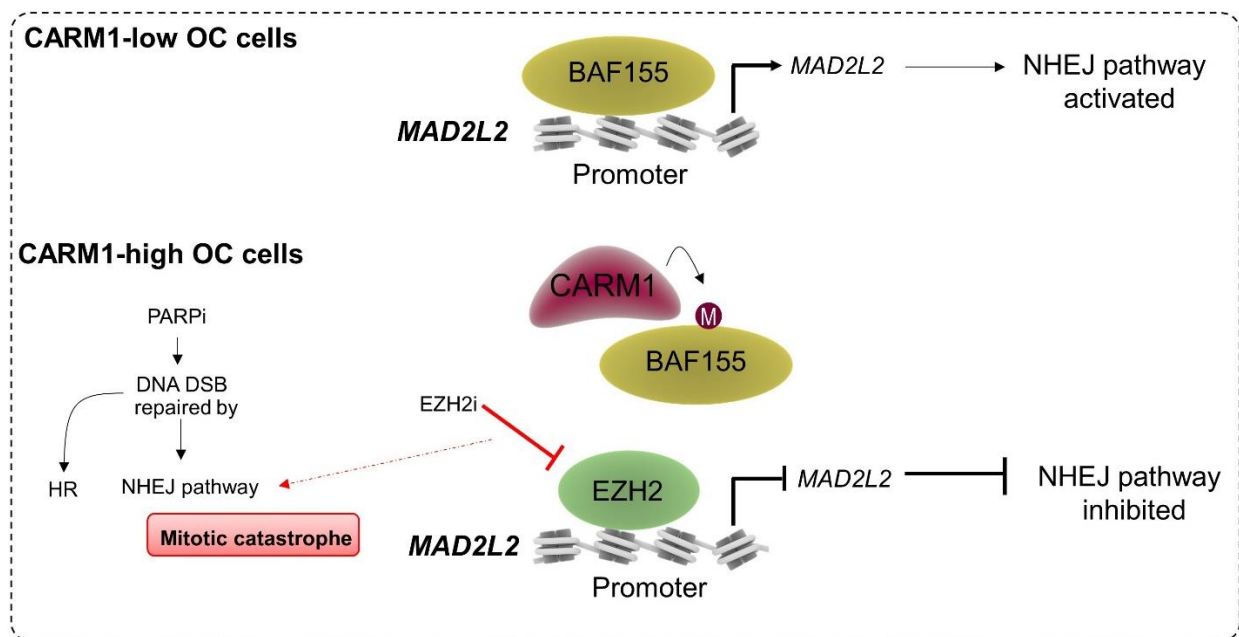


**Figure 45: CARM1 is a biomarker of response to EZH2 inhibition in ovarian cancer.** In CARM1 low ovarian cancer (OC) cells, BAF155 binds to the MAD2L2 promoter to activate its transcription and NHEJ. In CARM1 high OC cells, CARM1 methylates BAF155, leading to EZH2 binding to MAD2L2 promoter, inhibiting NHEJ. Inhibiting EZH2 activates the NHEJ pathway and cells depend on homologous recombination for

DNA repair which is inhibited by PARP inhibitors. DSB: double-strand break, NHEJ: non-homologous end-joining, PARP: Poly (ADP-ribose) polymerase; HR: homologous recombination.

DNA double-strand breaks (DSB) are repaired by either error-free HR or error-prone non-homologous end-joining (NHEJ) pathways. *MAD2L2*, which activates the NHEJ pathway, is either silenced by EZH2 or activated by unmethylated BAF155 [549]. Promoter occupancy of *MAD2L2* switches from BAF155 to EZH2 upon BAF155 methylation by CARM1, silencing *MAD2L2* expression and thus NHEJ [489, 549]. Therefore, high levels of CARM1 in cells will promote NHEJ silencing, which is reversed upon EZH2 inhibition [549] (**Figure 45**). Altogether, their results suggest that EZH2 and PARP inhibitors could be used in combination as a new treatment strategy for CARM1-high OC [549].

### 1.31.3 Other solid cancer

CARM1 depletion impairs colony formation and tumor growth in CRC [476]. The miRNAs - miR-195-5p and miR-195, target CARM1 for degradation in CRC, hence an overexpression of these miRNAs impair cell survival in CRC [476, 477]. Further, CARM1 interacts with  $\beta$ -catenin and/or androgen receptors to enhance their respective transcription programs in CRC, prostate, and bone cancer [201, 202, 537, 550].

In oral cancer, CARM1 depletion does not affect proliferation but rather impairs their migration [538]. Furthermore, CARM1 and the transcription factor YY1 co-regulate each other in oral cancer [538]. YY1 positively regulates the mRNA of CARM1, while CARM1 methylates YY1 and co-activates its transcription [538].

### 1.31.4 Hematopoietic cancer

CARM1 protein is overexpressed in Hodgkin Reed-Sternberg cells and Hodgkin's lymphoma [232] and CARM1 mRNA is upregulated in acute myelogenous leukemia (AML) patient samples [478]. CARM1 depletion minimally affects normal hematopoiesis but strongly impairs leukemogenesis by regulating cell-cycle progression, myeloid differentiation, and apoptosis [455, 478]. Small molecule CARM1 inhibitors (competitive for the substrate arginine binding pocket) impair proliferation, both *in vitro* and *in vivo*, in a multiple myeloma (MM) xenograft model [343], AML mouse model [455], and diffuse large B-cell lymphoma (DLBCL) model [551]; however, only a subset of MM [343, 344] or DLBCL cells [551] are sensitive. The mutation of CBP/p300 sensitizes DLBCL cells to CARM1 inhibition [551]. Unsurprisingly, combining CARM1 and CBP/p300 inhibitors is lethal for DLBCL WT cells [551], suggesting that CARM1 inhibition could be more effective in tumors with certain mutational statuses. CARM1 methylates PRMT5 in human erythroleukemia cells, *in vitro* and *in vivo*, and such methylation is necessary for PRMT5 homodimerization and activity [154]. Therefore, CARM1 inhibition may also inhibit PRMT5, suggesting crosstalk between the various PRMTs. It has been recently shown that targeting both Type I PRMTs and PRMT5 specifically kill AML cells mutated for splicing factors [436]. Overall,

these data suggest that targeting CARM1 could be a potential therapeutic strategy alone, or in combination, for a subset of hematopoietic tumors.

#### **1.31.5 Liver and pancreatic cancer**

In contrast to the above-mentioned cancer types, CARM1 protein is found at lower levels in human liver cancer [512] and pancreatic ductal adenocarcinoma (PDAC) [513] than in normal tissue. CARM1 regulates glycolysis in liver cancer through the methylation of GAPDH, delaying tumor cell proliferation *in vitro* and *in vivo* [512]. In pancreatic cancer, the inhibition of MDH1, through CARM1-mediated methylation, prevents glutamine metabolism and suppresses cell proliferation [513]. Thus, stimulating CARM1 activity has been proposed as a therapeutic approach against PDAC and liver cancer.

### **1.32 Concluding remarks**

In almost 60 years, the vital role of protein arginine methylation has been highlighted in numerous processes central to the normal functioning of cells. PRMTs as a family are gaining tremendous importance in both the field of basic and translational research given their contribution in diseases conditions, particularly cancer. Nevertheless, we have barely scratched the surface of their cellular roles and by discovering the entire methylome of these enzymes, we will uncover novel mechanisms and pathways.



## VI. ALIX: a multifunctional adaptor protein

A major finding in my thesis was identifying the protein ALIX as the principal protein partner of CARM1. Therefore, in this chapter, I will describe the structure, domains and known cellular functions of ALIX.

ALIX was first discovered by a yeast two-hybrid screen as an interacting protein to the apoptosis-linked gene 2 (ALG-2) and hence its name, ALG-2 interacting protein X (**ALIX**) [552, 553]. It is often also referred to as ALG-2 interacting protein 1 (**AIP1**), programmed cell death 6 interaction protein (**PDCD6IP**), or **Hp95**. ALIX localizes to the cytosol, and it is highly conserved through evolution having orthologues in fungi, yeast, worm, fruit flies, and amphibians [553, 554]. ALIX was identified to require the presence of calcium for its interaction with ALG-2 and the complex was involved in apoptosis [552]. It has now been described to play a role in apoptosis, multivesicular body (MVB) formation, organization of the actin network, budding of viruses, plasma membrane repair, and regulating mitotic spindle and cytokinesis [555, 556]. ALIX serves as an adaptor protein for many of these above-mentioned functions, acting as a bridging molecule for downstream effectors, but has no enzymatic activity of its own [557].

Although ALIX is important for cellular functions it is not essential for development, since ALIX knockout mice and drosophila are viable [558-560]. However, ALIX KO mice have severe microcephaly and decreased brain volume since ALIX is required for the growth of neuronal progenitor cells [558]. This can be perhaps explained by the fact that there are proteins similar to ALIX in the cell that compensate for ALIX function, such as Brox and HD-PTP, which have similar domains and protein partners as ALIX [561, 562] (**Figure 46**).

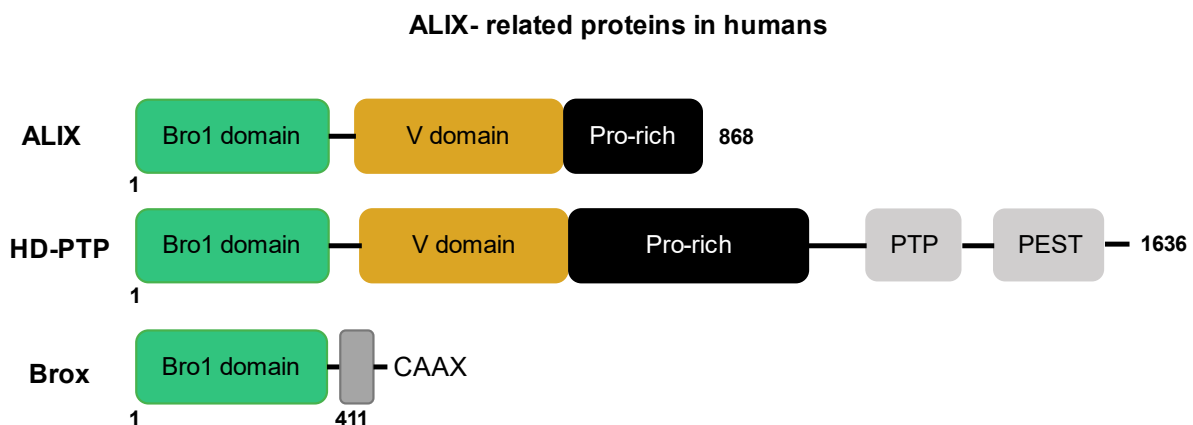


**Figure 46: ALIX-related proteins in humans.** Domain architecture of ALIX, HD-PTP, and Brox sharing homology domains (Bro1, V, and Pro-rich). HD-PTP contains a larger pro-rich domain than ALIX and an additional protein tyrosine phosphatase domain (PTP) and a PEST motif (Pro-Glu-Ser-Thr; putative signal

peptide for protein degradation). Brox contains a thioester-linkage site of isoprenoid lipid (CAAX motif; C, Cys; A aliphatic residue; X any residue).

### 1.33 Structure, domains and the interactome of ALIX

ALIX has 868 amino acids and sequence alignment shows that it was highly similar to the yeast protein, Bro1 [552]. It is composed of three domains: an N-terminal Bro1 domain (homologous to the yeast Bro1p), a central V domain and a C-terminal proline-rich domain (PRD or PRR – proline-rich region) [563] (**Figure 47**). The Bro1 and V domains are found to be discrete entities but none of the constructs that contained the PRD was well-expressed in *E. coli* suggesting that the PRD is disordered [563]. In fact, to date, the crystal structure of full-length ALIX (including all residues of the PRD) has not been solved owing to the disorderliness of the PRD. However, recently, Elias and colleagues successfully obtained the nuclear magnetic resonance (NMR) spectrum of the PRD by splitting it into two fragments, N-terminal (residues 703-800) and C-terminal (residues 800-868) [564].

**A**

#### ALIX domains

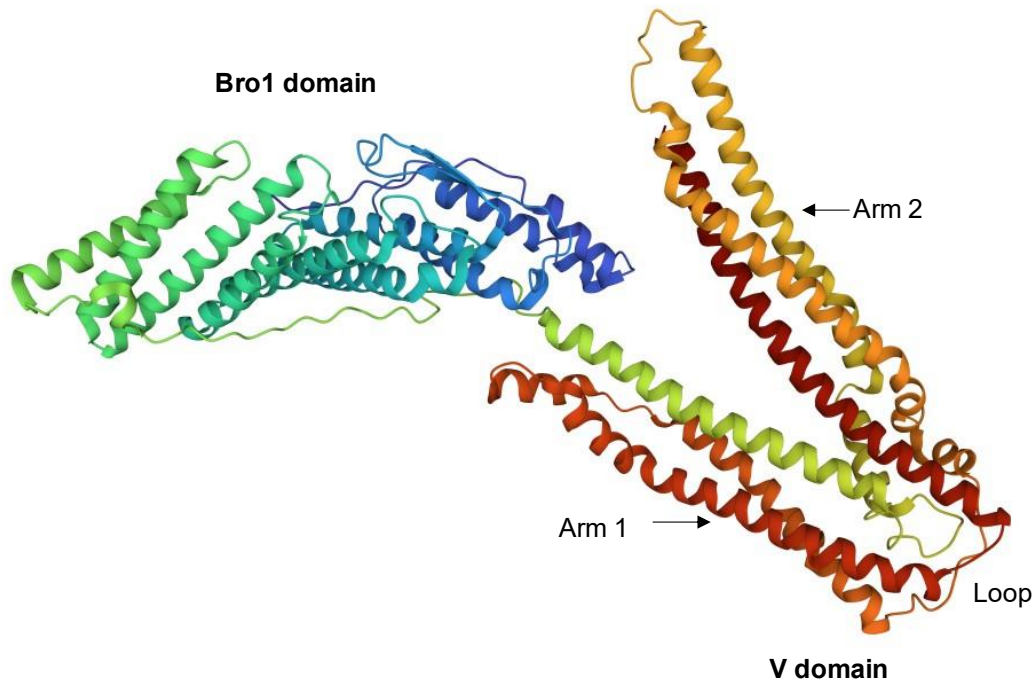


Protein partners :

CHMP4B  
Src (SH2)  
LBPA  
Nedd4-1

Syntenin-1  
GPCRs  
(PAR1, P2Y1)  
Viral Gag proteins

ESCRT-I  
(Vps37, TSG101)  
Src (SH3)  
CIN-85  
CD2AP  
Endophilins  
ALG-2  
Arrestins  
Cep55

**B****ALIX crystal structure (Bro1+V domain)**

**Figure 47: Domains and structure of ALIX.** (A) ALIX has 3 domains, an N-terminal Bro1, a central V domain, and a C-terminal proline-rich domain (PRD). Each domain has unique binding partners, with the PRD being the most important site for several of these interactions. The V domain contains a dimerization arm (indicated as D in the figure). (B) The crystal structure of ALIX<sub>Bro1-V</sub>, solved by Fisher and colleagues (PDB ID: 2OEV). The V-domain contains two arms connected by a linker loop [563].

### 1.33.1 Bro1 domain of ALIX

The Bro1 domain is highly similar in sequence and structure to Bro1p of yeast [565]. Like yeast Bro1p, ALIX<sub>bro1</sub> is organized around a core tetratricopeptide repeat (TPR) within its helical hairpin regions [563] (**Figure 48A**). The most crucial part of the Bro1 domain is the two exposed hydrophobic patches it contains that are centred around Phe199 (patch 1) and Tyr319 (patch 2) [563] (**Figure 48B**). Similar to Bro1p binding to Snf7, patch 1 of ALIX<sub>bro1</sub> binds to Endosomal Sorting Complex Required for Transport (ESCRT) III subunit, CHMP4B (the human homologue of Snf7) [565]. In addition, this region also binds to the paralogues of CHMP4B, CHMP4A and CHMP4C [566-568]. Notably, this hydrophobic patch recognizes the motif M/L/IxxLxxW in CHMP4, not present in the other CHMP proteins, explaining the specificity of ALIX towards CHMP4 [565, 566]. Moreover, among the CHMP4 paralogues, CHMP4B is the major partner of ALIX<sub>bro1</sub> [567]. The second hydrophobic patch acts as a docking site for the SH2 domain of Src kinase when it phosphorylates ALIX<sub>bro1</sub> at Tyr319 [569]. Bro1 domain is also the site of interaction with other partners like the lipid phospholipid lysobisphosphatidic acid (LBPA) [570] and the ubiquitin ligase Nedd4-1 [571].

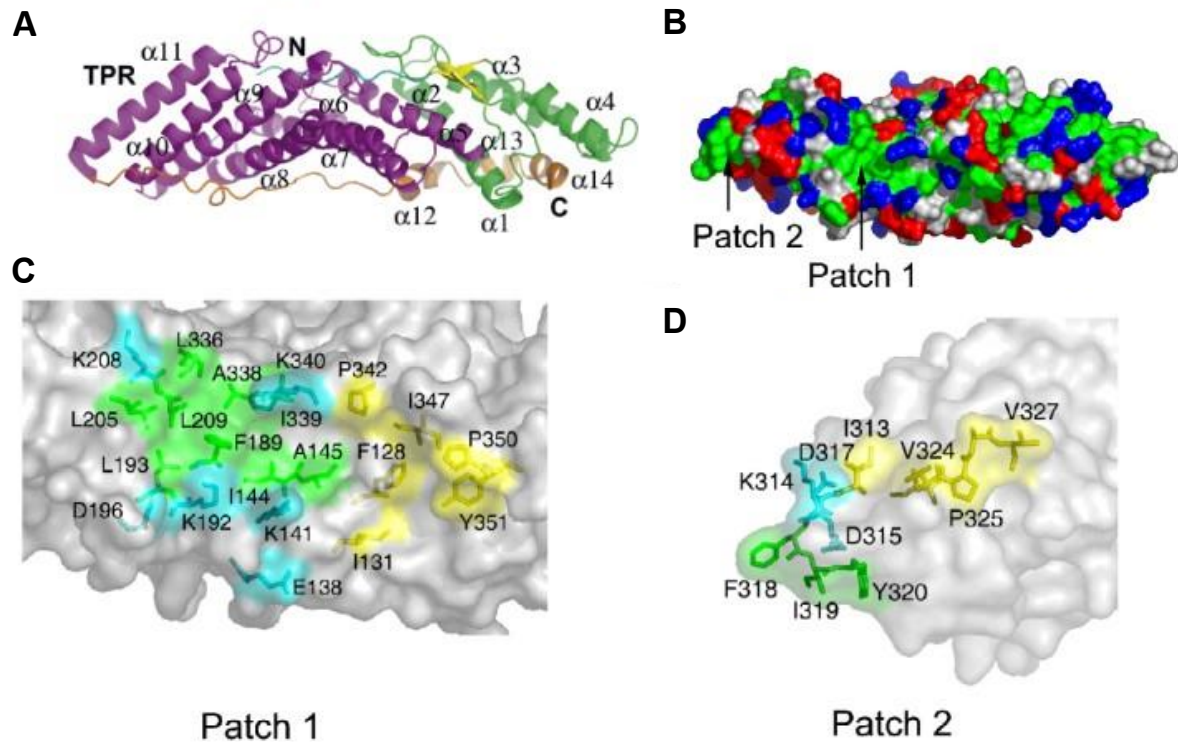


**Figure 48: Structural architecture of ALIX bro1 domain.** (A) Secondary structure of Bro1 domain where the N-terminal region is colored cyan; the N-terminal (non-TPR) region of the helical solenoid is colored green; the  $\beta$  sheet is colored yellow; the TPR domain is colored magenta; the C-terminal region is colored orange. (B) Molecular surface of the Bro1 domain colored according to residue property and indicating the two hydrophobic patches (green: hydrophobic, blue: basic, red: acidic, white: uncharged polar). (C) Close-up of hydrophobic patch 1. (D) Close-up of hydrophobic patch 2. Modified and adapted from [565].

### 1.33.2 V domain

The V domain of ALIX forms an actual “V-shaped” structure with two asymmetric “arms” connected by a loop region [563, 572, 573] and contains two coiled-coil (cc) regions [573]. The importance of this V-shaped structure is two-fold: (i) it provides flexibility to ALIX structure, giving it an open and closed conformation [574, 575], and (ii) brings the N-terminal Bro1 domain in close proximity to the C-terminal PRD [563] (**Figure 49**).

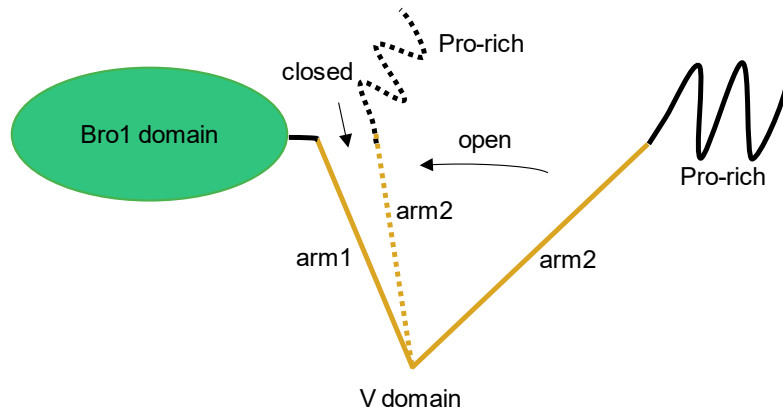


**Figure 49: Open and closed conformations of ALIX V domain.** Arm2 of the ALIX V domain rotates from an open to closed conformation.

Moreover, ALIX dimerizes via its V domain and mutating residues in this interface prevents dimerization leading to an elongated structure [574, 575]. ALIX function is thought to be regulated partially by its conformation state (open or closed) and dimerization [574, 575]. The open conformation and dimerized ALIX are considered as the active form, as they interact with their protein partners successfully for downstream functions [574, 575]. This domain has a high affinity for proteins containing the LYPX<sub>n</sub>LXXL motif, such as GAG proteins in retroviruses [563], G protein-coupled receptors (PAR1, P2Y1) [576, 577], and adaptor proteins (Syntenin) [578].

### 1.33.3 Proline-rich domain

Possibly, the most important domain for ALIX is its PRD, as this is the region where most of its protein-protein interactions occur. These interactions include **ALG-2** [579, 580], ESCRT-I complex (Vacuolar Protein Sorting factor 37- **VPS37**, Tumor Susceptibility Gene 101 - **TSG101**) [581, 582], **Src** (SH3 domain) [569], **Centrosomal protein 55 (Cep55)** [583-585], **CD2-associated protein (CD2AP)** [585, 586], **Cbl-interacting protein of 85kDa (CIN-85)** [587], **Endophilins** [588], and **Arrestins** [589] (**Figure 47A**). As previously mentioned, owing to the disordered nature of this region, there is no solved crystal structure containing this domain. In the recent NMR analysis of the PRD, they identified a few key features of the PRD in solution [564]. The N-terminal fragment (703-800) has three PTAP like motifs that all compete to bind to the UEV domain in the ESCRT-I protein, TSG101, and it is P<sup>717</sup>SAP<sup>720</sup> that is the primary contact site with TSG101 [564]. Further, the C-terminal fragment (800-868), rich in tyrosine residues appears to aggregate in solution forming rope-like structures [564]. Aggregation could possibly be important for enhancing ALIX's binding to the ESCRT proteins, CHMP4 and TSG101 [564], but remains to be elucidated *in vivo*. Interestingly, the tyrosine kinase Src not only binds to ALIX<sub>bro1</sub> but also to the PRD via its SH3 domain to phosphorylate this region [569].

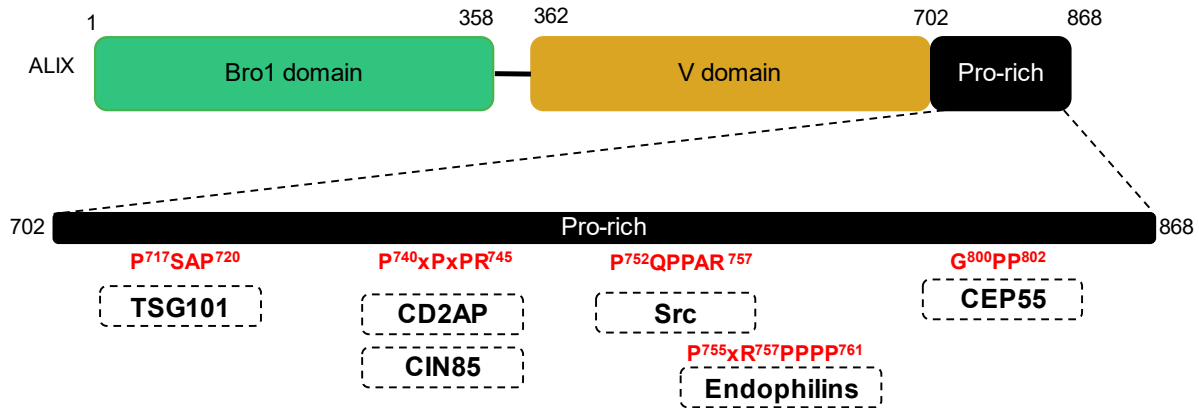


**Figure 50: Proteins interacting with the proline-rich domain of ALIX.** A close-up of the pro-rich shows the different motifs and binding regions for its protein partners.

### 1.33.4 Consequences of protein-protein interactions at the PRD

ALIX regulates cellular functions such as viral budding, biogenesis of exosomes or MVB formation and others by interacting/recruiting several effector proteins, particularly through its C-terminal PRD.

The PTAP motif, P<sup>717</sup>SAP<sup>720</sup> at the N-terminal of the PRD interacts with TSG101 (**Figure 50**) with a low affinity [564, 582, 585, 590, 591] but dimerization of ALIX significantly improves their binding [564, 584]. Further, ALG-2 has been shown to promote ALIX binding with TSG101 or indirectly with the other ESCRT-I complexes (VPS37) in a Ca<sup>2+</sup> dependent manner [581]. The interaction between ALIX and TSG101 is important for cytokinesis but dispensable for virus budding [584], suggesting that different combinatorial interactions between ALIX and its partners help in the regulation of these processes.

The residues surrounding Arg<sup>745</sup> (P<sup>740</sup>xPxPR<sup>745</sup>) are the binding region for two partners, CD2AP [585, 586] and CIN-85 (also known as SETA or Ruk) [587, 592, 593] (**Figure 50**). CD2AP and CIN-85 are homologues of each other, containing SH3 domains that aid in binding to the PRD of ALIX and function as adaptor proteins [586]. Despite their similarity, they aid in different downstream functions of ALIX. For example, by interacting with CIN-85, ALIX blocks the internalization/ubiquitination of EGFR [594]. CD2AP, on its own, is required for MVB biogenesis [595] and cytokinesis [596], but the functional impact of the interaction between ALIX and CD2AP is yet to be studied. The ALIX (P<sup>744</sup>→AR<sup>745</sup>→A) mutant which can no longer bind CD2AP, fully rescues cells cytokinetic defects, such as abnormal midbodies or multinucleated cells [584]. CD2AP can also interact with TSG101 [585], perhaps explaining why the ALIX/CD2AP interaction was dispensable for cytokinesis, leading to the speculation that when CD2AP can no longer bind to ALIX, it

interacts with TSG101, to perform the same function (although the function of CD2AP in cytokinesis is unknown).

Possibly the most crucial interaction occurring at the PRD is with Cep55, at least from the context of cytokinesis, since it is Cep55 that recruits ALIX to the midbody structure (**see Cytokinesis**) [583]. Cep55 binds to the c-terminal end of the PRD (G<sup>800</sup>PP<sup>802</sup>) (**Figure 50**) and when the proline is mutated (G<sup>800</sup>VD<sup>802</sup>), Cep55 can no longer recruit ALIX and causes major cytokinetic defects [584, 585].

The residues surrounding Arg757 (P<sup>755</sup>xR<sup>757</sup>PPPP<sup>761</sup>) provide the binding motif for the Endophilins, A1, A2, and A3 (**Figure 50**) and understandably, mutating R<sup>757</sup>→Ap<sup>758</sup>→A impairs this binding [563, 588].

Arrestin-related proteins (ARRDC 1, 2, and 3) bind to the PRD domain at an as yet unknown motif and could regulate viral budding [589], but has no implications in cytokinesis, yet.

Some protein partners that interact with the different domains of ALIX, such as Src kinase or Nedd4-1 ubiquitin ligase are also involved in regulating the function of ALIX by changing its conformation and this will be discussed in the next section.

### 1.34 Post-translational modifications and their repercussions

The major post-translational modifications occurring on ALIX are phosphorylation and ubiquitination, with one report suggesting palmitoylation (**Figure 51**).

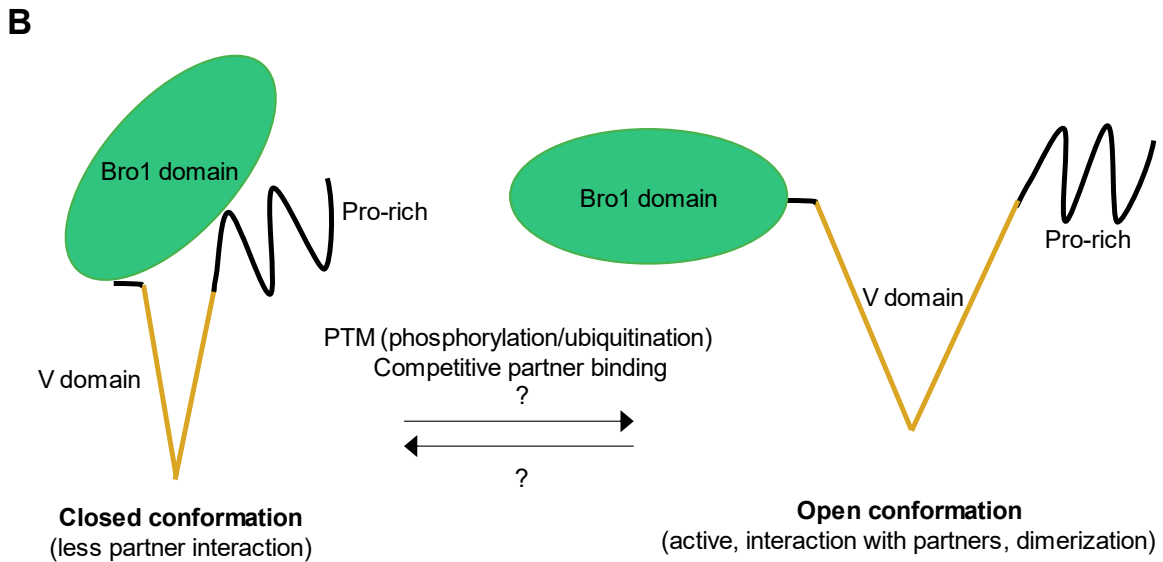
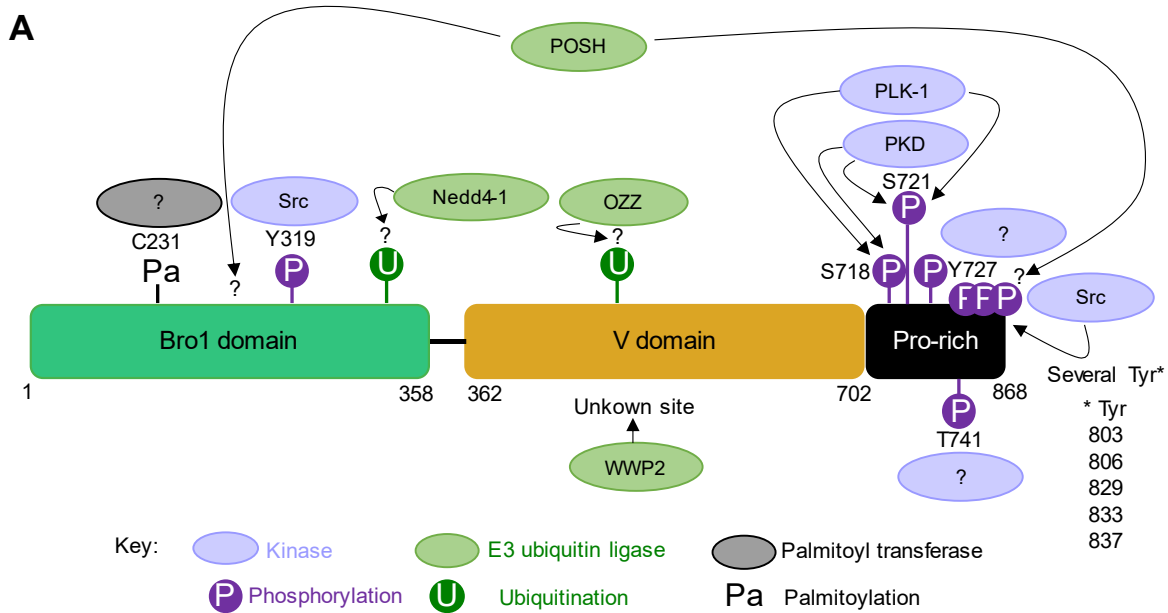


**Figure 51: Post-translational modifications and conformations of ALIX.** (A) Various PTMs occurring on ALIX in its different domains with the enzymes responsible indicated when known. (B) The closed conformation of ALIX where the hydrophobic patch 2 in its Bro1 domain binds to the TSG101 site in the PRD causing autoinhibition. Upon PTMs like phosphorylation or ubiquitination, ALIX adopts an open conformation making it active and allows access for its various binding partners. The events leading to a closed conformation are still unknown, *in vivo*.



### 1.34.1 Phosphorylation

The Src family kinases like Src [569, 597], Hck [598], and Fyn [598] have been shown to bind to the PRD region of ALIX, particularly via the motif P<sup>752</sup>QPPAR<sup>757</sup> [569] (**Figure 50**). However, apart from Y319 [569], no other tyrosine residue has been specifically mapped to be methylated by Src family kinases. However, the c-terminal region of the PRD (residues 800-868) is rich in tyrosines (14 residues), and is phosphorylated by Src, *in vitro*, and mapped to Tyr 803, 806, 829, 833, and 837 [564]. Further, Src-mediated phosphorylation on these residues helped in dissolving the aggregates observed in the solution [564]. This might have important physiological implications, particularly in binding to different partners to regulate cytokinesis/viral budding but is yet to be demonstrated. Notably, Y727 in the PRD is phosphorylated (102 references) by several large-scale studies as indicated in PhosphositePlus ([www.phosphosite.org](http://www.phosphosite.org)) [599], but the kinase responsible is yet to be identified. As mentioned above, Src binds to both the Bro1 and PRD domain of ALIX (and the V domain aids in bringing these two extremities close together), but when Y319 in the Bro1 domain is mutated (Y<sup>319→F</sup>), the interaction and phosphorylation are lost [569, 600]. In *Xenopus*, the homolog of ALIX (xp95) is phosphorylated on T745 by an unknown kinase, and sequence homology identified T741 of human ALIX<sub>PRD</sub> to be correspondingly modified [601]. This phosphorylation impaired xp95 binding to CIN-85 in *Xenopus* [601], but we do not know if this is true for human ALIX/CIN-85 interaction. During mitosis, two serine residues within the PRD (S718, S721) are phosphorylated by at least Polo-kinase 1 (PLK1) and Protein kinase D (PKD) (but also other kinases active during mitosis) [575]. This phosphorylation event causes the “activation” of ALIX by opening its conformation (**Figure 51B**). ALIX is shown to have an auto-inhibitory role when the hydrophobic patch 2 in its Bro1 domain intramolecularly binds to the TSG101 site within the PRD [575, 600, 602]. Thus, the open or closed conformation of ALIX affects its binding to partners like CHMP4B or TSG101, thereby impacting its role in cytokinesis or viral release [575, 600, 602].

### 1.34.2 Ubiquitination

Another PTM that “activates” ALIX is ubiquitination (**Figure 51B**). Several E3 ubiquitin ligases modify ALIX, such as Ned44-1 [571], POSH [603], Ozz [604], and WWP2 [605]. Although the exact lysine residues are still unknown, we know the domains ubiquitinated by some of these E3 ligases (WWP2 site is still unknown). Ned44-1 modifies in the Bro1 domain [571], Ozz possibly in the V domain [604], and POSH both in the Bro1 and PRD regions [603]. However, unlike the most common notion that ubiquitinated proteins are targeted for degradation, ubiquitinated ALIX serves several functions like enhancing the release of viruses [571, 603] or regulating remodeling of the cytoskeleton (ALIX dependent) [604]. Further, ALIX also interacts directly with ubiquitin monomers or polyubiquitin chains of Lys63 via its V domain [606, 607] and this interaction induces ALIX dimerization, *in vitro* [606], further reinforcing the idea that ubiquitin activates ALIX.

Notably, ALIX can bind to ubiquitinated EGFR to regulate its sorting through MVBs [608]. On the contrary, ALIX interacts with the deubiquitinase AMSH [601], possibly responsible for ALIX deubiquitination, and thus its deactivation, but yet to be demonstrated.

### 1.34.3 Palmitoylation

A recently identified modification is S-palmitoylation on Cys231 in the Bro1 domain by an unknown Palmitoyl transferase [609] (**Figure 51A**). This modification aids in the interaction between ALIX and the exosome membrane marker CD9, and possibly also in ALIX dimerization [609].

### 1.34.4 Methylation

Apart from the above-mentioned modifications, several large-scale proteomic studies have identified lysine and arginine residues on ALIX to be methylated and many of these (not all) have been documented on the Phosphosite website (<https://www.phosphosite.org>). However, it must be noted that these have not been manually validated and their functional relevance is not yet known. As my thesis focuses on arginine methylation and not lysine methylation, I will only list the arginine sites reported to be methylated (**Table 1**).

**Table 1: Summary of arginine methylation sites identified on ALIX**

Arg	Sequence	Domain	Methylation (MMA, DMA, both)	Refs
R322	NDFIyHDRV <b>P</b> DLkDL	Bro1	MMA	[114]
R456	EILDESL <b>R</b> LLDDEEEA	V	MMA	[114]
R606	LSVTELD <b>R</b> VyGGLtt	V	MMA	[114]
R745	tPPtPAP <b>R</b> <sup>3,4,5</sup> TMPPTkP	PRD	Both	[114, 147, 148, 610, 611]
R757	TkPQP <b>P</b> A <b>R</b> <sup>3,6,7</sup> PPPPVLP	PRD	Both	[114, 147, 148, 610-612]
R767	PPVLPAN <b>R</b> <sup>8</sup> APSATAP	PRD	MMA	[114, 613]

<sup>3</sup> MMA site is dependent on PRMT5 and PRMT7 [148].

<sup>4</sup> MMA site is lost in MCF7-CARM1 knockout cells [147].

<sup>5</sup> One of these sites are also DMA (not specified which) but the methylation is lost in MCF7-CARM1-KO cells [147].

<sup>6</sup> MMA site is abolished in cells depleted for CARM1 and is dependent on both CARM1 and PRMT7. DMA site is dependent on PRMT5 [148]

<sup>7</sup> MMA site is lost in MCF7-CARM1 knockout cells [147]

<sup>8</sup> MMA site is downregulated upon PRMT5 inhibition [613].

These arginine methylation sites, particularly those within the PRD suggest that ALIX could be a substrate for CARM1 or other PRMTs (see the footnotes) and that methylation could be a novel post-translational modification occurring on ALIX.

Together, this suggests that the PTMs occurring on ALIX are controlling its various protein-protein interactions and thus regulating its function in the different cellular processes.

### 1.35 Cellular functions

ALIX is a multifunctional protein and functions as an adaptor protein mainly to link the different ESCRT subunits to aid in different membrane deformation processes like the **budding of retroviruses, formation of exosomes and MVBs, membrane repair and cytokinetic abscission** (Figure 52). The major functions involving the ESCRT family and ALIX all share the same membrane topology, similar protein complexes and many parallels between these processes can be observed [555, 556, 614, 615]. Although most of the protein complexes are the same, there is usually one protein unique to each process. For instance, during viral budding, it is the viral Gag proteins that recruit ALIX and TSG101, which in turn recruit ESCRT-III subunits while during cytokinesis, it is Cep55 which does the function of the Gag proteins [584].

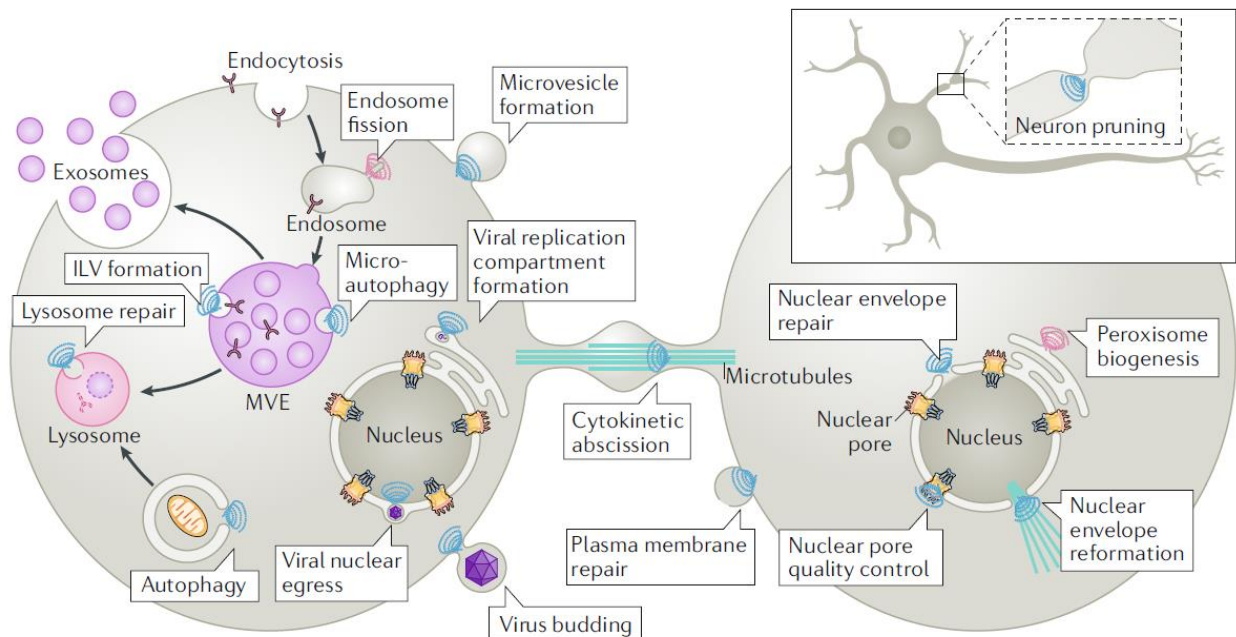


**Figure 52: The major functions of ESCRT proteins where ALIX is also involved.** The blue helices are indicative of the ESCRT-III at each of the shown processes and ALIX plays a role in all these functions by interacting with the ESCRT proteins. Adapted from [556]

Interestingly, all the cellular processes that ALIX is associated with depends on the function of its interacting partners. For example, ALIX is implicated in **apoptosis** (by interacting with ALG-2) [552, 553], **growth factor receptor recycling** (through CIN-85 binding) [594], and **cytoskeletal remodeling** (binding to actin/F-actin) [559, 592, 604, 616, 617]. ALIX directly binds to actin, cortactin, and alpha-actinin [592, 616] or perturbs the filamentous actin (F-actin) network [604, 616, 617]. In ALIX KO mice, several abnormalities in the epithelium are observed like asymmetrical size and shape of cells, the abnormal beating of cilia, and others indicating that ALIX is needed to ensure proper cell-cell junctions [559]. Further, ALIX negatively regulates cell adhesion [592]. Both ALIX and CIN-85 localize to focal adhesion points [587] and associate with the tyrosine kinases FAK and Pyk2 [592]. While overexpressing CIN-85 promotes cell adhesion, this effect is reversed when ALIX is overexpressed [592].

Similarly, by interacting with CIN-85, ALIX negatively regulates the recycling of growth factor receptors like EGFR [594] (**Figure 53**). Briefly, ALIX directly binds to CIN-85 via its PRD [587, 618], disrupting the interaction between the ubiquitin ligase Cbl and CIN-85 or another region in the PRD of ALIX interacts with the endophilin's [588], which could interrupt the CIN-85/endophilin complex (**Figure 53A**). Thereby, ALIX promotes signaling by EGFR. Conversely, activated EGFR binds to the ubiquitin ligase Cbl which ubiquitinates EGFR and recruits the adaptor CIN-85 and endophilins, causing downregulation of EGFR activity (by endocytosis and then lysosomal-mediated degradation) [619] (**Figure 53B**). This process occurs by Src-mediated hyperphosphorylation on the ALIX PRD which impairs its interaction with CIN-85, thereby promoting EGFR internalization [569] (**Figure 53B**).

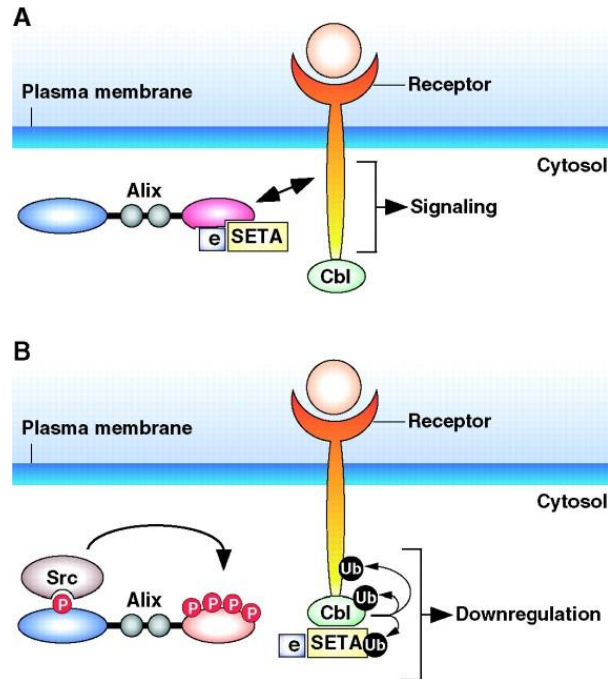


**Figure 53: Schematic of EGFR recycling mediated by ALIX and its partners.** (A) ALIX binds to SETA (CIN-85), endophilins (e), or indirectly to EGFR, enabling constitutive downstream signaling and preventing the degradation of EGFR. (B) Src binds to the phosphorylated Y319 at its Bro1 domain and hyperphosphorylates the PRD, preventing ALIX interaction with both CIN-85 and endophilins. Free CIN-85/endophilin complex can bind to Cbl to ubiquitinate EGFR and leads to its downregulation. Adapted from [557].

Since it was discovered as an interacting partner of ALG-2 [552, 553], a protein required for inducing apoptosis [552], ALIX is thought to promote apoptosis. While increased endogenous expression correlates with cell death, overexpressing ALIX elicits pro-apoptotic signals [580, 620]. Surprisingly, a truncated form of ALIX (lacking its Bro1 domain) shows anti-apoptotic activity [552, 580, 620]. But the exact mechanism behind this is still not understood, though there is speculation that this process could be mediated by endosomes [557].

### 1.35.1 Budding of viruses

We now know that viruses hijack several cellular machineries of the host cell for their replication cycle [621]. One such machinery that is hijacked is the ESCRT complex [622, 623]. Three types of mechanisms are used by the viruses, but ALIX is implicated only in two of these: (i) exit from the outer nuclear membrane (**Figure 54a**), and (ii) budding from the plasma membrane (**Figure 54c**) (not implicated in the formation of viral replication compartment, **Figure 54b**) [556]. The first mechanism is used by the herpes simplex virus (HSV) and Epstein-Barr virus (EBV) to bud across the nuclear membrane (**Figure 54a**). In HSV-1, several viral proteins form the nuclear egress complex (NEC) to aid in the membrane budding across the inner nuclear membrane (INM) [624, 625]. Membrane

deformation and its subsequent scission require the ESCRT-III subunit, CHMP4B, which is recruited by ALIX and the ATPase VPS4 [626]. Similarly, the NEC of EBV interacts with the bro1 domain and PRD of ALIX to aid in the nuclear membrane egression [627, 628]. Consequently, when ALIX is depleted, neither HSV-1 nor EBV can bud out of the INM and their viral capsid proteins accumulate at the edge of the nucleus [626, 628].

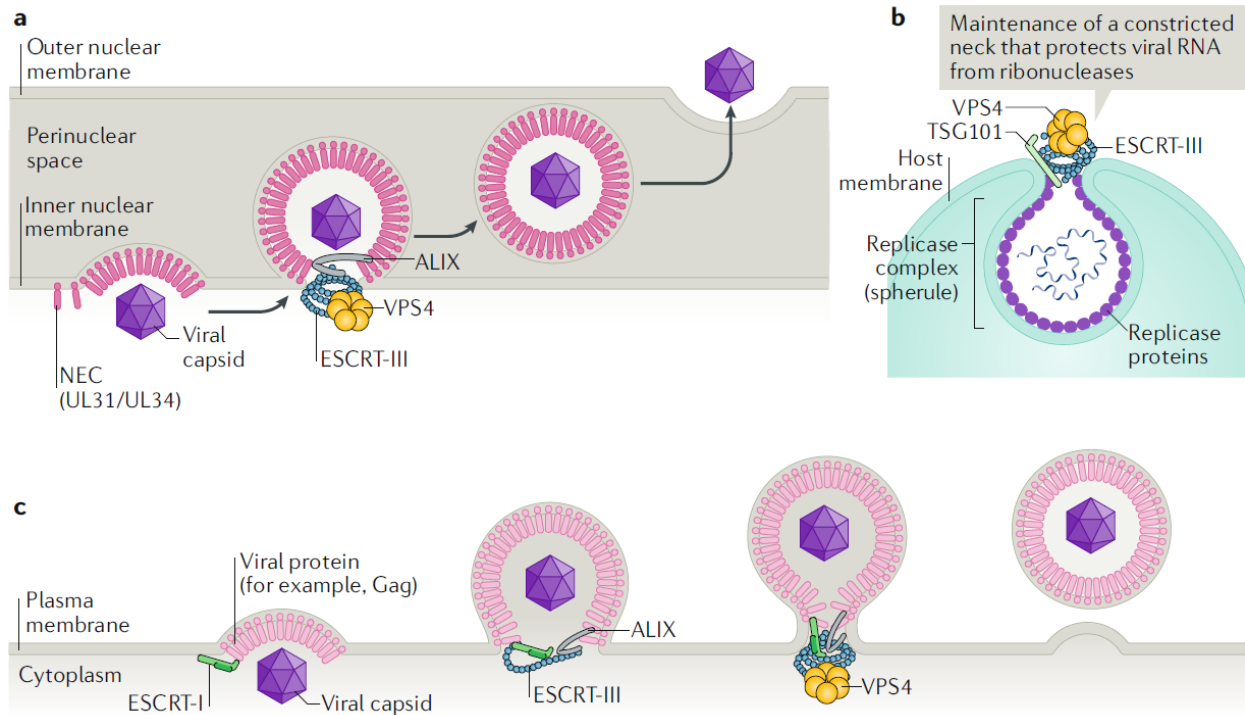


**Figure 54: Viral budding process using ESCRTs and ALIX.** The Gag proteins recruit ALIX via its V domain and ALIX acts as the adaptor for ESCRT-I and ESCRT-III subunits. This complex recruits the ATPase VPS4, and the ATPs generated are used as “fuel” for constricting and cutting the membrane, releasing the virus. Adapted from [556].

On the other hand, retroviruses like HIV-1 and EIAV or other pathogenic viruses (Ebola, hepatitis C) hijack the ESCRT machinery to bud out of the plasma membrane [556] (**Figure 54c**). In HIV-1, the P(T/S)AP motif located in the p6 region of its gag protein recruits TSG101 through its UEV domain (the region where ALIX interacts with TSG101 also) [629, 630]. TSG101 is thought to then recruit ESCRT-III and VPS4 for the scission and final release of the viral particles [631]. But, when either the Gag-TSG101 interaction is interrupted or TSG101 is depleted, the YPX<sub>n</sub>L motif in the Gag protein recruits the ALIX V domain to help in the completion of the above process [563, 590, 632]. Parallely, EIAV uses this ALIX-dependent mechanism by binding to the ALIX V domain through the YPX<sub>n</sub>L motif in its Gag protein to bud out of the cells [563, 566, 573, 590].

These examples illustrate how ALIX functions in the viral budding process but also reflects some compensatory effects between ALIX and TSG101, which as we will see in the upcoming sections, is a common observation.

### 1.35.2 Intracellular membrane vesicle trafficking

The similarity between ALIX and its yeast counterpart, Bro1p, implicates ALIX in cargo sorting through the MVBs (**Figure 55**). Like Bro1p, ALIX can directly bind to ubiquitin, which regulates ALIX activity (**see Ubiquitination**) but is also required for the budding of lentiviruses [606]. Alternatively, through its interaction with the lipid LBPA, ALIX is suggested to play a direct role in the intraluminal membrane (ILV) formation within the late endosomes (vesicles entering the cell) that depends on the ESCRT machinery [570, 633]. The counterpart of endosomes are vesicles secreted out of the cell, called exosomes, and ALIX is now a well-established protein found in exosomes [634, 635], that is often used as an exosome marker protein.

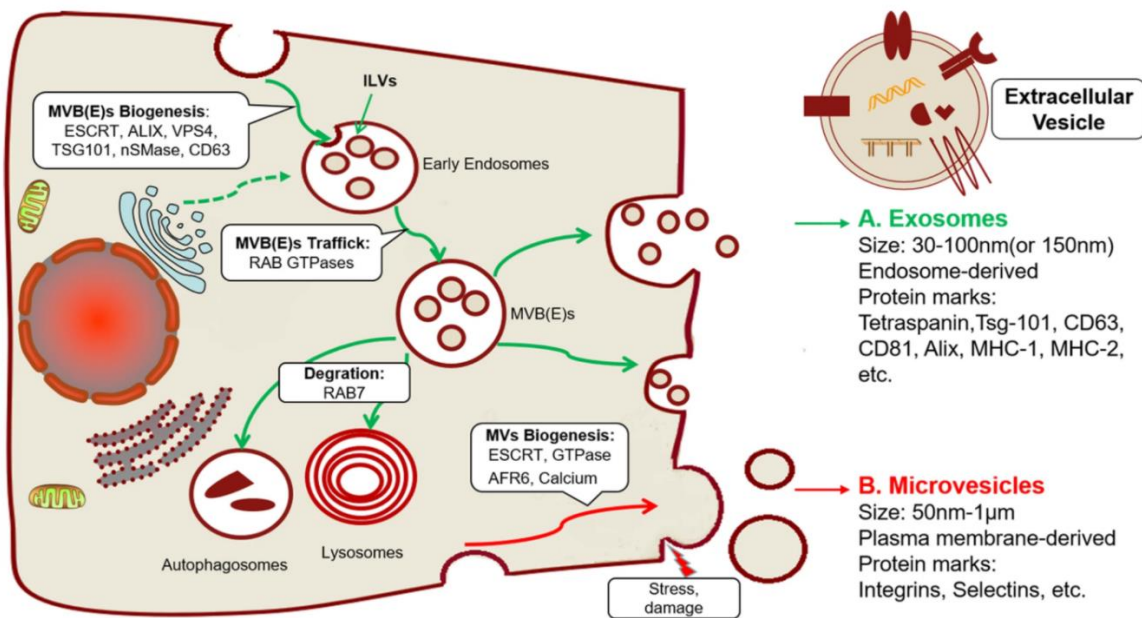


**Figure 55: Biogenesis of vesicles (MVBs, exosomes).** ALIX along with the ESCRT machinery is required for cargo (proteins/receptors) sorting through MVB biogenesis. ILV formation within late endosomes is ALIX-dependent, and this requires its interaction with LBPA. ALIX is also secreted out of the cell through exosomes. Adapted from [636].

A well-studied role of ALIX in receptor recycling is EGFR, as described in an earlier part of this section (**see Figure 53**). A recent study showed that ALIX regulated EGFR activity and the surface presentation of PD-L1 in breast cancer cells, and is the only one so far showing a direct role for ALIX in breast cancer [637] (**Figure 56**). It was previously shown that ALIX could indirectly bind to EGFR and sustain its downstream signaling, while ALIX depletion promoted the endocytosis of EGFR [594]. However, in this report, they show the

opposite wherein knocking down ALIX led to increased phosphorylation of EGFR, and therefore prolonged signaling [637]. Perhaps, this discrepancy could be explained using different cellular models or a cancer-specific role of ALIX.

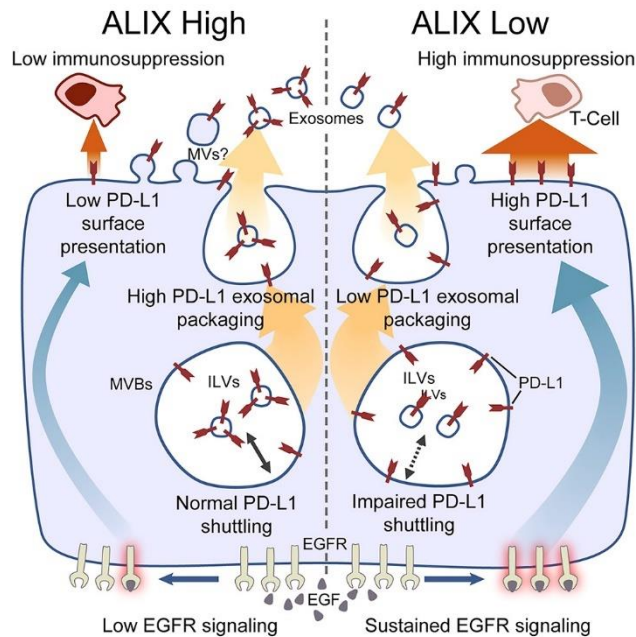


**Figure 56: Graphical abstract summarizing the key findings of Monnypenny et al. [637].**

Further, ALIX is shown to control the sorting of the receptor, PD-L1 into exosomes, and therefore its presentation on the cell surface [637]. In the absence of ALIX, more PD-L1 is presented on the surface of breast cancer cells leading to higher immunosuppression in these cells [637]. Given the clinical importance of both PD-L1 and EGFR for breast cancer (see page 44 and 50), it is interesting to note that ALIX is the protein that integrates these two signaling pathways. Moreover, ALIX depletion, *in vivo*, shows enhanced tumor growth due to both sustained EGFR signaling and high PD-L1 at the surface [637]. Therefore, it would be worth testing the efficacy of drug combinations using EGFR and PD-L1 in these breast tumors.

### 1.35.3 Cytokinesis

All mammalian cells undergo the process of cell division (mitosis). The final step during cell division is a process known as cytokinesis, through which the two daughter cells are physically separated (Figure 57). Cytokinesis is initiated by the formation of a cleavage furrow (driven by an actomyosin ring) which in turn leads to the formation of an intracellular bridge (ICB) composed of microtubules, and several proteins are required for this process [638]. At the center of this ICB is an electron-dense structure termed the midbody, which is highly rich in proteins, such as the ECSRT machinery, ALIX, VPS4, and others [638, 639]. The last step is membrane scission, called abscission, to divide the two daughter cells and the midbody structure could either remain in the extracellular matrix



as a remnant or sometimes can also be ingested by one of the daughter cells to be degraded [640]. The midbody remnant (MBR) has been purified by some groups where proteomic analysis has been performed and has been a gold mine for the community to identify novel proteins involved in cytokinesis. The first study was done in 2004 using CHO cells [641] and subsequently, in recent years three studies have been done in HeLa [642, 643] and the colon cancer cell line SW620 [644]. Interestingly, some PRMTs have been identified in the proteomes of these studies. Capalbo and colleagues used several known midbody proteins as baits to identify new interactors and found CARM1 when GFP-KIF14 was used as a bait (protein score: 33, number of peptides found: 1) [642]. Addi and colleagues characterized the proteome of the Flemming body (called the flemmingsome) and found PRMT1, PRMT3, and CARM1 in the total flemmingsome while PRMT5 was found in the enriched flemmingsome [643]. Similarly, Rai and colleagues identified PRMT1, PRMT3, CARM1 and PRMT5 in their midbody remnant proteome [644] and PRMT3 was categorized as enriched in the MBR (fold-change >2). Together, this suggests that the PRMTs might be involved in cytokinesis.

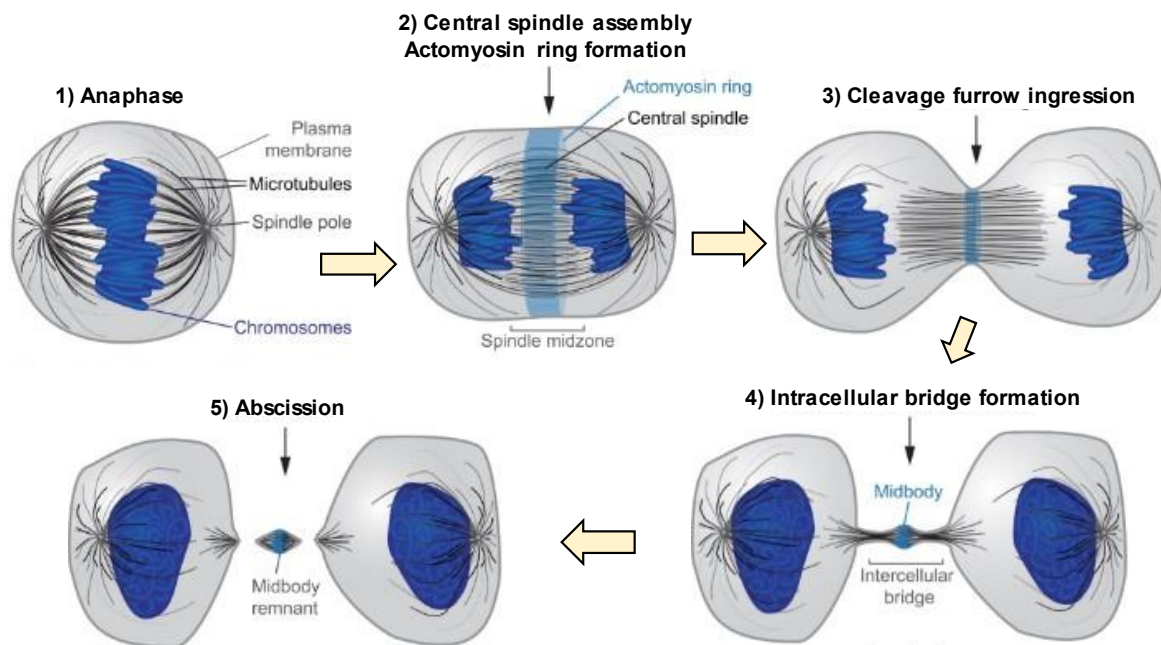


**Figure 57: Overview of cytokinesis.** (1) During the last stage of mitosis, anaphase, the sister chromatids are aligned in the central plane, (2) which then leads to the formation of the actomyosin ring in the midzone. (3) By contracting the actomyosin ring, the cell initiates a cleavage furrow formation that (4) subsequently narrows down to form the intracellular bridge, containing the midbody at its center. (5) The last step is to abscise the membrane to physically cut the two daughter cells resulting in the midbody remnant, thus completing cytokinesis. Modified and adapted from [638].

Unsurprisingly, the entire process of cytokinesis is highly concerted and tightly regulated to ensure proper completion. Cep55 accumulates to the midbody ring to

interact with the mitotic kinesin-like protein (MKLP1) [645, 646] (**Figure 58A**). Cep55 then recruits both TSG101 and ALIX [583-585, 614]. After this point, ALIX has been shown to have a dual role in mediating abscission. First, like its function in viral budding, ALIX binds to CHMP4B through its Bro1 domain and initiates **ESCRT-III polymerization** [647-649]. Recently, interactions between ALIX/syntenin and the membrane protein syndecan-4 has been shown to be the main players for proper localization of ESCRT-III at the site of abscission [643]. Like the process of viral release, the polymerization of ESCRT-III filaments causes membrane constriction and the membrane fission occurs using the ATPase activity of VPS4 [556] (**Figure 58B, C**).

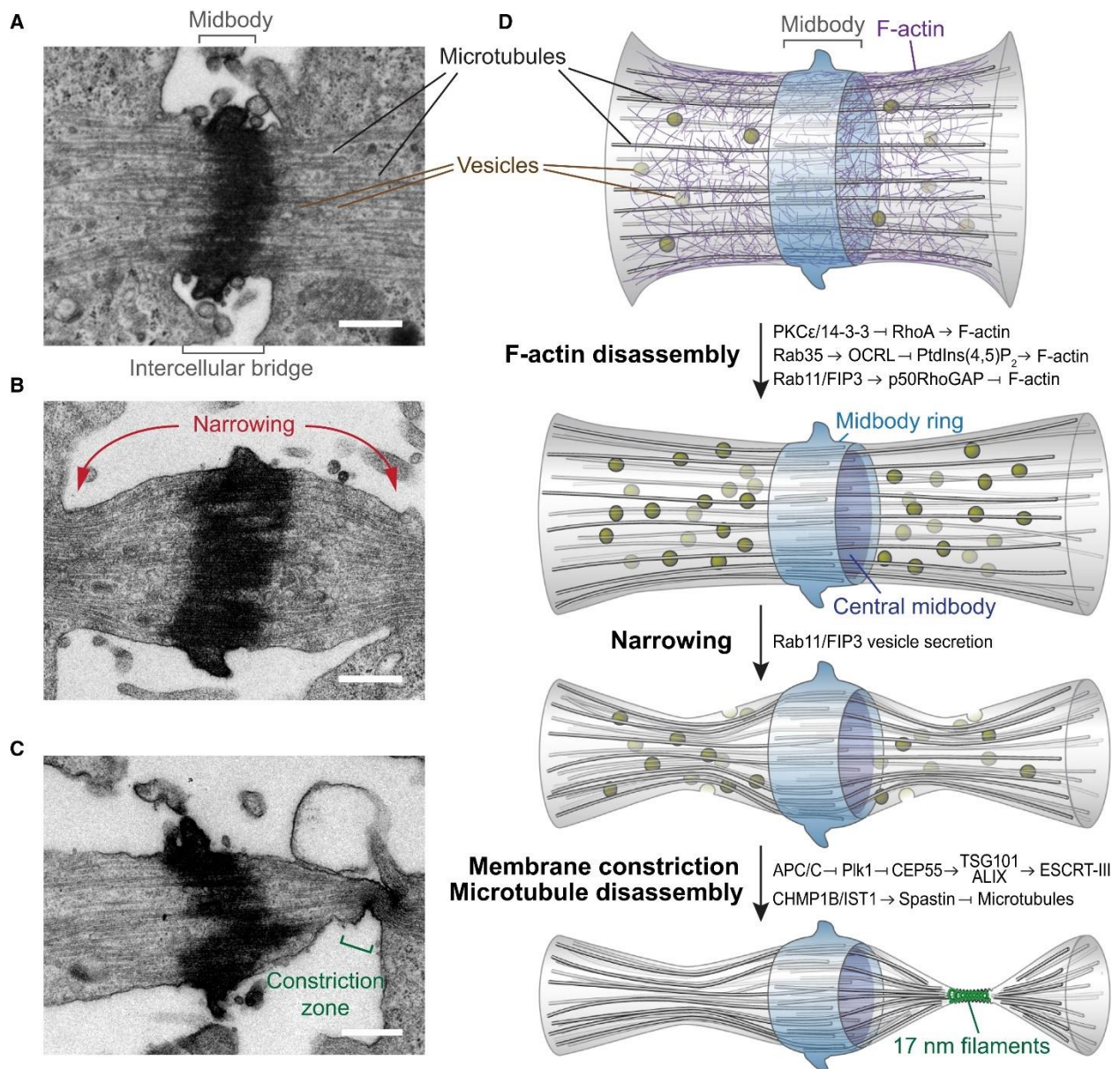
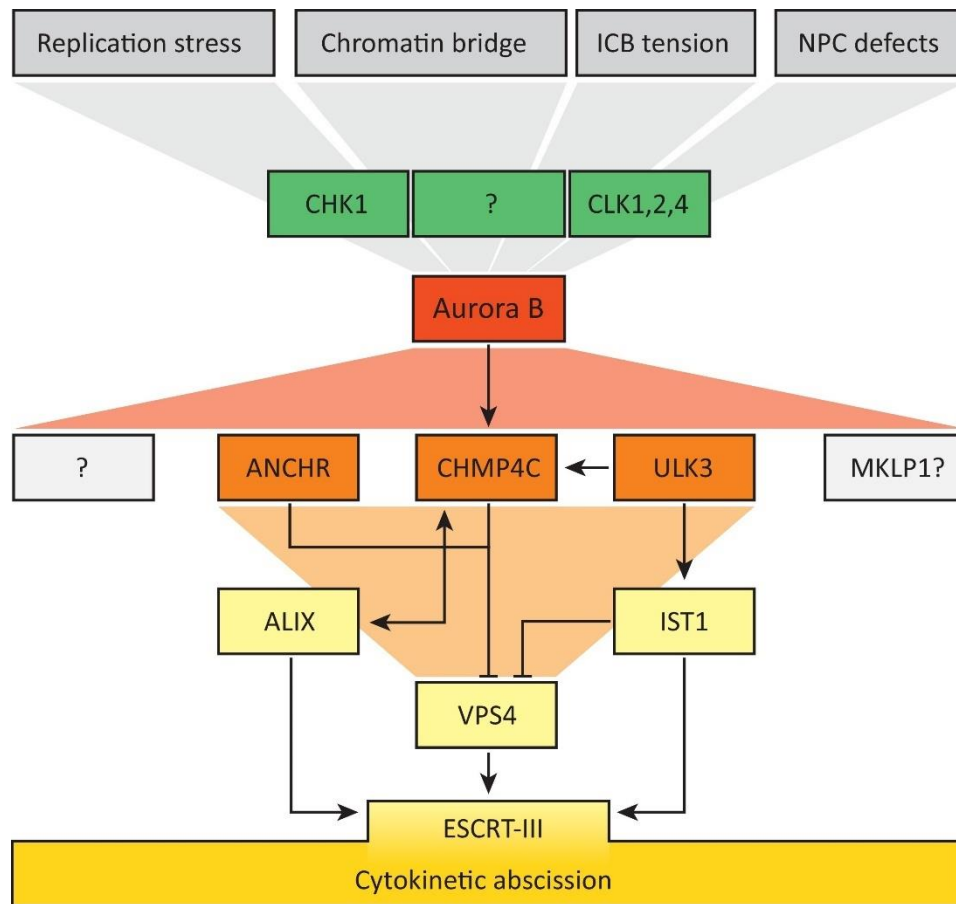


**Figure 58: Details of bridge maturation and abscission.** The transmission electron micrographs beautifully capture the different stages of the intracellular bridge maturation from (A) early bridge, (B)

middle bridge with the initiation of narrowing on either side of the midbody to the (C) late bridge with a well-defined constriction zone that is the site of abscission. (D) shows the same process in cartoon drawings along with the various proteins involved at each stage. Adapted from [638], the electron micrographs in (A) is from D.W Gerlich and T.Mueller-Reichert while (B) and (C) are from [650].

The second role of ALIX is in the **cytokinetic checkpoint** [648] (**Figure 59**). In the presence of lagging chromosomes (presence of DNA in the intracellular bridge) or defects during segregation, the cells employ a checkpoint to delay abscission [651-656]. The main player in the abscission checkpoint is Aurora B kinase. Aurora B phosphorylates CHMP4C and phosphorylated CHMP4C inhibits the ATPase activity of VPS4 on the ESCRT-III polymers at the abscission site, thereby preventing abscission [657, 658]. In this context, Christ and colleagues showed that it was ALIX which recruits CHMP4C to the midbody, highlighting its role in the abscission checkpoint [648].



Trends in Cell Biology

**Figure 59: Schematic of the cytokinetic abscission checkpoint signaling.** This checkpoint is triggered by DNA replication stress, chromatin in the bridges, high tension in the intercellular bridge (ICB), or defects in nuclear pore complex assembly (NPC). The key player is Aurora B kinase and is activated by Chk1, CLK1, CLK2, and CLK4. Aurora B phosphorylates CHMP4C and phosphorylated CHMP4C can then cooperate with ANCHR to inhibit VPS4 at the Flemming body, preventing VPS4 activity on ESCRT-III filaments to complete

abscission. ALIX recruits CHMP4C to the midbody when the abscission checkpoint is triggered. A double-headed arrow indicates direct binding. Adapted from [658].

Although we understand the spatial and temporal control of cytokinetic abscission, particularly those involving ALIX, as explained before, the cells do not rely completely on ALIX for the completion of this process, since TSG101 can act parallelly to recruit the downstream ESCRT proteins.

### 1.36 Concluding remarks

Since its discovery in 1999, ALIX is understood as a multifunction adaptor protein involved in fundamental cellular functions. One key aspect that has not been well-explored is other post-translational modifications occurring on ALIX or the downstream functional effect of already known modifications apart from impairing partner interactions. Exploring this could help us further understand the roles of ALIX in cellular contexts where it is essential, and not compensated for by similar proteins (like Brox, HD-PTP, see **Figure 46**) or TSG101. Notably, like ALIX, HD-PTP has also been found to be mono-methylated on several arginine residues within its pro-rich domain (R950, R1595, R1615, R1618) [114, 610, 611], but we did not identify this protein as a partner of CARM1.

# **CHAPTER 2**

## CHAPTER 2: RESULTS AND DISCUSSION

This chapter is divided into two parts, each part focusing on one PRMT studied in my thesis.

Part 1 is the manuscript entitled "**PRMT1 regulates the EGFR and Wnt signaling pathways**" which describes the results obtained for PRMT1 in the context of TNBC, followed by a discussion and conclusion and corresponding future direction.

Part 2 contains the manuscript entitled "**The ESCRT-binding protein ALIX is a novel CARM1 substrate**" which details the results obtained so far for the study regarding CARM1 in TNBC and followed by a discussion, conclusion, and future direction.

## CHAPTER 2: PART I

### *Preface*

Previous members of the lab (Dr. David Silvestre, Amélie Brisson, Bérengère Marty-Provoust) started this study that was initially submitted and in revision in Cancer Research. That initial study explored (1) PRMT1 as a therapeutic target using 2 poorly specific PRMT1 inhibitors (they were the only ones that were available at the time of the experiments; they have been removed in the new manuscript) and (2) the interaction between PRMT1 and EGFR (since it has now been published by others, has also been removed in the new version of the manuscript).

I have modified/continued that study focusing on another signaling pathway, the Wnt signaling pathway, and have used two recently developed Type I PRMT inhibitors, one of which is currently being evaluated in clinical trials (GSK3368715).

My contribution to this manuscript has been to validate the effect of PRMT1 on the Wnt pathway and uncover the mechanism. Further, with the help of Solène Huard, we performed all the experiments using the Type I PRMT inhibitors *in vitro* and drug combination analysis. Lastly, in collaboration with the preclinical investigation laboratory (LIP) at Institut Curie, we evaluated the *in vivo* efficacy of one of the Type I PRMT inhibitor.

# PRMT1 regulates the EGFR and Wnt signaling pathways

Samyuktha Suresh<sup>1,2,3</sup>, Solène Huard<sup>1,2,3</sup>, Amélie Brisson<sup>1,2,3</sup>, David C. Silvestre<sup>1,2,3</sup>, Fariba Nemati<sup>1,2,5</sup>, Coralie Poulard<sup>7</sup>, Mengliang Ye<sup>1,2,3</sup>, Bérengère Marty-Prouvost<sup>1,2,3</sup>, Elise Martel<sup>1,6</sup>, Didier Meseure<sup>1,4</sup>, André Nicolas<sup>1,4</sup>, Cécile Reyes<sup>1,2,6</sup>, David Gentien<sup>1,2,6</sup>, Didier Decaudin<sup>1,2,4</sup>, Muriel Le Romancer<sup>7</sup>, Gordon C. Tucker<sup>8</sup> and Thierry Dubois<sup>1,2,3</sup>

<sup>1</sup>Institut Curie, PSL Research University, Paris, France; <sup>2</sup>Translational Research Department; <sup>3</sup>Breast Cancer Biology Group; <sup>4</sup>Investigative Pathology Platform; <sup>5</sup>Pre-clinical investigation laboratory; <sup>6</sup>Genomic Platform; <sup>7</sup>Centre de Recherche en Cancérologie, Lyon, France; <sup>8</sup>Oncology Research and Development Unit, Institut de Recherches SERVIER, Croissy-sur-Seine, France.



## Abstract

Triple-negative breast cancer (TNBC) belong to the subgroup of breast cancer (BC) with the most aggressive behaviors. There is no targeted therapy for TNBC, and new treatments are needed to bypass resistance to chemotherapies and improve the survival rate of TNBC patients. Transcriptome and immunohistochemistry analyses revealed that protein arginine methyltransferase 1 (PRMT1) is more highly expressed in all BC subtypes than in healthy breast tissues. In a large panel of BC cell lines, RNAi-mediated PRMT1 depletion induced an increase in phosphorylated H2AX, and apoptosis, and decreased proliferation. Two recently developed Type I PRMT inhibitors decreased the proliferation of MDA-MB-468 cells. The type I PRMT inhibitor which is currently in clinical trial (GSK3368715) showed anti-tumor activity in mice engrafted with tumors derived from MDA-MB-468 cells. We discovered that PRMT1 activates the transcription of the Epidermal Growth Factor Receptor (EGFR), and two genes involved in the Wnt signaling pathway (LDL Receptor Related Protein 5- LRP5, and Porcupine – PORCN) by binding to their promoter regions. PRMT1 silencing and inhibition decrease Wnt signaling activity. The application of combination approaches to a TNBC cell line, MDA-MB-468, identified a synergistic association between PRMT1 and EGFR inhibition or chemotherapy treatments (cisplatin, cyclophosphamide, and camptothecin). Altogether, our results show that PRMT1 activity is necessary for BC cell survival. Targeting PRMT1, alone or in combination with specific chemo- or anti-EGFR- therapies, may represent novel therapeutic approaches for the treatment of TNBC patients.

## Introduction

Breast cancer (BC) is a heterogeneous disease with molecularly distinct subtypes having different clinical outcomes and responses to therapies [659]. However, the subgroup of patients with “triple-negative” BC (TNBC, lacking the expression of estrogen and progesterone receptors and Her2 overexpression) have a poor prognosis and has been challenging to treat, owing to their heterogeneity, high relapse rate and resistance to chemotherapy [660]. Therefore, alternative treatments are needed to bypass these challenges and to improve the survival rate of TNBC patients.

Protein arginine methylation, catalyzed by members of the Protein Arginine Methyltransferase (PRMT) family, is a post-translational modification regulating several fundamental cellular pathways including signal transduction and transcription regulation [161, 163]. PRMT1, the major type I PRMT, [352] that generates asymmetric dimethyl arginine (ADMA) and is overexpressed in various cancer types, including BC, and has been proposed as a potential therapeutic target [164, 272, 661]. However, the role of PRMT1 in estrogen receptor (ER) negative BC subtypes (such as Her2 and TNBC) is limited [291, 383].

A key signaling pathway that is responsible for chemoresistance of TNBC cells and in the renewal of TNBC cancer stem cells, is the Wnt/ $\beta$ -catenin signaling pathway [95, 662]. Wnt pathway is often dysregulated in TNBC, not through genetic mutations like in colorectal cancer, but rather through an overexpression of its transmembrane receptors, Frizzleds and co-receptors low-density lipoprotein receptor-related proteins (LRP6 and LRP5) [95]. Both FZD6 and FZD7 can be potential therapeutic targets for TNBC since reducing their expression decreases tumorigenic features like cell proliferation and invasion [100, 101]. We and others have previously shown that LRP5/6 [103-106] and LRP8 [108] could also be potential therapeutic targets for TNBC.

PRMTs regulate several signaling pathways, including the Wnt and EGFR signaling pathways [161, 163]. However, there are opposing reports for the role of PRMT1 in regulating the Wnt pathway. PRMT1 can both activate (via G3BP1, G3BP2) [388, 389] and inhibit (via Axin and Disheveled) [386, 387] Wnt signaling. PRMT1 regulates the EGFR signaling pathway by directly methylating it [194] and PRMT1-mediated methylation of EGFR was impaired upon PRMT1 knockdown, decreasing the proliferation of the MDA-MB-468 TNBC cells [383]. Further, PRMT1 inhibition using a nonspecific PRMT1 inhibitor (AMI-I) was shown to sensitize this TNBC cell line to an EGFR inhibitor (cetuximab) [383].

In this study, we found that PRMT1 is more expressed in the four BC subgroups than in normal tissue. Decreasing PRMT1 levels or inhibiting its activity reduces cell viability. We identified the EGFR and Wnt signaling pathways to be de-regulated upon PRMT1 depletion and described for the first time PRMT1-mediated regulation of two Wnt-pathway related genes (*LRP5* and *PORCN*). We observed synergistic effects, *in vitro*, between two type I PRMT inhibitors (MS023, GSK3368715) and the EGFR inhibitor

(Erlotinib). Additionally, we also observed synergy with different chemotherapies (such as cyclophosphamide, camptothecin, cisplatin) but not with others (doxorubicin, paclitaxel, and docetaxel) used to treat TNBC patients. Together, our results show that PRMT1 activity is necessary for BC cell survival and that targeting PRMT1, alone or in combination with other drugs, may represent a novel regimen for the management of BC, particularly in TNBC patients.

## Results

### PRMT1 is overexpressed in breast tumors

In the lab, we had previously performed gene expression profiling on a cohort of 154 human breast cancer (BC) biopsies composed of 35 luminal A, 40 luminal B, 46 triple-negative (TNBC), 33 Her2+ and 18 normal breast tissues and identified several novel therapeutic targets for TNBC [106, 108, 301, 663, 664]. Transcriptomic analysis showed that PRMT1 mRNA is more expressed in all BC tumors compared to normal tissues with the highest expression in TNBC (**Figure 60A, left panel**). Higher expression of PRMT1 mRNA in TNBC was also confirmed from the publicly available database - the cancer genome atlas (TCGA) cohort (**Figure 60A, right panel**). We examined whether variations in PRMT1 expression could arise from genomic alterations by analyzing DNA microarrays. The *PRMT1* locus showed more gains in TNBC than the other BC subtypes (**Figure 60B**). However, there was no significant correlation between PRMT1 mRNA and gene copy number within the TNBC subtype (**Figure 61A**), suggesting that the high levels of PRMT1 RNA is not linked to genomic gains.

To understand the clinical significance of PRMT1 expression, we plotted survival outcomes from the KM-plotter database ([www.kmplot.com](http://www.kmplot.com)) [665] and used the best performing threshold as the cut-off. High PRMT1 mRNA expression was associated with poor recurrence-free survival (RFS) in luminal B (LB,  $p < 0.01$ ), and luminal A (LA,  $p < 0.001$ ) (**Figure 61C, top panel**). Although this trend was seen in the Her2+ subtype, it was not statistically significant ( $p = 0.13$ ) perhaps due to a lesser sample size ( $n = 515$ ) (**Figure 61C, right bottom panel**). Conversely, in TNBC, high PRMT1 expression showed better RFS ( $p = 0.02$ ) (**Figure 61C, left bottom panel**) which may be linked to the highly proliferative nature of TNBC. In the curie cohort, PRMT1 mRNA positively correlated with the mRNA of the proliferation marker, Ki67 (**Figure 61B**,  $p < 0.001$ ) in the whole breast population, but the correlation was not significant within TNBC alone (**Figure 61B**,  $p = 0.382$ ). Since the survival outcomes were plotted using the KM-plotter database, we asked if there was a correlation between Ki67 and PRMT1 in this sample set which contained more TNBC tumors. Indeed, we found a positive correlation (**Table 2**) in the TNBC samples, suggesting the high PRMT1 tumors (more proliferative) might respond better to chemotherapy and display better survival outcomes.

**Table 2: Correlation between PRMT1<sup>1</sup> mRNA and Ki67<sup>2</sup> mRNA from KM-plotter database**

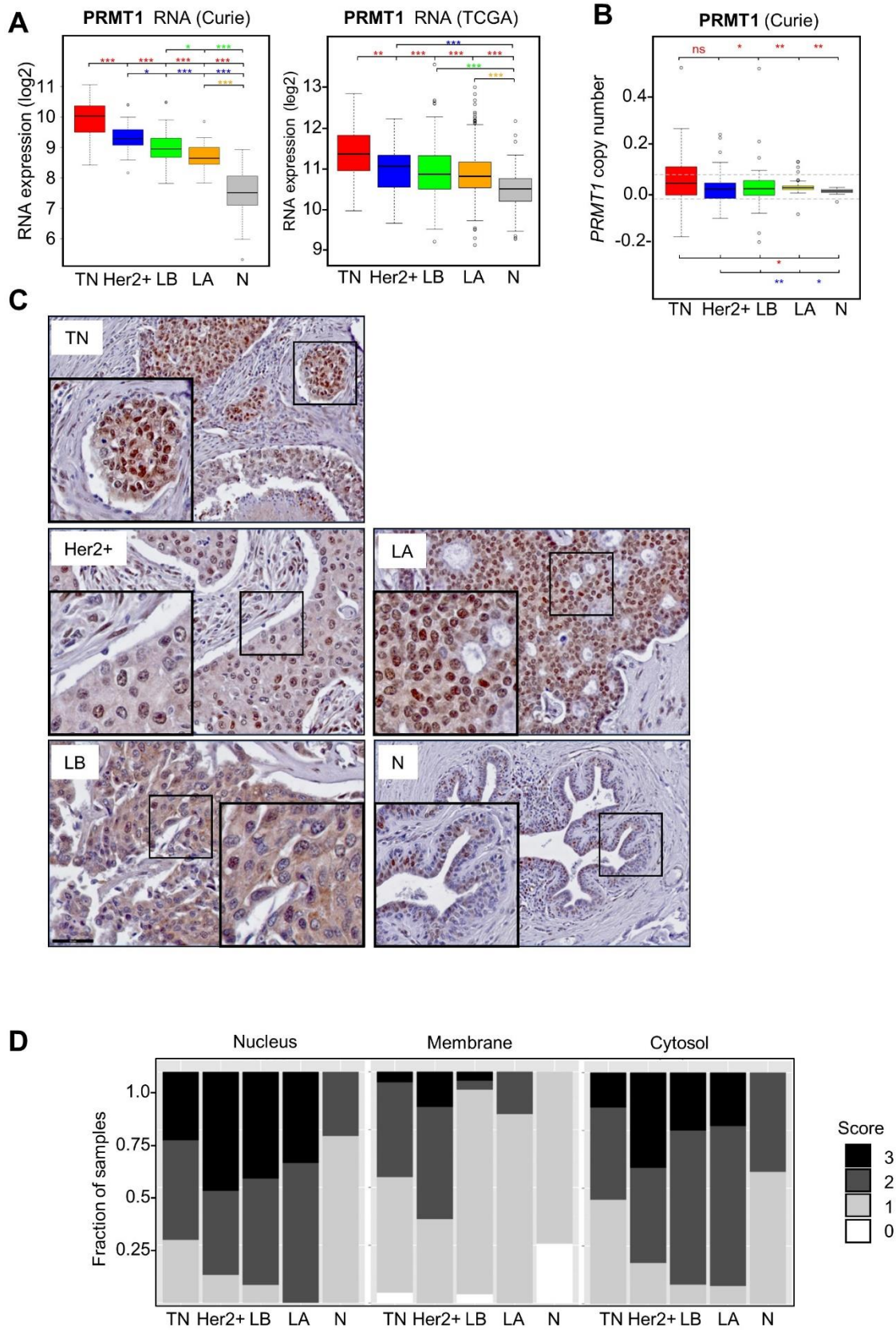
BC subtype	Spearman's correlation co-efficient	p-value
------------	--	---------

<b>All BC (n=4929)</b>	0.2168	$p < 1 \times 10^{-4}$
<b>TNBC (n=846)</b>	0.2665	$p < 1 \times 10^{-4}$
<b>Her2+ (n=515)</b>	0.1767	$p = 0.0016$
<b>Lum A (n=2277)</b>	0.1288	$p < 1 \times 10^{-4}$
<b>Lum B (n=1491)</b>	0.1082	$p < 1 \times 10^{-4}$

<sup>1</sup>PRMT1 affymetrix ID: 206445\_s\_at; <sup>2</sup>Ki67 affymetrix ID: 212023\_s\_at

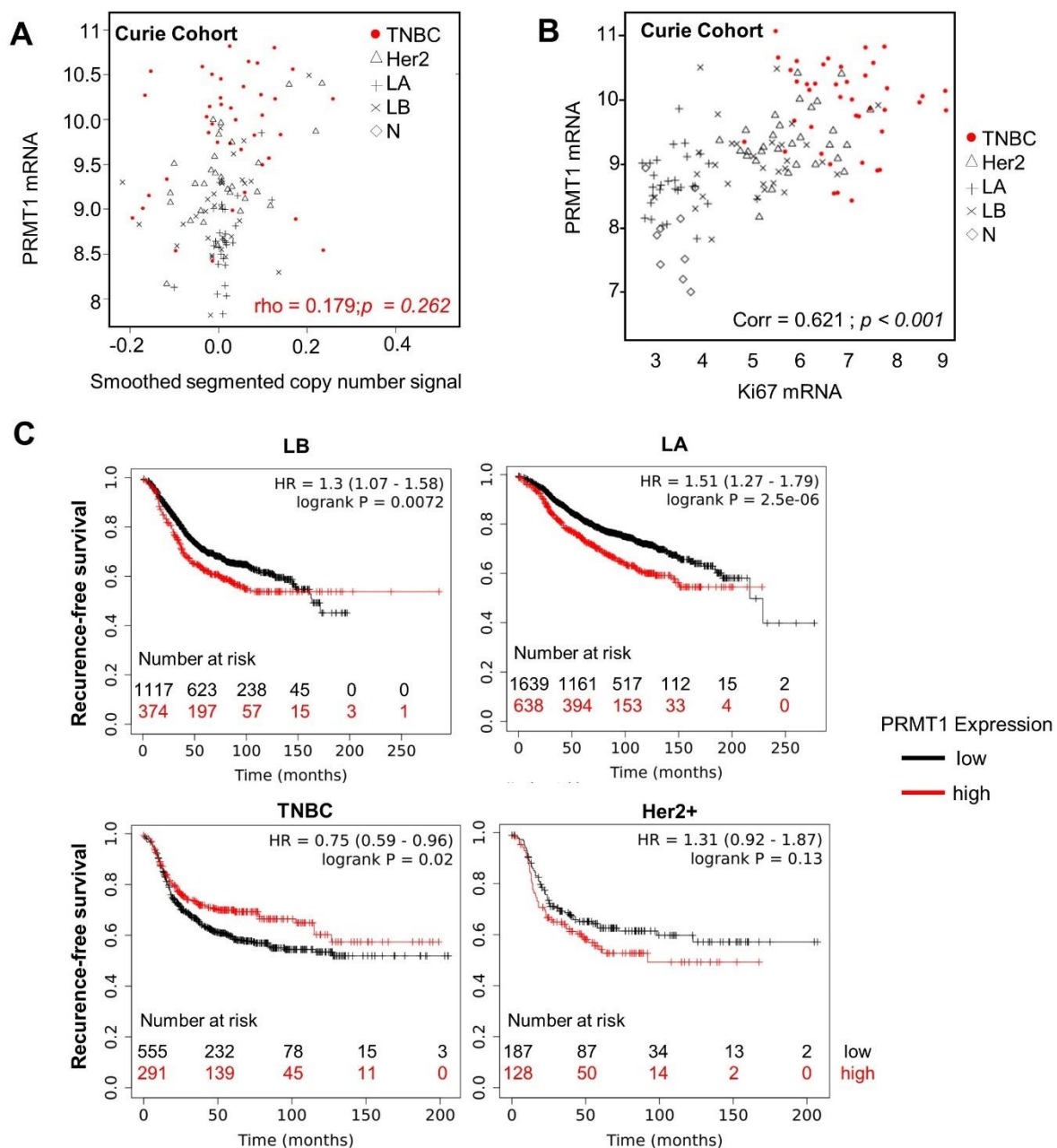
Next, we studied PRMT1 protein expression in BC and normal tumors. We first validated an anti-PRMT1 antibody for immunohistochemistry (IHC) staining in a TNBC cell line (MDA-MB-468) fixed in the same method as the tissue samples (**Figure 61D**). This antibody recognizes residues 298-318 located in the C-terminal region of human PRMT1. IHC analysis confirmed that PRMT1 is highly expressed in all BC subtypes compared to normal tissue (**Figure 60C**). In contrast to the mRNA expression levels, no significant difference was observed for PRMT1 protein expression between the different BC subtypes. PRMT1 was found localized mainly in the nucleus and the cytoplasm. However, membrane staining was also observed with a greater proportion of staining mainly in the ER-negative tumors, TNBC and Her2+ (**Figure 60C**).

Together, our results are in accordance with previously published data indicating that PRMT1 is overexpressed at the mRNA [133, 398] and protein [398, 399] levels in BC compared to normal breast tissue. In contrast to Mathioudaki et al. (who reported predominantly cytoplasmic staining for PRMT1), we observed both nuclear and cytoplasmic staining. This difference could be due to a difference in antibodies used or a difference in the tumor samples since breast cancer is highly heterogeneous. We used a commercially available antibody as described above while in their study, they used an in-house raised polyclonal antibody targeting amino acids 332-351 within the C-terminal region of PRMT1. Further, they do not specify the number of samples analyzed by IHC nor quantifications to support that PRMT1 was predominantly cytoplasmic. Furthermore, we are the first ones to report membrane staining of PRMT1 in these tumors.



**Figure 60: PRMT1 is more highly expressed in BC samples than normal breast tissue.** (A), Higher levels of PRMT1 mRNA in TNBC relative to other BC subtypes. The levels of PRMT1 RNA expression in TNBC (red), Her2+ (blue), Luminal B (LB, green), Luminal A (LA, orange), and healthy breast tissue (N,

grey) were determined by microarray analysis (Affymetrix) in the Curie cohort (Curie, left panel) or obtained from the publicly available dataset "The Cancer Genome Atlas" (TCGA, right panel). Relative RNA quantifications were logarithmically (log2) transformed and are illustrated by box plots. (B) Analysis of *PRMT1* DNA in the Curie cohort. The smoothed segmented copy number (CN) signal is presented in boxplots, with dashed lines indicating the thresholds retained to call CN gains and losses. Copy numbers were determined by microarray analysis. (C) Higher levels of PRMT1 protein in BC than in normal tissue. PRMT1 protein levels were analyzed by immunohistochemistry (IHC) in the Curie cohort. A representative image of PRMT1 staining is shown for the different BC subtypes. (Scale bar = 50µM). (D) Quantification of PRMT1 staining in the different cellular compartments (0: no staining, 3: the strongest staining). \* $p < 0.05$ ; \*\* $p < 0.01$ ; \*\*\* $p < 0.001$ , as calculated using the Student t-test.



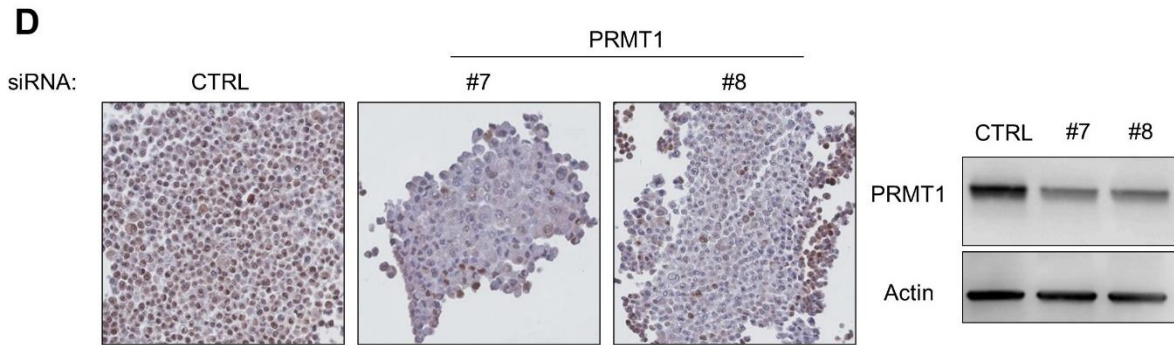


**Figure 61: Correlation, survival analysis and validation of PRMT1 antibody for IHC.** (A) Spearman correlation between the levels of PRMT1 transcript and *PRMT1* DNA copy number in the whole population of the Curie cohort. (B) Spearman correlation between the levels of PRMT1 transcript and Ki67 transcript (proliferative marker) in the whole Curie cohort population (values indicated in black) TNBC (O, red filled), Her2+ ( $\Delta$ ), LB (X), LA (+) breast tumors, and normal breast tissue (diamond) (A, B). (C) Recurrence-free survival was analyzed using the Kaplan-Meier (KM) plotter (<http://kmplot.com>) for PRMT1 (Affy probe ID: 206445\_s\_at). The auto-select best cutoff option was used for each plot. The different intrinsic subtypes were chosen such as Luminal B (LB, n=1491), Luminal A (LA, n=2277), Basal for TNBC (TN, n=846), and Her2+ (n=315). Hazard ratio with 95% confidence interval and log-rank P values were calculated and significance threshold was set at  $P < 0.05$ . (D) PRMT1 antibody validation was performed using AFA-fixed cell pellets from MDA-MB-468 cells treated with control siRNA (CTRL) or two PRMT1 siRNAs for 72 h (#7, #8). PRMT1 displays cytosolic and nuclear localization. PRMT1 depletion was verified by western-blotting using PRMT1 antibodies. Actin was used as a loading control.

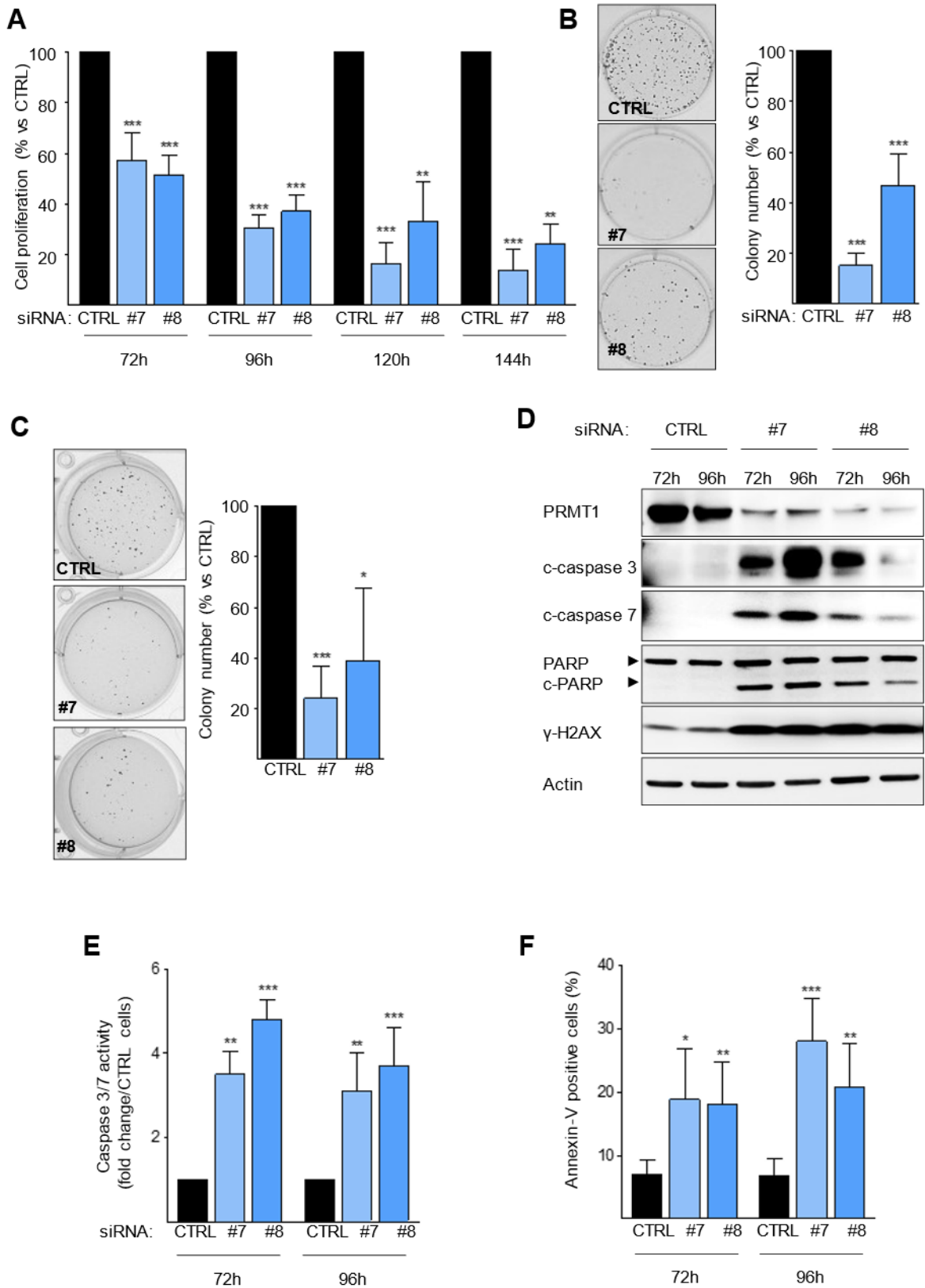
### RNAi-mediated depletion of PRMT1 decreases BC cell viability, clonogenicity and induces apoptosis

Next, we wanted to explore if PRMT1 could be a therapeutic target in BC. We depleted PRMT1 using two siRNAs (PRMT1#7, PRMT1#8) in a TNBC cell line MDA-MB-468, first validated for their specificity and efficiency in this cell line (**Figure 63A**). We observed that cell viability was significantly decreased upon PRMT1 depletion in MDA-MB-468 cells (**Figure 62A**), in a time-dependent manner, but also in other BC cell lines (3 TNBC, 2 Her2+, 2 luminal, and 2 non-tumorigenic) (**Figure 63B**), suggesting the effect was not specific to a BC subtype. PRMT1 depletion decreased colony number in MDA-MB-468 cells when they were cultured on plastic (**Figure 62B**) or in an anchorage-independent growth assay in soft-agar (**Figure 62C**), indicating that PRMT1 depletion decreased the tumorigenicity of this TNBC cell line. We also observed a decrease in colony number when other BC and non-tumorigenic cells were cultured on plastic (**Figure 63C**) indicating that PRMT1 was important for the proliferation of these cells. In order to understand the mechanism through which PRMT1 affected cell viability, we probed PRMT1-depleted cells for apoptotic markers such as the cleavage of caspases and PARP. We found that caspases 3, 7, and PARP were cleaved (**Figure 62D**) after 72 and 96h of PRMT1 depletion, indicating that PRMT1 depletion induced apoptosis. We further confirmed the induction of apoptosis by analyzing caspase 3/7 activity (**Figure 62E**) and the staining of annexin-V, present on the outer leaflet of the plasma

membrane (**Figure 62F**). Moreover, we observed that depleting PRMT1 also increased the phosphorylation of histone H2AX (on serine 139) which is a known marker of DNA damage, particularly DNA double-strand breaks (**Figure 62D**). Induction of apoptosis upon PRMT1 depletion has been verified in other BC cell lines (HCC70, MDA-MB-231 SKBr3, T47D) (**Figure 63D**).

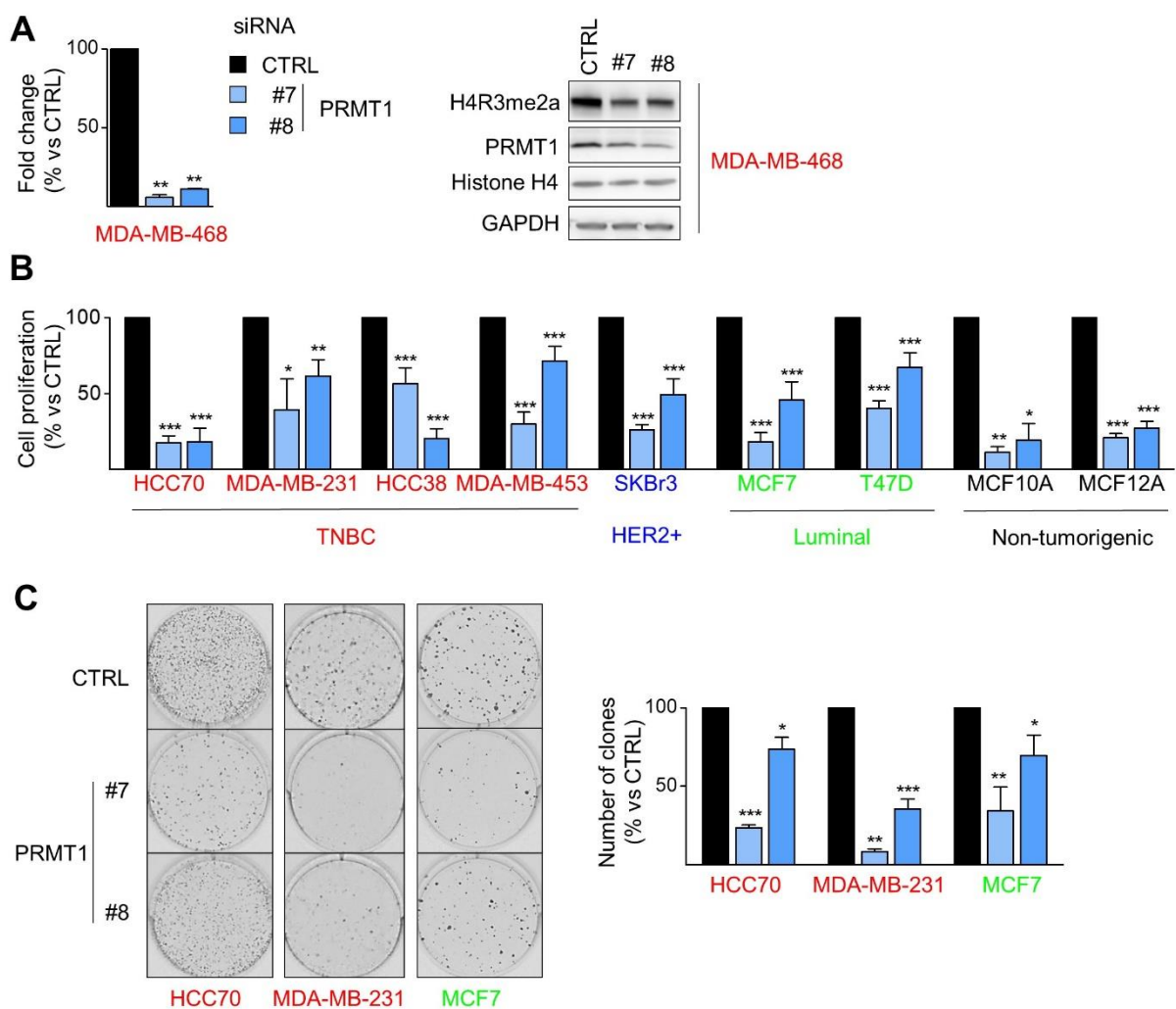
Depleting PRMT1 has been previously shown to decrease colony formation in MDA-MB-231 cells [399, 415] and a decrease in proliferation of MDA-MB-468 cells [383]. Here, we have shown that PRMT1 controlled cell proliferation in a larger panel of both BC and non-tumorigenic cell lines. Notably, these non-tumorigenic cell lines are the most proliferative cells in our culture conditions. We also demonstrate that PRMT1 depletion induces apoptosis in several BC cell lines. Together, this suggests that PRMT1 is an important protein required for BC cell survival.





**Figure 62: PRMT1 depletion using siRNA induces apoptosis and decreases the viability and clonogenicity of MDA-MB-468 cells.** (A) PRMT1 depletion impairs cell viability (MTT assay). Cells were

transfected with control siRNA (CTRL) and two different PRMT1 siRNAs (#7, #8) for the timepoint indicated. (B and C) PRMT1 depletion impairs colony formation when cells are grown on plastic after 13 days (B) or in soft-agar after four weeks (C) following siRNA treatment. (D, E, and F) PRMT1 depletion induces apoptosis. Apoptosis was analysed by western blotting using antibodies that recognize the cleaved forms of caspase 7 (c-caspase7), caspase 3 (c-caspase3) and PARP (c-PARP) 72 h and 96 h after PRMT1 depletion (D), a caspase 3/7 assay (E) or by performing an annexin-V binding assay (F) 72h and 96 h after siRNA treatment. PRMT1 depletion was verified using anti-PRMT1 antibodies (D) and actin (D) was used as loading control. Results are presented as the percentage (A, B, C, F) or fold change (E) relative to control cells (CTRL). For the quantifications, the data are expressed as the mean  $\pm$  SD from at least three independent experiments (A, B, C, E, F). Pictures are from a single experiment representative of three independent experiments (B, C, D). P values are represented as \* $p < 0.05$ ; \*\* $p < 0.01$ ; \*\*\* $p < 0.001$ .



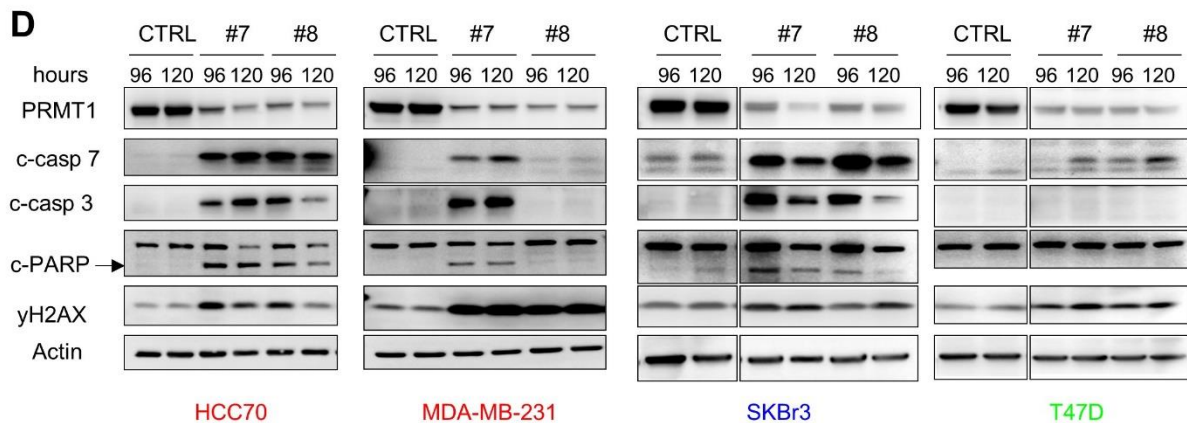


**Figure 63: PRMT1 depletion in a large panel of breast cancer cell lines decreases their viability, colony formation and induces apoptosis.** (A) siRNAs targeting PRMT1 were validated by RT-qPCR (left panel) normalised to actin expression or by western blotting (right panel) in MDA-MB-468 cells treated for 48h. The methylation of histone H4 on Arg 3 (H4R3me2a) was used to detect PRMT1 activity and histone H4 and GAPDH were used as loading controls (A, right panel). (B) PRMT1 depletion decreases cell viability measured by an MTT or WST1 assay. All cells were transfected with control siRNA (CTRL) or two PRMT1 siRNAs (#7, #8) for 144 h. (C) PRMT1 depletion decreases colony formation when cells were grown on plastic for 6 mitotic cycles equivalent to 14 (HCC70), 7 (MDA-MB-231) and 12 (MCF7) days, after siRNA transfection. Results are presented as the percentage (B, C) or fold change (A) relative to control cells (CTRL). (D) PRMT1 depletion induces apoptosis in BC cells. Apoptosis was analysed by western blotting using antibodies that recognize the cleaved forms of caspase 7 (c-casp7), caspase 3 (c-casp3) and PARP (c-PARP) 96h and 120h after PRMT1 depletion. Anti-GAPDH was used as a loading control for all cell lines. Arrow indicates the cleaved form of PARP, while the upper band corresponds to total PARP protein. All the data are expressed as the mean  $\pm$  SD from at least three independent experiments (A, B, C). Pictures are from a single experiment, representative of three independent experiments (A, C, D). P values are represented as \*p < 0.05; \*\*p < 0.01; \*\*\*p < 0.001.

### Type I PRMT inhibitors decrease cell viability, colony formation and show anti-tumor effects

Since we and others have shown that depleting PRMT1 impaired BC cell viability (this study, [383, 399]), we sought to explore if the enzymatic activity of PRMT1 was necessary for BC cell survival.

To answer this, we used two recently developed type I PRMT inhibitors – MS023 and GSK3368715. MS023 is a non-competitive inhibitor for both SAM and substrate binding regions [350] while GSK3368715 is a more potent and newly developed Type I inhibitor that is SAM uncompetitive [326]. GSK3368715 is in Phase I clinical trials for diffuse large B-cell lymphomas and solid cancers (NCT03666988). Both these inhibitors are known to target all type I PRMTs (PRMT1, PRMT2, PRMT3, CARM1, PRMT6, and PRMT8) but are more specific to PRMT1, PRMT6 and PRMT8 inhibition [326, 350]. Hence, we first verified their specificity against PRMT1 activity in MDA-MB-468 cells. Both inhibitors decreased the PRMT1-specific histone mark H4R3me2a from 62.5nM (Figure 64A) and showed no effect on H3R17me2a (histone mark specific to CARM1 and

PRMT6) or the methylation of PABP1 (CARM1-specific substrate) (**Figure 64A**), suggesting that PRMT1 activity was specifically inhibited at these concentrations. However, we did not check the methylation status of substrates specific to other type I PRMTs such as PRMT6 or PRMT8.

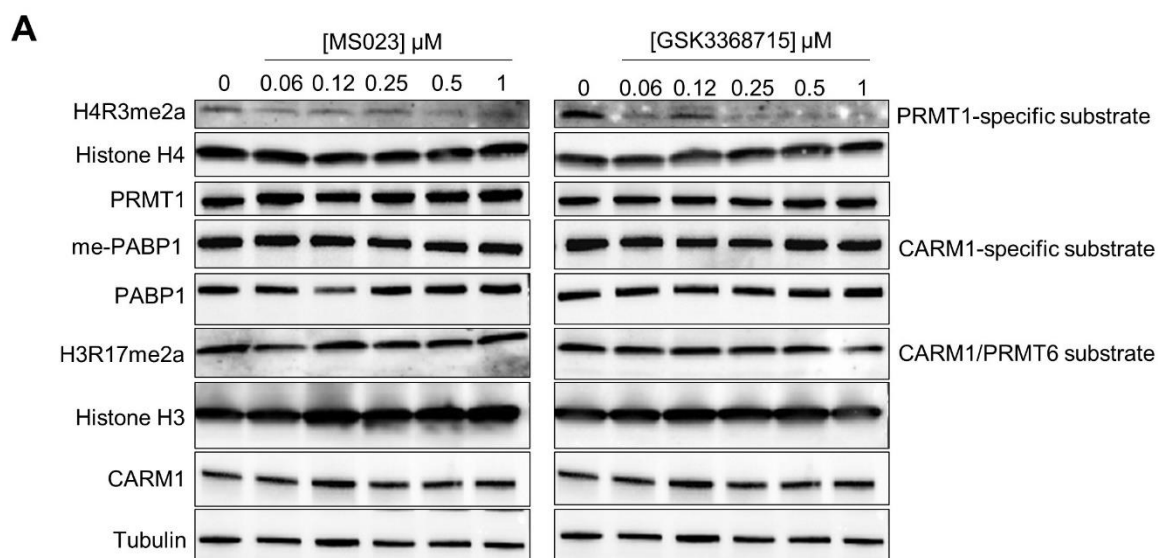
Both type I PRMT inhibitors decreased cell viability in MDA-MB-468 (**Figure 64B**) with half-maximal inhibitory ( $IC_{50}$ ) concentrations in the micromolar range:  $2.61 \pm 1.75 \mu\text{M}$  (MS023) and  $2.62 \pm 1.99 \mu\text{M}$  (GSK3368715). This indicated that there was a ten-fold difference between the concentration at which PRMT1 activity was inhibited (around 60nM) and the concentration at which these inhibitors affected cell viability ( $> 1 \mu\text{M}$ ). This implies that inhibiting PRMT1 activity alone was not sufficient to kill cells, and the effect we observe on cell viability could be due to the inhibition of several type I PRMTs.

In contrast, in a colony-forming assay when cells were cultured on plastic, we observed smaller sized colonies when MDA-MB-468 cells were treated with lower doses of the inhibitors (**Figure 64C**), at which they specifically target PRMT1 (**Figure 64A**). This suggests that inhibiting PRMT1 could decrease the colony-forming ability of MDA-MB-468 cells. Considering both these assays (i.e., cell viability and colony formation), we clearly see a difference in the concentrations at which the inhibitors exhibit an effect. In the first assay where the metabolic activity is used as a measure of cell viability (**Figure 64B**), we can speculate that inhibiting PRMT1 alone (i.e., low doses of the type I inhibitors) is not enough to impair active cell metabolism (maybe due to a compensatory mechanism by the other PRMTs), and thus required higher doses in the micromolar range to inhibit cell viability. In contrast, in the colony formation assay (**Figure 64C**), which is essentially a measure of cell survival (and proliferative ability of individual cells), PRMT1 inhibition (as seen at low inhibitor concentrations) was sufficient to impair colony formation, similar to the observation of PRMT1 depletion.

Then, we wanted to evaluate the anti-tumor effect of inhibiting PRMT1, *in vivo*. To do this, we have focused our study on the PRMT1 inhibitor (GSK3368715) which is currently being evaluated in clinical trials (NCT03666988) for other cancer types. First, we injected Swiss-nude mice with MDA-MB-468 cells and once the tumor was established (tumor size  $>60\text{mm}^3$ ), we grafted them into two groups of mice and randomly distributed them into the study (GSK3368715 treated) and control (vehicle-treated) groups. GSK3368715 was administered once daily at 80mg/kg once the tumors were palpable. We first tested this inhibitor at 100mg/kg for a period of 18 days and observed no visible toxicity in the mice in terms of mortality or body weight loss (**Figure 65B**). After 7 weeks of treatment, we observed a significant decrease in tumor growth (**Figure 65C, D**). The *in vivo* efficacy of this PRMT1 inhibitor (GSK3368715), has been previously tested in the same MDA-MB-468 model where the mice were administered with a higher dose (150mg/kg) of the inhibitor [326]. In our study, we confirm their results using lower doses (80mg/kg) of the same inhibitor, and by treating mice engrafted with tumors, instead of mice injected with cells [326]. Our

experiment shows that a lower dose of GSK3368715 was sufficient to delay tumor growth.

Altogether, our results show that depending on the readout used to measure cell proliferation (standard MTT assay or colony formation), the inhibitor concentrations at which we observe an effect varied. This suggested that maybe PRMT1 activity is required for BC cell survival, but we will have to test a larger panel of BC cells to extend this hypothesis. Most importantly, type I PRMT inhibition using GSK3368715 decreased tumor volume at half the dose than previously reported (80mg/kg in this study, 150mg/kg [326]), suggesting that this inhibitor could represent a new drug to treat BC patients, although this has to be verified in other *in vivo* models (to account for the heterogeneity of BC), by using in BC patient-derived xenograft models.



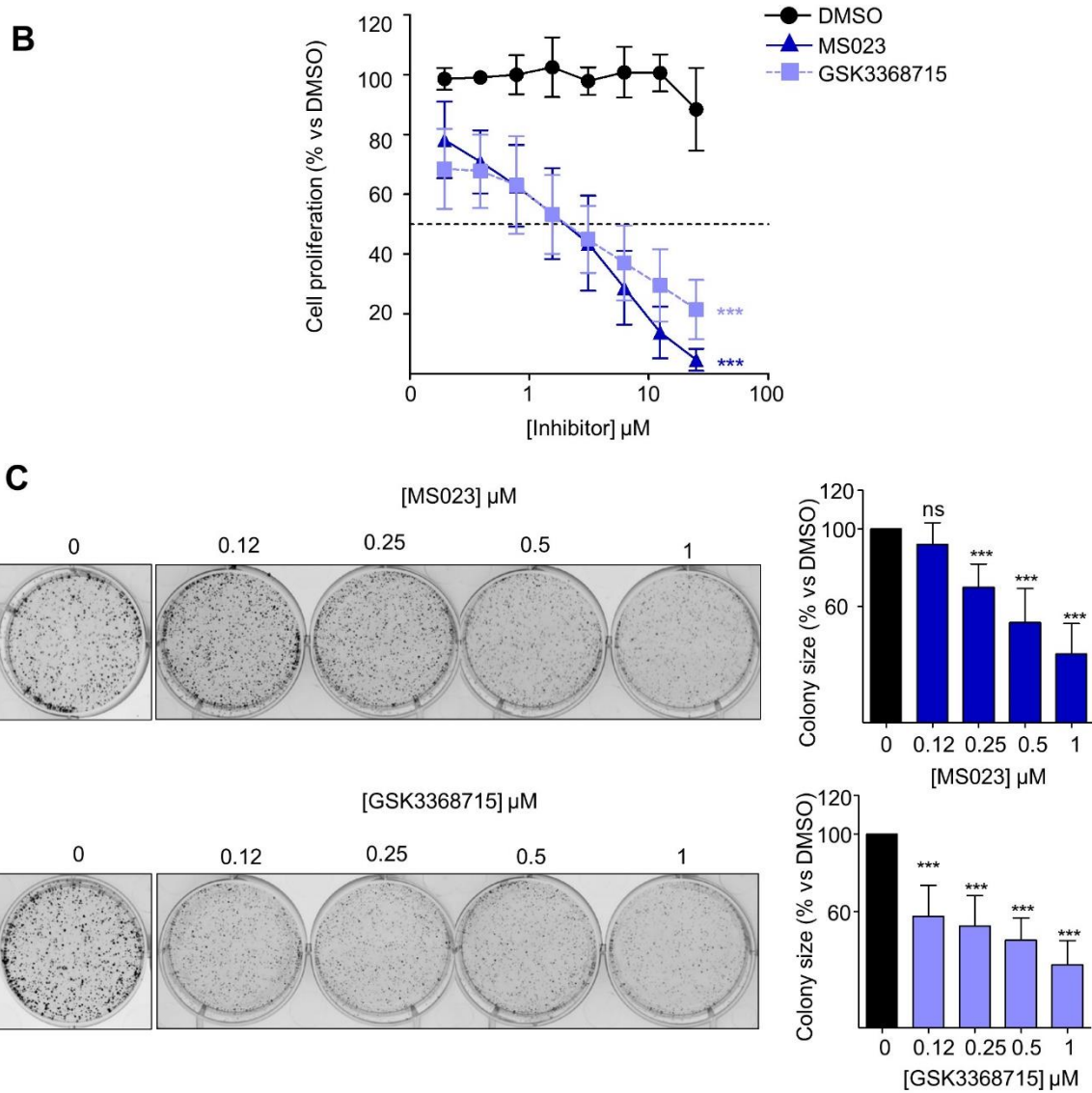


**Figure 64: PRMT1 inhibition decreases the BC cell proliferation in MDA-MB-468 cells.** (A) MDA-MB-468 cells were treated with MS023 and GSK3368715 for 48h. Methylation of histone H4 on R3 (H4R3me2a) was used to measure PRMT1 inhibition by western blotting. Methylation of PABP1 (me-PABP1) was used to measure CARM1 activity and histone H3 methylation (H3R17me2a) to assess CARM1 and PRMT6 activity. Anti-PABP1, histone H3, histone H4, CARM1, PRMT1 and tubulin were used as loading controls. (B) MS023 and GSK3368715 decrease MDA-MB-468 cell viability (MTT assay 7 days). Results are presented as the percentage of cell growth relative to DMSO-treated cells. The dotted line indicates the 50% cell proliferation mark. (C) PRMT1 inhibition decreases the size of colonies when MDA-MB-468 cells were cultured on plastic for 9 days after treatment. All the data are expressed as the mean  $\pm$  SD from at least three independent experiments (B, C). Pictures are from a single experiment, representative of three independent experiments (A, C). P values from a Student t-test are represented as \* $p < 0.05$ ; \*\* $p < 0.01$ ; \*\*\* $p < 0.001$ .

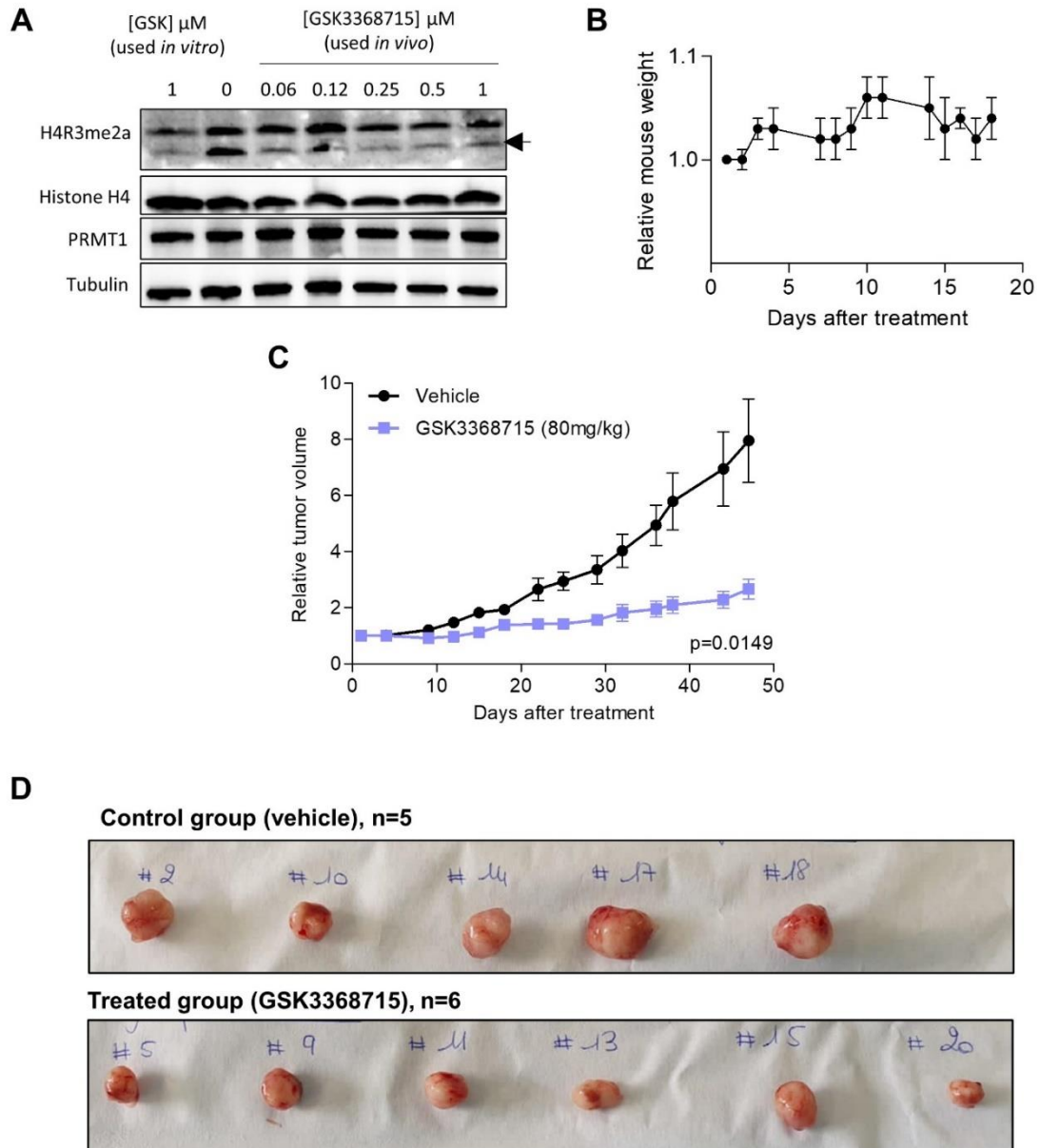


**Figure 65: GSK3368715 inhibits PRMT1 activity, shows no toxicity to mice and impairs tumor growth.** (A) GSK3368715 inhibitor used for the *in vivo* experiment was validated for efficient PRMT1 inhibition in MDA-MB-468 cells (48h treatment). GSK3368715 inhibitor used for the *in vitro* experiments was used as positive control (GSK). Anti-H4R3me2a was used to measure PRMT1 activity (arrow indicates the decrease in the methyl mark) and histone H4, PRMT1 and tubulin were used as loading controls. Pictures are from one experiment. (B) GSK3368715 shows no toxicity for mice. Swiss-nude mice (n=3) were administered GSK3368715 at 100 mg/kg per-os (p.o.), once daily. Treatment was not associated with any mortality or body weight loss over the 18-day experimental period. (C) PRMT1 inhibition impairs tumor growth, *in vivo*. MDA-MB-468 ( $12 \times 10^6$ ) cells were injected into three swiss-nude mice and once tumors grew to a reasonable size (60-80mm<sup>3</sup>), they were subcutaneously grafted onto 12 mice, then divided into two study groups. The mice (n=6) were administered GSK3368715 (80mg/kg), once daily (orally), and control mice were treated with vehicle (n=6). Tumor volume was measured twice weekly with calipers. Growth curves were obtained by plotting relative tumor volume mean versus time  $\pm$  SEM. P-value was calculated using a Mann-whitney U test. (D) Images of tumors excised from the two study groups, control (vehicle, n=5) and treated (GSK3368715, n=6) at the end of the 7-week treatment.

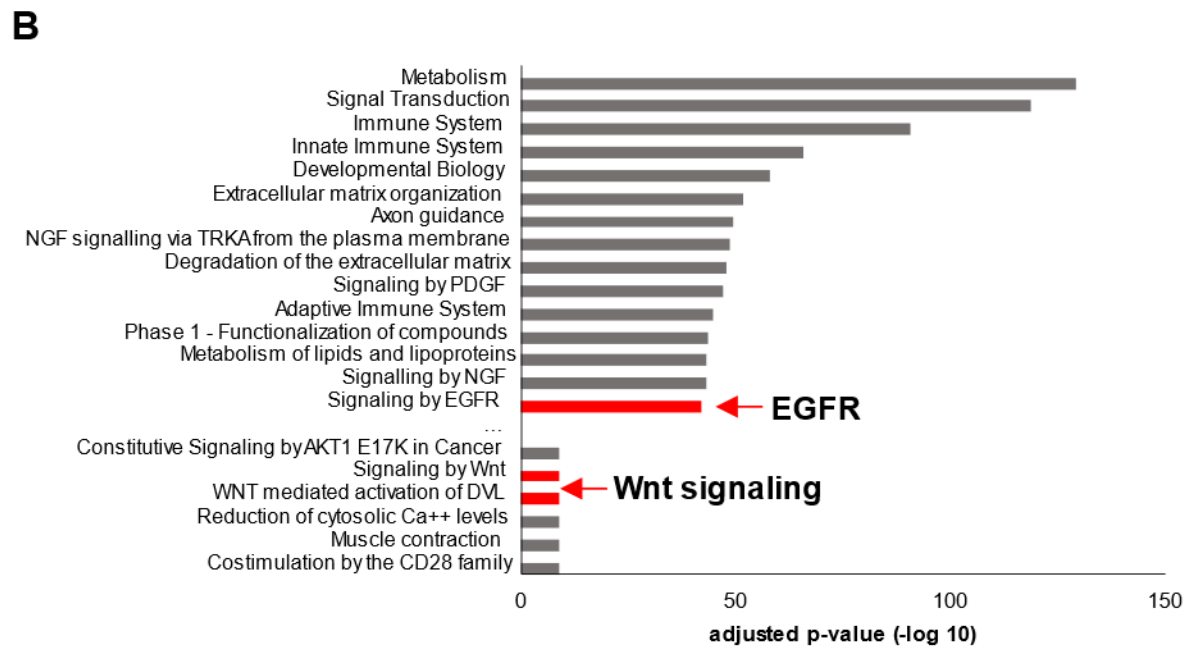
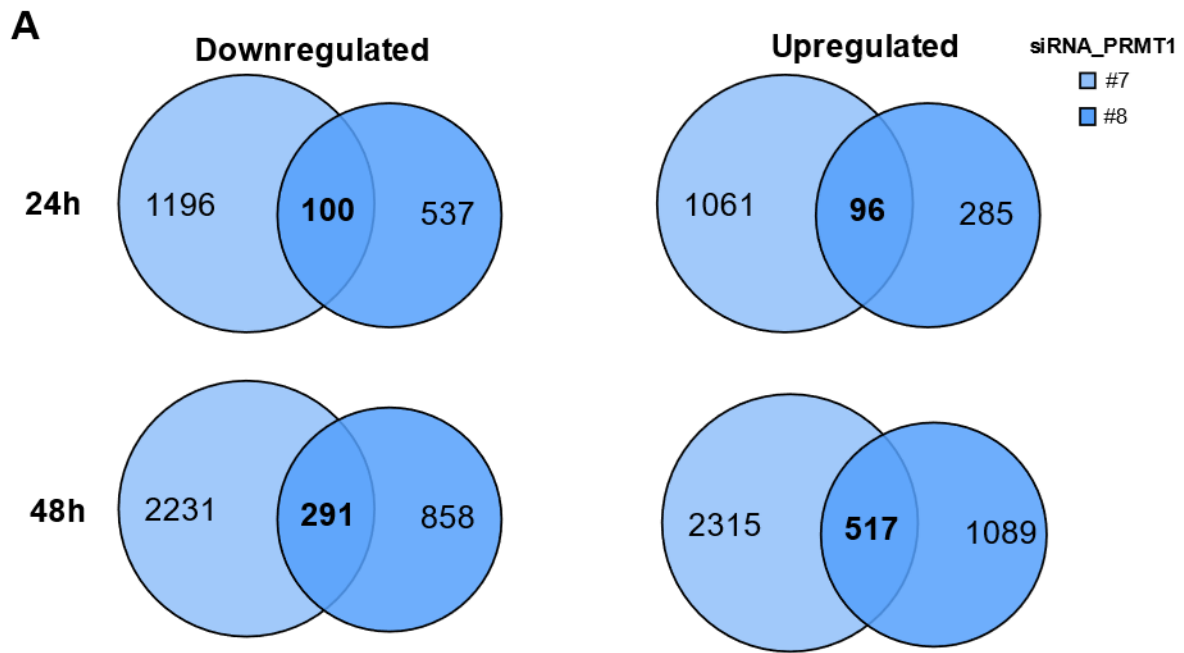
## **EGFR and Wnt pathway identified in the transcriptome of PRMT1-depleted cells**

Next, as one of the main functions to be reported for PRMT1 is in transcriptional regulation [164], we sought to understand the pathways that might be regulated by PRMT1 in TNBC cells and if they could contribute to BC cell survival. For this purpose, we performed a transcriptomic analysis in MDA-MB-468 cells depleted for PRMT1 using 2 different siRNAs for 24h and 48h using HTA 2.0 microarrays (Affymetrix). We found a greater number of genes up- and down-regulated using siRNA PRMT1#7 than PRMT1#8 (**Figure 66A**), most probably due to a more efficient knock-down using siRNA #7 (**Figure 66C**). Hence, we chose to focus on the genes that were commonly up- or down-regulated between both siRNAs.

We performed a gene enrichment pathway analysis on the list of genes that were differentially regulated (common to both siRNAs) after 48h using the REACTOME database. The top 15 pathways (ranked by adjusted p-value) revealed several that have been previously reported to be regulated by PRMT1 such as growth factor receptor signaling (like PDGF, EGFR), developmental biology, and immune system, to name a few [162, 163]. Notably, the EGFR signaling pathway ( $p = 1.16 \times 10^{-42}$ ; **Figure 66B**) is regulated by PRMT1 by either directly methylating EGFR [383] or controlling its transcription [381]. We observed that EGFR mRNA was downregulated after PRMT1 depletion in the Affymetrix analysis (**Figure 66C**) and we validated this observation by qPCR (**Figure 67A**). Further, we identified that PRMT1 was enriched on the promoter of *EGFR* when we immunoprecipitated the chromatin from MDA-MB-468 cells (which express high levels of EGFR) using an anti-PRMT1 antibody (**Figure 67B**). Our results are consistent with Yao and colleagues who described that PRMT1 depletion decreased EGFR mRNA in a colorectal cancer model and that PRMT1 co-operated with the transcription factor SMARCA4 to activate EGFR transcription [381]. Additionally, our results demonstrate a more direct role of PRMT1 in regulating EGFR transcription since we show directly its recruitment to the *EGFR* promoter.

Moreover, we also noticed that the Wnt signaling pathway, a pathway studied in our laboratory for several years [106, 108, 664], was significantly deregulated upon PRMT1 depletion ( $p = 1.12 \times 10^{-9}$ ) (**Figure 66B**). We found several genes involved in the Wnt pathway to be regulated by PRMT1 (**Figure 68**) and among these were LRP5 and Porcupine (PORCN) (**Figure 66C, Figure 68**), which are direct and important players in this pathway. LRP5 (with LRP6) is a co-receptor that interacts with the transmembrane protein Frizzled to activate Wnt signaling [95]. PORCN is a palmitoyl-transferase that acylates the Wnt ligands in the endoplasmic reticulum [95]. This modification aids in the transport and secretion of the Wnt ligands, thereby activating Wnt signaling by binding to Frizzled-LRP5/6 receptors [666]. As these two genes are important to Wnt signaling and were identified as commonly downregulated between the two PRMT1 siRNA, we pursued further analysis on these two genes.





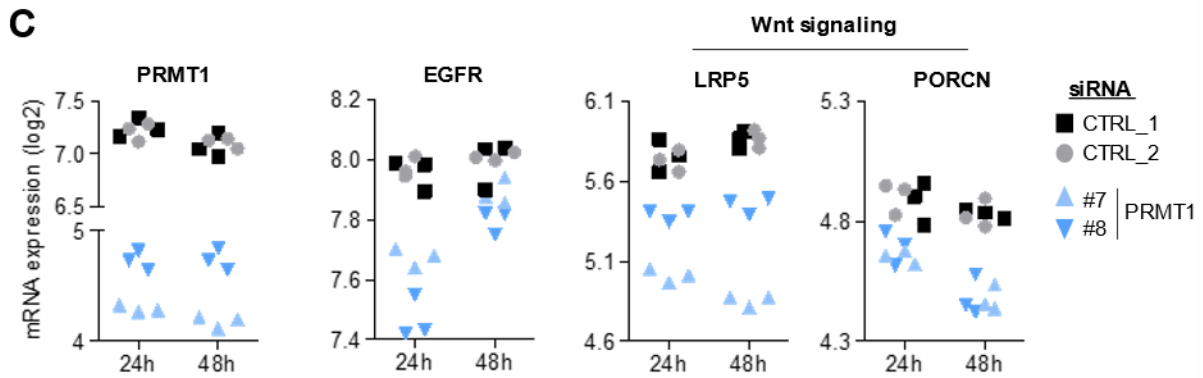


**Figure 66: PRMT1 regulates the transcription of EGFR and Wnt components (LRP5, PORCN).** (A) MDA-MB-468 cells were transfected with control and two siRNAs targeting PRMT1 (#7, #8) for 24h and 48h. Venn diagrams indicate the number of mRNAs, identified by Affymetrix microarrays, that were up- and down-regulated following PRMT1 depletion. (B) Gene enrichment pathway analysis was performed in the commonly down-regulated genes after PRMT1 depletion for 48h and ranked according to their significance (adjusted p values). The p-values were logarithmically transformed (-log base 10). EGFR and Wnt signaling pathways are highlighted by red bars and red arrows. (C) PRMT1, EGFR, LRP5, and PORCN gene expression as determined by the Affymetrix array. mRNA expression was logarithmically transformed (log 2) and each replicate is represented as a single point on the scatter plot. Two control siRNAs (CTRL\_1, black and CTRL\_2, grey) and two siRNAs targeting PRMT1 (#7, light blue and #8, dark blue) are shown.

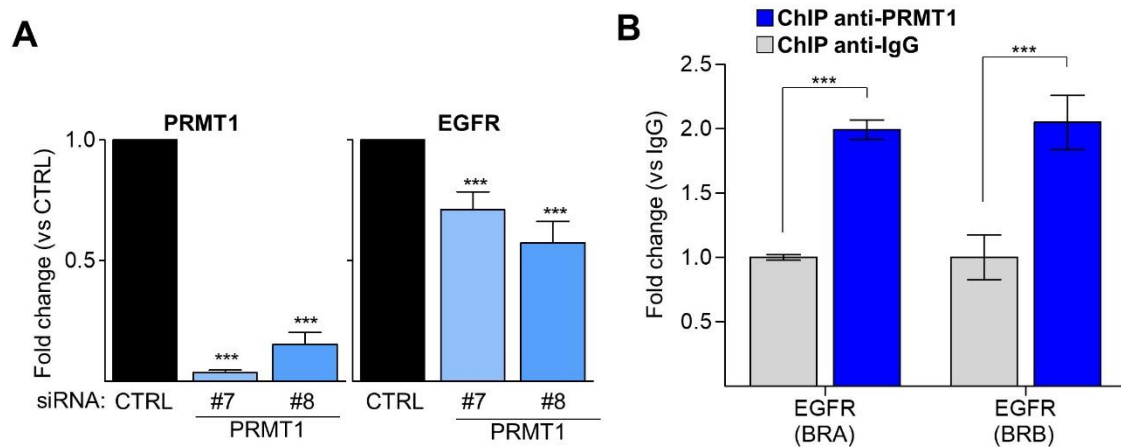


**Figure 67: PRMT1 regulates EGFR transcription by binding to its promoter.** (A) MDA-MB-468 cells were transfected with siRNA control (CTRL) or two siRNAs targeting PRMT1 (#7,#8) for 24h and gene expression was analyzed by qPCR and shown normalized to actin. The quantifications are represented as fold-change relative to siRNA control (CTRL) and presented as mean  $\pm$  SD from three independent experiments. (B) PRMT1 binds to the promoter region of EGFR. ChIP was performed using anti-PRMT1 (blue bars) or immunoglobulin (IgG, grey bars) antibodies, in MDA-MB-468 cells, followed by qPCR using primers for two promoter binding regions of EGFR (binding region A, BRA or binding region B, BRB) (see page 228 for details). The quantifications are represented as fold change relative to the IgG and presented as mean  $\pm$  SEM from three independent experiments. P values from Student t test are represented as \*p < 0.05; \*\*p < 0.01; \*\*\*p < 0.001.

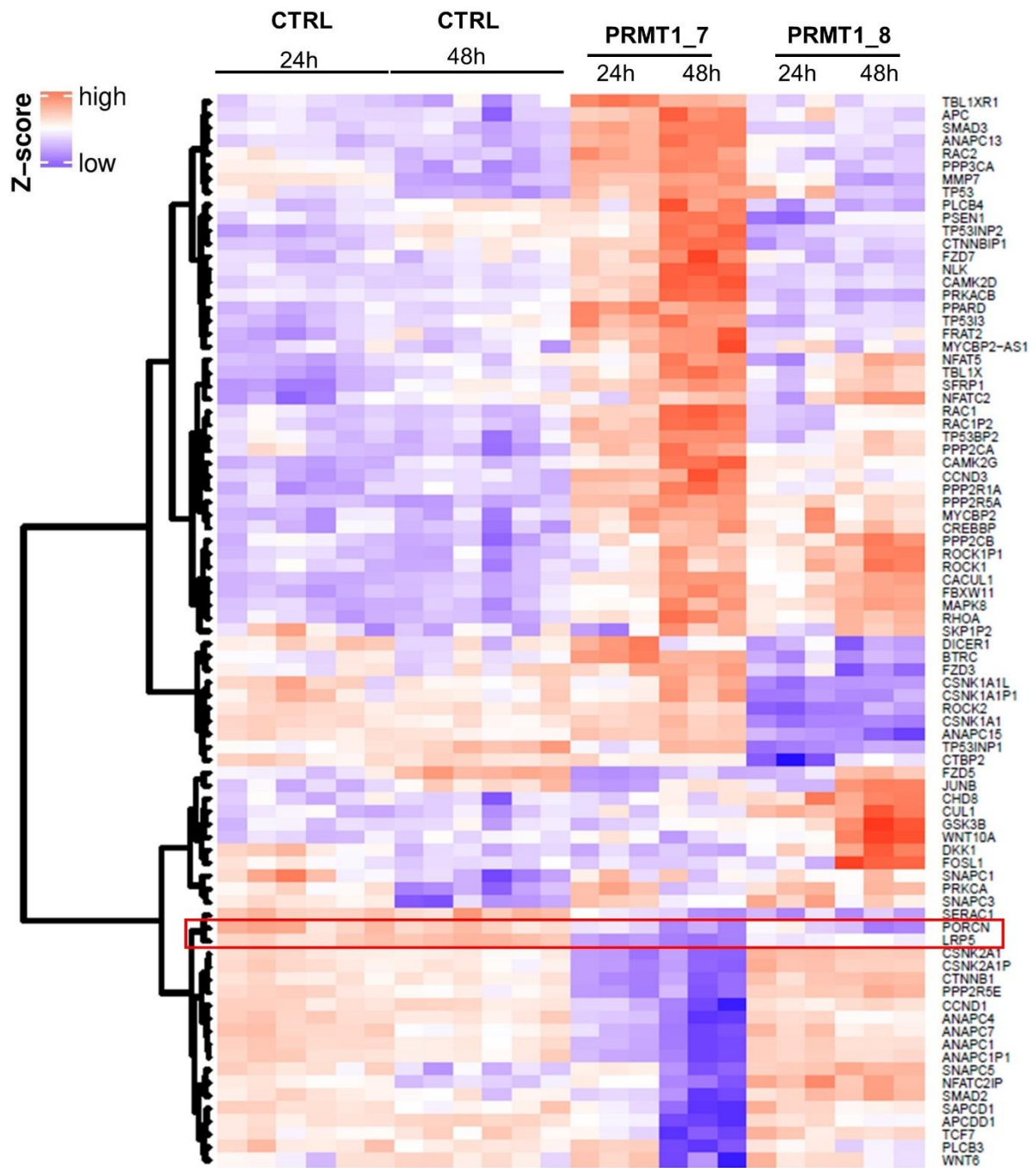


**Figure 68: Wnt pathway genes deregulated by PRMT1 depletion.** The genes that were differentially expressed in the PRMT1-depleted transcriptome were compared to the KEGG curated gene set for Wnt signaling pathway (gene set ID: hsa04310, from the GSEA website, <https://www.gsea-msigdb.org/gsea/index.jsp>; [667, 668]) and represented as a heatmap, showing only those genes that were significantly deregulated (adjusted p-value <0.05 and fold-change (FC) > 1.2). Fold-change <1.2 was not considered for the analysis here. LRP5 and PORCN are clustered together and down-regulated at 24h and 48h with both PRMT1 siRNAs (PRMT1\_7, PRMT1\_8) vs the control siRNA (CTRL). Color bar represents Z-score, with a low score in blue and a high score in red.

## **PRMT1 activates the canonical Wnt signaling pathway**

After identifying two crucial genes (LRP5 and PORCN) in the Wnt pathway to be regulated by PRMT1, we wanted to further understand how PRMT1 regulates their mRNA expression and what is the consequence of PRMT1 depletion on Wnt signaling activity. First, we confirmed that PRMT1 depletion decreased the mRNA level of LRP5 and PORCN by qPCR in the MDA-MB-468 cells (**Figure 70A**). We also validated this in another BC cell line, T47D (**Figure 70B**), showing a decrease in LRP5 mRNA upon PRMT1 depletion, but the results were inconclusive for PORCN expression (data not shown), due to a reproducibility issue between the two experiments (additional trials might yield conclusive results). As RNA and protein expression do not always match, we wanted to analyze the protein expression level of LRP5 and PORCN upon PRMT1 depletion. LRP5 protein level decreased when PRMT1 was silenced using siRNA in MDA-MB-468 (**Figure 69A**) and T47D (**Figure 70C**) cells. Unfortunately, we were unable to check the porcupine protein level since we did not find a specific antibody for western blotting. Together, this showed that PRMT1 controlled the expression of LRP5 at the mRNA and protein levels and PORCN at the mRNA level.

Next, we sought to understand how PRMT1 regulates the transcription of LRP5 and PORCN. Since the PRMT family are well-known for their function in transcriptional activation/repression [164], by directly or indirectly binding to the promoters of their target genes, we performed chromatin-immunoprecipitation (ChIP) in the MDA-MB-468 cells using an anti-PRMT1 antibody. For analyzing the ChIP by qPCR, we designed specific primers targeting regions upstream of both LRP5 and PORCN genes that were putative binding sites for PRMT1 based on previously published ChIP-sequencing (ChIP-seq) data [362]. Here, we observed an enriched binding of PRMT1 as compared to the control (IgG) on both *LRP5* and *PORCN* promoter regions (**Figure 69B**).

Therefore, these results suggested that PRMT1 was regulating LRP5 and PORCN expression by directly binding to their promoter regions.

As mentioned before, both LRP5 and PORCN are crucial genes that activate the Wnt signaling cascade. Given that PRMT1 regulates their expression, we sought to evaluate if PRMT1 could also control Wnt signaling activity. For this, we performed two different assays, (i) assessing Wnt target gene expression by qPCR and (ii) the gold-standard  $\beta$ -catenin activated reporter (BAR) assay. Our previous work revealed Axin2, APCDD1, and NKD1 as the three top Wnt target genes that were upregulated upon Wnt3a stimulation in MDA-MB-468 cells [664]. Hence, we chose these target genes and observed that depleting PRMT1 using siRNA decreased the expression of all three genes (**Figure 69C, top panel**). We further confirmed that PRMT1 depletion decreased Wnt signaling activity using the BAR assay (**Figure 69D**). We used siRNA targeting LRP6 as a positive control for both Wnt target gene expression and BAR assays. Therefore, our results indicated that PRMT1 positively regulates the canonical Wnt signaling pathway.

Next, to understand if the enzymatic activity of PRMT1 was required for regulating Wnt activity, we inhibited PRMT1 using MS023 and GSK3368715 (at 0.1 $\mu$ M and 0.5 $\mu$ M) for 72h in the MDA-MB-468 cells and measured Wnt activity by the BAR assay. We first verified that PRMT1 activity was inhibited in this assay by analyzing the expression of the histone mark H4R3me2a (**Figure 69E**). Similar to depleting PRMT1, inhibiting its activity also decreased Wnt signaling in a dose-dependent manner (**Figure 69F**). This suggests that PRMT1 enzymatic activity is required for Wnt signaling, maybe by methylating histones (to activate downstream target genes) or directly methylating Wnt players.

Collectively, our results showed that PRMT1 regulated the transcription of two important genes involved in the Wnt pathway: LRP5 and PORCN, by directly being recruited to their promoter regions. Further, PRMT1 silencing also decreased Wnt target gene expression and  $\beta$ -catenin dependent Wnt signaling. This implies that when PRMT1 protein is no longer present in the cell, Wnt signaling was inhibited by two mechanisms: (i) by regulating the transcription and protein expression of LRP5, therefore, decreasing the amount of LRP5 available at the membrane to activate downstream signaling, (ii) regulating the mRNA expression of PORCN, possibly leading to a decrease in its protein causing less Wnt ligand secretion. Moreover, we show that the methyltransferase activity of PRMT1 was required for its function in Wnt signaling activity, supporting previous work by Bikkavilli et al. where PRMT1-mediated methylation of two proteins (G3BP1, G3BP2) activated the Wnt pathway [388, 389]. This also suggests that PRMT1 activity could be important for regulating *LRP5* and *PORCN* expression, maybe by methylating histone H4 (H4R3me2a) on their promoter regions. This could be explored and validated in the future by performing a ChIP using an anti-H4R3me2a antibody.

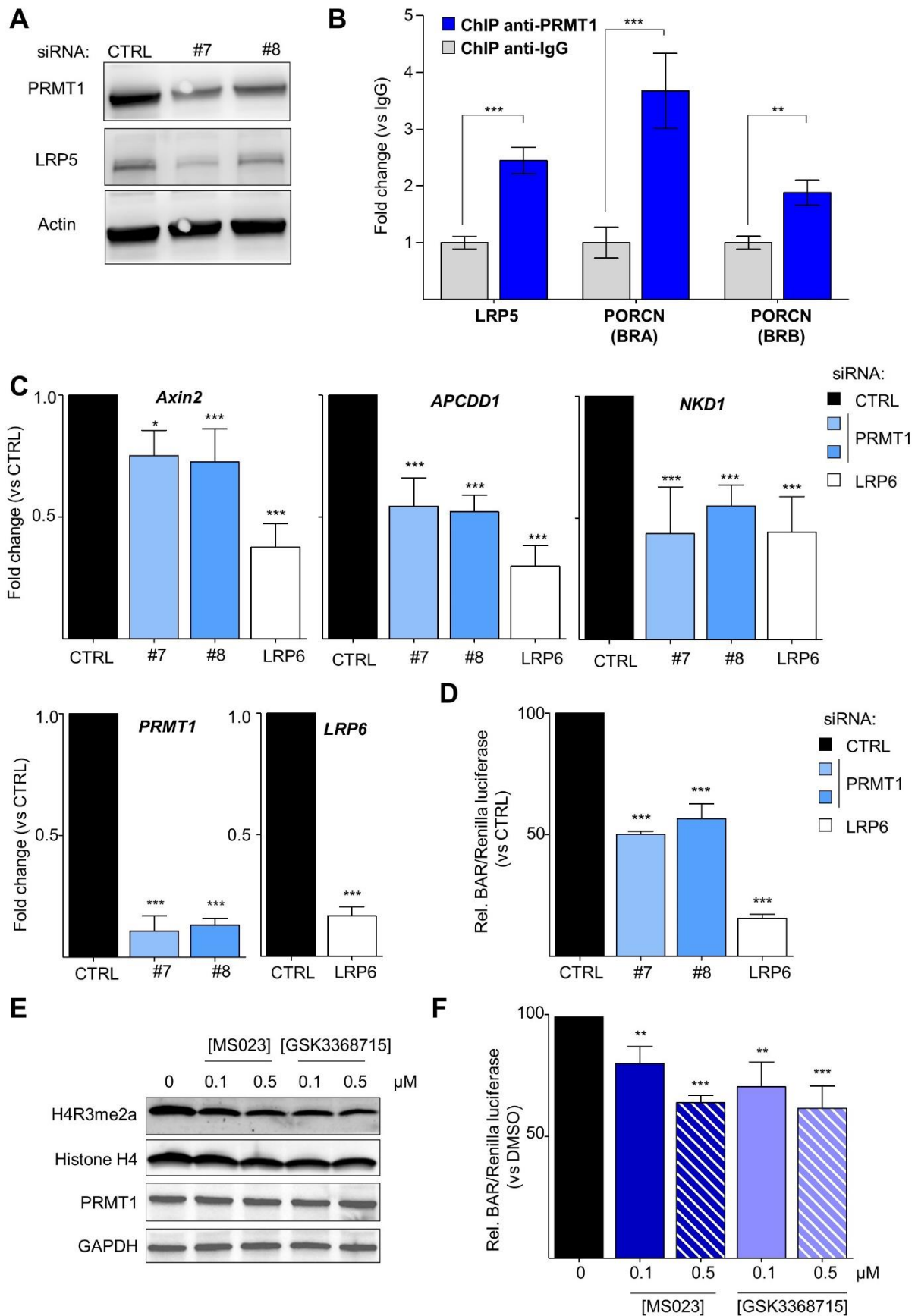


**Figure 69: PRMT1 positively regulates the Wnt signaling pathway.** (A) PRMT1 depletion decreases LRP5 protein level by western blotting. Antibody against actin was used as a loading control. (B) PRMT1

binds to the promoter region of LRP5 and PORCN. ChIP was performed using anti-PRMT1 (blue bars) or immunoglobulin (IgG, grey bars) antibodies, in MDA-MB-468 cells, followed by qPCR using primers for the promoter binding region of *LRP5* and *PORCN* (binding region A, BRA or binding region B, BRB). (C) PRMT1 depletion decreases Wnt target gene expression. MDA-MB-468 cells are transfected with siRNA control (CTRL), two siRNA targeting PRMT1 (#7, #8) or against LRP6 for 48h and stimulated with Wnt3a conditioned media for 6h. Axin2, APCDD1, NKD1 (Wnt target genes), PRMT1 and LRP6 expression were determined by qPCR normalized to actin. (D) PRMT1 depletion decreases Wnt signaling activity. MDA-MB-468 cells are transfected with siRNA control (CTRL) or two siRNA targeting PRMT1 (#7, #8) for 48h, co-transfected with plasmids coding for BAR-firefly luciferase and Renilla luciferase for 24h. The cells are stimulated with Wnt3a conditioned media for 6h and the relative luciferase signal (firefly luciferase divided by Renilla luciferase) is represented as a percentage normalised to the control siRNA (CTRL). (E) PRMT1 inhibition was verified by western blotting using anti-H4R3me2a antibody and histone H4, PRMT1, and GAPDH were used a loading controls in MDA-MB-468 cells inhibited for 72h using MS023 and GSK3368715. (F) PRMT1 inhibition decreases Wnt signaling activity. MDA-MB-468 cells were treated with type I inhibitors (MS023 and GSK3368715) for 72h using two concentrations as indicated, and then co-transfected with plasmids coding for BAR-firefly luciferase and Renilla luciferase for 24h. The cells are stimulated with Wnt3a conditioned media for 6h and the relative luciferase signal (firefly luciferase divided by Renilla luciferase) is represented as a percentage normalised to the DMSO treated cells (0). siRNA targeting LRP6 was used as a positive control (C, D). All quantifications are represented as fold change (B, C) or percentage (D, F) relative to the control. The data are expressed as the mean  $\pm$  SD from at least three independent experiments (B, D, F). For (C), the data are presented as mean  $\pm$  SEM. P values from Student t-test are represented as \* $p < 0.05$ ; \*\* $p < 0.01$ ; \*\*\* $p < 0.001$ . Pictures are representative of three independent (A) or one (E) experiment(s).

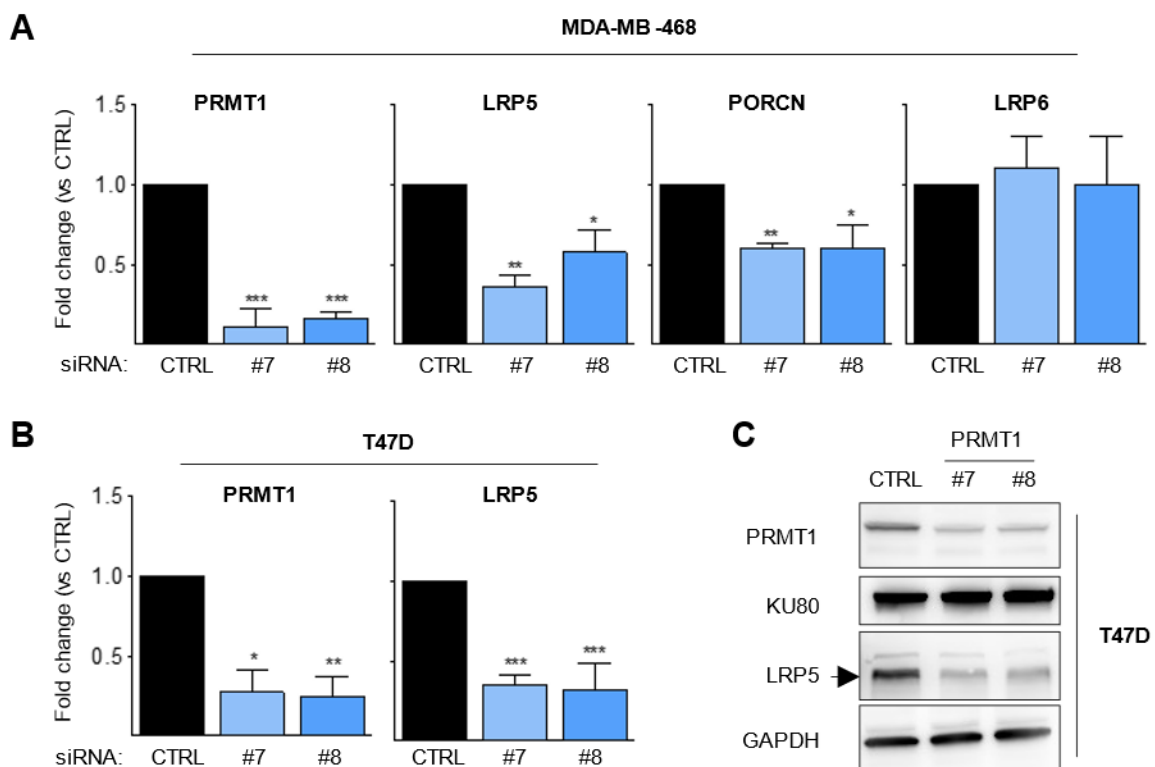


**Figure 70: PRMT1 depletion decreases LRP5 and PORCN expression.** MDA-MB-468 (A) or T47D (B, C) cells were transfected with control (CTRL) or two siRNAs against PRMT1 (#7, #8) for 48h and gene expression of indicated genes were assessed by qPCR (A, B) or by western-blotting (C). All gene expressions are represented as fold change relative to the siRNA control (CTRL), normalized to actin

expression. The data are expressed as the mean  $\pm$  SD from at least three (A) or two (B) independent experiments. P values were calculated using a Student t-test and are represented as \* $p < 0.05$ ; \*\* $p < 0.01$ ; \*\*\* $p < 0.001$ . (C) Antibodies against KU80 and GAPDH were used as a loading control. Arrow indicates band corresponding to LRP5. The image is representative of two independent experiments.

### **Synergistic interaction between Type I PRMT inhibitors and Erlotinib/standard of care chemotherapy**

A major challenge in treating TNBC patients is their acquired drug resistance and therefore, drug combination therapy has gained popularity to combat this issue. Our results indicated that depleting PRMT1 was sufficient to induce BC cell mortality. On the other hand, the concentration at which PRMT1 inhibition decreased cell proliferation depended on the type of assay used to determine cell viability. Nevertheless, PRMT1 inhibition decreased cell proliferation. Hence, we sought to investigate several drug combinations using these Type I PRMT inhibitors with the standard of care chemotherapies routinely used in the clinic to treat BC patients (such as cyclophosphamide, cisplatin, taxanes, doxorubicin, and camptothecin). We first identified the IC<sub>50</sub> concentration for each of the chemotherapeutic agents in the cell line of interest (MDA-MB-468, **Table 3**).

**Table 3: IC<sub>50</sub> values of drugs used in the combination analysis.**

<b>Inhibitor/drug (concentration)</b>	<b>IC<sub>50</sub> values (mean <math>\pm</math> SD)</b>	<b>Concentration range used for combination</b>
<b>Doxorubicin (nM)</b>	19.9 $\pm$ 6.75	0-70 nM
<b>Camptothecin (nM)</b>	7.74 $\pm$ 2.93	0-25 nM
<b>4-hydroperoxy cyclophosphamide (<math>\mu</math>M)</b>	1.22 $\pm$ 0.86	0-5 $\mu$ M
<b>Docetaxel (nM)</b>	0.6 $\pm$ 0.24	0-1 nM
<b>Paclitaxel (nM)</b>	5.36 $\pm$ 0.90	0-1 nM
<b>Cisplatin (nM)</b>	130 $\pm$ 50	0-200 nM
<b>Erlotinib (<math>\mu</math>M)</b>	1.95 $\pm$ 0.49	0-5 $\mu$ M
<b>LGK974 (<math>\mu</math>M)</b>	11.32 $\pm$ 1.62	0-10 $\mu$ M

MDA-MB-468 cells were treated with the following inhibitors/drugs for 7 days and cell viability was assessed by MTT or CellTiterGlo assay. Values are represented as mean  $\pm$  SD from at least two independent experiments.

Then, we treated the MDA-MB-468 cells with the different drug combinations using approximately twice the IC<sub>50</sub> values for the chemotherapy drugs and Type I PRMT inhibitors for 7 days (equivalent to 4 mitotic cycles) and measured cell viability using the CellTiterGlo assay. To calculate the synergy between each drug pair, we used the Combenefit software [669] and applied the Loewe additivity model since this model allows the possibility that the two drugs could have interacting modes of action [670]. The drug interaction matrix using the Loewe model showed additivity between the two Type I PRMT inhibitors and cyclophosphamide (**Figure 71A**), camptothecin (**Figure 71B**) and cisplatin (**Figure 71C**). It must be noted that we treated the MDA-MB-468 cells with the active metabolite form of cyclophosphamide known as 4-hydroperoxy cyclophosphamide (4-HPCy) because cyclophosphamide needs to be metabolized and

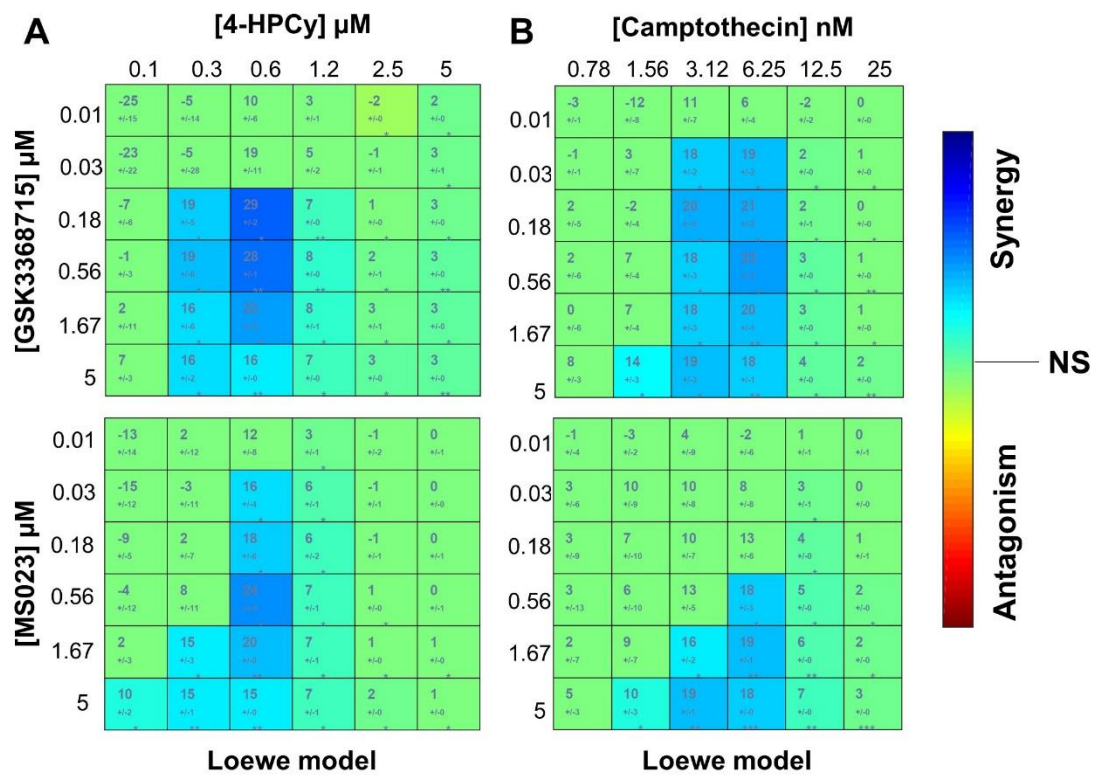


*in vivo*, this occurs in the liver [671]. More importantly, we observed additive interactions between the above-mentioned chemotherapies and the type I PRMT inhibitors at low doses (i.e., concentrations where PRMT1 activity is specifically inhibited), therefore indicating that the additive effects could be specific to PRMT1 inhibition.

On the other hand, for the other three chemotherapeutic agents (docetaxel, paclitaxel, and doxorubicin), the interaction matrix indicated no additivity as none of the values were statistically significant (cells colored in green, **Figure 72A, B, C**). To get a global overview (additivity/synergy) of the interactions occurring between each of these drug pairs, we exploited a metric that the Combenefit software generates, the "SUM\_SYN\_ANT" metric. This is defined as the sum of synergy and antagonism observed in concentration logarithmic space [669]. Then, we described net synergy based on another study [672], where scores  $> +2.0$  are considered to be synergistic,  $< -2.0$  to be antagonistic and between  $-2.0$  and  $+2.0$  to be neutral (**Figure 72D**). For the drug pairs that showed additivity, we observed "SUM\_SYN\_ANT" metric  $> 2.0$ , namely cisplatin (+29.0 with GSK3368715 and +5.9 with MS023), cyclophosphamide (+27.3 with GSK3368715 and +20.1 with MS023), and camptothecin (+31.1 with GSK3368715 and +27.7 with MS023) suggesting that they were highly synergistic (**Figure 72D**).

EGFR has been proposed as a potential therapeutic target for TNBC since it is overexpressed in  $>70\%$  of these tumors [673]. As we and others have shown that PRMT1 activates the transcription of EGFR in BC and CRC (**Figure 66, Figure 67**, [381]) and downstream signaling by methylating EGFR [382, 383], we sought to explore the drug interactions between the two Type I PRMT inhibitors and an EGFR inhibitor (erlotinib). Similar to the combination with the chemotherapies, we treated the MDA-MB-468 cells with twice the  $IC_{50}$  concentration of erlotinib (**Table 3**). The drug matrix showed several cells that were significantly additive (in blue, **Figure 71D**), suggesting that the interaction between erlotinib and the two Type I PRMT inhibitors were highly synergistic. Indeed, we obtained the highest SUM\_SYN\_ANT metric for this drug combination (+45 with GSK3368715, +54 with MS023, **Figure 72D**) as compared to all the other drug pairs tested. This concurs with the fact that PRMT1-mediated methylation of EGFR contributes to resistance against cetuximab treatment (a monoclonal antibody targeting EGFR) [194, 383]. Therefore, co-inhibiting PRMT1 and EGFR could prove beneficial to TNBC patients overexpressing EGFR.

Lastly, we tested another drug pair combination, Type I PRMT inhibitors with a Wnt pathway inhibitor (namely LGK-974, which inhibits PORCN) especially since the Wnt signaling pathway is a known contributor to chemoresistance in TNBC [95, 662]. We used LGK-974 as it is being evaluated in phase I clinical trials for several Wnt ligand-dependent solid cancer, including TNBC (NCT01351103). We treated the MDA-MB-468 cells at the  $IC_{50}$  value for LGK-974 (**Table 3**) and observed no significant additive interaction between the inhibitors (data not shown) indicating that the effect was neutral between PRMT1 inhibitor and the PORCN inhibitor.



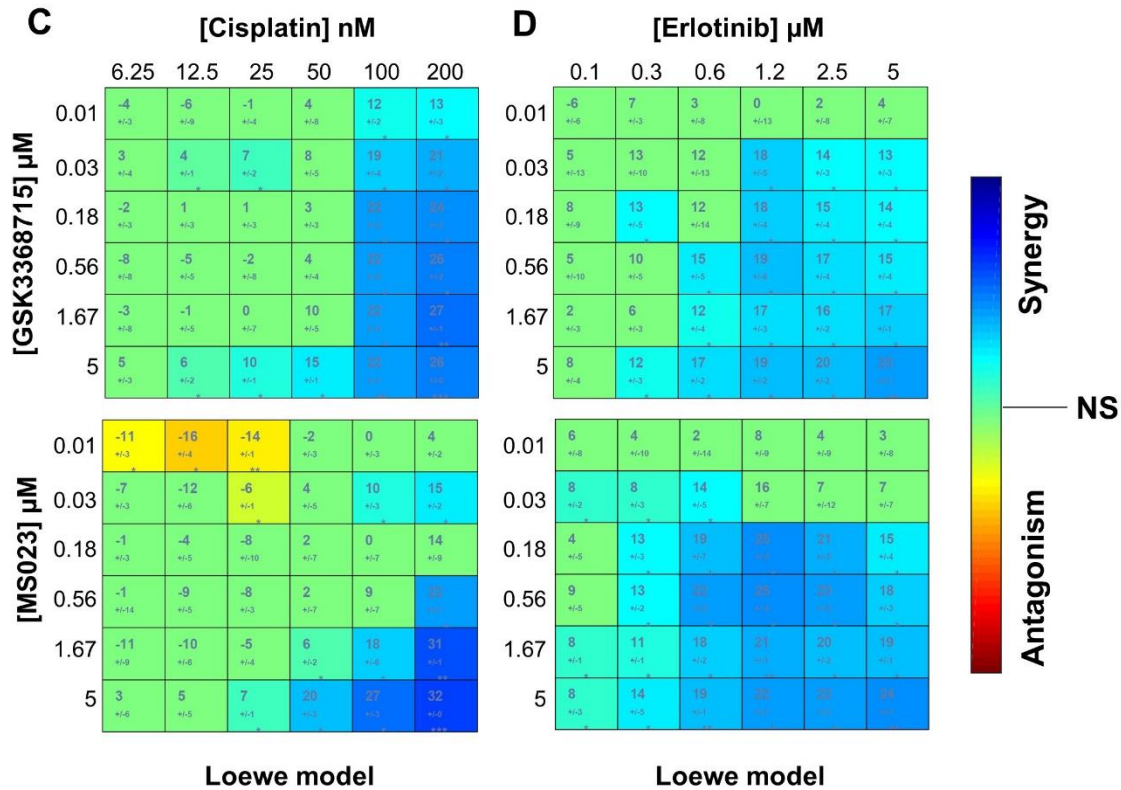


**Figure 71: Synergistic interaction between Type I PRMT inhibitors and chemotherapies or erlotinib.** MDA-MB-468 cells were seeded in 96-well plates, treated with the indicated drugs for 7 days (equivalent to 4 doubling times) and cell viability was measured by CellTiterglo assay. Type I PRMT inhibitors were serially diluted three-fold and the chemotherapies/erlotinib were serially diluted two-fold (concentrations indicated in the figure). The drug interactions were calculated using the Loewe model on the Combenefit software [669]. Synergy scores are represented as a matrix based on the Loewe additivity model. The larger numeral in each square of the matrix shows the mean synergy score from the three replicates of one experiment and the smaller numbers below indicate the standard deviation. Significance is calculated using a one-sample t-test and represented as \* $p < 0.05$ , \*\* $p < 0.01$ , \*\*\* $p < 0.0001$ . The matrix is colored as blue for synergy or red for antagonism only if the scores were significant. Scores that were not statistically significant (NS) are colored green. Synergy scores between the two Type I PRMT inhibitors (GSK3368715 and MS023) and standard chemotherapeutic agents used to treat breast cancer patients – 4-hydroperoxy cyclophosphamide (4-HPCy) (A), camptothecin (B), and cisplatin (C). (D) High synergy between the Type I PRMT inhibitors and erlotinib (an EGFR inhibitor). Presented data are representative of at least two (C) or three (A, B, D) independent experiments

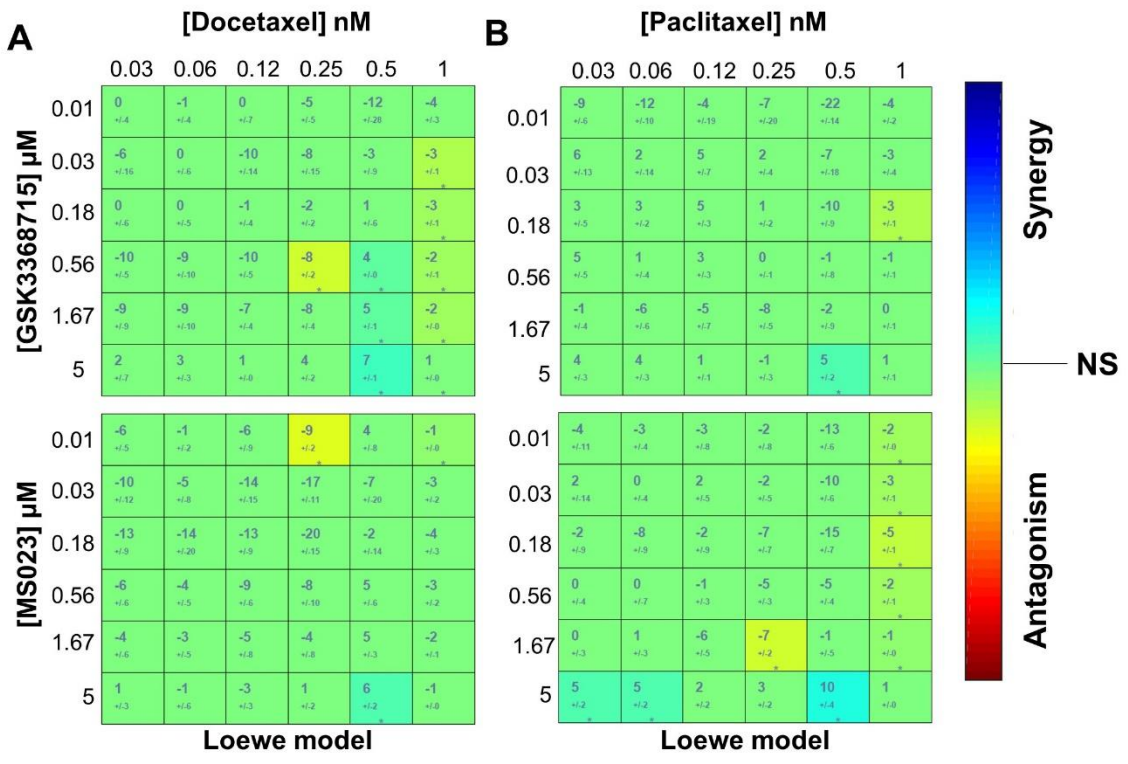


**Figure 72: Neutral effect between Type I PRMT inhibitors and certain chemotherapies (docetaxel, paclitaxel, doxorubicin).** See Figure 71 legend for a detailed description of the matrix representation. Presented matrices for each drug pair are from one experiment done in biological triplicates and are representative of three (A, B) independent experiments. The matrix in (C) shows one experiment done in biological triplicates out of two independent experiments. (D) The "SUM\_SYN\_ANT" metric is defined as the sum of synergy and antagonism observed in concentration logarithmic space [669]. This metric was used to define synergy or antagonism based on another study performing a similar analysis [672]. Synergy was defined when the SUM\_SYN\_ANT metric  $> +2.0$ , and antagonism when the metric was  $< -2.0$ . All scores between  $-2.0$  and  $+2.0$  were defined as neutral interactions, shown in the graph using the dashed lines on the y axis (at  $+2.0$ ). 4-HPCy: 4-hydroperoxy cyclophosphamide. The metric is calculated from one experiment done in triplicates but representative of two (for cisplatin) or three (all other chemotherapies) independent experiments.

## Discussion

Targeted therapy for breast cancer has greatly improved in recent years, but not for all subtypes, especially TNBC. The standard of care treatment is still chemotherapy and there is a dearth of therapeutic targets for this aggressive subtype. The PRMT family of enzymes have recently emerged as attractive druggable targets in various cancer types since they are often found overexpressed and several specific inhibitors have been developed [117]. In this study, we focused on PRMT1, the major type I PRMT and confirmed that it was indeed overexpressed in BC as compared to healthy breast tissue at the RNA and protein levels [133, 398, 399]. We report for the first time a membrane staining of PRMT1 in BC tumors more specifically with a higher proportion in TNBC and Her2+ BC subtypes. Further, we evaluated its therapeutic potential in breast cancer using siRNAs and the two recently developed type I inhibitors, MS023 and GSK3368715 [326, 350]. Indeed, we have demonstrated that PRMT1 depletion (i) decreased breast cancer cell viability, (ii) blocked their clonogenic potential and (iii) induced apoptosis in several breast cancer cell lines. This is concurrent with previous results in two TNBC cells [383, 399], luminal BC cells [409], and other cancer cell lines [381, 674-677].

To date, there are no PRMT1 specific small-molecule inhibitors, but rather inhibitors that target all type I PRMTs [326, 340, 350]. Unlike AMI-1 (a nonspecific pan PRMT inhibitor), the two newly developed type I inhibitors (MS023, GSK3368715) have been shown to be specific towards PRMT1 activity (but also PRMT6 and PRMT8) at low concentrations [326, 350]. Here, we validated the specificity of both inhibitors towards PRMT1 activity in MDA-MB-468 cells and ruled out the effect on PRMT8 as it is a neuronal-specific PRMT [132]. However, we never tested for the histone specific mark of PRMT6 and hence cannot exclude its influence on the observed cellular effects. Specifically, MDA-MB-468 cell viability (with  $IC_{50}$  concentration around  $2\mu M$ ) and colony-forming ability (around  $120nM$ ) were decreased, upon treatment with both inhibitors. MS023 has been shown to decrease cell viability in other cancer cell lines at

similar concentrations (between 1-4  $\mu\text{M}$  in leukaemia cells [434], 2-5  $\mu\text{M}$  in HT-29 colon cancer cells [678]) or greater concentrations (125  $\mu\text{M}$  in DLD1 and HCT116 colorectal cancer cells [679]) as our study. On the other hand, GSK3368715 has been shown to induce only cytostatic effects (and not cytotoxic) in a large panel of BC and several other cancer cell lines [326]. Moreover, this inhibitor (in phase I clinical trial) significantly decreases tumor volume in lymphoma, pancreatic and one BC tumor model (MDA-MB-468 derived xenograft) [326]. Here, we have shown that this inhibitor impairs tumor growth (in the same BC model) at half the inhibitor concentration as compared to Fedoriw and colleagues [326] and in mice grafted with tumors (not in mice injected with cells as in [326]).

Altogether, we propose that PRMT1 could be a potential therapeutic target in BC. PRMT1 has been previously proposed as a therapeutic target for other cancer types, such as renal cell carcinoma [674], hepatocellular cancer [676] and head and neck cancer [677].

A major function of PRMT1 lies in transcriptional regulation (activation/repression) [164]. Previously, PRMT1 has been shown to be important for cell survival, by regulating the transcription of relevant genes such as ATF5 in glioblastoma [680] or cyclin D1 in BC [399]. Hence, to explore how PRMT1 was responsible for BC cell survival in our study model, we analyzed the transcriptome of PRMT1 in MDA-MB-468 cells and identified several pathways involved in BC progression, such as constitutive Akt signaling, signaling by growth factor receptors (PDGF, EGFR) or Wnt signaling pathway. We chose to focus on the EGFR and Wnt signaling pathways as discussed below.

EGFR signaling is of clinical importance, especially for TNBC, since EGFR is overexpressed in more than 70% of TNBC patients [673], associated with a metastatic phenotype of TNBC and contains several oncogenes within this pathway (e.g., PI3KCA) that are pivotal in TNBC progression [681]. However, targeting EGFR alone (using available EGFR inhibitors) have shown only modest to low efficacy in clinical trials for TNBC patients [40]. PRMT1 has been previously observed to modulate EGFR signaling by two mechanisms: (i) activating transcription of EGFR in CRC and glioblastoma cells [196, 381] and (ii) methylating its extracellular domain in CRC and TNBC cells [194, 383]. We confirmed that EGFR mRNA expression was regulated by PRMT1 as previously described [381]. In addition, we show that PRMT1 was directly recruited to and enriched on the *EGFR* promoter, unlike previous studies where only the PRMT1-specific histone mark, H4R3me2a, was shown to be enriched [196, 381]. Besides, inhibiting PRMT1 using nonspecific inhibitors such as furamidine or AMI-1 has been shown to sensitize MDA-MB-468 cells [383], colorectal cancer cell lines [194], or non-small cell lung carcinoma [682] to EGFR inhibition (using erlotinib or cetuximab). Here, we found that combining PRMT1 and EGFR inhibitors displays high synergism on the viability of MDA-MB-468 cells, a TNBC cell line overexpressing EGFR. Similar synergistic interactions have been described using a PRMT5 inhibitor, as well [301]. This is not

surprising since EGFR is a substrate of both PRMT1 [194, 383] and PRMT5 [195]. To be able to generalize our findings to TNBC, we will have to test this combination in additional TNBC cell lines, as well as in TNBC patient-derived xenograft models. Overall, this indicates that combining anti-EGFR and anti-Type I PRMT inhibitors might be therapeutic for TNBC patients (at least those that overexpress EGFR), especially since anti-EGFR as a monotherapy is not efficient.

Moreover, we report for the first time, that targeting PRMT1 in combination with certain chemotherapeutic drugs (cisplatin, cyclophosphamide, and camptothecin) were synergistic, in the MDA-MB-468 TNBC cell line. Previous studies indicate that Type I PRMT inhibitors synergized with chemotherapies in other cancer cell line models. For instance, a study published last year showed that pretreating the ovarian cancer cell line SK-OV-3 with the PRMT1 inhibitor (MS023) sensitized these cells to cisplatin treatment and proposed PRMT1 inhibition as a mechanism to overcome cisplatin-resistance [364]. Therefore, the synergistic effects we demonstrate between PRMT1 inhibition and cisplatin treatment could possibly be extended beyond breast cancer cells and tested in other cancer types that are treated using cisplatin. Further, another study showed that PRMT1 inhibition using the nonspecific inhibitor AMI-1 enhanced the antitumor effect of doxorubicin in mice injected with MCF7 cells resistant to doxorubicin [417]. In our study, we observed no interaction between Type I PRMT inhibitors and doxorubicin, *in vitro*, suggesting that the effect observed by Li et al., might not be PRMT1 dependent since AMI-1 is not a PRMT1 specific inhibitor. In order to generalize our findings to all BC, we will have to test this combination in additional BC cell lines, as well as in BC patient-derived xenograft models. Taken together, this advocated that PRMT1 inhibition might prove beneficial to overcome chemotherapy-associated resistance in not only breast cancer but also other cancer types.

PRMT1 inhibition (using MS023) with PARP inhibitors was shown in a study published this year to be synergistic against non-small cell lung cancer cells and ovarian cancer cells resistant to PARP inhibition [683]. Overall, this indicates that combination therapy using Type I PRMT inhibitors with either chemotherapy or with targeted therapies is emerging as an attractive treatment strategy for many cancer types.

A major limitation while treating TNBC patients is their acquired resistance to chemotherapy. One of the underlying causes of chemoresistance has been attributed to the Wnt signaling pathway [94, 95]. Wnt signaling is required to maintain the stemness (i.e., self-renewing ability) of a subset of cancer cells (sometimes called tumor initiating cells (TIC), cancer stem cells (CSC), drug-resistant cells) [94, 95]. These CSCs are thought to be one of the drivers for intra-tumor heterogeneity in breast cancer [94]. In TNBC, overexpression of Wnt receptors (like Frizzleds and LRP6) causes activation of this pathway, rather than mutations of *CTNNB1* ( $\beta$ -catenin gene), which is rare in breast cancer [684]. Further, several genes involved in the EMT phenotype (e.g., Snail, Slug, Twist1, ZEB1) are downstream targets of Wnt signaling activity and

they contribute to the EMT (leading to metastasis) phenotypes in breast cancer [94, 95, 685]. Therefore, targeting the Wnt signaling pathway has been proposed to be beneficial for TNBC patients and one Wnt pathway inhibitor (LGK-974, a PORCN inhibitor) is in clinical trials for TNBC (NCT01351103). In our study, we tested this inhibitor in combination with the type I PRMT inhibitors but observed only neutral effects. Notably, LGK-974 alone did not induce cell death up to micromolar concentrations ( $IC_{50}$  around  $10\mu M$ ). PORCN inhibitors would only be effective in Wnt-ligand dependent cancer, since blocking PORCN, an enzyme that modifies Wnt ligands before their secretion, would essentially block the ligand-mediated activation. Given that we do not observe an efficient cytotoxic effect of LGK-974 in one TNBC cell line, maybe hints that targeting PORCN may not be efficient in TNBC. A possible reason could be that not all TNBC are Wnt-ligand dependent, and the pathway can be activated in a ligand-independent manner (for example, LRP6 overexpression). This could be verified by testing LGK-974 in a large panel of BC cell lines to check which cell lines are sensitive to this inhibitor. Maybe targeting the Wnt pathway using other Wnt inhibitors in combination with type I PRMT inhibitors might yield positive results.

In this study, we found the Wnt signaling pathway to be significantly de-regulated upon PRMT1 depletion. PRMT1 has been previously described to regulate Wnt signaling, but with opposing roles. The Wnt signaling is inhibited by PRMT1 when it methylates two antagonists of this pathway (i) Axin in HEK293 and L929 cell lines [386] and (ii) Dishevelled in HEK293, B2b, and F9 cell lines [387]. On the contrary, the same team has reported that PRMT1 activates the Wnt signaling pathway by methylating two Dishevelled-binding components: G3BP1 in F9 cells [388] and G3BP2 in F9, HEK293 and SW380 cells [389]. This indicated that maybe depending on the context, the role of PRMT1 on Wnt signaling since the above studies were performed in different cell lines (non-TNBC).

Notably, unlike previous studies, we investigated the function of PRMT1 on Wnt signaling at the transcriptional level without checking if any of the Wnt components mentioned above were substrates for PRMT1 in our cellular model. Here, we found that PRMT1 activated Wnt signaling in MDA-MB-468 cells and that it regulated the transcription of *LRP5* (a transmembrane receptor) and *PORCN* (enzyme modifying Wnt ligands), two important genes involved in activating the Wnt pathway. Further, inhibiting the methyltransferase activity of PRMT1 (using low doses of two Type I inhibitors) led to a decrease in Wnt signaling activity. It has been previously reported that the Wnt signaling activity was inhibited using Atox, a global inhibitor of methylation [392]. Also, the phosphorylation of LRP6 (required to activate Wnt signaling) was blocked when arginine methylation was inhibited using Atox [389]. However, it must be noted that Atox is a nonspecific inhibitor that impacts all cellular methylation events, including arginine, lysine and DNA methylation. Furthermore, in vascular smooth muscle cells, LRP6 was identified as a PRMT1 partner [391].



Altogether, this connoted that PRMT1 could regulate the Wnt signaling pathway by (i) transcriptional activation (this study) or (ii) post-translation modifications [386-389].

Recent research from the team of Prof. Edward De Robertis has shown a novel function for Wnt signaling, in nutrient scavenging and macropinocytosis [392-394]. They showed that within minutes of Wnt pathway stimulation using Wnt3a, there was a rapid formation of multivesicular bodies in which the kinase GSK3 was sequestered along with PRMT1 [392, 394]. This process was shown to be highly dependent on arginine methylation since adding Adox to cells completely blocked this process [392].

In addition, they have shown evidence involving the methionine cycle in Wnt signaling [394], which is highly relevant to our study because the methionine cycle generates the global methyl donor in cells, SAM, that is required by methyltransferases (including PRMTs) to catalyze the methylation reaction (**Figure 73**). Methionine deprivation or inhibition using methotrexate inhibited Wnt signaling [394]. This is interesting because both methionine-deprivation and using methotrexate could also inhibit PRMT activity by inhibiting SAM production (**Figure 73**). Considering this, it suggests that methotrexate (chemotherapy used to treat BC patients) might function as a dual inhibitor (Wnt pathway and PRMTs). Therefore, we can speculate that co-inhibiting PRMT1 with methotrexate might be beneficial in Wnt-dependent cancer.

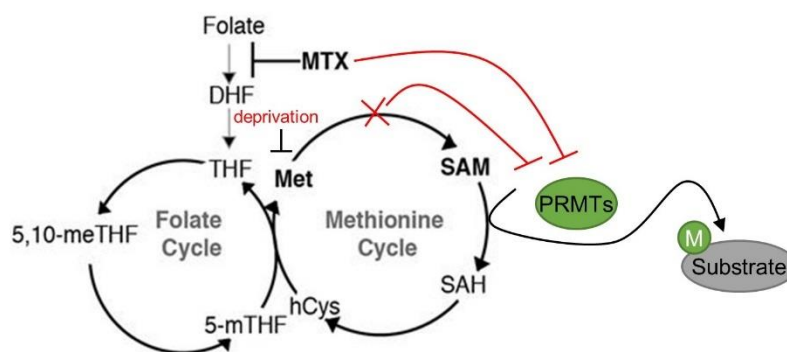


**Figure 73: Scheme of the methionine and folate cycles.** The folate and methionine cycles are coupled through homocysteine (hCys). The methionine cycle is responsible for the formation of S-adenosyl methionine (SAM), the methyl donor for PRMTs. Methotrexate (MTX) inhibits the enzyme that converts folate to dihydrofolate (DHF). Modified and adapted from [394].

## Conclusion and future perspectives

In conclusion, we have evidence supporting the idea that targeting PRMT1, alone or in combination with certain chemotherapeutic agents or targeted therapy, could be beneficial for the treatment of breast cancer patients. Further, we show an additional way by which PRMT1 regulates the Wnt signaling pathway (i.e., via transcription). Nevertheless, many follow-up questions remain to be answered.

**(i) Is PRMT1 inhibition effective as a monotherapy for all breast cancer patients?**

In our results, we observed that targeting PRMT1 alone, decreased tumor growth in MDA-MB-468, the only BC cell line we have examined. First, we would need to test this *in vitro*, in a large panel of BC cell lines (belonging to the different subtypes). Next, this would need to be validated, *in vivo*, in other mouse models such as using patient-derived xenografts (PDX) of breast cancer (including TNBC).

**(ii) Can anti-EGFR/anti-PRMT1 combination be used as a treatment for breast cancer patients?**

*In vitro*, we observed the highest synergistic interaction between anti-EGFR and anti-PRMT1 treatment in one TNBC cell line, MDA-MB-468. As these cells express high EGFR levels, it would be interesting to test if this synergy is limited to only high EGFR expressing cells or not by extending the study to other TNBC and BC cell lines, *in vitro*, and *in vivo*. This would help us to understand if this combination therapy would be beneficial to only a subset or all BC patients.

**(iii) Can PRMT1 inhibition be combined with chemotherapy in vivo?**

The synergy observed between Type I PRMT inhibitors and chemotherapeutic agents such as cisplatin, cyclophosphamide, and camptothecin warrant validation in other BC cell line models and *in vivo* in BC-PDX models. Especially since the above-mentioned chemotherapeutic drugs are routinely used in the clinic to treat BC.

**(iv) Does PRMT1 regulate the secretion of Wnt ligands?**

One result of this study was that PRMT1 regulated the transcription of PORCN, the enzyme modifying Wnt ligands. This raises the question whether PRMT1 could in turn modulate the secretion of the Wnt ligands. We tested out this hypothesis using an ELISA assay for Wnt3a ligands as previously described [686] but we were not successful to detect the Wnt3a ligands from the supernatant of the TNBC cell lines tested (MDA-MB-468 and SUM149, results were in the background range). However, if more sophisticated/sensitive assays are developed in the future, it would be interesting to test this. It would help us understand if PRMT1 can indeed affect the secretion of Wnt ligands, providing another mechanism by which PRMT1 can regulate the Wnt pathway.

**(v) Is the regulation of Wnt signaling by PRMT1 specific to MDA-MB-468? What is Wnt activity status in our BC cohort?**

We have shown here that PRMT1 regulated Wnt activity in the MDA-MB-468 cell line (or the luminal T47D for LRP5 expression). This would need to be investigated in other BC cell lines to exclude the possibility of a cell-type dependent phenotype.

By investigating the expression of activated  $\beta$ -catenin (nuclear  $\beta$ -catenin) in the Curie BC cohort, we can understand the status of Wnt signaling activation. Although

observing activated  $\beta$ -catenin has been challenging, it would help us to stratify the BC patients into Wnt-dependent and Wnt-independent.

**(vi) Does PRMT1 regulate the Wnt signaling pathway in colorectal cancer or hepatocellular carcinomas? Can Type I PRMT inhibitors be beneficial in these cancer types?**

PRMT1 has been shown to promote oncogenesis in colorectal cancer (CRC) by activating EGFR signaling [381], inducing CRC differentiation [678] or by methylating the protein NONO [675]. PRMT1 is also shown to be a prognostic marker in hepatocellular carcinoma (HCC) [687]. Further, the Wnt pathway is known to be hyperactivated in CRC or has increased activity in HCC owing to mutations in this pathway (e.g., *APC* for CRC or *CTNNB1* and *AXIN1* for HCC) [688]. Therefore, it would be interesting to explore if PRMT1 regulates the Wnt pathway in these cancer at the transcriptional level (as we have shown in this study) or by post-translational modifications (as shown by others, [386-389]). If yes, the Type I PRMT inhibitors could be tested in these cancer cells to see if they are efficient in inducing cell death.

## CHAPTER 2: PART II

### *Preface*

CARM1 is a type I PRMT like PRMT1 and is thought to be oncogenic in several cancer types, including breast cancer. However, the role of CARM1 in TNBC has not been studied so far. Therefore, the objective here was two-fold: (a) to analyze CARM1 expression pattern in TNBC and assess if it could be a potential therapeutic target and (b) characterize its function in TNBC. For the first objective, we investigated the RNA and protein expression of CARM1 in a large panel of breast tumors and evaluated the effect of depleting or inhibiting CARM1 on TNBC cell survival. For the second objective, we characterized the CARM1 interactome by mass spectrometry (MS) analysis in collaboration with the MS platform at Institut Curie and identified ALIX as the major partner of CARM1. As one of the main functions of ALIX is in cytokinesis (the final step in cell division), we explored the consequences of the interaction between CARM1 and ALIX on this function. For this purpose, we collaborated with the team of Dr. Arnaud Echard, Institut Pasteur, who has expertise in cytokinesis.

This entire work was conceived and started during this thesis. However, the full story is still incomplete, particularly in illustrating the role of CARM1 in cytokinesis and this is currently being pursued by another PhD student in our lab, Solène Huard.

# The ESCRT-binding protein ALIX is a novel CARM1 substrate

Samyuktha Suresh<sup>1,2,3</sup>, Solène Huard<sup>1,2,3</sup>, Nguyễn Huyền Nhung<sup>1,2,3</sup>, Vanessa Masson<sup>1,4</sup>, Florent Dingli<sup>1,4</sup>, Laetitia Lesage<sup>1,5</sup>, Anne Salomon<sup>1,6</sup>, André Nicolas<sup>1,5</sup>, Didier Meseure<sup>1,5</sup>, Damarys Loew<sup>1,4</sup>, Arnaud Echard<sup>7</sup> and Thierry Dubois<sup>1,2,3</sup>.

<sup>1</sup>Institut Curie, PSL Research University, Paris, France; <sup>2</sup>Translational Research Department; <sup>3</sup>Breast Cancer Biology Group; <sup>4</sup>Mass Spectrometry and Proteomics Facility; <sup>5</sup>Investigative Pathology Platform; <sup>6</sup>Department of Biopathology; <sup>7</sup>Membrane Traffic and Cell Division Lab, Institut Pasteur, UMR3691, CNRS, Paris, France.

## Abstract

Breast cancer is a heterogeneous disease comprised of distinct subtypes. Among them, triple-negative breast cancer (TNBC) is the most aggressive, with worse prognosis and lack of targeted therapy. Therefore, identifying novel treatments for TNBC is an unmet clinical need. Transcriptome and immunohistochemical analyses revealed that protein arginine methyltransferase 4 (PRMT4 also called CARM1) is more expressed in breast tumors than in healthy breast tissues. Silencing CARM1 expression impaired cell proliferation and induced apoptosis in two TNBC cell lines, BT-549 and MDA-MB-468. In contrast, CARM1 inhibition using two recently developed small-molecule inhibitors (TP-064 and EZM2302) did not affect cell viability in the tested cell lines, suggesting that its enzymatic activity may not be required for this function. Then, we searched for protein-protein interactions to comprehend the role of CARM1 on TNBC cell survival and identified the ESCRT accessory protein, ALIX, as the major CARM1 partner. Further, we demonstrate that ALIX is a substrate of CARM1 and is methylated on two major arginine residues, Arg745 and Arg757, within the c-terminal domain of ALIX. ALIX functions as an adaptor protein for the ESCRT family and aids in multiple cellular processes such as cytokinetic abscission, retroviral budding and multivesicular body biogenesis. In this study, we focused on cytokinetic abscission and observed that silencing CARM1 displayed phenotypes similar to ALIX depletion in causing cytokinetic defects. However, additional research is ongoing to fully understand the role of the CARM1/ALIX complex on cytokinetic abscission.

## Introduction

CARM1 (also known as PRMT4), belongs to the family of protein-arginine methyltransferases (PRMTs) and catalyzes the reaction of adding methyl groups on arginine residues [438]. It belongs to the type I PRMT as it generates asymmetric dimethylarginine (ADMA) and is involved in various cellular processes such as transcriptional regulation, RNA metabolism, and autophagy, to name a few [437]. Similar to other PRMTs, CARM1 is overexpressed in several cancer types, including breast tumors [147, 531-533].

Breast cancer (BC) is a heterogeneous disease that is comprised of different intrinsic subtypes, luminal (hormone receptor-positive, HR+ and human epidermal growth factor receptor-positive/negative, Her2+/-), Her2+ (HR- and Her2+), and triple-negative (TNBC, HR- and Her2-) [659]. CARM1 has been extensively studied in the luminal subtype, particularly because CARM1 functions as a co-activator for the estrogen receptor (ER) transcription factor (ER $\alpha$ ) [437]. However, very few studies have explored the role of CARM1 in the TNBC subtype. CARM1 has been shown to promote the migration in TNBC cell lines by methylating proteins like Protein kinase M2 or BAFF155 (a chromatin remodeler). TNBC is an aggressive subtype of BC and patients diagnosed with this disease have poor survival outcomes [660]. A major challenge in treating TNBC patients is their acquired resistance to chemotherapy and a high rate of relapse [660], thus, the identification of novel treatment strategies is crucial.

In this study, we found that CARM1 was highly expressed in BC as compared to normal tissue at the mRNA and protein levels. Silencing CARM1 levels decreased cell viability and induced apoptosis. However, inhibiting CARM1 activity did not affect the viability of cells. We identified a novel major partner of CARM1, ALIX, and this interaction was robust. ALIX is a multifunctional adaptor protein that is involved in several cellular processes like cytokinesis, budding of retroviruses, plasma membrane repair, biogenesis of multivesicular bodies [557]. We demonstrated that ALIX is mono- and di-methylated mainly on two arginine residues (Arg745 and Arg757) located within its C-terminal domain. We focused our study on cytokinesis and found that silencing CARM1 induces defects in cytokinesis, like binucleation. However, whether this role of CARM1 in cytokinesis is mediated through ALIX interaction and/or methylation remains to be demonstrated.

## Results

### **CARM1 mRNA is overexpressed breast tumors**

While analyzing the mRNA expression of the different PRMTs in our previously described curie cohort [301, 663], we observed that CARM1 was more expressed in breast tumors than in healthy breast tissue (**Figure 74, left panel**). Moreover, we observed a higher CARM1 expression in the two ER-negative subtypes (TNBC and Her2+) as

compared to the luminal subtypes and healthy breast (**Figure 74, left panel**). Further, given the heterogeneity of TNBC, we also explored if CARM1 mRNA was differentially expressed among the different TNBC subgroups, but no significant variation was observed (data not shown).

We confirmed that CARM1 mRNA was more expressed in all BC subtypes as compared to normal tissue (**Figure 74, right panel**) by analyzing the data from the publicly available TCGA sample set. Similar to the Curie cohort, both ER- subtypes expressed more CARM1 than the other subtypes, with higher expression in TNBC than Her2+ (**Figure 74, right panel**). We also observed that in contrast to the TCGA cohort, no difference was observed between the luminal subtypes and normal tissue in the Curie cohort (**Figure 74**). These differences could be due to the difference in sample sizes between the cohorts or the nature of the tumors in these sample sets.

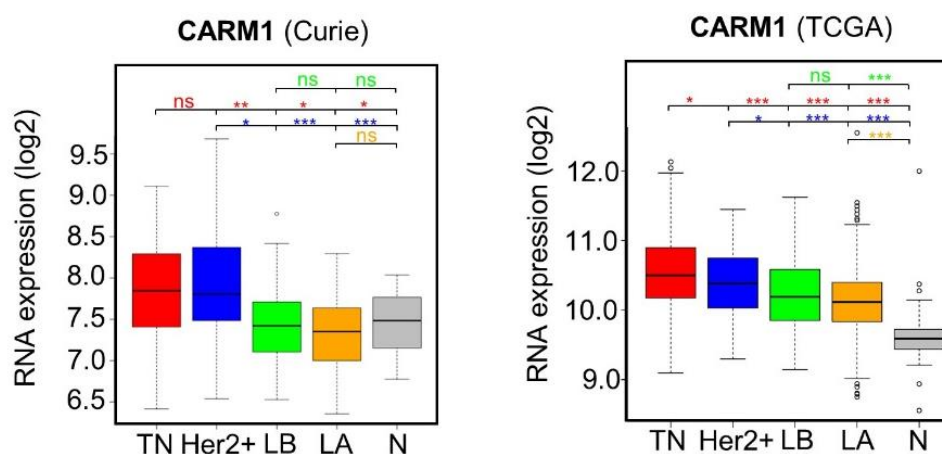


**Figure 74: CARM1 mRNA is more expressed in BC than normal breast tissue.** Higher levels of CARM1 mRNA in BC compared to normal tissue. The levels of CARM1 RNA expression in TNBC (red), Her2+ (blue), Luminal B (LB, green), Luminal A (LA, orange), and healthy breast tissue (Norm, grey) were determined by microarray analysis (Affymetrix) in the Curie cohort (Curie, left panel) or obtained from the publicly available dataset “The Cancer Genome Atlas” (TCGA, right panel). This curie cohort is composed of 35 luminal A, 40 luminal B, 46 TNBC, 33 Her2+ and 18 normal breast tissues [301, 663]. The TCGA cohort contains 157 TNBC, 41 Her2+, 153 luminal B, 663 luminal A, and 113 normal breast samples. The relative RNA quantifications were logarithmically (log<sub>2</sub>) transformed and are illustrated by box plots. \*p < 0.05; \*\*p < 0.01; \*\*\*p < 0.001, as calculated using the Student t-test.

### Higher CARM1 expression correlates with worse prognosis in Her2+ and LA BC subtypes

Next, we analyzed the distant metastasis-free survival outcomes for CARM1 using KM plotter ([www.kmplot.com](http://www.kmplot.com)), for each subtype individually, since they have different prognoses. We used the best performing threshold as the cut-off to stratify the samples into high and low CARM1 and observed that CARM1 expression did not correlate with prognosis in the TNBC subtype (p=0.63) or the luminal B (LB, 0.14) (**Figure 75**). In contrast, higher CARM1 showed a worse prognosis in the Her2+ (p=0.042) and Luminal A (LA, p=0.059) (**Figure 75**). Previously it has been shown that in ER+ tumors



(i.e., luminal subtype), higher CARM1 protein expression was associated with worse survival [532]. Here we observe the same for CARM1 mRNA expression in luminal A (**Figure 75**), but not luminal B, possibly because mRNA and protein expression may not always correlate. In another study, they reported that higher CARM1 mRNA correlated with worse prognosis in the whole breast population [147], similar to what we observe for LA and Her2+ (**Figure 75**). Together, this suggested that targeting CARM1 might have therapeutic value in a subset of BC.

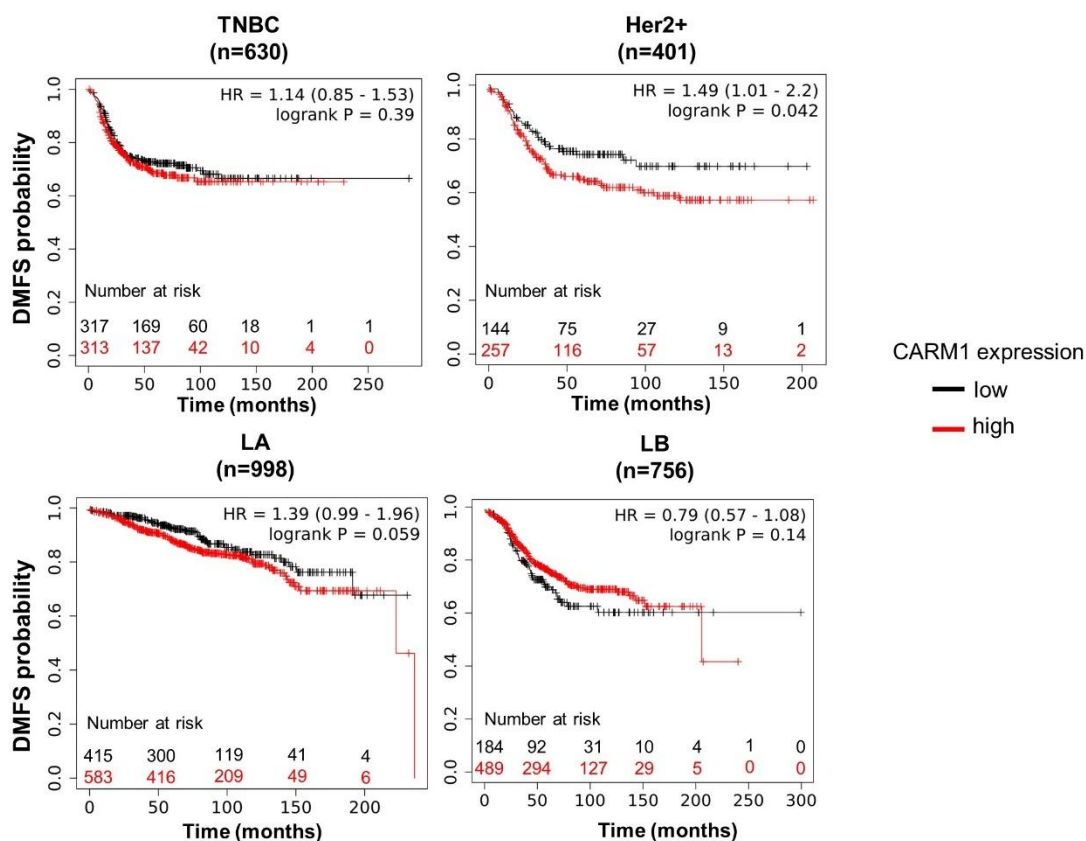


**Figure 75: Distant metastasis-free (DMFS) survival outcomes in CARM1 high and low BC patients.** DMFS was analyzed using the Kaplan-Meier (KM) plotter (<http://kmplot.com>) for CARM1 (Affy probe ID: 212512\_s\_at). An auto-select best cutoff option was used for each plot. The different intrinsic subtypes were chosen based on PAM50 option with Basal for TNBC (n=630), Her2+ (n=401), Luminal A (LA, n=998) and Luminal B (LB, n=673). Hazard ratio with 95% confidence interval and log-rank P value were calculated and significance threshold was set at  $P < 0.05$ .

Next, as RNA and protein expression levels do not always correlate, we examined CARM1 protein expression and its localization in BC samples and normal breast tissues. We used a cohort called the PIC-BIM from Institute curie (different from the curie cohort mentioned above) composed of 360 tumors (74 TNBC, 125 luminal A, 104 luminal B and 57 Her2+). We performed immunohistochemistry using an anti-CARM1 antibody that recognizes residues 550-585 located in the C-terminal domain of CARM1. We first validated the antibody in a TNBC cell line (BT-549), depleted or not for CARM1, that was fixed in a similar method as the tumor samples (**Figure 76A**). At the

protein level, CARM1 was more expressed in all the BC subtypes when compared to the normal tissue; however, unlike at the mRNA level, there were no significant differences between the BC subtypes (**Figure 76B**). Higher CARM1 protein level in BC than in normal tissues has been previously reported [531, 533, 544]. We observed nuclear and cytoplasmic staining of CARM1 as previously described [456, 531, 533]. Also, we observed CARM1 staining in the stroma in contrast to another study where they reported little to no stromal staining [456]. Interestingly, we found higher CARM1 nuclear staining in TNBC as compared to the other BC subtypes ( $p=0.026$ ) (**Figure 76C**). This is in an apparent contradiction with previous reports where high nuclear CARM1 was associated only with the Her2+ subtype ( $n=105$ , her2+ [533];  $n=23$ , her2+ [531];  $n=57$ , our study for Her2+ tumors). This could arise due to a few reasons, (i) difference in the tumor samples, (ii) difference in antibodies used, or (iii) difference in CARM1 isoforms recognized/stained. CARM1 is expressed in breast tumor cells as two main alternatively spliced isoforms, a full-length (FL) form or exon 15 deleted ( $\Delta E15$ ) form [454]. Our CARM1 antibody used for IHC recognizes residues 550-585 and therefore should recognize both CARM1 isoforms, whereas, we do not have this information for the antibodies used in the published studies (antibody used here has been discontinued by the supplier [533]; no reference of antibody stated [531]).

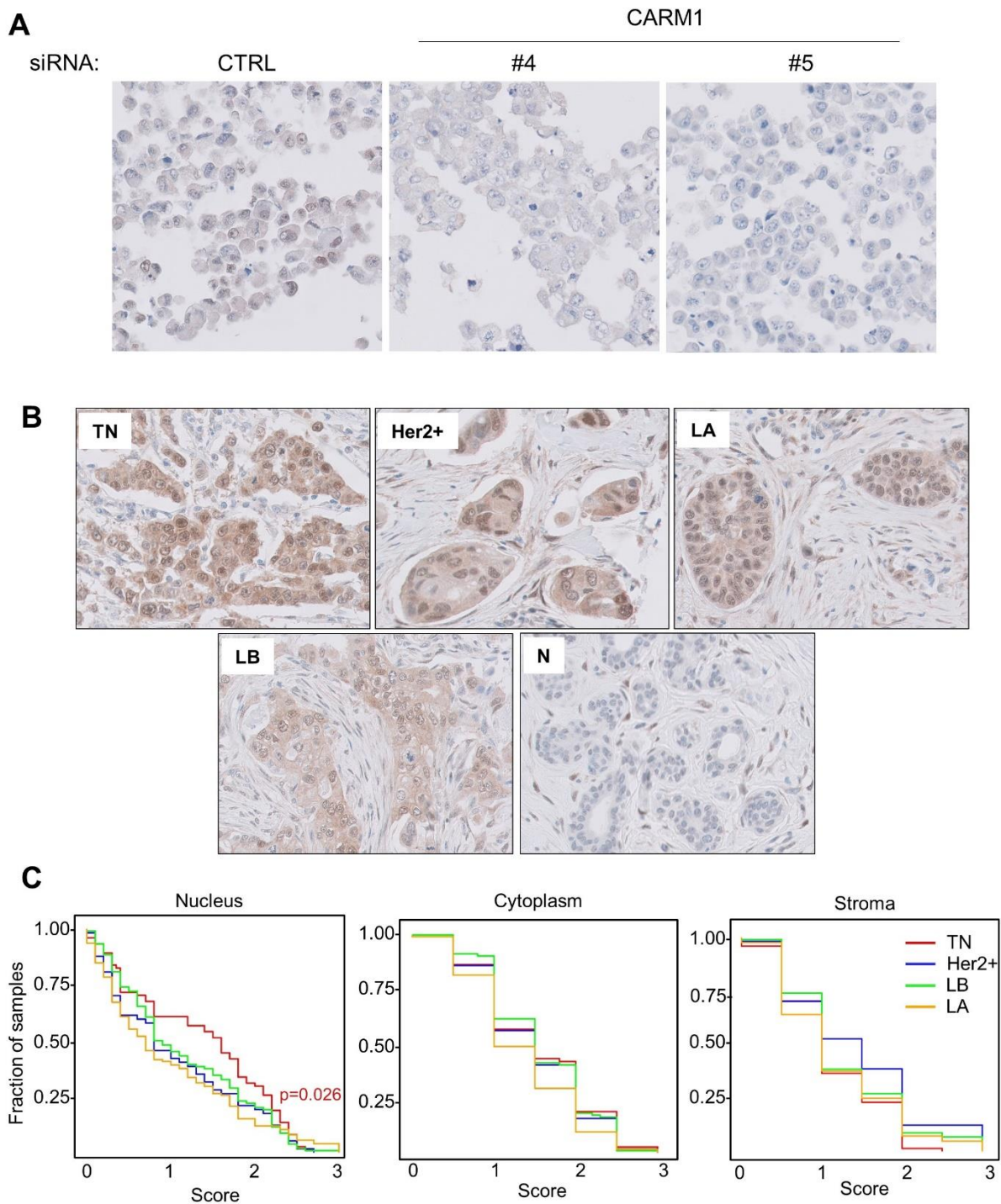


**Figure 76: CARM1 protein is overexpressed in all breast tumors than normal breast tissue by immunohistochemical staining.** (A) CARM1 antibody validation was performed using AFA-fixed cell pellets from BT-549 treated with control siRNA (CTRL) or two CARM1 siRNAs for 48 h (#4, #5). CARM1 displays cytosolic and nuclear localization. (B) Higher levels of CARM1 protein in BC than in normal tissue. CARM1 protein levels were analyzed by immunohistochemistry (IHC) in the PIC-BIM cohort from Institut Curie [689] which is a different sample set as compared to **Figure 74** as these samples were obtained from BC patients who underwent primary surgery at Institut Curie between 2005 and 2006 before any treatment (radiation/hormone/chemotherapy). A representative image of CARM1 staining is shown for the different BC subtypes. (C) Quantification of CARM1 staining in the different cellular compartments (0: no staining, 3: the strongest staining). p values calculated by Wilcox test.

Together, our data confirm previously observed results that CARM1 is indeed overexpressed in BC at the mRNA [147] and protein levels [531, 533, 544] as compared to healthy breast tissue. A striking observation from our IHC analysis of CARM1 protein is the higher nuclear expression in TNBC (compared to other subtypes) and the staining observed in stromal cells, which to our knowledge is being reported for the first time.

### **CARM1 depletion decreases cell proliferation, colony formation and induces apoptosis**

Given the overexpression of CARM1 in BC, particularly in TNBC, we wanted to evaluate its potential as a therapeutic target. We first validated two siRNAs targeting CARM1 (CARM1#4, CARM1#5) in MDA-MB-468 cells for their specificity and efficiency to deplete CARM1 (**Figure 78A, B**). Then, to account for TNBC heterogeneity, we chose two TNBC cell lines belonging to two different TNBC subtypes - mesenchymal (BT-549) and basal-like 1 (MDA-MB-468) - and observed that depleting CARM1 using siRNA decreased cell proliferation in a time-dependent manner (**Figure 77A**). This effect was not limited to these two cell lines but was also observed in other TNBC cell lines (**Figure 78C**). Noticeably, we observed a similar effect in the non-tumorigenic cell line, MCF10A (**Figure 78C**). This could be because these cells are highly proliferative in our culture conditions (in fact, the most proliferative cells, so not behaving like "normal" cells), suggesting that the depletion of CARM1 simply impairs the proliferation of any proliferative cell line. CARM1 silencing also decreased the colony-forming ability of TNBC cell lines when cultured on plastic (**Figure 77B**). To understand the mechanism through which CARM1 silencing impaired cell viability, we looked for apoptotic markers by western blotting. In both TNBC cell lines, cleavage of PARP was induced 48h following CARM1 depletion, suggesting an induction of apoptosis (**Figure 77C**). Moreover, we also observed an increase in the phosphorylation of histone H2AX, a known marker of DNA double-strand breaks (**Figure 77C**).

Depleting CARM1 has been reported by others to decrease cell proliferation in the luminal cell lines MCF7 [288, 547, 690] and ZR75 [288] while no effect was observed on cell proliferation in the TNBC cell line, MDA-MB-231 [690]. In contrast to Al-Dhaheri et al., we have shown that depleting CARM1 decreases cell proliferation in the MDA-MB-231 cells (also other TNBC cell lines, **Figure 78C**). This discrepancy might be due to the method used to deplete CARM1, transient transfection (our study) or stable infection with shCARM1 [690], and maybe these stably infected cells have found an alternative mechanism to divide independently of CARM1. This is the first report to evaluate the effect of CARM1 depletion on cell survival in more than one TNBC cell line. Therefore, our results indicate that CARM1 is important for the survival of all the BC cells tested.

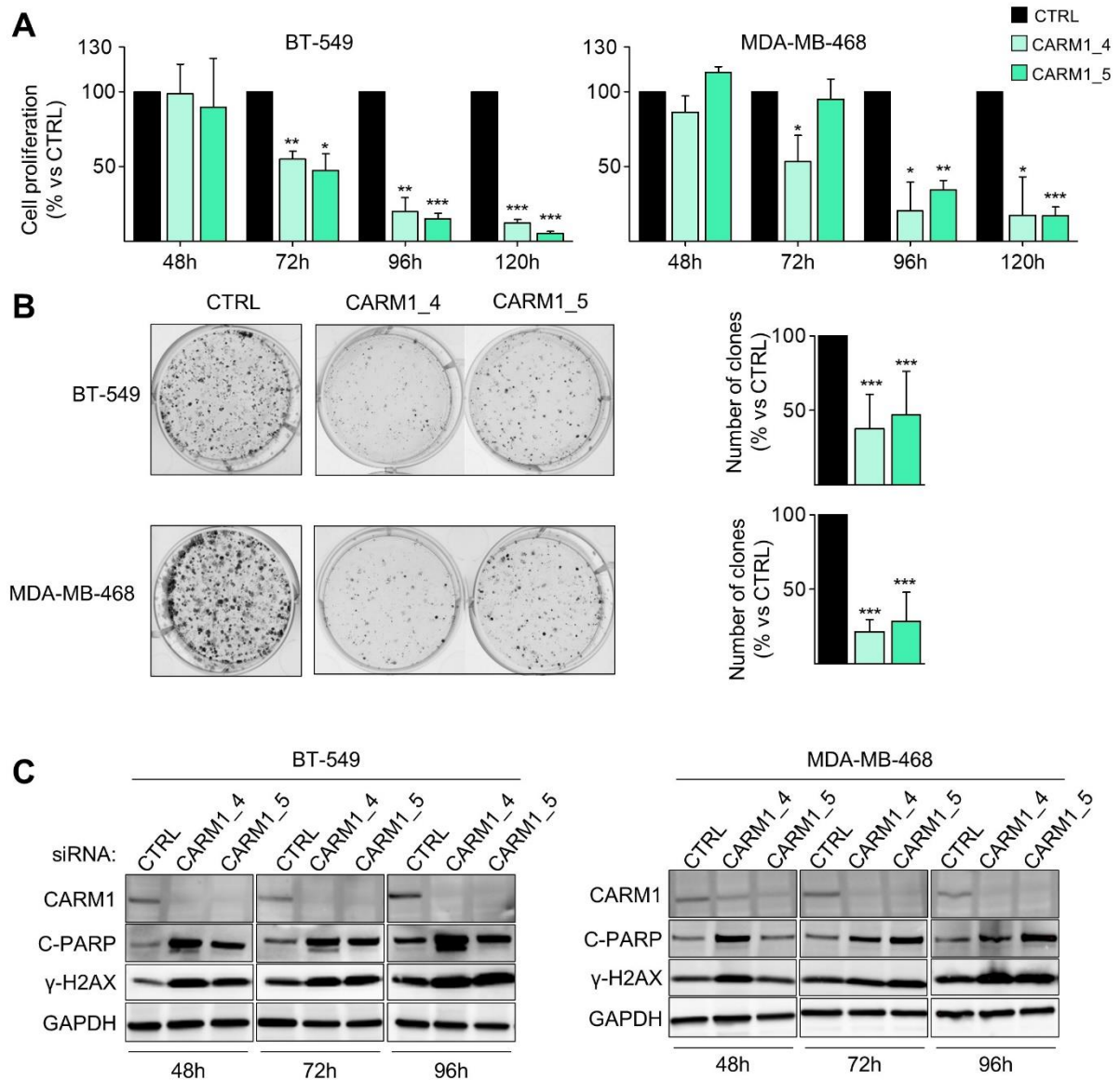


**Figure 77: CARM1 depletion impairs cell viability, colony formation and induces apoptosis.** (A) CARM1 depletion impairs cell viability (CellTiterGlo assay). Cells were transfected with control siRNA (CTRL) and two different CARM1 siRNAs (#4, #5) for the timepoint indicated. (B) CARM1 depletion impairs colony formation when cells are grown on plastic for 6 mitotic cycles which correspond to 7 (BT-549) or 9 (MDA-MB-468) days after siRNA treatment. (C) CARM1 depletion induces apoptosis and DNA damage. Apoptosis and DNA damage was analyzed by western blotting using an antibody that recognizes the cleaved form of PARP (c-PARP) or phosphorylated histone H2AX ( $\gamma$ -H2AX) 48 h, 72h and 96 h after CARM1 depletion. CARM1 depletion was verified using an anti-CARM1 antibody and GAPDH was used as a loading control. Results are presented as the percentage relative to control cells (CTRL, A, B). All the data are expressed as the mean  $\pm$  SD from at least three independent experiments (A, B). Pictures are from a single experiment representative of three independent experiments (B, C). P values from a Student t-test are represented as \* $p < 0.05$ ; \*\* $p < 0.01$ ; \*\*\* $p < 0.001$ .

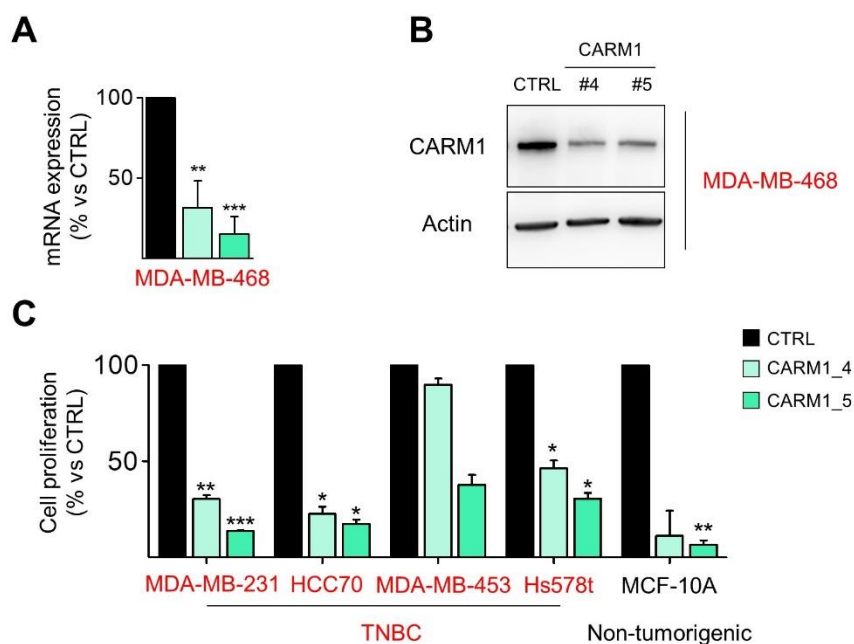


**Figure 78: Validation of CARM1 siRNA and CARM1 depletion decreases the viability of various breast cell lines.** MDA-MB-468 cells treated with siRNAs targeting CARM1 for 48h and were validated by RT-qPCR normalized to actin expression (A) or by western blotting using anti-CARM1 antibody and anti-actin antibodies were used as a loading control. (C) CARM1 depletion decreases cell viability measured by CellTiterGlo assay. All cells were transfected with control siRNA (CTRL) or one of two CARM1 siRNA (#4, #5) for 120 h. Results are presented as the percentage relative to control cells (CTRL) and expressed as the mean  $\pm$  SD from two (A) or three independent experiments (C). Pictures are representative of three independent experiments (A, right panel). P values from a Student t-test are represented as \* $p < 0.05$ ; \*\* $p < 0.01$ ; \*\*\* $p < 0.001$ .

### CARM1 inhibition does not impact cell viability of two TNBC cell lines

As CARM1 protein was shown to be important for TNBC cell survival (Figure 77), we sought to evaluate if its enzymatic activity could be required. For this, we used the two recently developed CARM1 specific inhibitors. TP-064 is >100 fold selective for CARM1 over the other PRMTs and binds to the substrate-binding pocket of CARM1, although it is unclear if it is substrate-competitive [344]. EZM2302, another specific CARM1 inhibitor, more potent than TP-064, is non-competitive for cofactor binding and binds in the substrate-binding region [343]. We also tested both inhibitors in one TNBC cell line (MDA-MB-468) to verify if they inhibited CARM1 activity. After 96h of inhibitor treatment, we could see a decrease in the methylation of PABP1 (a CARM1-specific substrate, [691]) by both inhibitors (Figure 79A), but at different inhibitor concentrations (i.e., around 5 $\mu$ M for TP-064 and 100nM for EZM2302). Then, we evaluated their potential on TNBC cell proliferation and observed that both TP-064 and EZM2302 had very high IC<sub>50</sub> values (>10 $\mu$ M, Figure 79B) suggesting that the cell lines tested (BT-549, MDA-MB-468) were resistant to CARM1 inhibition. This was concurrent with Drew and colleagues who developed EZM2302 as they reported that

IC<sub>50</sub> values were >20μM in the breast cancer cell lines tested (2 luminal: ZR75, MCF7, 1 Her2+: BT-474 and 1 TNBC: BT-20) [343]. Moreover, both CARM1 inhibitors have been shown to decrease cell proliferation only in a subset of myeloma cell lines (with no effect on other hematopoietic or solid cancer cell lines) [343, 344].

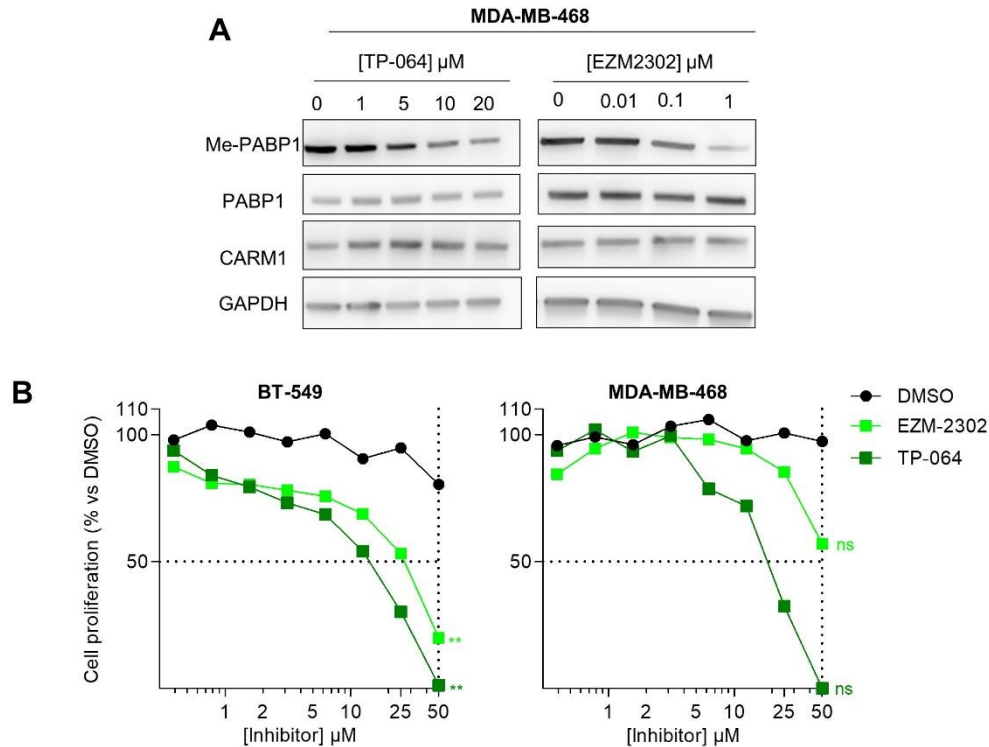


**Figure 79: CARM1 inhibition does not impair TNBC cell viability.** (A) MDA-MB-468 cells were treated with CARM1 inhibitors (TP-064 and EZM2302) for 96h and methylation of PABP1 was analyzed by western blotting. Antibodies against PABP1, CARM1, and GAPDH were used as loading controls. (B) Results are presented as the percentage of cell growth relative to DMSO-treated cells. The dotted line (y-axis) indicates the 50% cell proliferation mark, and the dotted line (x-axis) shows 50μM inhibitor concentration. Results are from two independent experiments and the p-value was calculated using a student t-test, shown as \*\*p<0.01.

Our results thus indicate that only CARM1 depletion and not its inhibition impaired BC cell proliferation implying that CARM1 was modulating TNBC cell survival in an enzyme independent manner. There is evidence to suggest that certain CARM1 functions are independent of its methyltransferase activity, for example when it acts as a co-activator for NF-κB mediated transcription, and its enzymatic activity is not required [503]. This raised the question of whether protein partners that interact with CARM1 might be involved in TNBC cell survival.

### **ALIX was identified as the principal protein partner of CARM1**

Since our results suggested that CARM1 could be modulating BC cell survival independent of its enzymatic activity and therefore perhaps through protein-protein

interactions (i.e., acting as a scaffolding protein, for example), we sought to search for its protein partners. For this purpose, we first chose a TNBC cell line that expresses high endogenous CARM1 levels (HCC1187, **Figure 81A**). Then, we used three antibodies against CARM1 that each recognized different domains/regions of CARM1 (**Figure 81B**). We immunoprecipitated (IPed) CARM1 using these three antibodies and used isotype-matched IgG antibodies as controls and subsequently analyzed the precipitated proteins by mass spectrometry. Surprisingly, we found very few partners of CARM1 that were common among the different antibodies (**Figure 80A**). On performing a gene ontology (GO) analysis for biological processes, we found several processes associated with cell cycle or mitosis (**Figure 80B**). The top partner identified with all three CARM1 antibodies, was the protein ALIX, with 48 (Ab1), 54 (Ab2), and 48 (Ab3) peptides (and >50% peptide coverage) (**Figure 80C**) and zero peptides in the IgG control. The number of peptides obtained for ALIX was almost equivalent to that obtained for CARM1 itself (63 – Ab1, 66 – Ab2, 59 – Ab3) suggesting that most of CARM1 was bound to ALIX. CARM1 is around 63kDa while ALIX is 100kDa, so the number of peptides obtained for each protein (when compared to their respective molecular weights), suggested almost a 1:1 molecular interaction between the two partners.

We performed a similar MS/MS analysis under stringent detergent conditions (1% of NP40), and the association between ALIX and CARM1 was still preserved (data not shown), indicating the robustness of the interaction. We analyzed the CARM1 interactome in another TNBC cell line (BT-549) that expressed lower endogenous CARM1 (**Figure 81A**). Similar to the interactome observed in HCC1187 cells, we obtained few partners (**Figure 81C**) and as expected, identified ALIX as the major partner, validating the robustness of this interaction (**Figure 81E**). Further, the GO analysis revealed processes involving ALIX, like exocytosis and vesicle-mediated transport (**Figure 81D**). As expected, we confirmed the interaction between endogenous CARM1 and ALIX by immunoblotting with an anti-ALIX antibody after IP-CARM1 (Ab1) in HCC1187 (**Figure 80D**), and BT-549 (**Figure 81F**) cells.

Next, as described before, CARM1 has two alternatively spliced isoforms (CARM1-FL and CARM1- $\Delta$ E15) and thus far only one protein, Pax7, has been identified as an isoform-specific partner (binding to CARM1- $\Delta$ E15) [458]. Therefore, we were curious to see if ALIX could be an isoform-specific partner and performed MS/MS analysis in HEK293T cells transfected with either Flag-CARM1-FL or Flag-CARM1- $\Delta$ E15. It must be noted here that we used the HEK293T cells instead of TNBC cells since TNBC cell lines are difficult to transfect with DNA. We found even fewer partners with exogenous CARM1 (**Figure 80E**), but ALIX emerged again as the top hit and bound equally to both CARM1 isoforms (**Figure 80E**). We confirmed this interaction by co-IP using an anti-Flag antibody in HEK239T cells transfected with both isoforms (**Figure 80F**).

Next, to characterize the cellular compartment where the interaction between ALIX and CARM1 was occurring, we performed *in situ* proximity ligation assays (PLA).



PLA is a powerful tool to detect protein-protein interactions if they are in close proximity (40nM) [692]. In this technique, two proteins are recognized by antibodies raised in different species (e.g., mouse and rabbit), and then coupled to specific probes conjugated with oligonucleotides that bind to these antibodies [692]. The oligonucleotides undergo hybridization and amplification by rolling-circle amplification, which is visualized by fluorescence microscopy [692]. For this, we depleted CARM1 and/or ALIX using siRNA in the BT-549 cells and used antibodies that recognized mouse-CARM1 and rabbit-ALIX. We observed the CARM1/ALIX complex in the cytosolic compartment (**Figure 80G**) and the fluorescent signal of the PLA dots (which represents the interaction between CARM1 and ALIX) was significantly decreased when either CARM1 or ALIX was depleted (**Figure 80G, right panel**), validating the specificity of the interaction.

Our results showed that ALIX interacted with both endogenous and exogenous CARM1. ALIX was found to interact with both the isoforms of CARM1 (CARM1-FL and CARM1- $\Delta$ E15) with an equal propensity, suggesting that it was not an isoform-specific partner. Further, given the number of peptides identified for ALIX in our MS/MS analysis, suggested that the majority of CARM1 was bound to ALIX, and it could be an important protein for CARM1 function. Previously, in some large-scale proteomic studies, ALIX has also been shown to interact with PRMT3 and PRMT5 (apart from CARM1) [153]. However, in our MS analysis performed after an IP anti-PRMT1 or IP anti-PRMT5/MEP50, we did not retrieve ALIX as a partner (data not shown); suggesting that in our hands and the cell lines studied, ALIX only interacted with CARM1 and not PRMT1 or PRMT5.

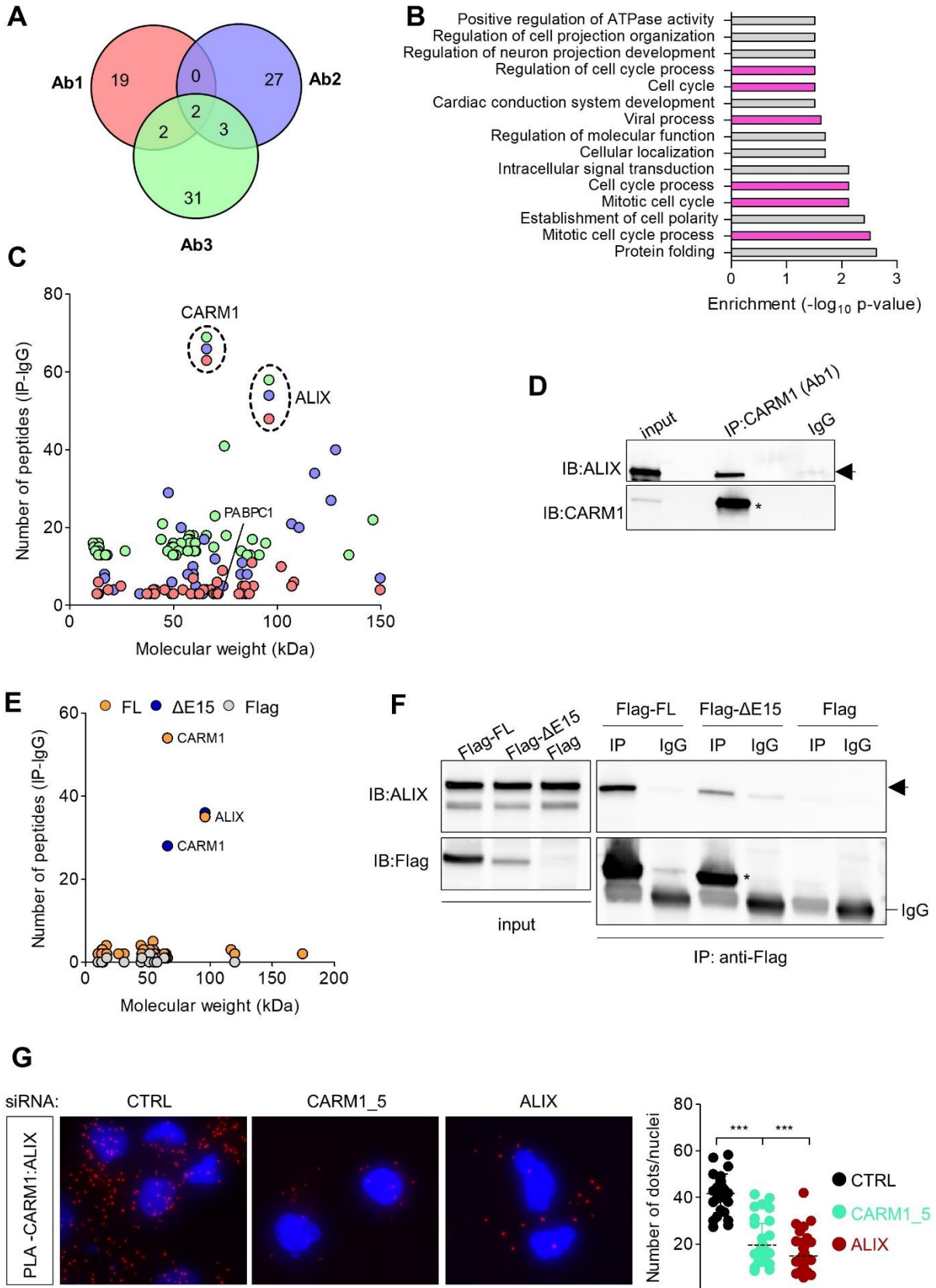


**Figure 80: CARM1 interactome reveals ALIX as its main partner.** (A) Venn-diagram of the enriched proteins found in MS analysis after immunoprecipitation (IP) in HCC1187 cells using three different CARM1 antibodies (Ab1 - red, Ab2 – blue, Ab3- green). The enriched proteins were defined as follows,

the number of peptides found in the IP was divided by the number of peptides found in the immunoglobulins (IgG) to obtain a ratio and only those proteins with a ratio  $\geq 3$  was considered. For the proteins where no peptides were found in the IgG, we replaced 0 with 1 to be able to calculate this ratio. (B) Gene ontology of biological processes using all the proteins found in enriched CARM1 interactome using ShinyGO (software developed by Institut Curie - <https://github.com/iDEP-SDSU/idep/tree/master/shinyapps/go>) [693]. The p-values were logarithmically transformed (-log base 10) and the pink bars represent all the processes involving ALIX. (C) CARM1 interactome plotted as a function of the molecular weight of the proteins identified (kDa) after subtracting the background (i.e., the number of peptides found in the IgG). The proteins found with each CARM1 antibody are shown in red (Ab1), blue (Ab2), and green (Ab3). CARM1 and ALIX are highlighted and an example of a known CARM1 partner (PABPC1) is marked. (D) CARM1 was IPed in HCC1187 cells using Ab1 and immunoblotted using anti-ALIX and anti-CARM1 antibodies. 1% of the total protein lysate was loaded as input control. (E) CARM1 interactome plotted as a function of the molecular weight of the proteins identified (kDa) from HEK293T cells transfected with either Flag-CARM1-FL (orange), Flag-CARM1- $\Delta$ E15 (blue), or Flag empty vector (grey) for 48h. CARM1 and ALIX are highlighted. (F) Co-immunoprecipitation using anti-Flag antibody in HEK293T cells transfected with Flag-CARM1-FL, Flag-CARM1- $\Delta$ E15, or Flag empty vector for 48h and immunoblotted with anti-ALIX and anti-Flag antibodies. 5% of the total protein lysate was loaded as input control. (G) Proximity-ligation assay using mouse-anti-CARM1 and rabbit-anti-ALIX antibodies. BT-549 cells were transfected with control siRNA (CTRL), or with siRNA targeting CARM1 (#5) and ALIX for 48h and fixed in 4% PFA, permeabilized with 0.1% triton. Images were captured at 40X magnification using a Deltavision epifluorescence microscope and the maximum intensity z-projection is presented. Quantifications of the PLA dots (which represents the interaction between CARM1/ALIX) were performed using ImageJ software from two independent experiments (n > 100 cells per experiment, per condition). P values from a Student t-test are represented as \*\*\*p < 0.001. Isotype matched immunoglobulins (IgG) were used as controls for the IP reactions (D, F).

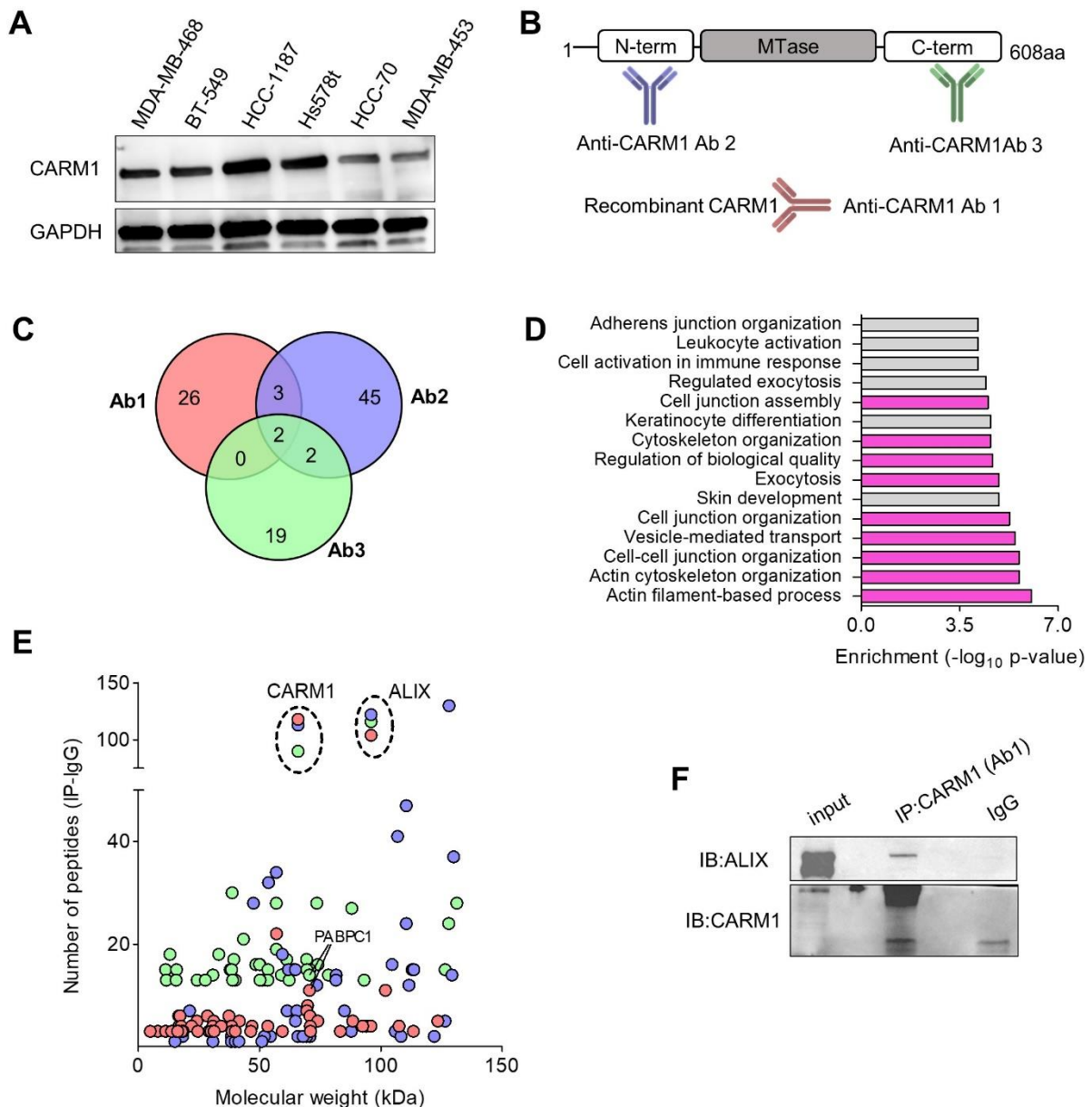


**Figure 81: ALIX interacts with CARM1 in the BT-549 TNBC cell line.** (A) Western blotting analysis of CARM1 in a panel of TNBC cell lines. (B) Schematic representation of the binding regions recognized by the three CARM1 antibodies used for immunoprecipitation followed by MS analysis. Ab1 recognizes recombinant full-length CARM1, Ab2 binds to the N-terminus and Ab3 recognizes amino acid residues between 550 and 585 in the c-terminal domain of CARM1. (C) Venn-diagram representing the enriched CARM1 interactome (defined in figure 3) in BT-549 cells with the three CARM1 antibodies. (D) Gene ontology of biological process using ShinyGO [693]. The p-values were logarithmically transformed ( $-\log_{10}$ ) and the pink bars represent all the GO terms where ALIX was found. (E) CARM1 interactome in BT-549 cells plotted as a function of the molecular weight of the proteins identified (kDa). The proteins found with each CARM1 antibody are shown in red (Ab1), blue (Ab2), and green (Ab3). CARM1 and ALIX are highlighted and an example of a known CARM1 partner (PABPC1) is marked. (F) Proteins from BT-549 cells were immunoprecipitated using an anti-CARM1 antibody and immunoblotted using anti-CARM1 or anti-ALIX antibodies. 1% of the protein lysate was loaded as input control. Isotype matched immunoglobulins (IgG) were used as a control for the IP reaction.

### **CARM1 interacts with the proline-rich domain of ALIX**

Next, we sought to characterize the domains within ALIX through which the interaction with CARM1 was occurring. ALIX contains three domains, an N-terminal Bro1 domain, a central V domain and a C-terminal proline-rich domain (PRD) and each domain is important for protein-protein interactions (**see page 113**). We co-transfected the HEK293T cells with the different ALIX domains containing an N-terminal mcherry tag (mcherry-ALIX-FL, mcherry-ALIX-Bro, and mcherry-ALIX-V-PRD) with Flag-CARM1-FL and immunoprecipitated ectopically expressed CARM1 using anti-Flag antibodies. CARM1-FL interacted with ALIX-FL and the construct containing the V-PRD domains but not with the construct containing the Bro1 domain (**Figure 82A**, indicated with the arrowhead). To narrow down the binding site within V-PRD, we designed constructs that expressed either the V or the PRD domain only and performed an immunoprecipitation as described above. We observed that CARM1-FL bound specifically to the PRD domain as no interaction was observed with the V domain (**Figure 82B**). This conclusively showed that CARM1 interacted with the C-terminal PRD domain of ALIX.

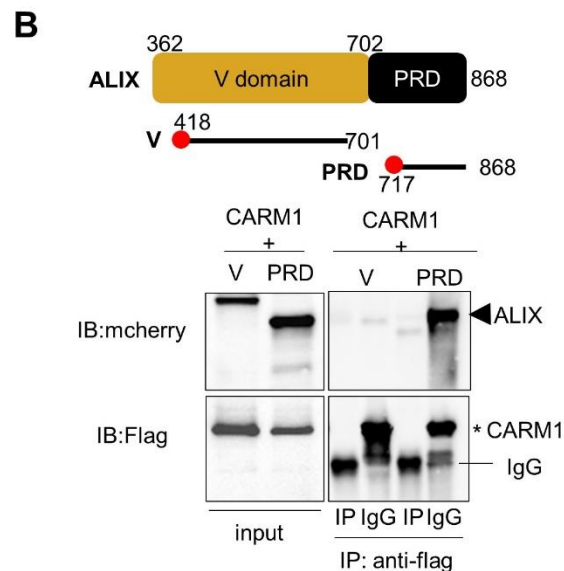
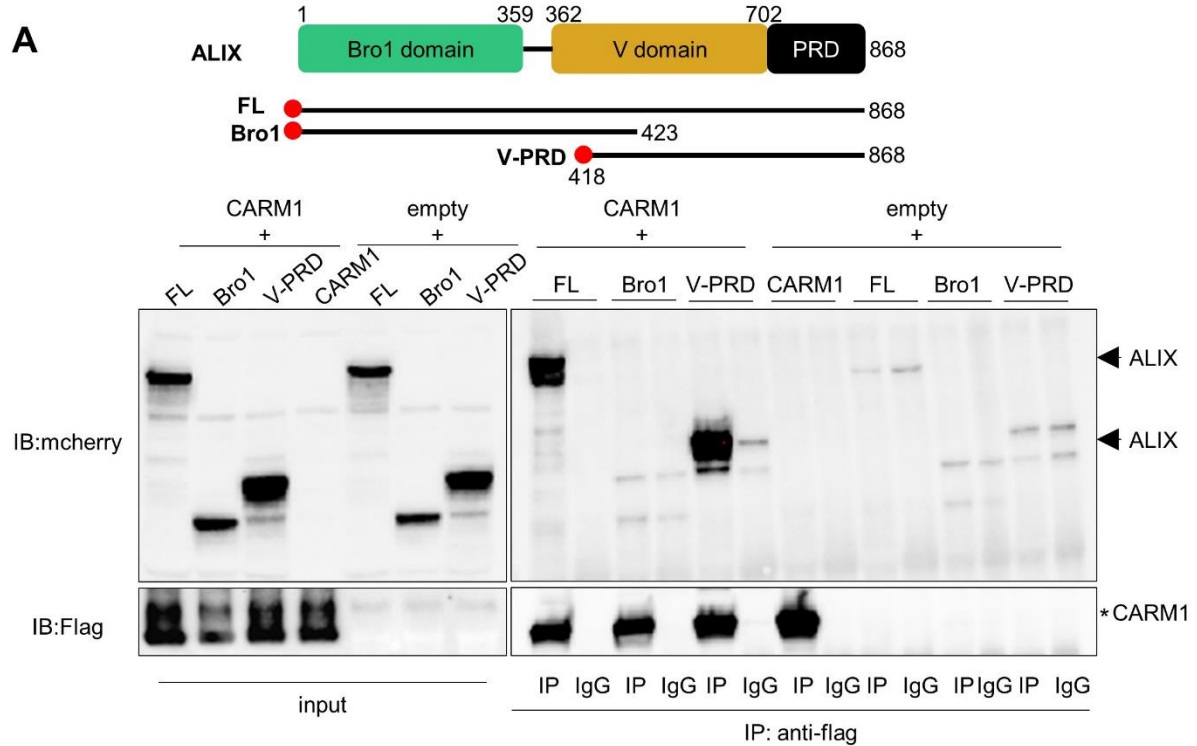


**Figure 82: ALIX interacts with CARM1 through its proline-rich domain.** (A) N-terminal mcherry tagged constructs of different ALIX domains, ALIX-FL (1-868), ALIX-Bro1 (1-423), and ALIX-V-PRD (418-868) were co-transfected with Flag-CARM1-FL or empty vector in HEK293T cells for 48h. Flag-CARM1 was immunoprecipitated using an anti-Flag antibody and immunoblotted with either anti-mcherry or anti-Flag antibodies. (B) HEK293T cells were co-transfected with Flag-CARM1-FL and mcherry-ALIX-V or mcherry-ALIX-PRD for 48h. CARM1 was immunoprecipitated using an anti-Flag antibody and immunoblotted using an anti-mcherry or anti-Flag antibody. 1% of total protein lysates were loaded as input controls. Isotype matched immunoglobulins (IgG) were used as controls for the IP reactions. Arrowhead indicates ALIX and asterisk marks CARM1 in all figures. Pictures are representative of at least two independent experiments.

### Enzymatic activity of CARM1 is required for interaction with ALIX

When we examined the exogenous CARM1 interactome in HEK293T cells, a surprising finding was that ALIX was not found to interact with the enzyme-dead mutant of CARM1 (irrespective of CARM1 isoforms, data not shown). We confirmed this observation in the HEK293T cells transfected with wild-type (CARM1-FL or CARM1- $\Delta$ E15) or the enzyme-dead mutant of CARM1 (CARM1-FL<sup>E266Q</sup> or CARM1- $\Delta$ E15<sup>E266Q</sup>; **Figure 83A and B**). These enzyme-dead mutants were generated by mutating the glutamic acid 266 residue to glutamine within the critical double E loop motif (common to all PRMTs) which is also the substrate-binding site for CARM1 (see page 85). We then generated another enzyme-dead mutant by changing arginine 168 to an alanine that is located within the cofactor (SAM) binding site and once again observed that ALIX only interacted with the wild-type and not the mutant (**Figure 83A, B**). This indicated that ALIX was binding within the substrate-binding region of CARM1 and might be methylated.

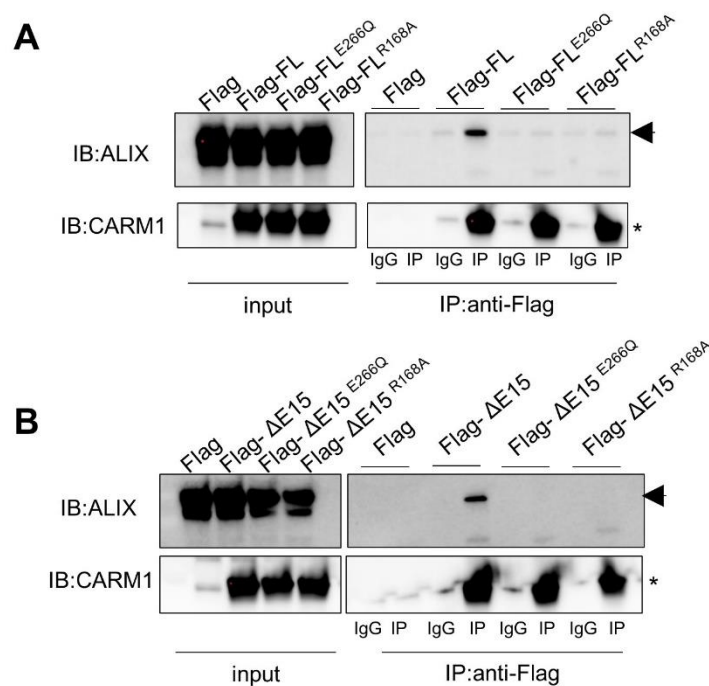


**Figure 83: ALIX does not interact with catalytically inactive CARM1 mutants.** (A) HEK293T cells transfected for 48h with an empty vector (Flag) or with a plasmid encoding for Flag-CARM1-FL wild-type or enzyme-dead mutants (Flag-CARM1-FL<sup>E266Q</sup> and Flag-CARM1-FL<sup>R168A</sup>). (B) HEK293T cells transfected for 48h with an empty vector (Flag) or with a plasmid encoding for Flag-CARM1- $\Delta$ E15 wild-type or enzyme-dead mutants (Flag-CARM1- $\Delta$ E15<sup>E266Q</sup> and Flag-CARM1- $\Delta$ E15<sup>R168A</sup>). (A, B) CARM1 was immunoprecipitated using anti-Flag antibody and the IP was immunoblotted using anti-ALIX or anti-CARM1 antibodies. 1% total protein lysate was loaded as input control and isotype-matched immunoglobulins (IgG) were used as controls for the IP reactions. Arrowhead marks ALIX and asterisk indicates CARM1. Pictures are representative of two independent experiments.

## ALIX is monomethylated in cells and the methylation is dependent on CARM1

From the above results (Figure 83), suggested that ALIX might be methylated and could be a substrate for CARM1. Indeed, several large-scale proteomic studies have previously shown that ALIX is methylated in non-BC cell lines [114, 148, 610, 611] or luminal BC cell lines [147]. Moreover, two of these studies showed that ALIX methylation was abolished in MCF7 CARM1 KO [147] cells or CARM1 depleted cells [148]. Given this evidence, we examined whether ALIX was methylated in our TNBC cell line, BT-549. For this, we performed immunoprecipitation using the same pan-monomethyl arginine (MMA) antibody used by the proteomic studies [610, 611]. Indeed, we observed endogenous ALIX was monomethylated in BT-549 cells (Figure 84A). Then, to verify if this methylation was CARM1-mediated in this cell line, we inhibited CARM1 (using TP-064 and EZM2302) and performed a similar IP as above and observed a decrease in ALIX monomethylation as compared to the DMSO-treated cells (Figure 84B). It must be noted here that initially we used high inhibitor concentrations (5 $\mu$ M of TP-064 and EZM2302) since we did not know the inhibitor concentration at which ALIX methylation might decrease considering the fact that these inhibitors decrease the methylation of different CARM1 substrates at different inhibitor concentrations (e.g., 0.67 $\mu$ M for BAF155 whereas only 74nM for MED12 [344]). Subsequently, we have also verified that ALIX monomethylation decreased at lower doses of the CARM1 inhibitor (EZM2302, 400nM, data not shown), showing that low inhibitor concentration was sufficient to inhibit ALIX methylation.

Altogether, we showed that endogenous ALIX was methylated in TNBC cells (BT-549) in agreement with previous studies and that this methylation was dependent on CARM1. A recent study has also shown that ALIX monomethylation was decreased upon PRMT5 or PRMT7 depletion [148]. As we have not tested the effect on ALIX methylation upon depletion (or inhibition) of these two PRMTs in our cells, we cannot rule out the possibility that ALIX is monomethylated by PRMTs in our cells.

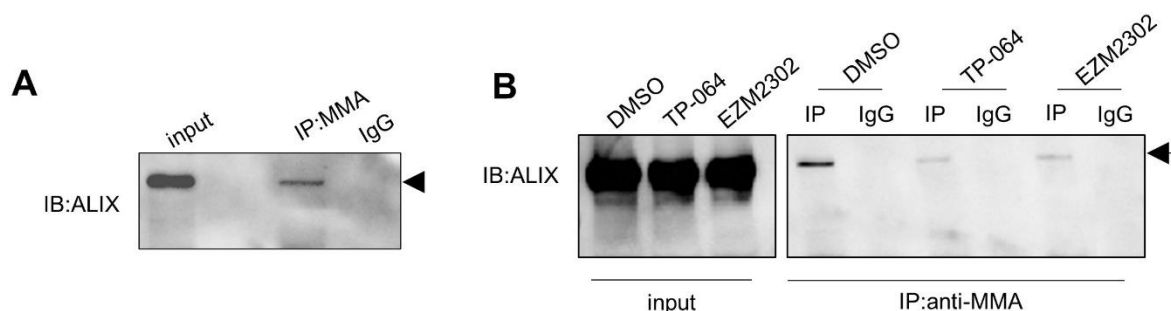


**Figure 84: ALIX methylation in cells is CARM1-mediated.** (A) Monomethylated arginine proteins were immunoprecipitated from untreated BT-549 cells using a pan-MMA antibody and immunoblotted using an anti-ALIX antibody. (B) CARM1 was inhibited in the BT-549 cells using two specific inhibitors at 5 $\mu$ M (TP-064, EZM2302) for 48h and monomethylated arginine proteins were immunoprecipitated using a pan-MMA antibody. The IPs were then immunoblotted using an anti-ALIX antibody. 1% of total



lysates were loaded as input control. Isotype matched immunoglobulins (IgG) were used as controls for the IP reactions. Pictures are representative of at least two independent experiments (A, B).

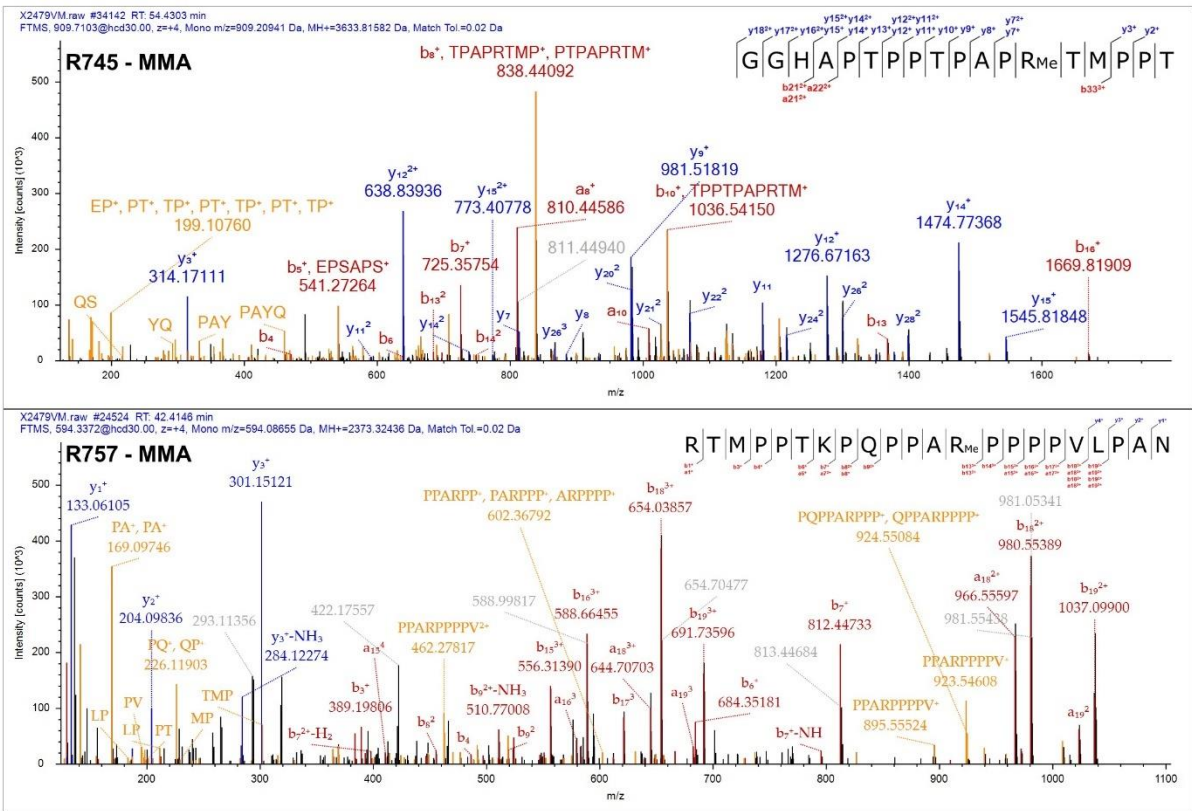
### **Endogenous ALIX is mono- and di-methylated on Arg745 and Arg757**

Once we showed that endogenous ALIX was monomethylated in our TNBC cells, we sought to identify the arginine residues on which the methylation occurred. The large-scale proteomic studies which have previously reported ALIX was methylated have shown that this methylation occurred on several arginine residues (e.g., Arg322, Arg456, Arg606, Arg745, Arg757, and Arg767), but only two of these residues were frequently found to be methylated [114, 147, 148, 610, 611]. As these sites were only identified by high throughput studies, we sought to specifically validate whether these two arginine sites (Arg745 and Arg757) were methylated in cells. We immunoprecipitated ALIX from HeLa<sup>9</sup> cells and then digested the samples using the enzyme LysargiNase (instead of the commonly used trypsin). This was because, unlike trypsin, LysargiNase could cleave peptides that contained methylated or dimethylated lysine/arginine residues, emerging as a valuable tool to identify methylated sites by MS [694]. Upon MS/MS analysis, we have demonstrated that the two arginine residues Arg745 and Arg757, located within the PRD of ALIX, were both monomethylated (**Figure 85A**) and dimethylated (**Figure 85B**), at the endogenous level. This experiment could be performed in cells inhibited for CARM1, to validate that both Arg sites are methylated by CARM1, endogenously.

---

<sup>9</sup> We used HeLa cells here because the later part of this thesis focused on one function of ALIX, i.e., cytokinesis and HeLa cells are a well-established model to study cytokinesis.

**A**



**B**

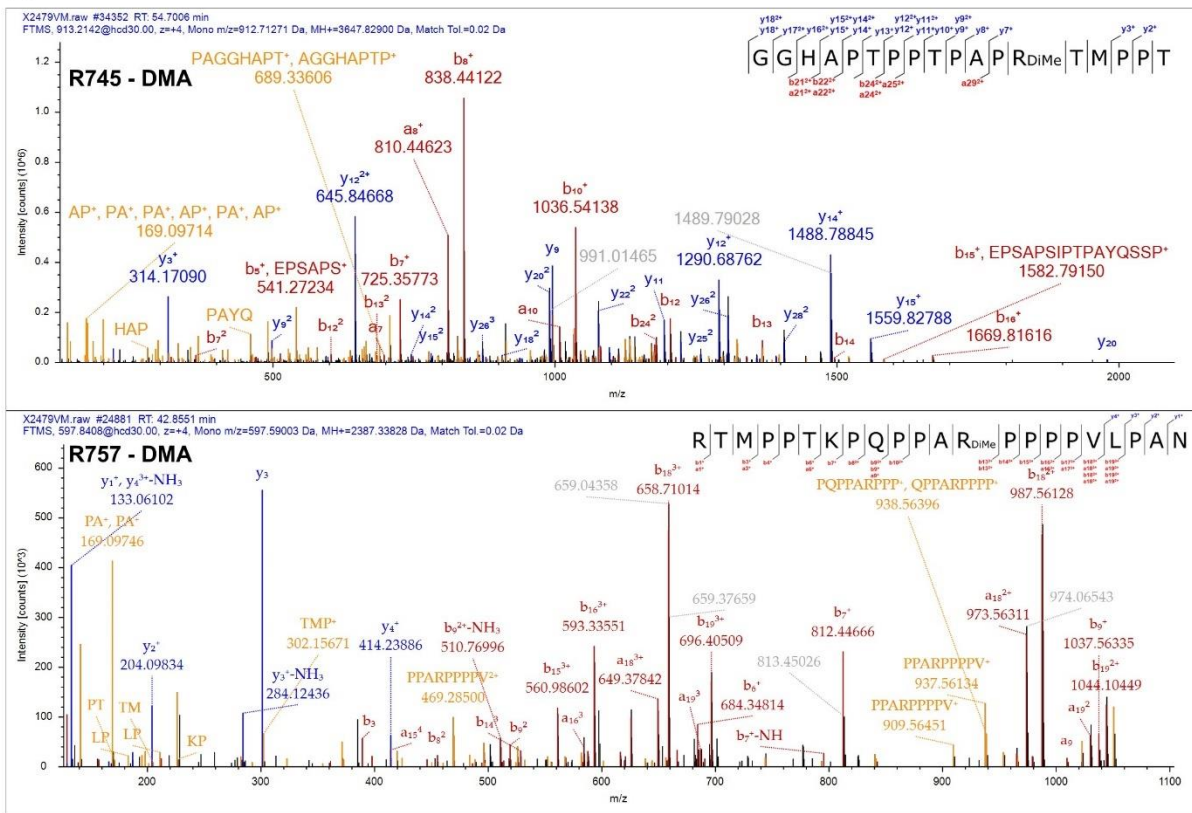
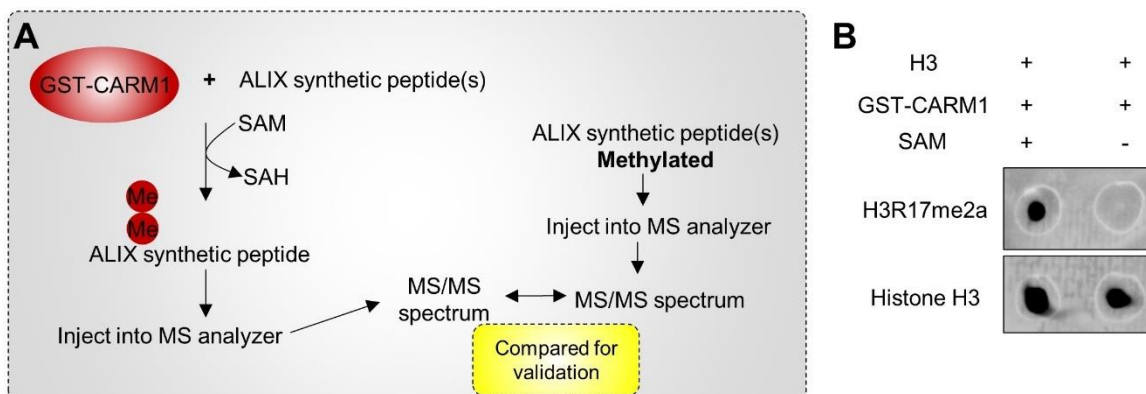


**Figure 85: Fragmentation MS/MS spectra of immunoprecipitated ALIX digested by LysargiNase.** The monomethylated and dimethylated peptide sequences and observed ions are indicated on top of

each spectrum. Singly, doubly and triply charged a, b and y ions, as well as ions corresponding to neutral losses of NH<sub>3</sub> groups, M, parent ion and internal fragments are shown. (A) Missed cleavage spectrum of monomethylated Arg745 (R745, top panel) and Arg757 (R757, bottom panel) is shown as intensity counts vs the mass/charge (m/z) ratio. (B) Missed cleavage spectrum of dimethylated Arg745 (R745, top panel) and Arg757 (R757, bottom panel) is shown as intensity counts vs the mass/charge (m/z) ratio.

### CARM1 mono- and di-methylates ALIX on Arg745 and Arg757, *in vitro*

Next, we wanted to verify, *in vitro*, if these two sites were methylated by CARM1. For this purpose, we produced recombinant GST-CARM1 in baculovirus-infected insect cells using the Bac-to-Bac system to generate an active enzyme with all its post-translational modifications intact. Using this GST-CARM1 as the enzyme source, we performed *in vitro* methylation reactions with short synthetic peptides of ALIX that contained either Arg745 or Arg757 and analyzed them by MS (**Figure 86A**). In parallel, we performed *in vitro* methylation reaction using recombinant histone H3 and GST-CARM1 in the presence (or absence) of SAM, to validate that the recombinant CARM1 was active. At the end of the incubation, the methylation reaction was verified by a dot blot using antibodies against the CARM1-specific histone mark (H3R17me2a) and total histone H3 (**Figure 86B**). The MS/MS spectrum obtained for each reaction using the ALIX peptides was compared to a spectrum of a synthetic peptide chemically modified to contain either a monomethylated or dimethylated arginine (i.e., Arg745-MMA/DMA or Arg757-MMA/DMA, **Figure 86A**). The spectrum obtained for each methylation reaction perfectly matched the spectrum of the synthetic methylated peptide (mono- and dimethylated) (**Figure 86C**), demonstrating unambiguously that both Arg745 and Arg757 were mono- and di-methylated by CARM1, *in vitro*, validating earlier proteomic studies [147, 148]. However, it remains to be shown if CARM1 methylates the full-length ALIX protein, *in vitro* (for example, by the classical radioactive *in vitro* methylation assay).



C

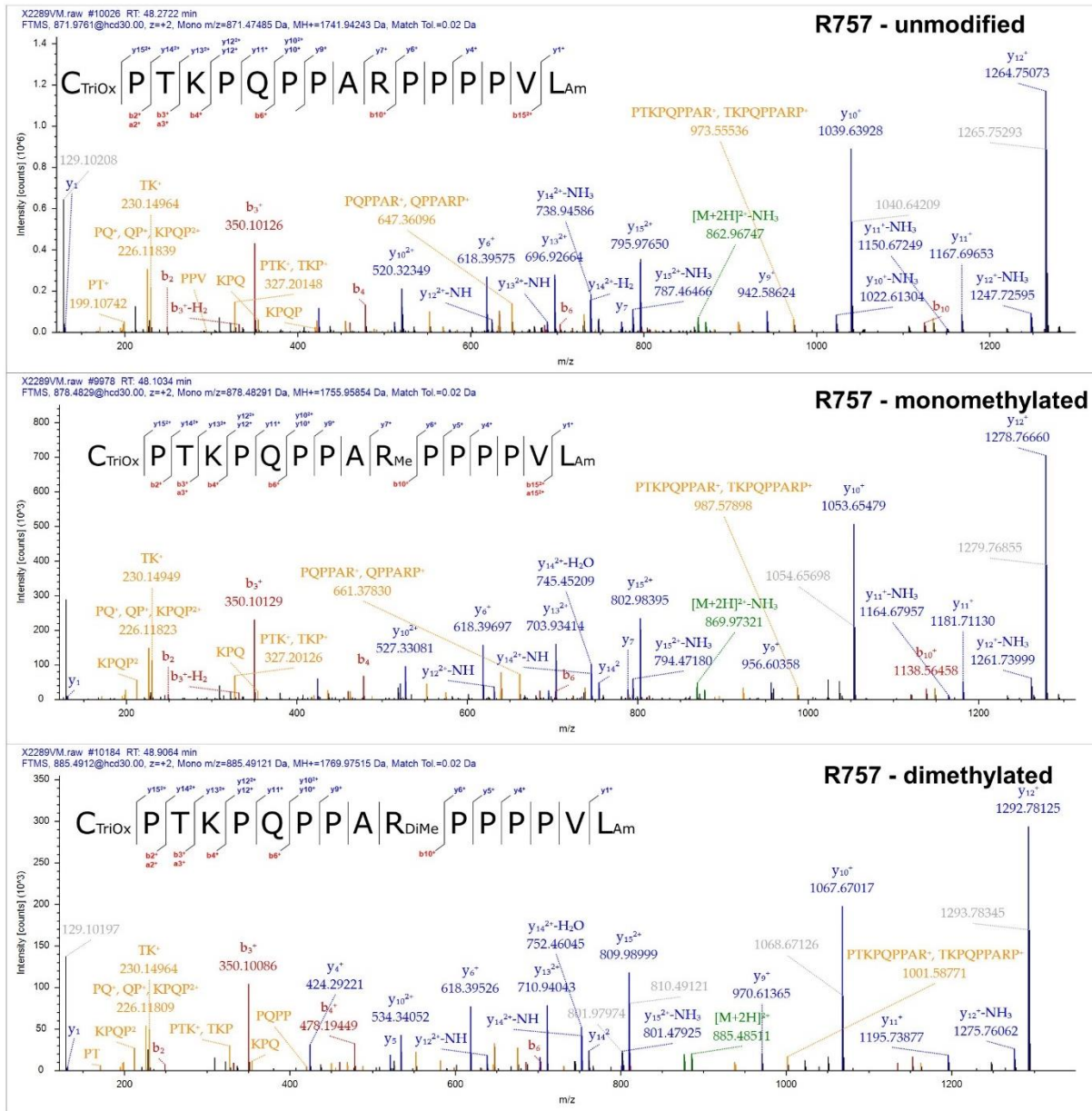


**Figure 86: CARM1 methylates *in vitro* ALIX on Arg745 and Arg757.** (A) Recombinant GST-CARM1-FL that was purified from baculovirus-infected insect cells (Sf9) was incubated with synthetic ALIX peptides in the presence of S-adenosyl methionine (SAM) for 90min and analyzed by MS spectrum. Mono- or di-methylated ALIX synthetic peptides were directly injected in an MS analyzer whose spectrum was used as a control to compare to those obtained from the *in vitro* methylation reaction. (B) Dot blot validating successful *in vitro* methylation reaction by GST-CARM1 with histone H3 incubated in the presence or absence of SAM. Immunoblotting was done using anti-H3R17me2a or anti-histone H3 antibodies. (C) Representative MS/MS spectra of unmodified (top panel), monomethylated (middle panel), and dimethylated (bottom panel) R757 in the presence of GST-CARM1 and SAM are shown as intensity counts vs mass/charge (m/z) ratio. The synthetic peptides are modified with an aminated C-terminus (Am) and trioxidation (TriOx) on the N-terminal cysteine. The unmodified, monomethylated and dimethylated peptides sequences and observed ions are indicated on top of each spectrum. Singly and doubly charged a, b, and y ions, as well as ions corresponding to neutral losses of water (H<sub>2</sub>O) and NH<sub>3</sub> groups, M, parent ion and internal fragments are shown.

## **CARM1 regulates cytokinetic abscission in HeLa cells**

Subsequently, we investigated the functional relevance of the interaction between CARM1 and ALIX. ALIX is implicated in several cellular processes, but its major functions are in topologically equivalent processes such as in vesicular trafficking, budding and release of retroviruses, and cytokinesis (**see page 118**). We explored all these functions in parallel by collaborating with different teams for the relevant expertise, including Dr. Clothilde Thery, Institut Curie (for exosome functions), Dr. Greg Towers, University College London (for HIV budding), and Dr. Arnaud Echard, Institut Pasteur (for cytokinesis). We focused on the role of CARM1 on cytokinesis as preliminary results were more promising compared to the others (**see CHAPTER 3: ADDITIONAL RESULTS AND DISCUSSIONS**).

Attempts to decipher the proteome of the midbody have revealed that few PRMTs, including CARM1, are present [642-644]. Addi and colleagues purified the midbody remnants (MBR) and identified CARM1 to be present in the total MBR fraction (termed total flemmingsome in their article) [643]. Rai and colleagues analyzed the proteome of secreted MBRs and found CARM1 in this fraction (with 16 spectral counts; KIF14 protein, a known midbody marker was found with 128 spectral counts) [644]. Capalbo and colleagues purified the midbody using HeLa cells that stably expressed GFP-KIF14 and found CARM1 (with a protein score of 33; KIF14 protein score was 36,060) [642]. Due to these pieces of evidence from the literature, we probed to see if endogenous CARM1 localized to the midbody. For this, by immunofluorescence (IF) technique, we stained HeLa cells (a well-established model to study cytokinesis) for CARM1 and used an anti-ALIX antibody to mark the midbody (**Figure 87**). Significant staining using the CARM1 antibody could be observed at the midbody (**Figure 87**). To validate the specificity of this staining, we depleted the HeLa cells using siRNA targeting CARM1. Unfortunately, depleting CARM1 only decreased the overall expression of CARM1 (within the nucleus and cytosol), but not its intensity at the midbody as compared to the control conditions (data not shown). The midbody is a highly protein rich region, therefore, it is possible that the CARM1 antibody recognizes another protein within this region and what we observe here (**Figure 87**) is an artefact. Another possible reason could be that the depletion of CARM1 was not adequate (i.e., transfection efficiency was not 100%), and the staining observed was that of the residual CARM1. Alternatively, we can hypothesize that the CARM1 remaining in the cell after depletion localizes to the midbody since it could be a crucial protein that is required for cytokinesis to complete. Therefore, the generation of a CARM1 knockout HeLa cell line would help us to validate the specificity of the staining towards CARM1 that we observed at the midbody (currently being investigated by Solène Huard).

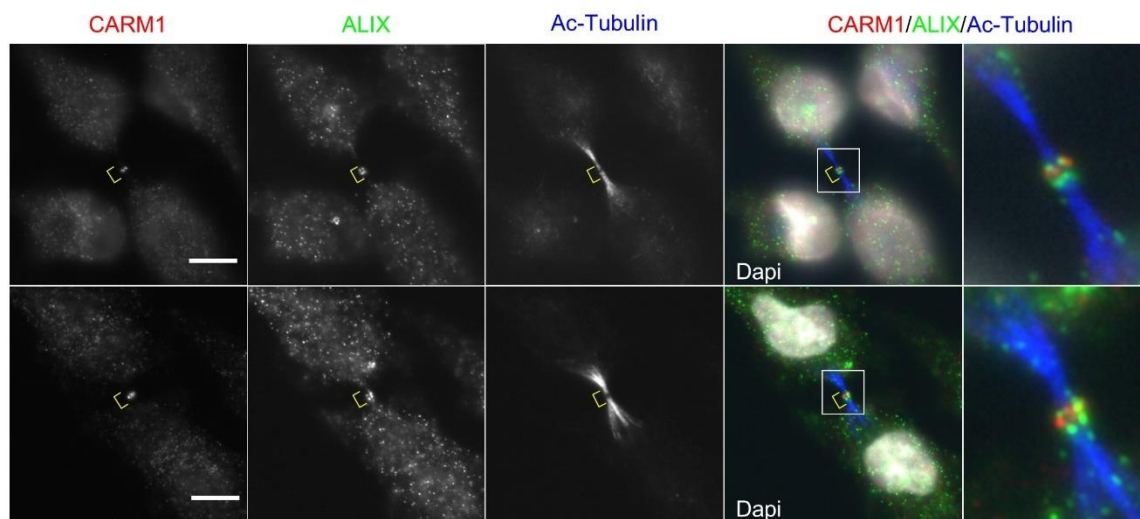


**Figure 87: Endogenous staining of CARM1 and ALIX in dividing HeLa cells.** Methanol fixed HeLa cells were stained for CARM1 (red), ALIX (green), acetylated tubulin (Ac-tubulin, blue) and counterstained with Dapi (white). Images were acquired using an Apotome microscope at 63X magnification. Scale bar = 9 $\mu$ M. Insets show a magnified intercellular bridge with the midbody. Brackets mark the midbody.

Until now, we have not been able to demonstrate unambiguously the presence of CARM1 at the midbody. However, as previous proteomic studies have indicated its presence at the midbody [642-644], we sought to evaluate if CARM1 could be involved in the process of cytokinetic abscission. Cytokinetic abscission has been previously shown to be regulated by ALIX [585, 643] where silencing ALIX causes severe defects in cytokinesis such as failure in abscission leading to binucleated/multinucleated cells [585]. Hence, to test if CARM1 was required for abscission, we depleted HeLa cells using control siRNA, or siRNAs targeting CARM1 or ALIX (as a positive control). We observed that CARM1 depleted HeLa cells displayed a reproducible (in four independent experiments) increase of binucleated cells compared to control cells (**Figure 88A**). As expected, we also observed a significant increase of binucleated cells upon ALIX depletion (**Figure 88A**), with a percentage of binucleated cells similar to the study from the team of Arnaud Echard [643], but lower from another study using another type of HeLa cells (HeLa-Kyoto) [585]. CARM1 depletion in these HeLa-Kyoto cells also increased the number of binucleated cells (**Figure 88B**). Together, our results suggested that CARM1, like ALIX, might regulate cytokinetic abscission.

Further, a recent study showed that ALIX was required for the localization of the ESCRT-III subunit, CHMP4B, to the abscission site (located on either side of the midbody where membrane scission occurs) and this was one mechanism by which ALIX regulated this process [643]. To understand if CARM1 was involved at this step, we depleted the HeLa cells for CARM1 or ALIX and quantified the percentage of

intercellular bridges (i) with no CHMP4B (corresponding to early bridges), (ii) with CHMP4B at the midbody (i.e., late bridges), and (iii) CHMP4B at the midbody and the abscission site (indicative of bridges about to undergo abscission), as done by [643]. CARM1 depleted HeLa cells showed a significant decrease of early bridges (i.e., with no CHMP4B staining) (**Figure 88C**). Then, similar to ALIX depletion, silencing CARM1 led to an increase in the proportion of bridges containing CHMP4B at the midbody and a decrease in the percentage of bridges with CHMP4B at the midbody + abscission site (**Figure 88C**). This suggested that CARM1, like ALIX, might regulate the localization of ESCRT-III subunits to the abscission site and therefore regulating cytokinetic abscission.

Altogether, our results show that CARM1 could regulate cytokinetic abscission. We observed similar phenotypes upon CARM1 and ALIX depletion i.e., (i) an increase in binucleated HeLa cells or (ii) preventing the localization of the ESCRT-III subunit, CHMP4B, to the abscission site (**Figure 91**). Additional work is needed to fully characterize the molecular mechanisms CARM1 regulate cytokinesis.

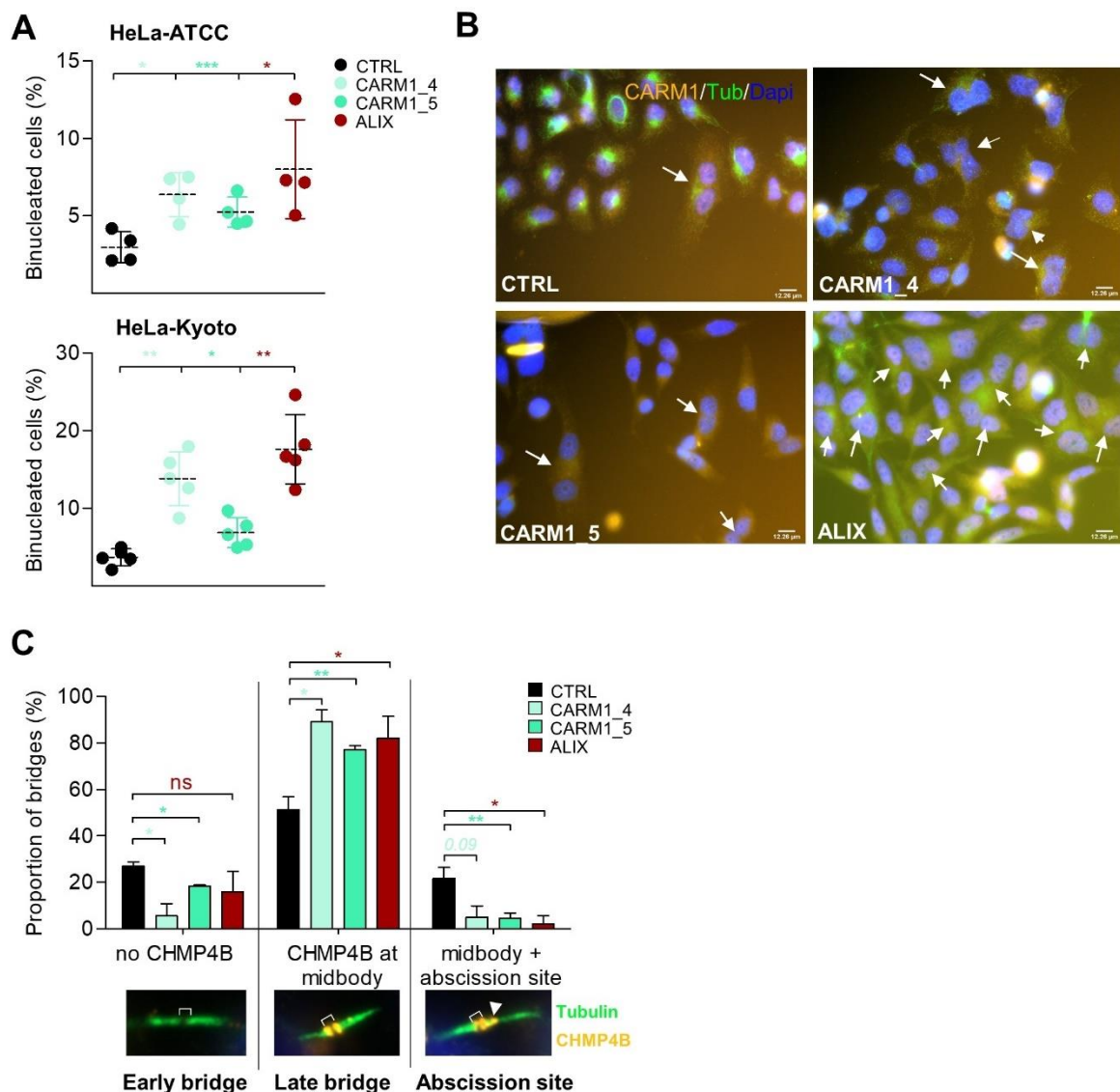


**Figure 88: CARM1 is involved in cytokinesis.** (A) Quantification of binucleated HeLa-ATCC (top panel) or HeLa-Kyoto (bottom panel) cells following depletion of CARM1 (CARM1\_4, CARM1\_5), ALIX or control siRNA (CTRL) for 48h. The data are presented as a percentage relative to the total number of cells counted from four (HeLa-ATCC, n>250 cells per experiment, per condition) or five (HeLa-Kyoto, n>300 cells per experiment, per condition) independent experiments. The dotted line represents the mean and the solid lines represent the range. (B) Representative images showing binucleated HeLa-Kyoto cells stained for endogenous CARM1, acetylated tubulin (Tub) and counterstained with Dapi. Scale bar = 12.26µM. Arrows mark the binucleated cells. (C) HeLa cells were treated with siRNAs (CTRL, CARM1\_4, CARM1\_5, and ALIX) for 48h and stained for endogenous CHMP4B and acetylated-tubulin. The presence of CHMP4B in cytokinetic bridges was classified into three categories: no CHMP4B, CHMP4B at the midbody, or CHMP4B at the midbody and the abscission site (see representative images). The proportion of bridges for each category are represented as a percentage relative to the total number of bridges counted and shown as mean ± SD from three independent experiments (n = 18-40 bridges per experiment, per condition). P values are calculated using Student t-test and shown as \*p < 0.05; \*\*p < 0.01; \*\*\*p < 0.001. All images were counterstained with Dapi and acquired on an Apotome microscope at 40X (B) or 63X (C) magnification. Brackets mark the midbody and arrowhead indicates the abscission site (C).

## Discussion

CARM1, a member of the protein arginine methyltransferase family, is overexpressed in several cancer types and has merited the need to understand its oncogenic potential in cancer progression. Also, CARM1 is one of the few members of the PRMT family for which specific and potent small-molecule inhibitors have been developed [343, 344].

### **CARM1 as a potential therapeutic target for TNBC**

Previously, CARM1 overexpression at the mRNA [147] and protein [531-533] level has been described in breast cancer, but functional and mechanistic aspects of its oncogenic potential have only been studied in the ER+ luminal subtype. The reason for this is that CARM1 binds to Erα (the main transcription factor of this pathway) and enhances/activates Erα-mediated transcription [147, 438, 462, 463, 497, 543]. In contrast, very few groups have studied the functions of CARM1 in Her2+ [291] or TNBC [531-533] BC subtypes. Therefore, the main aim of our study was to comprehend this aspect of CARM1 in TNBC, the most aggressive subtype of breast cancer. Indeed, we observed that CARM1 was overexpressed, as previously described, at the mRNA [147] and protein level [531, 533, 544] in BC as compared to healthy breast tissues.

More importantly, we report for the first time that higher CARM1 mRNA was found in the ER- tumors (i.e., Her2+ and TNBC), which was not explored by Peng et al. (they only compared BC vs normal without differentiating the subtypes) [147]. We also show that a higher CARM1 mRNA expression was associated with lower probabilities of distant metastasis-free survival in the Her2+ and luminal A subtype (not in TNBC or luminal B). Similar results were reported for higher CARM1 protein expression [532] in the luminal BC and for higher CARM1 mRNA in the whole breast population (without differentiating for the subtype) [147].



At the protein level, overall, we observed higher CARM1 expression in BC vs normal breast tissue. Whereas, when observing the expression among the BC subtypes, we saw no significant difference in the expression level, but certain variations (between our data and previous studies) in the sub-cellular localization of CARM1 protein. For instance, we report a higher nuclear CARM1 expression in TNBC when compared to the other subtypes but no difference in the cytoplasmic staining among the BC subtypes. In contrast, two studies showed that the highest nuclear CARM1 expression was found among the Her2+ subtype [531, 533]. This can be explained by few possible reasons: (i) difference in antibodies used, (ii) difference in the tumor samples (BC is known to be highly heterogeneous), or (iii) differential expression level of CARM1 isoforms. As previously discussed, CARM1 exists mainly as two alternatively spliced isoforms, CARM1-FL and CARM1-ΔE15 (**Figure 89**) in breast [454] and hematopoietic [455] cancer cell lines. Depending on the cell line, the isoform abundance can vary, for example: in AML cell lines, HEL cells have more CARM1-FL than CARM1-ΔE15 but HL-60 cells have more CARM1-ΔE15 than CARM1-FL [455]; in BC cell lines, BT-549 cells express 80% of CARM1-ΔE15 while CAL51 has an equal proportion of both [454]). However, overall, the predominant isoform has been shown to be CARM1-ΔE15 [454, 455]. We do not have sufficient information regarding the binding sites for the antibodies used by Cheng et al., and Davis et al. (no references indicated in their studies), but the CARM1 antibody used in our IHC analysis recognizes the C-terminus region. We hypothesize that this antibody might recognize both isoforms of CARM1. However, since a part of the sequence recognized by the antibody is located within the exon15, it suggests that this antibody might preferentially recognize CARM1-FL (**Figure 89**). We must verify whether this antibody recognizes both isoforms by performing a western blot using the recombinant proteins we generated (GST-CARM1-FL and GST-CARM1- ΔE15). This could potentially explain the difference in CARM1 sub-cellular localization between our study and others [531, 533]. Interestingly, CARM1-FL has been suggested to be predominantly nuclear while CARM1-ΔE15 to be cytoplasmic [456]. Perhaps the higher nuclear CARM1 observed in our analysis is indicative of CARM1-FL staining, but this would have to be confirmed using isoform-specific antibodies.

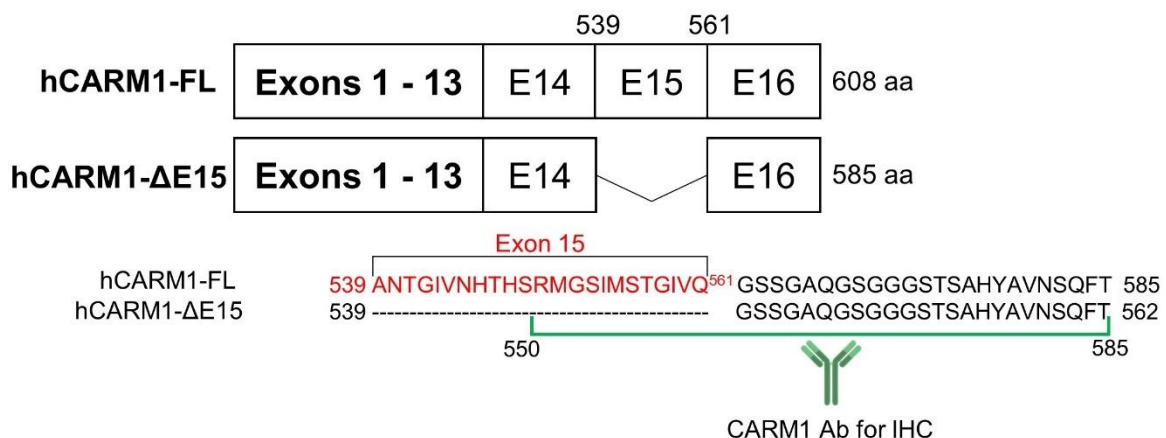


**Figure 89: Major CARM1 isoforms in human cell lines and binding site of CARM1 antibody used in our IHC analysis.** CARM1-FL contains 16 exons and produces a protein of 608 amino acids (aa). The alternatively spliced form, CARM1- $\Delta$ E15, is generated by exon15 skipping, corresponding to aa 539-561 and produces a shorter protein of 585 aa. The CARM1 antibody used in our immunohistochemistry (IHC) analysis is a polyclonal antibody that recognizes residues 550-585 as indicated (in green).

The novel finding of our IHC analysis is the staining of CARM1 in stromal cells, which has not been reported, so far. Shlensky and colleagues reported that they observed little staining in the stroma, but this might have been due to the very small sample size (12 tumors) or the antibody used in their study [456] as compared to ours (360 tumors). The identification of the specific cell types stained for CARM1 in the stroma is currently being pursued in collaboration with a team of pathologists at Institut Curie. This might help us understand if there is a contribution of CARM1 in the stroma to tumor progression.

As CARM1 was overexpressed in TNBC, our study is the first to evaluate its potential as a therapeutic target in TNBC. We observed that depleting CARM1 decreased cell proliferation and colony-forming ability in two TNBC cell lines (MDA-MB-468 and BT-549). We also observed similar effects on cell proliferation in other TNBC (MDA-MB-231, Hs578t, HCC70) and non-tumorigenic (MCF10A) cell lines. MCF10A cells are highly proliferative in our cell culture conditions (although non-tumorigenic), therefore suggesting that CARM1 affects cell proliferation of all cell lines tested. Similar to our findings, CARM1 depletion also impaired cell proliferation in other cancer types (OC – [489]; CRC [476]; prostate [536]; bone [537]; NSCLC [539]). Moreover, depleting CARM1 induced apoptosis and DNA damage in our two TNBC cell lines. This has been demonstrated in acute myeloid leukemia [455] cells, lung [695] and colorectal [477] cancer cells. Overall, this advocates that CARM1 could be an important protein for cell survival.

As mentioned above, two potent small-molecule inhibitors (TP-064 and EZM2302) have been recently developed, that specifically target CARM1 [343, 344]. Upon testing both these inhibitors in our TNBC cell lines, we observed no effect on cell proliferation (with  $IC_{50} > 10\mu M$ ). EZM2302 has been tested in a few BC cell lines (ZR751, BT-20, BT474, MCF7) and shows a similar effect as our data ( $IC_{50} > 20\mu M$ ). Notably, previous reports have shown that both CARM1 inhibitors are efficient in only very few cell lines, particularly those of hematopoietic lineages, with virtually no effect on any of the solid cancer cell lines tested [343, 344]. This suggested two hypotheses: (i) CARM1 enzymatic activity is not responsible for cell proliferation in these cancer cells or (ii) there is an underlying mechanism that is rendering some cells sensitive (and not others) to CARM1 inhibition. The second hypothesis was demonstrated by a study last year where non-Hodgkin lymphoma cells that were mutated for CREBBP and EP300 were more sensitive to CARM1 inhibition [551].

To summarize, CARM1 is overexpressed in various cancer types like ovarian [489, 534], colorectal [476, 535], prostate [536], bone [537], hematopoietic [232, 478], oral [538], non-small cell lung (NSCLC) [539], melanoma [540], and breast (our study, [147, 531-533]). Together, this suggests that depleting CARM1 could be an attractive therapeutic target; however, CARM1 inhibition, at least as a monotherapy, might be efficient only in a subset of hematopoietic cancer [343, 455, 551]. Therefore, identifying either underlying mechanisms or evaluating the available CARM1 inhibitors in combination with chemo- or targeted therapies (as previously described [551], might prove beneficial for breast and other cancer patients.

### **The CARM1-interactome reveals a novel partner and new function for CARM1**

As discussed above, the TNBC cells tested in this study were resistant to CARM1 inhibition, indicating that the proliferation of TNBC cells was independent of the methyltransferase activity of CARM1. Hence, we searched for the endogenous interactome of CARM1 in TNBC cells by immunoprecipitation followed by MS analysis. Here, we identified a major novel partner for CARM1, the protein ALIX, a multifunctional adaptor protein that is involved in endocytosis, multivesicular body biogenesis, membrane repair, cytokinesis, apoptosis, and maintenance of tight junction integrity [556]. The interaction observed between CARM1 and ALIX in our study is strong, and this interaction was not lost even under stringent detergent conditions.

Moreover, based on the number of peptides retrieved for each protein (when compared to their molecular weights) suggests that most molecules of CARM1 were bound to ALIX. A similar type of interaction is known for PRMT5 with its cofactor, MEP50, where they form a heterooctamer [696]. MEP50 functions as an adaptor protein between PRMT5 and its substrates and enhances PRMT5 activity [696]. Hence, ALIX may behave similarly to CARM1 (like MEP50 for PRMT5) especially since ALIX is an adaptor protein [557]. Here, we have confirmed their endogenous and exogenous binding in two TNBC cell lines (HCC1187 and BT-549) and the HeLa cells (data not shown) or the HEK293T cells, respectively. Further, we found that ALIX was a common partner for both the CARM1 isoforms (CARM1-FL and CARM1- $\Delta$ E15). Moreover, we also immunoprecipitated ALIX followed by MS analysis and indeed found CARM1 as a partner (data not shown). However, CARM1 was not the top hit in IP-ALIX, but we still retrieved 30 peptides (vs 221 peptides for ALIX) for CARM1. Taken together, we can infer that CARM1 might always be complexed to ALIX, but the inverse is not true, suggesting that some ALIX functions are independent of CARM1 interaction.

Besides, evidence from the literature suggested that ALIX could be a binding partner for other PRMTs, in particular, PRMT3, PRMT5 [153]. In our experience, ALIX was exclusively interacting with CARM1 (and not PRMT1 or PRMT5), but we have not verified for the other PRMTs. Therefore, without further experiments, we cannot exclude the possibility that ALIX interacts with other PRMTs.

Our study is the first, so far, to search for the endogenous CARM1 interactome. However, a major drawback from our MS analyses (endogenous or exogenous CARM1) was the limited number of partners retrieved commonly among all CARM1 antibodies. This could be because most of the protein-protein interactions occurring between CARM1, and its partners are transient and not captured during an IP/MS type of analysis. Recently developed techniques like the BioID or TurboID [697] which use a biotin-based proximity labeling might be better suited for CARM1 partner identification. This technique was employed by a study this year on all PRMTs and have identified numerous putative PRMT substrates [153]. Many of the earlier studies that searched for CARM1 substrates faced a similar problem i.e., few substrates were identified apart from two large-scale studies [146, 147]. All these high throughput studies performed immunoprecipitation using pan-methylarginine antibodies (that recognized glycine-arginine rich motifs) followed by MS analyses [114, 146, 147, 610, 611, 698-700]. This was their main limitation because we now know that CARM1 prefers to methylate arginines within a proline-rich region [146, 147] or a proline-glycine rich motif (PGM) [145, 691]. Thus far, less than 30 CARM1 substrates have been functionally validated (**see ANNEXE II: Known CARM1 substrates**). Therefore, identifying new partners and substrates of CARM1 will be of great help to the community.

An interesting finding in our study was that the novel CARM1 partner, ALIX, did not interact with the enzyme-dead mutants. We used two different CARM1 mutants here, one where the Glu266 was mutated to Gln (within the substrate-binding pocket of CARM1) and the other where Arg168 was mutated to Ala (located within the SAM binding pocket). Both mutants failed to bind to ALIX, suggesting that ALIX was binding to CARM1 through its substrate-binding pocket. We confirmed this by inhibiting CARM1 using one inhibitor (EZM2302) which has been shown to mimic substrate-binding [343] and observed that indeed the interaction between CARM1 and ALIX was lost (data not shown). Further, the fact that ALIX also failed to bind to the R168A mutant (located within the SAM binding site), hinted at the possibility that SAM binding may be required for ALIX to bind to CARM1. Kinetic studies have demonstrated that methylation by CARM1 is distributive meaning that CARM1 can either bind SAM first and then the substrate or vice-versa [448]. Given this distributive mechanism, we can speculate that the R168A mutant impairs SAM binding and therefore the interaction with ALIX. However, generating a crystal structure of CARM1 complexed with ALIX would be required to fully map these interactions. Further, the idea that ALIX binds within the substrate-binding pocket of CARM1, and that the majority of CARM1 is bound to ALIX suggests that ALIX might be an inhibitor of CARM1, like the SAM analogue molecule, MTA for PRMT5 [324]. It would be interesting to explore in the future if this is true.

Several large-scale proteomic studies have identified that ALIX is methylated on many arginine residues (e.g., Arg322, Arg456, Arg606, Arg745, Arg757, and Arg767) [114, 147, 148, 610, 611]. All these studies were performed mainly using a pan-

monomethyl arginine (MMA) antibody in non-BC cell lines [114, 148, 610, 611] or the luminal MCF7 cell line [147]. Arg745 and Arg757, have been found to be frequently methylated compared to the other sites. However, these sites were only identified by large-scale studies and have not been manually confirmed. Here, we confirmed that ALIX was methylated in TNBC cells and that these two sites (Arg745 and Arg757) were mono- and di-methylated. Further, upon CARM1 inhibition, ALIX monomethylation decreased, confirming previous studies where ALIX methylation (on Arg745 and Arg757) was abolished when CARM1 was knocked out [147] or depleted [148]. Decreased ALIX methylation on these two Arg sites has also been shown in PRMT5 or PRMT7 depleted cells [148]. Furthermore, by using synthetic peptides, we have demonstrated *in vitro* that CARM1 both mono- and dimethylated these residues. However, this still needs to be proved, *in vivo*. More importantly, Arg745 and Arg757 are located within a proline-rich motif (PPTPAPR<sup>745</sup>TMPP; PQPPAR<sup>757</sup>PPPP) suggesting that ALIX could preferentially be methylated by CARM1 and not the other PRMTs, as CARM1 prefers to methylate arginines within a proline-rich motif.

Interestingly, when we investigated the domains of ALIX that were bound to CARM1, we mapped it to its proline-rich domain (PRD). The PRD of ALIX is a rich hub of protein-protein interactions (**Figure 90**), through which ALIX mediates several cellular functions such as membrane trafficking, retroviral budding, cytokinesis, to name a few [557].

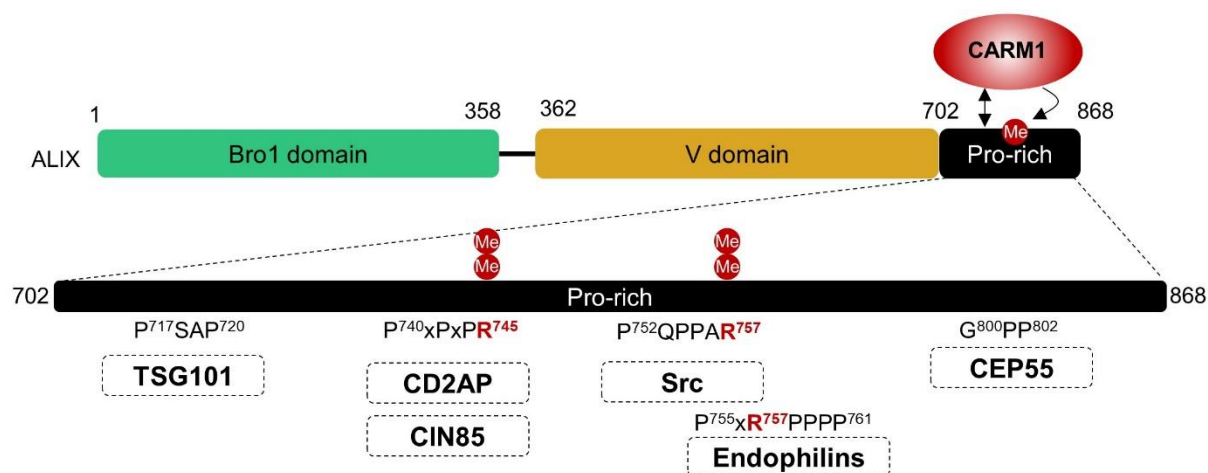


**Figure 90: Protein-protein interactions occurring through the PRD of ALIX.** The PRD (pro-rich) of ALIX mediates several interactions (see proteins indicated in the figure). Certain interactions take place at the Arg residues methylated by CARM1 (highlighted in red). CARM1 is shown to interact (by the double-headed arrow) and methylated the PRD of ALIX. Me: methylation.

Notably, some of the ALIX partner interactions like CD2AP/CIN85 [585-587, 592, 593] or Src/Endophilins [563, 569, 588] occur through the motif where CARM1 methylates ALIX, i.e., on Arg745 and Arg757, respectively. It has been shown that mutating these Arg residues can impair the binding to its partners, for example, when

Pro744 and Arg745 are mutated to Ala744,745, CD2AP can no longer bind to ALIX [584]. Otherwise, mutating Arg757Pro758 to Ala757,758 impaired ALIX binding to the three Endophilins (A1, A2, A3) [563, 588]. Thus far, the functional impact of these mutations is unknown. Given that CARM1 methylates both arginine residues, we can speculate that this methylation might also affect partner binding thereby regulating ALIX function. This will have to be explored in detail to understand the functional relevance of CARM1-mediated methylation on ALIX.

As mentioned above, one cellular function of ALIX is in cytokinesis, particularly during the last stage (i.e., cytokinetic abscission). Cytokinesis is the final step in mammalian cell division, where the two daughter cells physically separate. This is a highly concerted process where numerous proteins are involved to ensure proper division [638]. ALIX is recruited by a centrosomal protein, Cep55 to the midbody, located at the middle of the intercellular bridge (ICB) [583-585, 614]. Then, ALIX binds to the ESCRT-III subunit, CHMP4B to initiate ESCRT-III polymerization from the midbody to the site of abscission (the localization where the final membrane cut occurs) [643, 647-649]. In our study, we aimed to explore if CARM1 could be involved in this process of cytokinetic abscission. Recent evidence indicated that CARM1 (as well as a few other PRMTs, PRMT1, PRMT3, PRMT5) might be present in this midbody structure, from proteomic studies done on midbody remnants [642-644]. When we stained HeLa cells for CARM1, although we observed intense staining at the midbody, we have not been successful so far to demonstrate that this staining was specific to CARM1. Regardless of its presence at the midbody, we chose to explore if CARM1 regulated cytokinesis and observed cytokinetic defects when CARM1 was silenced. In CARM1 depleted HeLa cells there was an increase in binucleated cells (a common readout of a cytokinetic defect) as compared to control cells. This indicated that CARM1 might be required for the proper completion of cytokinesis (**Figure 91A**). As previously discussed, ALIX was required for recruiting CHMP4B to initiate ESCRT-III polymerization, a crucial step to ensure abscission completion [643]. Here, we demonstrated that CARM1 might also be involved in this process, because we observed a phenotype like ALIX depletion, i.e., an increase in the proportion of intercellular bridges (ICB) with CHMP4B at the midbody and a decrease in the proportion of ICB with CHMP4B at the midbody and abscission site when CARM1 was depleted. The implication was that CARM1 could be required for the correct localization of the ESCRT-III proteins at the abscission site (**Figure 91B**). As CARM1 depletion caused binucleated cells and hindered the localization of CHMP4B to the abscission site, it implied that CARM1, like ALIX, might be causing a delay in abscission, rather than a failure to cut. To confirm this hypothesis, we could perform live-imaging of HeLa cells depleted or not for CARM1 and calculate the time taken for cells to complete abscission (known as abscission timing). Altogether, we show evidence that implicates CARM1 in the process of cytokinetic abscission (a previously unknown role for CARM1), but further research is indeed needed to support this and to gain a comprehensive understanding of how CARM1 is regulating cytokinetic abscission.

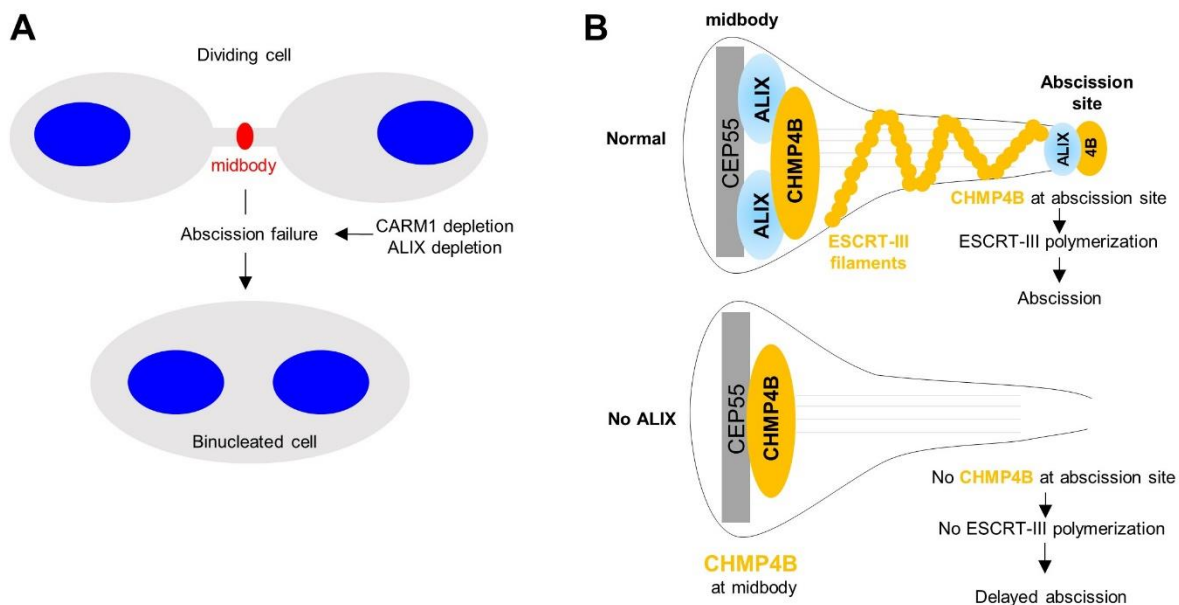


**Figure 91: Summary of cytokinetic defects caused by CARM1 depletion.** (A) HeLa cells depleted for CARM1 exhibit an increase in the number of binucleated cells, caused by a failure in abscission. This phenotype has been shown for ALIX [585, 643]. (B) For proper completion of abscission, ALIX-mediated recruitment of CHMP4B to the abscission site is required for ESCRT-III polymerization (top panel) [643]. When ALIX is depleted, CHMP4B remains at the midbody site and cannot be transported to the abscission site, causing a delay in abscission (bottom panel) [643]. We observe a similar phenotype (bottom panel) upon CARM1 depletion (CHMP4B at midbody), but we do not know yet if this induces a delay in abscission.

## Conclusion and future perspectives

In this study, we have explored two different aspects of CARM1, a clinically relevant function (as a potential therapeutic target for TNBC) and a fundamental cellular function (in cytokinetic abscission). Though both aspects have been individually explored in different cellular models (TNBC cells for the first and HeLa cells for the latter), we can speculate that both processes are linked. From our results, we can hypothesize that at early time points following CARM1 depletion, it causes defects in cytokinesis. Subsequently, maybe the accumulation of these cytokinetic defects become lethal to the cells causing them to undergo apoptosis-mediated death.

Further, there is evidence from the literature to support the notion that one of the causes of tumor progression is through the accumulation of cytokinetic defects [701]. For example, failure of cytokinesis leads to binucleated/multinucleated cells which can subsequently lead to aneuploidy (i.e., containing multiple copies of the chromosome). As aneuploidy is a trait observed in many cancer types [701], this can be thought to arise through cytokinetic failures. In contrast, excessive defects in cytokinesis may not be beneficial/sustainable for the tumor cells. Therefore, there could be a threshold level up to which tumor cells can tolerate (maybe even benefit from) cytokinetic failures. However, if this threshold is crossed, the accumulated

cytokinetic defects might become unsustainable for the tumor cells, and they undergo cell death. We may hypothesize that CARM1 is involved at this threshold (**Figure 92**).



**Figure 92: Schematic hypothesis of the effect of cytokinetic defects on tumor cell death.** CARM1 induces cytokinetic defects (such as binucleated/multinucleated cells). Upon prolonged CARM1 depletion, these cytokinetic defects could accumulate and induces apoptosis-mediated cell death.

Altogether, we have two main conclusions from our study:

(i) CARM1 is more expressed in breast cancer compared to normal tissue and its depletion impairs TNBC cell proliferation and induces apoptosis. Conversely, CARM1 inhibition exhibits no effect on TNBC cell proliferation. Therefore, CARM1 depletion may represent a potential therapeutic target but warrants the identification of the underlying reason for resistance to CARM1 inhibition in breast cancer cells.

(ii) CARM1 interactome revealed ALIX as the major partner of CARM1 and is a novel substrate. We have discovered a new function for CARM1 in the process of cytokinesis. This implies that cytokinesis may be regulated through post-translational modifications like arginine methylation.

Indeed, the results obtained and presented here require additional efforts and research for gaining a complete understanding of the molecular mechanisms at play.

### **(i) Is CARM1 important for the cell survival of all breast cancer cells?**

In our study, we depleted a subset of TNBC cells for CARM1 and observed a decrease in cell proliferation. However, TNBC and BC are highly heterogeneous. Therefore, we would need to verify if CARM1 depletion decreases cell proliferation in a large panel of BC cells to understand the importance of CARM1 on cell survival.

### **(ii) What are the cell types in the stroma that express CARM1? Does CARM1 in the stroma influence tumor progression?**

We observed staining of CARM1 in the stroma during our IHC analysis and observed a higher tendency in the Her2+ BC subtype ( $p > 0.05$ ). We would have to explore a larger cohort of Her2+ tumors to validate that CARM1 staining is indeed higher at the stroma in these tumors as compared to the others. Further, we are currently investigating with a team of Pathologists at Institut Curie to identify the cell types in the stroma that express CARM1. As a next step, we could explore how CARM1 present in the stroma might be regulating the surrounding tumor cells (in Her2+ subtype or all breast cancer).



**(iii) Are there underlying mechanisms contributing to CARM1 inhibition resistance in BC cells?**

We have shown that few TNBC cells are resistant to CARM1 inhibition. Previously, other BC cell lines (2 luminal, 1 Her2+, and 1 TNBC) [344] are also resistant to CARM1 inhibition, indicating BC cells, in general, might be resistant to CARM1 inhibition. Almost most of the cancer cell lines (particularly solid cancer) tested so far are resistant to CARM1 inhibition [343, 344]. Hence, it would be interesting to know the underlying cause that contributes to the resistance to CARM1 inhibition. Further, we could also test if CARM1 might function as a biomarker of drug response in these tumors as shown previously in ovarian cancer cells [549].

**(iv) Can CARM1 inhibition potentiate cell death when combined with other inhibitors/chemotherapies (used in the clinic)?**

CARM1 inhibition on its own has been efficient only in a subset of myeloma cell lines, but maybe co-inhibition with other inhibitors like PRMT5 inhibition or chemotherapies used in the clinic to treat BC patients might prove synergistic. For example, PRMT5 inhibition synergizes with type I PRMT inhibition in leukemia cells [326] and PRMT5 inhibition has proven to decrease cell proliferation in a subset of BC cells [301]. Hence, we can speculate that combining CARM1 and PRMT5 inhibition may be synergistic.

Moreover, high CARM1 expressing ovarian cancer cells are sensitive to PARP inhibition when combined with an EZH2 inhibitor [549]. This study also showed that ectopic expression of CARM1 homologous recombination activity [549]. Therefore, it would be interesting to check if CARM1 inhibitors can synergize with PARP inhibitors in HR-proficient breast cancer cells.

**(v) Does ALIX influence the methyltransferase activity of CARM1?**

We observed a strong interaction between CARM1 and ALIX in our study leading to the speculation that ALIX may function as an adaptor to mediate (similar to MEP50) the interaction between CARM1 and its substrate. We could explore if ALIX enhances/inhibits the methyltransferase activity of CARM1.

**(vi) What are the other cellular functions of the CARM1/ALIX complex besides cytokinesis?**

In our study, we only explored the role of the CARM1/ALIX complex in cytokinesis. We performed some preliminary experiments to study if this complex could be involved in the other known functions of ALIX such as multivesicular body biogenesis or budding of retroviruses (see **CHAPTER 3: ADDITIONAL RESULTS AND DISCUSSIONS**). This can be pursued further to fully understand the cellular role of the CARM1/ALIX complex.

**(vii) What is the role of CARM1 in cytokinesis?**

We have evidence now to suggest that CARM1 regulates cytokinetic abscission, but we still do not know the molecular mechanisms that are involved. Does CARM1

depletion delay abscission? Is the enzymatic activity of CARM1 required for its function in cytokinesis? These are some outstanding questions that need to be addressed (pursued by Solène Huard).

**(viii) Does ALIX methylation impact its partner interactions? Does the methylation impact the conformation of ALIX?**

The two arginine residues methylated by CARM1 (Arg745 and Arg757) are located within the proline-rich domain of ALIX where several important protein-protein interactions occur. We need to understand if the methylation on these residues impacts the interactions with these partners, such as CD2AP, CIN85, etc. Moreover, ALIX has been shown to exist in two conformations, an open and closed form which is mediated by post-translational modifications (see page 114). Does CARM1-mediated methylation of ALIX regulate this switch in conformation? This could be answered by crystalizing ALIX mutants (mutating Arg745 and/or Arg757 to Lys, to abolish methylation or Phe to mimic mutation).

**(ix) Can ALIX methylation be compensated for by other PRMTs (in CARM1 KO condition)?**

As there is evidence from the literature to suggest that ALIX could be methylated by other PRMTs, such PRMT5 or PRMT7, this aspect can be explored to understand if these methylation events only occur in the absence of CARM1 (as a compensatory mechanism) or if ALIX is a shared substrate between these PRMTs as is the case for few other proteins (e.g., histone H4 [156-158]).

**(x) What is the role of ALIX in BC? Does ALIX methylation correlate with BC progression?**

The function of ALIX in the context of cancer in general, or breast cancer, has not been studied thus far. Preliminary analysis from our cohort of tumors (Curie) suggests that like CARM1, ALIX is overexpressed in all BC as compared to the healthy breast samples at the mRNA level (data not shown). This can be explored further to understand the clinical relevance of ALIX and the CARM1/ALIX complex. For example, a previous report has shown that CARM1-mediated methylation of MED12 could be used to predict the sensitivity of breast cancer cells to chemotherapy [702]. We could thus analyze the methylation status of ALIX in tumors by performing IHC using antibodies that recognize mono- and dimethylated ALIX to see if this can be used as a biomarker. We attempted to generate antibodies that recognized mono- and dimethylated ALIX (on Arg 745 and Arg757) with Covalab, but only the monomethylated antibodies were successfully generated (not the dimethylated). These antibodies will have to be first validated for their specificity towards methylated ALIX and then for IHC technique, before we can answer the above question.

# **CHAPTER 3**

## **CHAPTER 3: ADDITIONAL RESULTS AND DISCUSSIONS**

In this chapter, I will discuss additional results obtained during this thesis that were not included in the two manuscripts described in chapter 2. This was because certain results were inconclusive, and more experiments were needed to answer the biological question or in other cases the topics were digressing away from the principal objective of the thesis. Nevertheless, the preliminary results described here are interesting and could be pursued further.

# The function of CARM1 isoforms in breast cancer

Human CARM1 pre-mRNA is known to be alternatively spliced resulting in two isoforms – CARM1-FL and CARM1- $\Delta$ E15. Most studies exploring CARM1 function in breast cancer, including the major part of this thesis, do not differentiate between the two isoforms [437]. However, the existence of these isoforms implies a functional need in the cells. The following work was done in collaboration with the team of Dr. Ivan Bieche, Genetics department, Diagnostic and Theranostic Medicine division at the Institut curie.

## Are both CARM1 isoforms expressed in BC?

The first question we asked was if both the CARM1 isoforms were well expressed in BC and if yes, which isoform was more expressed. Since there were no commercially available antibodies that recognized the isoforms individually, we chose to analyze the distribution of the CARM1 isoforms at the mRNA level. We analyzed a large panel of BC cell lines consisting of 11 luminal, 4 Her2+, 17 TNBC and 7 non-tumorigenic breast cell lines using primers designed to recognize CARM1-FL, CARM1- $\Delta$ E15 or both isoforms by qPCR (see **Table 14**). The first observation was that both isoforms were well expressed in BC cell lines and non-tumorigenic cells (**Figure 93, middle and right panels**). Further, we observed that CARM1-FL was more expressed in the BC cell lines vs non-tumorigenic cells (**Figure 93, middle panel**) while there was no difference for CARM1- $\Delta$ E15 expression (**Figure 93, right panel**). The total CARM1 expression did not vary between the BC cell lines and the non-tumorigenic cell lines (**Figure 93, right panel**). All the expression values (total CARM1, CARM1-FL and CARM1- $\Delta$ E15) were first normalized to the house-keeping gene expression (TATA-binding protein, TBP) and subsequently normalized to a threshold CT value (i.e.,  $CT^{35}$ ; **Figure 93**). Using these normalized values, we could observe that CARM1- $\Delta$ E15 (values ranging from 100-1200 units) was more expressed in both the BC cell lines and non-tumorigenic cell lines when compared with CARM1-FL (values ranging from 20-200 units) in these cell lines (**Figure 93, middle and right panels**). Further, as this pattern is reflected in the total CARM1 expression (**Figure 93, left panels**), these results suggested that CARM1- $\Delta$ E15 is the major CARM1 variant in BC and non-tumorigenic cell lines.

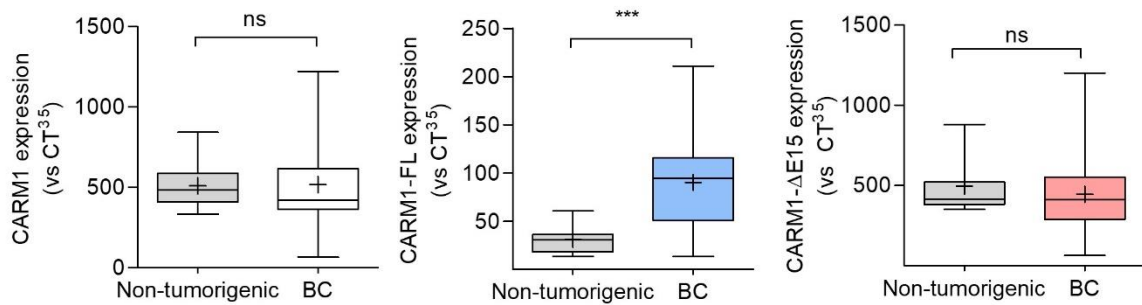


**Figure 93: CARM1 total and isoform mRNA expression in non-tumorigenic and breast cancer lines.** Total CARM1 (left panel), CARM1-FL (middle panel) and CARM1- $\Delta$ E15 (right panel), mRNA expression in non-tumorigenic (n=7) vs BC cell lines (n=32). The CT values for each expression (i.e., total CARM1, CARM1-FL and CARM1 $\Delta$ E15) were normalized to a threshold CT value (i.e., CT<sup>35</sup>, see page 245). The plus sign represents the mean. P-values were calculated from a student T-test and shown as \*\*\*p<0.001.

So far, only one group has explored the distribution of CARM1 isoforms in BC, where they analyzed a few BC cell lines (11 cell lines) [454] or 12 breast tumor samples [456]. Wang et al. reported that the major CARM1 isoform in BC cell lines was CARM1- $\Delta$ E15 [454]. Our results support their data and show that CARM1- $\Delta$ E15 was indeed the major variant in a larger panel of BC cell lines but also in non-tumorigenic breast cell lines.

To extend our question to tumors, we analyzed a large panel of breast tumors in an in-house cohort called "Saint Cloud", consisting of 514 samples (98 TNBC, 69 HER2+, 292 Luminal A, 55 Luminal B, and 16 normal breast tissues). Similar to the cell lines, both CARM1 isoforms were well expressed in the normal breast tissue and BC tumors (**Figure 94**). Upon individual isoform comparison in BC tumors vs normal tissue, we observed that CARM1-FL (**Figure 94, left panel**) and CARM1- $\Delta$ E15 (**Figure 94, middle panel**) were more expressed, perhaps mirroring total CARM1 expression (as we have shown before in two BC cohorts, see **Figure 74**). For these tumor samples, CARM1-FL and CARM1- $\Delta$ E15 expression were normalized to the TBP housekeeping gene expression. When we compare this normalized expression between CARM1-FL and CARM1- $\Delta$ E15, we observe that CARM1- $\Delta$ E15 (values ranging approximately from 1-50 units) was more expressed than CARM1-FL (values ranging from 0.1-7 units; **Figure 94**). This is similar to what we observed for the BC and non-tumorigenic cell lines indicating that CARM1- $\Delta$ E15 was the major variant in breast tumors, as well. Shlensky et al. previously explored the abundance of CARM1 isoforms in 12 breast tumors but reported that neither CARM1-FL nor CARM1- $\Delta$ E15 was more expressed than benign fibroadenomas [456]. In contrast, we indeed observe that both CARM1 isoforms were more expressed in BC than normal breast tissue and that CARM1- $\Delta$ E15 is the major isoform. This difference could be due to the variation in sample sizes between both studies (12 in [456] vs 514 in ours).

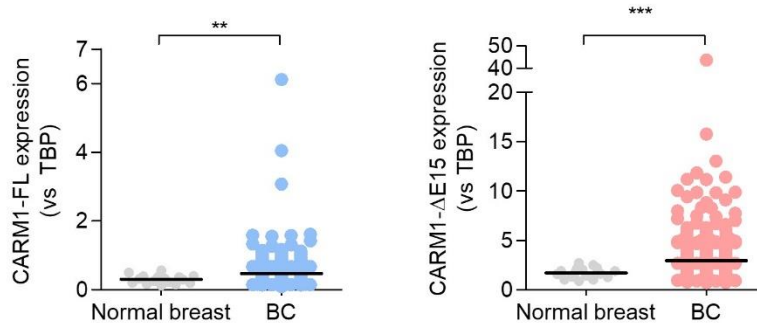


**Figure 94: Comparison of CARM1 isoform expression in breast tumors vs normal breast tissues.** CARM1-FL (left panel) or CARM1- $\Delta$ E15 mRNA in normal breast (n=16) and BC tumors (n=498). The expression was normalized to the housekeeping gene (TBP). P-values were calculated using a Mann Whitney test and shown as \*\*p<0.01 and \*\*\*p<0.001.

Next, when we stratified our BC samples according to their subtypes, the median expression of CARM1-FL was significantly different between all four subtypes (Kruskal Wallis test, p=0.0024; **Figure 95, left panel**). Further, the Her2+ subtype has a significantly higher CARM1-FL expression when compared to luminal A (Kruskal Wallis test, p<0.01; **Figure 95, left panel**) but did not statistically differ from the other subtypes (p>0.05). Median CARM1- $\Delta$ E15 expression also significantly differed between all four subgroups (p<0.0001; **Figure 95, right panel**) and luminal A expressed less CARM1- $\Delta$ E15 as compared to all the other subtypes (**Figure 95, right panel**). Shlensky et al. reported that the CARM1 isoform expression level was not different when the samples were stratified according to hormone receptor status [456]. However, in our study, we observed a significant difference for both CARM1-FL and CARM1- $\Delta$ E15 expression among the BC subtypes. These differences could probably be attributed to the skewness of their samples (6 luminal – HR+/HER2-; 6 TNBC – HR-/HER2-; no HER2+ tumors) [456].

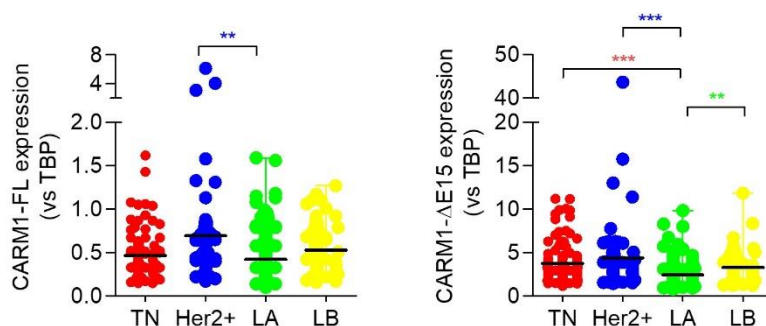


**Figure 95: Comparison of CARM1 isoform expression in the different BC subtypes.** CARM1-FL (left panel) or CARM1- $\Delta$ E15 (right panel) mRNA expression in the different BC subtypes (TN: red, n=98; Her2+: blue, n=69; LA: green, n=292; LB: yellow, n=55). The mRNA of CARM1 isoforms were normalized to the house-keeping gene expression (TBP). P values were calculated using the posthoc Dunn's multiple comparison test after a one-way ANOVA analysis and represented as \*\*<0.01, \*\*\*<0.001.

CARM1- $\Delta$ E15 has previously been proposed by Shlensky et al. to be the oncogenic variant in all BC due to the following observations. They showed it to be the major isoform expressed in BC cell lines [454]. Further, knocking out CARM1 in the MCF7 BC cell line (that expresses around 85% of CARM1- $\Delta$ E15) decreased cell proliferation while overexpressing CARM1-FL in MDA-MB-231 cells (also expressing around 85% of CARM1- $\Delta$ E15) also decreased cell proliferation [456]. Together, they proposed that CARM1- $\Delta$ E15 might be the oncogenic variant while CARM1-FL plays a protective role.

Similar to Wang et al. [454], we showed here that CARM1- $\Delta$ E15 was the major variant in BC cell lines (but also in non-tumorigenic cell lines). In addition, we show that both CARM1 isoforms are well-expressed in BC and normal breast tissue with CARM1- $\Delta$ E15 being the major variant in all breast tumors. Furthermore, we also show that CARM1-FL and CARM1- $\Delta$ E15 are more expressed in the Her2+ subtype as compared to the other BC subtypes. Together, our data suggest that CARM1- $\Delta$ E15 might be the oncogenic variant in breast tumors at least at the RNA level, aligning with the hypothesis of [456]. However, we would need to explore if CARM1- $\Delta$ E15 expression correlates with clinical parameters (such as tumor grade, tumor size, metastasis, etc.) in our sample set to support the idea that this isoform has oncogenic potential. Interestingly, the abundance of CARM1 isoforms has been studied in hematopoietic cancer cell lines (in one study) where they observed that the isoform expression varied greatly depending on the cell line analyzed, but CARM1- $\Delta$ E15 appeared to be the major variant in many cell lines [455]. They also reported that the isoform abundance did not predict the sensitivity of the hematopoietic cells to CARM1 inhibition.

Altogether, this indicates that at least at the RNA level, CARM1- $\Delta$ E15 is more expressed than CARM1-FL, suggesting that CARM1- $\Delta$ E15 could be the canonical form and not CARM1-FL. Further research will be needed to understand why both isoforms are required in the cell and how they contribute to tumor progression.



## Is CARM1 involved in other functions regulated by ALIX, apart from cytokinesis?

We identified the protein ALIX as a novel partner and substrate of CARM1 and focused on one cellular function of this complex, i.e., cytokinesis. Given the strength of their interaction and that this occurred in the cytosol, it is highly probable that the CARM1/ALIX complex could be involved in the other known roles of ALIX. Apart from regulating cytokinesis and abscission, ALIX also plays a role in the biogenesis of exosomes and the budding of HIV viral particles.

### Does CARM1 play a role in the biogenesis of exosomes?

To characterize if the CARM1/ALIX complex could be involved in the biogenesis of exosomes, we first asked if CARM1 localized to the exosome fraction. We collaborated with Dr. Clotilde Thèry (head of the extracellular vesicles, immune responses, and cancer Team at Institut Curie), an expert in the biology of exosomes.

The first step was to validate the isolation of exosomes and other extracellular vesicles (EVs). We successfully isolated the different types of EVs and exosomes from HEK293T (**Figure 96A**) and BT-549 (a TNBC cell line) (**Figure 96B**). However, we failed to observe CARM1 in any of the isolated EV/exosome fractions from both these cell lines (**Figure 96A, B**). A possible reason could be that there was an insufficient quantity of proteins within these fractions to detect a protein like CARM1 which may not be enriched in exosomes. This is supported by the observation that ALIX was faintly detected in the exosome fraction in the BT-549 cells (**Figure 96B**), as compared to the total cell lysate. On the other hand, CARM1 is expressed at low quantities in the HEK293T cells (data not shown), and therefore could be the reason why we do not observe CARM1 in the exosome fraction (**Figure 96A**). However, we had reason to believe that CARM1 is present in EVs since there is some evidence from different proteomic studies of extracellular vesicles (EV). Three peptides of CARM1 protein have been identified in a pull-down using antibodies against the tetraspanin proteins (known markers of exosomes), i.e., anti-CD9 and in the flow-through fraction using anti-CD63 antibodies [703]. Further, CARM1 was found in a secreted EV upon HIV infection of Jurkat cells [704]. Other evidence from the literature to support the localization of CARM1 to exosomes include [643, 644].

Then, we asked if CARM1 might be required for the localization of ALIX to the exosome. For this purpose, we depleted CARM1 using siRNA in the BT-549 cells, verified the efficiency of the depletion (**Figure 96C**) and isolated the EVs/exosomes. We observed a decrease of ALIX in the 100K fraction upon CARM1 depletion compared to the control-treated cells (**Figure 96D**), maybe suggesting that CARM1 was required for ALIX localization to the exosome, but this result needs to be confirmed. We also

observed a decrease in CD9 protein expression in the total cell lysate fraction (no change in exosome fraction) when CARM1 was depleted (**Figure 96D**), but no difference in the expression of the other exosome markers (**Figure 96D**). This suggests that maybe CARM1 was regulating CD9 expression but not its localization to the exosomes.

Altogether, though we were unable to demonstrate that CARM1 localized to the exosomes or EVs, there is evidence in the literature to suggest otherwise. It is possible that the cell lines we used here had low CARM1 expression (at least for HEK293T cells) and hence could not be detected using the CARM1 antibodies available. For the BT-549 cells, we know they express CARM1, but perhaps the quantity of EVs isolated from this cell line was not sufficient to detect CARM1 in this fraction. Otherwise, we can speculate that western blotting was not the most sensitive technique to assess CARM1 expression in the EVs, especially since it is not a protein that appears to be abundant in this fraction from previous proteomic studies of EVs [643, 644, 703, 704]. Therefore, we cannot rule out the possibility that the CARM1/ALIX complex co-localizes into the extracellular vesicles but further research is required to adequately confirm this.

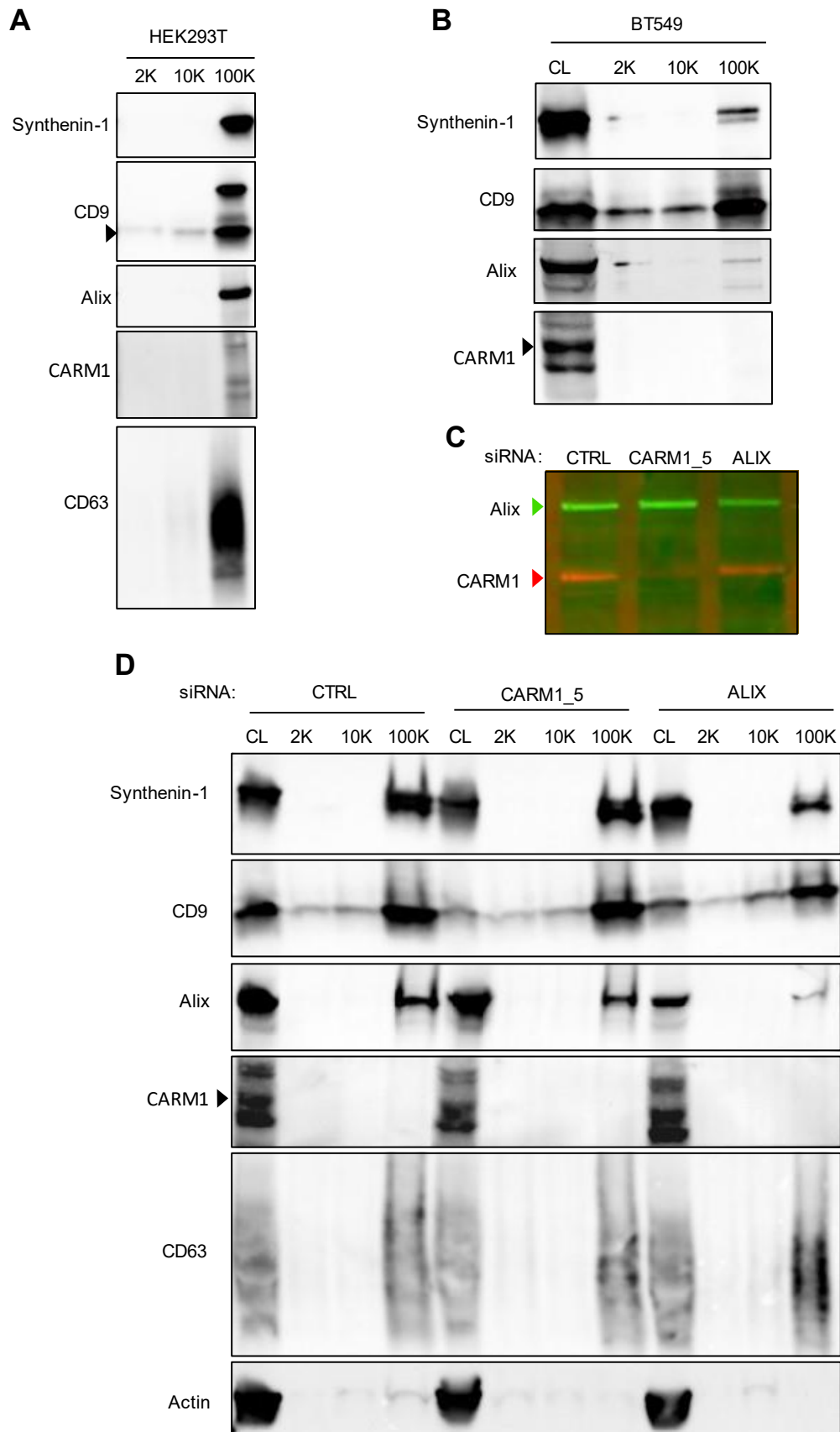


**Figure 96: Exosome/extracellular vesicles (EVs) isolation.** (A) EVs were isolated from the supernatant of untreated HEK293T by successive centrifugation steps (2K, 10K, and 100K) and immunoblotted using

bona fide EV markers (Syntenin-1, CD9, Alix, and CD63) and CARM1. The 2K pellet corresponds to EVs greater than 150nm in diameter and the 10K and 100K pellets correspond to exosomes [703]. Arrowhead indicates the band corresponding to CD9. (B) EVs were isolated from the TNBC cell line, BT-549 and the 2K, 10K, and 100K pellets were immunoblotted for the EV markers and CARM1 side-by-side with the total cell lysates (CL) that produced these EVs. Arrowhead indicates the band corresponding to CARM1. (C, D) BT-549 cells were transfected with siRNA control (CTRL), against CARM1 (CARM1\_5) or ALIX for 48h and the depletion was verified by fluorescent western-blotting using anti-CARM1 (shown in red) and anti-ALIX antibodies (in green) and fluorescent secondary antibodies (Starbright blue 520: green, Starbright blue 700: red) (C). (D) EVs isolated from the supernatant of the BT-549 cells depleted for CARM1 or ALIX were immunoblotted using the markers for EVs with the 2K, 10K, 100K pellets and corresponding CL fraction. Actin was used as a loading control for the CL fraction.

## Is CARM1 necessary for the budding of HIV from the cells?

The second function of ALIX we investigated was in the budding of the HIV virus. ALIX, along with an ESCRT-I component TGS101, are essential for aiding in the release of the HIV viral particles (**see page 120**). For this, we collaborated with experts in HIV biology, the team of Dr. Greg Towers (Division of Infection and Immunity, University College London), and they provided all the necessary tools (**see page 247**) and guidance to answer our biological question. The first step was to validate the technique to observe HIV viral-like particle (VLP) release. To do this, we transfected HEK293T cells with plasmids containing HIV-gag pol, ALIX (176-869), and an enzyme dead mutant of the ATPase complex, VPS4<sup>E233Q</sup> alone or together and analyzed the release of VLP by western blotting using an antibody that recognizes the HIV gag proteins (CA183). As expected, co-transfection of HIV-gag pol and ALIX exhibited a release of the VLP while the mutant VPS4<sup>E233Q</sup> inhibited the viral release since the ATPase activity of VPS4 is required for the membrane scission process (**Figure 97A**).

Next, we asked if CARM1 could impact the release of these VLPs. For this, we co-transfected the HEK293T cells with HIV-gag pol and either CARM1-FL or enzyme dead CARM1-FL<sup>E266Q</sup>. We observed that both CARM1-FL and its enzyme-dead mutant aided in the release of the VLP (**Figure 97B**), similar to ALIX (**Figure 97A**). As we previously showed that ALIX could bind to both the CARM1 isoforms (CARM1-FL and CARM1-ΔE15), we tested if we could observe any differences in HIV release between the two isoforms. Interestingly, we found that, unlike CARM1-FL, CARM1-ΔE15 appeared to prevent HIV VLP release, particularly with the enzyme dead mutant CARM1-ΔE15<sup>E266Q</sup> (**Figure 97B**) along with a decrease in the HIV-gag proteins inside the cell (**Figure 97B, cell lysates**). This suggested that the methyltransferase activity of CARM1-ΔE15 might be required in promoting HIV VLP release. The decrease in the HIV gag proteins produced inside the cells suggests that maybe CARM1 enzymatic activity might be needed for the assembly/oligomerization of these proteins within the cell, which is the first step prior to being released.

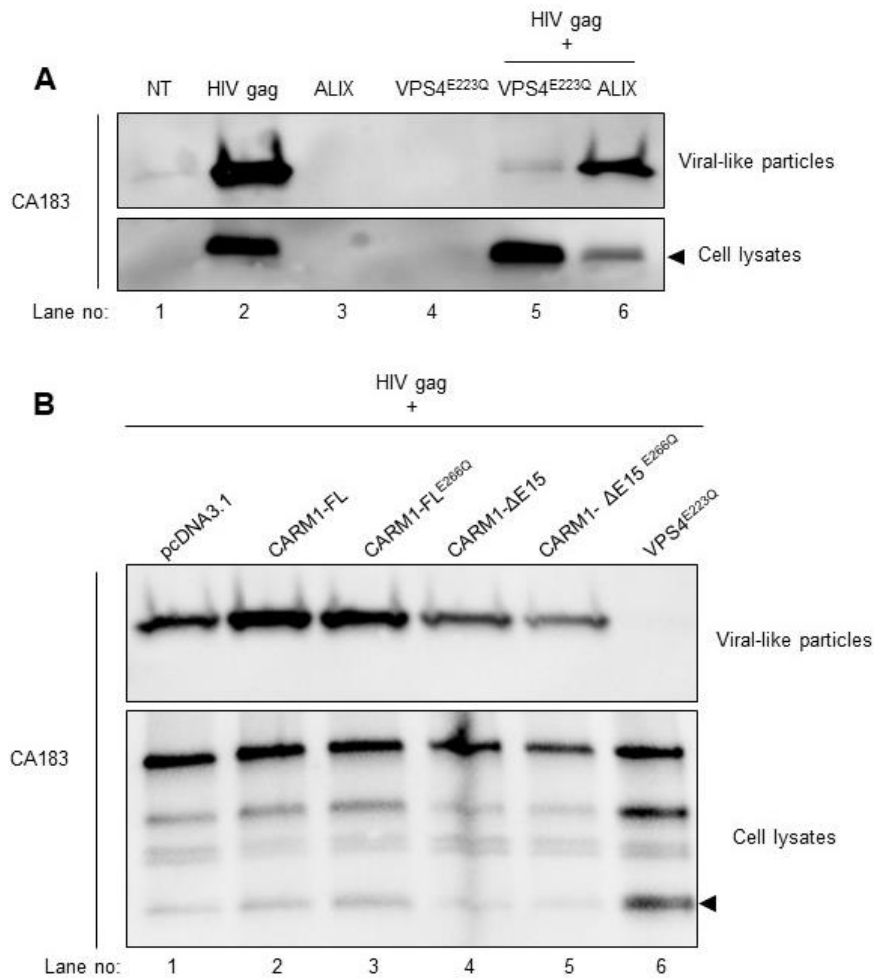


**Figure 97: Analysis of viral-like particle release in HEK293T cells.** (A) HEK293T cells were transfected with plasmids encoding for the HIV-gag protein, ALIX, or enzyme-dead mutant of VPS4<sup>E223Q</sup> (lanes 2, 3, and 4) or co-transfected with HIV-gag and VPS4<sup>E223Q</sup> or ALIX (lanes 5 and 6) in a 1:1 ratio. The viral-like particles (VLP) were isolated from the supernatant by ultracentrifugation at 100,000g and the VLPs with their corresponding cell lysates were immunoblotted for the HIV gag protein using an anti-CA183 antibody. (B) HEK293T cells were co-transfected with HIV-gag and empty vector (lane 1), CARM1-FL (lane 2), enzyme dead CARM1-FL (CARM1-FL<sup>E266Q</sup>, lane 3), CARM1-ΔE15 (lane 4), enzyme dead CARM1-ΔE15 (CARM1-ΔE15<sup>E266Q</sup>) or enzyme dead VPS4 (VPS4<sup>E223Q</sup>, lane 6) for 48h in a 1:1 ratio. VLP and cell lysates were immunoblotted using an anti-CA183 antibody, arrowhead indicates the band corresponding to p24 capsid protein. The other bands observed in (B) could represent other gag proteins such as p55 Gag [705]. NT: non-transfected.

We have chosen not to follow up further with this study since we decided at that time to focus on a cancer-related function (cytokinesis). Nevertheless, these preliminary results are encouraging, especially since the two CARM1 isoforms seem to have opposing roles in the release of VLP. So far, no studies have explored the function of PRMTs on the release of the HIV virus from infected cells. Rather, there is evidence to show that certain PRMTs are involved in the replicative cycle of HIV-1. For example, PRMT1 and PRMT5 decrease the translation of the HIV-1 Tat protein [217] while PRMT6-mediated methylation of Tat inhibits its transactivation [221]. PRMT6 is known to act as a restriction factor in HIV-1 infection by methylating HIV-1 proteins (Rev,

nucleocapsid protein p7) [223-227]. A recent study has shown that PRMT5 and PRMT7 could promote HIV-1 replication by stabilizing its Vpr protein [220]. The known role of CARM1 in HIV is that it decreases the transcription of the long-terminal repeat of HIV-1 by methylating histone H3 on R26 [219]. Therefore, it could be interesting to explore the direct function of CARM1 in HIV-1 release. In particular, how CARM1 is aiding/impairing the release of viral particles depending on the isoform in question and if this process is mediated in an ALIX-dependent function or not. This could potentially open a new area of research for CARM1.

# **CHAPTER 4**

# CHAPTER 4: MATERIALS AND METHODS

## Cell lines and Cell culture

MDA-MB-468, BT-549, HCC-1187, and HEK293T cells were purchased from the American Type Culture Collection (ATCC). Murine cell lines L-cells, and L-Wnt3a cells were obtained from Servier, France. HeLa-ATCC Clone 2 and HeLa-Kyoto were a kind gift from Dr. Arnaud ECHARD, Institut Pasteur. Mouse embryonic fibroblast (MEF) cell lines WT and knockout (KO) for CARM1 were a kind gift from Dr. Jocelyn COTE, Ottawa, Canada. Ovarian cancer cell lines A1847 (WT and KO for CARM1) were a kind gift from Dr. Rugang Zhang, Wistar University, USA. MDA-MB-468, A1847-WT and KO cells were maintained in RPMI-1640 glutamax (Gibco, Lifetechnologies) supplemented with 10% fetal bovine serum (FBS) and 1% pen/strep (Gibco, Lifetechnologies). BT-549 and HCC-1187 were maintained in RPMI-1640 glutamax supplemented with 10% FBS, 1% pen/strep, 1.5 g/L Sodium bicarbonate, 10 mM Hepes, 1 mM Sodium pyruvate. HEK293T, HeLa-ATCC clone2, HeLa-Kyoto, L, and L-wnt3a, MEF-WT and KO cells were maintained in DMEM glutamax (Gibco, Lifetechnologies) supplemented with 10% FBS and 1% penicillin/streptomycin. All cell lines were authenticated in 2018 [301] by short tandem repeats and tested for mycoplasma using MycoAlert Mycoplasma Detection Kit (Lonza Biosciences).

## Human samples and immunohistochemistry

Transcriptome microarray analysis for PRMT1 and PRMT4 were performed in the Curie cohort previously described [663] or in the publicly available TCGA breast invasive carcinoma (TCGA-BRCA) cohort [15]. The curie cohort was composed of 41 TNBC, 30 Her2+/ER-, 29 luminal A, 30 luminal B (chosen as Her2+), and 11 normal human samples. The TCGA-BRCA cohort was composed of TNBC (n = 157), Her2+ (n = 41), luminal B (n = 153, Her2+); luminal A (n = 663). The TCGA database includes 113 referenced normal breast tissue samples. Immunohistochemistry (IHC) was performed as previously described [301, 663]. Briefly, tissue microarrays (TMA) containing alcohol, formalin, and acetic acid (AFA)-fixed paraffin-embedded tissues were prepared and stained for either PRMT1 or PRMT4 using specific antibodies (see **Table 5**).

The Curie cohort (described above) was used for the IHC of PRMT1.

For the PRMT4 IHC, the PIC-BIM cohort [689, 706, 707] comprising 360 invasive ductal carcinoma samples (74 TNBC, 125 luminal A, 104 luminal B, 57 Her2+) were obtained from patients who underwent initial surgery (before radiation, hormone, or chemotherapy) at the Institut Curie between 2005 and 2006.

Analysis of all the above-mentioned human samples were performed in accordance with French Bioethics Law 2011–814, the French National Institute of Cancer Ethics Charter, and after approval by the Institut Curie Review Board and Ethics committee.



## Plasmid constructs

pcDNA3.1(+) plasmid was obtained from Lifetechnologies (V79020). pcDNA3.1(+)-FLAG-hCARM1-FL and pcDNA3.1(+)-FLAG-hCARM1-FL-E266Q encoding for the coding sequence (CDS) of full-length CARM1, and its corresponding enzyme dead mutant (E266Q) were synthesized by GENEWIZ. pcDNA3.1(+)-FLAG-hCARM1- $\Delta$ E15 and pcDNA3.1(+)-FLAG-hCARM1- $\Delta$ E15-E266Q were generated by site-directed mutagenesis (Quickchange II XL kit, Agilent) (**Table 6**). pmcherry-ALIX-FL, pmcherry-ALIX-Bro, and pmcherry-ALIX-V-PRD were a kind gift from Dr. Arnaud ECHARD, Institut Pasteur. pmcherry-ALIX-V was generated by introducing a stop codon after the V domain in the pmcherry-ALIX-V-PRD plasmid (Quickchange II XL kit, Agilent) (**Table 6**). pmcherry-ALIX-PRD was generated by PCR amplifying (**Table 6**) the PRD domain from the pmcherry-ALIX-V-PRD plasmid and cloned into a pmcherry-C1 vector using EcoRI and BamHI restriction enzymes.

## Small-interfering RNA (siRNA) transfection

Cells were seeded (**Table 4**) 24h (Day -1) prior to transfection in complete media to have 30-50% confluency for transfection. On Day 0, the seeding media was aspirated and replaced with fresh media. A 3X mix compared to the final concentration (20nM final for siRNAs and 1/500 for the transfectant interferin (PolyPlus)) is prepared in optiMEM (LifeTechnologies). One volume of transfectant mix is added to 1 volume of the siRNA mix and incubated for 10 min at room temperature (RT). Three volumes of optiMEM is added to the transfection mix, and the transfection mix is added slowly and homogeneously (dropwise) to the cells and cultured for the required timepoint.

For certain immunofluorescence experiments in the HeLa cells (ATCC and Kyoto), double shot of siRNA was used to sufficiently knockdown CARM1 protein level to observe cytokinetic defects such as binucleated cells and failure of CHMP4B to localize to the abscission site. Briefly, cells were seeded (**Table 4**) and transfected in complete media with 20nM of siRNA using Lipofectamine RNAimax reagent (LifeTechnologies). 24h after the first transfection, a second transfection was done using 20nM siRNA and cells were cultured for a total of 48h (starting from the first transfection) and 40nM final siRNA concentration.

## Plasmid transfection

Cells were seeded (**Table 4**) 24h prior to transfection in media with antibiotics to have 80% confluency. On the day of transfection, seeding media is aspirated and fresh media is added. Typically, 2 $\mu$ g of DNA is used for a 6-well plate. 2 $\mu$ g of DNA is added to optiMEM and Xtremegene-HP (Sigma) is added at a 4:1 ratio (i.e., 4 $\mu$ l for 1 $\mu$ g of DNA) and incubated at RT for 20 min. The transfection mix is added slowly to the cells and media is changed 4-5 hours after transfection.

## Wnt3a conditioned medium preparation

The murine fibroblast cell lines L-cells and L-Wnt3a cells were cultured to produce Wnt3a conditioned media. Once the cells reached ~ 80% confluency, they were split into 150cm<sup>2</sup> flasks and grown for 4 days (till confluency). The media was removed and filtered with a 0.22µm sterile filter (Sartorius) (called batch 1). 25ml fresh media (25 ml) was added and the cells were cultured for another 3 days. This media was removed and filtered using a 0.22µm sterile filter (called batch 2) and the cells were discarded. The media from batch 1 and batch 2 were mixed in a 1:1 proportion and the Wnt3a concentration in the conditioned media was measured by western blot using a standard curve of commercially available human recombinant Wnt3a (R&D systems). The conditioned media from both cell lines were appropriately aliquoted and stored at -80°C until further use.

## Wnt target gene expression assay

Cells are seeded (**Table 4**) 24h prior to siRNA transfection and transfected as described above. 24h after siRNA transfection, the cells are washed once with 1X PBS and three times in media without serum and serum-starved overnight. The next day, fresh media without serum is added to the cells and the cells are stimulated using Wnt3a conditioned media (and the control media) at 100ng/mL for 6h. RNA is extracted from these samples using the RNeasy Mini Kit (Qiagen) following the manufacturer's protocol. Wnt target gene expression is analyzed by performing an RT-qPCR (see below for details).

## Real-time – quantitative PCR assay (RT-qPCR)

RNA samples are diluted to 100ng/µl and 200ng of RNA are typically deposited into either MicroAmp Optical 96- or 384-well reaction plates (Applied Biosystems). Reverse-transcription and RT-qPCR are performed in a one-step reaction using the QuantiTect SYBR Green RT-PCR Kit (Qiagen). The reaction mix is set up using 2X QuantiTect SYBR Green RT-PCR Master Mix, 1X Quantitect Primer assay (Qiagen) or 0.2µM primers (forward and reverse) (**Table 6**), 1X QuantiTect RT Mix and RNase-free water to have a final volume of 15µl. The real-time cycler reaction is set up as 50°C, 30 min (for reverse transcription); 95°C, 15 min (initial PCR activation step); 94°C – 15sec, 60°C – 30sec, 72°C – 30sec for 40 cycles. The acquisition is done using QuantStudio™ 12K Flex Real-Time PCR System (Applied Biosystems).

## β-catenin-activated luciferase (BAR) assay

Cells were seeded (**Table 4**) 24h prior to siRNA transfection to have 50% confluency and transfected as described above (Small-interfering RNA (siRNA) transfection). After 5-6 hours of siRNA transfection, the media is replaced with antibiotic-free media and incubated overnight. Cells were transfected with the SuperTOPflash (7X Wnt response element containing plasmid) and pRL-TK-Renilla plasmids (obtained from Servier,

France) at a 10:1 ratio (2µg of DNA in total in a 6-well plate) as described above (see plasmid transfection). The cells were washed once with 1X PBS and three times with serum-free media 4-5h after DNA transfection and incubated overnight in serum-free media. The next morning, the cells were replaced with warm serum-free media and were stimulated with 100ng/mL of Wnt3a conditioned media or the control media (Wnt3a conditioned medium preparation) for 6h. The cells were washed once with 1X PBS and lysed using the 1X lysis buffer from the Dual-luciferase assay kit (Promega), passively. Passive lysis refers to adding the lysis buffer to the cells and placing the cell culture plates on a shaker for 20min, after which the lysates were collected into microcentrifuge tubes. The luminescence signal for SuperTOPflash and renilla luciferase was measured on the Infinite M200 spectrophotometer (Tecan) following the manufacturer's protocol. The ratio of the signal from firefly to renilla luciferase gives the normalized luciferase activity, representing  $\beta$ -catenin dependent Wnt activity.

### **Immunoprecipitation**

The cells were washed with 1X ice-cold PBS and collected into microcentrifuge tubes by adding 1X cold complete lysis buffer (**Table 11**) and detaching the cells using a cell scraper. Cells were lysed under rotation (40 rpm) in the cold room for 30 minutes. The cells were centrifuged at 4°C for 15 minutes at 13200 rpm to remove the cell debris and the supernatant was transferred into new tubes. The protein amount was quantified using the Pierce BCA assay kit (ThermoFisher). A final concentration of 1mg/ml of protein is prepared by dilution with lysis buffer for each immunoprecipitation condition. A small amount of the protein sample (input) is taken from the diluted tube and kept aside until further use. Antibodies of interest (2µg) are added in each tube and the same quantity of the isotype antibody (i.e., rabbit IgG or mouse IgG) is added in an additional tube and incubated overnight in a cold room under 40rpm rotation. Pre-washed (using incomplete lysis buffer, **Table 11**) Pierce Protein G agarose beads (40µl) (Life technologies) are added per condition and incubated for 1 hour in the cold room at 40rpm rotation. The samples are centrifuged for 1 minute at 13200 rpm, 4°C to pull down the beads and to remove the supernatant completely. The beads were washed three times and the proteins were eluted by adding boiling 1X laemmli buffer (**Table 10**) to the beads and denatured for 10 min at 100°C. The samples were centrifuged at 13200 rpm for 1 min and the supernatant was transferred into a new tube. 1% bromophenol blue was added to the samples prior to loading on an SDS-PAGE gel.

### **Western blotting**

Following the desired treatment, cells were washed with 1X PBS and then lysed in boiling 1X laemmli buffer (without bromophenol blue, **Table 10**) and scraped using a cell scraper, boiled for 10min at RT and centrifuged for 10min at 13200 rpm. Proteins were quantified using the Pierce BCA assay kit (ThermoFisher). Bromophenol blue (1%) is added prior to loading on an SDS-PAGE gel. Typically, unless specified otherwise,

Mini-PROTEAN TGX (4-15%) precast gels (Bio-Rad) are used for all western blotting experiments in this thesis. Protein samples along with molecular weight marker (Bio-Rad) are loaded on the TGX gels and migrated for 1h-1h30 at 120-150V. The gels are transferred onto Trans-Blot Turbo Mini 0.2  $\mu$ m nitrocellulose membranes (Bio-Rad) using a Trans-Blot Turbo Transfer System (BioRad). The membranes were blocked using 5% bovine serum albumin (BSA) (Sigma) in 1X Tris-Buffered Saline (Interchim) containing 0.1% Tween-20 (TBST) (Amresco) for 1h. Then, the membrane is incubated with the appropriate primary antibody (**Table 5**) diluted in 5% BSA + TBST overnight at 4°C on a rocker. After 3 washes using 1X TBST, the membranes are incubated with the secondary antibody coupled to HRP diluted in 5% BSA + TBST for 1h at RT. They are washed 3 times using 1X TBST and then revealed using the SuperSignal West Pico PLUS Chemiluminescent Substrate (ThermoFisher) and imaged using either the LAS-3000 imager (FujiFilm) or the ChemiDoc MP system (BioRad).

### Proximity ligation Assay (PLA)

Cells were seeded (**Table 4**) on glass coverslips in 6-well cell culture plates 24h prior to transfection. Cells were transfected with 20nM siRNA using interferin as previously described. After 48h of transfection, cells were fixed using 4% paraformaldehyde (Electron Microscopy Sciences) for 15min at RT. The cells were washed twice with 1X PBS and then permeabilized using 0.5% Triton X-100 in 1X PBS for 5min at RT and washed twice using 1X PBS. The proximity ligation assay was performed using the Duolink™ In Situ Red Starter Kit Mouse/Rabbit (Sigma, DUO92101) following the manufacturer's protocol. Images were acquired using an Inverted Widefield Deltavision microscope containing a CoolSNAP HQ2 camera and a 40x 1.3 NA objective. Quantifications are performed using ImageJ as previously described [708].

### Immunofluorescence

HeLa cells were grown and transfected with siRNA on glass coverslips in a 24-well cell culture plate (**Table 4**, Small-interfering RNA (siRNA) transfection). After 48h of siRNA treatments, the cells are washed twice with 1X PBS, fixed using either 100% cold methanol at -20°C for 3 min or 4% paraformaldehyde at RT for 15 min or 10% trichloroacetic acid at RT for 15min. After PFA and/or TCA fixation, cells are permeabilized using 0.1% Triton-X-100 in PBS for 5 min at RT. The coverslips are then washed twice using PBS and blocked using 0.2% or 1% BSA in PBS for 30 min at RT. The coverslips are incubated with the primary antibody diluted in PBS with 0.2% or 1% BSA for 1h at RT (see **Table 5** for dilutions). They are then washed with PBS + 0.2% or 1% BSA three times, 5 min each and incubated with the secondary antibody diluted as before. The washes are repeated as before, and the coverslips were incubated with 0.1 $\mu$ g/ml Dapi for 5-10min at RT. Final washes are performed using PBS+0.2% or 1%BSA and PBS before mounting the coverslips with Mowiol 4-88 (Sigma-Aldrich) solution. Images are acquired using an Upright Epifluorescence widefield microscope (Zeiss) at 40X (NA=1.3) or 63X (NA =1.4) and a CoolSnap HQ2 camera.

## Recombinant protein production

GST-CARM1-FL, GST-CARM1- $\Delta$ E15, GST and Flag-PABP1 recombinant proteins were produced in a Bac-to-Bac Baculovirus expression system using the kit from ThermoFisher. Prior to producing the recombinant proteins, they were first cloned as follows. GST fragment was first PCR amplified (**Table 6**) from the pGEX-4T-1 plasmid and cloned into the pFastBac vector using BamHI and EcoRI restriction enzymes. CARM1-FL and CARM1- $\Delta$ E15 fragments were PCR amplified (**Table 6**) from pcDNA3.1-CARM1-FL and pcDNA3.1-CARM1- $\Delta$ E15 plasmids and cloned into the pFastBac-GST vector generated using EcoRI and XbaI restriction enzymes. pFastBac-Flag-PABP1 plasmid was a kind gift from Dr. Micheal Rudnicki, Ottawa, Canada. The GST plasmids within the pFastbac vector were transformed into DH10Bac E.Coli cells to generate the recombinant bacmid containing the gene of interest. After verifying the successful transformation into the bacmid, it was transfected into the Sf9 insect cells to produce the baculovirus. Once produced, the viral stock was amplified (collecting and titrating the supernatant) and the recombinant protein was purified using a GST column.

Purified recombinant protein of ALIX (ALIX-FL, ALIX-Bro1, and ALIX- $\Delta$ PRD) was a kind gift from Dr. Aurelien Roux, Geneva, Switzerland. Recombinant human histone H3 (H3.1) was purchased from New England Biolabs.

## Immunoprecipitation followed by mass spectrometry analysis

HeLa cells were immunoprecipitated as described earlier (see Immunoprecipitation) using an anti-ALIX antibody (Table 5). The agarose beads were washed as before and resuspended in 100  $\mu$ l of 25 mM NH<sub>4</sub>HCO<sub>3</sub>, 10mM CaCl<sub>2</sub>. Samples were then digested by adding 0.4  $\mu$ g of LysArginase (Sigma EMS0008) for 1 hour at 37 °C. The resulting peptide mixtures were loaded onto homemade C18 StageTips packed with AttractSPE™ Disks Bio C18 (Affinisep™ SPE-Disks-Bio-C18-100.47.20) for desalting. Peptides were eluted using 40/60 CH<sub>3</sub>CN/H<sub>2</sub>O + 0.1% formic acid, vacuum concentrated to dryness and reconstituted in injection buffer in 2% MeCN/0.3% Trifluoroacetic acid (TFA) before Liquid chromatography-mass spectrometry (LC-MS/MS) analysis in data-dependent acquisition (DDA) mode.

## *In vitro* methylation assay (for mass spectrometry analysis)

All synthetic peptides used in this study were purchased from Covalab. 0.5 $\mu$ g of ALIX (716-775) synthetic peptide (83.33 picomoles) containing the three arginine (R745, R757, R767) was incubated with 1.56 $\mu$ g of GST-CARM1-FL (16.6 picomoles, to have a 5:1 molar ratio of peptide:CARM1) in the presence of 80 $\mu$ M S-adenosyl methionine (SAM, New England Biolabs) in 1X PBS buffer (final volume of 20 $\mu$ l) for 90min at 30°C. The methylation reaction was digested with LysArginase enzyme and injected into an MS analyzer. As a control for the methylation reaction, histone H3.1 (1.41  $\mu$ g which is equivalent to 83.3 picomoles, i.e., 0.5 $\mu$ g of peptide) was incubated with GST-CARM1

as mentioned above and verified by a dot blot using anti-H3R17me2a and anti-histone H3 antibodies.

Short synthetic peptides (~16aa) containing either R745 or R757 of ALIX (Covalab) were used to perform *in vitro* methylation assays. Non-modified peptides (i.e., the arginine residue was not chemically modified to be mono or dimethylated) were used to perform the *in vitro* methylation reaction using GST-CARM1 and SAM. 0.1µg of the non-modified peptide (62.5 picomoles) was incubated with 1.17µg of GST-CARM1-FL (12.5 picomoles to have a 5:1 molar ratio of peptide:CARM1) in the presence of 80µM SAM in 1X PBS (final volume of 20µl) for 90 min at 30°C. After the methylation reaction, peptides were purified on stage Tip to remove non-digested CARM1, peptides were eluted, vacuum concentrated to dryness and reconstituted in injection buffer as described above (see page 224). The equivalent of 1 pmol or 2 pmol of peptides (from the methylated reactions) were injected and analyzed in DDA and parallel reaction monitoring (PRM) mode.

### LC-MS/MS analysis

Online chromatography was performed with an RSLCnano system (Ultimate 3000, Thermo Scientific) coupled to an Orbitrap Exploris 480 mass spectrometer (Thermo Scientific). Peptides were trapped on a C18 column (75 µm inner diameter × 2 cm; nanoViper Acclaim PepMap™ 100, Thermo Scientific) with buffer A (2/98 CH<sub>3</sub>CN/H<sub>2</sub>O in 0.1% formic acid) at a flow rate of 3.0 µL/min over 4 min. Separation was performed on a 50 cm x 75 µm C18 column (nanoViper Acclaim PepMap™ RSLC, 2 µm, 100Å, Thermo Scientific) regulated to a temperature of 40°C with a linear gradient of 3% to 29% buffer B (100% CH<sub>3</sub>CN in 0.1% formic acid) at a flow rate of 300 nL/min over 91 min. Full scans MS were performed in the ultrahigh-field Orbitrap mass analyzer in ranges m/z 375–1500 with a resolution of 120 000 at m/z 200.

In the DDA mode, the top 15 intense ions were isolated and subsequently subjected to further fragmentation via high-energy collision dissociation (HCD) activation and acquired at a resolution of 15 000 with the auto gain control (AGC) target set to 100%. We selected ions with charge states from 2+ to 6+ for screening. Precursor ions were isolated with an isolation width of 1.6 m/z unite, normalized collision energy was set at 30% and the dynamic exclusion at 40s.

In PRM mode, acquisition list (Table 12) was generated from the peptides obtained from the synthetic unmodified, methylated and dimethylated arginine R745 and R757 peptides (Table 9) that contained an oxidated (Ox) methionine (Met), a trioxidated (TriOx) N-terminal cysteine (C) and an amidated C-terminal based on the DDA results.

### Data processing of LC-MS/MS

For protein identification from IPs, the data were searched against the Homo sapiens (UP000005640) UniProt database and the Escherichia coli database (LysArginase contamination) using SequestHT Proteome Discoverer (version 2.4). Enzyme specificity

was set to LysArginase (N-terminal cleavage of lysine and arginine) and a maximum of two missed cleavage sites were allowed. Oxidized methionine, Met-loss, Met-loss-Acetyl, N-terminal acetylation, methyl, and dimethyl arginine (R) were set as variable modifications.

For protein identification from *in vitro* methylated peptides, the data were searched against the synthetic peptide sequences using Mascot (version 2.5.1) through Sequest (version 2.4). Enzyme specificity was set to no cleavage. Oxidized methionine, N-terminal acetylation, amidated (C-Term), trioxodation (C), Methyl (R) and Dimethyl (R) were set as variable modifications.

Maximum allowed mass deviation was set to 10 ppm for monoisotopic precursor ions and 0.02 Da for MS/MS peaks. The resulting files were further processed using myProMS [709] (<https://github.com/bioinfo-pf-curie/myproms>) v3.9.3. The maximum false discovery rate (FDR) calculation was set to 1% at the peptide level (Percolator or QUALITY algorithm) and the spectra were checked manually.

PRM data analysis: raw files were processed using Skyline (version 20.2.0.343) MacCoss Lab Software (<https://skyline.ms/project/home/software/Skyline/begin.view>) for the generation of the extracted-ion chromatograms and peak integration. To robustly identify peptides in the skyline platform, we impose a mass accuracy of within 5 ppm for fragment ions. The targeted peptides were manually checked to ensure that the transitions for multiple fragment ions exhibit the same elution time in the pre-selected retention time window of the synthetic peptide. The data were then processed so that the distribution of relative intensities of multiple transitions associated with the same precursor ion must be correlated with the theoretical distribution in the MS/MS spectral library entry. The assessment of MS/MS matching was performed by Skyline and Mascot. It is worth noting that the same retention time and dot product (dotp) values [710] of at least 0.9 were found for all PRM transitions (4–6), thereby providing accurate peptide identification.

### **CellTiterGlo cell viability assay – for siRNA treatments**

The appropriate number of cells (**Table 4**) are seeded 24h prior to treatment in 96-well white transparent bottom (Greiner Bio-One, 655098) plates. Cells are transfected with 20nM siRNA using Interferin transfectant and incubated for the required time points. At time t (i.e., 48h, 72h, 96, or 120h), half-volume of the CelltiterGlo (Promega) reagent (i.e., if the well contains 150µl, 75µl of reagent) is added and incubated at 37°C for 15min. The luminescence signal is read using a Spark spectrophotometer (Tecan).

### **CellTiterGlo cell viability assay – for drug/inhibitor treatments**

The appropriate number of cells (**Table 4**) are seeded 48h prior to treatment in 96-well white transparent bottom (Greiner Bio-One, 655098) plates. On the day of the treatment, the inhibitors (150µl/well) to be tested were added in the 6 central wells of

column 11 in the 96-well plate. The inhibitor was then serially diluted from column 11 to column 3, (volume by volume) (**Figure 98**).

	1	2	3	4	5	6	7	8	9	10	11	12
A	○	○	○	○	○	○	○	○	○	○	○	○
B	○	○	○	○	○	○	○	○	○	○	○	○
C	○	○	○	○	○	○	○	○	○	○	○	○
D	○	○	○	○	○	○	○	○	○	○	○	○
E	○	○	○	○	○	○	○	○	○	○	○	○
F	○	○	○	○	○	○	○	○	○	○	○	○
G	○	○	○	○	○	○	○	○	○	○	○	○
H	○	○	○	○	○	○	○	○	○	○	○	○

**Figure 98: Scheme of a 96-well cell culture plate for IC50 calculations.** The plate shows schematically how the cells are treated with drugs/inhibitors. The max concentration is added to column 11 (darkest shade of orange) and then serially diluted into subsequent columns with the minimum concentration in column 3 (mildest shade of orange). Column 2 is non-treated cells and column 1 is blank with media-only.

After four doubling times for each cell line, half-volume of the CelltiterGlo (Promega) reagent (i.e., if the well contains 150µl, 75µl of reagent) is added and incubated at 37°C for 15min. The luminescence signal is measured using a Spark spectrophotometer (Tecan).

## 2D colony formation assay – for siRNA treatments

Cells were seeded (**Table 4**) and transfected with 20nM siRNA as previously described (Small-interfering RNA (siRNA) transfection). 24h post-transfection, cells were re-seeded into 6-well plates (**Table 4**). Cells are incubated at 37°C, 5% CO<sub>2</sub> for 6 mitotic cycles. Cells are then washed with 1X PBS and fixed using Coomassie solution (0.05% Coomassie® Brilliant Blue R-250 (ICN Biomedicals) dissolved in 50% methanol, 10% acetic acid, 40% H<sub>2</sub>O) for 15min. The staining solution is thoroughly removed by rinsing the plates using distilled water and the plates were left to dry overnight, before imaging using either the LAS-3000 imager (FujiFilm) or the ChemiDoc MP system (BioRad). The images are analyzed and quantified using ImageJ software (**Figure 100**).

## 2D colony formation assay – for drug/inhibitors treatments

The appropriate number of cells were seeded into 6-well plates (**Table 4**) 24h prior to drug/inhibitor treatment. Cells were treated with the desired drug/inhibitor concentrations for six mitotic cycles. The staining and analysis procedure was done as described above.



## Drug combinations

The appropriate number of cells (**Table 4**) were seeded 48h prior to treatment in a 96-well white transparent bottom (Greiner Bio-One, 655098) plate. Cells were treated with varying concentrations of each drug (**Table 8**) or DMSO alone as indicated (**Figure 99**).

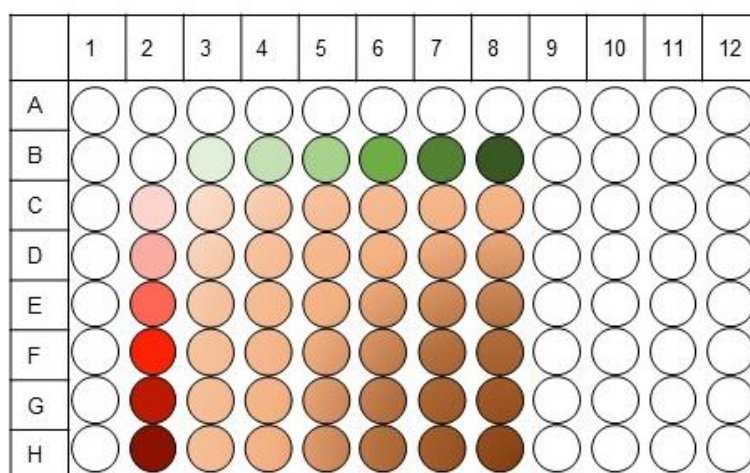


**Figure 99: Scheme of a 96-well cell culture plate for drug combination analysis.** Increasing concentrations of drug A are represented in varying shades of green and increasing concentrations of drug B in varying shades of red. The drug combination matrix is represented by shades of brown. Well number 2B indicates DMSO treatment alone (control).

Cell viability was determined after 7 days of treatment using CelltiterGlo reagent (Promega) incubated for 15min at 37°C. Luminescence signal was measured in Spark spectrophotometer (Tecan). Combenefit software was used for the drug-combination analysis [669]. All drug combinations were performed in triplicate reactions per experiment.

## Chromatin Immunoprecipitation (ChIP)

Cells were crosslinked using 1% formaldehyde (Sigma Aldrich) for 10 min at RT and then treated with 0.125M glycine for 5 min with gentle shaking. Chromatin was prepared from  $4 \times 10^6$  untreated MDA-MB-468 cells using the simpleChIP plus Enzymatic chromatin IP Kit (Cell signaling #9004). Chromatin is fragmented using both sonication and enzymatic digestion with Micrococcal Nuclease (around 150-500bp). The chromatin is immunoprecipitated using an anti-PRMT1 (**Table 5**) or control immunoglobulin (IgG) antibody overnight at 4°C under rotation. The chromatin/antibody complex was pulled down using the protein G agarose beads for 2h at 4°C under rotation. Following different washing steps, the chromatin is eluted, and the cross links are reversed using proteinase K. DNA is purified using the spin columns included in the kit and a qPCR was performed using specific primers for each promoter region (**Table 6**).

## Mice, treatment, and tumor growth measurements

Six-week-old female Swiss nude mice were purchased from Charles River and maintained in specific pathogen-free conditions. Their care and housing were per institutional guidelines as put forth by the French Ethical Committee. GSK3368715 (ChemScene LLC) was formulated in 10% DMSO (Sigma-Aldrich) at 80 mg/ml and subsequently diluted in water. GSK3368715 toxicity studies were performed by administration of 100 mg/kg daily, to nude mice. Treatment was not associated with any mortality or bodyweight loss.  $12 \times 10^6$  cells of the TNBC cell line, MDA-MB-468, were injected subcutaneously into three nude mice until tumors reached 700 mm<sup>3</sup>. The tumor fragments obtained from 2 xenografts were then grafted into the inter-scapular fat pad of nude mice. Xenografts were randomly assigned to control or treatment groups (n = 6/group) when tumors reached a volume comprised between 60 and 80 mm<sup>3</sup> and treated with vehicle or GSK3368715 at 80mg/kg once daily orally 5 days/week. During the weekends, the inhibitor was added to the drinking water of mice, full dose during the first 2 WE and then at half a dose (due to insufficient material). Tumor volume was evaluated by measuring two perpendicular tumor diameters with a caliper, twice a week. Mice were euthanized after 8 weeks of treatments. Tumor volumes were calculated as  $V = a \times b^2/2$ ,  $a$  being the largest diameter,  $b$  the smallest. Tumor volumes were then reported to the initial volume as Relative Tumor Volume (RTV). Means of RTV in the same treatment group were calculated, and growth curves were established as a function of time.

## Generation of methylated ALIX antibodies

Attempts to generate monomethylated and asymmetrically dimethylated (for Arg745 and Arg757) antibodies against ALIX were performed with Covalab. For the two monomethylated antibodies (i.e., R745-MMA and R757-MMA), the following peptides were injected into rabbits. For R745-MMA: NH<sub>2</sub>-C-H<sup>736</sup>ATPPTPAP (R<sup>745</sup>-MMA) TMPPT<sup>750</sup> – CONH<sub>2</sub> and for R757-MMA: NH<sub>2</sub>-C-P<sup>749</sup>TKPQPPA (R<sup>757</sup>-MMA) PPPPV<sup>763</sup>-CONH<sub>2</sub>. For the two asymmetrically demethylated antibodies (i.e., R745-ADMA and R757-ADMA), the rabbits were injected with the following peptides. For R745-ADMA: NH<sub>2</sub>-C-H<sup>736</sup>ATPPTPAP (R<sup>745</sup>-ADMA) TMPPT<sup>750</sup> – CONH<sub>2</sub> and for R757-ADMA: NH<sub>2</sub>-C-P<sup>749</sup>TKPQPPA (R<sup>757</sup>-MMA) PPPPV<sup>763</sup>-CONH<sub>2</sub>. For all the four antibodies, two different rabbits were injected and followed for 88 days, and the serum from the two rabbits were extracted at the end of this period, pooled together and immunopurified using columns. The specificity of the immunopurified antibodies were verified using an ELISA test. To note, the two ADMA antibodies (R745-ADMA and R757-ADMA) were not successful and only the two MMA antibodies (R745-MMA and R757-MMA) were successfully generated.

**Table 4: Cell culture conditions used**

<b>Cell line</b>	<b>Cell number</b> (culture dish)	<b>Application</b>	<b>Experiment type</b>	<b>Doubling time</b> (hours)	<b>Assay duration</b> (days)
MDA-MB-468	300,000 cells (6-well plates)	siRNA/ plasmid transfection	Wnt target gene expression, BAR assay, WB	-	-
MDA-MB-468	3000 cells/well (6-well plate)	After siRNA treatment	2D colony formation assay	35	9
MDA-MB-468	1500 cells/well (6-well plate)	Inhibitor treatment	2D colony formation assay	35	9
MDA-MB-468	10,000 cells/ml (96-well plate)	siRNA/inhibitor treatment	CellTiterGlo viability assay	35	7 (or timepoint indicated in the figure)
MDA-MB-468	10,000 cells/well (96-well plate)	Inhibitor treatment	Drug combination	35	7
BT-549	250,000 cells/well (6-well plate)	siRNA/inhibitor treatment	WB	-	-
BT-549	3000 cells/well (6-well plate)	After siRNA treatment	2D colony formation assay	30	9
BT-549	2000 cells/well (6-well plate)	Inhibitor treatment	2D colony formation assay	30	9
BT-549	5000 cells/ml (96-well plate)	siRNA/inhibitor treatment	CellTiterGlo viability assay	30	5 (or timepoint indicated in the figure)

BT-549	200,000 cells/well (6-well plate)	siRNA treatment	PLA		
BT-549	T150 flask	-	IP	-	-
HCC-1187	T150 flask	-	IP	-	-
HEK293T	1 × 10 <sup>6</sup> cells/dish (60.1cm <sup>2</sup> petri dish)	Plasmid transfection	IP	-	-
HEK293T	2 × 10 <sup>6</sup> cells/dish (60.1cm <sup>2</sup> petri dish)	Co-plasmid transfection	Co-IP	-	-
HeLa (ATCC)	T150 flask	-	IP	-	-
HeLa (ATCC)	40,000 cells/well (24-well plate)	Double-shot siRNA transfection	IF	-	-
HeLa (Kyoto)	35,000 cells/well (24-well plate)	Double-shot siRNA transfection	IF	-	-

**Table 5: List of antibodies used**

<b>Target</b>	<b>Company</b>	<b>Reference</b>	<b>Host species</b>	<b>Application</b>	<b>Dilution</b>
Actin	Sigma-Aldrich	A5441	Mouse	Wb	1/2000
Cleaved Caspase3	Sigma-Aldrich	C8487	Rabbit	Wb	1/1000
Cleaved Caspase7	Cell Signaling	9491	Rabbit	Wb	1/1000
Cleaved PARP	Cell Signaling	9546	Mouse	Wb	1/2000
GAPDH	Cell Signaling	2118	Rabbit	Wb	1/1000
H4R3me2 asymmetric	Active Motif	39705	Rabbit	Wb	1/500
Histone 4	Abcam	ab7311	Rabbit	Wb	1/1000
LRP5	Cell Signaling	5440	Rabbit	Wb	1/1000
LRP6	Cell Signaling	2560	Rabbit	Wb	1/1000
PRMT1	Millipore	07-404	Rabbit	Wb, IHC	1/1000, 1/1000
PRMT1	Bethyl	A300-722A	Rabbit	ChIP	5µg antibody/mg lysate
PRMT1	Cell Signaling	2449	Rabbit	Wb	1/1000
Tubulin	Sigma-Aldrich	T6074	Mouse	Wb	1/2000
γH2AX	Millipore	05-636	Mouse	Wb	1/1000
CARM1	Cell signaling	3379	Rabbit	WB,IP,IF (PFA/meOH)	1/1000,2µg/mg lysate,1/1000
CARM1	Cell Signaling	12495	Mouse	WB,IP,IF (PFA), PLA (PFA)	1/1000,2µg/mg lysate,1/1000, 1/1000
CARM1	Bethyl	A300-421A	Rabbit	IP	2µg/mg lysate
CARM1	Abcam	ab84370	Rabbit	IHC	1/500
ALIX	Cell signaling	92880	Rabbit	WB, IF (PFA), PLA (PFA)	1/1000
ALIX	Santacruz	sc-271975	Mouse	IF (meOH)	1/100

ALIX	Bethyl	A302-938A	Rabbit	IP	2µg/mg lysate
Acetyl-tubulin	Antibody platform – I. Curie	-	Human	IF (PFA, meOH)	1/50
PABP1	Cell Signaling	4992	Rabbit	WB	1/1000
Methyl-PABP1 (asymmetric R455/R460)	Cell Signaling	3505	Rabbit	WB	1/1000
Mono-methyl arginine	Cell Signaling	8015	Rabbit	WB, IP	1/1000, 2µg/mg lysate
Flag (clone M2)	Sigma-Aldrich	F3165	Mouse	WB, IP	1/1000 or 1/2000, 2µg/mg lysate
mcherry	Antibody platform – I. Curie	-	Rabbit	WB, IP	1/2500, 2µg/mg lysate
Histone H3	Cell signaling	9717	Rabbit	WB	1/1000
H3R17me2 asymmetric	Tebu-Bio	23613-0016	Rabbit	WB	1/500
H3R17me2 asymmetric	Upsate	07-214	Rabbit	Dot blot	1/1000
CHMP4B	Protein-tech (was a kind gift from Dr. Arnaud Echard, Institut Pasteur, France)	13683-1-AP	Rabbit	IF (meOH)	1/1000
Anti-Rabbit IgG-HRP	Interchim	111-035-045	Goat	Wb	1/20000

Anti-Mouse IgG-HRP	Interchim	115-035-062	Goat	Wb	1/20000
Anti-Human IgG Alexa Fluor 488	Invitrogen	A-11013	Goat	IF	1/1000
Anti-Mouse IgG Alexa Fluor 555	Invitrogen	A-21422	Goat	IF	1/1000
Anti-Rabbit IgG Alexa Fluor 555	Invitrogen	A-21428	Goat	IF	1/1000
Anti-rabbit IgG Alexa Fluor 647	Invitrogen	A-21244	Goat	IF	1/1000

**Table 6: List of primers used**

<b>Target</b>	<b>Target Sequence/name</b>	<b>Application</b>	<b>Company</b>	<b>Reference</b>
PRMT1	-	qPCR	Qiagen	QT0000581 7
LRP6	-	qPCR	Qiagen	QT0004317 6
LRP5 -F	5' GGACACCAACATGATCGAGTC G	qPCR	Eurogentec	This study
LRP5 -R	5' CGCTCAATGCTGTGCAGATTCC	qPCR	Eurogentec	This study
PORCN -F	5' TGGATGACACCACAGAGGAGC A	qPCR	Eurogentec	This study
PORCN -R	5' CTCAGCCTATGAGACGGTAGA	qPCR	Eurogentec	This study
GAPDH	-	qPCR	Qiagen	QT0119264 6
Actin	-	qPCR	Qiagen	QT0168047 6
Hsp90	-	qPCR	Qiagen	QT0167979 0
Axin 2	-	qPCR	Qiagen	QT0003763 9
APCDD1	-	qPCR	Qiagen	QT0004125 8
NKD1	-	qPCR	Qiagen	QT0003610 6
PORCN BRA -F	5' ATGTCCAGACCCCAGTTTGT	ChIP-qPCR	Eurofins	This study



PORCN BRA -R	5' GTGAACGCTGCTGAATTTGC	ChIP-qPCR	Eurofins	This study
PORCN BRB -F	5' TTAAGCCACCCAGTCTGAGG	ChIP-qPCR	Eurofins	This study
PORCN BRB -R	5' CCTTCAGCTAGACGAGGAGG	ChIP-qPCR	Eurofins	This study
LRP5-F	5' CACTTATCTCTTGGCGGTGC	ChIP-qPCR	Eurofins	This study
LRP5-R	5' TGGAGGAGCGTTCGTTTAGT	ChIP-qPCR	Eurofins	This study
EGFR BRA -F	5' CTCAAGCATGTTCAGCCCAC	ChIP-qPCR	Eurofins	This study
EGFR BRA -R	5' GGCATGCATCACCATACCTG	ChIP-qPCR	Eurofins	This study
EGFR BRB -F	5' TGTTGTCAGGGATGCTCAGT	ChIP-qPCR	Eurofins	This study
EGFR BRB -R	5' AGTGGGCTGAAGACTGACTC	ChIP-qPCR	Eurofins	This study
CARM1-Exon15- deletion-F	5'CCACAACAACCTGATTCCTTT AGGGTCCTCCG	Mutagenesis	Eurofins	This study
CARM1-Exon15- deletion-R	5' CGGAGGACCCTAAAGGAATCA GGTTGTTGTGG	Mutagenesis	Eurofins	This study
ALIX-V- stopcodon-F	5' CGGAAGACAGAAAGAGATTAA CTC TTAAAGGAC	Mutagenesis	Eurofins	This study
ALIX-V- stopcodon-R	5' GTCCTTTAAGAGTTAATCTCTTT CTGT CTCCG	Mutagenesis	Eurofins	This study
Alix-PRD-EcoRI -F	5' TGCTAGGAATTCAGATGAACTC TTAAAG GACTTGCAAC	Cloning	Eurofins	This study
Alix-PRD-BamHI- R	5'CTAGCAGGATCCCTACTGCTG TGG ATAGTAAGACTGC	Cloning	Eurofins	This study
GST-BamHI-F	5' TAGTCAGGATCCATGTCCCCTA TACTAGGTTATTG	Cloning	Eurofins	This study

GST-EcoRI-R	5' TGA CTAGAATTCCGATCCACGC GG AACCAGATCCG	Cloning	Eurofins	This study
CARM1-EcoRI-F	5' TGCTAGGAATTCATGGACAAG GCA GCGGCGGCGG	Cloning	Eurofins	This study
CARM1-XbaI-R	5' CTAGCATCTAGACTAGCTCCCG TAGTG CATGG	Cloning	Eurofins	This study

**Table 7: List of siRNAs used**

<b>siRNA</b>	<b>Target Sequence</b>	<b>Company</b>	<b>Reference</b>
AllStars Negative Control siRNA	-	Qiagen	0001027281
PRMT1_7	5' CACCATCGACCTGGACTTCAA	Qiagen	SI02663493
PRMT1_8	5' CCGGCAGTACAAAGACTACAA	Qiagen	SI02663500
LRP6	5' CTGGATGGTTCTGACCGTGTA	Qiagen	SI02628353
CARM1_4	5' TGAGGTCTTGGTGAAGAGTAA	Qiagen	SI00164493
CARM1_5	5' CAGGATAGAAATCCCATTCAA	Qiagen	SI02663815
ALIX	5' AAGAGCTGTGTGTTGTTCAAT	Qiagen	SI02655345

**Table 8: List of drugs and inhibitors used**

<b>Inhibitor/Drug</b>	<b>Concentration</b> (for drug combinations)	<b>Type/Target</b>	<b>Company</b>	<b>Reference</b>
4-hydroperoxy cyclophosphamide	0-5 $\mu$ M	DNA intercalant	Santacruz	sc-206885
Camptothecine (SN38)	0-25nM	DNA intercalant	Sigma-Aldrich	C9911
Docetaxel	0-1nM	Mitotic arrest	Selleckchem	S1148
Doxorubicin	0-70nM	Anthracycline	Sigma-Aldrich	D1515
Erlotinib	0-5 $\mu$ M	EGFR	Selleckchem	S7786
EZM-2302	NA	CARM1	Probechem Biochemicalls	PC-61030
TP-064	NA	CARM1	Tocris	6008
GSK3368715	0-5 $\mu$ M	Type I PRMT	MedChemExpress, ChemScene LLC	HY-128717A, CS-0100240
LGK-974	0-10 $\mu$ M	Porcupine	Selleckchem	S7143
Methotrexate	0-100nM	Dihydrofolate reductase	Calbiochem	454126
MS023	0-5 $\mu$ M	Type I PRMT	Tocris	5562
Paclitaxel	0-1nM	Mitotic arrest	Selleckchem	S1150

**Table 9: List of synthetic peptides used (from Covalab)**

Peptide name	Sequence
ALIX (716-775)	NH <sub>2</sub> - E <sup>716</sup> PSAPSIPTPAYQSLPAGGHAPTPTPAPR <sup>745</sup> TMPPTKPQPPAR <sup>757</sup> PPPPVLPANR <sup>767</sup> APSATAPS <sup>775</sup> - COOH
ALIX – R745 control	NH <sub>2</sub> -C-H <sup>736</sup> ATPPTPAPR <sup>745</sup> TMPPT <sup>750</sup> – CONH <sub>2</sub>
ALIX- R745 - MMA	NH <sub>2</sub> -C-H <sup>736</sup> ATPPTPAP (R <sup>745</sup> -MMA) TMPPT <sup>750</sup> – CONH <sub>2</sub>
ALIX- R745 - ADMA	NH <sub>2</sub> -C-H <sup>736</sup> ATPPTPAP (R <sup>745</sup> -ADMA) TMPPT <sup>750</sup> – CONH <sub>2</sub>
ALIX-R757- control	NH <sub>2</sub> -C-P <sup>749</sup> TKPQPPAR <sup>757</sup> PPPPVL <sup>763</sup> - CONH <sub>2</sub>
ALIX-R757-MMA	NH <sub>2</sub> -C-P <sup>749</sup> TKPQPPA (R <sup>757</sup> -MMA) PPPPVL <sup>763</sup> - CONH <sub>2</sub>
ALIX-R757- ADMA	NH <sub>2</sub> -C-P <sup>749</sup> TKPQPPA (R <sup>757</sup> -ADMA) PPPPVL <sup>763</sup> - CONH <sub>2</sub>

**Table 10: 1X laemmli sample buffer composition**

<b>Component</b>	<b>Final concentration</b>
Tris pH=6.8 (Sigma Aldrich)	50mM
SDS (Sigma Aldrich)	2%
Glycerol (Sigma Aldrich)	5%
Dithiothreitol (DTT) (Sigma Aldrich)	2mM
Ethylenediaminetetraacetic acid (EDTA) (Sigma Aldrich)	2.5mM
Ethylene glycol-bis ( $\beta$ -aminoethyl ether)-N,N,N',N'-tetraacetic acid (EGTA) (Sigma Aldrich)	2.5mM
Phosphatase inhibitors (ThermoScientific)	2X
Protease inhibitors (Roche)	1 tablet (per 5ml)
Sodium Orthovanadate (Sigma Aldrich)	4mM
Sodium Fluoride (Sigma Aldrich)	20mM
Water	to complete

**Table 11: 1X immunoprecipitation lysis buffer composition**

<b>Component</b>	<b>Final concentration</b>	<b>Complete lysis buffer</b>	<b>Incomplete lysis buffer</b>
Tris A (pH 7.4) (Sigma Aldrich)	50 mM	Yes	Yes
NaCl (VWR chemicals)	100 mM	Yes	Yes
EDTA (Sigma Aldrich)	1 mM	Yes	Yes
EGTA (Sigma Aldrich)	1 mM	Yes	Yes
Nonidet P-40 (Sigma Aldrich)	0.1%	Yes	Yes
DTT (Sigma Aldrich)	1 mM	Yes	Yes
Glycerol (Sigma Aldrich)	10%	Yes	Yes
Phosphatase inhibitors (ThermoScientific)	1%	Yes	No
Protease inhibitors (Roche)	1 tablet (every 10mL)	Yes	No

**Table 12: Acquisition list from the ALIX synthetic peptides generated in the parallel reaction monitoring mode during LC-MS/MS analysis.**

<b>PTM position</b>	<b>Peptide modification</b>	<b>Mass [m/z]</b>	<b>Charge</b>	<b>Extracted fragments</b>
R745	Unmethylated	869.4056	2	y12, y9, y12++, b2, b4, y12-64, y9-64, y12-64++, b3
	Monomethylated	876.4135	2	y12, y9, y12++, b2, b4, y12-64, y9-64, y12-64++, b4
	Dimethylated	883.4213	2	y12, y9, y12++, b2, b4, y12-64, y9-64, y12-64++, b5
R757	Unmethylated	871.4742	2	b3, b4, y12, y10, y4, y15++, y13++, y12++, y10++
	Monomethylated	878.48202	2	b3, b4, y12, y10, y4, y15++, y13++, y12++, y10++
	Dimethylated	885.4898	2	b3, b4, y12, y10, y4, y15++, y13++, y12++, y10++



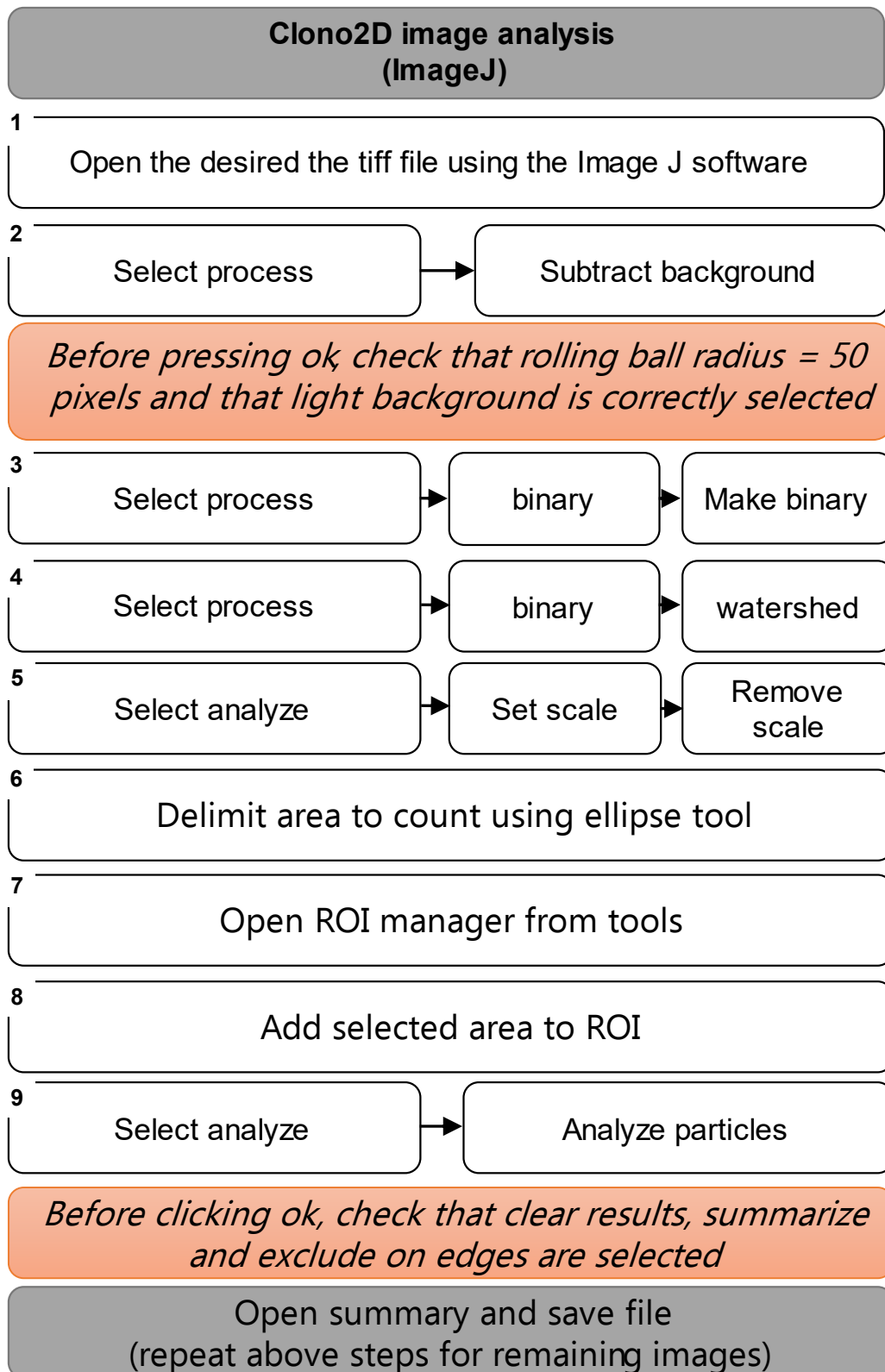


**Figure 100: Schematic process of image analysis for 2D colony formation assay using ImageJ software.**

# Supplementary materials and methods

## CARM1 isoform analysis in BC cell lines and human BC tumors

Primary unilateral invasive breast tumors excised from women managed at the Institut Curie-René Huguenin Hospital (Saint-Cloud, France) between 1978 and 2008 and analyzed. Each patient signed a written informed consent form, and this study was approved by the Institut Curie-René Huguenin Hospital Ethics Committee. Patients were followed at the Institut Curie-René Huguenin Hospital.

The cohort contained 41 BC cell lines and 514 patient samples. This was composed of 11 luminal, 4 Her2+, 17 TNBC and 7 non-cancerous cell lines subtypes and the patient samples contained 292 Luminal A, 55 Luminal B, 69 Her2+, 98 TNBC, and 16 normal breast tissues.

The expression of total CARM1 and the CARM1 isoforms – CARM1-FL and CARM1- $\Delta$ E15 – was analyzed from RNA samples by RT-qPCR using the Power SYBR Green PCR Master Mix kit (ThermoFisher Scientific) using specifically designed primers (see **Table 14**). Transcripts of the TATA box-binding protein (TBP) gene (Genbank accession NM\_003194) were used as an endogenous RNA control. The analysis was performed as previously described [711]. Briefly, each sample was normalized based on its TBP content. Results (expressed as N-fold differences in the CARM1 isoform expression relative to the TBP gene and termed  $N_{\text{CARM1 isoforms}}$ ) were determined as  $N_{\text{CARM1 isoforms}} = 2^{\Delta C_{\text{t sample}}}$ , where the  $\Delta C_{\text{t}}$  value of the sample was determined by subtracting the  $C_{\text{t}}$  value of CARM1 isoforms genes from the average  $C_{\text{t}}$  value of TBP gene. The  $N_{\text{CARM1 isoforms}}$  values were subsequently normalized to obtain a basal mRNA level (smallest amount of mRNA quantifiable,  $C_{\text{t}}=35$ ) equal to 1.

## Extracellular vesicles and exosome isolation

HEK293T cells were grown in a 150cm<sup>2</sup> cell culture flask until they reached 80% confluency. For BT-549 cells,  $4 \times 10^6$  cells were seeded in a 60mm petri dish for 48h. Four such petri-dishes were seeded for obtaining sufficient extracellular vesicles (EVs).

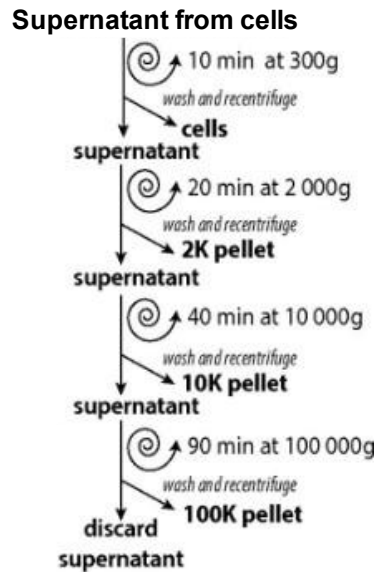


**Figure 101: Schema of extracellular vesicle isolation protocol.** The 2K pellet corresponds to EVs greater than 150nm in diameter and the 10K and 100K pellets correspond to exosomes. Modified and adapted from [703]

The EVs were isolated as previously described [703]. Briefly, the media was collected in a 50ml falcon tube. The cells were washed once with 1X PBS and collected into the same tube. The media was centrifuged at 300g for 10min at 4°C to remove the floating cells. This step was repeated two more times to completely remove all floating cells. After the last 300g centrifuge, the supernatant is transferred into a new 50ml tube and centrifuged at 2000g for 20min at 4°C. The pellet obtained after this step is referred to as the 2K pellet. The supernatant is then transferred into an ultra-centrifuge tube and centrifuged at 10,000g for 40min in an OPTIMA L-80 XP (Beckman Coulter Ultracentrifuge). The pellet obtained from this step is referred to as the 10K pellet. The remaining supernatant is transferred into a fresh ultra-centrifuge tube and centrifuged at 100,000g for 90min at 4°C in an OPTIMA L-80 XP (Beckman Coulter Ultracentrifuge). The pellet obtained from this step is referred to as the 100K pellet. The supernatant from the 100,000g centrifuge is discarded.

The 2K pellet was washed with 10ml PBS. This suspension was then completed to 50ml with PBS and centrifuged at 2000g for 20 minutes. The wash was discarded, the border of the tube dried, and the pellet was resuspended in 1X laemmli buffer (without bromophenol blue). The 10K pellet was washed in 6ml PBS and transferred into MLA-80 tubes and centrifuged at 10,000g for 20min in an OPTIMA MAX-XP using an MLA-80 rotor (Beckman Coulter Ultracentrifuge). The pellet was dried and resuspended as before. The 100K pellet was washed with 6ml PBS and centrifuged at 100,000g, 50min in an OPTIMA MAX-XP using an MLA-80 rotor (Beckman Coulter Ultracentrifuge). The pellet was dried and resuspended as before.

For the total cell lysates, after the wash using PBS, the cells were detached using TrypLE express reagent (ThermoFisher). The cell suspension was resuspended in PBS and centrifuged for 5 min at 300g. This pellet was resuspended in 1X laemmli buffer (without bromophenol blue).

All the pellets were boiled at 100°C for 10 min and bromophenol blue was added prior to loading an SDS-PAGE gel. Western blotting was performed as before.

For the siRNA treatments in BT549 cells,  $4 \times 10^6$  cells were seeded in a 60mm petri dish and five such dishes were seeded per siRNA condition. 24h after seeding, the cells were transfected with 40nM siRNA using Interferin for 48h. Downstream processing was done as before.

### **HIV viral-like particle production**

HEK293T cells (150,000 cells/well) were seeded in a 6-well (8.96cm<sup>2</sup>) cell culture plate in 2ml of media without antibiotic. 24h after seeding, cells were transfected with 2ug of total DNA (indicated plasmids were mixed in a 1:1 ratio) using Xtremegene HP DNA (Sigma-Aldrich) transfectant. 48h post-transfection, the supernatant from each condition was collected into separate 50ml falcon tubes. The cells were washed once with PBS and lysed using 1X laemmli buffer. The supernatant was filtered using a 0.22µM filter (Sartorius), transferred into ultracentrifuge tubes and centrifuged at 100,000g for 90min at 4°C in an OPTIMA MAX-XP using a MLA-80 rotor (Beckman Coulter Ultracentrifuge). The pellet (invisible) from the ultra-centrifugation was resuspended using sample loading buffer and loaded onto an SDS-PAGE gel. Western blotting was performed as described before.

HIV-gag pol, YFP-VPS4-E223Q, YFP-ALIX (176-869) which lacks a portion of the N-terminal Bro1 domain (1-176), YFP-VPS4, GFP-TSG101, YFP-Exn (murine leukemia retroviral vector), YFP-ΔVPS4, PK-GFP, PK-ΔCHMP3, and YFP-WWPI-ΔHECT plasmids were a kind gift from Dr. Greg Towers, UCL, UK.

**Table 13: Supplementary list of antibodies**

<b>Target</b>	<b>Company</b>	<b>Host species</b>	<b>Application</b>	<b>Dilution</b>	<b>Reference</b>
CA183	-	Mouse	WB	1/500	Kind gift from Dr. Greg Towers, UCL, UK
CD9	Millipore	Mouse	WB	1/1000	Kind gift from Dr. Clotilde Thery, Institut Curie
CD63	BD Biosciences	Mouse	WB	1/1000	Kind gift from Dr. Clotilde Thery, Institut Curie
Syntenin-1	Abcam	Rabbit	WB	1/1000	Kind gift from Dr. Clotilde Thery, Institut Curie

**Table 14: Supplementary list of primers**

<b>Target</b>	<b>Target Sequence/name</b>	<b>Application</b>	<b>Company</b>	<b>Reference</b>
PRMT2	-	RT-qPCR	Qiagen	QT00027314
PRMT3	-	RT-qPCR	Qiagen	QT00025123
PRMT5	-	RT-qPCR	Qiagen	QT00049938
PRMT6	-	RT-qPCR	Qiagen	QT00201411
CARM1- total - Fwd	5'CGGGCAGCACCTACAACCTCA	qPCR	Integrated DNA technologies	This study
CARM1- total - Rev	5'GGTTGTTGTGGCCACGCT	qPCR	Integrated DNA technologies	This study
CARM1- FL-Fwd	5'ACAACCTGATTCCTTTAGCCAACA	qPCR	Integrated DNA technologies	This study
CARM1- FL-Rev	5'TCGTGCTGCCACCACCACT	qPCR	Integrated DNA technologies	This study
CARM1- $\Delta$ E15-Fwd	5'GGGATGCCGACCGCCTATGA	qPCR	Integrated DNA technologies	This study
CARM1- $\Delta$ E15-Rev	5'GGCGCCGGAGGACCCTAAAG	qPCR	Integrated DNA technologies	This study

**Table 15: Supplementary list of siRNAs**

<b>siRNA</b>	<b>Target Sequence</b>	<b>Company</b>	<b>Reference</b>
PRMT2_3	5' CAGACCAGCCACGAACAATA	Qiagen	SI00441826
PRMT3_1	5' CACCGTGACCCTCACGTTGAA	Qiagen	SI03058699
PRMT3_2	5' TACCGAGATTTTCATATACCAA	Qiagen	SI03108938
PRMT5_1	5' TGCCGTGGTGACGCTAGAGAA	Qiagen	SI04216492
PRMT5_3	5' CTGGCGATGCAGCAATTCCAA	Qiagen	SI04308416
PRMT6_1	5' CCGCAGCGCTTTGCTCAGCTA	Qiagen	SI00120771
PRMT6_2	5' CACACCTTATCTAAGTCTGAA	Qiagen	SI00120778





# BIBLIOGRAPHY

## BIBLIOGRAPHY

1. Sung, H., et al., *Global Cancer Statistics 2020: GLOBOCAN Estimates of Incidence and Mortality Worldwide for 36 Cancer in 185 Countries*. CA Cancer J Clin, 2021. **71**(3): p. 209-249.
2. Society, A.C.; Available from: <https://www.cancer.org/>.
3. Institute, N.C.; Available from: <https://www.cancer.gov/>.
4. BreastCancer.org. Available from: <https://www.breastcancer.org/>.
5. Antoniou, A., et al., *Average risks of breast and ovarian cancer associated with BRCA1 or BRCA2 mutations detected in case Series unselected for family history: a combined analysis of 22 studies*. Am J Hum Genet, 2003. **72**(5): p. 1117-30.
6. Ban, K.A. and C.V. Godellas, *Epidemiology of breast cancer*. Surg Oncol Clin N Am, 2014. **23**(3): p. 409-22.
7. Kaminska, M., et al., *Breast cancer risk factors*. Prz Menopauzalny, 2015. **14**(3): p. 196-202.
8. Peart, O., *Breast intervention and breast cancer treatment options*. Radiol Technol, 2015. **86**(5): p. 535M-558M; quiz 559-62.
9. Apantaku, L.M., *Breast cancer diagnosis and screening*. Am Fam Physician, 2000. **62**(3): p. 596-602, 605-6.
10. Zoon, C.K., et al., *Current molecular diagnostics of breast cancer and the potential incorporation of microRNA*. Expert Rev Mol Diagn, 2009. **9**(5): p. 455-67.
11. Hortobagyi, G.N., S.B. Edge, and A. Giuliano, *New and Important Changes in the TNM Staging System for Breast Cancer*. Am Soc Clin Oncol Educ Book, 2018. **38**: p. 457-467.
12. Sorlie, T., et al., *Gene expression patterns of breast carcinomas distinguish tumor subclasses with clinical implications*. Proc Natl Acad Sci U S A, 2001. **98**(19): p. 10869-74.
13. Mathews, J.C., et al., *Robust and interpretable PAM50 reclassification exhibits survival advantage for myoepithelial and immune phenotypes*. NPJ Breast Cancer, 2019. **5**: p. 30.
14. Prat, A., et al., *Clinical implications of the intrinsic molecular subtypes of breast cancer*. Breast, 2015. **24 Suppl 2**: p. S26-35.
15. Cancer Genome Atlas, N., *Comprehensive molecular portraits of human breast tumours*. Nature, 2012. **490**(7418): p. 61-70.
16. Holm, K., et al., *Molecular subtypes of breast cancer are associated with characteristic DNA methylation patterns*. Breast Cancer Res, 2010. **12**(3): p. R36.
17. Eliyatkin, N., et al., *Molecular Classification of Breast Carcinoma: From Traditional, Old-Fashioned Way to A New Age, and A New Way*. J Breast Health, 2015. **11**(2): p. 59-66.

18. Perou, C.M., *Molecular stratification of triple-negative breast cancer*. *Oncologist*, 2011. **16 Suppl 1**: p. 61-70.
19. Liu, S.V., et al., *Neoadjuvant therapy for breast cancer*. *J Surg Oncol*, 2010. **101**(4): p. 283-91.
20. Early Breast Cancer Trialists' Collaborative, G., *Long-term outcomes for neoadjuvant versus adjuvant chemotherapy in early breast cancer: meta-analysis of individual patient data from ten randomised trials*. *Lancet Oncol*, 2018. **19**(1): p. 27-39.
21. Peart, O., *Mammography and Breast Imaging PREP*. Treatment options. In. 2012, New York, NY: McGrawHill. 397-436.
22. Decatris, M.P., S. Sundar, and K.J. O'Byrne, *Platinum-based chemotherapy in metastatic breast cancer: current status*. *Cancer Treat Rev*, 2004. **30**(1): p. 53-81.
23. Brana, M.F., et al., *Intercalators as anticancer drugs*. *Curr Pharm Des*, 2001. **7**(17): p. 1745-80.
24. Kaye, S.B., *New antimetabolites in cancer chemotherapy and their clinical impact*. *Br J Cancer*, 1998. **78 Suppl 3**: p. 1-7.
25. Heinemann, V., *Gemcitabine in metastatic breast cancer*. *Expert Rev Anticancer Ther*, 2005. **5**(3): p. 429-43.
26. Mitchison, T.J., *The proliferation rate paradox in antimetabolic chemotherapy*. *Mol Biol Cell*, 2012. **23**(1): p. 1-6.
27. Nabholz, J.M. and J. Gligorov, *The role of taxanes in the treatment of breast cancer*. *Expert Opin Pharmacother*, 2005. **6**(7): p. 1073-94.
28. Bonadonna, G., et al., *Combination chemotherapy as an adjuvant treatment in operable breast cancer*. *N Engl J Med*, 1976. **294**(8): p. 405-10.
29. Osborne, C.K., *Tamoxifen in the treatment of breast cancer*. *N Engl J Med*, 1998. **339**(22): p. 1609-18.
30. McKeage, K., M.P. Curran, and G.L. Plosker, *Fulvestrant: a review of its use in hormone receptor-positive metastatic breast cancer in postmenopausal women with disease progression following antiestrogen therapy*. *Drugs*, 2004. **64**(6): p. 633-48.
31. Schneider, R., et al., *Aromatase inhibitors in the treatment of breast cancer in post-menopausal female patients: an update*. *Breast Cancer (Dove Med Press)*, 2011. **3**: p. 113-25.
32. McCarthy, E.F., *The toxins of William B. Coley and the treatment of bone and soft-tissue sarcomas*. *Iowa Orthop J*, 2006. **26**: p. 154-8.
33. Behravan, J., A. Razazan, and G. Behravan, *Towards Breast Cancer Vaccines, Progress and Challenges*. *Curr Drug Discov Technol*, 2019. **16**(3): p. 251-258.
34. Fuentes-Antras, J., et al., *Adoptive Cell Therapy in Breast Cancer: A Current Perspective of Next-Generation Medicine*. *Front Oncol*, 2020. **10**: p. 605633.
35. Bu, X., Y. Yao, and X. Li, *Immune Checkpoint Blockade in Breast Cancer Therapy*. *Adv Exp Med Biol*, 2017. **1026**: p. 383-402.

36. Munagala, R., F. Aqil, and R.C. Gupta, *Promising molecular targeted therapies in breast cancer*. Indian J Pharmacol, 2011. **43**(3): p. 236-45.
37. Franklin, M.C., et al., *Insights into ErbB signaling from the structure of the ErbB2-pertuzumab complex*. Cancer Cell, 2004. **5**(4): p. 317-28.
38. Fang, L., et al., *Targeted therapy in breast cancer: what's new?* Swiss Med Wkly, 2011. **141**: p. w13231.
39. Hanahan, D. and R.A. Weinberg, *Hallmarks of cancer: the next generation*. Cell, 2011. **144**(5): p. 646-74.
40. Ju, J., A.J. Zhu, and P. Yuan, *Progress in targeted therapy for breast cancer*. Chronic Dis Transl Med, 2018. **4**(3): p. 164-175.
41. Samuels, Y. and V.E. Velculescu, *Oncogenic mutations of PIK3CA in human cancer*. Cell Cycle, 2004. **3**(10): p. 1221-4.
42. Marty, B., et al., *Frequent PTEN genomic alterations and activated phosphatidylinositol 3-kinase pathway in basal-like breast cancer cells*. Breast Cancer Res, 2008. **10**(6): p. R101.
43. Lee, J.J., K. Loh, and Y.S. Yap, *PI3K/Akt/mTOR inhibitors in breast cancer*. Cancer Biol Med, 2015. **12**(4): p. 342-54.
44. Scott, S.C., S.S. Lee, and J. Abraham, *Mechanisms of therapeutic CDK4/6 inhibition in breast cancer*. Semin Oncol, 2017. **44**(6): p. 385-394.
45. Gao, J.J., et al., *CDK4/6 inhibitor treatment for patients with hormone receptor-positive, HER2-negative, advanced or metastatic breast cancer: a US Food and Drug Administration pooled analysis*. Lancet Oncol, 2020. **21**(2): p. 250-260.
46. Spring, L.M., et al., *Cyclin-dependent kinase 4 and 6 inhibitors for hormone receptor-positive breast cancer: past, present, and future*. Lancet, 2020. **395**(10226): p. 817-827.
47. De Talhouet, S., et al., *Clinical outcome of breast cancer in carriers of BRCA1 and BRCA2 mutations according to molecular subtypes*. Sci Rep, 2020. **10**(1): p. 7073.
48. Mavaddat, N., et al., *Pathology of breast and ovarian cancer among BRCA1 and BRCA2 mutation carriers: results from the Consortium of Investigators of Modifiers of BRCA1/2 (CIMBA)*. Cancer Epidemiol Biomarkers Prev, 2012. **21**(1): p. 134-47.
49. Guha, M., *PARP inhibitors stumble in breast cancer*. Nat Biotechnol, 2011. **29**(5): p. 373-4.
50. Foulkes, W.D., I.E. Smith, and J.S. Reis-Filho, *Triple-negative breast cancer*. N Engl J Med, 2010. **363**(20): p. 1938-48.
51. Irvin, W.J., Jr. and L.A. Carey, *What is triple-negative breast cancer?* Eur J Cancer, 2008. **44**(18): p. 2799-805.
52. Herschkowitz, J.I., et al., *Identification of conserved gene expression features between murine mammary carcinoma models and human breast tumors*. Genome Biol, 2007. **8**(5): p. R76.

53. Pommier, R.M., et al., *Comprehensive characterization of claudin-low breast tumors reflects the impact of the cell-of-origin on cancer evolution*. Nat Commun, 2020. **11**(1): p. 3431.
54. Dent, R., et al., *Pattern of metastatic spread in triple-negative breast cancer*. Breast Cancer Res Treat, 2009. **115**(2): p. 423-8.
55. Foulkes, W.D., et al., *Germline BRCA1 mutations and a basal epithelial phenotype in breast cancer*. J Natl Cancer Inst, 2003. **95**(19): p. 1482-5.
56. Millikan, R.C., et al., *Epidemiology of basal-like breast cancer*. Breast Cancer Res Treat, 2008. **109**(1): p. 123-39.
57. Yang, X.R., et al., *Differences in risk factors for breast cancer molecular subtypes in a population-based study*. Cancer Epidemiol Biomarkers Prev, 2007. **16**(3): p. 439-43.
58. Trivers, K.F., et al., *The epidemiology of triple-negative breast cancer, including race*. Cancer Causes Control, 2009. **20**(7): p. 1071-82.
59. Lehmann, B.D., et al., *Identification of human triple-negative breast cancer subtypes and preclinical models for selection of targeted therapies*. J Clin Invest, 2011. **121**(7): p. 2750-67.
60. Bianchini, G., et al., *Triple-negative breast cancer: challenges and opportunities of a heterogeneous disease*. Nat Rev Clin Oncol, 2016. **13**(11): p. 674-690.
61. Burstein, M.D., et al., *Comprehensive genomic analysis identifies novel subtypes and targets of triple-negative breast cancer*. Clin Cancer Res, 2015. **21**(7): p. 1688-98.
62. Masuda, H., et al., *Differential response to neoadjuvant chemotherapy among 7 triple-negative breast cancer molecular subtypes*. Clin Cancer Res, 2013. **19**(19): p. 5533-40.
63. Bonsang-Kitzis, H., et al., *Biological network-driven gene selection identifies a stromal immune module as a key determinant of triple-negative breast carcinoma prognosis*. Oncoimmunology, 2016. **5**(1): p. e1061176.
64. Bertucci, F., et al., *Gene expression profiling shows medullary breast cancer is a subgroup of basal breast cancer*. Cancer Res, 2006. **66**(9): p. 4636-44.
65. Ridolfi, R.L., et al., *Medullary carcinoma of the breast: a clinicopathologic study with 10 year follow-up*. Cancer, 1977. **40**(4): p. 1365-85.
66. Limaïem, F. and M. Mlika, *Medullary Breast Carcinoma*, in *StatPearls*. 2021: Treasure Island (FL).
67. Lehmann, B.D., et al., *Refinement of Triple-Negative Breast Cancer Molecular Subtypes: Implications for Neoadjuvant Chemotherapy Selection*. PLoS One, 2016. **11**(6): p. e0157368.
68. Lee, J.S., S.E. Yost, and Y. Yuan, *Neoadjuvant Treatment for Triple Negative Breast Cancer: Recent Progresses and Challenges*. Cancer (Basel), 2020. **12**(6).
69. Lebert, J.M., et al., *Advances in the systemic treatment of triple-negative breast cancer*. Curr Oncol, 2018. **25**(Suppl 1): p. S142-S150.

70. Sun, L., et al., *Clinical efficacy and safety of anti-PD-1/PD-L1 inhibitors for the treatment of advanced or metastatic cancer: a systematic review and meta-analysis*. Sci Rep, 2020. **10**(1): p. 2083.
71. Sternschuss, M., et al., *Efficacy and safety of neoadjuvant immune checkpoint inhibitors in early-stage triple-negative breast cancer: a systematic review and meta-analysis*. J Cancer Res Clin Oncol, 2021.
72. Administration, U.S.F.a.D.
73. Sharom, F.J., *ABC multidrug transporters: structure, function and role in chemoresistance*. Pharmacogenomics, 2008. **9**(1): p. 105-27.
74. Nedeljkovic, M. and A. Damjanovic, *Mechanisms of Chemotherapy Resistance in Triple-Negative Breast Cancer-How We Can Rise to the Challenge*. Cells, 2019. **8**(9).
75. Raman, D., et al., *Editorial: The Role of Breast Cancer Stem Cells in Clinical Outcomes*. Front Oncol, 2020. **10**: p. 299.
76. Zhou, J., et al., *Stem Cells and Cellular Origins of Breast Cancer: Updates in the Rationale, Controversies, and Therapeutic Implications*. Front Oncol, 2019. **9**: p. 820.
77. Creighton, C.J., et al., *Residual breast cancer after conventional therapy display mesenchymal as well as tumor-initiating features*. Proc Natl Acad Sci U S A, 2009. **106**(33): p. 13820-5.
78. Shipitsin, M., et al., *Molecular definition of breast tumor heterogeneity*. Cancer Cell, 2007. **11**(3): p. 259-73.
79. Al-Hajj, M., et al., *Prospective identification of tumorigenic breast cancer cells*. Proc Natl Acad Sci U S A, 2003. **100**(7): p. 3983-8.
80. Ginestier, C., et al., *ALDH1 is a marker of normal and malignant human mammary stem cells and a predictor of poor clinical outcome*. Cell Stem Cell, 2007. **1**(5): p. 555-67.
81. Liu, S., et al., *Breast cancer stem cells transition between epithelial and mesenchymal states reflective of their normal counterparts*. Stem Cell Reports, 2014. **2**(1): p. 78-91.
82. Mani, S.A., et al., *The epithelial-mesenchymal transition generates cells with properties of stem cells*. Cell, 2008. **133**(4): p. 704-15.
83. Fabregat, I. and D. Caballero-Diaz, *Transforming Growth Factor-beta-Induced Cell Plasticity in Liver Fibrosis and Hepatocarcinogenesis*. Front Oncol, 2018. **8**: p. 357.
84. Massague, J., *TGFbeta signalling in context*. Nat Rev Mol Cell Biol, 2012. **13**(10): p. 616-30.
85. Neuzillet, C., et al., *Targeting the TGFbeta pathway for cancer therapy*. Pharmacol Ther, 2015. **147**: p. 22-31.
86. Asiedu, M.K., et al., *TGFbeta/TNF(alpha)-mediated epithelial-mesenchymal transition generates breast cancer stem cells with a claudin-low phenotype*. Cancer Res, 2011. **71**(13): p. 4707-19.

87. Bhola, N.E., et al., *TGF-beta inhibition enhances chemotherapy action against triple-negative breast cancer*. J Clin Invest, 2013. **123**(3): p. 1348-58.
88. Suresh, S. and A.E. Irvine, *The NOTCH signaling pathway in normal and malignant blood cell production*. J Cell Commun Signal, 2015. **9**(1): p. 5-13.
89. Bray, S.J., *Notch signalling: a simple pathway becomes complex*. Nat Rev Mol Cell Biol, 2006. **7**(9): p. 678-89.
90. Aster, J.C., W.S. Pear, and S.C. Blacklow, *The Varied Roles of Notch in Cancer*. Annu Rev Pathol, 2017. **12**: p. 245-275.
91. Locatelli, M.A., et al., *Phase I study of the gamma secretase inhibitor PF-03084014 in combination with docetaxel in patients with advanced triple-negative breast cancer*. Oncotarget, 2017. **8**(2): p. 2320-2328.
92. Schott, A.F., et al., *Preclinical and clinical studies of gamma secretase inhibitors with docetaxel on human breast tumors*. Clin Cancer Res, 2013. **19**(6): p. 1512-24.
93. Abe, Y. and N. Tanaka, *Roles of the Hedgehog Signaling Pathway in Epidermal and Hair Follicle Development, Homeostasis, and Cancer*. J Dev Biol, 2017. **5**(4).
94. Xu, X., et al., *Wnt signaling in breast cancer: biological mechanisms, challenges and opportunities*. Mol Cancer, 2020. **19**(1): p. 165.
95. Pohl, S.G., et al., *Wnt signaling in triple-negative breast cancer*. Oncogenesis, 2017. **6**(4): p. e310.
96. de Sousa, E.M.F. and L. Vermeulen, *Wnt Signaling in Cancer Stem Cell Biology*. Cancer (Basel), 2016. **8**(7).
97. Kahn, M., *Wnt Signaling in Stem Cells and Cancer Stem Cells: A Tale of Two Coactivators*. Prog Mol Biol Transl Sci, 2018. **153**: p. 209-244.
98. Clevers, H., *Wnt/beta-catenin signaling in development and disease*. Cell, 2006. **127**(3): p. 469-80.
99. Geyer, F.C., et al., *beta-Catenin pathway activation in breast cancer is associated with triple-negative phenotype but not with CTNNB1 mutation*. Mod Pathol, 2011. **24**(2): p. 209-31.
100. Corda, G., et al., *Functional and prognostic significance of the genomic amplification of frizzled 6 (FZD6) in breast cancer*. J Pathol, 2017. **241**(3): p. 350-361.
101. Yang, L., et al., *FZD7 has a critical role in cell proliferation in triple negative breast cancer*. Oncogene, 2011. **30**(43): p. 4437-46.
102. Yin, S., et al., *Tumor-initiating cells and FZD8 play a major role in drug resistance in triple-negative breast cancer*. Mol Cancer Ther, 2013. **12**(4): p. 491-8.
103. Liu, C.C., et al., *LRP6 overexpression defines a class of breast cancer subtype and is a target for therapy*. Proc Natl Acad Sci U S A, 2010. **107**(11): p. 5136-41.
104. Wang, H., et al., *SOX9 regulates low density lipoprotein receptor-related protein 6 (LRP6) and T-cell factor 4 (TCF4) expression and Wnt/beta-catenin activation in breast cancer*. J Biol Chem, 2013. **288**(9): p. 6478-87.

105. Lindvall, C., et al., *The Wnt co-receptor Lrp6 is required for normal mouse mammary gland development*. PLoS One, 2009. **4**(6): p. e5813.
106. Maubant, S., et al., *LRP5 regulates the expression of STK40, a new potential target in triple-negative breast cancer*. Oncotarget, 2018. **9**(32): p. 22586-22604.
107. Zhang, J., et al., *LRP8 mediates Wnt/beta-catenin signaling and controls osteoblast differentiation*. J Bone Miner Res, 2012. **27**(10): p. 2065-74.
108. Maire, V., et al., *LRP8 is overexpressed in estrogen-negative breast cancer and a potential target for these tumors*. Cancer medicine, 2019. **8**(1): p. 325-336.
109. Lee, A. and M.B.A. Djamgoz, *Triple negative breast cancer: Emerging therapeutic modalities and novel combination therapies*. Cancer Treat Rev, 2018. **62**: p. 110-122.
110. Shi, Y., et al., *Therapeutic landscape in mutational triple negative breast cancer*. Mol Cancer, 2018. **17**(1): p. 99.
111. Dickler, M.N., et al., *Efficacy and safety of erlotinib in patients with locally advanced or metastatic breast cancer*. Breast Cancer Res Treat, 2009. **115**(1): p. 115-21.
112. Ambler, R.P. and M.W. Rees, *Epsilon-N-Methyl-lysine in bacterial flagellar protein*. Nature, 1959. **184**: p. 56-7.
113. Paik, W.K. and S. Kim, *Protein methylase I. Purification and properties of the enzyme*. J Biol Chem, 1968. **243**(9): p. 2108-14.
114. Larsen, S.C., et al., *Proteome-wide analysis of arginine monomethylation reveals widespread occurrence in human cells*. Sci Signal, 2016. **9**(443): p. rs9.
115. Gary, J.D. and S. Clarke, *RNA and protein interactions modulated by protein arginine methylation*. Prog Nucleic Acid Res Mol Biol, 1998. **61**: p. 65-131.
116. Bedford, M.T. and S.G. Clarke, *Protein arginine methylation in mammals: who, what, and why*. Mol Cell, 2009. **33**(1): p. 1-13.
117. Wu, Q., et al., *Protein arginine methylation: from enigmatic functions to therapeutic targeting*. Nat Rev Drug Discov, 2021.
118. Morales, Y., et al., *Biochemistry and regulation of the protein arginine methyltransferases (PRMTs)*. Arch Biochem Biophys, 2016. **590**: p. 138-152.
119. Zhang, X., L. Zhou, and X. Cheng, *Crystal structure of the conserved core of protein arginine methyltransferase PRMT3*. EMBO J, 2000. **19**(14): p. 3509-19.
120. Antonysamy, S., et al., *Crystal structure of the human PRMT5:MEP50 complex*. Proc Natl Acad Sci U S A, 2012. **109**(44): p. 17960-5.
121. Toma-Fukai, S., et al., *Novel helical assembly in arginine methyltransferase 8*. J Mol Biol, 2016. **428**(6): p. 1197-1208.
122. Tewary, S.K., Y.G. Zheng, and M.C. Ho, *Protein arginine methyltransferases: insights into the enzyme structure and mechanism at the atomic level*. Cell Mol Life Sci, 2019. **76**(15): p. 2917-2932.
123. Troffer-Charlier, N., et al., *Functional insights from structures of coactivator-associated arginine methyltransferase 1 domains*. EMBO J, 2007. **26**(20): p. 4391-401.



124. Cura, V., et al., *Structural studies of protein arginine methyltransferase 2 reveal its interactions with potential substrates and inhibitors*. FEBS J, 2017. **284**(1): p. 77-96.
125. Zhang, X. and X. Cheng, *Structure of the predominant protein arginine methyltransferase PRMT1 and analysis of its binding to substrate peptides*. Structure, 2003. **11**(5): p. 509-20.
126. Cura, V., et al., *Structural insight into arginine methylation by the mouse protein arginine methyltransferase 7: a zinc finger freezes the mimic of the dimeric state into a single active site*. Acta Crystallogr D Biol Crystallogr, 2014. **70**(Pt 9): p. 2401-12.
127. Lee, W.C., et al., *Protein Arginine Methyltransferase 8: Tetrameric Structure and Protein Substrate Specificity*. Biochemistry, 2015. **54**(51): p. 7514-23.
128. Herrmann, F., et al., *Human protein arginine methyltransferases in vivo--distinct properties of eight canonical members of the PRMT family*. J Cell Sci, 2009. **122**(Pt 5): p. 667-77.
129. Tang, J., et al., *PRMT3, a type I protein arginine N-methyltransferase that differs from PRMT1 in its oligomerization, subcellular localization, substrate specificity, and regulation*. J Biol Chem, 1998. **273**(27): p. 16935-45.
130. Hadjikyriacou, A., et al., *Unique Features of Human Protein Arginine Methyltransferase 9 (PRMT9) and Its Substrate RNA Splicing Factor SF3B2*. J Biol Chem, 2015. **290**(27): p. 16723-43.
131. Frankel, A., et al., *The novel human protein arginine N-methyltransferase PRMT6 is a nuclear enzyme displaying unique substrate specificity*. J Biol Chem, 2002. **277**(5): p. 3537-43.
132. Lee, J., et al., *PRMT8, a new membrane-bound tissue-specific member of the protein arginine methyltransferase family*. J Biol Chem, 2005. **280**(38): p. 32890-6.
133. Goulet, I., et al., *Alternative splicing yields protein arginine methyltransferase 1 isoforms with distinct activity, substrate specificity, and subcellular localization*. J Biol Chem, 2007. **282**(45): p. 33009-21.
134. Ohkura, N., et al., *Coactivator-associated arginine methyltransferase 1, CARM1, affects pre-mRNA splicing in an isoform-specific manner*. J Biol Chem, 2005. **280**(32): p. 28927-35.
135. Gros, L., et al., *Characterization of prmt7alpha and beta isozymes from Chinese hamster cells sensitive and resistant to topoisomerase II inhibitors*. Biochim Biophys Acta, 2006. **1760**(11): p. 1646-56.
136. Pawlak, M.R., et al., *Arginine N-methyltransferase 1 is required for early postimplantation mouse development, but cells deficient in the enzyme are viable*. Mol Cell Biol, 2000. **20**(13): p. 4859-69.
137. Tee, W.W., et al., *Prmt5 is essential for early mouse development and acts in the cytoplasm to maintain ES cell pluripotency*. Genes Dev, 2010. **24**(24): p. 2772-7.

138. Yoshimoto, T., et al., *The arginine methyltransferase PRMT2 binds RB and regulates E2F function*. Exp Cell Res, 2006. **312**(11): p. 2040-53.
139. Swiercz, R., et al., *Ribosomal protein rpS2 is hypomethylated in PRMT3-deficient mice*. J Biol Chem, 2007. **282**(23): p. 16917-23.
140. Neault, M., et al., *Ablation of PRMT6 reveals a role as a negative transcriptional regulator of the p53 tumor suppressor*. Nucleic Acids Res, 2012. **40**(19): p. 9513-21.
141. Yadav, N., et al., *Specific protein methylation defects and gene expression perturbations in coactivator-associated arginine methyltransferase 1-deficient mice*. Proc Natl Acad Sci U S A, 2003. **100**(11): p. 6464-8.
142. Najbauer, J., et al., *Peptides with sequences similar to glycine, arginine-rich motifs in proteins interacting with RNA are efficiently recognized by methyltransferase(s) modifying arginine in numerous proteins*. J Biol Chem, 1993. **268**(14): p. 10501-9.
143. Thandapani, P., et al., *Defining the RGG/RG motif*. Mol Cell, 2013. **50**(5): p. 613-23.
144. Feng, Y., et al., *Mammalian protein arginine methyltransferase 7 (PRMT7) specifically targets RXR sites in lysine- and arginine-rich regions*. J Biol Chem, 2013. **288**(52): p. 37010-25.
145. Cheng, D., et al., *The arginine methyltransferase CARM1 regulates the coupling of transcription and mRNA processing*. Mol Cell, 2007. **25**(1): p. 71-83.
146. Shishkova, E., et al., *Global mapping of CARM1 substrates defines enzyme specificity and substrate recognition*. Nat Commun, 2017. **8**: p. 15571.
147. Peng, B.L., et al., *A hypermethylation strategy utilized by enhancer-bound CARM1 to promote estrogen receptor alpha-dependent transcriptional activation and breast carcinogenesis*. Theranostics, 2020. **10**(8): p. 3451-3473.
148. Li, W.J., et al., *Profiling PRMT methylome reveals roles of hnRNPA1 arginine methylation in RNA splicing and cell growth*. Nat Commun, 2021. **12**(1): p. 1946.
149. Gayatri, S., et al., *Using oriented peptide array libraries to evaluate methylarginine-specific antibodies and arginine methyltransferase substrate motifs*. Sci Rep, 2016. **6**: p. 28718.
150. Yang, Y., et al., *PRMT9 is a type II methyltransferase that methylates the splicing factor SAP145*. Nat Commun, 2015. **6**: p. 6428.
151. Fulcher, A.J., et al., *The protein arginine methyltransferase PRMT6 inhibits HIV-1 Tat nucleolar retention*. Biochim Biophys Acta, 2016. **1863**(2): p. 254-62.
152. Dhar, S., et al., *Loss of the major Type I arginine methyltransferase PRMT1 causes substrate scavenging by other PRMTs*. Sci Rep, 2013. **3**: p. 1311.
153. Wei, H.-H., et al., *A systematic survey of PRMT interactomes reveals the key roles of arginine methylation in the global control of RNA splicing and translation*. Science Bulletin, 2021.

154. Nie, M., et al., *CARM1-mediated methylation of protein arginine methyltransferase 5 represses human gamma-globin gene expression in erythroleukemia cells*. J Biol Chem, 2018. **293**(45): p. 17454-17463.
155. Pak, M.L., et al., *A protein arginine N-methyltransferase 1 (PRMT1) and 2 heteromeric interaction increases PRMT1 enzymatic activity*. Biochemistry, 2011. **50**(38): p. 8226-40.
156. Strahl, B.D., et al., *Methylation of histone H4 at arginine 3 occurs in vivo and is mediated by the nuclear receptor coactivator PRMT1*. Curr Biol, 2001. **11**(12): p. 996-1000.
157. Wang, H., et al., *Methylation of histone H4 at arginine 3 facilitating transcriptional activation by nuclear hormone receptor*. Science, 2001. **293**(5531): p. 853-7.
158. Zhao, Q., et al., *PRMT5-mediated methylation of histone H4R3 recruits DNMT3A, coupling histone and DNA methylation in gene silencing*. Nat Struct Mol Biol, 2009. **16**(3): p. 304-311.
159. Schurter, B.T., et al., *Methylation of histone H3 by coactivator-associated arginine methyltransferase 1*. Biochemistry, 2001. **40**(19): p. 5747-56.
160. Pal, S., et al., *Human SWI/SNF-associated PRMT5 methylates histone H3 arginine 8 and negatively regulates expression of ST7 and NM23 tumor suppressor genes*. Mol Cell Biol, 2004. **24**(21): p. 9630-45.
161. Blanc, R.S. and S. Richard, *Arginine Methylation: The Coming of Age*. Mol Cell, 2017. **65**(1): p. 8-24.
162. Jarrold, J. and C.C. Davies, *PRMTs and Arginine Methylation: Cancer's Best-Kept Secret?* Trends Mol Med, 2019. **25**(11): p. 993-1009.
163. Guccione, E. and S. Richard, *The regulation, functions and clinical relevance of arginine methylation*. Nature Reviews Molecular Cell Biology, 2019. **20**(10): p. 642-657.
164. Yang, Y. and M.T. Bedford, *Protein arginine methyltransferases and cancer*. Nat Rev Cancer, 2013. **13**(1): p. 37-50.
165. Raposo, A.E. and S.C. Piller, *Protein arginine methylation: an emerging regulator of the cell cycle*. Cell Div, 2018. **13**: p. 3.
166. Meister, G. and U. Fischer, *Assisted RNP assembly: SMN and PRMT5 complexes cooperate in the formation of spliceosomal UsnRNPs*. EMBO J, 2002. **21**(21): p. 5853-63.
167. Meister, G., et al., *Methylation of Sm proteins by a complex containing PRMT5 and the putative U snRNP assembly factor pICln*. Curr Biol, 2001. **11**(24): p. 1990-4.
168. Zhang, L., et al., *Cross-talk between PRMT1-mediated methylation and ubiquitylation on RBM15 controls RNA splicing*. Elife, 2015. **4**.
169. Boisvert, F.M., et al., *The GAR motif of 53BP1 is arginine methylated by PRMT1 and is necessary for 53BP1 DNA binding activity*. Cell Cycle, 2005. **4**(12): p. 1834-41.

170. Boisvert, F.M., et al., *Methylation of MRE11 regulates its nuclear compartmentalization*. Cell Cycle, 2005. **4**(7): p. 981-9.
171. Boisvert, F.M., et al., *Arginine methylation of MRE11 by PRMT1 is required for DNA damage checkpoint control*. Genes Dev, 2005. **19**(6): p. 671-6.
172. Hamard, P.J., et al., *PRMT5 Regulates DNA Repair by Controlling the Alternative Splicing of Histone-Modifying Enzymes*. Cell Rep, 2018. **24**(10): p. 2643-2657.
173. Clarke, T.L., et al., *PRMT5-Dependent Methylation of the TIP60 Coactivator RUVBL1 Is a Key Regulator of Homologous Recombination*. Mol Cell, 2017. **65**(5): p. 900-916 e7.
174. Tan, D.Q., et al., *PRMT5 Modulates Splicing for Genome Integrity and Preserves Proteostasis of Hematopoietic Stem Cells*. Cell Rep, 2019. **26**(9): p. 2316-2328 e6.
175. El-Andaloussi, N., et al., *Arginine methylation regulates DNA polymerase beta*. Mol Cell, 2006. **22**(1): p. 51-62.
176. Dolezal, E., et al., *The BTG2-PRMT1 module limits pre-B cell expansion by regulating the CDK4-Cyclin-D3 complex*. Nat Immunol, 2017. **18**(8): p. 911-920.
177. Yang, H., et al., *PRMT5 competitively binds to CDK4 to promote G1-S transition upon glucose induction in hepatocellular carcinoma*. Oncotarget, 2016. **7**(44): p. 72131-72147.
178. Lu, Y., et al., *The interplay between p16 serine phosphorylation and arginine methylation determines its function in modulating cellular apoptosis and senescence*. Sci Rep, 2017. **7**: p. 41390.
179. Kumar, B., et al., *Nuclear PRMT5, cyclin D1 and IL-6 are associated with poor outcome in oropharyngeal squamous cell carcinoma patients and is inversely associated with p16-status*. Oncotarget, 2017. **8**(9): p. 14847-14859.
180. Wang, X., et al., *Suppression of PRMT6-mediated arginine methylation of p16 protein potentiates its ability to arrest A549 cell proliferation*. Int J Biochem Cell Biol, 2012. **44**(12): p. 2333-41.
181. Oh, T.G., et al., *PRMT2 and RORgamma expression are associated with breast cancer survival outcomes*. Mol Endocrinol, 2014. **28**(7): p. 1166-85.
182. Kim, K.Y., et al., *PRMT4-mediated arginine methylation negatively regulates retinoblastoma tumor suppressor protein and promotes E2F-1 dissociation*. Mol Cell Biol, 2015. **35**(1): p. 238-48.
183. Nakakido, M., et al., *PRMT6 increases cytoplasmic localization of p21CDKN1A in cancer cells through arginine methylation and makes more resistant to cytotoxic agents*. Oncotarget, 2015. **6**(31): p. 30957-67.
184. Zhang, Y., et al., *The impact of R213 mutation on p53-mediated p21 activity*. Biochimie, 2014. **99**: p. 215-8.
185. Kleinschmidt, M.A., et al., *Cell cycle regulation by the PRMT6 arginine methyltransferase through repression of cyclin-dependent kinase inhibitors*. PLoS One, 2012. **7**(8): p. e41446.

186. Jansson, M., et al., *Arginine methylation regulates the p53 response*. Nat Cell Biol, 2008. **10**(12): p. 1431-9.
187. Wei, H., et al., *PRMT5 dimethylates R30 of the p65 subunit to activate NF-kappaB*. Proc Natl Acad Sci U S A, 2013. **110**(33): p. 13516-21.
188. Covic, M., et al., *Arginine methyltransferase CARM1 is a promoter-specific regulator of NF-kappaB-dependent gene expression*. EMBO J, 2005. **24**(1): p. 85-96.
189. Hassa, P.O., et al., *Protein arginine methyltransferase 1 coactivates NF-kappaB-dependent gene expression synergistically with CARM1 and PARP1*. J Mol Biol, 2008. **377**(3): p. 668-78.
190. Gou, Y., et al., *Protein Arginine Methyltransferase PRMT1 Is Essential for Palatogenesis*. J Dent Res, 2018. **97**(13): p. 1510-1518.
191. Li, Q., et al., *Histone arginine methylation by Prmt5 is required for lung branching morphogenesis through repression of BMP signaling*. J Cell Sci, 2018. **131**(14).
192. Tamiya, H., et al., *SHARPIN-mediated regulation of protein arginine methyltransferase 5 controls melanoma growth*. J Clin Invest, 2018. **128**(1): p. 517-530.
193. Tabata, T., et al., *Ski co-repressor complexes maintain the basal repressed state of the TGF-beta target gene, SMAD7, via HDAC3 and PRMT5*. Genes Cells, 2009. **14**(1): p. 17-28.
194. Liao, H.W., et al., *PRMT1-mediated methylation of the EGF receptor regulates signaling and cetuximab response*. J Clin Invest, 2015. **125**(12): p. 4529-43.
195. Hsu, J.M., et al., *Crosstalk between Arg 1175 methylation and Tyr 1173 phosphorylation negatively modulates EGFR-mediated ERK activation*. Nat Cell Biol, 2011. **13**(2): p. 174-81.
196. Takai, H., et al., *5-Hydroxymethylcytosine plays a critical role in glioblastomagenesis by recruiting the CHTOP-methylosome complex*. Cell Rep, 2014. **9**(1): p. 48-60.
197. Calabretta, S., et al., *Loss of PRMT5 Promotes PDGFRalpha Degradation during Oligodendrocyte Differentiation and Myelination*. Dev Cell, 2018. **46**(4): p. 426-440 e5.
198. Blythe, S.A., et al., *beta-Catenin primes organizer gene expression by recruiting a histone H3 arginine 8 methyltransferase, Prmt2*. Dev Cell, 2010. **19**(2): p. 220-31.
199. Su, X., et al., *Molecular basis underlying histone H3 lysine-arginine methylation pattern readout by Spin/Ssty repeats of Spindlin1*. Genes Dev, 2014. **28**(6): p. 622-36.
200. Yang, C.K., et al., *Differential use of functional domains by coiled-coil coactivator in its synergistic coactivator function with beta-catenin or GRIP1*. J Biol Chem, 2006. **281**(6): p. 3389-97.

201. Ou, C.Y., et al., *A coactivator role of CARM1 in the dysregulation of beta-catenin activity in colorectal cancer cell growth and gene expression*. Mol Cancer Res, 2011. **9**(5): p. 660-70.
202. Lee, E., et al., *Inhibition of androgen receptor and beta-catenin activity in prostate cancer*. Proc Natl Acad Sci U S A, 2013. **110**(39): p. 15710-5.
203. Kleszcz, R., et al., *Inhibition of CBP/beta-catenin and porcupine attenuates Wnt signaling and induces apoptosis in head and neck carcinoma cells*. Cell Oncol (Dordr), 2019. **42**(4): p. 505-520.
204. Jin, Y., et al., *Targeting methyltransferase PRMT5 eliminates leukemia stem cells in chronic myelogenous leukemia*. J Clin Invest, 2016. **126**(10): p. 3961-3980.
205. Chung, J., et al., *Protein arginine methyltransferase 5 (PRMT5) promotes survival of lymphoma cells via activation of WNT/beta-catenin and AKT/GSK3beta proliferative signaling*. J Biol Chem, 2019. **294**(19): p. 7692-7710.
206. Zhu, K., et al., *Metadherin-PRMT5 complex enhances the metastasis of hepatocellular carcinoma through the WNT-beta-catenin signaling pathway*. Carcinogenesis, 2020. **41**(2): p. 130-138.
207. Wang, N., et al., *PRMT5/Wnt4 axis promotes lymph-node metastasis and proliferation of laryngeal carcinoma*. Cell Death Dis, 2020. **11**(10): p. 864.
208. Shailesh, H., K.S. Siveen, and S. Sif, *Protein arginine methyltransferase 5 (PRMT5) activates WNT/beta-catenin signalling in breast cancer cells via epigenetic silencing of DKK1 and DKK3*. J Cell Mol Med, 2021. **25**(3): p. 1583-1600.
209. Paul, C., C. Sardet, and E. Fabbri, *The Wnt-target gene Dlk-1 is regulated by the Prmt5-associated factor Copr5 during adipogenic conversion*. Biol Open, 2015. **4**(3): p. 312-6.
210. Stuhlinger, M.C., et al., *Homocysteine impairs the nitric oxide synthase pathway: role of asymmetric dimethylarginine*. Circulation, 2001. **104**(21): p. 2569-75.
211. Loscalzo, J. and G. Welch, *Nitric oxide and its role in the cardiovascular system*. Prog Cardiovasc Dis, 1995. **38**(2): p. 87-104.
212. Couto, E.S.A., et al., *Protein Arginine Methyltransferases in Cardiovascular and Neuronal Function*. Mol Neurobiol, 2020. **57**(3): p. 1716-1732.
213. Pyun, J.H., et al., *Cardiac specific PRMT1 ablation causes heart failure through CaMKII dysregulation*. Nat Commun, 2018. **9**(1): p. 5107.
214. Wang, Y., et al., *PRMT4 overexpression aggravates cardiac remodeling following myocardial infarction by promoting cardiomyocyte apoptosis*. Biochem Biophys Res Commun, 2019. **520**(3): p. 645-650.
215. Beltran-Alvarez, P., et al., *Protein arginine methyl transferases-3 and -5 increase cell surface expression of cardiac sodium channel*. FEBS Lett, 2013. **587**(19): p. 3159-65.
216. Chen, X., et al., *Expression of nitric oxide related enzymes in coronary heart disease*. Basic Res Cardiol, 2006. **101**(4): p. 346-53.

217. Kwak, Y.T., et al., *Methylation of SPT5 regulates its interaction with RNA polymerase II and transcriptional elongation properties*. Mol Cell, 2003. **11**(4): p. 1055-66.
218. Jeong, S.J., et al., *Coactivator-associated arginine methyltransferase 1 enhances transcriptional activity of the human T-cell lymphotropic virus type 1 long terminal repeat through direct interaction with Tax*. J Virol, 2006. **80**(20): p. 10036-44.
219. Zhang, Z., et al., *Crosstalk between histone modifications indicates that inhibition of arginine methyltransferase CARM1 activity reverses HIV latency*. Nucleic Acids Res, 2017. **45**(16): p. 9348-9360.
220. Murakami, H., et al., *Protein Arginine N-methyltransferases 5 and 7 Promote HIV-1 Production*. Viruses, 2020. **12**(3).
221. Boulanger, M.C., et al., *Methylation of Tat by PRMT6 regulates human immunodeficiency virus type 1 gene expression*. J Virol, 2005. **79**(1): p. 124-31.
222. Sivakumaran, H., et al., *Overexpression of PRMT6 does not suppress HIV-1 Tat transactivation in cells naturally lacking PRMT6*. Virol J, 2013. **10**: p. 207.
223. Singhroy, D.N., et al., *Automethylation of protein arginine methyltransferase 6 (PRMT6) regulates its stability and its anti-HIV-1 activity*. Retrovirology, 2013. **10**: p. 73.
224. Invernizzi, C.F., et al., *PRMT6 diminishes HIV-1 Rev binding to and export of viral RNA*. Retrovirology, 2006. **3**: p. 93.
225. Willemsen, N.M., et al., *Protein methylation is required to maintain optimal HIV-1 infectivity*. Retrovirology, 2006. **3**: p. 92.
226. Xie, B., et al., *Arginine methylation of the human immunodeficiency virus type 1 Tat protein by PRMT6 negatively affects Tat Interactions with both cyclin T1 and the Tat transactivation region*. J Virol, 2007. **81**(8): p. 4226-34.
227. Invernizzi, C.F., et al., *Arginine methylation of the HIV-1 nucleocapsid protein results in its diminished function*. AIDS, 2007. **21**(7): p. 795-805.
228. Liu, C.D., et al., *Modulation of Epstein-Barr virus nuclear antigen 2-dependent transcription by protein arginine methyltransferase 5*. Biochem Biophys Res Commun, 2013. **430**(3): p. 1097-102.
229. Gross, H., et al., *Asymmetric Arginine dimethylation of Epstein-Barr virus nuclear antigen 2 promotes DNA targeting*. Virology, 2010. **397**(2): p. 299-310.
230. Shire, K., et al., *Regulation of the EBNA1 Epstein-Barr virus protein by serine phosphorylation and arginine methylation*. J Virol, 2006. **80**(11): p. 5261-72.
231. Barth, S., et al., *Epstein-Barr virus nuclear antigen 2 binds via its methylated arginine-glycine repeat to the survival motor neuron protein*. J Virol, 2003. **77**(8): p. 5008-13.
232. Leonard, S., et al., *Arginine Methyltransferases Are Regulated by Epstein-Barr Virus in B Cells and Are Differentially Expressed in Hodgkin's Lymphoma*. Pathogens, 2012. **1**(1): p. 52-64.

233. Hsu, C.H., et al., *The HPV E6 oncoprotein targets histone methyltransferases for modulating specific gene transcription*. *Oncogene*, 2012. **31**(18): p. 2335-49.
234. Melar-New, M. and L.A. Laimins, *Human papillomaviruses modulate expression of microRNA 203 upon epithelial differentiation to control levels of p63 proteins*. *J Virol*, 2010. **84**(10): p. 5212-21.
235. Souki, S.K., P.D. Gershon, and R.M. Sandri-Goldin, *Arginine methylation of the ICP27 RGG box regulates ICP27 export and is required for efficient herpes simplex virus 1 replication*. *J Virol*, 2009. **83**(11): p. 5309-20.
236. Friedrich, S., et al., *Arginine methylation enhances the RNA chaperone activity of the West Nile virus host factor AUF1 p45*. *RNA*, 2016. **22**(10): p. 1574-91.
237. Cai, T., et al., *Arginine Methylation of SARS-Cov-2 Nucleocapsid Protein Regulates RNA Binding, its Ability to Suppress Stress Granule Formation and Viral Replication*. *J Biol Chem*, 2021: p. 100821.
238. Tradewell, M.L., et al., *Arginine methylation by PRMT1 regulates nuclear-cytoplasmic localization and toxicity of FUS/TLS harbouring ALS-linked mutations*. *Hum Mol Genet*, 2012. **21**(1): p. 136-49.
239. Nolan, M., K. Talbot, and O. Ansorge, *Pathogenesis of FUS-associated ALS and FTD: insights from rodent models*. *Acta Neuropathol Commun*, 2016. **4**(1): p. 99.
240. Scaramuzzino, C., et al., *Protein arginine methyltransferase 1 and 8 interact with FUS to modify its sub-cellular distribution and toxicity in vitro and in vivo*. *PLoS One*, 2013. **8**(4): p. e61576.
241. Jun, M.H., et al., *Sequestration of PRMT1 and Nd1-L mRNA into ALS-linked FUS mutant R521C-positive aggregates contributes to neurite degeneration upon oxidative stress*. *Sci Rep*, 2017. **7**: p. 40474.
242. Suarez-Calvet, M., et al., *Monomethylated and unmethylated FUS exhibit increased binding to Transportin and distinguish FTLD-FUS from ALS-FUS*. *Acta Neuropathol*, 2016. **131**(4): p. 587-604.
243. Yang, Q., B. Jiao, and L. Shen, *The Development of C9orf72-Related Amyotrophic Lateral Sclerosis and Frontotemporal Dementia Disorders*. *Front Genet*, 2020. **11**: p. 562758.
244. Liu, Y. and J. Wang, *C9orf72-dependent lysosomal functions regulate epigenetic control of autophagy and lipid metabolism*. *Autophagy*, 2019. **15**(5): p. 913-914.
245. Suganuma, T., et al., *MPTAC Determines APP Fragmentation via Sensing Sulfur Amino Acid Catabolism*. *Cell Rep*, 2018. **24**(6): p. 1585-1596.
246. Quan, X., et al., *The protein arginine methyltransferase PRMT5 regulates Abeta-induced toxicity in human cells and Caenorhabditis elegans models of Alzheimer's disease*. *J Neurochem*, 2015. **134**(5): p. 969-77.
247. Ratovitski, T., et al., *PRMT5-mediated symmetric arginine dimethylation is attenuated by mutant huntingtin and is impaired in Huntington's disease (HD)*. *Cell Cycle*, 2015. **14**(11): p. 1716-29.
248. Migazzi, A., et al., *Huntingtin-mediated axonal transport requires arginine methylation by PRMT6*. *Cell Rep*, 2021. **35**(2): p. 108980.



249. Scaramuzzino, C., et al., *Protein arginine methyltransferase 6 enhances polyglutamine-expanded androgen receptor function and toxicity in spinal and bulbar muscular atrophy*. *Neuron*, 2015. **85**(1): p. 88-100.
250. Ljubcic, V., et al., *Chronic AMPK stimulation attenuates adaptive signaling in dystrophic skeletal muscle*. *Am J Physiol Cell Physiol*, 2012. **302**(1): p. C110-21.
251. Hubers, L., et al., *HuD interacts with survival motor neuron protein and can rescue spinal muscular atrophy-like neuronal defects*. *Hum Mol Genet*, 2011. **20**(3): p. 553-79.
252. Sanchez, G., et al., *A novel function for the survival motoneuron protein as a translational regulator*. *Hum Mol Genet*, 2013. **22**(4): p. 668-84.
253. Sanchez, G., et al., *A novel role for CARM1 in promoting nonsense-mediated mRNA decay: potential implications for spinal muscular atrophy*. *Nucleic Acids Res*, 2016. **44**(6): p. 2661-76.
254. Tadesse, H., et al., *KH-type splicing regulatory protein interacts with survival motor neuron protein and is misregulated in spinal muscular atrophy*. *Hum Mol Genet*, 2008. **17**(4): p. 506-24.
255. Boisvert, F.M., et al., *Symmetrical dimethylarginine methylation is required for the localization of SMN in Cajal bodies and pre-mRNA splicing*. *J Cell Biol*, 2002. **159**(6): p. 957-69.
256. Markowitz, J.A., P. Singh, and B.T. Darras, *Spinal muscular atrophy: a clinical and research update*. *Pediatr Neurol*, 2012. **46**(1): p. 1-12.
257. Liu, Y., et al., *CARM1 contributes to skeletal muscle wasting by mediating FoxO3 activity and promoting myofiber autophagy*. *Exp Cell Res*, 2019. **374**(1): p. 198-209.
258. Iwasaki, H. and T. Yada, *Protein arginine methylation regulates insulin signaling in L6 skeletal muscle cells*. *Biochem Biophys Res Commun*, 2007. **364**(4): p. 1015-21.
259. Iwasaki, H., *Impaired PRMT1 activity in the liver and pancreas of type 2 diabetic Goto-Kakizaki rats*. *Life Sci*, 2009. **85**(3-4): p. 161-6.
260. Choi, D., et al., *Protein arginine methyltransferase 1 regulates hepatic glucose production in a FoxO1-dependent manner*. *Hepatology*, 2012. **56**(4): p. 1546-56.
261. Ojima, A., et al., *Glucagon-like peptide-1 receptor agonist inhibits asymmetric dimethylarginine generation in the kidney of streptozotocin-induced diabetic rats by blocking advanced glycation end product-induced protein arginine methyltransferase-1 expression*. *Am J Pathol*, 2013. **182**(1): p. 132-41.
262. Chen, Y., et al., *PRMT-1 and DDAHs-induced ADMA upregulation is involved in ROS- and RAS-mediated diabetic retinopathy*. *Exp Eye Res*, 2009. **89**(6): p. 1028-34.
263. Kim, J.K., et al., *PRMT4 is involved in insulin secretion via the methylation of histone H3 in pancreatic beta cells*. *J Mol Endocrinol*, 2015. **54**(3): p. 315-24.

264. Kim, D., et al., *Ubiquitination-dependent CARM1 degradation facilitates Notch1-mediated podocyte apoptosis in diabetic nephropathy*. *Cell Signal*, 2014. **26**(9): p. 1774-82.
265. Wang, S.C., et al., *CARM1/PRMT4 is necessary for the glycogen gene expression programme in skeletal muscle cells*. *Biochem J*, 2012. **444**(2): p. 323-31.
266. Tsai, W.W., et al., *PRMT5 modulates the metabolic response to fasting signals*. *Proc Natl Acad Sci U S A*, 2013. **110**(22): p. 8870-5.
267. Huang, L., et al., *Inhibition of protein arginine methyltransferase 5 enhances hepatic mitochondrial biogenesis*. *J Biol Chem*, 2018. **293**(28): p. 10884-10894.
268. Akawi, N., et al., *Discovery of four recessive developmental disorders using probabilistic genotype and phenotype matching among 4,125 families*. *Nat Genet*, 2015. **47**(11): p. 1363-9.
269. Agolini, E., et al., *Expanding the clinical and molecular spectrum of PRMT7 mutations: 3 additional patients and review*. *Clin Genet*, 2018. **93**(3): p. 675-681.
270. Kernohan, K.D., et al., *Loss of the arginine methyltransferase PRMT7 causes syndromic intellectual disability with microcephaly and brachydactyly*. *Clin Genet*, 2017. **91**(5): p. 708-716.
271. Jeong, H.J., et al., *Prmt7 Deficiency Causes Reduced Skeletal Muscle Oxidative Metabolism and Age-Related Obesity*. *Diabetes*, 2016. **65**(7): p. 1868-82.
272. Morettin, A., R.M. Baldwin, and J. Cote, *Arginine methyltransferases as novel therapeutic targets for breast cancer*. *Mutagenesis*, 2015. **30**(2): p. 177-89.
273. Le Romancer, M., et al., *Regulation of estrogen rapid signaling through arginine methylation by PRMT1*. *Mol Cell*, 2008. **31**(2): p. 212-21.
274. Qi, C., et al., *Identification of protein arginine methyltransferase 2 as a coactivator for estrogen receptor alpha*. *J Biol Chem*, 2002. **277**(32): p. 28624-30.
275. Chen, D., S.M. Huang, and M.R. Stallcup, *Synergistic, p160 coactivator-dependent enhancement of estrogen receptor function by CARM1 and p300*. *J Biol Chem*, 2000. **275**(52): p. 40810-6.
276. Wei, T.Y., et al., *Methylosome protein 50 promotes androgen- and estrogen-independent tumorigenesis*. *Cell Signal*, 2014. **26**(12): p. 2940-50.
277. Harrison, M.J., Y.H. Tang, and D.H. Dowhan, *Protein arginine methyltransferase 6 regulates multiple aspects of gene expression*. *Nucleic Acids Research*, 2010. **38**(7): p. 2201-2216.
278. Singh, V., et al., *DAL-1/4.1B tumor suppressor interacts with protein arginine N-methyltransferase 3 (PRMT3) and inhibits its ability to methylate substrates in vitro and in vivo*. *Oncogene*, 2004. **23**(47): p. 7761-71.
279. Jiang, W. and I.F. Newsham, *The tumor suppressor DAL-1/4.1B and protein methylation cooperate in inducing apoptosis in MCF-7 breast cancer cells*. *Mol Cancer*, 2006. **5**: p. 4.
280. Zhong, J., et al., *Identification and characterization of novel spliced variants of PRMT2 in breast carcinoma*. *FEBS J*, 2012. **279**(2): p. 316-35.

281. Zhong, J., et al., *Identification and expression analysis of a novel transcript of the human PRMT2 gene resulted from alternative polyadenylation in breast cancer*. *Gene*, 2011. **487**(1): p. 1-9.
282. Zhong, J., et al., *Nuclear loss of protein arginine N-methyltransferase 2 in breast carcinoma is associated with tumor grade and overexpression of cyclin D1 protein*. *Oncogene*, 2014. **33**(48): p. 5546-58.
283. Zhong, J., et al., *PRMT2beta, a C-terminal splice variant of PRMT2, inhibits the growth of breast cancer cells*. *Oncol Rep*, 2017. **38**(2): p. 1303-1311.
284. Shen, Y., et al., *Protein arginine N-methyltransferase 2 reverses tamoxifen resistance in breast cancer cells through suppression of ER-alpha36*. *Oncol Rep*, 2018. **39**(6): p. 2604-2612.
285. Lee, L.M., et al., *ER-alpha36, a novel variant of ER-alpha, is expressed in ER-positive and -negative human breast carcinomas*. *Anticancer Res*, 2008. **28**(1B): p. 479-83.
286. Sun, Y., et al., *Protein arginine methyltransferase 6 enhances ligand-dependent and -independent activity of estrogen receptor alpha via distinct mechanisms*. *Biochim Biophys Acta*, 2014. **1843**(9): p. 2067-78.
287. Dowhan, D.H., et al., *Protein arginine methyltransferase 6-dependent gene expression and splicing: association with breast cancer outcomes*. *Endocr Relat Cancer*, 2012. **19**(4): p. 509-26.
288. Mann, M., et al., *PELP1 oncogenic functions involve alternative splicing via PRMT6*. *Mol Oncol*, 2014. **8**(2): p. 389-400.
289. Phalke, S., et al., *p53-Independent regulation of p21Waf1/Cip1 expression and senescence by PRMT6*. *Nucleic Acids Res*, 2012. **40**(19): p. 9534-42.
290. Kim, N.H., et al., *PRMT6 overexpression upregulates TSP-1 and downregulates MMPs: its implication in motility and invasion*. *Biochem Biophys Res Commun*, 2013. **432**(1): p. 60-5.
291. Bao, J., et al., *Mouse Models of Overexpression Reveal Distinct Oncogenic Roles for Different Type I Protein Arginine Methyltransferases*. *Cancer Res*, 2019. **79**(1): p. 21-32.
292. Thomassen, M., Q. Tan, and T.A. Kruse, *Gene expression meta-analysis identifies chromosomal regions and candidate genes involved in breast cancer metastasis*. *Breast Cancer Res Treat*, 2009. **113**(2): p. 239-49.
293. Geng, P., et al., *Automethylation of protein arginine methyltransferase 7 and its impact on breast cancer progression*. *FASEB J*, 2017. **31**(6): p. 2287-2300.
294. Baldwin, R.M., et al., *Protein arginine methyltransferase 7 promotes breast cancer cell invasion through the induction of MMP9 expression*. *Oncotarget*, 2015. **6**(5): p. 3013-32.
295. Yao, R., et al., *PRMT7 induces epithelial-to-mesenchymal transition and promotes metastasis in breast cancer*. *Cancer Res*, 2014. **74**(19): p. 5656-67.

296. Liu, Y., et al., *Arginine methylation of SHANK2 by PRMT7 promotes human breast cancer metastasis through activating endosomal FAK signalling*. Elife, 2020. **9**.
297. Liu, L., et al., *Arginine and lysine methylation of MRPS23 promotes breast cancer metastasis through regulating OXPLOS*. Oncogene, 2021. **40**(20): p. 3548-3563.
298. Han, X., L. Wei, and B. Wu, *PRMT5 Promotes Aerobic Glycolysis and Invasion of Breast Cancer Cells by Regulating the LXRalpha/NF-kappaBp65 Pathway*. Onco Targets Ther, 2020. **13**: p. 3347-3357.
299. Yang, F., et al., *Proliferative role of TRAF4 in breast cancer by upregulating PRMT5 nuclear expression*. Tumour Biol, 2015. **36**(8): p. 5901-11.
300. Rengasamy, M., et al., *The PRMT5/WDR77 complex regulates alternative splicing through ZNF326 in breast cancer*. Nucleic Acids Res, 2017. **45**(19): p. 11106-11120.
301. Vinet, M., et al., *Protein arginine methyltransferase 5: A novel therapeutic target for triple-negative breast cancer*. Cancer Med, 2019. **8**(5): p. 2414-2428.
302. Wu, Y., et al., *Elevated expression of protein arginine methyltransferase 5 predicts the poor prognosis of breast cancer*. Tumour Biol, 2017. **39**(4): p. 1010428317695917.
303. Huang, S., et al., *CAPG enhances breast cancer metastasis by competing with PRMT5 to modulate STC-1 transcription*. Theranostics, 2018. **8**(9): p. 2549-2564.
304. Wu, D., et al., *Circ-PRMT5 promotes breast cancer by the miR-509-3p/TCF7L2 axis activating the PI3K/AKT pathway*. J Gene Med, 2021. **23**(2): p. e3300.
305. Wang, X., et al., *Arginine methyltransferase PRMT5 methylates and stabilizes KLF5 via decreasing its phosphorylation and ubiquitination to promote basal-like breast cancer*. Cell Death Differ, 2021.
306. Chiang, K., et al., *PRMT5 Is a Critical Regulator of Breast Cancer Stem Cell Function via Histone Methylation and FOXP1 Expression*. Cell Rep, 2017. **21**(12): p. 3498-3513.
307. Wang, Z., et al., *PRMT5 determines the sensitivity to chemotherapeutics by governing stemness in breast cancer*. Breast Cancer Res Treat, 2018. **168**(2): p. 531-542.
308. Hu, D., et al., *Interplay between arginine methylation and ubiquitylation regulates KLF4-mediated genome stability and carcinogenesis*. Nat Commun, 2015. **6**: p. 8419.
309. Zhou, Z., et al., *A novel small-molecule antagonizes PRMT5-mediated KLF4 methylation for targeted therapy*. EBioMedicine, 2019. **44**: p. 98-111.
310. Chen, H., et al., *A TGFbeta-PRMT5-MEP50 axis regulates cancer cell invasion through histone H3 and H4 arginine methylation coupled transcriptional activation and repression*. Oncogene, 2017. **36**(3): p. 373-386.
311. Lattouf, H., et al., *LKB1 regulates PRMT5 activity in breast cancer*. Int J Cancer, 2019. **144**(3): p. 595-606.

312. Liu, R., et al., *PHD finger protein 1 (PHF1) is a novel reader for histone H4R3 symmetric dimethylation and coordinates with PRMT5-WDR77/CRL4B complex to promote tumorigenesis*. Nucleic Acids Res, 2018. **46**(13): p. 6608-6626.
313. Powers, M.A., et al., *Protein arginine methyltransferase 5 accelerates tumor growth by arginine methylation of the tumor suppressor programmed cell death 4*. Cancer Res, 2011. **71**(16): p. 5579-87.
314. Chatterjee, B., et al., *Curcumin ameliorates PRMT5-MEP50 arginine methyltransferase expression by decreasing the Sp1 and NF- $\kappa$ B transcription factors in the A549 and MCF-7 cells*. Mol Cell Biochem, 2019. **455**(1-2): p. 73-90.
315. Hernandez, S.J., D.M. Dolivo, and T. Dominko, *PRMT8 demonstrates variant-specific expression in cancer cells and correlates with patient survival in breast, ovarian and gastric cancer*. Oncol Lett, 2017. **13**(3): p. 1983-1989.
316. Branscombe, T.L., et al., *PRMT5 (Janus kinase-binding protein 1) catalyzes the formation of symmetric dimethylarginine residues in proteins*. J Biol Chem, 2001. **276**(35): p. 32971-6.
317. Liu, F., et al., *JAK2V617F-mediated phosphorylation of PRMT5 downregulates its methyltransferase activity and promotes myeloproliferation*. Cancer Cell, 2011. **19**(2): p. 283-94.
318. Koh, C.M., et al., *MYC regulates the core pre-mRNA splicing machinery as an essential step in lymphomagenesis*. Nature, 2015. **523**(7558): p. 96-100.
319. Chung, J., et al., *Protein arginine methyltransferase 5 (PRMT5) inhibition induces lymphoma cell death through reactivation of the retinoblastoma tumor suppressor pathway and polycomb repressor complex 2 (PRC2) silencing*. J Biol Chem, 2013. **288**(49): p. 35534-47.
320. Pal, S., et al., *Low levels of miR-92b/96 induce PRMT5 translation and H3R8/H4R3 methylation in mantle cell lymphoma*. EMBO J, 2007. **26**(15): p. 3558-69.
321. Gulla, A., et al., *Protein arginine methyltransferase 5 has prognostic relevance and is a druggable target in multiple myeloma*. Leukemia, 2018. **32**(4): p. 996-1002.
322. Marjon, K., et al., *MTAP Deletions in Cancer Create Vulnerability to Targeting of the MAT2A/PRMT5/RIOK1 Axis*. Cell Rep, 2016. **15**(3): p. 574-587.
323. Mavrakis, K.J., et al., *Disordered methionine metabolism in MTAP/CDKN2A-deleted cancer leads to dependence on PRMT5*. Science, 2016. **351**(6278): p. 1208-13.
324. Kryukov, G.V., et al., *MTAP deletion confers enhanced dependency on the PRMT5 arginine methyltransferase in cancer cells*. Science, 2016. **351**(6278): p. 1214-8.
325. Barbarino, M., et al., *PRMT5 silencing selectively affects MTAP-deleted mesothelioma: In vitro evidence of a novel promising approach*. J Cell Mol Med, 2020. **24**(10): p. 5565-5577.

326. Fedoriw, A., et al., *Anti-tumor Activity of the Type I PRMT Inhibitor, GSK3368715, Synergizes with PRMT5 Inhibition through MTAP Loss*. *Cancer Cell*, 2019. **36**(1): p. 100-114 e25.
327. Guccione, E., et al., *Cancer synthetic vulnerabilities to protein arginine methyltransferase inhibitors*. *Curr Opin Pharmacol*, 2021. **59**: p. 33-42.
328. Solari, C., et al., *Protein arginine Methyltransferase 8 gene is expressed in pluripotent stem cells and its expression is modulated by the transcription factor Sox2*. *Biochem Biophys Res Commun*, 2016. **473**(1): p. 194-199.
329. Kim, J.D., et al., *PRMT8 as a phospholipase regulates Purkinje cell dendritic arborization and motor coordination*. *Sci Adv*, 2015. **1**(11): p. e1500615.
330. Simandi, Z., et al., *PRMT1 and PRMT8 regulate retinoic acid-dependent neuronal differentiation with implications to neuropathology*. *Stem Cells*, 2015. **33**(3): p. 726-41.
331. Tan, Z., et al., *Overexpression of HOXC10 promotes angiogenesis in human glioma via interaction with PRMT5 and upregulation of VEGFA expression*. *Theranostics*, 2018. **8**(18): p. 5143-5158.
332. Lu, Y.F., et al., *LncRNA SNHG16 Functions as an Oncogene by Sponging MiR-4518 and Up-Regulating PRMT5 Expression in Glioma*. *Cell Physiol Biochem*, 2018. **45**(5): p. 1975-1985.
333. Holmes, B., et al., *The protein arginine methyltransferase PRMT5 confers therapeutic resistance to mTOR inhibition in glioblastoma*. *J Neurooncol*, 2019. **145**(1): p. 11-22.
334. Banasavadi-Siddegowda, Y.K., et al., *PRMT5-PTEN molecular pathway regulates senescence and self-renewal of primary glioblastoma neurosphere cells*. *Oncogene*, 2017. **36**(2): p. 263-274.
335. Mongiardi, M.P., et al., *Myc and Omomyc functionally associate with the Protein Arginine Methyltransferase 5 (PRMT5) in glioblastoma cells*. *Sci Rep*, 2015. **5**: p. 15494.
336. Han, X., et al., *Expression of PRMT5 correlates with malignant grade in gliomas and plays a pivotal role in tumor growth in vitro*. *J Neurooncol*, 2014. **118**(1): p. 61-72.
337. Yan, F., et al., *Genetic validation of the protein arginine methyltransferase PRMT5 as a candidate therapeutic target in glioblastoma*. *Cancer Res*, 2014. **74**(6): p. 1752-65.
338. Chaturvedi, N.K., et al., *Role of protein arginine methyltransferase 5 in group 3 (MYC-driven) Medulloblastoma*. *BMC Cancer*, 2019. **19**(1): p. 1056.
339. Sachamitr, P., et al., *PRMT5 inhibition disrupts splicing and stemness in glioblastoma*. *Nat Commun*, 2021. **12**(1): p. 979.
340. Cheng, D., et al., *Small molecule regulators of protein arginine methyltransferases*. *J Biol Chem*, 2004. **279**(23): p. 23892-9.
341. Chan-Penebre, E., et al., *A selective inhibitor of PRMT5 with in vivo and in vitro potency in MCL models*. *Nat Chem Biol*, 2015. **11**(6): p. 432-7.

342. Kaniskan, H.U., et al., *A potent, selective and cell-active allosteric inhibitor of protein arginine methyltransferase 3 (PRMT3)*. *Angew Chem Int Ed Engl*, 2015. **54**(17): p. 5166-70.
343. Drew, A.E., et al., *Identification of a CARM1 Inhibitor with Potent In Vitro and In Vivo Activity in Preclinical Models of Multiple Myeloma*. *Sci Rep*, 2017. **7**(1): p. 17993.
344. Nakayama, K., et al., *TP-064, a potent and selective small molecule inhibitor of PRMT4 for multiple myeloma*. *Oncotarget*, 2018. **9**(26): p. 18480-18493.
345. Duncan, K.W., et al., *Structure and Property Guided Design in the Identification of PRMT5 Tool Compound EPZ015666*. *ACS Med Chem Lett*, 2016. **7**(2): p. 162-6.
346. Gerhart, S.V., et al., *Activation of the p53-MDM4 regulatory axis defines the anti-tumour response to PRMT5 inhibition through its role in regulating cellular splicing*. *Sci Rep*, 2018. **8**(1): p. 9711.
347. Bonday, Z.Q., et al., *LLY-283, a Potent and Selective Inhibitor of Arginine Methyltransferase 5, PRMT5, with Antitumor Activity*. *ACS Med Chem Lett*, 2018. **9**(7): p. 612-617.
348. Palte, R.L., et al., *Allosteric Modulation of Protein Arginine Methyltransferase 5 (PRMT5)*. *ACS Med Chem Lett*, 2020. **11**(9): p. 1688-1693.
349. Mitchell, L.H., et al., *Aryl Pyrazoles as Potent Inhibitors of Arginine Methyltransferases: Identification of the First PRMT6 Tool Compound*. *ACS Med Chem Lett*, 2015. **6**(6): p. 655-9.
350. Eram, M.S., et al., *A Potent, Selective, and Cell-Active Inhibitor of Human Type I Protein Arginine Methyltransferases*. *ACS Chem Biol*, 2016. **11**(3): p. 772-781.
351. Katsanis, N., M.L. Yaspo, and E.M. Fisher, *Identification and mapping of a novel human gene, HRMT1L1, homologous to the rat protein arginine N-methyltransferase 1 (PRMT1) gene*. *Mamm Genome*, 1997. **8**(7): p. 526-9.
352. Tang, J., et al., *PRMT1 is the predominant type I protein arginine methyltransferase in mammalian cells*. *J Biol Chem*, 2000. **275**(11): p. 7723-30.
353. Weiss, V.H., et al., *The structure and oligomerization of the yeast arginine methyltransferase, Hmt1*. *Nat Struct Biol*, 2000. **7**(12): p. 1165-71.
354. Rust, H.L., et al., *Mechanistic studies on transcriptional coactivator protein arginine methyltransferase 1*. *Biochemistry*, 2011. **50**(16): p. 3332-45.
355. Gui, S., et al., *Investigation of the molecular origins of protein-arginine methyltransferase I (PRMT1) product specificity reveals a role for two conserved methionine residues*. *J Biol Chem*, 2011. **286**(33): p. 29118-29126.
356. Lakowski, T.M., et al., *Neta-substituted arginyl peptide inhibitors of protein arginine N-methyltransferases*. *ACS Chem Biol*, 2010. **5**(11): p. 1053-63.
357. Scott, H.S., et al., *Identification and characterization of two putative human arginine methyltransferases (HRMT1L1 and HRMT1L2)*. *Genomics*, 1998. **48**(3): p. 330-40.

358. Scorilas, A., et al., *Genomic organization, physical mapping, and expression analysis of the human protein arginine methyltransferase 1 gene*. *Biochem Biophys Res Commun*, 2000. **278**(2): p. 349-59.
359. Herrmann, F., et al., *Dynamics of human protein arginine methyltransferase 1 (PRMT1) in vivo*. *J Biol Chem*, 2005. **280**(45): p. 38005-10.
360. Patounas, O., et al., *A novel splicing isoform of protein arginine methyltransferase 1 (PRMT1) that lacks the dimerization arm and correlates with cellular malignancy*. *J Cell Biochem*, 2018. **119**(2): p. 2110-2123.
361. Adamopoulos, P.G., et al., *Novel alternative splice variants of the human protein arginine methyltransferase 1 (PRMT1) gene, discovered using next-generation sequencing*. *Gene*, 2019. **699**: p. 135-144.
362. Bao, X., et al., *CSNK1a1 Regulates PRMT1 to Maintain the Progenitor State in Self-Renewing Somatic Tissue*. *Dev Cell*, 2017. **43**(2): p. 227-239 e5.
363. Rust, H.L., et al., *Using unnatural amino acid mutagenesis to probe the regulation of PRMT1*. *ACS Chem Biol*, 2014. **9**(3): p. 649-55.
364. Musiani, D., et al., *PRMT1 Is Recruited via DNA-PK to Chromatin Where It Sustains the Senescence-Associated Secretory Phenotype in Response to Cisplatin*. *Cell Rep*, 2020. **30**(4): p. 1208-1222 e9.
365. Hirata, Y., et al., *TRIM48 Promotes ASK1 Activation and Cell Death through Ubiquitination-Dependent Degradation of the ASK1-Negative Regulator PRMT1*. *Cell Rep*, 2017. **21**(9): p. 2447-2457.
366. Bhuripanyo, K., et al., *Identifying the substrate proteins of U-box E3s E4B and CHIP by orthogonal ubiquitin transfer*. *Sci Adv*, 2018. **4**(1): p. e1701393.
367. Lai, Y., et al., *Lipopolysaccharide modulates p300 and Sirt1 to promote PRMT1 stability via an SCF(Fbx17)-recognized acetyldegron*. *J Cell Sci*, 2017. **130**(20): p. 3578-3587.
368. Mertins, P., et al., *Integrated proteomic analysis of post-translational modifications by serial enrichment*. *Nat Methods*, 2013. **10**(7): p. 634-7.
369. Huang, S., M. Litt, and G. Felsenfeld, *Methylation of histone H4 by arginine methyltransferase PRMT1 is essential in vivo for many subsequent histone modifications*. *Genes Dev*, 2005. **19**(16): p. 1885-93.
370. Kleinschmidt, M.A., et al., *The protein arginine methyltransferases CARM1 and PRMT1 cooperate in gene regulation*. *Nucleic Acids Res*, 2008. **36**(10): p. 3202-13.
371. Mowen, K.A., et al., *Arginine methylation of STAT1 modulates IFNalpha/beta-induced transcription*. *Cell*, 2001. **104**(5): p. 731-41.
372. Inamitsu, M., et al., *Methylation of Smad6 by protein arginine N-methyltransferase 1*. *FEBS Lett*, 2006. **580**(28-29): p. 6603-11.
373. Katsuno, Y., et al., *Arginine methylation of SMAD7 by PRMT1 in TGF-beta-induced epithelial-mesenchymal transition and epithelial stem-cell generation*. *J Biol Chem*, 2018. **293**(34): p. 13059-13072.



374. Tan, C.P. and S. Nakielny, *Control of the DNA methylation system component MBD2 by protein arginine methylation*. Mol Cell Biol, 2006. **26**(19): p. 7224-35.
375. Dery, U., et al., *A glycine-arginine domain in control of the human MRE11 DNA repair protein*. Mol Cell Biol, 2008. **28**(9): p. 3058-69.
376. Chen, Y., et al., *Arginine methylation of hnRNP K enhances p53 transcriptional activity*. FEBS Lett, 2008. **582**(12): p. 1761-5.
377. Rho, J., et al., *Arginine methylation of Sam68 and SLM proteins negatively regulates their poly(U) RNA binding activity*. Arch Biochem Biophys, 2007. **466**(1): p. 49-57.
378. Hwang, J.W., et al., *Protein arginine methyltransferases: promising targets for cancer therapy*. Exp Mol Med, 2021. **53**(5): p. 788-808.
379. Xu, J., et al., *Arginine Methylation Initiates BMP-Induced Smad Signaling*. Mol Cell, 2013. **51**(1): p. 5-19.
380. Zhang, T., et al., *Smad6 Methylation Represses NFkappaB Activation and Periodontal Inflammation*. J Dent Res, 2018. **97**(7): p. 810-819.
381. Yao, B., et al., *PRMT1-mediated H4R3me2a recruits SMARCA4 to promote colorectal cancer progression by enhancing EGFR signaling*. Genome Med, 2021. **13**(1): p. 58.
382. Wang, W.J., et al., *An essential role of PRMT1-mediated EGFR methylation in EGFR activation by ribonuclease 5*. Am J Cancer Res, 2019. **9**(1): p. 180-185.
383. Nakai, K., et al., *The role of PRMT1 in EGFR methylation and signaling in MDA-MB-468 triple-negative breast cancer cells*. Breast Cancer, 2018. **25**(1): p. 74-80.
384. Yamagata, K., et al., *Arginine methylation of FOXO transcription factors inhibits their phosphorylation by Akt*. Mol Cell, 2008. **32**(2): p. 221-31.
385. Wang, Y., et al., *Oncogenic Functions of Gli1 in Pancreatic Adenocarcinoma Are Supported by Its PRMT1-Mediated Methylation*. Cancer Res, 2016. **76**(23): p. 7049-7058.
386. Cha, B., et al., *Methylation by protein arginine methyltransferase 1 increases stability of Axin, a negative regulator of Wnt signaling*. Oncogene, 2011. **30**(20): p. 2379-89.
387. Bikkavilli, R.K., et al., *Dishevelled3 is a novel arginine methyl transferase substrate*. Sci Rep, 2012. **2**: p. 805.
388. Bikkavilli, R.K. and C.C. Malbon, *Arginine methylation of G3BP1 in response to Wnt3a regulates beta-catenin mRNA*. J Cell Sci, 2011. **124**(Pt 13): p. 2310-20.
389. Bikkavilli, R.K. and C.C. Malbon, *Wnt3a-stimulated LRP6 phosphorylation is dependent upon arginine methylation of G3BP2*. J Cell Sci, 2012. **125**(Pt 10): p. 2446-56.
390. Zhao, Y., et al., *PRMT1 regulates the tumour-initiating properties of esophageal squamous cell carcinoma through histone H4 arginine methylation coupled with transcriptional activation*. Cell Death Dis, 2019. **10**(5): p. 359.

391. Cheng, S.L., et al., *Vascular smooth muscle LRP6 limits arteriosclerotic calcification in diabetic LDLR<sup>-/-</sup> mice by restraining noncanonical Wnt signals*. *Circ Res*, 2015. **117**(2): p. 142-56.
392. Albrecht, L.V., et al., *Arginine methylation is required for canonical Wnt signaling and endolysosomal trafficking*. *Proc Natl Acad Sci U S A*, 2018. **115**(23): p. E5317-E5325.
393. Tejada-Munoz, N., et al., *Wnt canonical pathway activates macropinocytosis and lysosomal degradation of extracellular proteins*. *Proc Natl Acad Sci U S A*, 2019. **116**(21): p. 10402-10411.
394. Albrecht, L.V., M.H. Bui, and E.M. De Robertis, *Canonical Wnt is inhibited by targeting one-carbon metabolism through methotrexate or methionine deprivation*. *Proc Natl Acad Sci U S A*, 2019. **116**(8): p. 2987-2995.
395. Desterke, C., et al., *Embryonic Program Activated during Blast Crisis of Chronic Myelogenous Leukemia (CML) Implicates a TCF7L2 and MYC Cooperative Chromatin Binding*. *Int J Mol Sci*, 2020. **21**(11).
396. Sun, Y., et al., *The Development of Tetrazole Derivatives as Protein Arginine Methyltransferase I (PRMT I) Inhibitors*. *Int J Mol Sci*, 2019. **20**(15).
397. Guendel, I., et al., *Methylation of the tumor suppressor protein, BRCA1, influences its transcriptional cofactor function*. *PLoS One*, 2010. **5**(6): p. e11379.
398. Mathioudaki, K., et al., *Clinical evaluation of PRMT1 gene expression in breast cancer*. *Tumour Biol*, 2011. **32**(3): p. 575-82.
399. Liu, L.M., et al., *Methylation of C/EBPalpha by PRMT1 Inhibits Its Tumor-Suppressive Function in Breast Cancer*. *Cancer Res*, 2019. **79**(11): p. 2865-2877.
400. Seligson, D.B., et al., *Global histone modification patterns predict risk of prostate cancer recurrence*. *Nature*, 2005. **435**(7046): p. 1262-6.
401. Yoshimatsu, M., et al., *Dysregulation of PRMT1 and PRMT6, Type I arginine methyltransferases, is involved in various types of human cancer*. *Int J Cancer*, 2011. **128**(3): p. 562-73.
402. Papadokostopoulou, A., et al., *Colon cancer and protein arginine methyltransferase 1 gene expression*. *Anticancer Res*, 2009. **29**(4): p. 1361-6.
403. Mathioudaki, K., et al., *The PRMT1 gene expression pattern in colon cancer*. *Br J Cancer*, 2008. **99**(12): p. 2094-9.
404. Zou, L., et al., *Correlation of SRSF1 and PRMT1 expression with clinical status of pediatric acute lymphoblastic leukemia*. *J Hematol Oncol*, 2012. **5**: p. 42.
405. Shia, W.J., et al., *PRMT1 interacts with AML1-ETO to promote its transcriptional activation and progenitor cell proliferative potential*. *Blood*, 2012. **119**(21): p. 4953-62.
406. Cheung, N., et al., *Protein arginine-methyltransferase-dependent oncogenesis*. *Nat Cell Biol*, 2007. **9**(10): p. 1208-15.
407. Mirsadeghi, L., et al., *EARN: an ensemble machine learning algorithm to predict driver genes in metastatic breast cancer*. *BMC Med Genomics*, 2021. **14**(1): p. 122.

408. Montenegro, M.F., et al., *PRMT1-dependent methylation of BRCA1 contributes to the epigenetic defense of breast cancer cells against ionizing radiation*. Sci Rep, 2020. **10**(1): p. 13275.
409. Malbeteau, L., et al., *PRMT1 Is Critical for the Transcriptional Activity and the Stability of the Progesterone Receptor*. iScience, 2020. **23**(6): p. 101236.
410. Choucair, A., et al., *The arginine methyltransferase PRMT1 regulates IGF-1 signaling in breast cancer*. Oncogene, 2019. **38**(21): p. 4015-4027.
411. Le Romancer, M., et al., *Methylation, a key step for nongenomic estrogen signaling in breast tumors*. Steroids, 2010. **75**(8-9): p. 560-4.
412. Izumikawa, K., et al., *Modulating the expression of Chtop, a versatile regulator of gene-specific transcription and mRNA export*. RNA Biol, 2018. **15**(7): p. 849-855.
413. Singh, P., et al., *Pharmacologic downregulation of protein arginine methyltransferase1 expression by adenosine dialdehyde increases cell senescence in breast cancer*. Eur J Pharmacol, 2021. **891**: p. 173697.
414. Baldwin, R.M., et al., *Identification of the PRMT1v1 and PRMT1v2 specific interactomes by quantitative mass spectrometry in breast cancer cells*. Proteomics, 2015. **15**(13): p. 2187-97.
415. Baldwin, R.M., et al., *Alternatively spliced protein arginine methyltransferase 1 isoform PRMT1v2 promotes the survival and invasiveness of breast cancer cells*. Cell Cycle, 2012. **11**(24): p. 4597-612.
416. Bondy-Chorney, E., et al., *RNA binding protein RALY promotes Protein Arginine Methyltransferase 1 alternatively spliced isoform v2 relative expression and metastatic potential in breast cancer cells*. Int J Biochem Cell Biol, 2017. **91**(Pt B): p. 124-135.
417. Li, T., et al., *Protein arginine methyltransferase 1 may be involved in pregnane x receptor-activated overexpression of multidrug resistance 1 gene during acquired multidrug resistant*. Oncotarget, 2016. **7**(15): p. 20236-48.
418. Cho, J.H., et al., *Arginine methylation-dependent regulation of ASK1 signaling by PRMT1*. Cell Death Differ, 2012. **19**(5): p. 859-70.
419. Tang, L., et al., *PAK4 phosphorylating RUNX1 promotes ERalpha-positive breast cancer-induced osteolytic bone destruction*. Int J Biol Sci, 2020. **16**(12): p. 2235-2247.
420. Sala, L., et al., *Abrogation of myofibroblast activities in metastasis and fibrosis by methyltransferase inhibition*. Int J Cancer, 2019. **145**(11): p. 3064-3077.
421. Gao, Y., et al., *The dual function of PRMT1 in modulating epithelial-mesenchymal transition and cellular senescence in breast cancer cells through regulation of ZEB1*. Sci Rep, 2016. **6**: p. 19874.
422. Li, Z., et al., *Macrophages-stimulated PRMT1-mediated EZH2 methylation promotes breast cancer metastasis*. Biochem Biophys Res Commun, 2020. **533**(4): p. 679-684.

423. Li, Z., et al., *Methylation of EZH2 by PRMT1 regulates its stability and promotes breast cancer metastasis*. Cell Death Differ, 2020. **27**(12): p. 3226-3242.
424. Favia, A., et al., *The Protein Arginine Methyltransferases 1 and 5 affect Myc properties in glioblastoma stem cells*. Sci Rep, 2019. **9**(1): p. 15925.
425. Avasarala, S., et al., *PRMT1 Is a Novel Regulator of Epithelial-Mesenchymal-Transition in Non-small Cell Lung Cancer*. J Biol Chem, 2015. **290**(21): p. 13479-89.
426. Zhang, T., et al., *Inhibition of Nonsmall Cell Lung Cancer Cell Migration by Protein Arginine Methyltransferase 1-small Hairpin RNA Through Inhibiting Epithelial-mesenchymal Transition, Extracellular Matrix Degradation, and Src Phosphorylation In Vitro*. Chin Med J (Engl), 2015. **128**(9): p. 1202-8.
427. Nichols, R.C., et al., *The RGG domain in hnRNP A2 affects subcellular localization*. Exp Cell Res, 2000. **256**(2): p. 522-32.
428. Madreiter-Sokolowski, C.T., et al., *UCP2 and PRMT1 are key prognostic markers for lung carcinoma patients*. Oncotarget, 2017. **8**(46): p. 80278-80285.
429. Gao, G., et al., *PRMT1 loss sensitizes cells to PRMT5 inhibition*. Nucleic Acids Res, 2019. **47**(10): p. 5038-5048.
430. Cheng, C., et al., *CRISPR/Cas9 library screening uncovered methylated PKP2 as a critical driver of lung cancer radioresistance by stabilizing beta-catenin*. Oncogene, 2021. **40**(16): p. 2842-2857.
431. He, L., et al., *PRMT1 is critical to FEN1 expression and drug resistance in lung cancer cells*. DNA Repair (Amst), 2020. **95**: p. 102953.
432. Zhu, L., et al., *Protein arginine methyltransferase 1 is required for maintenance of normal adult hematopoiesis*. Int J Biol Sci, 2019. **15**(13): p. 2763-2773.
433. He, X., et al., *PRMT1-mediated FLT3 arginine methylation promotes maintenance of FLT3-ITD(+) acute myeloid leukemia*. Blood, 2019. **134**(6): p. 548-560.
434. Zhu, Y., et al., *Targeting PRMT1-mediated FLT3 methylation disrupts maintenance of MLL-rearranged acute lymphoblastic leukemia*. Blood, 2019. **134**(15): p. 1257-1268.
435. Yuniati, L., et al., *Tumor suppressor BTG1 promotes PRMT1-mediated ATF4 function in response to cellular stress*. Oncotarget, 2016. **7**(3): p. 3128-43.
436. Fong, J.Y., et al., *Therapeutic Targeting of RNA Splicing Catalysis through Inhibition of Protein Arginine Methylation*. Cancer Cell, 2019. **36**(2): p. 194-209 e9.
437. Suresh, S., S. Huard, and T. Dubois, *CARM1/PRMT4: Making Its Mark beyond Its Function as a Transcriptional Coactivator*. Trends Cell Biol, 2021.
438. Chen, D., et al., *Regulation of transcription by a protein methyltransferase*. Science, 1999. **284**(5423): p. 2174-7.
439. Teyssier, C., D. Chen, and M.R. Stallcup, *Requirement for multiple domains of the protein arginine methyltransferase CARM1 in its transcriptional coactivator function*. J Biol Chem, 2002. **277**(48): p. 46066-72.

440. Yue, W.W., et al., *Insights into histone code syntax from structural and biochemical studies of CARM1 methyltransferase*. EMBO J, 2007. **26**(20): p. 4402-12.
441. Higashimoto, K., et al., *Phosphorylation-mediated inactivation of coactivator-associated arginine methyltransferase 1*. Proc Natl Acad Sci U S A, 2007. **104**(30): p. 12318-23.
442. Lee, Y.H., et al., *Synergy among nuclear receptor coactivators: selective requirement for protein methyltransferase and acetyltransferase activities*. Mol Cell Biol, 2002. **22**(11): p. 3621-32.
443. Zika, E., et al., *Interplay among coactivator-associated arginine methyltransferase 1, CBP, and CIITA in IFN-gamma-inducible MHC-II gene expression*. Proc Natl Acad Sci U S A, 2005. **102**(45): p. 16321-6.
444. Kim, D., et al., *Enzymatic activity is required for the in vivo functions of CARM1*. J Biol Chem, 2010. **285**(2): p. 1147-52.
445. Zhao, H.Y., et al., *CARM1 mediates modulation of Sox2*. PLoS One, 2011. **6**(10): p. e27026.
446. Yu, Y.S., et al., *Pontin arginine methylation by CARM1 is crucial for epigenetic regulation of autophagy*. Nat Commun, 2020. **11**(1): p. 6297.
447. Boriack-Sjodin, P.A., et al., *Structural Insights into Ternary Complex Formation of Human CARM1 with Various Substrates*. ACS Chem Biol, 2016. **11**(3): p. 763-71.
448. Jacques, S.L., et al., *CARM1 Preferentially Methylates H3R17 over H3R26 through a Random Kinetic Mechanism*. Biochemistry, 2016. **55**(11): p. 1635-44.
449. van Haren, M.J., et al., *Transition state mimics are valuable mechanistic probes for structural studies with the arginine methyltransferase CARM1*. Proc Natl Acad Sci U S A, 2017. **114**(14): p. 3625-3630.
450. Sack, J.S., et al., *Structural basis for CARM1 inhibition by indole and pyrazole inhibitors*. Biochem J, 2011. **436**(2): p. 331-9.
451. Gunnell, E.A., et al., *Structural and biochemical evaluation of bisubstrate inhibitors of protein arginine N-methyltransferases PRMT1 and CARM1 (PRMT4)*. Biochem J, 2020. **477**(4): p. 787-800.
452. Gupta, N., et al., *Mapping of Post-translational Modifications of Transition Proteins, TP1 and TP2, and Identification of Protein Arginine Methyltransferase 4 and Lysine Methyltransferase 7 as Methyltransferase for TP2*. J Biol Chem, 2015. **290**(19): p. 12101-22.
453. Matsuda, H., et al., *Contrasting effects of two alternative splicing forms of coactivator-associated arginine methyltransferase 1 on thyroid hormone receptor-mediated transcription in Xenopus laevis*. Mol Endocrinol, 2007. **21**(5): p. 1082-94.
454. Wang, L., et al., *CARM1 automethylation is controlled at the level of alternative splicing*. Nucleic Acids Res, 2013. **41**(14): p. 6870-80.

455. Greenblatt, S.M., et al., *CARM1 Is Essential for Myeloid Leukemogenesis but Dispensable for Normal Hematopoiesis*. *Cancer Cell*, 2018. **33**(6): p. 1111-1127
456. Shlensky, D., et al., *Differential CARM1 Isoform Expression in Subcellular Compartments and among Malignant and Benign Breast Tumors*. *PLoS One*, 2015. **10**(6): p. e0128143.
457. Wang, X. and C.W. Roberts, *CARMA: CARM1 methylation of SWI/SNF in breast cancer*. *Cancer Cell*, 2014. **25**(1): p. 3-4.
458. Chang, N.C., et al., *The Dystrophin Glycoprotein Complex Regulates the Epigenetic Activation of Muscle Stem Cell Commitment*. *Cell Stem Cell*, 2018. **22**(5): p. 755-768 e6.
459. Li, X., et al., *Oxidative stress destabilizes protein arginine methyltransferase 4 via glycogen synthase kinase 3beta to impede lung epithelial cell migration*. *Am J Physiol Cell Physiol*, 2017. **313**(3): p. C285-C294.
460. Feng, Q., et al., *Biochemical control of CARM1 enzymatic activity by phosphorylation*. *J Biol Chem*, 2009. **284**(52): p. 36167-74.
461. Lim, C.S. and D.L. Alkon, *Protein kinase C stimulates HuD-mediated mRNA stability and protein expression of neurotrophic factors and enhances dendritic maturation of hippocampal neurons in culture*. *Hippocampus*, 2012. **22**(12): p. 2303-19.
462. Carascossa, S., et al., *CARM1 mediates the ligand-independent and tamoxifen-resistant activation of the estrogen receptor alpha by cAMP*. *Genes Dev*, 2010. **24**(7): p. 708-19.
463. Benesch, M.A., et al., *LSD1 engages a corepressor complex for the activation of the estrogen receptor alpha by estrogen and cAMP*. *Nucleic Acids Res*, 2016. **44**(18): p. 8655-8670.
464. Winter, D.L., G. Hart-Smith, and M.R. Wilkins, *Characterization of Protein Methyltransferases Rkm1, Rkm4, Efm4, Efm7, Set5 and Hmt1 Reveals Extensive Post-Translational Modification*. *J Mol Biol*, 2018. **430**(1): p. 102-118.
465. Cheung, W.D., et al., *O-linked beta-N-acetylglucosaminyltransferase substrate specificity is regulated by myosin phosphatase targeting and other interacting proteins*. *J Biol Chem*, 2008. **283**(49): p. 33935-41.
466. Charoensuksai, P., et al., *O-GlcNAcylation of co-activator-associated arginine methyltransferase 1 regulates its protein substrate specificity*. *Biochem J*, 2015. **466**(3): p. 587-99.
467. Sakabe, K. and G.W. Hart, *O-GlcNAc transferase regulates mitotic chromatin dynamics*. *J Biol Chem*, 2010. **285**(45): p. 34460-8.
468. Shin, H.J., et al., *AMPK-SKP2-CARM1 signalling cascade in transcriptional regulation of autophagy*. *Nature*, 2016. **534**(7608): p. 553-7.
469. Li, C., et al., *Nuclear AMPK regulated CARM1 stabilization impacts autophagy in aged heart*. *Biochem Biophys Res Commun*, 2017. **486**(2): p. 398-405.
470. Kuhn, P., et al., *Automethylation of CARM1 allows coupling of transcription and mRNA splicing*. *Nucleic Acids Res*, 2011. **39**(7): p. 2717-26.

471. Qin, H., et al., *The long noncoding RNA ST7-AS1 promotes laryngeal squamous cell carcinoma by stabilizing CARM1*. *Biochem Biophys Res Commun*, 2019. **512**(1): p. 34-40.
472. Wang, D. and Y. Hu, *Long Non-coding RNA PVT1 Competitively Binds MicroRNA-424-5p to Regulate CARM1 in Radiosensitivity of Non-Small-Cell Lung Cancer*. *Mol Ther Nucleic Acids*, 2019. **16**: p. 130-140.
473. Wang, J., et al., *Asymmetric Expression of LincGET Biases Cell Fate in Two-Cell Mouse Embryos*. *Cell*, 2018. **175**(7): p. 1887-1901 e18.
474. Hu, S.B., et al., *Protein arginine methyltransferase CARM1 attenuates the paraspeckle-mediated nuclear retention of mRNAs containing IRAIus*. *Genes Dev*, 2015. **29**(6): p. 630-45.
475. Hupalowska, A., et al., *CARM1 and Paraspeckles Regulate Pre-implantation Mouse Embryo Development*. *Cell*, 2018. **175**(7): p. 1902-1916 e13.
476. Zhang, M., et al., *Coactivator-associated arginine methyltransferase 1 promotes cell growth and is targeted by microRNA-195-5p in human colorectal cancer*. *Tumour Biol*, 2017. **39**(3): p. 1010428317694305.
477. Zheng, L., et al., *miR-195 enhances the radiosensitivity of colorectal cancer cells by suppressing CARM1*. *Onco Targets Ther*, 2017. **10**: p. 1027-1038.
478. Vu, L.P., et al., *PRMT4 blocks myeloid differentiation by assembling a methyl-RUNX1-dependent repressor complex*. *Cell Rep*, 2013. **5**(6): p. 1625-38.
479. Bauer, U.M., et al., *Methylation at arginine 17 of histone H3 is linked to gene activation*. *EMBO Rep*, 2002. **3**(1): p. 39-44.
480. Yang, G., et al., *Base-Editing-Mediated R17H Substitution in Histone H3 Reveals Methylation-Dependent Regulation of Yap Signaling and Early Mouse Embryo Development*. *Cell Rep*, 2019. **26**(2): p. 302-312 e4.
481. Torres-Padilla, M.E., et al., *Histone arginine methylation regulates pluripotency in the early mouse embryo*. *Nature*, 2007. **445**(7124): p. 214-8.
482. El Messaoudi, S., et al., *Coactivator-associated arginine methyltransferase 1 (CARM1) is a positive regulator of the Cyclin E1 gene*. *Proc Natl Acad Sci U S A*, 2006. **103**(36): p. 13351-6.
483. Goolam, M., et al., *Heterogeneity in Oct4 and Sox2 Targets Biases Cell Fate in 4-Cell Mouse Embryos*. *Cell*, 2016. **165**(1): p. 61-74.
484. Cheng, D., et al., *Genetic evidence for partial redundancy between the arginine methyltransferases CARM1 and PRMT6*. *J Biol Chem*, 2020. **295**(50): p. 17060-17070.
485. Xu, W., et al., *A transcriptional switch mediated by cofactor methylation*. *Science*, 2001. **294**(5551): p. 2507-11.
486. Daujat, S., et al., *Crosstalk between CARM1 methylation and CBP acetylation on histone H3*. *Curr Biol*, 2002. **12**(24): p. 2090-7.
487. Xu, W., et al., *A methylation-mediator complex in hormone signaling*. *Genes Dev*, 2004. **18**(2): p. 144-56.

488. Wang, L., et al., *CARM1 methylates chromatin remodeling factor BAF155 to enhance tumor progression and metastasis*. *Cancer Cell*, 2014. **25**(1): p. 21-36.
489. Karakashev, S., et al., *CARM1-expressing ovarian cancer depends on the histone methyltransferase EZH2 activity*. *Nat Commun*, 2018. **9**(1): p. 631.
490. Koh, S.S., et al., *Synergistic enhancement of nuclear receptor function by p160 coactivators and two coactivators with protein methyltransferase activities*. *J Biol Chem*, 2001. **276**(2): p. 1089-98.
491. Koh, S.S., et al., *Synergistic coactivator function by coactivator-associated arginine methyltransferase (CARM) 1 and beta-catenin with two different classes of DNA-binding transcriptional activators*. *J Biol Chem*, 2002. **277**(29): p. 26031-5.
492. Lee, Y.H., M.T. Bedford, and M.R. Stallcup, *Regulated recruitment of tumor suppressor BRCA1 to the p21 gene by coactivator methylation*. *Genes Dev*, 2011. **25**(2): p. 176-88.
493. Bao, J., et al., *The arginine methyltransferase CARM1 represses p300\*ACT\*CREMtau activity and is required for spermiogenesis*. *Nucleic Acids Res*, 2018. **46**(9): p. 4327-4343.
494. Lee, Y.H., et al., *Regulation of coactivator complex assembly and function by protein arginine methylation and demethylation*. *Proc Natl Acad Sci U S A*, 2005. **102**(10): p. 3611-6.
495. Chevillard-Briet, M., D. Trouche, and L. Vandell, *Control of CBP co-activating activity by arginine methylation*. *EMBO J*, 2002. **21**(20): p. 5457-66.
496. Ceschin, D.G., et al., *Methylation specifies distinct estrogen-induced binding site repertoires of CBP to chromatin*. *Genes Dev*, 2011. **25**(11): p. 1132-46.
497. Naeem, H., et al., *The activity and stability of the transcriptional coactivator p/CIP/SRC-3 are regulated by CARM1-dependent methylation*. *Mol Cell Biol*, 2007. **27**(1): p. 120-34.
498. Feng, Q., et al., *Signaling within a coactivator complex: methylation of SRC-3/AIB1 is a molecular switch for complex disassembly*. *Mol Cell Biol*, 2006. **26**(21): p. 7846-57.
499. Purcell, D.J., et al., *Novel CARM1-Interacting Protein, DZIP3, Is a Transcriptional Coactivator of Estrogen Receptor-alpha*. *Mol Endocrinol*, 2015. **29**(12): p. 1708-19.
500. Zhao, X. and E.N. Benveniste, *Transcriptional activation of human matrix metalloproteinase-9 gene expression by multiple co-activators*. *J Mol Biol*, 2008. **383**(5): p. 945-56.
501. An, W., J. Kim, and R.G. Roeder, *Ordered cooperative functions of PRMT1, p300, and CARM1 in transcriptional activation by p53*. *Cell*, 2004. **117**(6): p. 735-48.
502. Chen, S.L., et al., *The coactivator-associated arginine methyltransferase is necessary for muscle differentiation: CARM1 coactivates myocyte enhancer factor-2*. *J Biol Chem*, 2002. **277**(6): p. 4324-33.



503. Jayne, S., K.M. Rothgiesser, and M.O. Hottiger, *CARM1 but not its enzymatic activity is required for transcriptional coactivation of NF-kappaB-dependent gene expression*. J Mol Biol, 2009. **394**(3): p. 485-95.
504. Lin, W., et al., *Regulation of Nrf2 transactivation domain activity by p160 RAC3/SRC3 and other nuclear co-regulators*. J Biochem Mol Biol, 2006. **39**(3): p. 304-10.
505. Hernando, C.E., et al., *Genome wide comparative analysis of the effects of PRMT5 and PRMT4/CARM1 arginine methyltransferases on the Arabidopsis thaliana transcriptome*. BMC Genomics, 2015. **16**: p. 192.
506. Fox, A.H., et al., *Paraspeckles: Where Long Noncoding RNA Meets Phase Separation*. Trends Biochem Sci, 2018. **43**(2): p. 124-135.
507. Morishita, H. and N. Mizushima, *Diverse Cellular Roles of Autophagy*. Annu Rev Cell Dev Biol, 2019. **35**: p. 453-475.
508. Bento, C.F., et al., *Mammalian Autophagy: How Does It Work?* Annu Rev Biochem, 2016. **85**: p. 685-713.
509. Liu, Y., et al., *A C9orf72-CARM1 axis regulates lipid metabolism under glucose starvation-induced nutrient stress*. Genes Dev, 2018. **32**(21-22): p. 1380-1397.
510. Wei, X., et al., *SKP2 Promotes Hepatocellular Carcinoma Progression Through Nuclear AMPK-SKP2-CARM1 Signaling Transcriptionally Regulating Nutrient-Deprived Autophagy Induction*. Cell Physiol Biochem, 2018. **47**(6): p. 2484-2497.
511. Liu, F., et al., *PKM2 methylation by CARM1 activates aerobic glycolysis to promote tumorigenesis*. Nat Cell Biol, 2017. **19**(11): p. 1358-1370.
512. Zhong, X.Y., et al., *CARM1 Methylates GAPDH to Regulate Glucose Metabolism and Is Suppressed in Liver Cancer*. Cell Rep, 2018. **24**(12): p. 3207-3223.
513. Wang, Y.P., et al., *Arginine Methylation of MDH1 by CARM1 Inhibits Glutamine Metabolism and Suppresses Pancreatic Cancer*. Mol Cell, 2016. **64**(4): p. 673-687.
514. Ito, T., et al., *Arginine methyltransferase CARM1/PRMT4 regulates endochondral ossification*. BMC Dev Biol, 2009. **9**: p. 47.
515. Kim, J., et al., *Loss of CARM1 results in hypomethylation of thymocyte cyclic AMP-regulated phosphoprotein and deregulated early T cell development*. J Biol Chem, 2004. **279**(24): p. 25339-44.
516. Li, J., et al., *Coactivator-associated arginine methyltransferase 1 regulates fetal hematopoiesis and thymocyte development*. J Immunol, 2013. **190**(2): p. 597-604.
517. Yadav, N., et al., *CARM1 promotes adipocyte differentiation by coactivating PPARgamma*. EMBO Rep, 2008. **9**(2): p. 193-8.
518. Kawabe, Y., et al., *Carm1 regulates Pax7 transcriptional activity through MLL1/2 recruitment during asymmetric satellite stem cell divisions*. Cell Stem Cell, 2012. **11**(3): p. 333-45.

519. O'Brien, K.B., et al., *CARM1 is required for proper control of proliferation and differentiation of pulmonary epithelial cells*. *Development*, 2010. **137**(13): p. 2147-56.
520. Parfitt, D.E. and M. Zernicka-Goetz, *Epigenetic modification affecting expression of cell polarity and cell fate genes to regulate lineage specification in the early mouse embryo*. *Mol Biol Cell*, 2010. **21**(15): p. 2649-60.
521. Panamarova, M., et al., *The BAF chromatin remodelling complex is an epigenetic regulator of lineage specification in the early mouse embryo*. *Development*, 2016. **143**(8): p. 1271-83.
522. Sun, H., et al., *CARM1 is heterogeneous in mouse four-cell embryo and important to blastocyst development*. *Reproduction*, 2020. **159**(1): p. 91-104.
523. Shi, J., et al., *Dynamic transcriptional symmetry-breaking in pre-implantation mammalian embryo development revealed by single-cell RNA-seq*. *Development*, 2015. **142**(20): p. 3468-77.
524. Xu, Z., et al., *MicroRNA-181 regulates CARM1 and histone arginine methylation to promote differentiation of human embryonic stem cells*. *PLoS One*, 2013. **8**(1): p. e53146.
525. Choi, S., et al., *Regulation of Pluripotency-related Genes and Differentiation in Mouse Embryonic Stem Cells by Direct Delivery of Cell-penetrating Peptide-conjugated CARM1 Recombinant Protein*. *Dev Reprod*, 2013. **17**(1): p. 9-16.
526. Wu, Q., et al., *CARM1 is required in embryonic stem cells to maintain pluripotency and resist differentiation*. *Stem Cells*, 2009. **27**(11): p. 2637-2645.
527. Quintero, C.M., et al., *CARM1 (PRMT4) Acts as a Transcriptional Coactivator during Retinoic Acid-Induced Embryonic Stem Cell Differentiation*. *J Mol Biol*, 2018. **430**(21): p. 4168-4182.
528. Selvi, B.R., et al., *CARM1 regulates astroglial lineage through transcriptional regulation of Nanog and posttranscriptional regulation by miR92a*. *Mol Biol Cell*, 2015. **26**(2): p. 316-26.
529. Dacwag, C.S., et al., *Distinct protein arginine methyltransferases promote ATP-dependent chromatin remodeling function at different stages of skeletal muscle differentiation*. *Mol Cell Biol*, 2009. **29**(7): p. 1909-21.
530. Mallappa, C., et al., *The expression of myogenic microRNAs indirectly requires protein arginine methyltransferase (Prmt)5 but directly requires Prmt4*. *Nucleic Acids Res*, 2011. **39**(4): p. 1243-55.
531. Cheng, H., et al., *Overexpression of CARM1 in breast cancer is correlated with poorly characterized clinicopathologic parameters and molecular subtypes*. *Diagn Pathol*, 2013. **8**: p. 129.
532. Habashy, H.O., et al., *The oestrogen receptor coactivator CARM1 has an oncogenic effect and is associated with poor prognosis in breast cancer*. *Breast Cancer Res Treat*, 2013. **140**(2): p. 307-16.

533. Davis, M.B., et al., *Expression and sub-cellular localization of an epigenetic regulator, co-activator arginine methyltransferase 1 (CARM1), is associated with specific breast cancer subtypes and ethnicity*. Mol Cancer, 2013. **12**(1): p. 40.
534. Nakayama, N., et al., *Cancer-related transcription regulator protein NAC1 forms a protein complex with CARM1 for ovarian cancer progression*. Oncotarget, 2018. **9**(47): p. 28408-28420.
535. Kim, Y.R., et al., *Differential CARM1 expression in prostate and colorectal cancer*. BMC Cancer, 2010. **10**: p. 197.
536. Hong, H., et al., *Aberrant expression of CARM1, a transcriptional coactivator of androgen receptor, in the development of prostate carcinoma and androgen-independent status*. Cancer, 2004. **101**(1): p. 83-9.
537. Li, S., et al., *The Overexpression of CARM1 Promotes Human Osteosarcoma Cell Proliferation through the pGSK3beta/beta-Catenin/cyclinD1 Signaling Pathway*. Int J Biol Sci, 2017. **13**(8): p. 976-984.
538. Behera, A.K., et al., *Functional interplay between YY1 and CARM1 promotes oral carcinogenesis*. Oncotarget, 2019. **10**(38): p. 3709-3724.
539. Elakoum, R., et al., *CARM1 and PRMT1 are dysregulated in lung cancer without hierarchical features*. Biochimie, 2014. **97**: p. 210-8.
540. Limm, K., et al., *Deregulation of protein methylation in melanoma*. Eur J Cancer, 2013. **49**(6): p. 1305-13.
541. Buljan, M., et al., *Systematic characterization of pan-cancer mutation clusters*. Molecular systems biology, 2018. **14**(3): p. e7974.
542. Liu, J., et al., *Arginine methylation-dependent LSD1 stability promotes invasion and metastasis of breast cancer*. EMBO Rep, 2020. **21**(2): p. e48597.
543. Hiken, J.F., et al., *Epigenetic activation of the prostaglandin receptor EP4 promotes resistance to endocrine therapy for breast cancer*. Oncogene, 2017. **36**(16): p. 2319-2327.
544. Mann, M., V. Cortez, and R. Vadlamudi, *PELP1 oncogenic functions involve CARM1 regulation*. Carcinogenesis, 2013. **34**(7): p. 1468-75.
545. Sanders, D.A., et al., *Genome-wide mapping of FOXM1 binding reveals co-binding with estrogen receptor alpha in breast cancer cells*. Genome Biol, 2013. **14**(1): p. R6.
546. Shirley, S.H., et al., *Transcriptional regulation of estrogen receptor-alpha by p53 in human breast cancer cells*. Cancer Res, 2009. **69**(8): p. 3405-14.
547. Fietze, S., et al., *CARM1 regulates estrogen-stimulated breast cancer growth through up-regulation of E2F1*. Cancer Res, 2008. **68**(1): p. 301-6.
548. Gao, W.W., et al., *JMJD6 Licenses ERalpha-Dependent Enhancer and Coding Gene Activation by Modulating the Recruitment of the CARM1/MED12 Co-activator Complex*. Mol Cell, 2018. **70**(2): p. 340-357 e8.
549. Karakashev, S., et al., *EZH2 Inhibition Sensitizes CARM1-High, Homologous Recombination Proficient Ovarian Cancer to PARP Inhibition*. Cancer Cell, 2020. **37**(2): p. 157-167 e6.

550. Majumder, S., et al., *Involvement of arginine methyltransferase CARM1 in androgen receptor function and prostate cancer cell viability*. Prostate, 2006. **66**(12): p. 1292-301.
551. Veazey, K.J., et al., *CARM1 inhibition reduces histone acetyltransferase activity causing synthetic lethality in CREBBP/EP300-mutated lymphomas*. Leukemia, 2020.
552. Vito, P., et al., *Cloning of AIP1, a novel protein that associates with the apoptosis-linked gene ALG-2 in a Ca<sup>2+</sup>-dependent reaction*. J Biol Chem, 1999. **274**(3): p. 1533-40.
553. Missotten, M., et al., *Alix, a novel mouse protein undergoing calcium-dependent interaction with the apoptosis-linked-gene 2 (ALG-2) protein*. Cell Death Differ, 1999. **6**(2): p. 124-9.
554. Che, S., et al., *Identification and cloning of xp95, a putative signal transduction protein in Xenopus oocytes*. J Biol Chem, 1999. **274**(9): p. 5522-31.
555. Bissig, C. and J. Gruenberg, *ALIX and the multivesicular endosome: ALIX in Wonderland*. Trends Cell Biol, 2014. **24**(1): p. 19-25.
556. Vietri, M., M. Radulovic, and H. Stenmark, *The many functions of ESCRTs*. Nat Rev Mol Cell Biol, 2020. **21**(1): p. 25-42.
557. Odorizzi, G., *The multiple personalities of Alix*. J Cell Sci, 2006. **119**(Pt 15): p. 3025-32.
558. Laporte, M.H., et al., *Alix is required during development for normal growth of the mouse brain*. Sci Rep, 2017. **7**: p. 44767.
559. Campos, Y., et al., *Alix-mediated assembly of the actomyosin-tight junction polarity complex preserves epithelial polarity and epithelial barrier*. Nat Commun, 2016. **7**: p. 11876.
560. Eikenes, A.H., et al., *ALIX and ESCRT-III coordinately control cytokinetic abscission during germline stem cell division in vivo*. PLoS Genet, 2015. **11**(1): p. e1004904.
561. Ichioka, F., et al., *Brox, a novel farnesylated Bro1 domain-containing protein that associates with charged multivesicular body protein 4 (CHMP4)*. FEBS J, 2008. **275**(4): p. 682-92.
562. Ichioka, F., et al., *HD-PTP and Alix share some membrane-traffic related proteins that interact with their Bro1 domains or proline-rich regions*. Arch Biochem Biophys, 2007. **457**(2): p. 142-9.
563. Fisher, R.D., et al., *Structural and biochemical studies of ALIX/AIP1 and its role in retrovirus budding*. Cell, 2007. **128**(5): p. 841-52.
564. Elias, R.D., et al., *Proline-rich domain of human ALIX contains multiple TSG101-UEV interaction sites and forms phosphorylation-mediated reversible amyloids*. Proc Natl Acad Sci U S A, 2020. **117**(39): p. 24274-24284.
565. Kim, J., et al., *Structural basis for endosomal targeting by the Bro1 domain*. Dev Cell, 2005. **8**(6): p. 937-47.

566. McCullough, J., et al., *ALIX-CHMP4 interactions in the human ESCRT pathway*. Proc Natl Acad Sci U S A, 2008. **105**(22): p. 7687-91.
567. Katoh, K., et al., *CHMP4b is a major binding partner of the ALG-2-interacting protein Alix among the three CHMP4 isoforms*. Arch Biochem Biophys, 2004. **421**(1): p. 159-65.
568. Katoh, K., et al., *The ALG-2-interacting protein Alix associates with CHMP4b, a human homologue of yeast Snf7 that is involved in multivesicular body sorting*. J Biol Chem, 2003. **278**(40): p. 39104-13.
569. Schmidt, M.H.H., I. Dikic, and O. Bogler, *Src phosphorylation of Alix/AIP1 modulates its interaction with binding partners and antagonizes its activities*. J Biol Chem, 2005. **280**(5): p. 3414-25.
570. Matsuo, H., et al., *Role of LBPA and Alix in multivesicular liposome formation and endosome organization*. Science, 2004. **303**(5657): p. 531-4.
571. Sette, P., et al., *The ESCRT-associated protein Alix recruits the ubiquitin ligase Nedd4-1 to facilitate HIV-1 release through the LYPXnL L domain motif*. J Virol, 2010. **84**(16): p. 8181-92.
572. Pashkova, N., et al., *The yeast Alix homolog Bro1 functions as a ubiquitin receptor for protein sorting into multivesicular endosomes*. Dev Cell, 2013. **25**(5): p. 520-33.
573. Lee, S., et al., *Structural basis for viral late-domain binding to Alix*. Nat Struct Mol Biol, 2007. **14**(3): p. 194-9.
574. Pires, R., et al., *A crescent-shaped ALIX dimer targets ESCRT-III CHMP4 filaments*. Structure, 2009. **17**(6): p. 843-56.
575. Sun, S., et al., *Phosphorylation-Dependent Activation of the ESCRT Function of ALIX in Cytokinetic Abscission and Retroviral Budding*. Dev Cell, 2016. **36**(3): p. 331-43.
576. Dores, M.R., et al., *ALIX Regulates the Ubiquitin-Independent Lysosomal Sorting of the P2Y1 Purinergic Receptor via a YPX3L Motif*. PLoS One, 2016. **11**(6): p. e0157587.
577. Dores, M.R., et al., *ALIX binds a YPX(3)L motif of the GPCR PAR1 and mediates ubiquitin-independent ESCRT-III/MVB sorting*. J Cell Biol, 2012. **197**(3): p. 407-19.
578. Baietti, M.F., et al., *Syndecan-syntenin-ALIX regulates the biogenesis of exosomes*. Nat Cell Biol, 2012. **14**(7): p. 677-85.
579. Shibata, H., et al., *The penta-EF-hand protein ALG-2 interacts with a region containing PxY repeats in Alix/AIP1, which is required for the subcellular punctate distribution of the amino-terminal truncation form of Alix/AIP1*. J Biochem, 2004. **135**(1): p. 117-28.
580. Trioulier, Y., et al., *Alix, a protein regulating endosomal trafficking, is involved in neuronal death*. J Biol Chem, 2004. **279**(3): p. 2046-52.

581. Okumura, M., et al., *VPS37 isoforms differentially modulate the ternary complex formation of ALIX, ALG-2, and ESCRT-I*. *Biosci Biotechnol Biochem*, 2013. **77**(8): p. 1715-21.
582. von Schwedler, U.K., et al., *The protein network of HIV budding*. *Cell*, 2003. **114**(6): p. 701-13.
583. Lee, H.H., et al., *Midbody targeting of the ESCRT machinery by a noncanonical coiled coil in CEP55*. *Science*, 2008. **322**(5901): p. 576-80.
584. Carlton, J.G., M. Agromayor, and J. Martin-Serrano, *Differential requirements for Alix and ESCRT-III in cytokinesis and HIV-1 release*. *Proc Natl Acad Sci U S A*, 2008. **105**(30): p. 10541-6.
585. Morita, E., et al., *Human ESCRT and ALIX proteins interact with proteins of the midbody and function in cytokinesis*. *EMBO J*, 2007. **26**(19): p. 4215-27.
586. Rouka, E., et al., *Differential Recognition Preferences of the Three Src Homology 3 (SH3) Domains from the Adaptor CD2-associated Protein (CD2AP) and Direct Association with Ras and Rab Interactor 3 (RIN3)*. *J Biol Chem*, 2015. **290**(42): p. 25275-92.
587. Chen, B., et al., *The glioma-associated protein SETA interacts with AIP1/Alix and ALG-2 and modulates apoptosis in astrocytes*. *J Biol Chem*, 2000. **275**(25): p. 19275-81.
588. Chatellard-Cause, C., et al., *Alix (ALG-2-interacting protein X), a protein involved in apoptosis, binds to endophilins and induces cytoplasmic vacuolization*. *J Biol Chem*, 2002. **277**(32): p. 29108-15.
589. Rauch, S. and J. Martin-Serrano, *Multiple interactions between the ESCRT machinery and arrestin-related proteins: implications for PPXY-dependent budding*. *J Virol*, 2011. **85**(7): p. 3546-56.
590. Strack, B., et al., *AIP1/ALIX is a binding partner for HIV-1 p6 and EIAV p9 functioning in virus budding*. *Cell*, 2003. **114**(6): p. 689-99.
591. Martin-Serrano, J., T. Zang, and P.D. Bieniasz, *Role of ESCRT-I in retroviral budding*. *J Virol*, 2003. **77**(8): p. 4794-804.
592. Schmidt, M.H.H., et al., *SETA/CIN85/Ruk and its binding partner AIP1 associate with diverse cytoskeletal elements, including FAKs, and modulate cell adhesion*. *J Cell Sci*, 2003. **116**(Pt 14): p. 2845-55.
593. Kurakin, A.V., S. Wu, and D.E. Bredesen, *Atypical recognition consensus of CIN85/SETA/Ruk SH3 domains revealed by target-assisted iterative screening*. *J Biol Chem*, 2003. **278**(36): p. 34102-9.
594. Schmidt, M.H.H., et al., *Alix/AIP1 antagonizes epidermal growth factor receptor downregulation by the Cbl-SETA/CIN85 complex*. *Mol Cell Biol*, 2004. **24**(20): p. 8981-93.
595. Kim, J.M., et al., *CD2-associated protein haploinsufficiency is linked to glomerular disease susceptibility*. *Science*, 2003. **300**(5623): p. 1298-300.
596. Monzo, P., et al., *Clues to CD2-associated protein involvement in cytokinesis*. *Mol Biol Cell*, 2005. **16**(6): p. 2891-902.

597. Hikita, T., et al., *Src in endosomal membranes promotes exosome secretion and tumor progression*. Sci Rep, 2019. **9**(1): p. 3265.
598. Shi, X., et al., *Structural recognition mechanisms between human Src homology domain 3 (SH3) and ALG-2-interacting protein X (Alix)*. FEBS Lett, 2012. **586**(13): p. 1759-64.
599. Hornbeck, P.V., et al., *PhosphoSitePlus, 2014: mutations, PTMs and recalibrations*. Nucleic Acids Res, 2015. **43**(Database issue): p. D512-20.
600. Zhou, X., et al., *Decoding the intrinsic mechanism that prohibits ALIX interaction with ESCRT and viral proteins*. Biochem J, 2010. **432**(3): p. 525-34.
601. Dejournett, R.E., et al., *Phosphorylation of the proline-rich domain of Xp95 modulates Xp95 interaction with partner proteins*. Biochem J, 2007. **401**(2): p. 521-31.
602. Zhou, X., et al., *The CHMP4b- and Src-docking sites in the Bro1 domain are autoinhibited in the native state of Alix*. Biochem J, 2009. **418**(2): p. 277-84.
603. Votteler, J., et al., *Exploring the functional interaction between POSH and ALIX and the relevance to HIV-1 release*. BMC Biochem, 2009. **10**: p. 12.
604. Bongiovanni, A., et al., *Alix protein is substrate of Ozz-E3 ligase and modulates actin remodeling in skeletal muscle*. J Biol Chem, 2012. **287**(15): p. 12159-71.
605. Does, M.R., et al., *The alpha-arrestin ARRDC3 mediates ALIX ubiquitination and G protein-coupled receptor lysosomal sorting*. Mol Biol Cell, 2015. **26**(25): p. 4660-73.
606. Keren-Kaplan, T., et al., *Structure-based in silico identification of ubiquitin-binding domains provides insights into the ALIX-V:ubiquitin complex and retrovirus budding*. EMBO J, 2013. **32**(4): p. 538-51.
607. Dowlatshahi, D.P., et al., *ALIX is a Lys63-specific polyubiquitin binding protein that functions in retrovirus budding*. Dev Cell, 2012. **23**(6): p. 1247-54.
608. Sun, S., et al., *Unravelling the pivotal role of Alix in MVB sorting and silencing of the activated EGFR*. Biochem J, 2015. **466**(3): p. 475-87.
609. Romancino, D.P., et al., *Palmitoylation is a post-translational modification of Alix regulating the membrane organization of exosome-like small extracellular vesicles*. Biochim Biophys Acta Gen Subj, 2018. **1862**(12): p. 2879-2887.
610. Geoghegan, V., et al., *Comprehensive identification of arginine methylation in primary T cells reveals regulatory roles in cell signalling*. Nat Commun, 2015. **6**: p. 6758.
611. Guo, A., et al., *Immunoaffinity enrichment and mass spectrometry analysis of protein methylation*. Mol Cell Proteomics, 2014. **13**(1): p. 372-87.
612. Wang, K., et al., *Antibody-Free Approach for the Global Analysis of Protein Methylation*. Anal Chem, 2016. **88**(23): p. 11319-11327.
613. Lehman, S.M., et al., *Transcriptomic and proteomic regulation through abundant, dynamic, and independent arginine methylation by Type I and Type II PRMTs*. bioRxiv, 2020.

614. Carlton, J.G. and J. Martin-Serrano, *Parallels Between Cytokinesis and Retroviral Budding: A Role for the ESCRT Machinery*. Science, 2007. **316**: p. 1908-1912.
615. McDonald, B. and J. Martin-Serrano, *No strings attached: the ESCRT machinery in viral budding and cytokinesis*. J Cell Sci, 2009. **122**(Pt 13): p. 2167-77.
616. Pan, S., et al., *Involvement of the conserved adaptor protein Alix in actin cytoskeleton assembly*. J Biol Chem, 2006. **281**(45): p. 34640-50.
617. Cabezas, A., et al., *Alix regulates cortical actin and the spatial distribution of endosomes*. J Cell Sci, 2005. **118**(Pt 12): p. 2625-35.
618. Kowanetz, K., et al., *Identification of a novel proline-arginine motif involved in CIN85-dependent clustering of Cbl and down-regulation of epidermal growth factor receptors*. J Biol Chem, 2003. **278**(41): p. 39735-46.
619. Soubeyran, P., et al., *Cbl-CIN85-endophilin complex mediates ligand-induced downregulation of EGF receptors*. Nature, 2002. **416**(6877): p. 183-7.
620. Mahul-Mellier, A.L., et al., *Alix, making a link between apoptosis-linked gene-2, the endosomal sorting complexes required for transport, and neuronal death in vivo*. J Neurosci, 2006. **26**(2): p. 542-9.
621. Lopez, S. and C. Arias, *How viruses hijack endocytic machinery*. Nature Education, 2010. **3**(9): p. 16.
622. Scourfield, E.J. and J. Martin-Serrano, *Growing functions of the ESCRT machinery in cell biology and viral replication*. Biochem Soc Trans, 2017. **45**(3): p. 613-634.
623. Votteler, J. and W.I. Sundquist, *Virus budding and the ESCRT pathway*. Cell Host Microbe, 2013. **14**(3): p. 232-41.
624. Zeev-Ben-Mordehai, T., et al., *Crystal Structure of the Herpesvirus Nuclear Egress Complex Provides Insights into Inner Nuclear Membrane Remodeling*. Cell Rep, 2015. **13**(12): p. 2645-52.
625. Bigalke, J.M., et al., *Membrane deformation and scission by the HSV-1 nuclear egress complex*. Nat Commun, 2014. **5**: p. 4131.
626. Arii, J., et al., *ESCRT-III mediates budding across the inner nuclear membrane and regulates its integrity*. Nat Commun, 2018. **9**(1): p. 3379.
627. Yadav, S., et al., *EBV early lytic protein BFRF1 alters emerin distribution and post-translational modification*. Virus Res, 2017. **232**: p. 113-122.
628. Lee, C.P., et al., *The ESCRT machinery is recruited by the viral BFRF1 protein to the nucleus-associated membrane for the maturation of Epstein-Barr Virus*. PLoS Pathog, 2012. **8**(9): p. e1002904.
629. Martin-Serrano, J., T. Zang, and P.D. Bieniasz, *HIV-1 and Ebola virus encode small peptide motifs that recruit Tsg101 to sites of particle assembly to facilitate egress*. Nat Med, 2001. **7**(12): p. 1313-9.
630. Garrus, J.E., et al., *Tsg101 and the vacuolar protein sorting pathway are essential for HIV-1 budding*. Cell, 2001. **107**(1): p. 55-65.
631. Bleck, M., et al., *Temporal and spatial organization of ESCRT protein recruitment during HIV-1 budding*. Proc Natl Acad Sci U S A, 2014. **111**(33): p. 12211-6.



632. Zhai, Q., et al., *Structural and functional studies of ALIX interactions with YPX(n)L late domains of HIV-1 and EIAV*. Nat Struct Mol Biol, 2008. **15**(1): p. 43-9.
633. Falguieres, T., et al., *In vitro budding of intraluminal vesicles into late endosomes is regulated by Alix and Tsg101*. Mol Biol Cell, 2008. **19**(11): p. 4942-55.
634. Mathivanan, S., et al., *ExoCarta 2012: database of exosomal proteins, RNA and lipids*. Nucleic Acids Res, 2012. **40**(Database issue): p. D1241-4.
635. Thery, C., M. Ostrowski, and E. Segura, *Membrane vesicles as conveyors of immune responses*. Nat Rev Immunol, 2009. **9**(8): p. 581-93.
636. Xie, C., et al., *The role of extracellular vesicles from different origin in the microenvironment of head and neck cancer*. Mol Cancer, 2019. **18**(1): p. 83.
637. Monypenny, J., et al., *ALIX Regulates Tumor-Mediated Immunosuppression by Controlling EGFR Activity and PD-L1 Presentation*. Cell Rep, 2018. **24**(3): p. 630-641.
638. Mierzwa, B. and D.W. Gerlich, *Cytokinetic abscission: molecular mechanisms and temporal control*. Dev Cell, 2014. **31**(5): p. 525-38.
639. Fremont, S. and A. Echard, *Membrane Traffic in the Late Steps of Cytokinesis*. Curr Biol, 2018. **28**(8): p. R458-R470.
640. Dionne, L.K., X.J. Wang, and R. Prekeris, *Midbody: from cellular junk to regulator of cell polarity and cell fate*. Curr Opin Cell Biol, 2015. **35**: p. 51-8.
641. Skop, A.R., et al., *Dissection of the mammalian midbody proteome reveals conserved cytokinesis mechanisms*. Science, 2004. **305**(5680): p. 61-6.
642. Capalbo, L., et al., *The midbody interactome reveals unexpected roles for PP1 phosphatases in cytokinesis*. Nat Commun, 2019. **10**(1): p. 4513.
643. Addi, C., et al., *The Flemmingsome reveals an ESCRT-to-membrane coupling via ALIX/syntenin/syndecan-4 required for completion of cytokinesis*. Nat Commun, 2020. **11**(1): p. 1941.
644. Rai, A., et al., *Secreted midbody remnants are a class of extracellular vesicles molecularly distinct from exosomes and microparticles*. Commun Biol, 2021. **4**(1): p. 400.
645. Bastos, R.N. and F.A. Barr, *Plk1 negatively regulates Cep55 recruitment to the midbody to ensure orderly abscission*. J Cell Biol, 2010. **191**(4): p. 751-60.
646. Zhao, W.M., A. Seki, and G. Fang, *Cep55, a microtubule-bundling protein, associates with centralspindlin to control the midbody integrity and cell abscission during cytokinesis*. Mol Biol Cell, 2006. **17**(9): p. 3881-96.
647. Tang, S., et al., *ESCRT-III activation by parallel action of ESCRT-I/II and ESCRT-0/Bro1 during MVB biogenesis*. Elife, 2016. **5**.
648. Christ, L., et al., *ALIX and ESCRT-I/II function as parallel ESCRT-III recruiters in cytokinetic abscission*. J Cell Biol, 2016. **212**(5): p. 499-513.
649. Goliand, I., et al., *Inhibition of ESCRT-II-CHMP6 interactions impedes cytokinetic abscission and leads to cell death*. Mol Biol Cell, 2014. **25**(23): p. 3740-8.

650. Guizetti, J., et al., *Cortical constriction during abscission involves helices of ESCRT-III-dependent filaments*. *Science*, 2011. **331**(6024): p. 1616-20.
651. Bhowmick, R., et al., *The RIF1-PP1 Axis Controls Abscission Timing in Human Cells*. *Curr Biol*, 2019. **29**(7): p. 1232-1242 e5.
652. Maciejowski, J., et al., *Chromothripsis and Kataegis Induced by Telomere Crisis*. *Cell*, 2015. **163**(7): p. 1641-54.
653. Bembenek, J.N., et al., *Condensin and the spindle midzone prevent cytokinesis failure induced by chromatin bridges in *C. elegans* embryos*. *Curr Biol*, 2013. **23**(11): p. 937-46.
654. Mendoza, M., et al., *A mechanism for chromosome segregation sensing by the NoCut checkpoint*. *Nat Cell Biol*, 2009. **11**(4): p. 477-83.
655. Steigemann, P., et al., *Aurora B-mediated abscission checkpoint protects against tetraploidization*. *Cell*, 2009. **136**(3): p. 473-84.
656. Norden, C., et al., *The NoCut pathway links completion of cytokinesis to spindle midzone function to prevent chromosome breakage*. *Cell*, 2006. **125**(1): p. 85-98.
657. Thoresen, S.B., et al., *ANCHR mediates Aurora-B-dependent abscission checkpoint control through retention of VPS4*. *Nat Cell Biol*, 2014. **16**(6): p. 550-60.
658. Nahse, V., et al., *The Abscission Checkpoint: Making It to the Final Cut*. *Trends Cell Biol*, 2017. **27**(1): p. 1-11.
659. Loibl, S., et al., *Breast cancer*. *Lancet*, 2021. **397**(10286): p. 1750-1769.
660. Manjunath, M. and B. Choudhary, *Triple-negative breast cancer: A run-through of features, classification and current therapies*. *Oncol Lett*, 2021. **22**(1): p. 512.
661. Poulard, C., L. Corbo, and M. Le Romancer, *Protein arginine methylation/demethylation and cancer*. *Oncotarget*, 2016. **7**(41): p. 67532-67550.
662. Mohammed, M.K., et al., *Wnt/beta-catenin signaling plays an ever-expanding role in stem cell self-renewal, tumorigenesis and cancer chemoresistance*. *Genes Dis*, 2016. **3**(1): p. 11-40.
663. Maire, V., et al., *Polo-like Kinase 1: A Potential Therapeutic Option in Combination with Conventional Chemotherapy for the Management of Patients with Triple-Negative Breast Cancer*. *Cancer Research*, 2013. **73**: p. 813-823.
664. Maubant, S., et al., *Transcriptome analysis of Wnt3a-treated triple-negative breast cancer cells*. *PLoS One*, 2015. **10**(4): p. e0122333.
665. Gyorffy, B., et al., *An online survival analysis tool to rapidly assess the effect of 22,277 genes on breast cancer prognosis using microarray data of 1,809 patients*. *Breast Cancer Res Treat*, 2010. **123**(3): p. 725-31.
666. Torres, V.I., J.A. Godoy, and N.C. Inestrosa, *Modulating Wnt signaling at the root: Porcupine and Wnt acylation*. *Pharmacol Ther*, 2019. **198**: p. 34-45.

667. Subramanian, A., et al., *Gene set enrichment analysis: a knowledge-based approach for interpreting genome-wide expression profiles*. Proc Natl Acad Sci U S A, 2005. **102**(43): p. 15545-50.
668. Mootha, V.K., et al., *PGC-1alpha-responsive genes involved in oxidative phosphorylation are coordinately downregulated in human diabetes*. Nat Genet, 2003. **34**(3): p. 267-73.
669. Di Veroli, G.Y., et al., *Combenefit: an interactive platform for the analysis and visualization of drug combinations*. Bioinformatics, 2016. **32**(18): p. 2866-8.
670. Tang, J., K. Wennerberg, and T. Aittokallio, *What is synergy? The Saariselka agreement revisited*. Front Pharmacol, 2015. **6**: p. 181.
671. Shrivastav, S., et al., *Activation of cyclophosphamide for in vitro testing of cell sensitivity*. Cancer Res, 1980. **40**(12): p. 4443-5.
672. Khandelwal Gilman, K.A., et al., *Complex interactions of lovastatin with 10 chemotherapeutic drugs: a rigorous evaluation of synergism and antagonism*. BMC Cancer, 2021. **21**(1): p. 356.
673. Corkery, B., et al., *Epidermal growth factor receptor as a potential therapeutic target in triple-negative breast cancer*. Ann Oncol, 2009. **20**(5): p. 862-7.
674. Wang, J., et al., *PRMT1 is a novel molecular therapeutic target for clear cell renal cell carcinoma*. Theranostics, 2021. **11**(11): p. 5387-5403.
675. Yin, X.K., et al., *PRMT1 enhances oncogenic arginine methylation of NONO in colorectal cancer*. Oncogene, 2021. **40**(7): p. 1375-1389.
676. Zhang, X.P., et al., *PRMT1 Promoted HCC Growth and Metastasis In Vitro and In Vivo via Activating the STAT3 Signalling Pathway*. Cell Physiol Biochem, 2018. **47**(4): p. 1643-1654.
677. Chuang, C.Y., et al., *PRMT1 expression is elevated in head and neck cancer and inhibition of protein arginine methylation by adenosine dialdehyde or PRMT1 knockdown downregulates proliferation and migration of oral cancer cells*. Oncol Rep, 2017. **38**(2): p. 1115-1123.
678. Plotnikov, A., et al., *PRMT1 inhibition induces differentiation of colon cancer cells*. Sci Rep, 2020. **10**(1): p. 20030.
679. Lim, Y., et al., *Proteome-wide identification of arginine methylation in colorectal cancer tissues from patients*. Proteome Sci, 2020. **18**: p. 6.
680. Hua, Z.Y., et al., *PRMT1 promotes neuroblastoma cell survival through ATF5*. Oncogenesis, 2020. **9**(5): p. 50.
681. Ali, R. and M.K. Wendt, *The paradoxical functions of EGFR during breast cancer progression*. Signal Transduct Target Ther, 2017. **2**.
682. Iderzorig, T., et al., *Comparison of EMT mediated tyrosine kinase inhibitor resistance in NSCLC*. Biochem Biophys Res Commun, 2018. **496**(2): p. 770-777.
683. Dominici, C., et al., *Synergistic effects of type I PRMT and PARP inhibitors against non-small cell lung cancer cells*. Clin Epigenetics, 2021. **13**(1): p. 54.

684. van Schie, E.H. and R. van Amerongen, *Aberrant WNT/CTNNB1 Signaling as a Therapeutic Target in Human Breast Cancer: Weighing the Evidence*. *Front Cell Dev Biol*, 2020. **8**: p. 25.
685. Bai, X., et al., *Cancer stem cell in breast cancer therapeutic resistance*. *Cancer Treat Rev*, 2018. **69**: p. 152-163.
686. Lopez Almeida, L., et al., *The SCRIB Paralog LANO/LRRC1 Regulates Breast Cancer Stem Cell Fate through WNT/beta-Catenin Signaling*. *Stem Cell Reports*, 2018. **11**(5): p. 1040-1050.
687. Ryu, J.W., et al., *Novel prognostic marker PRMT1 regulates cell growth via downregulation of CDKN1A in HCC*. *Oncotarget*, 2017. **8**(70): p. 115444-115455.
688. Schatoff, E.M., B.I. Leach, and L.E. Dow, *Wnt Signaling and Colorectal Cancer*. *Curr Colorectal Cancer Rep*, 2017. **13**(2): p. 101-110.
689. Marchesin, V., et al., *ARF6-JIP3/4 regulate endosomal tubules for MT1-MMP exocytosis in cancer invasion*. *J Cell Biol*, 2015. **211**(2): p. 339-58.
690. Al-Dhaheeri, M., et al., *CARM1 is an important determinant of ERalpha-dependent breast cancer cell differentiation and proliferation in breast cancer cells*. *Cancer Res*, 2011. **71**(6): p. 2118-28.
691. Lee, J. and M.T. Bedford, *PABP1 identified as an arginine methyltransferase substrate using high-density protein arrays*. *EMBO Rep*, 2002. **3**(3): p. 268-73.
692. Poulard, C., et al., *Proximity ligation assay to detect and localize the interactions of ERalpha with PI3-K and Src in breast cancer cells and tumor samples*. *Methods Mol Biol*, 2014. **1204**: p. 135-43.
693. Ge, S.X., D. Jung, and R. Yao, *ShinyGO: a graphical gene-set enrichment tool for animals and plants*. *Bioinformatics*, 2020. **36**(8): p. 2628-2629.
694. Huesgen, P.F., et al., *LysargiNase mirrors trypsin for protein C-terminal and methylation-site identification*. *Nat Methods*, 2015. **12**(1): p. 55-8.
695. Zheng, M., et al., *ESRP1 regulates alternative splicing of CARM1 to sensitize small cell lung cancer cells to chemotherapy by inhibiting TGF-beta/Smad signaling*. *Aging (Albany NY)*, 2021. **13**(3): p. 3554-3572.
696. Antonysamy, S., *The Structure and Function of the PRMT5:MEP50 Complex*. *Subcell Biochem*, 2017. **83**: p. 185-194.
697. Cho, K.F., et al., *Proximity labeling in mammalian cells with TurboID and split-TurboID*. *Nat Protoc*, 2020. **15**(12): p. 3971-3999.
698. Ong, S.E., G. Mittler, and M. Mann, *Identifying and quantifying in vivo methylation sites by heavy methyl SILAC*. *Nat Methods*, 2004. **1**(2): p. 119-26.
699. Uhlmann, T., et al., *A method for large-scale identification of protein arginine methylation*. *Mol Cell Proteomics*, 2012. **11**(11): p. 1489-99.
700. Boisvert, F.M., et al., *A proteomic analysis of arginine-methylated protein complexes*. *Mol Cell Proteomics*, 2003. **2**(12): p. 1319-30.
701. Lens, S.M.A. and R.H. Medema, *Cytokinesis defects and cancer*. *Nat Rev Cancer*, 2019. **19**(1): p. 32-45.

702. Wang, L., et al., *MED12 methylation by CARM1 sensitizes human breast cancer cells to chemotherapy drugs*. *Sci Adv*, 2015. **1**(9): p. e1500463.
703. Kowal, J., et al., *Proteomic comparison defines novel markers to characterize heterogeneous populations of extracellular vesicle subtypes*. *Proc Natl Acad Sci U S A*, 2016. **113**(8): p. E968-77.
704. Martin-Jaular, L., et al., *Unbiased proteomic profiling of host cell extracellular vesicle composition and dynamics upon HIV-1 infection*. *EMBO J*, 2021. **40**(8): p. e105492.
705. Chukwuma, V.U., et al., *Association of VH4-59 Antibody Variable Gene Usage with Recognition of an Immunodominant Epitope on the HIV-1 Gag Protein*. *PLoS One*, 2015. **10**(7): p. e0133509.
706. Shen, W.W., et al., *EHD2 is a Predictive Biomarker of Chemotherapy Efficacy in Triple Negative Breast Carcinoma*. *Sci Rep*, 2020. **10**(1): p. 7998.
707. Lodillinsky, C., et al., *p63/MT1-MMP axis is required for in situ to invasive transition in basal-like breast cancer*. *Oncogene*, 2016. **35**(3): p. 344-57.
708. Poulard, C., et al., *Using proximity ligation assay to detect protein arginine methylation*. *Methods*, 2020. **175**: p. 66-71.
709. Pouillet, P., S. Carpentier, and E. Barillot, *myProMS, a web server for management and validation of mass spectrometry-based proteomic data*. *Proteomics*, 2007. **7**(15): p. 2553-6.
710. de Graaf, E.L., et al., *Improving SRM assay development: a global comparison between triple quadrupole, ion trap, and higher energy CID peptide fragmentation spectra*. *J Proteome Res*, 2011. **10**(9): p. 4334-41.
711. Vacher, S., et al., *High AHR expression in breast tumors correlates with expression of genes from several signaling pathways namely inflammation and endogenous tryptophan metabolism*. *PLoS One*, 2018. **13**(1): p. e0190619.

# ANNEXES

# **ANNEXE I: CARM1/PRMT4: Making Its Mark beyond Its Function as a Transcriptional Coactivator**

## Review

# CARM1/PRMT4: Making Its Mark beyond Its Function as a Transcriptional Coactivator

Samyuktha Suresh,<sup>1</sup> Solène Huard,<sup>1</sup> and Thierry Dubois <sup>1,\*</sup>

**Coactivator-associated arginine methyltransferase 1 (CARM1), identified 20 years ago as a coregulator of transcription, is an enzyme that catalyzes arginine methylation of proteins. Beyond its well-established involvement in the regulation of transcription, the physiological functions of CARM1 are still poorly understood. However, recent studies have revealed novel roles of CARM1 in autophagy, metabolism, paraspeckles, and early development. In addition, CARM1 is emerging as an attractive therapeutic target and a drug response biomarker for certain types of cancer. Here, we provide a comprehensive overview of the structure of CARM1 and its post-translational modifications, its various functions, apart from transcriptional coactivation, and its involvement in cancer.**

## CARM1 Was Discovered as a Transcriptional Coactivator

CARM1 (also known as PRMT4) was discovered by the group of Stallcup [1] as the first **protein arginine methyltransferase (PRMT; see Glossary)** to be linked to transcriptional activation by methylating and/or regulating histone H3 and non-histone proteins, such as coactivators and transcription factors [2–7]. CARM1 was believed to be mainly involved in transcription until recently; however, studies have now uncovered new roles for this enzyme in cellular pathways. In this review, we will not address the well-known role of CARM1 in transcription, but rather focus on its newly emerging functions, such as its role in mammalian development and cell differentiation, autophagy and metabolism, RNA regulation (pre-mRNA splicing, mRNA retention, mRNA stability), and its involvement in cancer. We also outline its structure and post-translational modifications and provide a complete list of CARM1 substrates identified thus far.

## Insights into the X-Ray Structure of CARM1

The first crystallographic structures of CARM1 revealed the presence of an N-terminal **pleckstrin homology-like domain (PH-like)**, a C-terminal transactivase domain, and a central catalytic domain containing the four conserved PRMT motifs: motif I (YFxxY), motif II (DVGxGxG), motif III (SE<sup>257</sup>xMGxxLxxE<sup>266</sup>xM, also called double E-loop), and motif IV (TH<sup>414</sup>WxQ; amino acids are numbered according to human CARM1, hereafter; Figure 1A, Key Figure). These motifs are essential for binding of the cofactor SAM (S-adenosyl methionine) and the substrate arginine in two adjacent distinct pockets [8,9]. The N- and C-terminal domains of CARM1 are not necessary for its methyltransferase activity but essential for substrate recognition [10] and its transcription-mediated activation [11]. CARM1 exists as a dimer [8,9] and dimerization may be necessary for its methyltransferase activity [12], like other PRMTs [13]. The dimerization arm of CARM1, within its catalytic domain, contains a unique insertion of 9–10 residues that generates a larger and less negatively charged central cavity than the PRMT1 dimer [8,9], perhaps explaining why CARM1 has distinctive substrates.

The structure of the CARM1 catalytic domain complexed with a peptide substrate has been challenging to obtain but was recently solved using a non-hydrolyzable SAM mimic [14] or a

## Highlights

In addition to the initially described activity as a transcriptional coactivator, the emerging functions of CARM1 include autophagy, metabolism, early development, pre-mRNA splicing and export, and localization to paraspeckles.

Aside from post-translationally modifying its substrates, CARM1 itself undergoes several modifications, such as phosphorylation, O-GlcNAcylation, ubiquitination, and auto-methylation.

CARM1 is composed of a central catalytic and unique N- and C-terminal domains that are important for binding to its partners.

CARM1 is the only known PRMT to preferentially methylate a proline-rich sequence.

A spliced isoform of *CARM1* is the major variant expressed in BCs.

CARM1 has now emerged as an attractive therapeutic target/biomarker of response for various types of cancer.

Specific CARM1 inhibitors show anti-tumor activity *in vivo* in myeloma models.

<sup>1</sup>Institut Curie – PSL Research University, Translational Research Department, Breast Cancer Biology Group, 75005 Paris, France

\*Correspondence: [thierry.dubois@curie.fr](mailto:thierry.dubois@curie.fr) (T. Dubois).





peptide-based transition-state mimic [15]. The guanidine moiety of the substrate arginine is oriented by the two glutamate residues (E257 and E266) of the double E-loop and binds to H414 of motif IV via several hydrogen bonds. Additional residues within the substrate-binding pocket permit interactions with the conformationally constrained proline residues surrounding the substrate arginine, thus explaining the preference of CARM1 for proline-rich motifs in substrates [14].

Obtaining the structure of full-length CARM1, alone or with partners, having failed thus far, is an ongoing challenge in the field.

### Alternatively Spliced Isoforms of CARM1

Several spliced forms of *CARM1* have been reported, which may explain apparent discrepancies in the literature concerning the function of CARM1 and its potential involvement in cancer (reviewed in [16]).

Five rat *CARM1* isoforms (v1–v5) have been isolated [17,18]: *CARM1*-v1 is the full-length version of *CARM1* (referred to later as CARM1-FL), containing all 16 exons, whereas *CARM1*-v2 is generated by the retention of intron 15, *CARM1*-v3 by the retention of introns 14 and 15, *CARM1*-v4 by exon 15 skipping (referred to later as *CARM1*- $\Delta E15$ ), and *CARM1*-v5 includes a part of intron 15. In *Xenopus*, CARM1a (exon 14 skipping) and CARM1b (equivalent to CARM1-FL) have been reported, and only CARM1a activates the transcription of liganded thyroid hormone receptor [19].

By contrast, only two variants, CARM1-FL and CARM1- $\Delta E15$  (Figure 1A), are well expressed in breast [20] and hematopoietic [21] cell lines and capable of forming homo and heterodimers [20]. CARM1-FL is the most highly expressed form of CARM1 in healthy brain, heart, skeletal muscle, and testis [17,20], whereas CARM1- $\Delta E15$  is predominant in a panel of **breast cancer (BC)** cell lines and breast tumors [20,22]. The overexpression of CARM1-FL (and not CARM1- $\Delta E15$ ) [22] or the knockout (KO) of all CARM1 isoforms impairs cell proliferation of a BC cell line that mainly expresses CARM1- $\Delta E15$  [22,23]. Thus, the authors suggest that CARM1- $\Delta E15$  may be the oncogenic CARM1 variant, but it is unclear to what extent this can be generalized. The use of antibodies that recognize either CARM1-FL or all CARM1 isoforms suggests differential localization of CARM1 isoforms in two cancer cell lines (breast and ovarian): mainly nuclear for CARM1-FL, and potentially mainly cytosolic for CARM1- $\Delta E15$  [22]. However, such localization may vary depending on the cell type and/or tissue studied. Histone H3 [17,18,20,24], TP2 [18], and PABP1 [20] are methylated *in vitro* by both isoforms, whereas Pax7 is preferentially methylated by CARM1- $\Delta E15$  [24], possibly due to constrained accessibility to CARM1-FL.

Although cells can express differential levels of various CARM1 isoforms, the majority of studies and their conclusions, thus far, have not taken into account their existence.

### CARM1 Itself Is Post-translationally Modified

CARM1 catalyzes the methylation of proteins but is itself subjected to various post-translational modifications, such as phosphorylation, O-GlcNAcylation, ubiquitination, and methylation (Figure 1A).

CARM1 is phosphorylated on several residues, T131 [25], S216 [26], S228 [12,27], S447 [28], and S595 (corresponding to S572 of CARM1- $\Delta E15$ ) [24]. Glycogen synthase kinase 3 beta (GSK3 $\beta$ ) phosphorylates CARM1 on T131, within the PH-like domain, to protect it from ubiquitin-mediated proteasomal degradation [25]. S216 [26] and S228 [12,27] are located within the catalytic domain and are phosphorylated by an unknown kinase and protein kinase C [27],

### Glossary

**Adipogenesis:** the process of the development of fat cells or adipocytes in the body.

**Asymmetric dimethyl arginine (ADMA):** the addition of two methyl groups to the same guanidino nitrogen by type I PRMTs (PRMT1–3, CARM1, PRMT6, and PRMT8).

**Autophagy:** the process of lysosome-mediated cellular self-digestion, which guarantees the quality of proteins and organelles by eliminating those that are damaged and allows cell survival during starvation and stress.

**Breast cancer (BC):** a heterogeneous disease categorized into subtypes depending on the expression of hormone receptors [ER and progesterone receptor (PR)] and HER2 (human epidermal growth factor 2). These include luminal (ER+/PR+), HER2, and triple-negative breast cancer (ER-/PR-/HER2-).

**CARM1 speckles:** membraneless bodies in the nucleus, apart from paraspeckles, that contain CARM1, as reported by Hupalowska *et al.* [51]. Their components and functions have not yet been studied.

**Embryonic stem cells (ESCs):** stem cells derived from the undifferentiated ICM that are pluripotent, with the ability to self-renew and give rise to the three germ layers of the body – ectoderm, endoderm, and mesoderm.

**Endochondral ossification:** one of the essential processes in the development of the mammalian skeletal system, in which cartilage is replaced by bone.

**H3R17me2a:** asymmetrically dimethylated arginine 17 of histone H3, of which the reaction is catalyzed by CARM1.

**H3R26me2a:** asymmetrically dimethylated arginine 26 of histone H3, of which the reaction is catalyzed by CARM1.

**Hematopoiesis:** the process by which all cellular components of the blood and blood plasma are produced by the body.

**Homologous recombination (HR):** pathway for the repair of DNA double-strand breaks in an error-free manner using the homologous DNA sequence of the sister chromatid as a template to repair the break.

**Inner cell mass (ICM):** mass of cells located on the inside of the developing embryo that will eventually generate the entire body of the fetus.

respectively. Mutants mimicking their phosphorylated state (S216E and S228E) impair CARM1 methyltransferase activity by interfering with SAM binding, as well as transactivation of estrogen receptor (ER)-dependent transcription [12,26,27]. Although S228E affects CARM1 dimerization [12,26], S216E neither affects CARM1 dimerization nor its interaction with coactivators such as p300 [26]. Both S216 and S228 have been shown to be phosphorylated during mitosis [12,26], suggesting CARM1 is involved in cell-cycle progression. The phosphorylation of S447 by protein kinase A (PKA) promotes the interaction of CARM1 with the hormone-binding domain of unliganded ER $\alpha$ , leading to its cAMP (cyclic adenosine monophosphate)-dependent transcriptional activity [28], which is further enhanced by PKA-mediated phosphorylation of LSD1 (lysine-specific histone demethylase 1) [29]. p38 $\gamma$  MAPK (mitogen-activated protein kinase) phosphorylates S572 of CARM1- $\Delta$ E15 (and S595 of CARM1-FL) within its C-terminal domain without affecting its methyltransferase activity [24]. Phosphorylation of S216 [26] and S572 (CARM1- $\Delta$ E15) [24] has been shown to prevent nuclear localization of CARM1, leading to its accumulation in the cytosol. Furthermore, the authors of a study in *Saccharomyces cerevisiae* hypothesized that T413 (within motif IV) of human CARM1 could be phosphorylated, but this is yet to be demonstrated [30].

Another post-translational modification of S/T residues is O-GlcNAcylation, catalyzed by O-GlcNAc transferase, which is also a CARM1 protein partner [31]. CARM1 is highly O-GlcNAcylated at four residues: S595 (corresponding to S572 of CARM1- $\Delta$ E15, also phosphorylated by p38 $\gamma$  MAPK), S598, T601, and T603 [32]. O-GlcNAcylation of CARM1 does not alter its stability, nuclear-cytoplasmic distribution, dimerization capacity, or coactivator activity but may affect substrate specificity [32]. The overexpression of O-GlcNAc transferase prevents CARM1 phosphorylation (possibly on S216 and S228) and affects its localization (possibly on S572/S595 of CARM1- $\Delta$ E15/CARM1-FL) during mitosis [24,32,33]. Such crosstalk between phosphorylation and O-GlcNAcylation regulates the ability of CARM1 to methylate histone H3 at R17 [33]. CARM1 is also ubiquitinated [34–36], particularly on K470, by the SKP2-containing SCF (SKP1–cullin 1–F-box protein) E3 ligase complex, for proteasomal degradation [35,36]. Finally, nearly 100% of CARM1-FL is auto-methylated on R550 (absent in CARM1- $\Delta$ E15) [20,37]. This modification has no effect on methyltransferase activity [20,37] but is required for ER $\alpha$ -mediated transcription and pre-mRNA splicing [20,37].

### The Repertoire of CARM1 Substrates

Over the past 20 years, numerous large-scale studies have aimed to identify PRMT substrates. Here, we provide a comprehensive summary of all the validated CARM1 substrates identified thus far (Supplemental Table S1). The first attempts to detect CARM1 substrates involved the screening of cDNA libraries and found a limited number of substrates, such as PABP1 and TARPP [38] and CA150, SmB, SF3B4, and U1C [39], but showed that CARM1 methylates an arginine within a PGM (proline, glycine, methionine) motif rather than within the GAR (glycine, arginine rich) motif like the other PRMTs [38,39]. More recently, several antibody-based and antibody-free approaches coupled to mass spectrometry (MS) analysis have identified a large number of substrates of PRMTs (Box 1). Among them, two studies that discovered a large number of potential CARM1 substrates in BC cells confirmed that CARM1 indeed prefers to methylate substrates within a proline-rich motif [10,40].

### CARM1 Regulates Autophagy via Two Independent Pathways

Two major studies recently highlighted a role for CARM1 in the regulation of **autophagy** [35,41]. Under normal/nutrient-rich conditions, CARM1 is degraded via two different mechanisms: (i) nuclear CARM1 through SKP2-mediated ubiquitination (K470) and subsequent proteasomal degradation [35,36] and (ii) cytosolic CARM1 through C9orf72-dependent lysosomal proteolysis

**Leukemogenesis:** the process of developing leukemia, a cancer of the blood and bone marrow.

**Long non-coding RNA (lncRNA):** RNA molecules longer than 200 nucleotides that are transcribed and do not encode proteins but have the ability to interact with proteins, DNA, and RNA.

**MicroRNA (miRNA):** small non-coding RNA molecules (~22 nucleotides) that are mainly involved in the post-transcriptional regulation of protein expression.

**Monomethyl arginine (MMA):** addition of a single methyl group to a guanidino nitrogen, which is the first step in the catalytic reaction by PRMTs.

**Non-homologous end-joining (NHEJ):** a DNA double-strand break repair mechanism that is error prone, as the break ends are directly ligated without the use of a template (like in HR).

**Nonsense-mediated decay pathway:** surveillance pathway to reduce errors in gene expression by eliminating mRNA transcripts that contain premature stop codons.

**Paraspeckles:** membraneless structures located in the interchromatin space inside the nucleus organized around the lncRNA *NEAT1*, which recruits several RNA-binding proteins, such as paraspeckles protein 1 (PSPC1), p54nrb (also known as NonO), splicing factor Pro/Glu-rich (SFPQ), and CARM1. They are rich hubs of RNA–protein interactions involved in the regulation of gene expression.

**Pleckstrin homology-like (PH-like) domain:** a domain involved in protein–protein interactions. The domain present in the N terminus of CARM1 diverges from other members of this family. It forms a dimer when crystallized on its own.

**Protein arginine methyltransferases (PRMTs):** family of nine enzymes (PRMT1–9) that catalyze the addition of a methyl group to the guanidino nitrogen of an arginine residue. They are categorized as type I (PRMT1–3, CARM1, PRMT6, PRMT8), type II (PRMT5 and PRMT9), and type III (PRMT7) PRMTs. All nine PRMTs monomethylate their substrates. Type I PRMTs asymmetrically dimethylate, while type II symmetrically dimethylate the substrate arginine.

**Thymopoiesis:** the maturation process of thymocytes into mature T cells.

**Trophectoderm (TE):** the polarized layer of epithelial cells forming the wall of the growing embryo that can give rise to

[41]. By contrast, CARM1 accumulates in the nucleus under glucose-starved conditions [35,41] (Figure 1B).

Upon glucose starvation, 5' AMP-activated protein kinase (AMPK) level increases in the nucleus and it phosphorylates FOXO3a, which is then recruited to the promoter of SKP2, leading to its repression; nuclear CARM1 is no longer degraded and interacts with transcription factor EB (*TFEB*), inducing the expression of various autophagy and lysosomal target genes by methylating histone H3 (**H3R17me2a**; Figure 1B) [35]. This pathway has since been reported as the AMPK–SKP2–CARM1 signaling pathway [35,36,42].

By contrast, C9orf72, which interacts with the PH-like domain of CARM1, regulates lipid metabolism upon glucose starvation [41]. The loss of C9orf72 prevents lysosomal-mediated degradation of CARM1, leading to its accumulation in the cytoplasm and nucleus (Figure 1B) [41]. The nuclear localization signal identified within CARM1 (Figure 1A) is responsible for its translocation to the nucleus to induce the *de novo* biogenesis of lipids as a stress response [41].

### Regulation of RNA Metabolism: Pre-mRNA Splicing and Paraspeckle-Dependent mRNA Export

In addition to its function as a transcriptional coactivator, nuclear CARM1 regulates mRNA stability by promoting mRNA degradation of a subset of transcripts via the **nonsense-mediated decay** pathway [43], pre-mRNA splicing [17,37,39,43–48], and mRNA export through **paraspeckles** [49].

#### Pre-mRNA Splicing

The first study implying a role for CARM1 in splicing showed that among the five rat isoforms, only the minor isoform *CARM1-v3* regulates splicing by promoting the use of a 5' distal splice site, independent of its methyltransferase activity [17]. By contrast, Cheng *et al.* [39] showed that CARM1-FL regulates splicing, possibly due to different experimental conditions, and depends on its methyltransferase activity [39] (Figure 1C). CARM1-FL methylates several splicing factors (SmB, SF3B4, U1C, and CA150) and promotes exon skipping through the methylation of CA150 (Figure 1C) [39]. More recently, additional studies have highlighted the involvement of CARM1 in splicing: (i) methylation of the splicing factor SRSF2 (Figure 1C) [44], (ii) exon skipping of VEGF [45], (iii) requirement of auto-methylation of CARM1-FL for its splicing activity (Figure 1C) [37], and (iv) involvement in other splicing events, such as intron retention in *Arabidopsis thaliana* [46]. Moreover, two major studies have shown that type I PRMT inhibitors and PRMT5 inhibitors alter splicing events and act synergistically when targeting cancer cells mutated for splicing factors [47,48]. However, the importance of specifically inhibiting CARM1 (a type I PRMT) in this context is yet to be determined.

#### mRNA Export through Paraspeckles

Paraspeckles are organized around the **long non-coding RNA (lncRNA) NEAT1** (Box 2), which recruits several RNA-binding proteins, such as PSPC1, p54nrb, SFPQ [50], and CARM1 [7,49,51]. These structures regulate gene expression by sequestering specific mRNA molecules, such as those containing inverted repeated Alu elements (IRAlus) in their 3' untranslated region, through their binding to p54nrb [49].

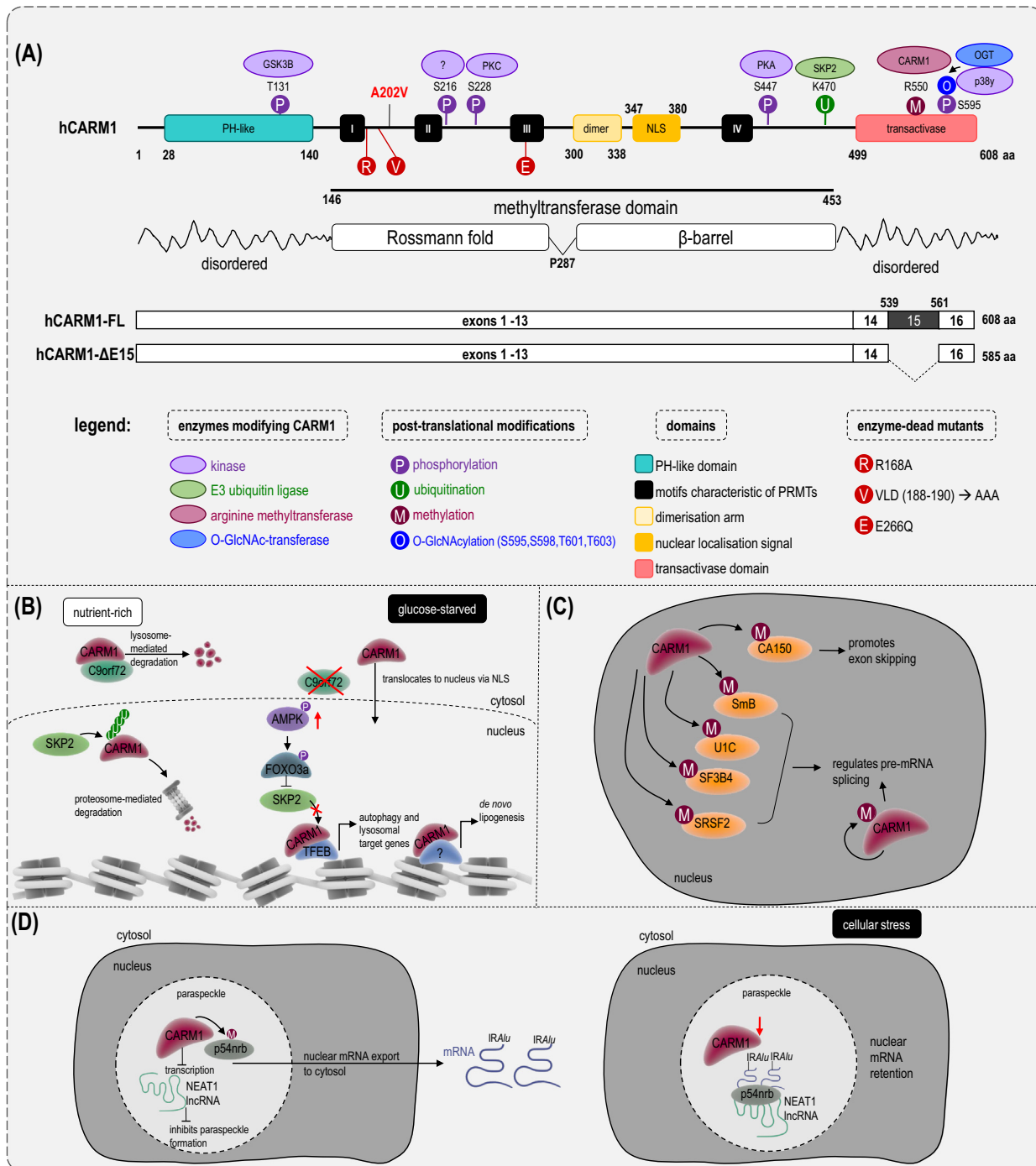
CARM1 regulates paraspeckle formation and function. On the one hand, CARM1 represses the transcription of *NEAT1* by binding to its promoter, thus impairing paraspeckle formation (Figure 1D) [49,51]. On the other hand, CARM1 methylates p54nrb, decreasing its binding affinity to IRAlus-containing mRNAs (Figure 1D) [49]. This allows the export of these mRNAs from the

extra-embryonic structures (such as the placenta) at later developmental stages.

**Tudor domain:** a domain that has the ability to interact with methylated arginine or lysine. CARM1-mediated methylation facilitates the binding of some substrates with Tudor domain-containing proteins.

Key Figure

Summary of the Structure and Functions of CARM1



Trends in Cell Biology

(See figure legend at the bottom of the next page.)

nucleus to the cytosol, leading to their translation, and represents an additional molecular mechanism for CARM1 to regulate gene expression [49]. Inducing stress by treatment with polyinosine-polycytidylic acid [poly (I:C)] reduces CARM1 levels in paraspeckles, leading to the nuclear retention of IRALus containing mRNAs (Figure 1D) [49]. In addition, CARM1 appears to regulate the localization of p54nrb [51] and the splicing factor SRSF2, which is a potential CARM1 substrate [44], in paraspeckle.

## CARM1 in Development and Differentiation

### CARM1 Activity Is Essential for Embryonic Development

CARM1 regulates early mouse development and plays a role in the determination of cell fate. In contrast to PRMT1 and PRMT5 (the major type I and type II PRMTs), of which the KO causes embryonic lethality [52,53], CARM1 KO mice display recessive neonatal lethality, with pups dying at birth due to breath failure [54,55] (Figure 2A). Furthermore, CARM1 KO mice are smaller than their wild-type littermates [54]; show delayed **endochondral ossification** and decreased chondrocyte proliferation [56]; reduced **thymopoiesis**, resulting from a defect in the fetal hematopoietic compartment [57,58]; impaired adipocyte differentiation [59], muscle regeneration deficit [60]; and hyperproliferation of alveolar type II cells [61] (Figure 2A). Interestingly, a CARM1 enzyme-dead knock-in mutant mouse phenocopies CARM1 KO mice [55], showing blocked thymocyte differentiation [55,57,58] and defective **adipogenesis** [55,59], indicating CARM1 activity is essential for development (Figure 2A). In parallel, substituting R17 on histone H3 with a histidine causes developmental retardation at embryo day E4.5 (Figure 2B) [62]. A similar phenotype was observed with a C-terminal-truncated CARM1 mutant (Figure 2B) [62], suggesting that certain CARM1 partners may also be involved in early embryogenesis.

### CARM1 Biases Cells toward an Inner Cell Mass Fate in Early Embryos

The function of CARM1 at earlier stages of mammalian development was unknown until an elegant study by Torres-Padilla *et al.* [63] showed that CARM1 can contribute to cell fate decisions in the mouse four-cell-stage embryo. CARM1 levels, along with its specific histone marks (H3R17me2a and **H3R26me2a**), varied between the four-cell blastomeres and higher levels of H3R26me2a were associated with a global increase in transcription [63]. During mammalian embryo development, the blastomeres have two lineages or fates, either to become part of the **inner cell mass (ICM)** or **trophectoderm (TE)**, contributing to embryonic and extra-embryonic cells, respectively. CARM1 activity and expression bias the blastomeres toward an ICM fate by inducing the expression of *Nanog*, *Sox2*, *Sox21*, and *Oct4* [63,64], while repressing the expression of *Cdx2*, a transcription factor for TE differentiation (Figure 2C) [64,65]. In addition, CARM1-mediated methylation of BAF155 influences the cell fate toward ICM [66]. Unmethylated BAF155 induces the expression of TE differentiation markers, whereas methylated BAF155 switches on the expression of pluripotent markers, such as *Nanog* (Figure 2C) [66]. The heterogeneous distribution of CARM1 in the four-cell-stage embryo is also regulated by the **microRNA**

**Figure 1.** (A) Schematic representation of human CARM1 (hCARM1) and its main isoform (hCARM1- $\Delta$ E15) showing the domains and post-translational modifications. CARM1 has an N-terminal PH-like domain, a C-terminal transactivase domain, and a central methyltransferase domain containing the four PRMT motif signatures, motif I (YFxxY), motif II (DVGxGxG), motif III (SE<sup>257</sup>xMGxxLxxE<sup>266</sup>xM, double E-loop), and motif IV (TH<sup>414</sup>WxQ), and a dimerization arm. Enzymatic activity is lost upon mutation of E266Q, VLD(188-190)AAA, and R168A. Human and mouse CARM1 amino acid numbering differ by one. All amino acid residues are numbered according to hCARM1 throughout the review to avoid confusion. (B) CARM1 regulates autophagy. Under nutrient-rich conditions, nuclear and cytosolic CARM1 are degraded by SKP2 and C9orf72, respectively. Conversely, under glucose-starved conditions, CARM1 induces the expression of autophagy and lysosomal target genes via TFEB or genes responsible for *de novo* lipogenesis. (C) CARM1 regulates pre-mRNA splicing by methylating splicing factors and promotes exon skipping. Auto-methylation of CARM1-FL also regulates pre-mRNA splicing. (D) CARM1 mediates the export of nuclear mRNA by regulating the formation of paraspeckles via two mechanisms. (i) CARM1 inhibits the transcription of lncRNA *NEAT1*, (ii) CARM1 methylates p54nrb, thus decreasing its affinity for IRALus-containing mRNAs. Cellular stress decreases CARM1 levels inside paraspeckles, enabling nuclear mRNA retention. Abbreviations: aa, amino acid; CARM1, coactivator-associated arginine methyltransferase 1; lncRNA, long non-coding RNA; PH, pleckstrin homology; PRMT, protein arginine methyltransferase.

**Box 1. Methods to Identify CARM1 Substrates**

Methylation of CARM1 substrates can be evaluated either *in vitro* or *in vivo* (previously reviewed in [103]). The *in vitro* assay includes CARM1 (endogenous from cell lysates or recombinant from bacteria and insect cells), the substrate (recombinant or a peptide), and the methyl group donor (SAM) [103].

Several methods can be used to detect the methylation of substrates (Figure 1), *in vivo*, usually by coupling various techniques with MS analysis [10,40,44,104–107]. First, cells can be metabolically labeled with radioactive methionine and the potential substrate can be immunoprecipitated [38,108]. Otherwise, immunoprecipitation using pan-methylated {**asymmetric dimethyl arginine (ADMA)** [10,40,104,105,109] and **monomethyl arginine (MMA)** [40,44,104–106,110]} antibodies and MS can detect a larger number of methylated peptides. Notably, although existing ADMA and MMA antibodies recognize a GAR motif, a large proportion of arginine residues within proline-rich sequences have also been discovered (corresponding to known and putative CARM1 substrates) [10,40,44,104–107]. Other antibody approaches include the use of ADMA antibodies generated against a peptide cocktail of various reported CARM1 methylated substrates [111] or the use of custom antibodies that recognize the methylated substrate arginine (Supplemental Table S1). To overcome the limitation of using antibodies, antibody-free approaches, using strong cation-exchange chromatography and/or hydrophilic interaction liquid chromatography, can be performed and can identify approximately 20% of methylated peptides that harbor a proline-rich sequence [105,107,112–114]. However, these methods only indicate that a protein was methylated *in vivo* and not specifically by CARM1. To ensure specificity toward CARM1, these experiments must be performed in CARM1 wild-type and depleted and/or inhibited cells [10,40,44].

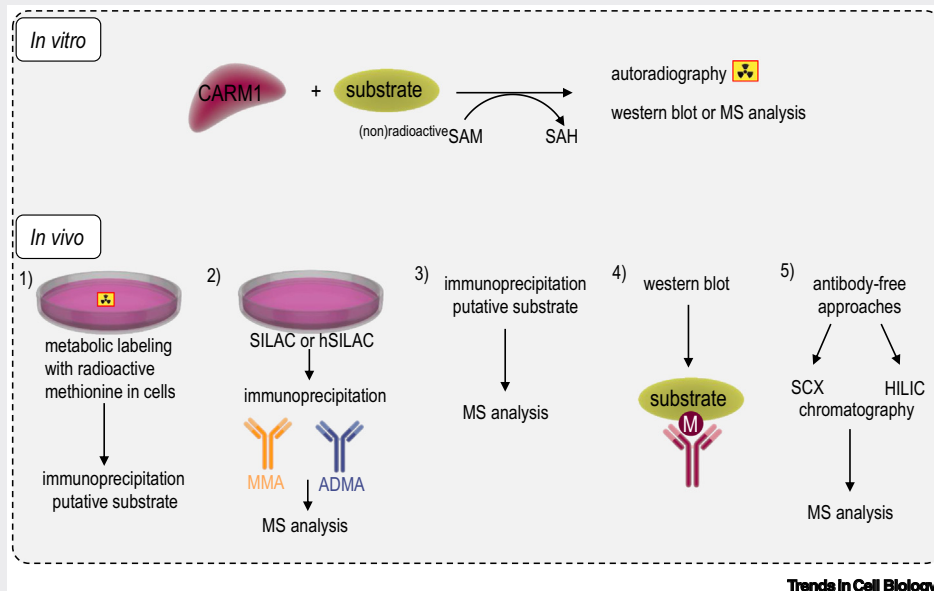


**Figure 1. Techniques to Identify CARM1 Substrates *In Vitro* and in Cells.** *In vitro* methylation assays use recombinant CARM1 and the putative substrate in the presence of tritiated/cold SAM to visualize the methylated protein by autoradiography or identify the methylated residue(s) by MS. *In vivo*, methylated proteins can be (1) metabolically labeled with radioactive methionine; (2) immunoprecipitated using pan-methyl antibodies for MS analysis, after stable isotope labeling by amino acids in cell culture (SILAC) or heavy-SILAC (hSILAC); (3) immunoprecipitated for MS analysis; (4) detected by western blot using antibodies that specifically recognize the methylated arginine; or (5) enriched using antibody-free strong cation exchange (SCX) or hydrophilic liquid interaction (HILIC) chromatography for MS analysis. Abbreviation: SAH, S-adenosyl-L-homocysteine.

miR-181a (Box 2) [67]. Interestingly, it is a balance in CARM1 levels that determines the resulting fate of the blastomeres [63–65,68].

Recent evidence suggests that CARM1 is involved in cell fate determination at earlier stages of the mouse embryo (two to four cells) by interacting with *LincGET*, an endogenous retroviral lncRNA (Box 2) [69] and localizing to the membrane-free nuclear body – paraspeckles (Figure 2C) [51]. *LincGET* induces nuclear localization of CARM1 by interacting with its

transactivation domain, resulting in high H3R26me2a levels and ICM-specific gene expression [69]. Moreover, the presence of CARM1 in paraspeckles is required for the methylation of histone H3 at R26 and to ensure proper lineage allocation to facilitate normal embryo development (Figure 2C) [51]. CARM1 is also present in other nuclear bodies called **CARM1 speckles** [51], but its function in such structures is yet to be elucidated.

#### CARM1 Maintains the Pluripotency of Embryonic Stem Cells

Mirroring its function in embryonic cell fate determination, CARM1 induces the expression of pluripotency genes (*Oct4* and *Sox2*) through the methylation of histone H3, impairing **embryonic stem cell (ESC)** differentiation [70–72]. Conversely, the miR-181 family promotes ESC differentiation by regulating CARM1 expression [70].

#### CARM1 Controls Neuronal and Skeletal Muscle Differentiation

CARM1 is also involved in neuronal and skeletal muscle differentiation (reviewed in [73]). For example, CARM1-mediated methylation of histone H3 (H3R17me2a) enhances miR-92 expression, which is essential for the maintenance of the astroglial lineage [74]. CARM1-dependent methylation of *Pax7* activates *Myf5* expression, inducing the myogenic differentiation program [60].

#### CARM1 and Cancer: A Therapeutic Target and/or a Biomarker of Drug Response?

A hotspot mutation at A202V, located in its methyltransferase domain, has been recently identified in *CARM1*, supporting it as a cancer driver gene [75]. CARM1 is overexpressed in several cancer types, such as breast [40,76,77], ovarian [78,79], hematopoietic [80,81], liver [82], pancreatic [83], colorectal [84,85], prostate [86], bone [87], oral [88], lung [89], and melanoma [90]. Because of space constraints, we will only focus on breast, ovarian, hematopoietic, liver, and pancreatic cancer.

#### Breast Cancer

BC express higher CARM1 RNA [40] and protein [76,77] levels than normal tissue. CARM1 protein expression is associated with hormone-negative tumors and HER2 status [76,77,91]. The two CARM1 isoforms (FL and  $\Delta E15$ ) do not differ at the RNA level between BC and normal tissue and are not associated with hormone receptors [22]. In addition, the CARM1-FL and CARM1- $\Delta E15$  proteins are suggested to be mainly nuclear and cytosolic in BC, respectively [22]. HER2 tumors contain the highest nuclear CARM1 protein levels (presumably CARM1-FL) [76,77]. Cytoplasmic CARM1 protein (presumably CARM1- $\Delta E15$ ) expression is associated with both triple-negative BC and HER2 tumors [77].

#### Box 2. lncRNA and miRNA – Friends and Foes of CARM1

It was previously thought that CARM1 could only interact with proteins and not RNA, but recent studies have shown that it associates with several lncRNAs (Figure 1A). Indeed, the lncRNA called suppressor of tumorigenicity 7 antisense RNA 1 (*S77-AS1*) interacts with the N terminus of CARM1 and protects it from ubiquitin-dependent degradation [115]. *S77-AS1* further promotes CARM1-induced Sox-2 methylation/self-association, thus acting as an oncogenic factor in laryngeal squamous cell carcinoma [115]. CARM1 coexpresses and binds to lncRNA *PVT1* in non-small-cell lung carcinoma (NSCLC) and is associated with radiosensitivity [116]. *LincGET* [endogenous retrovirus (ERV)-associated lncRNA] induces the nuclear localization of CARM1, which induces the expression of ICM-specific genes to bias embryo development [69]. Finally, the lncRNA *NEAT1* recruits CARM1 to paraspeckles and is itself negatively transcriptionally regulated by CARM1 [49,51]. In addition, CARM1 is regulated by another subset of RNA – miRNA/miR (Figure 1B). CARM1 has been shown to be targeted by miR-195 and miR-195-5p in colorectal cancer [85,117], miR-424-5p in NSCLC [116], and miR-223 in hematopoietic stem progenitor cells (HSPCs) [81]. In HSPCs, CARM1 also represses miR-223 expression by methylating *RUNX1* as part of a feedback loop [81]. The overexpression of miR-195, miR-195-5p, and miR-424-5p impairs cell proliferation [85,116,117]. Whether CARM1 interacts with other lncRNAs or other subsets of RNA is still unknown.

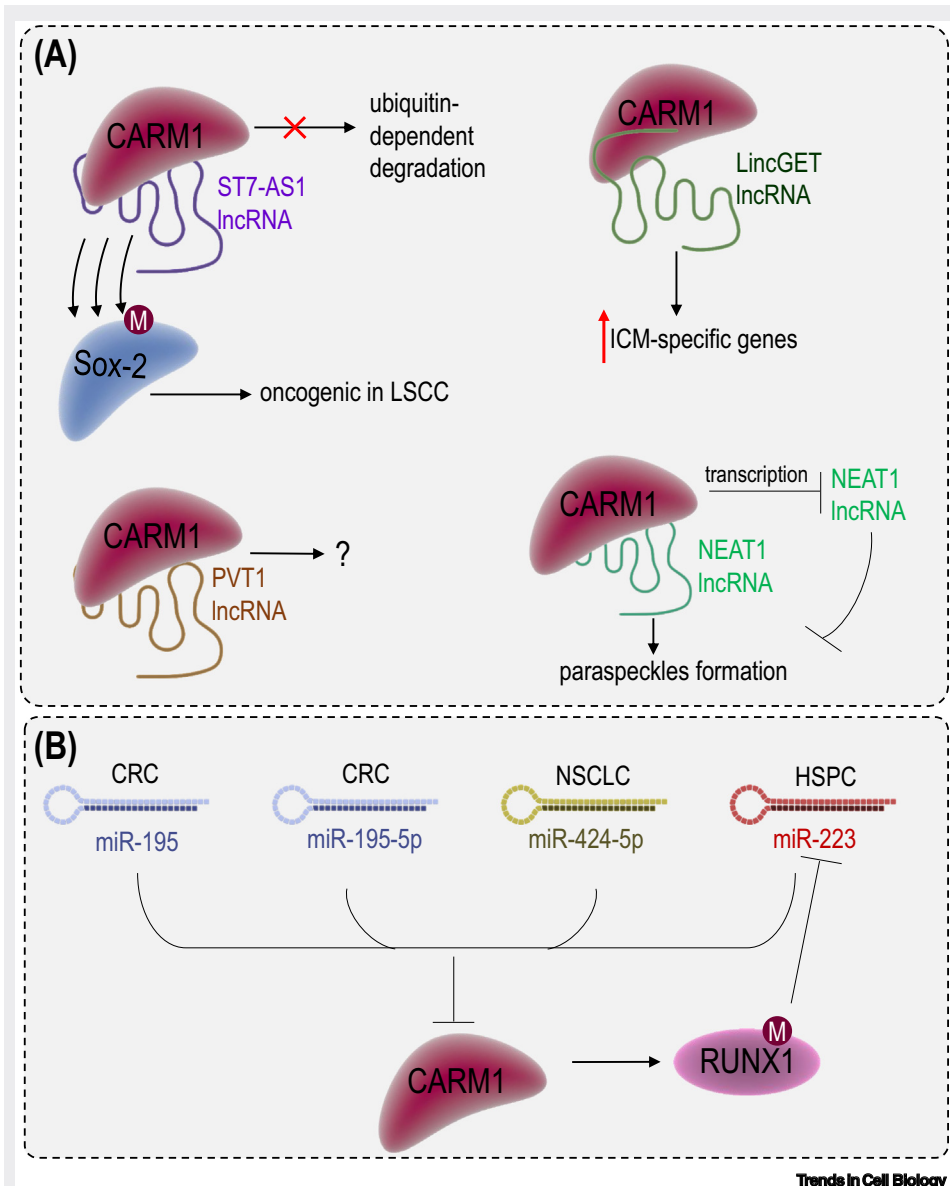


**Figure 1. CARM1 binds to lncRNAs and Is Targeted by miRNAs.** (A) CARM1 interacts with *ST7-AS1* to protect it from degradation while also methylating *Sox2* in laryngeal-squamous carcinoma cells (LSCCs). It binds to *PVT1* lncRNA for an unknown function. *LincGET* lncRNA induces nuclear localization of CARM1 in early blastomeres to upregulate the expression of ICM transcription factors. *NEAT1* lncRNA recruits CARM1 to induce paraspeckle formation and CARM1 binds to the *NEAT1* promoter to repress its transcription in a negative feedback mechanism. (B) CARM1 is degraded by miR-195 and miR195-5p in colorectal cancer cells (CRCs), miR-424-5p in NSCLCs, and miR-223 in HSPCs. Methylation of RUNX1 by CARM1 inhibits miR-223 as a feedback mechanism.

Among the various types of BC, CARM1 has been extensively studied in luminal BC, particularly in the liganded nuclear receptor signaling pathways [92]. CARM1 is essential for estrogen-induced cell-cycle progression (through *E2F1*) [93] and its depletion delays tumor growth [40]. The demethylase JMJD6 facilitates binding between CARM1 and MED12 [94] and methylated MED12 recruits TDRD3 (a **Tudor domain**-containing protein) to CARM1-bound active enhancers to



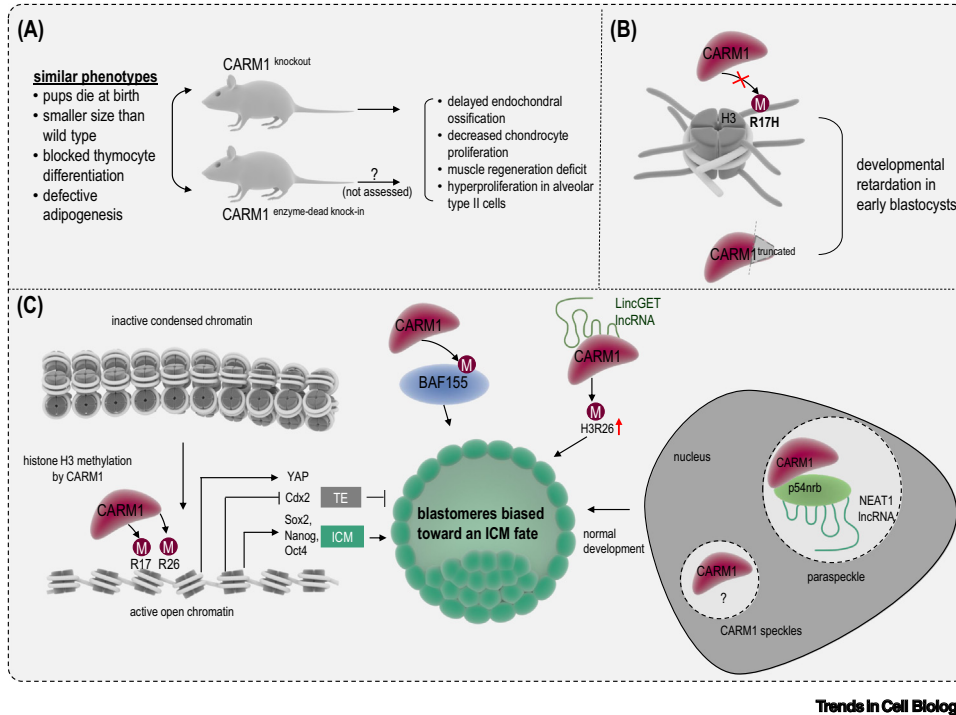


**Figure 2. CARM1 Controls Early Embryo Development through Several Mechanisms and Biases the Cell Fate Toward ICM.** (A) Phenotypes of CARM1 knockout and enzyme-dead (R168A; equivalent to R169A in mouse CARM1) knock-in mice. (B) Substituting R17 of H3 or truncating CARM1 at its C terminus causes developmental retardation. (C) CARM1-mediated methylation of histone H3 and/or BAF155 induces the expression of ICM-specific factors and blocks TE differentiation. Paraspeckles are necessary for normal development dependent on H3R26 methylation by CARM1. Abbreviations: CARM1, coactivator-associated arginine methyltransferase 1; ICM, inner cell mass; lncRNA, long non-coding RNA; TE, trophoblast.

activate estrogen/ $ER\alpha$ -target genes [40].  $ER\alpha$  can also be activated in a ligand-independent manner through PKA. PKA-mediated phosphorylation of CARM1 and LSD1 activates transactivation of unliganded  $ER\alpha$  [28,29]. CARM1 is also involved in epithelial-to-mesenchymal transition by methylating LSD1 and methylated LSD1 correlates with tumor grade in human BC [95].

Very little is known about the role of CARM1 in the other BC subtypes. In HER2-overexpressing BC cells, CARM1 is phosphorylated upon growth factor stimulation [12]. Furthermore, CARM1 delays tumor initiation in an HER2-driven mammary gland tumorigenesis model, but the tumors grew more quickly once established, demonstrating the oncogenic potential of CARM1 [96]. In triple-negative BC cells, CARM1 promotes migration [23,40,97] and metastasis through the methylation of PKM2 [97] (Box 3) or BAF155 (a core subunit of the chromatin remodeling complex) [23].

### Ovarian Cancer

The overexpression of CARM1 mRNA [78] or protein [79] in a subset of ovarian cancers (OCs) is associated with a poor prognosis and CARM1 deletion/inhibition impairs OC cell growth. Furthermore, CARM1 amplification appears to be mutually exclusive with the mutation of *BRCA1/2* [79,98], key players in **homologous recombination (HR)**. *MAD2L2*, which activates the **non-homologous end-joining (NHEJ)** pathway, is either silenced by EZH2 or activated by unmethylated BAF155 [98]. Promoter occupancy of *MAD2L2* switches from

**Box 3. CARM1 Controls Metabolic Pathways in Tumors**

CARM1 regulates various metabolic pathways, such as oxidative phosphorylation, glycolysis, and glutamine metabolism in breast, liver, and pancreatic cancer, respectively. CARM1-dependent methylation of PKM2 decreases the expression of inositol-1,4,5-trisphosphate receptors (InsP3Rs), thereby switching the metabolism from oxidative phosphorylation to aerobic glycolysis [97]. Blocking PKM2 methylation increases the calcium flux from the endoplasmic reticulum to mitochondria, leading to oxidative phosphorylation (Figure 1A) [97].

In liver cancer cells, upon glucose starvation, CARM1 is upregulated in an AMPK-dependent manner and inhibits glycolysis through the methylation of GAPDH (Figure 1B) [82].

Under normal conditions, CARM1-mediated methylation of MDH1 inhibits its activity and thus glutamine metabolism [83]. Conversely, under stress conditions, the inhibition of CARM1 activity by reactive oxygen species (ROS) activates glutamine metabolism in PDAC (Figure 1C) [83].

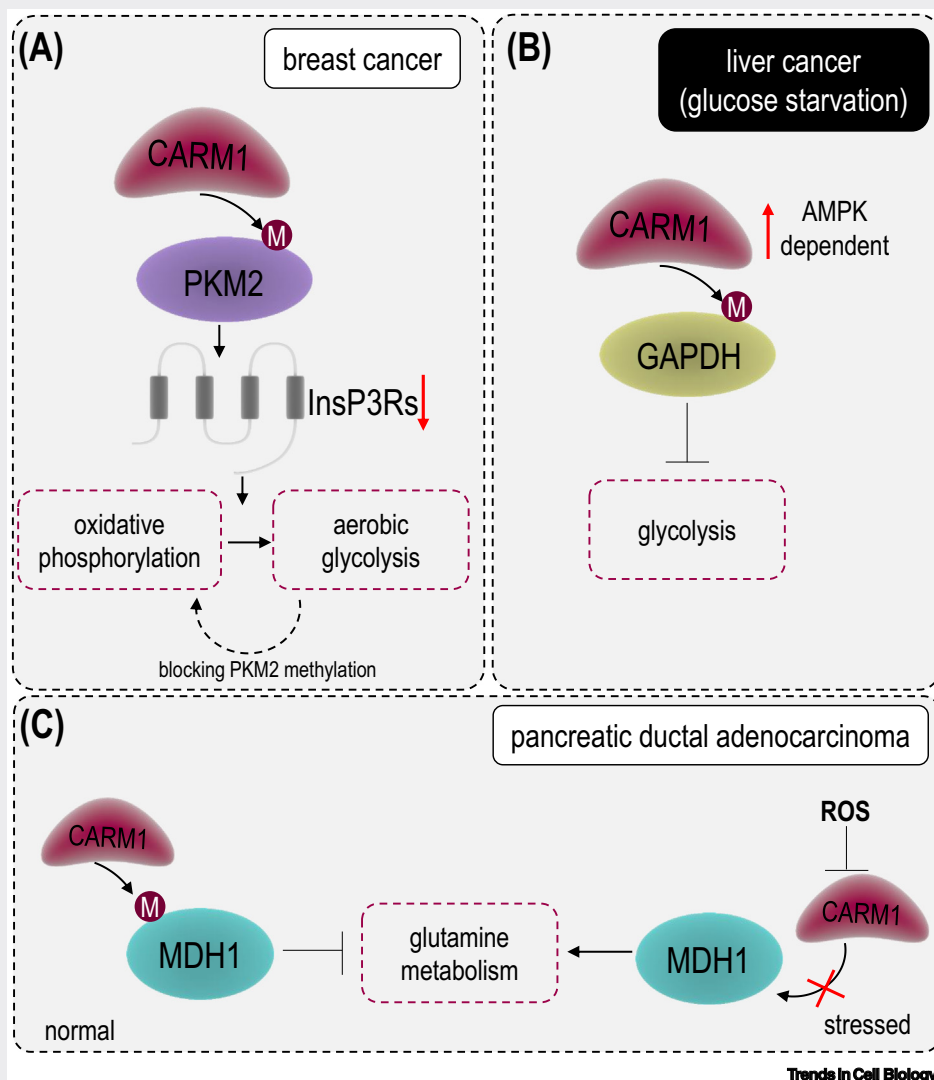


**Figure 1. CARM1 Mediates Metabolic Pathways in Certain Cancer Types.** A) CARM1-mediated methylation of PKM2 switches metabolism from oxidative phosphorylation to aerobic glycolysis, which is reversed upon blocking PKM2 methylation. B) Methylation of GAPDH by CARM1 blocks glycolysis in glucose-starved liver cancer cells. C) Methylation of MDH1 inhibits its activity and glutamine metabolism under normal conditions, whereas stress conditions, such as the presence of ROS, inhibit CARM1, preventing MDH1 methylation and activating glutamine metabolism.

BAF155 to EZH2 upon BAF155 methylation by CARM1, silencing MAD2L2 expression and thus NHEJ [79,98]. Therefore, high levels of CARM1 in cells will promote NHEJ silencing, which is reversed upon EZH2 inhibition [98]. OC cells with high CARM1 expression are therefore sensitive to EZH2 inhibitors alone [79] or in combination with poly(ADP-ribose) polymerase (PARP) inhibitors [98]. Indeed, high CARM1 expression also decreases HR activity [98]. This combination strategy may be applied to other HR-proficient cancers.

### Hematopoietic Cancers

CARM1 protein is overexpressed in Hodgkin Reed–Sternberg cells and Hodgkin’s lymphoma [80] and CARM1 mRNA is upregulated in acute myelogenous leukemia (AML) patient samples [81]. CARM1 depletion minimally affects normal **hematopoiesis** but strongly impairs **leukemogenesis** by regulating cell-cycle progression, myeloid differentiation, and apoptosis [21,81]. Small-molecule CARM1 inhibitors (competitive for the substrate arginine-binding pocket) impaired proliferation, both *in vitro* and *in vivo*, in a multiple myeloma xenograft model [99], AML mouse model [21], and diffuse large B-cell lymphoma (DLBCL) model [100]; however, only a subset of multiple myeloma [99,101] or DLBCL cells [100] are sensitive to these inhibitors. The mutation of *CBP/p300* sensitizes DLBCL cells to CARM1 inhibition, whereas the combination of CARM1 and CBP/p300 bromodomain inhibitors is lethal for DLBCL wild-type cells, highlighting the necessity of finding biomarkers of responses to CARM1 inhibitors [100]. CARM1 methylates PRMT5 in human erythroleukemia cells, *in vitro* and *in vivo*, and such methylation is necessary for PRMT5 homodimerization and activity [102]. Therefore, CARM1 inhibition may also inhibit PRMT5, suggesting crosstalk between the various PRMTs. It has been recently shown that targeting both type I PRMTs and PRMT5 specifically kills AML cells mutated for splicing factors [48]. Overall, these data suggest that targeting CARM1 could be a potential therapeutic strategy alone, or in combination, for a subset of hematopoietic tumors.

### Liver and Pancreatic Cancers

In contrast to the aforementioned cancer types, CARM1 protein is found at lower levels in human liver cancer [82] and pancreatic ductal adenocarcinoma (PDAC) [83] than in normal tissue. CARM1 regulates glycolysis in liver cancer through the methylation of GAPDH, delaying tumor cell proliferation *in vitro* and *in vivo* [82] (Box 3). In pancreatic cancers, the inhibition of malate dehydrogenase 1 (MDH1), through CARM1-mediated methylation, prevents glutamine metabolism and suppresses cell proliferation [83] (Box 3). Thus, stimulating CARM1 activity has been proposed as a therapeutic approach against PDAC and liver cancer.

### Concluding Remarks

CARM1 is unique among the PRMTs, as it is the only one that methylates arginine within a proline-rich sequence. Although studies over the past 5 years have highlighted novel roles for CARM1, several key areas still need to be explored to fully comprehend its physiological and pathological functions (see [Outstanding Questions](#)).

First, it is likely that the list of CARM1 substrates is incomplete and unraveling the entire methylome of CARM1 would be an important step to better mechanistically characterize its cellular functions. A major drawback is the difficulty to identify methylated arginine without enriching for methylated peptides using pan-methyl antibodies prior to MS analysis. The generation of pan-methyl antibodies that can detect methylated arginine within a proline-rich motif would significantly improve the chances of recognizing specific CARM1 substrates.

Second, solving the full-length crystal structure of CARM1, alone or complexed with a protein substrate, may reveal key residues from the N-terminus PH-like and C-terminal domains

### Outstanding Questions

Why is CARM1- $\Delta$ E15 mRNA more highly expressed than CARM1-FL in BC? Is the protein also highly expressed? Is the CARM1- $\Delta$ E15 mRNA more highly expressed in other cancer types? What are their common/specific partners/substrates in normal and cancer cells? Are their functions redundant or compensatory? What are the structural similarities/differences between CARM1-FL and CARM1- $\Delta$ E15 in terms of their binding to their substrates?

What are the ‘CARM1 speckles’ and their function? Does CARM1 localize to other nuclear structures apart from paraspeckles and ‘CARM1 speckles’? Are these related to its known functions in RNA metabolism?

Is the PH-like fold the only domain that interacts with RNA? Can CARM1 interact with other nucleic acids? Is there competition between nucleic acids and proteins in binding to the PH-like domain? Do the CARM1 PTMs regulate binding to RNA/proteins?

What CARM1 functions are affected by its post-translational modifications (PTMs)? Are there any additional PTMs that occur on CARM1? Which kinase phosphorylates S216? Why does CARM1-FL have to be auto-methylated? Is this methylation dynamic?

By what molecular mechanism does CARM1 regulate pre-mRNA splicing? Does CARM1 self-regulate its splicing to generate CARM1- $\Delta$ E15?

Is CARM1 enzymatic activity required for every function or can it act as a scaffolding protein under certain conditions? What are the cytosolic functions of CARM1?

Why are certain hematopoietic cancer cells more sensitive to CARM1 inhibition than others? Is it due to the presence of specific mutations and what are they? Is there synergy between the inhibition of CARM1 and that of other PRMTs in cancers mutated for splicing factors?

Why are cancer cell lines derived from solid tumors not sensitive to CARM1 inhibition? Would it be beneficial to combine CARM1 inhibitors with

important for protein–protein interactions. Moreover, we now know that the PH domain of CARM1 not only interacts with proteins but also several lncRNAs. Identifying the interactome (proteins and nucleic acids) of CARM1 could thus uncover novel functions.

Third, nuclear CARM1 is present in various types of speckles, including paraspeckles. Future efforts are needed to characterize the nature of such speckles and to understand how and why CARM1 is present in these structures.

Fourth, CARM1 has emerged as an attractive therapeutic target for a subset of hematopoietic cancers and PDAC/liver cancer and as a biomarker of response to therapy in OC. Recently developed specific and potent CARM1 small-molecule inhibitors are efficient in only a subset of hematopoietic cancer cell lines. Future studies could focus on understanding why only very few cancer cell lines are sensitive to these inhibitors when used as a single agent.

Finally, an unexplored area in CARM1 biology is the cellular function of its two isoforms, namely, CARM1-FL and CARM1- $\Delta$ E15. CARM1- $\Delta$ E15 is predominantly expressed in BC at the RNA level but we do not know whether this is true for other types of cancer. Isoform-specific antibodies would be a vital tool to explore the expression and localization of CARM1- $\Delta$ E15 in various types of cancer and normal tissue. Furthermore, the functions of the CARM1- $\Delta$ E15 isoform (proposed to be an oncogenic variant) can be explored by searching for its unique partners/substrates.

Our understanding of the biology of CARM1 has come a long way since its discovery 20 years ago. This is certainly not the end of the road, but rather the beginning of exciting breakthroughs in the characterization of CARM1 functions.

### Acknowledgments

This work was supported by the Institut Curie and by the European Union's Horizon 2020 Research and Innovation Programme (Marie Skłodowska-Curie grant agreement No 666003). We are grateful to Dr Marc-Henri Stern (Institut Curie, Department of Genetics, INSERM U830), Dr Sergio Roman-Roman (Institut Curie, Translational Research Department), and Raquel Vivet-Noguer (Institut Curie, Translational Research Department, Uveal Melanoma group) for their critical review of the manuscript. Figures were generated using the illustrations from Somersault 18:24 under the Creative Commons license (CC BY-NC-SA 4.0). We apologize to the authors whose work could not be cited due to space constraints.

### Supplemental Information

Supplemental information associated with this article can be found online at <https://doi.org/10.1016/j.tcb.2020.12.010>.

### References

- Chen, D. *et al.* (1999) Regulation of transcription by a protein methyltransferase. *Science* 284, 2174–2177
- Stallcup, M.R. *et al.* (2003) The roles of protein–protein interactions and protein methylation in transcriptional activation by nuclear receptors and their coactivators. *J. Steroid Biochem. Mol. Biol.* 85, 139–145
- Bedford, M.T. and Richard, S. (2005) Arginine methylation an emerging regulator of protein function. *Mol. Cell* 18, 263–272
- Lee, Y.H. and Stallcup, M.R. (2009) Minireview: protein arginine methylation of nonhistone proteins in transcriptional regulation. *Mol. Endocrinol.* 23, 425–433
- Yang, Y. and Bedford, M.T. (2013) Protein arginine methyltransferases and cancer. *Nat. Rev. Cancer* 13, 37–50
- Jarrod, J. and Davies, C.C. (2019) PRMTs and arginine methylation: cancer's best-kept secret? *Trends Mol. Med.* 25, 993–1009
- Guccione, E. and Richard, S. (2019) The regulation, functions and clinical relevance of arginine methylation. *Nat. Rev. Mol. Cell Biol.* 20, 642–657
- Troffer-Charlier, N. *et al.* (2007) Functional insights from structures of coactivator-associated arginine methyltransferase 1 domains. *EMBO J.* 26, 4391–4401
- Yue, W.W. *et al.* (2007) Insights into histone code syntax from structural and biochemical studies of CARM1 methyltransferase. *EMBO J.* 26, 4402–4412
- Shishkova, E. *et al.* (2017) Global mapping of CARM1 substrates defines enzyme specificity and substrate recognition. *Nat. Commun.* 8, 15571
- Teyssier, C. *et al.* (2002) Requirement for multiple domains of the protein arginine methyltransferase CARM1 in its transcriptional coactivator function. *J. Biol. Chem.* 277, 46066–46072
- Higashimoto, K. *et al.* (2007) Phosphorylation-mediated inactivation of coactivator-associated arginine methyltransferase 1. *Proc. Natl. Acad. Sci. U. S. A.* 104, 12318–12323
- Morales, Y. *et al.* (2016) Biochemistry and regulation of the protein arginine methyltransferases (PRMTs). *Arch. Biochem. Biophys.* 590, 138–152

chemotherapies or targeted therapies in certain types of cancer?

Are all HR-proficient cancer cells that highly express CARM1 sensitive to PARP and/or EZH2 inhibitors? What is the function of CARM1 in the DNA damage response?

14. Boriack-Sjodin, P.A. *et al.* (2016) Structural insights into ternary complex formation of human CARM1 with various substrates. *ACS Chem. Biol.* 11, 763–771
15. van Haren, M.J. *et al.* (2017) Transition state mimics are valuable mechanistic probes for structural studies with the arginine methyltransferase CARM1. *Proc. Natl. Acad. Sci. U. S. A.* 114, 3625–3630
16. Baldwin, R.M. *et al.* (2014) Role of PRMTs in cancer: could minor isoforms be leaving a mark? *World J. Biol. Chem.* 5, 115–129
17. Ohkura, N. *et al.* (2005) Coactivator-associated arginine methyltransferase 1, CARM1, affects pre-mRNA splicing in an isoform-specific manner. *J. Biol. Chem.* 280, 28927–28935
18. Gupta, N. *et al.* (2015) Mapping of post-translational modifications of transition proteins, TP1 and TP2, and identification of protein arginine methyltransferase 4 and lysine methyltransferase 7 as methyltransferase for TP2. *J. Biol. Chem.* 290, 12101–12122
19. Matsuda, H. *et al.* (2007) Contrasting effects of two alternative splicing forms of coactivator-associated arginine methyltransferase 1 on thyroid hormone receptor-mediated transcription in *Xenopus laevis*. *Mol. Endocrinol.* 21, 1082–1094
20. Wang, L. *et al.* (2013) CARM1 automethylation is controlled at the level of alternative splicing. *Nucleic Acids Res.* 41, 6870–6880
21. Greenblatt, S.M. *et al.* (2018) CARM1 is essential for myeloid leukemogenesis but dispensable for normal hematopoiesis. *Cancer Cell* 33, 1111–1127
22. Shlensky, D. *et al.* (2015) Differential CARM1 isoform expression in subcellular compartments and among malignant and benign breast tumors. *PLoS One* 10, e0128143
23. Wang, L. *et al.* (2014) CARM1 methylates chromatin remodeling factor BAF155 to enhance tumor progression and metastasis. *Cancer Cell* 25, 21–36
24. Chang, N.C. *et al.* (2018) The dystrophin glycoprotein complex regulates the epigenetic activation of muscle stem cell commitment. *Cell Stem Cell* 22, 755–768
25. Li, X. *et al.* (2017) Oxidative stress destabilizes protein arginine methyltransferase 4 via glycogen synthase kinase 3beta to impede lung epithelial cell migration. *Am. J. Physiol. Cell Physiol.* 313, C285–C294
26. Feng, Q. *et al.* (2009) Biochemical control of CARM1 enzymatic activity by phosphorylation. *J. Biol. Chem.* 284, 36167–36174
27. Lim, C.S. and Alkon, D.L. (2012) Protein kinase C stimulates HuD-mediated mRNA stability and protein expression of neurotrophic factors and enhances dendritic maturation of hippocampal neurons in culture. *Hippocampus* 22, 2303–2319
28. Carascossa, S. *et al.* (2010) CARM1 mediates the ligand-independent and tamoxifen-resistant activation of the estrogen receptor alpha by cAMP. *Genes Dev.* 24, 708–719
29. Bennesch, M.A. *et al.* (2016) LSD1 engages a corepressor complex for the activation of the estrogen receptor alpha by estrogen and cAMP. *Nucleic Acids Res.* 44, 8655–8670
30. Winter, D.L. *et al.* (2018) Characterization of protein methyltransferases Rkm1, Rkm4, Efm4, Efm7, Set5 and Hmt1 Reveals extensive post-translational modification. *J. Mol. Biol.* 430, 102–118
31. Cheung, W.D. *et al.* (2008) O-linked beta-N-acetylglucosaminyltransferase substrate specificity is regulated by myosin phosphatase targeting and other interacting proteins. *J. Biol. Chem.* 283, 33935–33941
32. Charoensuksai, P. *et al.* (2015) O-GlcNAcylation of coactivator-associated arginine methyltransferase 1 regulates its protein substrate specificity. *Biochem. J.* 466, 587–599
33. Sakabe, K. and Hart, G.W. (2010) O-GlcNAc transferase regulates mitotic chromatin dynamics. *J. Biol. Chem.* 285, 34460–34468
34. Kim, D. *et al.* (2014) Ubiquitination-dependent CARM1 degradation facilitates Notch1-mediated podocyte apoptosis in diabetic nephropathy. *Cell. Signal.* 26, 1774–1782
35. Shin, H.J. *et al.* (2016) AMPK-SKP2-CARM1 signalling cascade in transcriptional regulation of autophagy. *Nature* 534, 553–557
36. Li, C. *et al.* (2017) Nuclear AMPK regulated CARM1 stabilization impacts autophagy in aged heart. *Biochem. Biophys. Res. Commun.* 486, 398–405
37. Kuhn, P. *et al.* (2011) Automethylation of CARM1 allows coupling of transcription and mRNA splicing. *Nucleic Acids Res.* 39, 2717–2726
38. Lee, J. and Bedford, M.T. (2002) PABP1 identified as an arginine methyltransferase substrate using high-density protein arrays. *EMBO Rep.* 3, 268–273
39. Cheng, D. *et al.* (2007) The arginine methyltransferase CARM1 regulates the coupling of transcription and mRNA processing. *Mol. Cell* 25, 71–83
40. Peng, B.L. *et al.* (2020) A hypermethylation strategy utilized by enhancer-bound CARM1 to promote estrogen receptor alpha-dependent transcriptional activation and breast carcinogenesis. *Theranostics* 10, 3451–3473
41. Liu, Y. *et al.* (2018) A C9orf72-CARM1 axis regulates lipid metabolism under glucose starvation-induced nutrient stress. *Genes Dev.* 32, 1380–1397
42. Wei, X. *et al.* (2018) SKP2 promotes hepatocellular carcinoma progression through nuclear AMPK-SKP2-CARM1 signaling transcriptionally regulating nutrient-deprived autophagy induction. *Cell. Physiol. Biochem.* 47, 2484–2497
43. Sanchez, G. *et al.* (2016) A novel role for CARM1 in promoting nonsense-mediated mRNA decay: potential implications for spinal muscular atrophy. *Nucleic Acids Res.* 44, 2661–2676
44. Larsen, S.C. *et al.* (2016) Proteome-wide analysis of arginine monomethylation reveals widespread occurrence in human cells. *Sci. Signal* 9, rs9
45. Harrison, M.J. *et al.* (2010) Protein arginine methyltransferase 6 regulates multiple aspects of gene expression. *Nucleic Acids Res.* 38, 2201–2216
46. Hernando, C.E. *et al.* (2015) Genome wide comparative analysis of the effects of PRMT5 and PRMT4/CARM1 arginine methyltransferases on the *Arabidopsis thaliana* transcriptome. *BMC Genomics* 16, 192
47. Fedoriv, A. *et al.* (2019) Anti-tumor activity of the type I PRMT inhibitor, GSK3368715, synergizes with PRMT5 inhibition through MTAP loss. *Cancer Cell* 36, 100–114
48. Fong, J.Y. *et al.* (2019) Therapeutic targeting of RNA splicing catalysis through inhibition of protein arginine methylation. *Cancer Cell* 36, 194–209
49. Hu, S.B. *et al.* (2015) Protein arginine methyltransferase CARM1 attenuates the paraspeckle-mediated nuclear retention of mRNAs containing IRAlus. *Genes Dev.* 29, 630–645
50. Fox, A.H. *et al.* (2018) Paraspeckles: where long noncoding RNA meets phase separation. *Trends Biochem. Sci.* 43, 124–135
51. Hupalowska, A. *et al.* (2018) CARM1 and paraspeckles regulate pre-implantation mouse embryo development. *Cell* 175, 1902–1916
52. Pawlak, M.R. *et al.* (2000) Arginine N-methyltransferase 1 is required for early postimplantation mouse development, but cells deficient in the enzyme are viable. *Mol. Cell. Biol.* 20, 4859–4869
53. Tee, W.W. *et al.* (2010) Prmt5 is essential for early mouse development and acts in the cytoplasm to maintain ES cell pluripotency. *Genes Dev.* 24, 2772–2777
54. Yadav, N. *et al.* (2003) Specific protein methylation defects and gene expression perturbations in coactivator-associated arginine methyltransferase 1-deficient mice. *Proc. Natl. Acad. Sci. U. S. A.* 100, 6464–6468
55. Kim, D. *et al.* (2010) Enzymatic activity is required for the *in vivo* functions of CARM1. *J. Biol. Chem.* 285, 1147–1152
56. Ito, T. *et al.* (2009) Arginine methyltransferase CARM1/PRMT4 regulates endochondral ossification. *BMC Dev. Biol.* 9, 47
57. Kim, J. *et al.* (2004) Loss of CARM1 results in hypomethylation of thymocyte cyclic AMP-regulated phosphoprotein and deregulated early T cell development. *J. Biol. Chem.* 279, 25339–25344
58. Li, J. *et al.* (2013) Coactivator-associated arginine methyltransferase 1 regulates fetal hematopoiesis and thymocyte development. *J. Immunol.* 190, 597–604
59. Yadav, N. *et al.* (2008) CARM1 promotes adipocyte differentiation by coactivating PPARgamma. *EMBO Rep.* 9, 193–198
60. Kawabe, Y. *et al.* (2012) CARM1 regulates Pax7 transcriptional activity through MLL1/2 recruitment during asymmetric satellite stem cell divisions. *Cell Stem Cell* 11, 333–345

61. O'Brien, K.B. *et al.* (2010) CARM1 is required for proper control of proliferation and differentiation of pulmonary epithelial cells. *Development* 137, 2147–2156
62. Yang, G. *et al.* (2019) Base-editing-mediated R17H substitution in histone H3 reveals methylation-dependent regulation of Yap signaling and early mouse embryo development. *Cell Rep.* 26, 302–312
63. Torres-Padilla, M.E. *et al.* (2007) Histone arginine methylation regulates pluripotency in the early mouse embryo. *Nature* 445, 214–218
64. Goolam, M. *et al.* (2016) Heterogeneity in Oct4 and Sox2 targets biases cell fate in 4-cell mouse embryos. *Cell* 165, 61–74
65. Parfitt, D.E. and Zernicka-Goetz, M. (2010) Epigenetic modification affecting expression of cell polarity and cell fate genes to regulate lineage specification in the early mouse embryo. *Mol. Biol. Cell* 21, 2649–2660
66. Panamurova, M. *et al.* (2016) The BAF chromatin remodelling complex is an epigenetic regulator of lineage specification in the early mouse embryo. *Development* 143, 1271–1283
67. Sun, H. *et al.* (2020) CARM1 is heterogeneous in mouse four-cell embryo and important to blastocyst development. *Reproduction* 159, 91–104
68. Shi, J. *et al.* (2015) Dynamic transcriptional symmetry-breaking in pre-implantation mammalian embryo development revealed by single-cell RNA-seq. *Development* 142, 3468–3477
69. Wang, J. *et al.* (2018) Asymmetric expression of LincGET biases cell fate in two-cell mouse embryos. *Cell* 175, 1887–1901
70. Xu, Z. *et al.* (2013) MicroRNA-181 regulates CARM1 and histone arginine methylation to promote differentiation of human embryonic stem cells. *PLoS One* 8, e53146
71. Choi, S. *et al.* (2013) Regulation of pluripotency-related genes and differentiation in mouse embryonic stem cells by direct delivery of cell-penetrating peptide-conjugated CARM1 recombinant protein. *Dev. Reprod.* 17, 9–16
72. Wu, Q. *et al.* (2009) CARM1 is required in embryonic stem cells to maintain pluripotency and resist differentiation. *Stem Cells* 27, 2637–2645
73. Blanc, R.S. and Richard, S. (2017) Regenerating muscle with arginine methylation. *Transcription* 8, 175–178
74. Selvi, B.R. *et al.* (2015) CARM1 regulates astroglial lineage through transcriptional regulation of Nanog and posttranscriptional regulation by miR92a. *Mol. Biol. Cell* 26, 316–326
75. Buljan, M. *et al.* (2018) Systematic characterization of pan-cancer mutation clusters. *Mol. Syst. Biol.* 14, e7974
76. Cheng, H. *et al.* (2013) Overexpression of CARM1 in breast cancer is correlated with poorly characterized clinicopathologic parameters and molecular subtypes. *Diagn. Pathol.* 8, 129
77. Davis, M.B. *et al.* (2013) Expression and sub-cellular localization of an epigenetic regulator, co-activator arginine methyltransferase 1 (CARM1), is associated with specific breast cancer subtypes and ethnicity. *Mol. Cancer* 12, 40
78. Nakayama, N. *et al.* (2018) Cancer-related transcription regulator protein NAC1 forms a protein complex with CARM1 for ovarian cancer progression. *Oncotarget* 9, 28408–28420
79. Karakashev, S. *et al.* (2018) CARM1-expressing ovarian cancer depends on the histone methyltransferase EZH2 activity. *Nat. Commun.* 9, 631
80. Leonard, S. *et al.* (2012) Arginine methyltransferases are regulated by Epstein-Barr virus in B cells and are differentially expressed in Hodgkin's lymphoma. *Pathogens* 1, 52–64
81. Vu, L.P. *et al.* (2013) PRMT4 blocks myeloid differentiation by assembling a methyl-RUNX1-dependent repressor complex. *Cell Rep.* 5, 1625–1638
82. Zhong, X.Y. *et al.* (2018) CARM1 methylates GAPDH to regulate glucose metabolism and is suppressed in liver cancer. *Cell Rep.* 24, 3207–3223
83. Wang, Y.P. *et al.* (2016) Arginine methylation of MDH1 by CARM1 inhibits glutamine metabolism and suppresses pancreatic cancer. *Mol. Cell* 64, 673–687
84. Kim, Y.R. *et al.* (2010) Differential CARM1 expression in prostate and colorectal cancers. *BMC Cancer* 10, 197
85. Zhang, M. *et al.* (2017) Coactivator-associated arginine methyltransferase 1 promotes cell growth and is targeted by microRNA-195-5p in human colorectal cancer. *Tumour Biol.* 39, 1010428317694305
86. Hong, H. *et al.* (2004) Aberrant expression of CARM1, a transcriptional coactivator of androgen receptor, in the development of prostate carcinoma and androgen-independent status. *Cancer* 101, 83–89
87. Li, S. *et al.* (2017) The overexpression of CARM1 promotes human osteosarcoma cell proliferation through the pGSK3beta/beta-Catenin/cyclinD1 signaling pathway. *Int. J. Biol. Sci.* 13, 976–984
88. Behera, A.K. *et al.* (2019) Functional interplay between YY1 and CARM1 promotes oral carcinogenesis. *Oncotarget* 10, 3709–3724
89. Elakoum, R. *et al.* (2014) CARM1 and PRMT1 are dysregulated in lung cancer without hierarchical features. *Biochimie* 97, 210–218
90. Limm, K. *et al.* (2013) Deregulation of protein methylation in melanoma. *Eur. J. Cancer* 49, 1305–1313
91. Habashy, H.O. *et al.* (2013) The oestrogen receptor coactivator CARM1 has an oncogenic effect and is associated with poor prognosis in breast cancer. *Breast Cancer Res. Treat.* 140, 307–316
92. Moretti, A. *et al.* (2015) Arginine methyltransferases as novel therapeutic targets for breast cancer. *Mutagenesis* 30, 177–189
93. Frieze, S. *et al.* (2008) CARM1 regulates estrogen-stimulated breast cancer growth through up-regulation of E2F1. *Cancer Res.* 68, 301–306
94. Gao, W.W. *et al.* (2018) JMJD6 licenses ERalpha-dependent enhancer and coding gene activation by modulating the recruitment of the CARM1/MED12 co-activator complex. *Mol. Cell* 70, 340–357
95. Liu, J. *et al.* (2020) Arginine methylation-dependent LSD1 stability promotes invasion and metastasis of breast cancer. *EMBO Rep.* 21, e48597
96. Bao, J. *et al.* (2019) Mouse models of overexpression reveal distinct oncogenic roles for different type I protein arginine methyltransferases. *Cancer Res.* 79, 21–32
97. Liu, F. *et al.* (2017) PKM2 methylation by CARM1 activates aerobic glycolysis to promote tumorigenesis. *Nat. Cell Biol.* 19, 1358–1370
98. Karakashev, S. *et al.* (2020) EZH2 inhibition sensitizes CARM1-high, homologous recombination proficient ovarian cancers to PARP inhibition. *Cancer Cell* 37, 157–167
99. Drew, A.E. *et al.* (2017) Identification of a CARM1 inhibitor with potent *in vitro* and *in vivo* activity in preclinical models of multiple myeloma. *Sci. Rep.* 7, 17993
100. Veazey, K.J. *et al.* (2020) CARM1 inhibition reduces histone acetyltransferase activity causing synthetic lethality in CREBBP/EP300-mutated lymphomas. *Leukemia* 34, 3269–3285
101. Nakayama, K. *et al.* (2018) TP-064, a potent and selective small molecule inhibitor of PRMT4 for multiple myeloma. *Oncotarget* 9, 18480–18493
102. Nie, M. *et al.* (2018) CARM1-mediated methylation of protein arginine methyltransferase 5 represses human gamma-globin gene expression in erythroleukemia cells. *J. Biol. Chem.* 293, 17454–17463
103. Cheng, D. *et al.* (2012) Methods applied to the study of protein arginine methylation. *Methods Enzymol.* 512, 71–92
104. Ong, S.E. *et al.* (2004) Identifying and quantifying *in vivo* methylation sites by heavy methyl SILAC. *Nat. Methods* 1, 119–126
105. Uhlmann, T. *et al.* (2012) A method for large-scale identification of protein arginine methylation. *Mol. Cell. Proteomics* 11, 1489–1499
106. Geoghegan, V. *et al.* (2015) Comprehensive identification of arginine methylation in primary T cells reveals regulatory roles in cell signalling. *Nat. Commun.* 6, 6758
107. Wang, K. *et al.* (2016) Antibody-free approach for the global analysis of protein methylation. *Anal. Chem.* 88, 11319–11327
108. Naeem, H. *et al.* (2007) The activity and stability of the transcriptional coactivator p/CIP/SRC-3 are regulated by CARM1-dependent methylation. *Mol. Cell. Biol.* 27, 120–134
109. Boisvert, F.M. *et al.* (2003) A proteomic analysis of arginine-methylated protein complexes. *Mol. Cell. Proteomics* 2, 1319–1330

110. Guo, A. *et al.* (2014) Immunoaffinity enrichment and mass spectrometry analysis of protein methylation. *Mol. Cell. Proteomics* 13, 372–387
111. Cheng, D. *et al.* (2018) CARM1 methylates MED12 to regulate its RNA-binding ability. *Life Sci. Alliance* 1, e201800117
112. Ma, M. *et al.* (2017) Strategy based on deglycosylation, multiprotease, and hydrophilic interaction chromatography for large-scale profiling of protein methylation. *Anal. Chem.* 89, 12909–12917
113. Hartel, N.G. *et al.* (2019) Deep protein methylation profiling by combined chemical and immunoaffinity approaches reveals novel PRMT1 targets. *Mol. Cell. Proteomics* 18, 2149–2164
114. Wang, Q. *et al.* (2019) A new chromatographic approach to analyze methylproteome with enhanced lysine methylation identification performance. *Anal. Chim. Acta* 1068, 111–119
115. Qin, H. *et al.* (2019) The long noncoding RNA ST7-AS1 promotes laryngeal squamous cell carcinoma by stabilizing CARM1. *Biochem. Biophys. Res. Commun.* 512, 34–40
116. Wang, D. and Hu, Y. (2019) Long non-coding RNA PVT1 competitively binds microRNA-424-5p to regulate CARM1 in radiosensitivity of non-small-cell lung cancer. *Mol. Ther. Nucleic Acids* 16, 130–140
117. Zheng, L. *et al.* (2017) miR-195 enhances the radiosensitivity of colorectal cancer cells by suppressing CARM1. *Oncotargets Ther.* 10, 1027–1038





## **ANNEXE II: Known CARM1 substrates**

**List of CARM1 substrates identified so far.** Modified from Suresh et al., 2021, *Trends in Cell Biology*

<b>Substrate</b>	<b>Methylated arginine residue</b> (human amino-acid numbering)	<b>Sequence</b> (corresponding to the human protein)	<b>Residue shown to be methylated <i>in vitro/in vivo</i></b>	<b>Arginine residue methylated by other PRMTs?</b>	<b>CARM1-isoform specific methylation?</b>	<b>Impact of the methylation on the function of the substrate</b>	<b>Refs</b>
AIB1 (= p/CIP, SRC-3, ACTR, RAC3, NCOA3)	R849 R854 R1171 R1177 R1188	QS <b>IR</b> <sup>1</sup> PPYNRA PYN <b>RA</b> VSLDS PKQL <b>RM</b> QLQ LQQ <b>RL</b> QGQQ NQ <b>S</b> RQALELK	both	Not PRMT1	ND <sup>2</sup>	impairs association to CBP	[1, 2]
BAF155	R1064 <sup>*3</sup>	PGNILG <b>P</b> RVPL	both	No	ND	switches promoter occupancy	[3, 4]

<sup>1</sup> The methylated arginine is indicated in bold

<sup>2</sup> ND: not determined

<sup>3</sup> If a custom antibody detecting the methylated arginine was generated is indicated with an asterisk (\*)

						from BAF155 to EZH2	
CA150 (= TCERG1)	R28 R30 R41 R48	QAL <b>R</b> FRGP LRF <b>R</b> GPAPP VM <b>R</b> GPPP PPPLM <b>R</b> PPPP	both	Yes, PRMT5	ND	allows interaction with the tudor domain of SMN	[5]
CARM1	R550*	NHTHS <b>R</b> MGSIMS	both	No	CARM1-FL only	affects pre-mRNA splicing	[6, 7]
CBP	KIX domain: R601 R625	TQDL <b>R</b> SHLV LKDR <b>R</b> MENL	by sequence homology to p300	ND	ND	blocks CREB activation by disabling the binding between KIX and the kinase inducible domain of CREB.	[8]
	R714* R742*	PLSLPVN <b>R</b> MQVSQ QAPMG <b>P</b> RAASP	both	ND	ND	induces for GRIP-1- and	[9, 10]

	R768* R2151*	MAISPS <b>R</b> MPQPP QAGV <b>P</b> RPGVPP				steroid hormone- mediated gene activation; increases histone- acetyltransferas e activity	
GAPDH	R234*	GMAF <b>R</b> VPTA	both	No	ND	inhibits glycolysis	[11]
Histone H3	R2*	<b>A</b> RTKQTARK	both	No	No	ND	[12-14]
	R17*	GGKAP <b>R</b> KQL	both	PRMT6	No	transcriptional activation	[12-18]
	R26*	ATKA <b>A</b> RSAPAT	both	No	No	transcriptional activation and repression	[12, 14, 19, 20]

	R42	KKPHRY <b>R</b> PGTVA	<i>in vitro</i>	PRMT6	No	transcriptional activation	[21]
HSP70	R469*	IPPAP <b>R</b> GV PQI	both	No	ND	regulates retinoid acid- mediated RAR $\beta$ 2 gene activation	[22]
HuD	R248	QAQ <b>R</b> FRLDN	both	Not PRMT1	ND	affects mRNA turnover of p21cip1/waf1	[23]
HuR	R217*	QAQ <b>R</b> FRFSP	both	Not PRMT1,2,3	ND	affects subcellular localization and stability	[24-26]
LSD1	R838*	MYTL <b>R</b> QATP	both	Not PRMT1/5/ 6/7	ND	affects stabilization	[27]

MDH1	R248*	TTVQQ <b>R</b> GAAVIK	<i>in vivo</i>	Not PRMT1/2/ 3	ND	inhibits activity	[28]
MED12	R1782 R1792 R1854 R1859 R1862* R1871 R1899* R1910 R1912 R1994 R2015	PPSTEER <b>K</b> KKK TKGKK <b>R</b> SQPA PAGGP <b>R</b> VDP VDPY <b>R</b> PVRLP PV <b>R</b> LPMQKL KLPT <b>R</b> P TYP TSVY <b>R</b> QQQP PQGQ <b>R</b> LRQQ PQGQ <b>R</b> LRQQ HLQQ <b>R</b> PSGY TSTQ <b>R</b> FSHQ	both	No	ND	suppresses p21 transcription  mediates interaction with TDRD3  important for ER- $\alpha$ mediated gene transcription	[29-32]
NOTCH1	R2263 R2272 R2313 R2327 R2372*	GGG <b>R</b> LAFET GPP <b>R</b> LSHLP WLS <b>R</b> LQSGM YNPL <b>R</b> GSVAP LPST <b>R</b> LATQP	both	possibly PRMT6	ND	controls stability	[33]

p300	R580 R604 R651 (minor)	TQDL <b>R</b> NHLV LKDR <b>R</b> MENL RR <b>R</b> LQK	<i>in vitro</i>	ND	ND	blocks CREB activation by disabling the interaction between KIX and the kinase inducible domain of CREB.	[8]
	R754*	YG <b>P</b> RMQQP	both	ND	ND	important for binding to BRCA1	[34]
	R2142*	AGVQ <b>R</b> AGLP	both	ND	ND	impairs binding to GRIP1 and ACT	[35, 36]
p54nrb (= NonO)	R357* R365* R378	EM <b>R</b> RQQEE MM <b>R</b> RQQEG FPD <b>A</b> REQEI	both	PRMT1/6 (less than CARM1)	ND	reduces binding to mRNAs	[37]

						containing IRAlus	
PABP1	R455* R460* R506	PGAI <b>R</b> PAAP PAAP <b>R</b> PPFST TPAV <b>R</b> TVPQY	both	No	No	no impact on stability or distribution	[38-40]
Pax7	R10 R13 R22 R37	PGTV <b>P</b> RMMRP PRMM <b>R</b> PAPGQ PGQNY <b>P</b> RTGFP PLGQ <b>G</b> RVNQ	both	No	CARM1- $\Delta$ E15 only	induces <i>Myf5</i> expression	[41, 42]
PKM2	R445* R447* R455	VARY <b>R</b> PR RYR <b>P</b> RAPIIA PIIAV <b>T</b> RNPQ	both	No	ND	increases activity	[43, 44]
pRb	R775 R787* R798	QYAST <b>R</b> PPTLS PIPHIP <b>R</b> SPYKFP PSSPL <b>R</b> IPGG	<i>in vitro</i> both <i>in vitro</i>	ND	ND	negatively regulates tumor suppressor function	[45]
PRMT5	R505*	PYVV <b>R</b> LHNF	Both	Not PRMT1 or PRMT5	ND	essential for oligomerization and	[46]



				(auto-methylation)		methyltransferase activity	
Pontin	R333* R339*	FASN <b>R</b> GNCV NCV <b>I</b> RGTED	both both	Not PRMT5 or PRMT6	ND	enhances interaction to FoxO3, to initiate autophagy gene transcription	[47]
Ribose-5-phosphate isomerase A (RPIA)	R42	PGSHV <b>R</b> LPGR	both	ND	ND	promotes the catalytic activity of RPIA upon glucose-starvation	[48]
RNA Pol II	R1810*	YSPSS <b>P</b> RYTPQS	Both	ND	ND	facilitates expression of select small nuclear RNAs	[49]

RUNX1	R223*	PTPN <b>P</b> RASLN	both	ND	ND	regulates binding to DPF2	[50]
Sox2	R113*	PDYKY <b>R</b> PRRK	both	No	ND	enhances self-association	[51]
TARPP	R655	TQQY <b>R</b> PMAP	both	ND	ND	exact function unknown	[52]
YY1	R281 R294 R323 R342 R363 R381	AEFAR <b>M</b> KP DDAP <b>R</b> TIACP THGPR <b>V</b> HV KLK <b>R</b> HQLV GCGK <b>R</b> FSLDF TGDR <b>P</b> YVCP	<i>in vitro</i>	ND	ND	unknown	[53]
Potential CARM1 substrates that are yet to be functionally validated can be found in [5, 30, 32, 38, 54, 55]							

1. Naeem, H. et al. (2007) The activity and stability of the transcriptional coactivator p/CIP/SRC-3 are regulated by CARM1-dependent methylation. Mol Cell Biol 27 (1), 120-34.

2. Feng, Q. et al. (2006) Signaling within a coactivator complex: methylation of SRC-3/AIB1 is a molecular switch for complex disassembly. *Mol Cell Biol* 26 (21), 7846-57.
3. Wang, L. et al. (2014) CARM1 methylates chromatin remodeling factor BAF155 to enhance tumor progression and metastasis. *Cancer Cell* 25 (1), 21-36.
4. Karakashev, S. et al. (2018) CARM1-expressing ovarian cancer depends on the histone methyltransferase EZH2 activity. *Nat Commun* 9 (1), 631.
5. Cheng, D. et al. (2007) The arginine methyltransferase CARM1 regulates the coupling of transcription and mRNA processing. *Mol Cell* 25 (1), 71-83.
6. Kuhn, P. et al. (2011) Automethylation of CARM1 allows coupling of transcription and mRNA splicing. *Nucleic Acids Res* 39 (7), 2717-26.
7. Wang, L. et al. (2013) CARM1 automethylation is controlled at the level of alternative splicing. *Nucleic Acids Res* 41 (14), 6870-80.
8. Xu, W. et al. (2001) A transcriptional switch mediated by cofactor methylation. *Science* 294 (5551), 2507-11.
9. Chevillard-Briet, M. et al. (2002) Control of CBP co-activating activity by arginine methylation. *EMBO J* 21 (20), 5457-66.
10. Ceschin, D.G. et al. (2011) Methylation specifies distinct estrogen-induced binding site repertoires of CBP to chromatin. *Genes Dev* 25 (11), 1132-46.
11. Zhong, X.Y. et al. (2018) CARM1 Methylates GAPDH to Regulate Glucose Metabolism and Is Suppressed in Liver Cancer. *Cell Rep* 24 (12), 3207-3223.
12. Schurter, B.T. et al. (2001) Methylation of histone H3 by coactivator-associated arginine methyltransferase 1. *Biochemistry* 40 (19), 5747-56.
13. Yang, Y. et al. (2010) TDRD3 is an effector molecule for arginine-methylated histone marks. *Mol Cell* 40 (6), 1016-23.
14. Jacques, S.L. et al. (2016) CARM1 Preferentially Methylates H3R17 over H3R26 through a Random Kinetic Mechanism. *Biochemistry* 55 (11), 1635-44.
15. Ma, H. et al. (2001) Hormone-dependent, CARM1-directed, arginine-specific methylation of histone H3 on a steroid-regulated promoter. *Curr Biol* 11 (24), 1981-5.
16. Bauer, U.M. et al. (2002) Methylation at arginine 17 of histone H3 is linked to gene activation. *EMBO Rep* 3 (1), 39-44.
17. Yang, G. et al. (2019) Base-Editing-Mediated R17H Substitution in Histone H3 Reveals Methylation-Dependent Regulation of Yap Signaling and Early Mouse Embryo Development. *Cell Rep* 26 (2), 302-312 e4.

18. Cheng, D. et al. (2020) Genetic evidence for partial redundancy between the arginine methyltransferases CARM1 and PRMT6. *J Biol Chem* 295 (50), 17060-17070.
19. Goolam, M. et al. (2016) Heterogeneity in Oct4 and Sox2 Targets Biases Cell Fate in 4-Cell Mouse Embryos. *Cell* 165 (1), 61-74.
20. Zhang, Z. et al. (2017) Crosstalk between histone modifications indicates that inhibition of arginine methyltransferase CARM1 activity reverses HIV latency. *Nucleic Acids Res* 45 (16), 9348-9360.
21. Casadio, F. et al. (2013) H3R42me2a is a histone modification with positive transcriptional effects. *Proc Natl Acad Sci U S A* 110 (37), 14894-9.
22. Gao, W.W. et al. (2015) Arginine methylation of HSP70 regulates retinoid acid-mediated RARbeta2 gene activation. *Proc Natl Acad Sci U S A* 112 (26), E3327-36.
23. Fujiwara, T. et al. (2006) CARM1 regulates proliferation of PC12 cells by methylating HuD. *Mol Cell Biol* 26 (6), 2273-85.
24. Li, H. et al. (2002) Lipopolysaccharide-induced methylation of HuR, an mRNA-stabilizing protein, by CARM1. Coactivator-associated arginine methyltransferase. *J Biol Chem* 277 (47), 44623-30.
25. Battaglia-Hsu, S.F. et al. (2018) Inherited disorders of cobalamin metabolism disrupt nucleocytoplasmic transport of mRNA through impaired methylation/phosphorylation of ELAVL1/HuR. *Nucleic Acids Res* 46 (15), 7844-7857.
26. Calvanese, V. et al. (2010) Sirtuin 1 regulation of developmental genes during differentiation of stem cells. *Proc Natl Acad Sci U S A* 107 (31), 13736-41.
27. Liu, J. et al. (2020) Arginine methylation-dependent LSD1 stability promotes invasion and metastasis of breast cancer. *EMBO Rep* 21 (2), e48597.
28. Wang, Y.P. et al. (2016) Arginine Methylation of MDH1 by CARM1 Inhibits Glutamine Metabolism and Suppresses Pancreatic Cancer. *Mol Cell* 64 (4), 673-687.
29. Wang, L. et al. (2015) MED12 methylation by CARM1 sensitizes human breast cancer cells to chemotherapy drugs. *Sci Adv* 1 (9), e1500463.
30. Cheng, D. et al. (2018) CARM1 methylates MED12 to regulate its RNA-binding ability. *Life Sci Alliance* 1 (5), e201800117.
31. Gao, W.W. et al. (2018) JMJD6 Licenses ERalpha-Dependent Enhancer and Coding Gene Activation by Modulating the Recruitment of the CARM1/MED12 Co-activator Complex. *Mol Cell* 70 (2), 340-357 e8.
32. Peng, B.L. et al. (2020) A hypermethylation strategy utilized by enhancer-bound CARM1 to promote estrogen receptor alpha-dependent transcriptional activation and breast carcinogenesis. *Theranostics* 10 (8), 3451-3473.

33. Hein, K. et al. (2015) Site-specific methylation of Notch1 controls the amplitude and duration of the Notch1 response. *Sci Signal* 8 (369), ra30.
34. Lee, Y.H. et al. (2011) Regulated recruitment of tumor suppressor BRCA1 to the p21 gene by coactivator methylation. *Genes Dev* 25 (2), 176-88.
35. Bao, J. et al. (2018) The arginine methyltransferase CARM1 represses p300\*ACT\*CREMtau activity and is required for spermiogenesis. *Nucleic Acids Res* 46 (9), 4327-4343.
36. Lee, Y.H. et al. (2005) Regulation of coactivator complex assembly and function by protein arginine methylation and demethylination. *Proc Natl Acad Sci U S A* 102 (10), 3611-6.
37. Hu, S.B. et al. (2015) Protein arginine methyltransferase CARM1 attenuates the paraspeckle-mediated nuclear retention of mRNAs containing IRAlus. *Genes Dev* 29 (6), 630-45.
38. Lee, J. and Bedford, M.T. (2002) PABP1 identified as an arginine methyltransferase substrate using high-density protein arrays. *EMBO Rep* 3 (3), 268-73.
39. Cheng, D. and Bedford, M.T. (2011) Xenoestrogens regulate the activity of arginine methyltransferases. *Chembiochem* 12 (2), 323-9.
40. Brook, M. et al. The multifunctional poly(A)-binding protein (PABP) 1 is subject to extensive dynamic post-translational modification, which molecular modelling suggests plays an important role in co-ordinating its activities. (1470-8728 (Electronic)).
41. Kawabe, Y. et al. (2012) Carm1 regulates Pax7 transcriptional activity through MLL1/2 recruitment during asymmetric satellite stem cell divisions. *Cell Stem Cell* 11 (3), 333-45.
42. Chang, N.C. et al. (2018) The Dystrophin Glycoprotein Complex Regulates the Epigenetic Activation of Muscle Stem Cell Commitment. *Cell Stem Cell* 22 (5), 755-768 e6.
43. Abeywardana, T. et al. (2018) CARM1 suppresses de novo serine synthesis by promoting PKM2 activity. *J Biol Chem* 293 (39), 15290-15303.
44. Liu, F. et al. (2017) PKM2 methylation by CARM1 activates aerobic glycolysis to promote tumorigenesis. *Nat Cell Biol* 19 (11), 1358-1370.
45. Kim, K.Y. et al. (2015) PRMT4-mediated arginine methylation negatively regulates retinoblastoma tumor suppressor protein and promotes E2F-1 dissociation. *Mol Cell Biol* 35 (1), 238-48.



46. Nie, M. et al. (2018) CARM1-mediated methylation of protein arginine methyltransferase 5 represses human gamma-globin gene expression in erythroleukemia cells. *J Biol Chem* 293 (45), 17454-17463.
47. Yu, Y.S. et al. (2020) Pontin arginine methylation by CARM1 is crucial for epigenetic regulation of autophagy. *Nat Commun* 11 (1), 6297.
48. Guo, J. et al. (2020) Arginine methylation of ribose-5-phosphate isomerase A senses glucose to promote human colorectal cancer cell survival. *Sci China Life Sci* 63 (9), 1394-1405.
49. Sims, R.J., 3rd et al. (2011) The C-terminal domain of RNA polymerase II is modified by site-specific methylation. *Science* 332 (6025), 99-103.
50. Vu, L.P. et al. (2013) PRMT4 blocks myeloid differentiation by assembling a methyl-RUNX1-dependent repressor complex. *Cell Rep* 5 (6), 1625-38.
51. Zhao, H.Y. et al. (2011) CARM1 mediates modulation of Sox2. *PLoS One* 6 (10), e27026.
52. Kim, J. et al. (2004) Loss of CARM1 results in hypomethylation of thymocyte cyclic AMP-regulated phosphoprotein and deregulated early T cell development. *J Biol Chem* 279 (24), 25339-44.
53. Behera, A.K. et al. (2019) Functional interplay between YY1 and CARM1 promotes oral carcinogenesis. *Oncotarget* 10 (38), 3709-3724.
54. Guo, A. et al. (2014) Immunoaffinity enrichment and mass spectrometry analysis of protein methylation. *Mol Cell Proteomics* 13 (1), 372-87.
55. Shishkova, E. et al. (2017) Global mapping of CARM1 substrates defines enzyme specificity and substrate recognition. *Nat Commun* 8, 15571.



# **ANNEXE III: Protein arginine methyltransferase 5: A novel therapeutic target for triple-negative breast cancer**



# Protein arginine methyltransferase 5: A novel therapeutic target for triple-negative breast cancers

Mathilde Vinet<sup>1,2</sup>  | Samyuktha Suresh<sup>1,2</sup> | Virginie Maire<sup>1,2</sup> | Clarisse Monchecourt<sup>1,2</sup> | Fariba Némati<sup>1,3</sup> | Laetitia Lesage<sup>4</sup> | Fabienne Pierre<sup>1,2,5</sup> | Mengliang Ye<sup>1,2</sup> | Auriane Lescure<sup>1,5</sup> | Amélie Brisson<sup>1,2</sup> | Didier Meseure<sup>4</sup> | André Nicolas<sup>4</sup> | Guillem Rigail<sup>6,7</sup> | Elisabetta Marangoni<sup>1,3</sup> | Elaine Del Nery<sup>1,5</sup> | Sergio Roman-Roman<sup>1</sup> | Thierry Dubois<sup>1,2</sup> 

<sup>1</sup>Translational Research Department, Institut Curie, PSL Research University, Paris, France

<sup>2</sup>Breast Cancer Biology Group, Institut Curie, Paris, France

<sup>3</sup>Preclinical Investigation Laboratory, Institut Curie, Paris, France

<sup>4</sup>Platform of Investigative Pathology, Department of Pathology, Institut Curie, Paris, France

<sup>5</sup>Biophenics High-Content Screening Laboratory, Cell and Tissue Imaging Facility (PICT-IBiSA), Institut Curie, Paris, France

<sup>6</sup>Institute of Plant Sciences Paris-Saclay (IPS2), UMR 9213, UMR1403, CNRS, INRA, Université Paris-Sud, Université d'Evry, Université Paris-Diderot, Sorbonne, Paris-Cité, Orsay, France

<sup>7</sup>Laboratoire de Mathématiques et Modélisation d'Evry (LaMME), Université d'Evry Val d'Essonne, UMR CNRS 8071, ENSIIE, USC INRA, Evry, France

## Correspondence

Thierry Dubois, Translational Research Department, Institut Curie, PSL Research University, Paris, France.  
Email: thierry.dubois@curie.fr

## Funding information

Institut Curie; Cancéropôle Île-de-France; Institut National Du Cancer; Université de Recherche Paris Sciences et Lettres; European Union's Horizon 2020 Research and Innovation Programme under the Marie Skłodowska-Curie Grant

## Abstract

TNBC is a highly heterogeneous and aggressive breast cancer subtype associated with high relapse rates, and for which no targeted therapy yet exists. Protein arginine methyltransferase 5 (PRMT5), an enzyme which catalyzes the methylation of arginines on histone and non-histone proteins, has recently emerged as a putative target for cancer therapy. Potent and specific PRMT5 inhibitors have been developed, but the therapeutic efficacy of PRMT5 targeting in TNBC has not yet been demonstrated. Here, we examine the expression of PRMT5 in a human breast cancer cohort obtained from the Institut Curie, and evaluate the therapeutic potential of pharmacological inhibition of PRMT5 in TNBC. We find that PRMT5 mRNA and protein are expressed at comparable levels in TNBC, luminal breast tumors, and healthy mammary tissues. However, immunohistochemistry analyses reveal that PRMT5 is differentially localized in TNBC compared to other breast cancer subtypes and to normal breast tissues. PRMT5 is heterogeneously expressed in TNBC and high PRMT5 expression correlates with poor prognosis within this breast cancer subtype. Using the small-molecule inhibitor EPZ015666, we show that PRMT5 inhibition impairs cell proliferation in a subset of TNBC cell lines. PRMT5 inhibition triggers apoptosis, regulates cell cycle progression and decreases mammosphere formation. Furthermore, EPZ015666 administration to a patient-derived xenograft model of TNBC significantly deters tumor progression. Finally, we reveal potentiation between EGFR and PRMT5 targeting, suggestive of a beneficial combination therapy. Our findings highlight a distinctive subcellular localization of PRMT5 in TNBC, and uphold PRMT5 targeting, alone or in combination, as a relevant treatment strategy for a subset of TNBC.

## KEY WORDS

breast cancer, molecular biology, targeted therapy, translational research

This is an open access article under the terms of the Creative Commons Attribution License, which permits use, distribution and reproduction in any medium, provided the original work is properly cited.

© 2019 The Authors. *Cancer Medicine* published by John Wiley & Sons Ltd.

## 1 | INTRODUCTION

The efficacy of breast cancer therapeutic management has considerably improved in recent years, however, the subgroup of patients with triple-negative breast cancers (TNBC), defined by the absence of expression of estrogen (ER) and progesterone (PR) receptors and of HER2 overexpression, maintain a poor prognosis.<sup>1</sup> One of the major problematics in TNBC therapeutic management is the heterogeneity of the disease, and the absence of clear molecular targets.<sup>2</sup> To account for this heterogeneity, several groups have classified TNBC into distinct subtypes based on DNA, RNA, epigenetic and proteomic profiling, with the aim of providing therapeutic guidance. TNBC patients generally respond well to conventional chemotherapies, but suffer high recurrence rates due to residual, resistant tumor cells, and continually represent a large proportion of breast cancer deaths. TNBC thus remain a major challenge for oncologists, and the development of alternative treatments is warranted to bypass resistance to chemotherapies and improve patient survival rates.<sup>3,4</sup>

Protein arginine methylation is a key post-translational modification implicated in gene transcription and signal transduction.<sup>5</sup> Protein arginine methyltransferase 5 (PRMT5) is the main type II PRMT, which catalyzes the symmetric dimethylation of arginine residues of histone and non-histone proteins.<sup>6</sup> PRMT5 functions as part of a complex coined the methylosome, along with its binding partner and co-activator methylosome protein 50 (MEP50). PRMT5 is overexpressed in a number of cancers including melanoma, multiple myeloma, glioblastoma, lung, gastric, prostate, ovarian, and colorectal cancers,<sup>6</sup> and high expression of PRMT5 often correlates with poor patient prognosis.<sup>6</sup>

Moreover, PRMT5 regulates the expression and activity of key players in oncogenic and apoptotic signaling, and was shown to participate in stem cell maintenance.<sup>6,7</sup> PRMT5-mediated H3R8 and H4R3 methylation, for example, repress the transcription of a number of tumor suppressors including RB-family genes, ST7, and NM23, leading to increased cell survival and proliferation.<sup>8,9</sup> PRMT5 also directly methylates p53, PI3K, and E2F-1, thereby influencing the transcriptional activity of these essential cell fate regulators to promote cell growth and inhibit apoptosis.<sup>10-12</sup> Given this, PRMT5 has been attributed oncogenic functions and has recently received considerable attention as a potential therapeutic target in cancer. Several selective and potent small-molecule inhibitors have been developed against PRMT5 and their effects on cancer development are now being assessed in vitro, in vivo,<sup>13-15</sup> as well as in a clinical trial.<sup>15,16</sup> Among these is the inhibitor EPZ015666, which competes with the PRMT5 peptide substrate binding pocket to impede PRMT5-substrate interaction and subsequent methylation.<sup>13</sup> In this study, we evaluate the therapeutic potential of PRMT5 inhibition in TNBC in vitro and in vivo using the specific and potent inhibitor

EPZ015666,<sup>13</sup> and analyze the expression and localization of PRMT5 in a cohort of human breast cancer biopsies.

## 2 | MATERIALS AND METHODS

### 2.1 | Human samples, transcriptome microarray, and immunohistochemistry

Our cohort has been described previously.<sup>17</sup> Briefly, transcriptome microarray (U133 Plus 2.0 Affymetrix chips) was performed on TNBC (n = 41), HER2+/ER- (n = 30), luminal A (LA, n = 29), luminal B (LB, n = 30), and normal human samples (n = 11).<sup>17</sup> Immunohistochemistry (IHC) was performed as described<sup>17,18</sup> on the following number of tumors (TNBC: n = 41; HER2+/ER-: n = 29; LA: n = 22; LB: n = 27) and on normal breast tissues (n = 7). For PRMT5 staining, tissue microarrays (TMA) containing alcohol, formalin and acetic acid (AFA)-fixed paraffin-embedded tissues were made as described.<sup>17,18</sup> Antigen retrieval was performed in EDTA buffer pH = 6 (PRMT5). The PRMT5 antibody (Table S1) was validated for IHC using cell pellets fixed in the same way than the tumors from cell lines depleted or not of PRMT5. To assess whether the mean percentage of stained cells differs between any two subtypes, we performed Student *t* tests.

The TCGA breast invasive carcinoma (TCGA-BRCA) cohort is publicly available.<sup>19</sup> The RNA-SeqV2 Level 3 data (Jan 2015) were downloaded from the TCGA Research Network (<http://cancergenome.nih.gov/>) and integrated into a platform in knowledge data integration (KDI) at Institut Curie (<https://bioinfo-portal.curie.fr>). Subtype classification was based on immunohistochemical status for the estrogen receptor (ER), progesterone receptor (PR) and HER2, as follows. TNBC: ER-, PR- and HER2-negative (n = 157); HER2+/ER-: ER- and PR-negative, HER2-positive (n = 41); luminal B: ER- and/or PR-positive, HER2-positive (n = 153); luminal A: ER- and/or PR-positive, HER2-negative (n = 663). The TCGA database includes 113 referenced normal breast tissue samples.

### 2.2 | Cell culture

Cell lines were purchased between 2005 and 2009 from the American Type Culture Collection (ATCC, LGC Promochem) and authenticated by short tandem repeat profiling in 2018, using the Powerplex 16 system (Promega). All cell lines were cultured as described.<sup>20,21</sup> MDA-MB-468 cells were cultured in RPMI-1640 (LifeTechnologies) supplemented with 10% (vol/vol) fetal bovine serum (FBS, LifeTechnologies), 100 U/mL penicillin and 100 µg/mL streptomycin (P/S, LifeTechnologies). HCC38, HCC70, HCC1937, and HCC1954 cells were cultured using the same media, complemented with 1.5 g/L sodium bicarbonate (LifeTechnologies), 10 mmol/L

Hepes (LifeTechnologies), and 1 mmol/L sodium pyruvate (LifeTechnologies). MDA-MB-157 and Hs578-T cells were cultured in DMEM (Life Technologies) supplemented with 10% FBS and 1% P/S. MCF-10A and MCF-12A cells were cultured in the same media, supplemented with 0.01 mg/mL insulin, 100 ng/mL cholera toxin (Sigma), 500 ng/mL hydrocortisone (SERB Laboratories), and 20 ng/mL epidermal growth factor (Sigma). MDA-MB-453 cells were cultured in DMEM-F12 (LifeTechnologies) supplemented with 10% FBS and 1% P/S. BT-20 and MCF-7 cells were cultured in MEM (Sigma-Aldrich) containing 10% FBS, 1% P/S, 1.5 g/L sodium bicarbonate, 0.1 mmol/L non-essential amino-acids (NEAA, LifeTechnologies) and 1 mmol/L sodium pyruvate. SK-BR-3 cells (HTB-30) were cultured in McCoy5a (LifeTechnologies) containing 10% FBS and 1% P/S. All cell lines were maintained at 37°C in a humidified atmosphere with 5% CO<sub>2</sub>.

### 2.3 | PRMT5 inhibitors, antibodies, and small interfering RNAs (siRNAs)

PRMT5 inhibitor EPZ015666 was purchased from Clinisciences and DC Chemicals. EPZ015938 was purchased from Selleckchem. Antibodies used are listed in Table S1. All siRNAs were purchased from Qiagen: Allstars negative control (SI03650318); PRMT5\_1 (SI04216492), target sequence 5'-TGCCGTGGTGACGCTAGAGAA-3'; PRMT5\_2 (SI04248951), target sequence 5'-CAGAGATCCTATGATTGACAA-3'; PRMT5\_3 (SI04308416), target sequence 5'-CTGGCGATGCAGCAATTCCAA-3'; PRMT5\_4 (SI00719432), target sequence 5'-CAGCCATAACGGTACGTGAA-3'.

### 2.4 | Cellular assays

Cell assays were performed as already described.<sup>17,18,20-22</sup> Briefly, cells were incubated with DMSO or a PRMT5 inhibitor (EPZ015666, EPZ015938), or transfected with 40 nmol/L siRNA (Qiagen) using INTERFERin (Polyplus Transfection) (BT-20, Hs578T, MCF-10A, MDA-MB-453, MDA-MB-468) or Lipofectamine RNAiMAX (Life Technologies) (HCC38, HCC70). Cell proliferation determined by MTT (Sigma). Apoptotic activity was determined by the Caspase-Glo 3/7 luminescent assay (Promega) or by Western blot analysis. Caspase activity using the luminescent assay was normalized to cell viability, measured by a concomitant MTT assay. Cell-cycle analysis was carried out with LSRII (Becton Dickinson) using BD FACSDIVA Software™ (BD Bioscience) to determine cellular DNA content, and analyzed using FlowJo and Modfit LT softwares. For the colony formation assay, cells were treated with drugs or siRNA, and incubated for 5 (MCF10A), 9 (MDA-MB-468) or 14 days (BT20, HCC38, HCC70, MDA-MB-453). Colonies were then stained with a solution

containing 0.05% Coomassie Brilliant Blue R-250, 50% methanol, 10% acetic acid, 40% ultrapure water for 20 minutes and rinsed with water. For the mammosphere formation assay, 2000 HCC38 cells were seeded in six-well ultra-low attachment plates (Corning, VWR, ref. 734-1582) and cultured in MEBM basal medium (Lonza) supplemented with 1% B27 (Invitrogen), 4 µg/mL insulin, 2 µg/mL hydrocortisone (SERB Laboratories), 20 ng/mL epidermal growth factor (Sigma), 10 µmol/L 2-mercaptoethanol (Invitrogen), 100 U/mL penicillin and 100 µg/ml streptomycin (P/S, LifeTechnologies). The number of mammospheres in each well was counted under a microscope after 14 days. All the experiments were repeated at least three times.

### 2.5 | Screening of the Prestwick drug library

MDA-MB-453 cells were seeded into 384-well plates (ViewPlate-384 Black Perkin Elmer) in 40 µL of media, using a MultiDrop combi (Thermo Fisher Scientific). Twenty-four hours later, cells were incubated with 1200 clinically licensed compounds from the Prestwick Chemical Library (Prestwick Chemical) (final concentration: 10 µmol/L), or one of six additional compounds were added (Table S2; later referred to as “Prestwick” along with the Prestwick Chemical library drugs; final concentration as indicated), mixed or not with EPZ015666 (DC Chemicals) (final concentration: 10 µmol/L). Liquid handling was performed using the MultiChannel Arm™ 384 (MCA 384) (TECAN). For controls, DMSO alone (0.5%) and EPZ015666 (10 µmol/L) were added to the cells as single agents. Cell viability was monitored using the CellTiter-Glo (Promega) assay after 96 hours using a CLARIOStar (BMG Labtech). The experiment was carried out in duplicates. Positive hits for each compound were identified as follows: data were first transformed with log functions; B-score normalization was then applied to each replicate separately, and includes corrections for plates, rows, and columns. Median and median absolute deviation (MAD) were computed and used to calculate Robust Z-scores (RZ-scores) for each sample, according to the formula: score = (value – median)/(1.4826 × Median MAD). RZ-scores were calculated for the comparison of each compound against the DMSO-treated cells. A compound was identified as a ‘hit’, if the RZ-score was <–2 in the two replicates. The correspondence between RZ-score and cell proliferation is given by the following formula:

$$\% \text{ proliferation} = \frac{\exp(\text{RZscore} \times 1.4826 \times \text{MAD} + \text{median (all treated wells)})}{\exp(\text{median (all treated wells)})} \times 100$$

A  $\Delta\text{RZscore} = \text{RZscore (Prestwick + EPZ015666)} - \text{RZscore (Prestwick)}$  was calculated for each ‘hit’ to quantify the effect of the Prestwick + EPZ015666 drug combination.

## 2.6 | Combination analysis

Cells were seeded into 96-well plates and treated with various concentrations ranging from 0 to 5 or 10  $\mu\text{mol/L}$  of EPZ015666 (DC Chemicals) and/or Erlotinib (Cayman Chemical) or with DMSO alone after 24 hours. Cell viability was determined after 3 days (MDA-MB-453), as in the screen for experimental validation, or 7 days (BT-20, HCC70, MDA-MB-468, HCC38) by CellTiter-Glo (CTG, Promega) assay. Luminescent signals were measured using an Infinite 200 spectrophotometer (Tecan). Chalice Analyzer (<http://chalice.horizondiscovery.com/analyzer-server/cwr/analyze.jsp>) was used to calculate the Loewe excess. Synerdrug Analyzer (<https://github.com/bioinfo-pf-curie/synerdrug>) was used to calculate Chou-Talalay Combination Indexes. Experiments were repeated at least three times.

## 2.7 | Mice, compounds, treatment, and tumor growth measurement

Six-week-old Female Swiss nude mice were purchased from Charles River (Les Arbresles, France) and maintained in specific pathogen-free conditions. Their care and housing were in accordance with institutional guidelines as put forth by the French Ethical Committee. EPZ015666 (DC Chemicals) was formulated at 1 mg/mL in 0.5% Methylcellulose (Sigma Aldrich) + 0.5% Tween 20 (Sigma Aldrich). EPZ015666 toxicity studies were performed by administration of 100 mg/kg, per-os (po), twice daily, 5 days per week, to nude mice. Treatment was not associated with any mortality or body weight loss (Figure S1). The patient-derived xenograft model HBCx-17 was established from a triple-negative breast cancer as detailed elsewhere<sup>23,24</sup> and chosen on the basis of high mRNA expression of PRMT5. Briefly, tumor fragments (30–60 mm<sup>3</sup>) were grafted into the inter-scapular fat pad of nude mice. When tumors reached 60–100 mm<sup>3</sup> (day 1 of the analysis), mice were randomly assigned to control or treatment groups ( $n = 7/\text{group}$ ). Tumor volume was evaluated by measuring two perpendicular tumor diameters with a caliper, twice a week, as described.<sup>17,23</sup> Mice were ethically killed at the end of the experiment (5 weeks).

## 2.8 | Statistical analyses

For caspase activity assay, sub-G1 cell cycle analysis, colony formation, and mammosphere formation assays, differences between groups were assessed using Student *t* tests and were considered significant if the *P* value was below 0.05. For the cell cycle experiment, we used cell counts to evaluate the difference between DMSO-treated cells and EPZ015666-treated cells for each population (G1 vs not G1, S vs not S, G2/M vs not G2/M), in a Fisher-exact test. We adjusted for multiple testing using the Benjamini-Hochberg method. Differences

were considered significant if the adjusted *P* value was below 0.05. For the in vivo experiment, differences observed between treated mice RTV and control group RTV were calculated using a two-tailed Mann-Whitney test. Differences were considered significant if the *P* value was below 0.05.

## 3 | RESULTS

### 3.1 | PRMT5 is differentially localized in TNBC compared to other breast cancer subtypes and to normal mammary tissues

We examined the expression of PRMT5 in a previously generated cohort of 150 breast cancer biopsy specimens and normal breast tissues from the Institut Curie Hospital (Curie cohort).<sup>17</sup> We find that TNBC express similar levels of PRMT5 mRNA compared to luminal breast cancers and healthy breast tissues, and higher levels of PRMT5 mRNA compared to HER2+ breast cancers (Figure 1A, left panel). To confirm these observations, we analyzed publically available data from the TCGA breast invasive carcinoma cohort.<sup>19</sup> We find that PRMT5 is overexpressed in breast cancers—encompassing all subtypes—compared to normal breast tissues (data not shown), as previously reported.<sup>25</sup> In contrast with the Curie cohort, the TCGA data shows no difference in PRMT5 mRNA expression between TNBC and HER2+ breast cancers (Figure 1A, right panel). However, Curie and TCGA cohort analyses indicate that TNBC, luminal breast tumors, and healthy breast tissues express comparable levels of PRMT5 mRNA (Figure 1A).

As mRNA and protein expression do not always concur, we next evaluated the expression of PRMT5 at the protein level in the samples from the Curie cohort by IHC using TMA, after validating an anti-PRMT5 antibody for IHC staining (Figure S2). We observe that, as for mRNA, PRMT5 protein is expressed at similar levels in the different breast cancer subtypes and in healthy breast tissues (Figure 1B,C). However, the subcellular localization of PRMT5 varies (Figure 1B,C; Figure S3). Healthy breast tissues display significantly high levels of PRMT5 at the cell plasma membrane compared to cancerous tissues from all breast cancer subtypes (Figure 1B; Figure S3, left panel). Importantly, TNBC exhibit a distinctive PRMT5 subcellular distribution, with significantly lower levels of nuclear PRMT5 than healthy breast tissues and all other breast cancer subtypes (Figure 1C).

### 3.2 | High PRMT5 expression is associated with poor prognosis in TNBC

Our analysis of PRMT5 mRNA expression in TNBC shows up to eightfold variability between samples (Figure 1A), paralleling TNBC heterogeneity.<sup>2</sup> To determine the clinical significance of PRMT5 in TNBC, we analyzed PRMT5

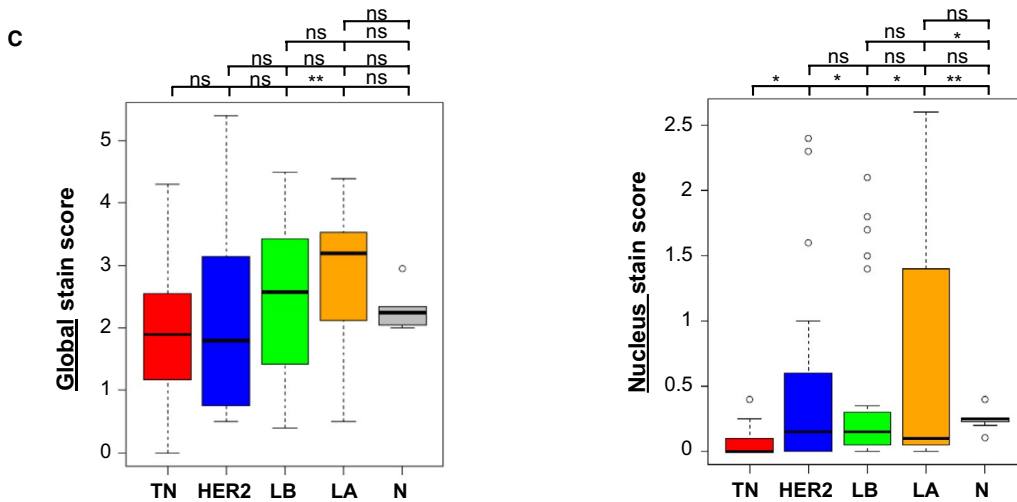
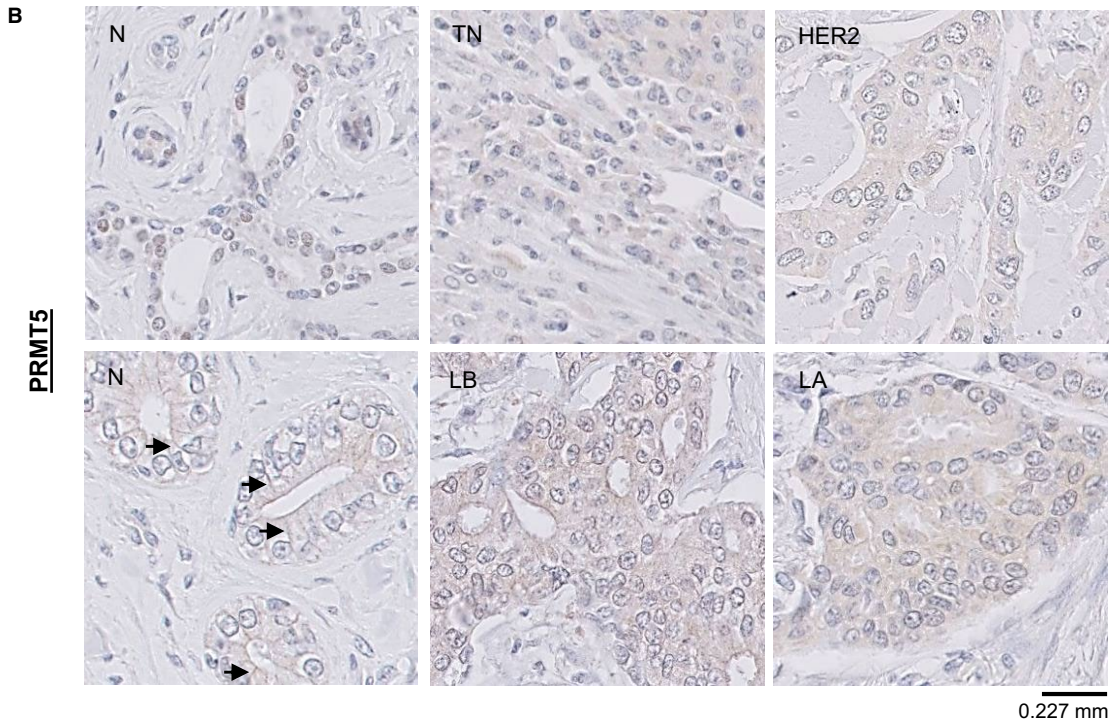
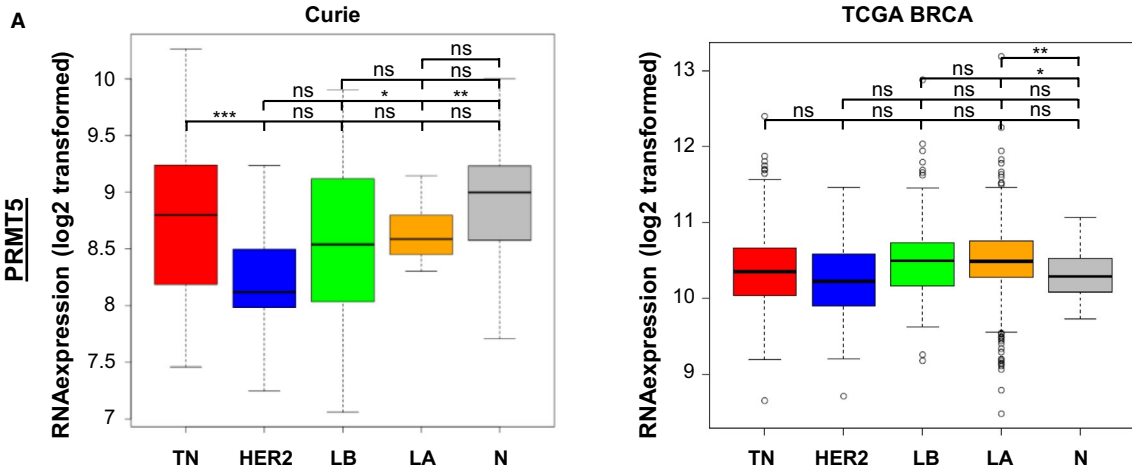


**FIGURE 1** PRMT5 is differentially localized in breast cancer subtypes and healthy mammary tissues. A, PRMT5 mRNA expression in the different breast cancer subtypes and in normal breast tissues in the Curie<sup>17</sup> (left panel) and TCGA BRCA<sup>19</sup> (right panel) cohorts. The breast cancer subtypes rank from the most to the less proliferative tumors: TNBC (TN, red), ER-/HER2+ (HER2, blue), luminal B (LB, green), luminal A (LA, orange). Normal breast tissues (N) are in grey. RNA relative quantifications are logarithmic (log2) transformed and illustrated by boxplots. Outliers are shown within each studied population (open circles). *P* values were calculated using ANOVA test and are indicated as follows: \**P* < 0.05, \*\**P* < 0.01, \*\*\**P* < 0.001. B and C, PRMT5 protein levels were analyzed by immunohistochemistry (IHC) in the samples from the Curie cohort<sup>17</sup>: (B) Representative images of PRMT5 staining in the different breast cancer subtypes and in normal breast tissues (×40). Two images of normal breast tissues (N) are shown to better visualize nuclear (upper image) and transmembrane (bottom image) localization. Arrows indicate transmembrane staining. C, Global (left panel) and nuclear-only (right panel) quantification of PRMT5 staining (0: no staining, 3: the strongest staining) in the different breast cancer subtypes (TN, red; HER2, blue; LB, green; LA, orange) and in normal breast tissues (N, grey). Boxplots show median, upper and lower quartiles of each studied population. Outliers are represented as open circles. *P* values were calculated using Student *t* test and are indicated as follows: \**P* < 0.05, \*\**P* < 0.01, \*\*\**P* < 0.001

expression and survival outcomes in TNBC using data from the Kaplan-Meier plotter online database<sup>26</sup> (www.kmplot.com) (Figure 2). Kaplan-Meier analyses indicate an association between high PRMT5 expression and lower probabilities of distant metastasis-free survival (DMFS, *P* = 0.085) and overall survival (OS, *P* = 0.012) (Figure 2), outlining the potential therapeutic value of PRMT5 targeting in a subset of TNBC.

### 3.3 | Pharmacological inhibition of PRMT5 impairs breast cancer cell viability

To explore the potential of PRMT5 targeting in TNBC, we first examined the effect of PRMT5 depletion on six TNBC cell lines using two PRMT5 siRNAs. PRMT5 silencing significantly decreases viability (Figure S4A), and colony formation (Figure S4B) of all tested cell lines.

To better assess the therapeutic relevance of PRMT5 targeting in TNBC, we next examined the effect of PRMT5

inhibition on a panel of breast cell lines using the PRMT5-specific inhibitor EPZ015666.<sup>13,14,27</sup> First, we confirmed that EPZ015666 inhibits PRMT5 activity by analyzing PRMT5-specific methylation marks on histones H3 (H3R8me2s) and H4 (H4R3me2s) (Figure 3A; Figure S5). We then conducted a cell viability assay on 13 breast cell lines, comprising eight TNBC-derived cell lines (ER-/PR-/HER-) from the different TNBC molecular subtypes defined by Lehmann<sup>2</sup> (Table S3), but also one ER+ (MCF-7), two ER-/HER2+ (HCC1954, SKBR3), and two non-tumorigenic mammary cell lines (MCF-10A, MCF-12A), for comparison purposes. EPZ015666 treatment impairs cell viability of all tested cell lines (Figure 3B). More precisely, we distinguish two groups of cell lines that we deem “sensitive” or “resistant” to the inhibitor based on the IC50 values calculated from the assay (0.5 μmol/L < IC50 < 4 μmol/L and IC50 > 30 μmol/L, respectively) (Figure 3B, Table S3). Three of the eight TNBC (ER-/PR-/HER-) cell lines tested are sensitive. These three cell lines—MDA-MB-453,

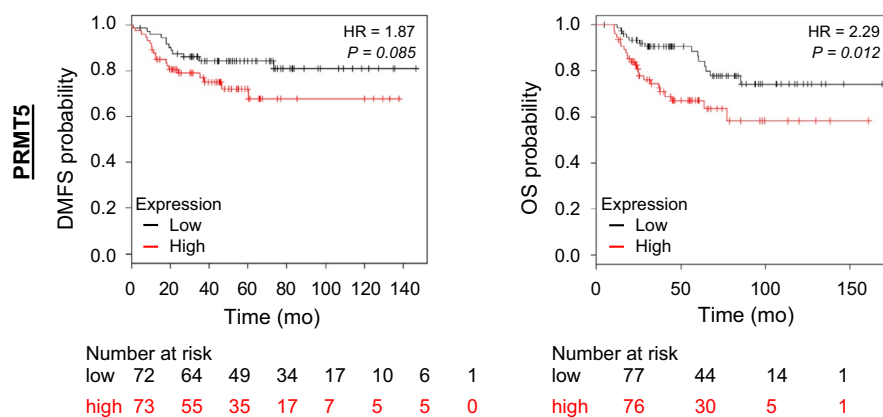


**FIGURE 2** High PRMT5 expression associates with poor prognosis in TNBC. Distant metastasis free survival (DMFS, left panel) and overall survival (OS, right panel) according the RNA expression of PRMT5 (Affy probe ID: 1564520\_s\_at) was analyzed by Kaplan-Meier (KM) Plotter<sup>52</sup> (<http://kmplot.com>). Because the breast cancer subtypes have different prognoses, the analysis was restricted to TNBC patients: the group “basal” (ER-/HER2-) was selected from the intrinsic subtypes. TNBC samples were split into high and low groups according to the expression level of the selected probe (median cutoff). Hazard ratio with 95% confidence interval and log rank *P* value were calculated and significance threshold was set at *P* < 0.05. A similar figure of TNBC patient OS as a function of high vs low PRMT5 RNA expression is presented in Wu Y et al,<sup>25</sup> with a lower number of samples (248 in our study compared to 220 in that article)

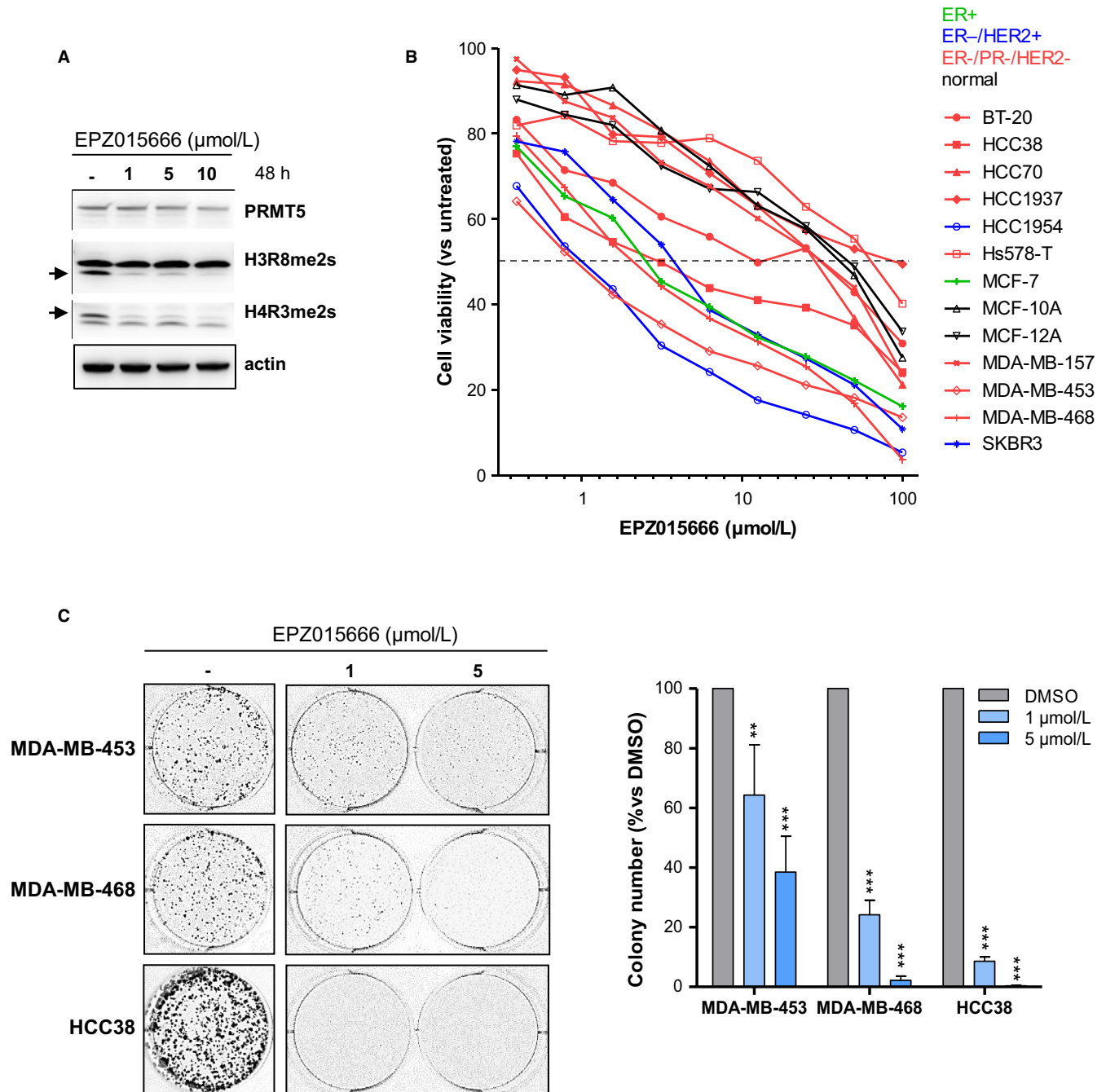


**FIGURE 3** PRMT5 inhibition impairs cell viability. A, EPZ015666 inhibits PRMT5 activity. MDA-MB-468 cells were treated with the indicated concentration of the PRMT5 inhibitor EPZ015666 or with vehicle (DMSO). PRMT5 activity was assessed 48 h later by Western-Blot analysis using antibodies that recognize symmetric dimethyl-arginine on histones H3 (H3R8me2s) and H4 (H4R3me2s). PRMT5 expression was verified. Actin was used as a loading control. Images are from a single experiment representative of three independent experiments. B, Treatment of breast cell lines with PRMT5 inhibitor EPZ015666 identifies a group of sensitive cell lines and a group of resistant cell lines. Cell viability was determined by MTT assay after four doubling times. Results are expressed as the percentage of cell growth relative to vehicle-treated cells. The mean of at least three independent experiments for each cell line is presented. Breast cancer subtypes are indicated as follows: green (ER+), blue (ER-/HER2+), red (ER-/PR-/HER2-). The non-tumorigenic breast cells, MCF-10A and MCF-12A, are in black. C, PRMT5 inhibition reduces colony formation. MDA-MB-453, MDA-MB-468 and HCC38 TNBC cells, seeded at low-confluency, were treated with DMSO (-) or with 1 or 5  $\mu\text{mol/L}$  EPZ015666 for 9–14 d, until colony formation. A representative image of one well is shown for all conditions (left panel). The number of colonies, counted using ImageJ Software (NIH) is presented as a percentage relative to DMSO-treated cells (right panel). Grey bars: DMSO-treated cells; blue bars: EPZ015666-treated cells. Represented are means + SD from at least three independent experiments. *P* values were calculated using Student *t* test and are indicated as follow: \*\**P* < 0.01, \*\*\**P* < 0.001 (ie decrease relative to the control DMSO)

MDA-MB-468, and HCC38—are among the four most sensitive to the PRMT5 inhibitor and therefore represent good models to study the impact of PRMT5 inhibition on TNBC. The two HER2+ cell lines (HCC1954, SKBR3) and the single luminal cell line (MCF-7) tested are sensitive. The non-tumorigenic mammary cell lines MCF-10A and MCF-12A are resistant (Figure 3B). This differential sensitivity to EPZ015666 is not due to marked differences in PRMT5 expression nor in global PRMT5 activity (Figure S6).

A newer more potent PRMT5 inhibitor (biochemical IC<sub>50</sub> of  $6.2 \pm 0.8$  nmol/L<sup>16</sup> vs  $22 \pm 14$  nmol/L for EPZ015666<sup>27</sup>), GSK3326595 (EPZ015938), is currently evaluated in a phase I clinical trial.<sup>16,28</sup> In order to confirm the specificity of EPZ015666, we examined its effect on four TNBC cell lines—two sensitive (MDA-MB-453, MDA-MB-468) and two resistant (BT-20, HCC70) to EPZ015666. We first validated the inhibition of PRMT5 activity by EPZ015938 in the four cell lines (Figure S7A). Like EPZ015666, EPZ015938 impairs the viability of MDA-MB-453 and MDA-MB-468 cells (Figure S7B), but with more efficacy. Indeed, we calculate IC<sub>50</sub> values of 124 nmol/L and 162 nmol/L for MDA-MB-453 and MDA-MB-468 cells, respectively (vs 1  $\mu$ mol/L and 2.2  $\mu$ mol/L for EPZ015666). BT-20 and HCC70 cells are resistant to EPZ015938 (IC<sub>50</sub> >35  $\mu$ mol/L for both cell lines) (Figure S7A), like to EPZ015666 (Figure 3B, Table S3).

### 3.4 | PRMT5 inhibition impairs colony formation in TNBC cells

We pursued our study by investigating the molecular mechanisms of the PRMT5-dependent cell survival in the three TNBC cell lines sensitive to EPZ015666: MDA-MB-453, MDA-MB-468, and HCC38.

To further validate the deleterious effect of PRMT5 inhibition on cell viability (Figure 3B), we examined the effect of PRMT5 inhibition on colony formation. In the three tested cell lines, 1  $\mu$ mol/L EPZ015666 treatment results in 35%-90% less colonies (Figure 3C) compared to untreated cells. EPZ015666 treatment at 5  $\mu$ mol/L results in 60%-100% less colonies (Figure 3C).

### 3.5 | PRMT5 inhibition induces apoptosis and G2/M cell cycle arrest

We first evaluated the activation of apoptotic pathways in EPZ015666-treated cells. Western blot analyses confirm PRMT5 inhibition (decreased pan-SDMA), and show dose-dependent increases in PARP, caspase-7, and caspase-8 cleavage following treatment (Figure 4A). These results are supported by the detection of increased caspase-3 and caspase-7 activity in a luminescent assay (Figure 4B).

Next, we examined the effect of PRMT5 inhibition on breast cancer cell cycle progression using flow cytometry. EPZ015666-treated MDA-MB-453, MDA-MB-468, and HCC38 cells display a higher proportion of cells in the sub-G1 phase 96 hours post-treatment compared to untreated cells (Figure 4C), confirming the above results regarding apoptosis. In all three cell lines, we also observe a significant decrease in the G1 population and an increase of the G2/M population following EPZ015666 treatment (Figure 4D). Collectively, our data show that PRMT5 inhibition induces apoptosis and impedes cell cycle progression.

### 3.6 | PRMT5 inhibition impairs mammosphere formation in TNBC cells

In addition, because breast cancer stem cells (BCSCs) are enriched in TNBC<sup>8</sup> and play a role in resistance to chemotherapies,<sup>29</sup> we investigated the effect of PRMT5 inhibition on an indicator of breast cancer cell stemness. Specifically, we assessed the propensity of HCC38 cells to form mammospheres following EPZ015666 treatment. PRMT5 inhibition significantly impairs HCC38 mammosphere formation in a dose-dependent manner (Figure 5A), suggesting a potential role for PRMT5 in the maintenance of BCSC properties.

### 3.7 | PRMT5 targeting slows tumor progression in vivo in a TNBC patient-derived xenograft model

We evaluated the potential anti-tumor effects of PRMT5 targeting in a preclinical study involving a TNBC patient-derived xenograft model, selected for its high PRMT5 mRNA expression. EPZ015666 was administered twice daily, at 100 mg/kg *per-os* (*po*). Treatment significantly slows tumor growth, with 39% tumor growth inhibition (TGI,  $P = 0.02$ ) after 4 weeks (Figure 5B, left panel), and no observed toxicity (Figure S1). We verified that PRMT5 inhibition had indeed occurred in the tumors at the end of the experiment by assessing PRMT5 activity by Western Blot, using pan symmetric dimethyl-arginine (pan-SDMA) and H4R3me2s antibodies (Figure 5B, right panel).

### 3.8 | Synergistic interaction between PRMT5 and EGFR inhibitors

Drug combinations have gained interest in cancer therapeutics, as means for increased treatment efficacy, decreased toxicity, and reduced risk of drug resistance. To address this, we screened the Prestwick Chemical Library—consisting of 1,200 FDA-approved molecules<sup>30</sup>—and six additional drugs (Table S2), alone or in combination with EPZ015666 on MDA-MB-453 cell viability. Following



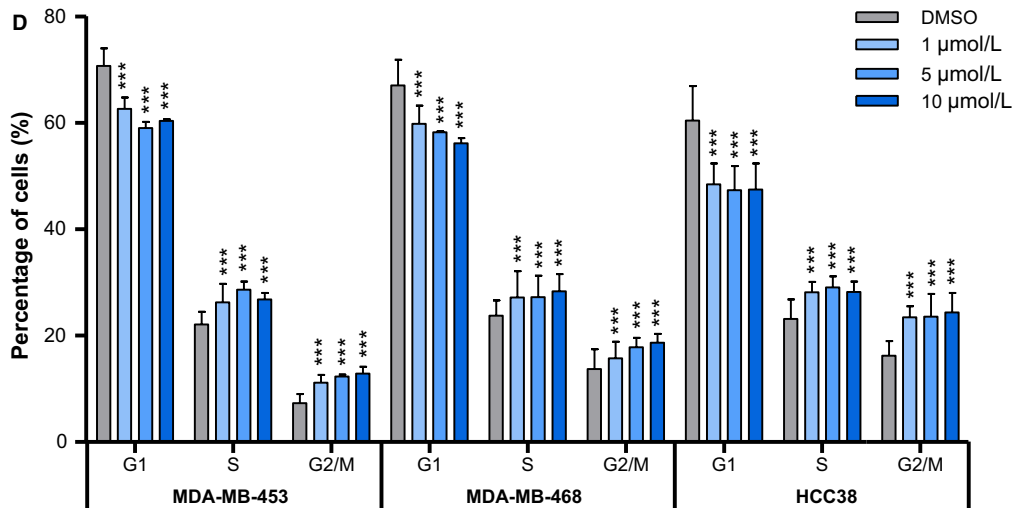
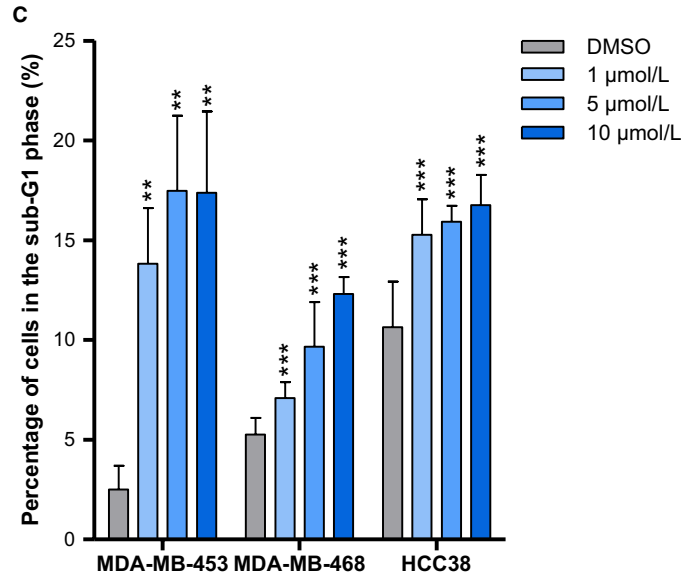
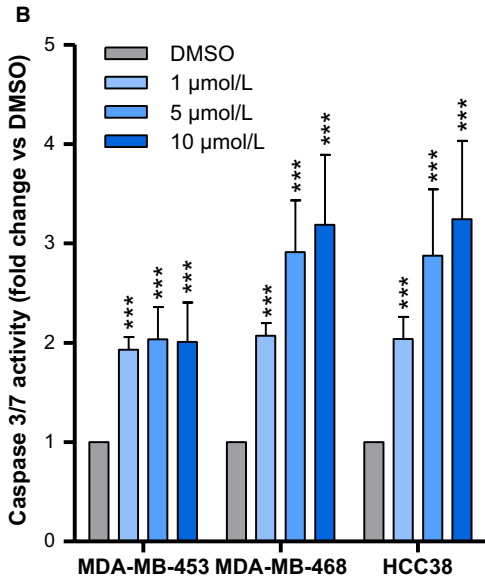
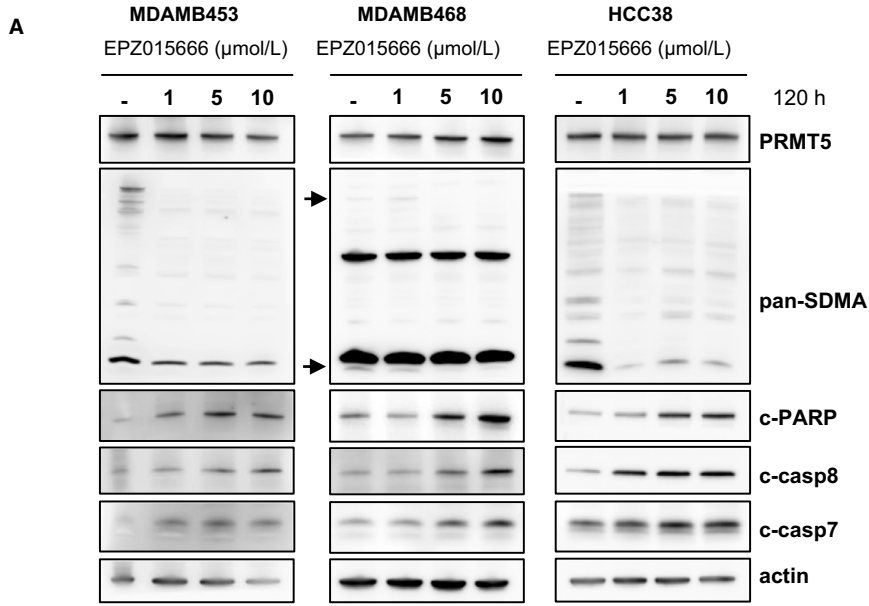


**FIGURE 4** PRMT5 inhibition leads to apoptosis and affects cell cycle progression. A-D, MDA-MB-453, MDA-MB-468 and HCC38 TNBC cells were treated with DMSO (- or grey bars) or with the indicated concentration of EPZ015666 (1-10  $\mu\text{mol/L}$ , blue bars) (A-C) PRMT5 inhibition induces apoptosis. A, Apoptosis was analyzed by western blotting using antibodies that recognize the cleaved forms of caspase 7 (c-casp7), caspase 8 (c-casp8) and PARP (c-PARP) 120 h after PRMT5 inhibition. PRMT5 and actin were used as controls. General symmetric arginine dimethylation (pan-SDMA) was examined to validate PRMT5 inhibition following cell treatment with EPZ015666. Pictures are from a single experiment representative of two or three independent experiments. B, Apoptosis was assessed by a luminescence assay to detect caspase 3/7 activity of viable cells 120h after PRMT5 inhibition. Results are expressed as fold-change compared to vehicle-treated cells. *P* values were calculated using Student *t* test. C and D, Cell cycle was monitored 96 hours following PRMT5 inhibition or treatment with DMSO by FACs analysis following PI staining. C, Percentage of cells in the sub-G1 phase are represented. Data are expressed as means from three to four independent experiments. *P* values were calculated using Student *t* test. D, PRMT5 inhibition impairs cell cycle progression. Percentages of live cells in G1, S and G2/M phases are represented. *P* values were calculated based on cell count using a Fisher-exact test and adjusted for multiple testing using the Benjamini-Hochberg method. B-D, Means + SD of at least three independent experiments are represented. *P* values (B and C) and adjusted *P* values (D) are indicated as follows: \*\**P* < 0.01; \*\*\**P* < 0.001

the selection criteria, Erlotinib, an EGFR inhibitor, was identified twice in the top 25 compounds for which there is at least some additivity with EPZ015666 (Figure S8). We validated the results of our screen by treating MDA-MB-453 cells with variable combinations of EPZ015666 and Erlotinib and measuring cell viability after 3 days, as for the screen (Figure 5, left panel). We calculated Loewe excess inhibition values and Chou-Talalay combination indexes (CI) as measures of synergy (Figure 5, middle and right panels, respectively). We considered Loewe excess values greater than 10% and Chou-Talalay CI lower than 1 to be suggestive of additivity. Both Loewe excess and Chou-Talalay CI suggest additivity, if not synergy, between EPZ015666 and Erlotinib, confirming the results from our screen (Figure 6A). We next sought to determine whether an EPZ015666/Erlotinib drug combination would be efficient on all TNBC cell lines or, as for EPZ015666 treatment alone, in a subset of TNBC cell lines. We hence tested combinations of EPZ015666 and Erlotinib on four additional cell lines, two of which (MDA-MB-468, HCC38) were sensitive to EPZ015666 in our initial cell viability assay (Figure 3A), and two of which (BT20, HCC70) were resistant. We found the drug combination to be beneficial on MDA-MB-468 and BT20 cells especially (Figure 6B), both of which express high levels of EGFR (Figure S5B), as well as on HCC70 cells (Figure 6B). EPZ015666/Erlotinib combination had no additive effect on HCC38 cells (data not shown).

## 4 | DISCUSSION

Despite considerable improvement in breast cancer therapeutic management, no targeted therapy yet exists for the treatment of TNBC, and this breast cancer subtype remains a challenge for oncologists. PRMTs have recently received considerable attention as potential therapeutic targets in various types of cancer,<sup>31</sup> and several specific PRMT inhibitors have recently been described.<sup>14</sup> The present study suggests

a promising therapeutic potential for PRMT5 targeting in a subset of TNBC, using the small-molecule inhibitor EPZ015666.<sup>13,14,27</sup> Indeed, we show that PRMT5 inhibition (a) impairs breast cancer cell viability, (b) triggers apoptosis, (c) impedes colony formation (d) affects CSC properties, and (e) slows tumor growth in a TNBC patient-derived xenograft model (PDX). In doing so, we align with previous studies which underline the potential value of PRMT5 inhibition as a therapeutic approach in glioblastoma<sup>32,33</sup> and mantle cell lymphoma.<sup>8,13</sup>

The 13 breast cell lines we tested display differential sensitivity to PRMT5 inhibition. Six of the cell lines examined are sensitive whereas seven are resistant to EPZ015666. Interestingly, the non-tumorigenic cell lines MCF-10A and MCF-12A belong to the group that is resistant to PRMT5 inhibition. Although non-tumorigenic, these cell lines are the most proliferative in our in vitro assays, demonstrating that the sensitivity to the inhibitor is not related to cell proliferation rate. This consideration suggests that side-effects of PRMT5 targeting could be minimal. We confirmed specificity and differential sensitivity to PRMT5 inhibition using a newly available inhibitor, EPZ015938. Using this same inhibitor, Gerhart et al also observe variable sensitivity to PRMT5 inhibition across a panel of 240 cancer cell lines.<sup>16</sup> They find p53 status to be determinant to EPZ015938 sensitivity. We, however, observe no correlation between p53 mutation and sensitivity to PRMT5 inhibition in the TNBC cell lines we tested, and were unable to trace sensitivity back to the expression of transcriptomic biomarkers. Enlarging our analysis to a larger number of TNBC cell lines would be necessary to do so, and could, in turn, help stratify patients who could benefit from treatment with a PRMT5 inhibitor.

In contrast, PRMT5 depletion impairs the viability of all the TNBC cell lines tested in this study, thus aligning with previous research conducted on cell lines derived from other cancer types<sup>10,34</sup> or on MDA-MB-468<sup>16</sup> and another TNBC-derived cell line, MDA-MB-231.<sup>8,25</sup> It thus appears that the effect of PRMT5 depletion on cell viability is independent from cell sensitivity to EPZ015666. Indeed, inhibiting an

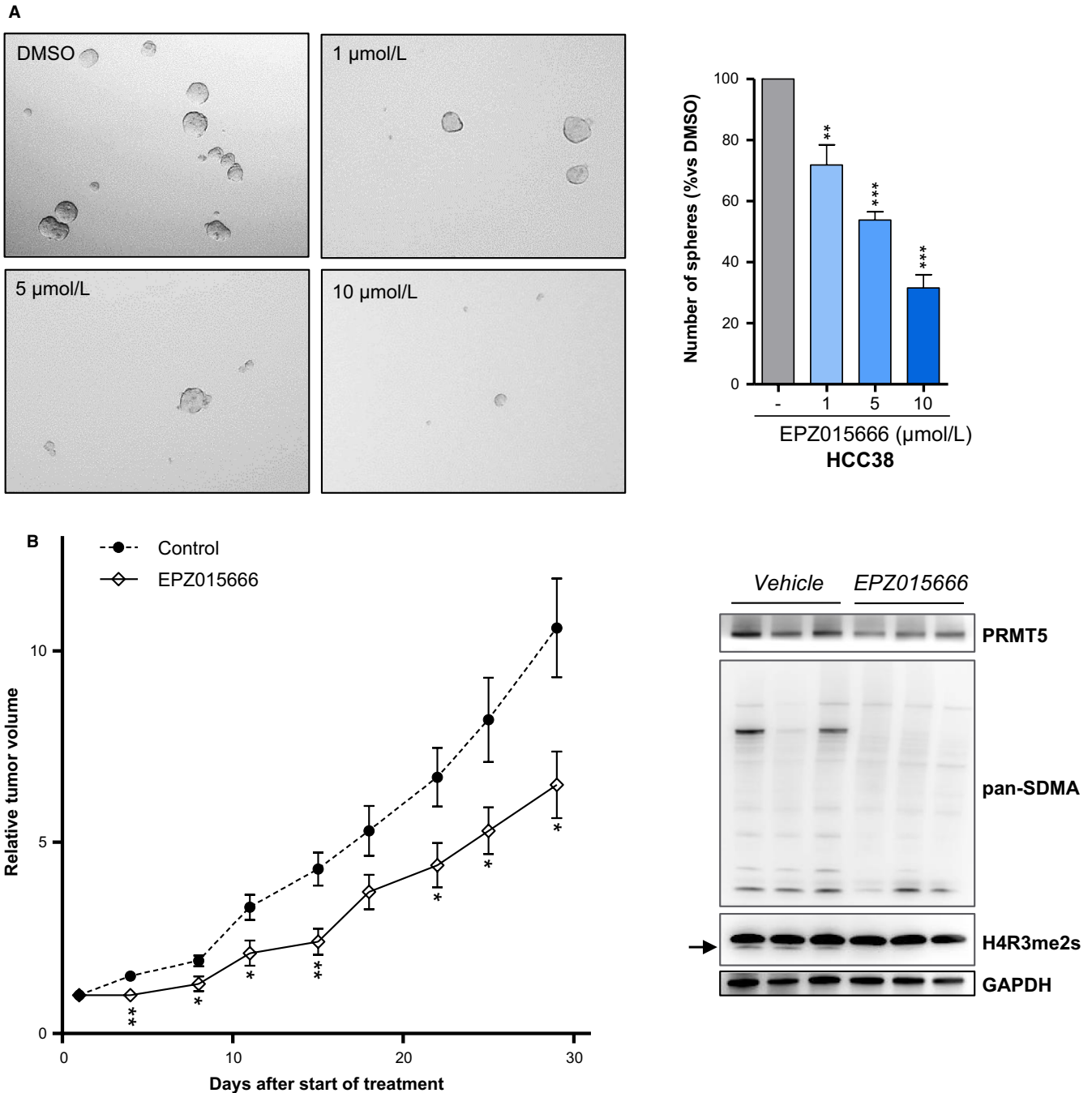


**FIGURE 5** PRMT5 inhibition impairs, mammosphere formation, and slows tumor growth in a TNBC PDX model. **A**, PRMT5 inhibition impairs mammosphere formation. HCC38 cells were seeded in 6-well low-binding plates and treated with DMSO (-) or with the indicated concentration of EPZ015666 for 14 d. Mammospheres were then examined and counted under a microscope. A representative image of one well is also shown for all conditions ( $\times 100$ ). Mammosphere count for each EPZ015666-treated condition is expressed as a percentage relative to vehicle-treated cells. Grey bars: DMSO-treated cells; blue bars: EPZ015666-treated cells. Represented are means + SD from at least three independent experiments. *P* values were calculated using Student *t* test and are indicated as follows: \**P* < 0.05, \*\**P* < 0.01, \*\*\**P* < 0.001 (ie, decrease relative to the control DMSO). **B**, PRMT5 inhibition slows tumor growth in vivo. EPZ015666 (200 mg/kg BID, *po*) was administered to a TNBC PDX model ( $n = 7$  mice) during one month. Control mice were treated with EPZ015666 vehicle ( $n = 7$  mice). (left panel) Tumor volume was measured twice weekly with calipers. Growth curves were obtained by plotting relative tumor volume mean versus time  $\pm$  SEM *P* values were calculated using Mann-Whitney test are indicated as follow: \**P* < 0.05, \*\**P* < 0.01, \*\*\**P* < 0.001. (right panel) PRMT5 inhibition reduces symmetric arginine dimethylation (SDMA) in tumors. Western blot analysis of tumors at the end of the treatment shows lower PRMT5 activity in the tumors derived from EPZ015666-treated mice compared to those derived from vehicle-treated mice. Symmetric arginine dimethylation was detected using anti-pan-SDMA and anti-H3R8me2s antibodies. PRMT5 expression was verified. GAPDH was used as loading control

enzyme is different from removing its expression. Such a difference was also observed by Mavrakis et al,<sup>35</sup> who found that cancer cell sensitivity to PRMT5 depletion, but not to PRMT5 inhibition using EPZ015666, is contingent upon low-MTAP expression. These observations demonstrate that inhibiting the activity of PRMT5 has a different impact on cell viability than silencing PRMT5 expression. The mode of PRMT5 targeting is therefore key. More generally, these observations underline the importance of validating potential therapeutic targets using pharmacological inhibitors, and not only using siRNA.

Furthermore, we find that PRMT5 is required for cell proliferation. Pharmacological inhibition of PRMT5 slows cell cycling, leading towards a G2/M cell cycle arrest in the three TNBC cell lines examined. G2/M arrest was previously observed in U-87 MG human glioma cells<sup>36</sup> treated with EPZ015666, and in NIH-3T3 cells stably expressing an anti-sense PRMT5.<sup>9</sup> Some studies have shown that following PRMT5 knockdown, Huh7, MCF-7, and MDA-MB-231 cells also exhibit decreased proliferation, but associated to a G1/S growth arrest.<sup>12,25,37</sup> The mode of PRMT5 targeting is likely determinant here. It is also possible that the role of PRMT5 in cell cycle progression be dependent on cell-type and context.

Previous studies demonstrate that PRMT5 activity is essential for cell stemness.<sup>7,38,39</sup> In breast cancers specifically, PRMT5 was shown to play a critical role in the proliferation and self-renewal of stem-like cells via the regulation of C-MYC, OCT4/A, and FOXP1 expression.<sup>7,38,39</sup> Our study supports these findings as we show that PRMT5 inhibition impairs the formation of mammospheres—an indicator of cancer cell stemness—in a TNBC cell line. Since TNBC are enriched in stem-like cells, and this subpopulation is linked to resistance to chemotherapy and relapse,<sup>29</sup> our observations further support the coherence of targeting PRMT5 in TNBC and suggest that PRMT5 targeting could potentiate the effects of conventional therapy, potentially avoiding relapses, the main concern for current treatments of TNBC patients.

Our screening of the Prestwick Chemical Library in the presence or in the absence of the PRMT5 inhibitor EPZ015666 reveals that targeting EGFR potentiates the effect of PRMT5 inhibition on cell viability. In four TNBC cell lines, we thus show potentiation between Erlotinib and EPZ015666 using Loewe excess quantification and Chou-Talalay combination index. TNBC cell line sensitivity to the drug combination was independent from sensitivity to EPZ015666 treatment alone, suggesting that PRMT5 targeting may be valuable on a different set—and perhaps wider number—of TNBC when used in combination than when used as monotherapy. In our cell line panel, we noted that the EPZ015666/Erlotinib combination is most effective on, but not limited to, the two cell lines expressing high levels of EGFR. EGFR inhibitors on their own have shown only a modest effect in clinical trials in TNBC patients,<sup>40</sup> their use in combination could be beneficial. PRMT5 has been shown to interact with EGFR and to modulate its activity.<sup>41</sup>

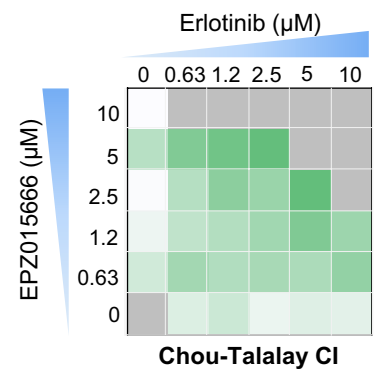
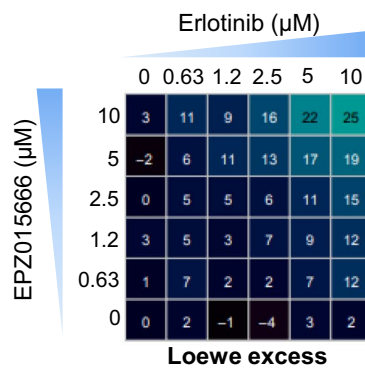
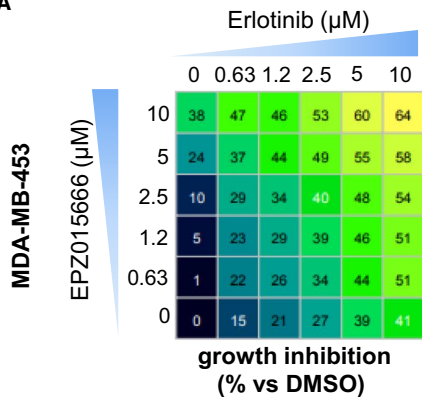
EGFR is also a substrate of PRMT1,<sup>42</sup> the main PRMT generating asymmetric dimethylation.<sup>31</sup> The methylation of EGFR by PRMT1 is reported to play a role in resistance to treatment with Cetuximab, an anti-EGFR antibody.<sup>42</sup> Recently, inhibition of PRMT1 using the nonspecific inhibitor Furamidine was reported to increase Erlotinib sensitivity in MDA-MB-468 cells,<sup>43</sup> further endorsing anti-EGFR/anti-PRMT therapeutic combination strategies in the context EGFR-overexpressing TNBC. Previous reports have shown that PRMT5 silencing slows tumor growth in vivo, using xenograft models from cancer-derived cell lines, including the breast cancer-derived MCF7.<sup>39,44</sup> In alignment with these reports, we here show that pharmacological inhibition of PRMT5 slows tumor growth in a TNBC PDX model. Our study constitutes a first approach to PRMT5 inhibition in vivo in TNBC PDX models. Applying this approach to additional PDX models would be essential to strengthen this initial observation, as well as to evaluate in vivo the potential of EGFR and PRMT5 combinatorial targeting.

Parallely, using Kaplan-Meier plotter online survival analyses in TNBC, we associate the high PRMT5 expression and poor patient prognosis in TNBC, as observed in a wide range of cancers (Stopa, Krebs, and Shechter 2015, 2041-2059), including breast cancers.<sup>25,45</sup> We do not, however, observe elevated PRMT5 mRNA expression in TNBC from our breast cancer cohort nor from TCGA-BRCA. In our cohort, PRMT5 is not overexpressed at the protein level either, contrarily to reports from distinct groups.<sup>45,46</sup> These discrepancies may be due to the use of different TMA fixation and staining techniques, as well as to the use of different PRMT5 antibodies.

We further show here that PRMT5 is differentially localized in breast cancers and healthy mammary tissue, and that some important subcellular localization differences can be noted between breast cancer subtypes. Indeed, PRMT5 is expressed at lower levels in the nucleus of TNBC than in those of healthy breast tissues, HER2+, and luminal breast cancers. We thus posit that PRMT5 activity has different biological outcomes depending on PRMT5 subcellular localization and/or substrate specificity.

Several studies have already pointed out the importance of PRMT5 localization in determining substrate specificity and resultant cell fate. During mouse embryogenesis, Prmt5 is predominantly found in the cytoplasm, where it maintains cell pluripotency via methylation of predeposited H2AR3.<sup>7</sup> The onset of cell differentiation is contingent on the nuclear translocation of Prmt5 and concurrent decrease of the H2AR3 methylation mark.<sup>7</sup> Likewise, PRMT5 localizes in the cytoplasm of human prostate cancer cells where it supports cell proliferation.<sup>47,48</sup> Forced nuclear localization of PRMT5 is associated with epithelial cell differentiation and inhibits prostate cancer development in tissue culture and in prostate tumor xenograft models.<sup>49</sup> More recently, Lattouf et al found that in a cohort of 390 breast invasive carcinomas, high nuclear PRMT5 was associated with longer OS

**A**



**B**

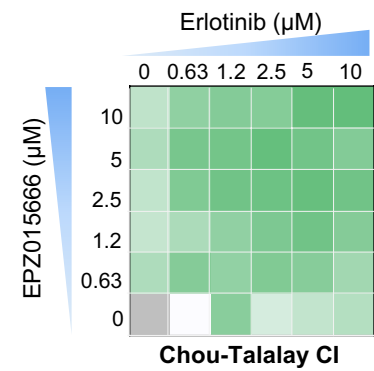
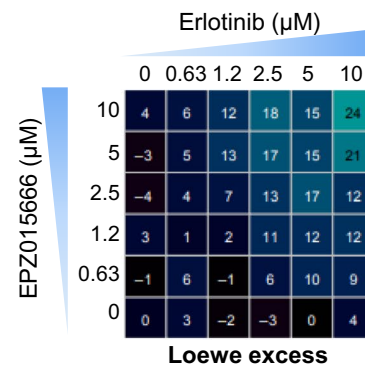
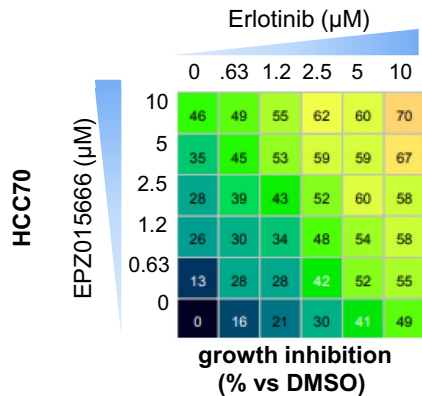
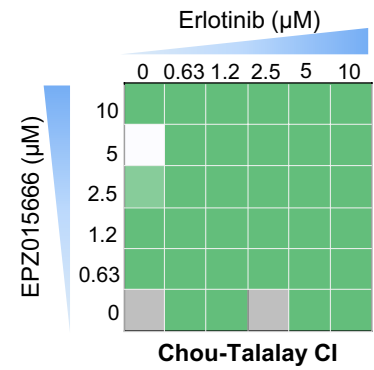
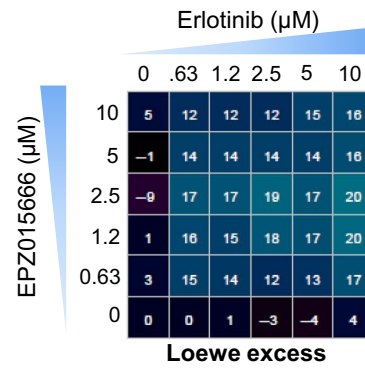
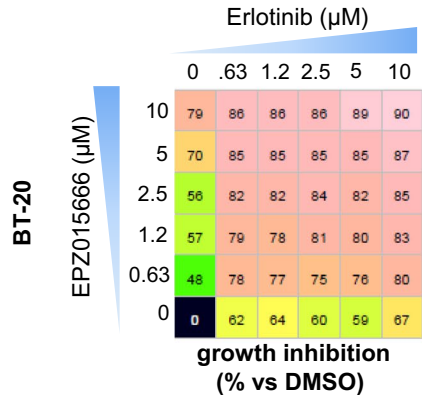
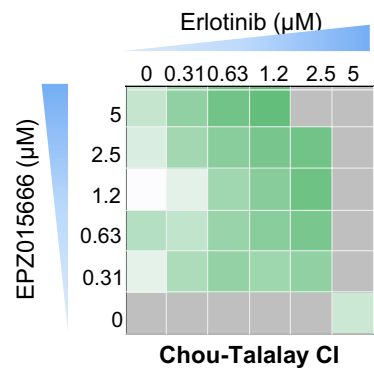
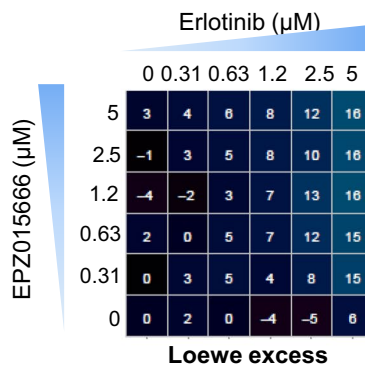
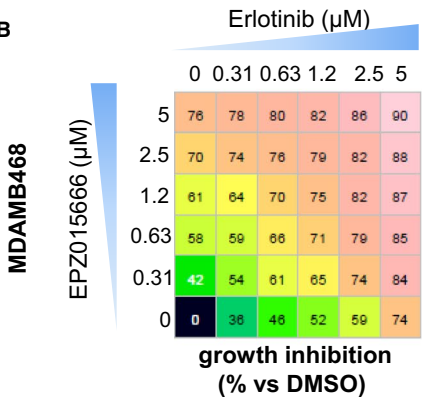


**FIGURE 6** Synergistic interaction between PRMT5 and EGFR inhibition. A and B, Potentiation between EPZ015666 and Erlotinib. Cells were seeded into 96-well plates and treated with EPZ015666 and/or Erlotinib for 7 d at 5–two-fold–serial diluted concentrations (excluding a drug-less control; concentrations as indicated). Cell viability was measured after 3 d, as in the drug combination screen (A), or 7 d (B) using CellTiter-Glo (CTG). The nature of the interaction between EPZ015666 and Erlotinib was assessed by Loewe excess and Chou-Talalay combination index (CI). Cell viability inhibition (% compared to DMSO-treated cells) is indicated for each combination (left panel, dose matrix). Chalice Analyzer (<http://chalice.horizondiscovery.com/analyzer-server/cwr/analyze.jsp>) was used to calculate the Loewe excess (middle panel). Synderdrug Analyzer (<https://github.com/bioinfo-pf-curie/synderdrug>) was used to calculate Chou-Talalay CIs (right panel). CIs are not calculated where the effect of the drug combination is superior to that of either drug alone (grey quadrants). Data are representative of at least three independent experiments

and longer DFS, thus concurring with our study.<sup>50</sup> Broadly, the majority of cancer-related studies interested in PRMT5 localization and substrate specificity associates cytoplasmic PRMT5 activity to tumor development or bad prognosis. We further this observation by suggesting that the localization of PRMT5 may be a determinant of TNBC.

What controls the subcellular localization of PRMT5? A 2007 study by Teng et al may give a first element of response.<sup>51</sup> In this study, Teng et al show that treatment of prostate cancer cells using the nucleolin octamer AS1411, leads to a nucleolin-mediated redistribution of PRMT5 from the nucleus to the cytoplasm. Teng et al thus posit that nucleolin plays a role in PRMT5 shuttling between these subcellular compartments. It is likely, however, that the mechanism proposed by Teng et al not be the sole at work, and that other PRMT5 partners may be involved in its nuclear/cytosolic shuttling.

Which additional signals and/or protein-protein interactions are involved? These interrogations must be addressed to better understand PRMT5 substrate specificity and to further decipher the role of PRMT5 in cancers. Such knowledge could, in turn, allow the design of efficient therapeutic strategies targeting PRMT5 in a substrate-specific manner. In conclusion, the present study highlights the importance of the subcellular localization of PRMT5 in determining TNBC prognosis and upholds continued attention for PRMT5 targeting, alone or in combination, as a potential treatment option in a subset of TNBC.

## ORCID

Mathilde Vinet  <https://orcid.org/0000-0002-8251-013X>

Thierry Dubois  <https://orcid.org/0000-0003-4739-6164>

## REFERENCES

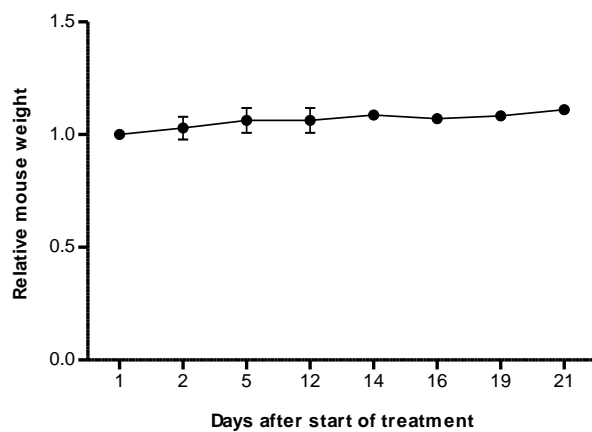
- Denkert C, Liedtke C, Tutt A, von Minckwitz G. Molecular alterations in triple-negative breast cancer—the road to new treatment strategies. *Lancet*. 2017;389(10087):2430-2442.
- Lehmann BD, Bauer JA, Chen Xi, et al. Identification of human triple-negative breast cancer subtypes and preclinical models for selection of targeted therapies. *J Clin Invest*. 2011;121(7):2750-2767.
- Bianchini G, Balko JM, Mayer IA, Sanders ME, Gianni L. Triple-negative breast cancer: challenges and opportunities of a heterogeneous disease. *Nat Rev Clin Oncol*. 2016;13(11):674-690.
- Shao F, Sun H, Deng C. Potential therapeutic targets of triple-negative breast cancer based on its intrinsic subtype. *Oncotarget*. 2017;8(42):73329-73344.
- Blanc RS, Richard S. Arginine methylation: the coming of age. *Mol Cell*. 2017;65(1):8-24.
- Stopa N, Krebs JE, Shechter D. The PRMT5 arginine methyltransferase: many roles in development, cancer and beyond. *Cell Mol Life Sci*. 2015;72(11):2041-2059.
- Tee WW, Pardo M, Theunissen TW, et al. Prmt5 is essential for early mouse development and acts in the cytoplasm to maintain ES cell pluripotency. *Genes Dev*. 2010;24(24):2772-2777.
- Wang Z, Kong J, Wu Y, et al. PRMT5 determines the sensitivity to chemotherapeutics by governing stemness in breast cancer. *Breast Cancer Res Treat*. 2017;162(2):531-542.
- Pal S, Vishwanath SN, Erdjument-Bromage H, Tempst P, Sif S. Human SWI/SNF-associated PRMT5 methylates histone H3 arginine 8 and negatively regulates expression of ST7 and NM23 tumor suppressor genes. *Mol Cell Biol*. 2004;24(21):9630-9645.
- Gu Z, Gao S, Zhang F, et al. Protein arginine methyltransferase 5 is essential for growth of lung cancer cells. *Biochem J*. 2012;446(2):235-241.
- Cho EC, Zheng S, Munro S, et al. Arginine methylation controls growth regulation by E2F-1. *EMBO J*. 2012;31(7):1785-1797.
- Scoumanne A, Zhang J, Chen X. PRMT5 is required for cell-cycle progression and p53 tumor suppressor function. *Nucleic Acids Res*. 2009;37(15):4965-4976.
- Chan-Penebre E, Kuplast KG, Majer CR, et al. A selective inhibitor of PRMT5 with in vivo and in vitro potency in MCL models. *Nat Chem Biol*. 2015;11(6):432-437.
- Kaniskan HÜ, Jin J. Recent progress in developing selective inhibitors of protein methyltransferases. *Curr Opin Chem Biol*. 2017;39:100-108.
- Gerhart SV, Kellner WA, Thompson C, et al. Activation of the p53-MDM4 regulatory axis defines the anti-tumour response to PRMT5 inhibition through its role in regulating cellular splicing. *Sci Rep*. 2018;8(1):9711.
- Wu T, Millar H, Gaffney D, et al. JNJ-64619178, a selective and pseudo-irreversible PRMT5 inhibitor with potent in vitro and in vivo activity, demonstrated in several lung cancer models [abstract]. In *Proceedings of the American Association for Cancer Research Annual Meeting 2018; 2018 Apr 14-18; Chicago, IL*. Philadelphia, PA: AACR; *Cancer Res*. 2018;78(13 Suppl):Abstract nr 4859.
- Maire V, Nemati F, Richardson M, et al. Polo-like kinase 1: a potential therapeutic option in combination with conventional chemotherapy for the management of patients with triple-negative breast cancer. *Cancer Res*. 2013;73(2):813-823.
- Maire V, Baldeyron C, Richardson M, et al. TTK/hMPS1 is an attractive therapeutic target for triple-negative breast cancer. *PLoS One*. 2013;8(5):e63712.
- Cancer Genome Atlas Network. Comprehensive molecular portraits of human breast tumours. *Nature*. 2012;490(7418):61-70.

20. Baldeyron C, Brisson A, Tesson B, et al. TIPIN depletion leads to apoptosis in breast cancer cells. *Mol Oncol*. 2015;9(8):1580-1598.
21. Maubant S, Tesson B, Maire V, et al. Transcriptome analysis of Wnt3a-treated triple-negative breast cancer cells. *PLoS One*. 2015;10(4):e0122333.
22. Marty B, Maire V, Gravier E, et al. Frequent PTEN genomic alterations and activated phosphatidylinositol 3-kinase pathway in basal-like breast cancer cells. *Breast Cancer Res*. 2008;10(6):R101.
23. Marangoni E, Vincent-Salomon A, Auger N, et al. A new model of patient tumor-derived breast cancer xenografts for preclinical assays. *Clin Cancer Res*. 2007;13(13):3989-3998.
24. de Plater L, Laugé A, Guyader C, et al. Establishment and characterisation of a new breast cancer xenograft obtained from a woman carrying a germline BRCA2 mutation. *Br J Cancer*. 2010;103(8):1192-1200.
25. Wu Y, Wang Z, Zhang J, Ling R. Elevated expression of protein arginine methyltransferase 5 predicts the poor prognosis of breast cancer. *Tumor Biol*. 2017;1-11.
26. Lánckzy A, Nagy Á, Bottai G, et al. miRpower: a web-tool to validate survival-associated miRNAs utilizing expression data from 2178 breast cancer patients. *Breast Cancer Res Treat*. 2016;160(3):439-446.
27. Duncan KW, Rioux N, Boriack-Sjodin PA, et al. Structure and property guided design in the identification of PRMT5 tool compound EPZ015666. *ACS Med Chem Lett*. 2015;7(2):162-166.
28. Rasco D, Tolcher A, Siu LL, et al. A phase I, open-label, dose-escalation study to investigate the safety, pharmacokinetics, pharmacodynamics, and clinical activity of GSK3326595 in subjects with solid tumors and non-Hodgkin's lymphoma [abstract]. In *Proceedings of the American Association for Cancer Research Annual Meeting 2017; 2017 Apr 1-5; Washington, DC*. Philadelphia, PA: AACR; *Cancer Res*. 2017;77(13 Suppl):Abstract nr CT038.
29. Singh A, Settleman J. EMT, cancer stem cells and drug resistance: an emerging axis of evil in the war on cancer. *Oncogene*. 2010;29(34):4741-4751.
30. Chauvin C, Leruste A, Tauziède-Espariat A, et al. High-throughput drug screening identifies pazopanib and clofilium tosylate as promising treatments for malignant rhabdoid tumors. *Cell Rep*. 2017;21(7):1737-1745.
31. Yang Y, Bedford MT. Protein arginine methyltransferases and cancer. *Nat Rev Cancer*. 2013;13(1):37-50.
32. Yan F, Alinari L, Lustberg ME, et al. Genetic validation of the protein arginine methyltransferase PRMT5 as a candidate therapeutic target in glioblastoma. *Cancer Res*. 2014;74(6):1752-1765.
33. Banasavadi-Siddegowda YK, Welker AM, An M, et al. PRMT5 as a druggable target for glioblastoma therapy. *Neuro Oncol*. 2018;20(6):753-763.
34. Wang L, Pal S, Sif S. Protein arginine methyltransferase 5 suppresses the transcription of the RB family of tumor suppressors in leukemia and lymphoma cells. *Mol Cell Biol*. 2008;28(20):6262-6277.
35. Mavrakis KJ, McDonald ER, Schlabach MR, et al. Disordered methionine metabolism in MTAP/CDKN2A-deleted cancers leads to dependence on PRMT5. *Science*. 2016;351(6278):1208-1213.
36. Braun CJ, Stanciu M, Boutz PL, et al. Splicing of regulatory detained introns within oncogenic transcripts creates an exploitable vulnerability in malignant glioma. *Cancer cell*. 2017;32(4):426.e11.
37. Jiang H, Zhu Y, Zhou Z, et al. PRMT5 promotes cell proliferation by inhibiting BTG2 expression via the ERK signaling pathway in hepatocellular carcinoma. *Cancer Med*. 2018;7(3):869-882.
38. Jin Y, Zhou J, Xu F, et al. Targeting methyltransferase PRMT5 eliminates leukemia stem cells in chronic myelogenous leukemia. *J Clin Invest*. 2016;126(10):3961-3980.
39. Chiang K, Zielinska AE, Shaaban AM, et al. PRMT5 is a critical regulator of breast cancer stem cell function via histone methylation and FOXP1 expression. *Cell Rep*. 2017;21(12):3498-3513.
40. Tomao F, Papa A, Zaccarelli E, et al. Triple-negative breast cancer: new perspectives for targeted therapies. *Onco Targets Ther*. 2015;16(8):177-193.
41. Hsu J, Chen C, Chou C, et al. Crosstalk between Arg 1175 methylation and Tyr 1173 phosphorylation negatively modulates EGFR-mediated ERK activation. *Nat Cell Biol*. 2011;13(2):174-181.
42. Liao H-W, Hsu J-M, Xia W, et al. PRMT1-mediated methylation of the EGF receptor regulates signaling and cetuximab response. *J Clin Invest*. 2015;125(12):4529-4543.
43. Iderzorig T, Kellen J, Osude C, et al. Comparison of epithelial mesenchymal transition mediated tyrosine kinase inhibitor resistance in non-small cell lung cancer cell lines with wild type EGFR and mutant type EGFR. *Biochem Biophys Res Commun*. 2018;496(2):770-777.
44. Powers MA, Fay MM, Factor RE, Welm AL, Ullman KS. Protein arginine methyltransferase 5 accelerates tumor growth by arginine methylation of the tumor suppressor programmed cell death 4. *Cancer Res*. 2011;71(16):5579-5587.
45. Yang F, Wang J, Ren H-Y, et al. Proliferative role of TRAF4 in breast cancer by upregulating PRMT5 nuclear expression. *Tumor Biol*. 2015;36(8):5901-5911.
46. Hu D, Gur M, Zhou Z, et al. Interplay between arginine methylation and ubiquitylation regulates KLF4-mediated genome stability and carcinogenesis. *Nat Commun*. 2015;6:11-21.
47. Zhou L, Wu H, Lee P, Wang Z. Roles of the androgen receptor cofactor p44 in the growth of prostate epithelial cells. *J Mol Endocrinol*. 2006;37(2):283-300.
48. Gu Z, Li Y, Lee P, Liu T, Wan C, Wang Z. Protein arginine methyltransferase 5 functions in opposite ways in the cytoplasm and nucleus of prostate cancer cells. *PLoS One*. 2012;7(8):e44033.
49. Peng Y, Chen F, Melamed J, et al. Distinct nuclear and cytoplasmic functions of androgen receptor cofactor p44 and association with androgen-independent prostate cancer. *Proc Natl Acad Sci U S A*. 2008;105(13):5236-5241.
50. Lattouf H, Kassem L, Jacquemetton J, et al. LKB1 regulates PRMT5 activity in breast cancer. *Int J Cancer*. 2018;144(3):595-606.
51. Teng Y, Girvan AC, Casson LK, et al. AS1411 alters the localization of a complex containing protein arginine methyltransferase 5 and nucleolin. *Cancer Res*. 2007;67(21):10491-10500.
52. Györfy B, Lánckzy A, Eklund AC, et al. An online survival analysis tool to rapidly assess the effect of 22,277 genes on breast cancer prognosis using microarray data of 1,809 patients. *Breast Cancer Res Treat*. 2010;123(3):725-731.

## SUPPORTING INFORMATION

Additional supporting information may be found online in the Supporting Information section at the end of the article.

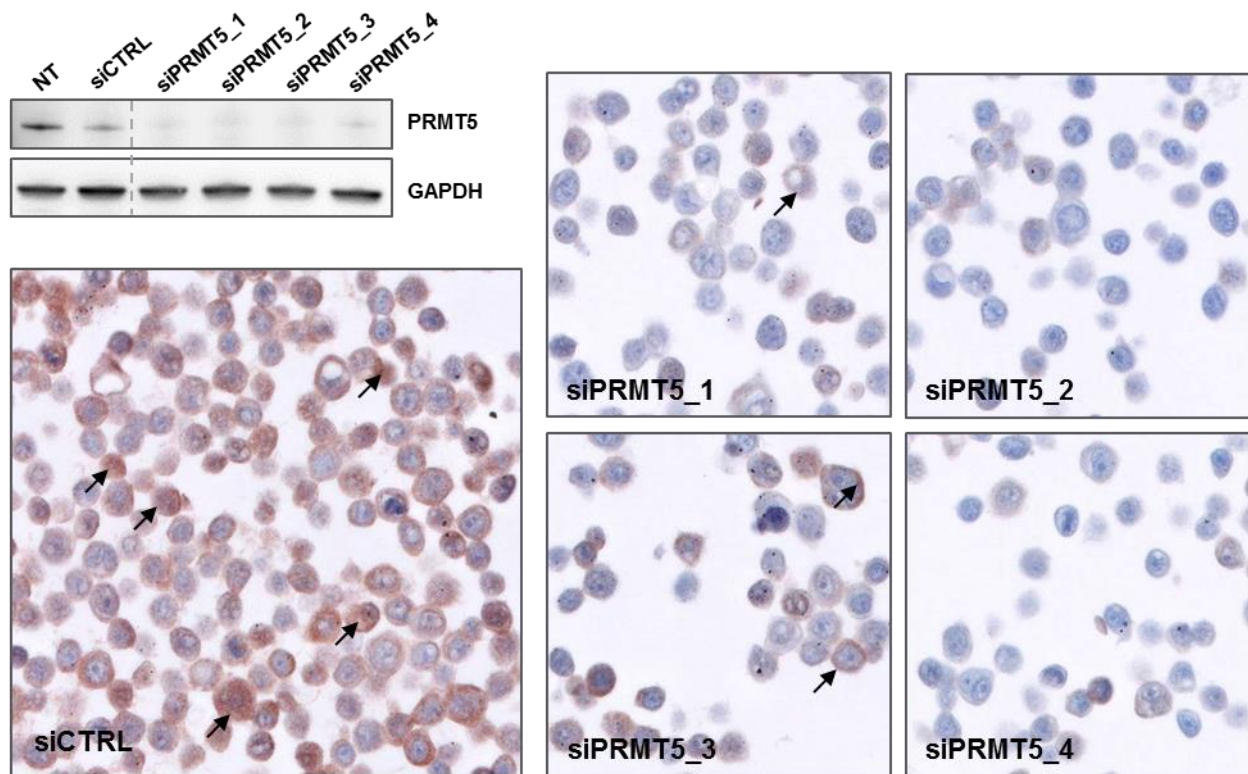
**How to cite this article:** Vinet M, Suresh S, Maire V, et al. Protein arginine methyltransferase 5: A novel therapeutic target for triple-negative breast cancers. *Cancer Med*. 2019;8:2414–2428. <https://doi.org/10.1002/cam4.2114>



**Supplementary Figure S1.** EPZ015666 shows no toxicity for mice.

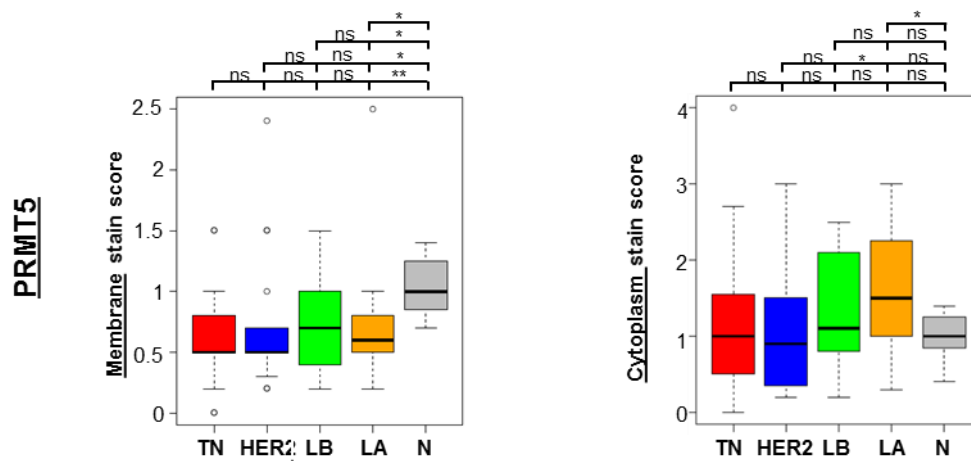
Nude mice (n=3) were administered EPZ015666 at 100 mg/kg *per-os* (*p.o.*), twice daily. Treatment was not associated with any mortality or body weight loss over the 21-day experimental period.





**Supplementary Figure S2.** PRMT5 antibody validation for IHC staining.

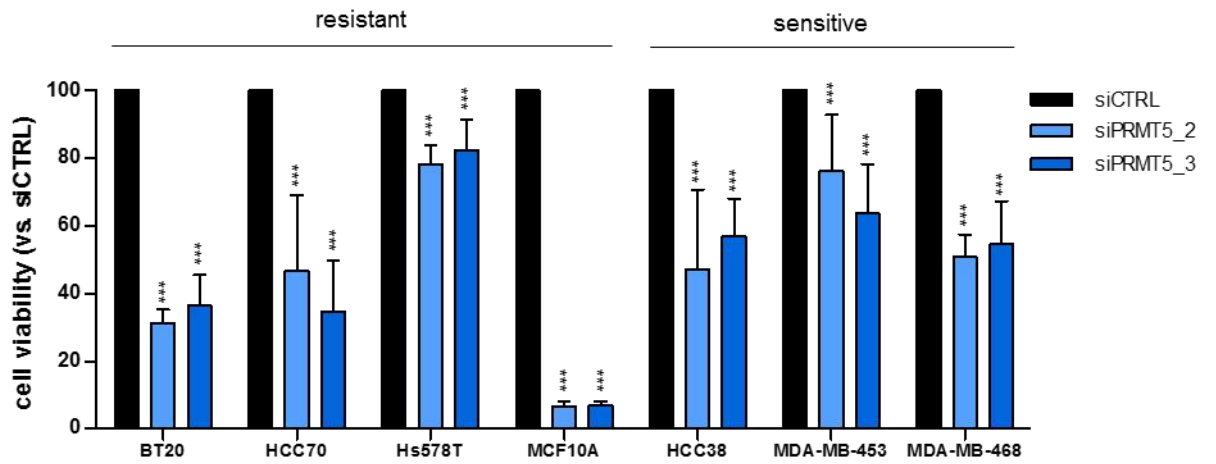
MDA-MB-468 cells were transfected with 20nM siRNA targeted against PRMT5 or with a control siRNA (siCTRL), or left untreated (NT). PRMT5 expression was assessed 72 hours later by western blotting. GAPDH was used as loading control. Part of the cells were collected, pelleted, frozen and fixed for IHC staining, as previously described<sup>17,19</sup>.



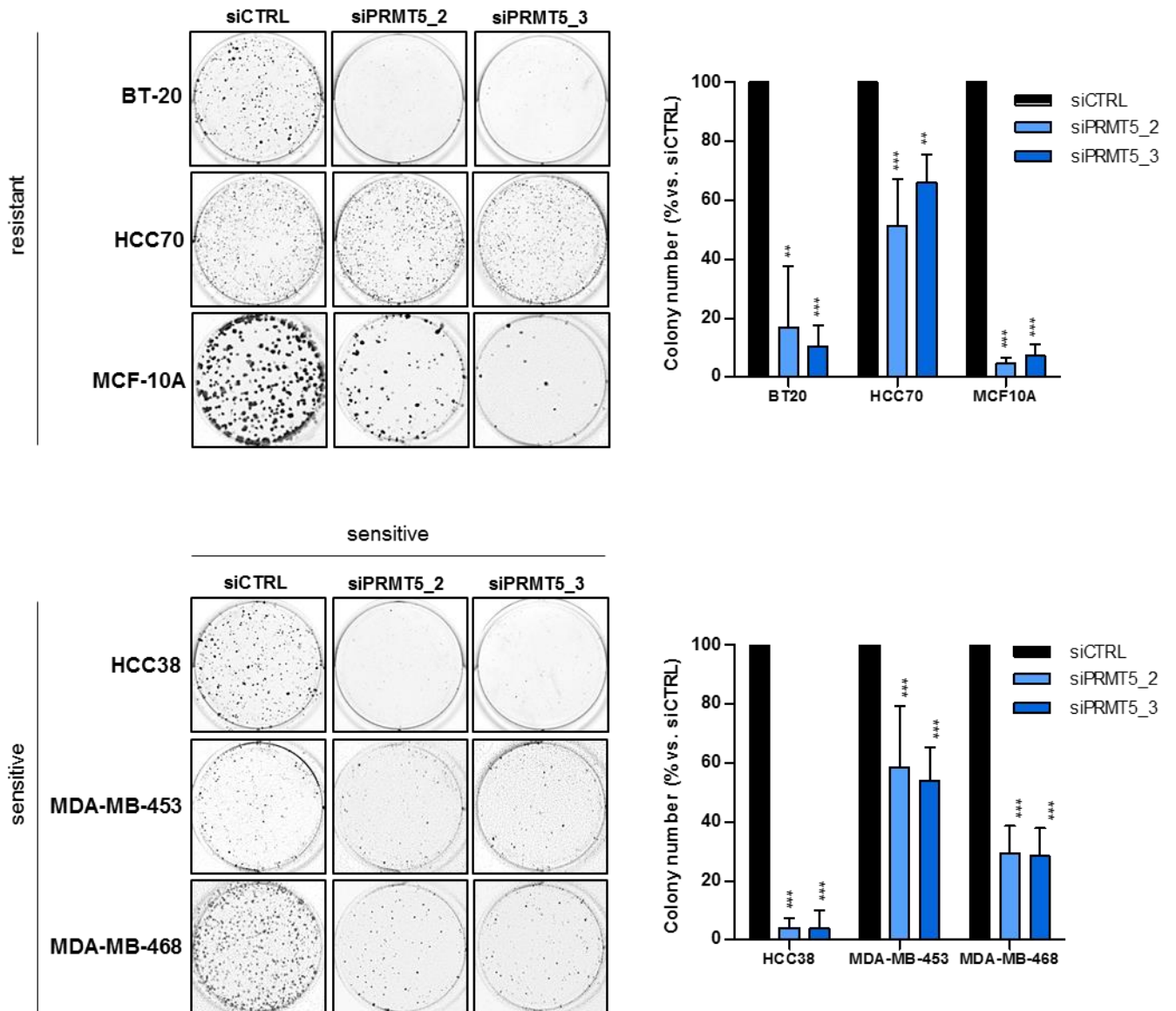
**Supplementary Figure S3.** Subcellular localization of PRMT5 in the Curie cohort.

PRMT5 protein levels were analyzed by immunohistochemistry (IHC) in the samples from the Curie cohort<sup>16</sup>: TNBC (TN, red), ER<sup>-</sup>/HER2<sup>+</sup> (HER2, blue), luminal B (LB, green), luminal A (LA, orange), and normal breast tissues (N, grey). Staining was quantified (0: no staining, 3: the strongest staining) at the cell membrane (left panels), and in the cytoplasm (right panels). Boxplots show median, upper and lower quartiles of each studied population. Outliers are represented as open circles. *P* values were calculated using Student t-test and are indicated as follows: \* $P < 0.05$ , \*\* $P < 0.01$ , \*\*\* $P < 0.001$ .

**a**

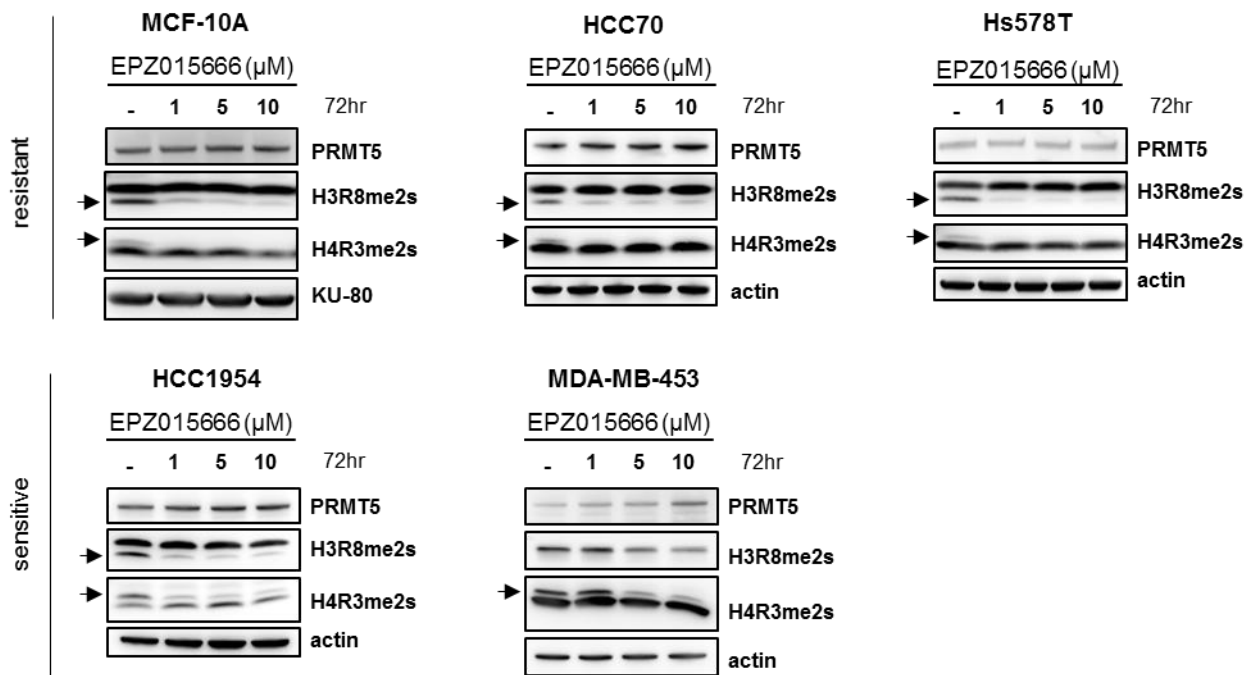


**b**



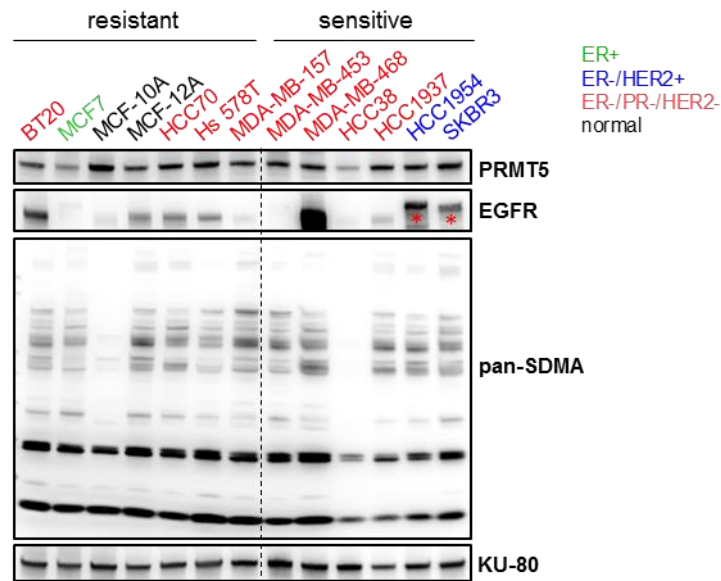
**Supplementary Figure S4.** PRMT5 depletion impairs TNBC cell viability and clonogenicity.

( a ) Cells were transfected with one of two PRMT5 siRNAs (PRMT5\_2, PRMT5\_3), chosen for their high efficacy, or control siRNA (siCTRL). Depletion was validated in all cell lines, and cell viability was determined by MTT assay after 6 days. Results are expressed as the percentage of cell growth relative to siCTRL-transfected cells. Presented is the mean of at least three independent experiments for each cell line. Cell lines are distributed according to their sensitivity to PRMT5 inhibitor EPZ015666. ( b ) TNBC cells were transfected with the indicated siRNA and seeded at low confluency for 5-14 days, until colony formation. A representative image of one well is shown for all conditions (left panel) Average colony number was evaluated using ImageJ Software (NIH) and is represented as a percentage relative to siCTRL-transfected cells. Represented are means + SD from at least three independent experiments (right panel). Black bars: siCTRL-transfected cells; blue bars: siPRMT5-transfected cells. *P* values were calculated using Student t-test and are indicated as follow: \**P*<0.05, \*\**P*<0.01, \*\*\**P*<0.001 (*i.e.* decrease relative to siCTRL). Cell lines are grouped according to their sensitivity to PRMT5 inhibitor EPZ015666.



**Supplementary Figure S5.** EPZ015666 inhibits PRMT5 activity in breast cell lines.

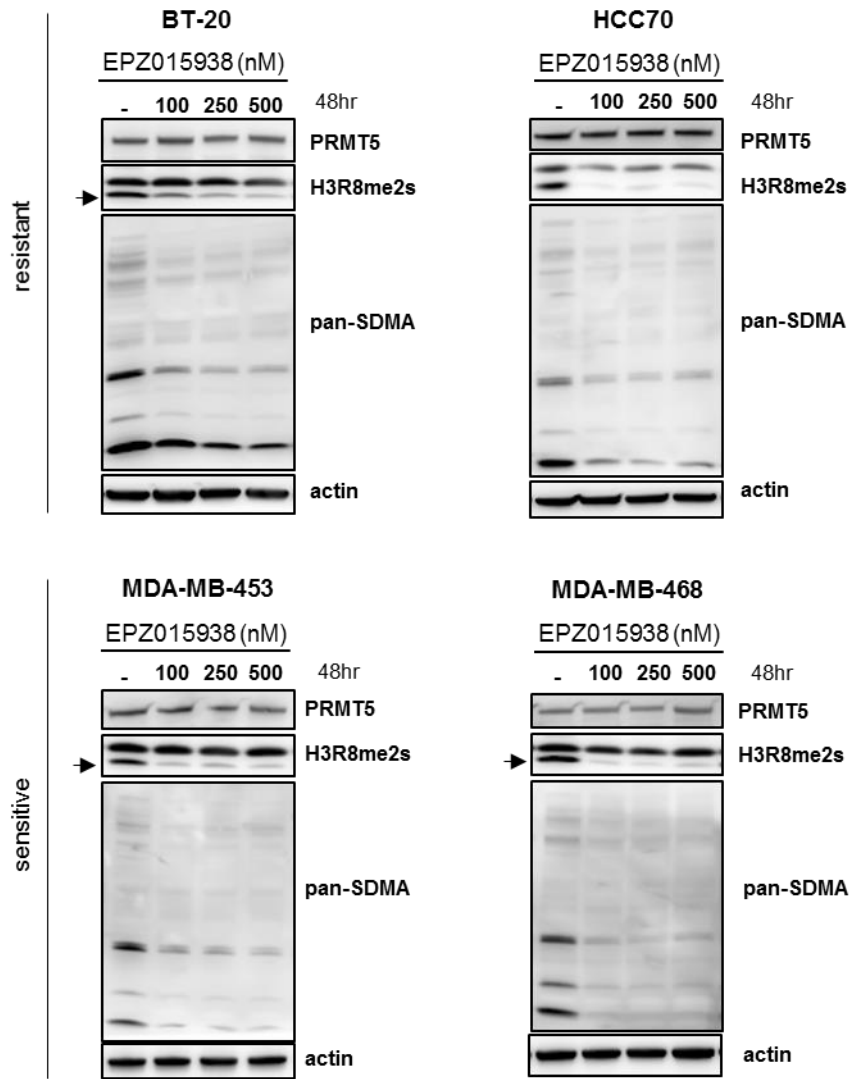
Cells were treated with the indicated concentration of the PRMT5 inhibitor EPZ015666 or with vehicle (DMSO). PRMT5 activity was assessed 72 hours later by Western-Blot analysis using antibodies that recognize symmetric dimethyl-arginine on histones H3 (H3R8me2s) and H4 (H4R3me2s). PRMT5 expression was verified. Actin or KU-80 were used as loading controls. Pictures are from a single experiment representative of at least two independent experiments.



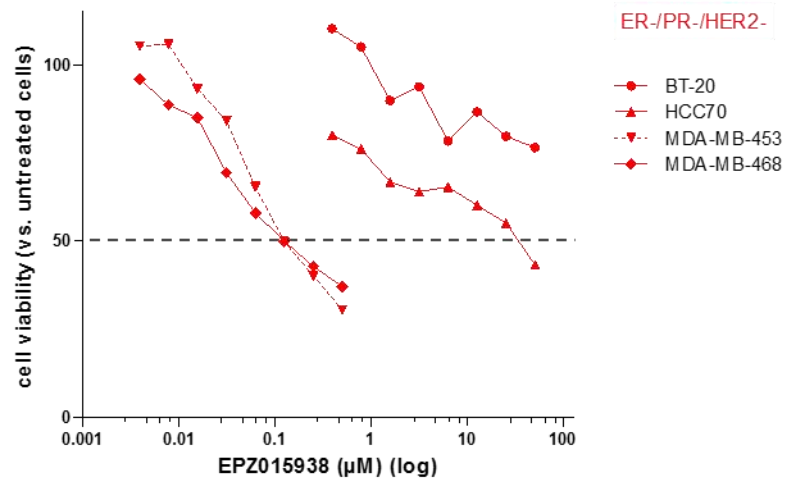
**Supplementary Figure S6.** PRMT5 expression, activity, and EGFR expression across a panel of breast cancer cell lines.

Western Blot analysis of PRMT5 expression and activity (total symmetric dimethylation of arginines; pan-SDMA), and of EGFR expression in a panel of breast cancer cell lines. KU-80 was used as a loading control. Cell lines are distributed according to their sensitivity to PRMT5 inhibitor EPZ015666. Breast cancer subtypes are indicated as follows: green (ER<sup>+</sup>), blue (ER<sup>-</sup>/HER2<sup>+</sup>), red (ER<sup>-</sup>/PR<sup>-</sup>/HER2<sup>-</sup>). The non-tumorigenic breast cells, MCF-10A and MCF-12A, are in black. Pictures are from a single experiment representative of three independent experiments. \* corresponds to HER2, as the EGFR antibody used is known to cross-react with HER2.

**a**



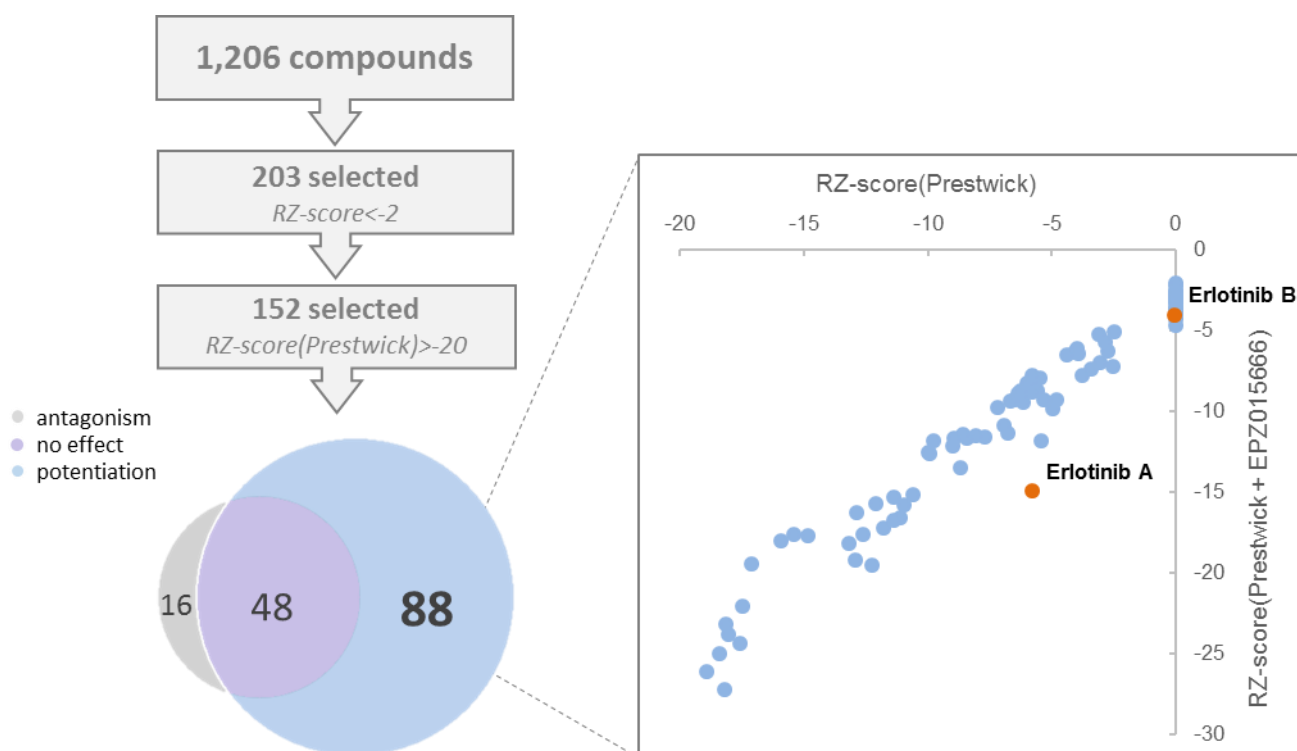
**b**



**Supplementary Figure S7.** EPZ015038 inhibits PRMT5 activity of 4 TNBC cell lines and identifies sensitive and resistant cells lines

( *a* ) EPZ015938 inhibits PRMT5 activity. Cells were treated with the indicated concentration of the PRMT5 inhibitor EPZ015938 or with vehicle (DMSO). PRMT5 activity was assessed 48 hours later by Western-Blot analysis using antibodies that recognize symmetric dimethyl-arginine on histones H3 (H3R8me2s) and total symmetric dimethyl-arginine (pan-SDMA). PRMT5 expression was verified. Actin was used as loading control. Pictures are from a single experiment representative of three independent experiments. ( *b* ) EPZ015938 identifies sensitive and resistant cells lines. Cell viability was determined by MTT assay after four doubling times. Results are expressed as the percentage of cell growth relative to untreated cells. The mean of at least three independent experiments for each cell line is represented.





**Supplementary Figure S8.** Drug combination screen identifies Erlotinib as candidate for dual therapy with EPZ015666.

A screening with a panel of 1,200 FDA approved drugs (Prestwick Chemical Library) and six additional compounds including Erlotinib (Sup. Table 2) reveals a benefit to combining PRMT5 and EGFR inhibitors. MDA-MB-453 cells were seeded into 384-well plates and treated with the Prestwick Chemical Library (10 $\mu$ M) or one of six additional compounds (Sup. Table 2; concentration as indicated) alone, or in combination with EPZ015666 (10 $\mu$ M). After 3 days, cell viability was assessed by CellTiter-Glo (CTG) assay. Of the 1,206 screened compounds, 203 were identified as detrimental to MDA-MB-453 cell viability ( $RZ\text{score} < -2$ ). Compounds which alone inhibited cell viability by 90% or more ( $RZ\text{score}(\text{Prestwick}) \leq -20$ ) were excluded from this first selection, leaving 152 hits. The 152 hits were then sorted by  $\Delta RZ\text{score}$  using the following thresholds to delineate the effect of the Prestwick+EPZ015666 combination:  $\Delta RZ\text{score} > 0$ : antagonism;  $-2 < \Delta RZ\text{score} \leq 0$ : no effect;  $-2 \leq \Delta RZ\text{score}$ : potentiation. Represented on the graphic are RZ-scores of Prestwick

alone vs. Prestwick+EPZ015666 for the 88 compounds for which the combination potentiates the effect of each compound alone, according to the described analysis. Erlotinib A (Prestwick Chemical) and Erlotinib B (Caiman Chemical) are highlighted in orange.

**Supplementary Table 1.** Antibodies used in this study.

<b>Target</b>	<b>Cat. #</b>	<b>Manufacturer</b>	<b>Use</b>
PRMT5	2252	CST	WB
PRMT5	ab109451	Abcam	IHC
c-casp7 (Asp198)	9491	CST	WB
c-casp8 (Asp391)	9496 (18C8)	CST	WB
c-PARP (Asp214) p89	ab32561	Abcam	WB
PARP/c-PARP (Asp214) p89	9546	CST	WB
pan-SDMA	13222	CST	WB
H3R8me2s	23613-0018	Epiccypher	WB
H4R3me2s	ab5823	Abcam	WB
Actin Beta (Clone AC-15)	A5441	Sigma	WB
GAPDH	2118	CST	WB
KU-80 (C48E7)	2180	CST	WB
anti-Rabbit IgG (H+L) HRP	111-035-045	Interchim	WB
anti-Mouse IgG (H+L) HRP	115-035-062	Interchim	WB

**Supplementary Table 2.** Additional drugs to the Prestwick Chemical Library+EPZ015666 screening and concentration.

	final concentration ( $\mu\text{M}$ )
<b>Erlotinib (Caiman Chemicals)</b>	10
<b><i>B12536</i> (PLK1 inhibitor - Selleck Chemicals)</b>	0.1
<b><i>BAY1217389</i> (TTK inhibitor - Selleck Chemicals)</b>	0.2
<b>Cisplatin (Mylan)</b>	10
<b>Doxorubicin (Sigma)</b>	0.1
<b>Paclitaxel (Selleck Chemicals)</b>	0.01

**Supplementary Table 3.** IC50 values for EPZ015666 in breast cancer cell lines. Cell lines are listed from most to least sensitive. IC50 values are calculated from at least three independent experiments. BC subtypes are indicated as follows: green (ER+), blue (ER-/HER2+), red (ER-/PR-/HER2-). The “normal” breast cells, MCF-10A and MCF-12A, are in black. ER-/PR-/HER2- cell lines encompass the different TNBC subtypes: BL1 (basal-like 1); BL2 (basal-like 2); LAR (luminal androgen receptor); MSL (mesenchymal stem like); UN (unclassified), as previously defined (2).

	ER-/PR-/HER2-subtype	EPZ015666 IC50 ( $\mu$ M)	Standard deviation	
HCC1954		<b>0.8</b>	0.1	<b>SENSITIVE</b>
MDA-MB-453	LAR	<b>1.0</b>	0.3	
HCC38	BL1	<b>2.2</b>	1.6	
MDA-MB-468	BL1	<b>2.2</b>	0.9	
MCF7		<b>2.6</b>	1.0	
SKBr3		<b>3.9</b>	1.9	
BT-20	UN	<b>12.3</b>	7.8	<b>RESISTANT</b>
HCC70	BL2	<b>29.9</b>	5.7	
MDA-MB-157	MSL	<b>33.4</b>	1.7	
MCF10A		<b>42.7</b>	14.2	
MCF12A		<b>47.1</b>	11.2	
Hs578T	MSL	<b>67.8</b>	17.6	
HCC1937	BL1	<b>74.7</b>	32.4	

**Titre:** Analyse des protéines arginine méthyltransférases 1 (PRMT1) et 4 (PRMT4) dans les cancers du sein triple-négatifs

**Mots clés:** Cancer du sein; PRMT; thérapie ciblée; modification post-traductionnelle ; Voie de signalisation Wnt ; Cytokinèse

**Résumé:** L'identification de nouvelles stratégies de traitement pour les patientes atteintes d'un cancer du sein triple-négatifs (TNBC) reste une priorité en oncologie. Les protéines arginine méthyltransférases (PRMTs) sont surexprimées dans de nombreux cancers, et émergent actuellement comme des cibles thérapeutiques de grand intérêt. L'objectif de ma thèse était centré sur l'étude des PRMT1 et PRMT4 dans les cancers du sein TNBC. Nous avons constaté que ces deux PRMTs sont exprimées plus abondamment dans les cancers du sein que dans les tissus mammaires normaux, et que la déplétion de PRMT1 ou de PRMT4 freine la prolifération cellulaire et induit l'apoptose. Nous avons montré que PRMT1 régule les voies de signalisation Wnt et EGFR en se liant d'une part au promoteur de LRP5 et porcupine et d'autre part à celui de l'EGFR. L'inhibition de PRMT1 (avec des inhibiteurs contre les PRMTs de type I) réduit la taille des colonies (dans un test de formation de colonie) et l'activité de la voie Wnt in vitro, et la croissance tumorale chez la souris. Nous avons observé une interaction synergique entre ces inhibiteurs des PRMTs et certaines chimiothérapies (mais pas avec d'autres) utilisées en clinique pour le traitement des patientes avec un cancer TNBC, ainsi qu'avec un inhibiteur anti-EGFR, mettant en avant le potentiel thérapeutique de ces combinaisons. En revanche, l'inhibition de PRMT4 n'a aucun effet sur la prolifération d'une lignée TNBC, suggérant que PRMT4 pourrait réguler la viabilité cellulaire indépendamment de son activité enzymatique mais au travers de son interaction avec certains de ses partenaires. Nous avons alors entrepris de caractériser l'interactome de PRMT4 dans des lignées cellulaires TNBC et avons identifié ALIX comme son partenaire principal. PRMT4 se lie avec le domaine C-terminal d'ALIX et le méthyle ; un domaine clé interagissant avec de nombreuses protéines. La déplétion de PRMT4 entraîne des défauts de cytokinèse, similaires à ceux observés à la suite de la déplétion d'ALIX. Des travaux en cours devraient permettre de caractériser les mécanismes moléculaires du contrôle de la cytokinèse par PRMT4.

**Title:** Analysis of the protein arginine methyltransferases 1 (PRMT1) and 4 (PRMT4) in triple-negative breast cancer

**Keywords:** Breast cancer; PRMT; Targeted therapy; post-translational modification; Wnt signaling pathway; Cytokinesis

**Abstract:** Breast cancer is a highly heterogenous disease comprising of different subtypes. Triple-negative breast cancer (TNBC) is associated with the worst prognosis. Identification of novel treatment strategies for TNBC patients is an unmet clinical need. Protein arginine methyltransferases (PRMTs), the family of enzymes that methylate histone and non-histone proteins are overexpressed in several cancer types and are currently emerging as attractive therapeutic targets. The goal of my thesis was to study PRMT1 and PRMT4 in TNBC. We found both PRMTs are more expressed in breast cancer compared to normal breast tissue, and that depleting PRMT1 or PRMT4 impaired cell proliferation and induced apoptosis. We found that PRMT1 regulates the Wnt or the EGFR signaling pathway by binding to the promoter of LRP5 and porcupine or EGFR. PRMT1 inhibition (Type I PRMT inhibitors) decreases colony formation and Wnt activity in vitro and delays tumor growth in mice. Type I PRMT inhibitors exhibit synergistic interactions with some chemo- or targeted- (anti-EGFR) therapies, highlighting the therapeutic potential of these combinations. In contrast, PRMT4 inhibition shows no effect on TNBC cell proliferation, indicating that PRMT4 regulates cell viability independently of its enzymatic activity. Hence, we characterized the PRMT4 interactome in a TNBC cell line and identified ALIX as its major partner. PRMT4 binds to and methylates the c-terminal domain of ALIX, the hub for its protein-protein interactions. The depletion of PRMT4 shows cytokinetic defects, similar to the known phenotype induced upon ALIX depletion. Additional ongoing work will uncover the molecular mechanisms by which PRMT4 regulates cytokinesis.